Technical Feasibility of Compressed Air Energy Storage (CAES) Utilizing a Porous Rock Reservoir

Final Report Appendix — Chapter 6

March 2018

Report Number DOE-PGE-00198-5

Prepared by

Pacific Gas & Electric Company

San Francisco, CA 94105

Authors
Michael Medeiros, Robert Booth, James Fairchild, Doug Imperato, Charles Stinson, Mark Ausburn, Mike Tietze, Saeed Irani, Alan Burzlaff, Hal Moore, James Day, Ben Jordan, Trent Holsey, Doug Davy, Kevin Plourde

For the United States Department of Energy under Contract DOE-OE0000198, Executed December 2009

And, the California Public Utilities Commission under Decision 10-01-025, Executed January 2010

And, the California Energy Commission under Grant Award PIR-12-001, Executed July 2013

Principal Investigator

Michael Medeiros, Program Manager, Pacific Gas & Electric Company, mjml@pge.com

Acknowledgments

We would like to acknowledge the many organizations and individuals who contributed their time and unique expertise to the overall Compressed Air Energy Storage (CAES) Study effort and in creating the basis for this final report. These included PG&E contractors Worley Parsons, MHA Petroleum Consultants, Irani Engineering, Vox Planning, CH2M Hill, Hal Moore Energy Consulting Services, Bluewater Energy Solutions, Day Carter Murphy LLP, King Island Gas Storage, Robert Booth, James Fairchild, Doug Imperato, and Charles Stinson. As well, we would like to acknowledge Lawrence Berkeley National Labs and the public agencies of San Joaquin County and the City of Lodi for their contributions and support. Reviewing and editing by Jonas Weisel are also gratefully acknowledged.

Citation

Medeiros, M, Booth, R, Fairchild, J, Imperato, D, Stinson, C, Ausburn, M, Tietze, M, Irani, S, Burzlaff, A, Moore, H, Day, J, Jordan, B, Holsey, T, Davy, D, Plourde, K. 2018. Technical Feasibility of Compressed Air Energy Storage (CAES) Utilizing a Porous Rock Reservoir, Final Report. DOE-PGE-00198-1. Pacific Gas & Electric Company, San Francisco, CA, March 2018.

Legal Disclaimer

This report was prepared by Pacific Gas and Electric Company. Neither Pacific Gas and Electric Company nor any of its employees and agents: makes any written or oral warranty, expressed or implied, including, but not limited to those concerning merchantability or fitness for a particular purpose; assumes any legal liability or responsibility for the accuracy, completeness, or usefulness of any information, apparatus process, method, or policy contained herein; or represents that its use would not infringe any privately owned rights, including, but not limited to, patents, trademarks, or copyrights.

This report was prepared as an account of work sponsored by agencies of the United States government. Neither the United States government nor any agency thereof, nor any of their employees, makes any warranty, express or implied, or assumes any legal liability or responsibility for the accuracy, completeness, or usefulness of any information, apparatus, product, or process disclosed, or represents that its use would not infringe privately owned rights.

Reference herein to any specific commercial product, process, or service by trade name, trademark, manufacturer, or otherwise does not necessarily constitute or imply its endorsement, recommendation, or favoring by the United States government or any agency thereof. The views and opinions of authors expressed herein do not necessarily state or reflect those of the United States government or any agency thereof.

Abstract

Pacific Gas & Electric Company (PG&E) conducted a project to explore the viability of underground compressed air energy storage (CAES) technology.

CAES uses low-cost, off-peak electricity to compress air into a storage system in an underground space such as a rock formation or salt cavern. When electricity is needed, the air is withdrawn and used to drive a generator for electricity production.

The project screened potential sites in California and selected two locations: King Island, near Stockton, and East Island in San Joaquin County. All necessary rights were acquired at both sites to conduct tests and develop a CAES facility. Core drilling provided information on reservoir rock properties, caprock properties, reservoir pressure, and reservoir fluid. Results found the conditions at the King Island site to be more favorable than East Island. Air injection testing at King Island produced data on flow dynamics, rock mechanics, and other factors. Finally, the project team developed a conceptual engineering design for a CAES facility and reservoir infrastructure, and analyzed the environmental impacts and permitting requirements.

To determine the interest and qualifications of potential third parties, the project issued a Request for Offer (RFO), which required applicants to describe their technical qualifications to develop, construct, own, operate, and maintain a CAES facility at the King Island site, and to estimate their costs for participation in the project. Offers were received, but the best offer was not economically competitive with alternative storage technologies.

The project demonstrated the technical feasibility of using an abandoned natural gas reservoir for storing high-pressure compressed air for a 300-MW-by-10-hour CAES facility. The reservoir at the King Island site was shown to be capable of accommodating the flow rates and pressures necessary for the operation of the facility. However, the estimated high cost of a CAES facility will have to be addressed in the context of the cost of alternative energy storage technologies.

Chapter 6 Attachments

A601: Final Tech Memo for CAES: Reservoir Characterization and Full Field Development Model
A602: Flammability Characteristics of Combustible Cases and Vapors
A603: Limiting Oxygen - Impacts on Flammability
A604: Methane Lower Flammability Limit as Function of Pressure
A605: USBM Bulletin 680 - Investigation of Fire & Explosion

A601: Final Tech Memo for CAES: Reservoir Characterization and Full Field Development Model

WorleyParsons
resources & energy

PACIFIC GAS AND ELECTRIC

Final Technical Memorandum For Compressed Air Energy Storage Reservoir Characterization and Full Field Development Model

King Island Gas Field

San Joaquin County, California

108010-00365 – PGCS-1-LI-022-018_Rev 0

25 September 2015

Power
WorleyParsons Limited
2330 East Bidwell Street, Sacramento (Folsom) CA 95630, United States of America
Tel: +1 916 817 3920
Fax: +1 916 983 1935

WorleyParsons
resources & energy

PACIFIC GAS AND ELECTRIC

CERTIFICATION AND DISCLAIMER

This report has been prepared under the review and supervision of Alan Burzlaff, P. E. as an employee of MHA Petroleum Consultants, and with expertise in reservoir engineering and numerical simulation. The report was prepared with the assistance of Mark Ausburn, P.G., as an employee of WorleyParsons and with expertise in petroleum geology. Their signatures and professional registration stamps appear below. The findings, recommendations, specifications and/or professional opinions presented herein have been prepared in accordance with generally accepted professional geologic and petroleum engineering practice for similar projects, and within the scope of the project. There is no warranty, express or implied, and no assumption of any legal liability or responsibility for the accuracy, completeness, or usefulness of any information or process disclosed in this report. The reservoir modeling results in this report should not be regarded as exact quantities or predictions of actual reservoir performance.

MHA Petroleum Consultants
Alan A. Burzlaff, P. E.
Vice-President

WorleyParsons Group
Mark Ausburn, P.G.
Senior Supervising Geologist

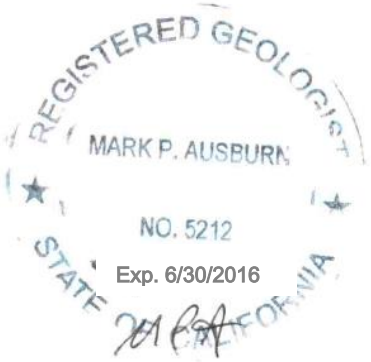

WorleyParsons

resources & energy

PACIFIC GAS AND ELECTRIC

PROJECT: FINAL TECHNICAL MEMORANDUM: COMPRESSED AIR ENERGY STORAGE RESERVOIR CHARACTERIZATION AND FULL FIELD DEVELOPMENT MODEL

REV	DESCRIPTION	ORIG	REVIEW	WORLEY-PARSONS APPROVAL	DATE	CLIENT COMMENTS/ APPROVAL	DATE
0	Issued for final client review	MPA, AAB A. Burzlaff, M. Ausburn	J.Chan, C. Stinson, J. Fairchild	MPA M. Ausburn	Sep 2015		

FINAL TECHNICAL MEMORANDUM FOR COMPRESSED AIR ENERGY STORAGE RESERVOIR CHARACTERIZATION AND FULL FIELD DEVELOPMENT MODEL

KING ISLAND GAS FIELD SAN JOAQUIN COUNTY, CALIFORNIA

TABLE OF CONTENTS

1. INTRODUCTION 1

2. PURPOSE 2

3. SUMMARY OF PREVIOUS WORK 3

4. SUMMARY OF CURRENT FINDINGS 5

5. COMPRESSION TESTING PROGRAM 7

5.1 PG&E Test Injection/Withdrawal Well 1 7

5.1.1 Well Construction 7
5.1.2 Reservoir Characterization 10
5.1.3 Reservoir Conditions 16

5.2 Observation Wells 17

5.3 Compression Test Overview 19

5.3.1 Testing, Logging and Sampling Data Collection 20
5.3.2 EPA Permit Required Testing, Analyses and Reporting 20

5.4 Temporary Site Facility 23

5.4.1 Surface Compression/Withdrawal System 23
5.4.2 Test Instrumentation 25
5.4.3 Data Acquisition System (DAS) 27

5.5 Phase 1 – Oxygen-Depleted Air Bubble Build 27

5.5.1 Test Bubble Development 28
5.5.2 Reservoir Pressure Response 29
5.5.3 Pressure Fall-off Testing 30
5.5.4 Thermal Multi-gate Decay Lithology (TMDL) Logging Results 31

5.6 Phase 2 – Oxygen-Depleted Air Cycling 33

5.6.1Deliverability Testing 33
5.6.2Bubble Performance 34
5.6.3Reservoir Pressure Response 36
5.7 Phase 3 – Data Evaluation 36
5.7.1Sampling Results 37
5.8 Phase 4 – Ambient Air Testing 37
5.8.1Deliverability Testing 37
5.8.2Withdrawal Testing 38
6. RESERVOIR SIMULATION 39
6.1 Model Update 42
6.2 ECLIPSE Compositional Simulator 42
6.2.1History Match Pre-Compression Testing 43
6.2.2History Match Compression Testing 44
6.3 Full Field Development 45
7. CAES REFINED RESERVOIR DEVELOPMENT SCENARIOS 46
7.1 Design Criteria 46
7.2 Well Plan 48
7.3 Bubble Build 49
7.4 Simulated CAES Operations 49
8. REFERENCES 52

TABLE OF CONTENTS (Cont'd)

LIST OF TABLES

TABLE NO.	DESCRIPTION
1	General Details for I/W Well
2	Casing/Tubing Detail for I/W Well
3	Packer Details for I/W Well
4	Bottom Hole Completion Details for I/W Well
5	Logging/Sidewall Coring Program for I/W Well
6	Routine Sidewall Core Analyses Results for I/W Well
7	MRF Reservoir Properties in I/W Well
8	Sidewall Core Porosity and Permeability in MRF Reservoir in I/W Well
9	Fall-off Test Results from I/W Well
10	Depth Discrete Pressure Measurements from I/W Well
11	General Details for Observation Wells
12	Casing/Tubing Details for Observation Wells
13	Packer Details for Observation Wells
14	Compression Test Phases
15	Testing and Sampling Required by EPA UIC Permit
16	PG&E Submittals to EPA
17	Temporary Site Facility (TSF) Surface Equipment
18	Specifications for Gauges, Meters and Sensors
19	Oxygen-Depleted Air Injectate Composition
20	Compression Test Bubble Build Schedule
21	Results of Pressure Gradient Surveys for Piacentine 1-27
22	Results of Pressure Gradient Surveys for Citizen Green 1
23	Results of Fall-off Tests in Injection/Withdrawal Well
24	Results of Simulated Fall-off Test in Injection/Withdrawal Well
25	Thermal Multi-gate Decay Lithology (TMDL) Logging Summary
26	Oxygen-Depleted Air Cycle Testing Program
27	Compression Test Cycle-Testing Data
28	Data Evaluation in Consideration of Ambient Air Testing
29	Analytical Results of I/W Well Gas Samples during Depleted Air Cycle Testing

TABLE NO.	DESCRIPTION
30	Ambient Air Flow Testing Program
31	Ambient Air Injectate Composition
32	Analytical Results of I/W Well Gas Samples during Ambient Air Testing
33	King Island – Native Gas Components in Field and Model
34	King Island CAES Full Field Development Design Parameters
35	CAES 300 MW Plant Weekly Injection/Withdrawal Schedule

TABLE OF CONTENTS (Cont'd)

LIST OF FIGURES

FIGURE NO.	DESCRIPTION
1	King Island Reservoir and Well Locations
2	Planned and Actual I/W and Observation Well Coordinates and Actual Well Bore Path
3	Injection/Withdrawal Well 1 Wellbore Diagram
4	Geological Structure Cross-Section Across East Lobe
5	Structure Map of Top Upper MR1
6	Structure Map of Top Lower MR1
7	Structure Map of Base Lower MR1
8	Piacentine 2-27 and I/W Well Core Results – Porosity vs. Permeability
9	King Island Gas Field Compression Testing Program
10	Reservoir Pressure Response vs. Bubble Build Volume
11	Results of Isochronal Tests in Injection/Withdrawal Well During Depleted Air Cycle Testing - Bottomhole Absolute Open Flow Plot
12	Results of Isochronal Tests in Injection/Withdrawal Well During Depleted Air Cycle Testing - Wellhead Absolute Open Flow Plot
13	Reservoir Pressure Response During Depleted Air Cycle Testing
14	King Island Model Forecast of Methane Concentration During Ambient Air Flow Testing
15	Results of Isochronal Tests in Injection/Withdrawal Well During Depleted Air Cycle Testing and Ambient Air Flow Testing - Bottomhole Absolute Open Flow Plot
16	Results of Isochronal Tests in Injection/Withdrawal Well During Depleted Air Cycle Testing and Ambient Air Flow Testing - Wellhead Absolute Open Flow Plot
17	Grid Display – Cross-Section Locations
18	Porosity Aerial
19	Porosity Cross-Section
20	Permeability Aerial
21	Permeability Cross-Section
22	King Island Gas Field – Initial Gas-in-Place – Aerial Gas Saturation
23	Initial Gas-in-Place – Cross-Section Gas Saturation
24	Moresco A1 History Match – Gas Production
25	Moresco A1 History Match – Water Production
26	Moresco A1 History Match – BHP

FIGURE NO.	DESCRIPTION
27	Piacentine 1-27 History Match – Gas Production
28	Piacentine 1-27 History Match – Water Production
29	Piacentine 1-27 History Match – BHP
30	Citizen Green RD1 History Match – Gas Production
31	Citizen Green RD1 History Match – Water Production
32	Citizen Green RD1 History Match – BHP
33	King Island HCPV vs. Depth, Used to Define Strength and Volume of Aquifer Influx
34	Compression Test History Match – I/W Well Gas Production/Injection
35	Compression Test History Match BHP – I/W Well
36	Compression Test History Match BHP – Piacentine 1-27
37	Compression Test History Match BHP – Citizen Green RD1
38	Compression Test History Match - I/W Well - % Methane in Withdrawal Stream
39	Compression Test History Match - I/W Well - % Oxygen in Withdrawal Stream
40	Compression Test History Match - I/W Well - Water Production
41	Reservoir Pressure Response and Aquifer Influx / Efflux During King Island – Compression Testing and SI Period
42	LGR vs. No LGR Methane Concentration
43	Compression Testing Bubble Build (Beginning) Methane Composition Mole Fraction
44	Compression Testing Bubble Build (Beginning) – Cross-Section – Methane Composition Mole Fraction
45	Compression Testing Bubble Build (Beginning) Methane Composition Mole Fraction
46	Compression Testing Bubble Build (Beginning) – Cross-Section Methane Composition Mole Fraction
47	Compression Testing Bubble Build (Middle) Methane Composition Mole Fraction
48	Compression Testing Bubble Build (Middle) – Cross-Section – Methane Composition Mole Fraction
49	Compression Testing Bubble Build (End) Methane Composition Mole Fraction
50	Compression Testing Bubble Build (End) – Cross-Section – Methane Composition Mole Fraction
51	Compression Testing Program (End) Methane Composition Mole Fraction
52	Compression Testing Program (End) – Cross-Section – Methane Composition Mole Fraction
53	Compression Testing Program (End) – Zoom CT1 – Methane Composition Mole Fraction

FIGURE NO.	DESCRIPTION
54	Compression Testing Program End of Ambient Air Injection – Methane Composition Mole Fraction
55	Compression Testing Program End of Ambient Air Injection – Cross-Section - Methane Composition Mole Fraction
56	Compression Testing Program (End) Methane Composition Mole Fraction
57	Compression Testing Program (End) – Cross-Section - Methane Composition Mole Fraction
58	CAES Full Field Well Plan – Aerial View
59	CAES Full Field Well Plan – Cross-Sections
60	CAES Full Field Well Plan – Completion Interval – Cross-Section
61	King Island Full Field CAES Simulation – Bubble Build Period
62	CAES Full Field Well Plan – Beginning of Bubble Build – Methane Composition Mole Fraction
63	CAES Full Field Well Plan – End of Bubble Build – Methane Composition Mole Fraction
64	CAES Full Field Well Plan – End of Bubble Build – Cross-Section Views – Methane Composition Mole Fraction
65	CAES Full Field Well Plan End of Bubble Build – Cross-Section View Zoom – Methane Composition Within Air Bubble
66	CAES Full Field Development – B – Field Methane Concentration in Produced Gas Stream, and Field Average Pressure
67	CAES Full Field Development – B – Field Methane Concentration in Produced Gas Stream, and Field Water Production
68	CAES Full Field Development – B – Maximum Methane Concentration
69	CAES Full Field Development – B – Aerial View – Methane Composition Mole Fraction, January 7, 2022
70	CAES Full Field Development – B – Cross-Section Views – Methane Composition Mole Fraction, January 7, 2022
71	CAES Full Field Development – B – Aerial View – Methane Composition Mole Fraction, March 11, 2022
72	CAES Full Field Development – B – Cross-Section Views – Methane Composition Mole Fraction, March 11, 2022
73	CAES Full Field Development – B – Aerial View – Methane Composition Mole Fraction, December 23, 2022
74	CAES Full Field Development – B – Cross-Section Views – Methane Composition Mole Fraction, December 23, 2022
75	CAES Full Field Development – B – Cross-Section View Zoom – Methane Composition Within Air Bubble, December 23, 2022

TABLE OF CONTENTS (Cont'd)

LIST OF PHOTOS

PHOTO NO.	DESCRIPTION
1	Drilling Rig and Halliburton Pump Trucks - Step Rate Test, October 2014
2	Water Storage Tanks in Use at Well Site during Step Rate Test, October 2014
3	Temporary Site Facility – Surface Equipment

TABLE OF CONTENTS (Cont'd)

LIST OF APPENDICES

APPENDIX	DESCRIPTION
A	I/W Well Directional Program and Survey
B	I/W Well Mud Log
C	I/W Well Geophysical Logs
D	I/W Well Depth Discrete Pressure Measurements
E	I/W Well Sidewall Core Analyses
F	I/W Well Composite Logs and Interpretation Reports
G	I/W Well Step Rate Test and Initial Fall-off Test Report
H	Observation Wells As-build Schematics
I	EPA UIC Permit R9UIC-CAS5-FY13-1
J	Compression Test Daily Data and Information
K	Thermal Multi-gate Decay Lithology Logs and Report
L	Compression Test Laboratory Analyses
M	Stantec Drawing M00-01-001, Rev 0
N-1	Stantec drawings P00-02-001, Rev 1
N-2	Stantec drawings P00-02-002, Rev 1
O	Compression Test Hourly Data
P	Compression Test Fall-off Test Reports
Q	Isochronal Test Analyses

FINAL TECHNICAL MEMORANDUM FOR COMPRESSED AIR ENERGY STORAGE RESERVOIR CHARACTERIZATION AND FULL FIELD DEVELOPMENT MODEL

KING ISLAND GAS FIELD
SAN JOAQUIN COUNTY, CALIFORNIA

1. INTRODUCTION

Compressed Air Energy Storage (CAES) is a technique that stores, in the form of air, excess energy generated during times of low loads and then utilizes the pressurized air to generate electricity during periods of high demands. In the case of renewable energy resources, such as wind and solar power, the energy generated by these resources is intermittent and highly dependent on the resource (i.e. wind and sun); the energy generated by those resources, does not always match the time periods when customers need it most. Therefore, CAES technology is being investigated as one potential opportunity for storing this intermittent energy for use during higher demand periods.

Under California's existing Renewable Portfolio Standard, utilities must supply 33 percent of all electricity retail sales from eligible renewable resources by the year 2020. Much of this renewable generation is expected to be derived from the addition of new solar and wind power generation. As such, energy storage is a potential strategy to mitigate the intermittent effects and enable greater entry of wind and solar power into the existing electrical power generation and transmission system. CAES is a key technology for expanding reliance on wind and solar renewable resources for electricity production.

The United States Department of Energy (DOE), the California Public Utilities Commission (CPUC), and the California Energy Commission (CEC) have funded Pacific Gas and Electric Company (PG&E) to investigate the viability of using a nearly depleted natural gas field to store energy by injecting compressed air into a subsurface reservoir, during periods of excess and/or low-cost generation, and recovering it by generating electricity using turbo-generation equipment during high demand periods. The application of CAES using a depleted gas reservoir for storage provides several distinct advantages. First, depleted gas reservoirs are proven geologic traps that formerly held natural gas reserves for millions of years and are therefore capable of containing compressed air to power a CAES facility. Second, the subsurface data, including well logs, production, and seismic imaging data, that are needed for characterization of the reservoir and predicting its performance in a CAES application are typically available for natural gas fields. Finally, the Sacramento Valley Basin contains many natural gas fields that are situated along California's power transmission backbone, and thus ideally located to provide utility-scale power storage to facilitate integration and distribution of renewable energy throughout the state.

The first phase of the PG&E CAES project involved screening of depleted gas reservoirs throughout Northern California to select a subset of fields with the most favorable characteristics for further evaluation. Three gas field reservoirs were selected for computer modeling to further assess their suitability to support a CAES plant, and two of these were selected for drilling core wells to investigate reservoir and cap rock characteristics through well logging and laboratory analysis of core samples. Based on the core well data, subsequent reservoir model refinements and simulations and the expected ability of the reservoir to support a permanent 300 megawatt (MW)/10-hour storage facility, the King Island Gas Field emerged as the preferred location to perform the compression test.

The criteria and process that led to the selection of the King Island Gas Field reservoir for CAES compression testing and details of preliminary reservoir model development and planned compression test simulations are provided in WorleyParsons document PGCS-1-LI-022-017: *Preliminary Reservoir Characterization and Testing for Compressed Air Energy Storage* dated June 4, 2014 (WorleyParsons, 2014a). The June 2014 report also described the regional geologic setting and history of King Island Gas Field reservoir production and conditions, and provided preliminary reservoir characterization results through drilling, logging and completion of the Piacentine 2-27 core well in March 2013.

The second phase of the PG&E CAES project was the drilling and completion of the PG&E Test Injection/Withdrawal Well 1 (hereafter in this report referred to as the I/W Well) in October and November 2014 and the compression testing of the I/W well from February to June 2015. This phase was conducted in accordance with the requirements of an Underground Injection Control (UIC) Permit issued by the United State Environmental Protection Agency (EPA) on August 20, 2015 (EPA, 2014). The data collected from the I/W well and the compression test were used to further characterize the reservoir; to assess the reservoir performance on a pilot scale; to refine the computer model of the reservoir and develop a conceptual design for full scale reservoir development to support a CAES plant; and to support subsequent engineering, economic and environmental evaluations and conclude the project feasibility analysis.

2. PURPOSE

The purpose of this report is to document the following:

1. Final characterization and model update of the King Island Gas Field reservoir based on drilling and testing of the PG&E Test Withdrawal/Injection Well 1 (I/W well) in October-November 2014 and I/W well compression testing from February-June 2015; and

2. Running of reservoir model simulations to provide recommendations for CAES reservoir full field development at King Island Gas Field.

The refined reservoir development recommendations will meet the conceptual CAES Energy Conversion Facility (ECF) design requirements specified in WorleyParsons document PGCS-1-LI-027-0001 (WorleyParsons, 2014b), which are 2,300 pounds per square inch absolute (psia) maximum withdrawal air pressure at the wellhead and 1,100 million standard cubic feet per day (MMscfd) maximum withdrawal air flow rate to support an ECF nominal capacity of 300 MW with 10-hour withdrawal cycles and 12-hour injection Monday through Friday and 39-hour injection over the weekend.

3. SUMMARY OF PREVIOUS WORK

A. The King Island Gas Field was discovered in 1985. The gas-productive area encompasses about 235 acres (**Figure 1**). The field is an elliptical anticlinal structure, an erosional remnant of Cretaceous age Mokelumne River Formation (MRF) strata created by deep erosion of the Meganos submarine canyon in the surrounding area. The reservoir had an initial apparent depletion drive mechanism subsequently supported by a bottomwater drive component. High porosity and permeability of the upper MRF reservoir have yielded high gas production rates for this area. Due to the water drive, the reservoir pressure in February 2015 was about 1,900 psia or within 180 psi of the discovery pressure.

B. The target zone for compression testing at King Island Gas Field consists of gas-depleted (i.e., water invaded) sands of the Upper MRF reservoir. The field has produced over 10.5 billion standard cubic feet (Bscf) of natural gas with a BTU content of 930 Btu from three wells. Four wells have penetrated the gas pool, Piacentine 1-27, Piacentine 2-27 (PGE's core-well has not produced), Moresco A1 and Citizen-Green 1. Approximately 75 percent of the initial gas-in-place has been recovered from three wells. The Citizen-Green 1 and Piacentine 1-27 wells were producing small volumes of dry gas until February 2015. The Citizen-Green 1 produced very small volumes of gas in May and June 2015 before returning to full production in July 2015 following completion of the compression test.

C. PG&E prepared and submitted an application to the EPA for a UIC Permit to install and test an I/W well and operate the well during the compression test. The document titled *Underground Injection Control Permit Application and Technical Attachments, PG&E Compressed Air Energy Storage Project, Compression Testing Program, King Island Gas Field, San Joaquin County, California*, dated April 28, 2014 and revised June 26, 2014 (PG&E, 2014a) included a description of the regional and King Island Field geology, and I/W well construction, logging, stimulation, testing, operating and monitoring procedures. The report also included a Zone of Endangering Influence (ZEI) evaluation that involved reservoir modeling to demonstrate that I/W well injection would not negatively impact Underground Sources of Drinking Water (USDWs). EPA issued the permit to construct and operate the I/W well on August 20, 2014 (EPA, 2014). Final authorization to inject

was contingent upon submittal and approval of the Well Completion Report prepared in accordance with EPA form 7520-9 (see below).

D. Details of the King Island Gas Field reservoir model development and planned compression test simulations are presented in WorleyParsons document PGCS-1-LI-022-017: *Preliminary Reservoir Characterization and Testing for Compressed Air Energy Storage* dated June 4, 2014 (WorleyParsons2014a). The three-dimensional (3D) geologic (static) model was developed using Schlumberger's Petrel software (2012.4) based on several geologic reports, maps, cross-sections, and well data including digitized well logs for the King Island Gas Field. The King Island static model was exported from Petrel and input into Schlumberger's ECLIPSE reservoir simulation software. The ECLIPSE model was calibrated (history-matched) to the historical gas and water production and reservoir pressure performance for the three producing gas wells in the field. Once an acceptable match was achieved, model simulations were run to assist in finalizing the planned compression testing program, and to develop preliminary CAES full field development recommendations.

E. Preliminary full-field development modeling was performed to provide guidance for future full-field development simulations (after the compression testing and final model updating are completed), and for input to the conceptual design of the air transmission system (discussed below). The final preferred full-field development case in this report included the following elements:

- 1,100 MMscfd withdrawal over 10-hour cycle and 550 MMscfd injection over 12-hour cycle Monday through Friday and 550 MMscfd over 39-hour cycle on weekends.
- Maximum well bottomhole pressure (WBHP) of 3,000 psia.
- Minimum well tubing head pressure (WTHP) of 850 psia.
- 1.5-year build time of 9.6 billion cubic feet (bcf) bubble using 28 injection wells and 4 water withdrawal wells.

F. The preliminary CAES full field development recommendations derived from the model simulations regarding the number and type of injection/withdrawal wells and water withdrawal wells and withdrawal pressures at the wellhead formed the basis for the conceptual design of the air transmission system presented in WorleyParsons document PGCS-1-LI-027-0001: (WorleyParsons, 2014b). The air transmission system includes the following design components:

- Two well pads, one each on the east and west reservoir structures, with a combined area of less than 10 acres;

- Well locations for 29 I/W wells, four water withdrawal wells and two water disposal wells (combined numbers for two well pads);
- Production separation equipment at each I/W wellhead to remove water and particulates;
- 12-inch headers at the east well pad and 24-inch headers at the west well pad;
- 6-inch diameter injection lines from each I/W wellhead to the headers;
- Each well pad stream connects to two 30-inch air headers (one for injection air and one for withdrawal air) common to both pads;
- Connection piping from the headers to a three mile long 30-inch diameter air transmission pipeline to the ECF;
- Collection piping to transfer water from water separation vessel at each wellhead and the air transmission pipeline to a sump tank and water disposal well located at each well pad.

G. The I/W Well was spud on October 8, 2014 and drilled to a total depth (TD) of 4,963 feet (ft) MD (4,950 ft MD based on wireline logs). A full suite open hole and cased hole logs were run over the surface and long-string cased intervals and sidewall cores were taken in the reservoir and confining zone. In accordance with requirements of the August 20, 2014 EPA Permit, a step rate test (SRT) and fall-off test (FOT) to derive reservoir parameters and determine the formation parting pressure were performed on the I/W well. Details and results of the I/W well are presented in the *Well Completion Report, PG&E CAES Injection/Withdrawal Well and Observation Wells, In Accordance with EPA Form 7520-9*, dated January 28, 2015 (PG&E, 2015a). Based on their review and approval of the Well Completion Report, EPA provided final authorization to inject on February 9, 2015.

4. SUMMARY OF CURRENT FINDINGS

A. The King Island Gas Field is a nearly depleted natural gas reservoir that is suitable for a commercial CAES application provided measures are implemented to mitigate the presence of not insignificant quantities of natural gas (methane) within the reservoir. An air bubble can be developed and cycled in this depleted gas field using natural gas engineering principles.

B. A compression testing program (CTP) was successfully conducted in the field to evaluate the reservoir's injectivity, productivity, storage capability, methane content in the withdrawal stream, oxygen depletion and chemical reactions during short-term air storage and cycling. Numerous digital measurements and gas/water samples were acquired during the testing program. The focus of the monitoring activity was the I/W Well, but additional measurements were also taken at the three observation wells: Piacentine 1-27 (pressure, temperature and water saturation), Piacentine 2-27 (water saturation) and Citizen Green 1 (pressure). The I/W Well was used to build a moderate

0.5 bcf air bubble (oxygen-depleted air) in the reservoir and to perform air-cycle testing. The bubble seemed to be very stable around the I/W Well based on the less than expected water production during cycle testing. The air-cycling operations demonstrated that air may be injected and withdrawn at sufficient rates and pressures for a viable CAES plant operation. The entire CTP lasted a total of 110 days.

C. The field test was run in a portion of the field where the geologic structure of the reservoir helped maintain the air bubble integrity, but which still contained *in-situ* natural gas comprising greater than 90 percent methane. The presence of methane in parts of the reservoir presents the risk of combustion if oxygen is above the Limiting Oxygen Concentration (LOC) and methane is above the Lower Explosive Limit (LEL), and constraints on maximum inlet methane concentrations for the surface power generation equipment. Oxygen-depleted air (with less than 5 percent oxygen) was used to build the air bubble to eliminate problems with flammability. The injected air was effective in displacing any *in-situ* natural gas away from the I/W Well. As a result, the quantities of methane produced during the cycle testing period were very small (less than 0.5 mole percent in the withdrawal gas) and much less than the LEL. Higher concentrations of methane (still below the LEL) were present in the withdrawal gas during the partial blowdown of the air bubble. While the methane factor cannot be fully eliminated, this study found that it is manageable subject to the aforementioned producing and surface equipment constraints.

D. The byproducts of oxidation of iron-bearing reservoir minerals were observed during the CTP, including oxygen depletion, precipitated iron oxide solids, lowered pH in the produced water, and a localized increase in reservoir temperature. Based on the available test data, however, a reduction in reservoir porosity and/or permeability was not indicated or detected during the test. Further details and analysis of the geochemical reactions are given in the report, *Evaluation of Geochemical Effects Resulting from Air Injection into a Partially Depleted Gas Reservoir*, prepared by Jacobson James and Associates, dated September 2015 (JJ&A, 2015).

E. The data obtained from the CTP, together with the data from I/W Well construction, geophysical logging, sidewall core analysis and testing (SRT/FOT), were used to update the existing King Island compositional reservoir dynamic simulation model. The model was re-calibrated (history-matched) to the field test operations and production information by making some adjustments to the reservoir porosity and permeability in and around the I/W Well. The model was able to closely match the observed methane concentration in the withdrawal gas. It also indicated preferential migration of air through higher-permeability reservoir zones that was confirmed by changes in water saturation determined from geophysical logging in an offsetting observation well.

F. Once the updated King Island simulation model was available, several scenarios for a full field CAES development and operation were simulated. The information upon which these simulations was based included the well locations, completions, injection and withdrawal rates, and the amount of cushion air from the previous full-field development modeling described above in the Summary of Previous Findings (**Section 3.E.**). The simulated CAES plant was a 300 MW/10-hour withdrawal cycle facility. Field group controls and manual interventions were used to minimize the methane concentrations in the withdrawal air during a two-year simulated CAES plant operation. The methane concentration in the plant inlet air stream peaked at two mole percent followed by a gradual decline to below one mole percent after two-years of plant operation. For the individual wells, the highest methane concentrations reached during the two-year period stayed below the LEL at less than 4 mole percent.

G. The methane concentrations for the withdrawal cycles are very sensitive to the frequency and volume of the re-injection cycles. Subsequent full field sensitivity cases with the King Island model found that the plant may operate for only about two withdrawal cycles (two days) without re-injection before the methane concentrations become elevated above the specified threshold levels in some wells and in the inlet air stream. The simulation model showed that re-injection of make-up gas for those missed re-injection cycles helped to re-establish the lower levels of methane concentration.

5. COMPRESSION TESTING PROGRAM

CTP was conducted as a field test for air injection and withdrawal from the King Island Gas Field. The CTP involved the injection of oxygen-depleted air into the I/W Well over a period of several months to build an “air bubble” approximately 500 million standard cubic feet (MMscf) in size and to perform a series of injection, flow and pressure transient tests while observing the reservoir response and methane concentration in the withdrawal stream. Based on the successful testing with oxygen-depleted air, a short test involving the injection and withdrawal of ambient was conducted for the I/W Well.

5.1 PG&E Test Injection/Withdrawal Well 1

5.1.1 *Well Construction*

All of the data for the drilling, installation, logging and testing of the I/W Well, and a complete discussion of the results, are provided in the *Well Completion Report, PG&E CAES Injection/Withdrawal Well and Observation Wells, In Accordance with EPA Form 7520-9*, dated January 28, 2015 (PG&E, 2015a). The I/W Well was spud on October 8, 2014 and drilled vertically to a depth of 3,450’ MD. The borehole kicked-off at 3,463’ MD, built angle at 3° to 5.77° per 100’ and attained a maximum inclination of 20° at 4,132’ MD that was held to total depth (TD) at 4,963’ MD (4950’ MD wireline [WL]). The I/W Well reached TD at a surface projected location

291' north and 258' east of the surface location. **Figure 2** depicts an aerial view of the planned and actual directional wellbore paths for the I/W well using coordinates presented in the Halliburton directional program (pre-drill) and directional survey (**Appendix A**), as well as the surveyed locations for the compression test observation wells (Piacentine 1-27 and 2-27). The approximate intersection of the top of the MRF (representing the top of the compression test injection zone) with the ground surface is located 349 ft northeast of Piacentine 2-27 and 171 ft northeast of Piacentine 1-27.

After the borehole was logged to TD, it was plugged back to 4,815' MD and 9-5/8" casing was set and cemented to 4,716'. The interval from 4,722' to 4,815' MD was under-reamed to 17" and completed with gravel pack and 5-1/2" liner with wire wrapped screen (WWS) to 4,814' MD. The drilling rig was released on November 4, 2014. From November 20-26, 2014, a workover rig was used to complete the well with 5-1/2" tubing and packer, and perform hydro-testing, internal mechanical integrity testing (MIT) and acid stimulation.

"As-build" construction details for the I/W Well are provided below in **Tables 1** through **4**. An as-built well schematic is provided in **Figure 3**.

Table 1: General Details for I/W Well

API No.	7720739
Surface Location Coordinates (Lat-Long)	38.081988814 121.422161054 (NAD 83)
Spud Date	8-Oct-14
Rig Release Date	4-Nov-14
Surface Elevation (ft MSL)	-3.75'
KB Elevation (ft MSL)	8.25'
Total Drilled Depth (ft MD)	4963'
Total Wireline Logger Depth (ft MD WL)	4950'
Completed Well Depth (ft MD)	4815'

Definitions
ft MD = Measured depth below Kelly Bushing in feet
ft MD WL = Wireline logger measured depth
ft MSL = Elevation in feet relative to mean sea level
KB = Kelly Bushing
NAD 83 = North American Datum of 1983

Table 2: Casing/Tubing Details for I/W Well

Specifications	Casing / Tubing			
	Surface	Long-String	Liner	Tubing
Material	Steel	Steel	Steel	Steel
Size (in OD)	13-3/8"	9-5/8"	5-1/2"	5-1/2"
Weight (lb/ft)	54.5#	40#	17#	17#
Grade	J-55	J-55 & N-80	N-80	J-55
Depth Interval (ft)	0 - 630'	0 - 4716'	4687' - 4814'	0 - 4614'

Definitions
in OD = Outside diameter in inches
lb/ft = pounds per foot

Table 3: Packer Details for I/W Well

Type	Permanent
Name/Model	Baker Model SC-1
Setting Depth (ft MD)	4614'
Type of Annular Fluid	4% KCL with biocide and corrosion inhibitor

Definitions
ft MD= Measured depth below Kelly Bushing in feet
KCL = Potassium Chloride

Table 4: Bottom Hole Completion Details for I/W Well

in OD of Pipe	in ID of Pipe	Length of Pipe (feet)	To Depth (ft MD)	Description
5-1/2"	4.767"	4614'	4614'	5-1/2", 17#, J-55
8.6"	6"	4.56'	4618.56'	Baker SC-1 Packer
7.63"	6.969"	5.99'	4624.55'	7-5/8", 26#, Upper Extension
8.13"	6"	2.12'	4626.67'	Baker Model S Sliding Sleeve
7.63"	6"	1.7'	4628.37'	Baker Seal Bore
7"	6.366"	19.63'	4648'	Lower Extension
5.5"	4.892"	38.30'	4686.3'	Blank 5-1/2", 17#, N-80
6"	4.892"	122.68'	4808.98'	5-1/2" wire wrapped screen
5.5"	3.5"	2.63'	4811.61'	O-ring seal sub
5.5"	N/A	1.9'	4813.51'	shoe

Definitions
ft MD = Measured depth below Kelly Bushing in feet
in OD = Outside diameter in inches
in ID = Inside diameter in inches
= lb/ft

5.1.2 *Reservoir Characterization*

Log and Core Analysis

The borehole logging and coring program for the I/W Well is outlined below in **Table 5**. The program consisted of mud logging (Geolog), open-hole and cased-hole geophysical logging (Halliburton), discrete-depth formation pressure measurements and pressure transient analysis (Halliburton) and sidewall coring (Halliburton). The mud log, geophysical logs, formation pressure data and sidewall core analyses results are provided in **Appendices B, C, D** and **E**, respectively.

Table 5: Logging / Sidewall Coring Program for I/W Well

Logging / Coring Program		Halliburton Tool	Primary Purpose	Depth Range (ft MD)
Open-hole	Mud Log	N/A (Geolog)	lithology, rate of penetration, gas shows	70' - 4938'
	Spontaneous Potential (SP) log	Spontaneous Potential (SP)	Sand layer definition, formation water salinity	
	Dual induction log (DIL)	Array Compensated True Resistivity (ACRt)	Formation water salinity, hydrocarbon indicator, water/hydrocarbon saturation (with porosity measurements)	
	Micro-resistivity Tool (MRT)	Micro Log (ML)	Flushed and invaded zone resistivity, permeability indicator	
	Gamma Ray (GR) log	Gamma Ray (GR)	Shale indicator	
	Formation Density Compensated (FDC) log	Spectral Density Log (SDL)	Porosity measurement, water/hydrocarbon saturation (with resistivity measurements)	
	Compensated Neutron Log (CNL)	Dual Spaced Neutron Log (DSN)	Porosity measurement, water/hydrocarbon saturation (with resistivity measurements)	
	Caliper log (CAL)	ICT Multi-arm Caliper	Show variations in borehole size and geometry	
	Sonic log (SL)	Wave Sonic Semblance (dipole) Tool (WSST)	Formation velocity, synthetic seismograms. Can be used for porosity determination.	620' - 4898'
	Repeat Formation Tester (RFT)	Reservoir Description Tool (RDT)	Depth-discrete pressure measurement, permeability determination	4610' - 4915'
	Sidewall coring (SWC)	Percussion Sidewall Coring Tool	Reservoir and confining zone parameters. Compare results to those from Piacentine 2-27 conventional core.	4645' - 4903'
Cased-hole	Cement bond log (CBD)	Radial cement bond log (RCBL) NL/GR	Evaluate integrity of annular cement seal and identify channels that might allow fluids to migrate between formations	12' - 4692'

Definitions
ft MD = measured depth in feet below kelly bushing

Analysis and interpretation of the I/W Well geophysical logs was performed by Digital Formation, a petrophysical consulting company located in Denver, Colorado. The Digital Formation report, which includes analytical methodologies, formulas and rock property results, as well as composite interpretation logs, is provided in **Appendix F**.

Physical, textural, mineralogical and hydraulic properties of the target injection zone (MRF reservoir) and overlying confining zone (Capay Shale) were determined through petrophysical analysis of I/W Well sidewall core plugs performed by CoreLab in its Bakersfield, California facility. The routine core analyses performed by CoreLab are listed and described below in **Table 6**.

Table 6: Routine Sidewall Core Analyses Results for I/W Well

Core Analyses	Description
Porosity	Total pore space in sample as a percentage of total sample volume. Used in all reservoir volumetric calculations.
Grain density	Density of reservoir solids whose value determined by rock mineralogy. Input to formula relating sample porosity and bulk density.
Horizontal permeability to air	Intrinsic characteristic of rock that determines how easily air can pass through it. Measured parallel to rock layering, which is preferential flow direction in reservoir. High horizontal permeability is an indicator of good reservoir quality.
Fluid saturation	Percentage of rock porosity occupied by water. Affects the relative permeability of reservoir with respect to air, with permeability to air decreasing as fluid saturation increases.
V-clay	Ratio of clay (or shale) volume to total rock matrix volume; expressed as a decimal. High V-clay usually indicates low reservoir. Used as correction factor in log porosity calculations.

The top of the MRF was penetrated in the I/W Well at a sub-sea depth of 4,650 ft, approximately 23 ft high to the pre-drill estimated depth, approximately 11 ft high to the top of the MRF in the Piacentine 1-27, and approximately 26 ft high to the top of the MRF in the Piacentine 2-27.

The MRF reservoir consists of an upper sand lobe called the upper MR1 and a lower sand lobe called the lower MR1 (see structure cross-section - **Figure 4**). The upper MR-1 sand is well developed at the Piacentine 1-27 but is interpreted to mostly shale-out a short distance to the south and west (note poor sand quality in Piacentine 2-27) and to further bifurcate into upper and lower sand lobes at the location of the I/W well. The upper MR1 and the lower MR1 are separated by a thin shale layer that is continuous across the King Island Field, but is not a sealing hydraulic barrier. The lower MR1 sand is better developed than the upper MR1, with a consistently high net-to-gross sand ratio.

Structure maps for MRF Reservoir presented in the June 2014 preliminary reservoir characterization report (WorleyParsons, 2014a; Figures 23-25) have been updated with geophysical log tops from the I/W well. The re-mapped levels are the top of the upper MR1 (**Figure 5**), top of the lower MR1 (**Figure 6**) and base of the lower MR1 (**Figure 7**).

The I/W well MRF reservoir tops did not change appreciably the structural contours and interpretation in the three maps. At the top of the MRF, the field is interpreted as an anticlinal feature with two structural closures.

The structure cross-section (**Figure 4**) shows that the top of the MRF reservoir in the I/W well is high to the Piacentine 1-27 and that the southeastward directed arcuate slump feature that cuts the Piacentine 2-27 also cuts the I/W well and removed section in the Capay Shale. Since the slump fault soles out in the Capay Shale, it does not cut the MRF and, therefore, is not seen on the three MRF structure maps. A detailed discussion of the structural geology and stratigraphy of the King Island Gas Field is provided in the June 2014 preliminary reservoir characterization report (WorleyParsons, 2014a).

A description of the reservoir in the I/W Well injection zone is provided in **Table 7** below, and is based on I/W Well borehole geophysical logs, mud log and SWC analyses, supplemented with the Piacentine 2-27 conventional core lithologic descriptions. Injection zone depth and thickness are from I/W Well geophysical logs, based on correlations with nearby King Island Gas Field wells (primarily Piacentine 1-27 and Piacentine 2-27). The injection zone is from the top of the under-reamed (to 17" diameter) and gravel packed interval at 4,722' measured depth (MD) (4,671' true vertical depth [TVD]) to the bottom of the gravel pack at 4,815' MD (4,759' TVD).

Table 7: MRF Reservoir Properties in I/W Well

Formation; Age	Injection Zone	Lithology	Depth to top of gravel packed completion interval (feet)			Interval Thickness (feet)		Net Reservoir Thickness (feet)		Avg. Porosity (%) [1]	Avg. Permeability (mD) [2]	Bottom Hole Temperature (Deg. F) [3]	Bottom Hole Pressure (psi) [4]	Fracture Pressure (psi) [5]	Formation Fluid Pressure (psi) [6]	Formation Fluid Pressure Gradient (psi/ft) [6]
			MD	TVD	SS	MT	TVT	MT	TVT							
Mokelumne River Formation; Upper Cretaceous	King Island Gas Reservoir	Interlayered sand and mudstone, comprised of 3 sand lobes and 2 intervening mudstone layers of approx. 16 and 12 feet thickness. Sand is predominantly medium-grained, friable, with common cross-laminations defined by biotite and carbonaceous material. Small igneous and lignite fragments; trace of kaolite and glauconite.	4,722	4,671	-4,663	93	88	60	57	31	140	147	1,932	3,758	1,908	0.406

Definitions
Deg. F = Degree Fahrenheit
KB = kelly bushing
PB = Plug-back depth
mD = Milli-Darcy
MT = Measured Thickness
psi = Pounds per square inch
MD = Measured Depth from KB
TVD = True Vertical Depth from KB
TVT = True Vertical Thickness
SS = Subsea; relative to mean sea level
ft = Feet

Footnotes
1 From I/W well sidewall core analyses
2 From I/W well Falloff Test (FOT)
3 Logging Temperature at 4,950 ft MD (from I/W well wireline log header)
4 Based on PB depth (TVD) and pressure gradient established by RDT discrete depth pressures
5 From I/W well Step Rate Test (SRT), corresponding to Instantaneous Shut-in Pressure (ISIP)
6 Measured in I/W well with Halliburton's Reservoir Description Tool (RDT); average across interval

Datums

Ground elev.	-3.75	feet relative to mean sea level
KB height	12.0	feet above ground surface
KB elev.	8.25	feet relative to mean sea level

A brief summary of the results of core and log analysis for the MRF reservoir injection zone and the Capay Shale confining unit is provided below. A detailed discussion of the core and log analysis based on the results of the Piacentine 2-27 core well drilling in March 2013 is provided in the June 2014 preliminary reservoir characterization report (WorleyParsons, 2014a).

I/W well sidewall core samples were collected in the Domengine (1 sample), Capay (4 samples), MRF reservoir (11 recovered samples), sub-reservoir shale (2 samples) and MR-2 (1 sample). I/W well sidewall core porosity and horizontal permeability (to air) measurements (fractured sample measurements removed) were cross-plotted, along with sidewall core and conventional core

porosity and permeability measurements from approximately the same stratigraphic intervals in the Piacentine 2-27 (**Figure 8**). The Piacentine 2-27 had several samples that plotted farther to the upper-right and the lower-left in **Figure 8** compared to the I/W Well samples (green crosses), indicating the presence of both higher and lower porosity/permeability sand layers in the Piacentine 2-27, but all sample results from both wells plotted along the same trend.

The permeabilities of the I/W Well sidewall core samples from the MRF reservoir interval that was subsequently under-reamed to 17" diameter and gravel packed from 4,722' to 4,815' MD (corresponding to the compression test injection zone) ranged from 9.2 to 225.4 milliDarcies (mD) (see **Appendix E**), with an arithmetic average permeability of 115 mD and a geometric mean permeability of 72 mD (**Table 8**). Porosity in the injection interval ranges from 28.6 percent to 32.0 percent. There is very good agreement between the I/W Well sidewall core porosities and the porosity log curve on the Digital Formation composite logs (**Appendix F**). This confirmation of I/W Well core porosities supports the validity of I/W Well permeabilities because they fall along the same porosity/permeability cross-plot trend as the Piacentine 2-27 samples (**Figure 8**). The generally lower permeability of the MRF in the I/W Well compared to the Piacentine 2-27 is believed to represent sedimentological heterogeneity in the formation (i.e. lateral facies change), with average porosity and permeability increasing away from the I/W Well towards the Piacentine 1-27 and Piacentine 2-27.

Table 8: Sidewall Core Porosity and Permeability in MRF Reservoir in I/W Well

	Permeability (mD)						Porosity (%)	
Ft-MD	MRF Reservoir		MRF Reservoir (low & high outliers removed)		MRF Injection Zone (4722' - 4815')		MRF Injection Zone (4722' - 4815')	
4713	11.2		11.2		-		-	
4754	9.2		-		9.2		28.6	
4765	141.5		141.5		141.5		31.4	
4771	42.1		42.1		42.1		31.6	
4794	225.4		225.4		225.4		32.0	
4810	159.1		159.1		159.1		30.9	
4817	118.2		118.2		-		-	
4821	31.5		31.5		-		-	
4830	119.0		119.0		-		-	
4840	194.6		194.6		-		-	
4846	1029.3		-		-		-	
	Arithmetic Average	Geometric Mean	Arithmetic Average	Geometric Mean	Arithmetic Average	Geometric Mean	Arithmetic Average	Geometric Mean
	189	86	116	84	115	72	31	31

Definitions
Hyphen (-) where value not presented because not applicable to interval of interest or is removed outlier
ft MD = Measured depth from kelly bushing
mD = milli-Darcy
MRF = Mokelumne River Formation
' = Foot
% = Percent

Horizontal permeabilities measured in the four Capay Shale sidewall cores samples (4,665' to 4,698' MD) ranged from 102.7 to 305.9 mD. These permeabilities are much higher than those measured in Capay Shale core plugs sub-sampled from the Piacentine 2-27 conventional core, which showed a harmonic mean of 17 horizontal permeabilities (at ambient stress) of 0.27 mD and a harmonic mean of 4 vertical permeabilities (at confining stress) of 0.04 mD (PG&E, 2014; Table G-6).

The CoreLab report (**Appendix E**) shows that visible fractures were present in all four of the Capay sidewall cores in the I/W Well, probably produced by the percussion sidewall coring technique, which explains the anomalously high permeability measurements. Note that the sidewall core samples from the comparatively more silty-sandy sub-reservoir shale interval (samples at 4,857' and 4,870'), which are not fractured, have permeabilities of 4.2 and 14.7 mD, approximately one order of magnitude lower than for the four Capay Shale samples. In the absence of induced fractures, it would be expected that the Capay Shale would have lower permeability that the sub-reservoir shale. Rock physics modeling performed by Digital Formation (**Appendix F**) using the dipole sonic log and based on a cross-plot relationship between Young's Modulus and Poisson's ratio indicates that the Capay Shale is ductile, which is a favorable characteristic for a seal rock.

Step Rate and Fall-Off Testing

On October 27, 2014, a SRT and FOT were conducted on the I/W Well for the injection zone by Irani Engineering and MHA Petroleum Consultants (MHA) in accordance with the EPA approved procedures outlined in: *Plan to Conduct Step-Rate Test (SRT) and Initial Fall-Off Test (FOT)*, prepared for PG&E by MHA and WorleyParsons and dated September 25, 2014 (PG&E, 2014b).

The pre-SRT activities included several attempts to establish water injection into the MRF without success and as a result, the well had to be deepened twice to increase the test interval beyond the original 10 ft proposed in the testing plan. The MRF reservoir interval tested was 4,722' to 4,780' MD. The tested interval gross thickness was 58' measured thickness (MT) (55' TVT) and the net sand thickness was 34' MT (31' TVT) (Digital Formation Petrophysical Report, **Appendix F**). Pressures were collected both at the surface and bottomhole during the entire SRT/FOT procedure.

The SRT was performed using pump trucks and 4 percent potassium chloride (KCL) water (**Photos 1** and **2**). The total injection period was 5.38 hours and there were at least three injection rates that generated pressures greater than the formation breakdown pressure. After the SRT, the well was shut-in for 12 hours to record the pressure fall-off, representing the FOT. The formation breakdown pressure based on the slope change on the pressure vs. injection rate plot was 3,940 psia (measured in bottomhole gauge set at 4,687' MD), corresponding to a fracture pressure gradient of 0.847 psi/ft. The instantaneous shut-in pressure (ISIP), representing the minimum pressure required to hold open a fracture, was determined to be 3,757.5 psi (bottomhole), corresponding to a fracture gradient of 0.808 psi/ft. The two fracture gradients are fairly close in magnitude but the lower fracture gradient (0.808 psi/ft) is adopted as the standard for the field.

Photo 1: Drilling Rig and Halliburton Pump Trucks - Step Rate Test, October 2014

Photo 2: Water Storage Tanks in Use at Well Site during Step Rate Test, October 2014

The pressure transient data from the bottomhole pressure gauge was input into a commercial well test software program marketed and supported by IHS called *WellTest*. A summary of the *WellTest* FOT analyses results is provided in **Table 9** below:

Table 9: Fall-Off Results from I/W Well

Well / Test Date	PGE Test Well 1 / 27-28Oct2014
Test Type	Injection / Fall-off
Flow Capacity (kh)	4,340 mD-ft
Effective Thickness (h)	31 feet
Effective Permeability (k)	140 mD
Total Skin Factor (s')	0.59
Radius of Investigation (r_{inv})	379 feet
Reservoir (Formation) Compressibility (c_f)	3.3243e-06 1/psi
Total Compressibility ($c_{t)}$	8.8397e-05 1/psi

Definitions
mD = milliDarcy
mD-ft = milliDarcy * feet

The effective permeability derived from the FOT data (140 mD) is within the range of sidewall core permeabilities for the injection zone (**Table 8**). Some difference can be expected between the two permeability measurements because the FOT measurement is effective to water flow while the sidewall core measurements are effective to air flow. In addition, the permeability calculated from the FOT is an average permeability for the 31 ft effective thickness. Nevertheless the FOT and sidewall core permeabilities are in reasonable agreement. There is no indication on a

log-log diagnostic plot of linear flow (1/2 slope) associated with a fractured wellbore (refer to MHA FOT/SRT report in **Appendix G)**. The induced fracture during the SRT must have closed immediately after the water injection ended because there was nothing to keep it open (no proppant).

5.1.3 *Reservoir Conditions*

Depth Discrete Pressure Measurements using Reservoir Description Tool

When the I/W Well was drilled, reservoir pressure measurements were taken in the Domengine Formation and the MRF injection zone using Halliburton's Reservoir Description Tool (RDT™). This tool allows multiple in-situ pressure measurements to be made at various depths using a special probe. The measured pressures are provided in **Appendix D** and shown in **Table 10**. The RDT pressures for the MRF (including the MR2 sand below the MRF injection zone) ranged from 1,891.7 pounds per square inch, atmospheric (psia) to 1974.2 psia. The average pressure gradient in the Domengine Formation is 0.4374 pounds per square inch per foot (psi/ft) and in the MRF injection zone (4,671' – 4,759' TVD) is 0.4057 psi/ft (after elimination of one pressure outlier at 4,702.7 ft). The average pressure gradient in the underlying MR2 is 0.4067 psi/ft, just slightly higher than in the MRF injection zone, indicating that the MR2 is in pressure communication with the MRF injection zone.

Table 10: Depth-Discrete Pressure Measurements from I/W Well

Formation Zone	Depth (feet-TVD)	Original Pressure (psi)[1]	Pressure Test Data (psi)[2]	Pressure Gradient at time of RDT (psi/feet)	Pressure Deviation from Hydrostatic Gradient (psi)[3]
Domengine Sand	4564.73		1997.1	0.4375	20.6
	4602.5		2013	0.4374	20.1
MRF Reservoir Zone	4663.83	2080 (0.438 psi/ft)	1891.7	0.4056	-127.7
	4672.56		1894.6	0.4055	-128.6
	4678.02		1897.5	0.4056	-128.1
	4702.7		1949*	0.4144	-87.3
	4715.9		1914.2	0.4059	-127.8
	4740.5		1924.6	0.4060	-128.0
	4763.3		1934.4	0.4061	-128.1
	4778.5		1940.8	0.4062	-128.3
	4787.1		1944.6	0.4062	-128.2
MR2 Sand (Below Sub Reservoir Shale)	4843.3	--	1969.7	0.4067	-127.4
	4853.8		1974.2	0.4067	-127.5

Footnotes and Definitions

1 Discovery pressure in Moresco et al. Unit A 1 at 4744'-4760'

2 Pressure measurements taken using Halliburton Reservoir Description Tool (RDT™) on October 18, 2014.

3 Hydrostatic gradient is calculated as 0.433 psi/ft assuming the density of fresh water. Actual gradient in saline formations will be slightly higher.

psi = pounds per square inch

TVD = True vertical depth from Kelly bushing

* Outlier pressure measurement

The pressure data indicate that the MRF injection zone and the underlying MR2 sand were pressure depleted relative to normal hydrostatic by -127 to -128 psia due to historical natural gas production in the King Island MRF gas reservoir, and that the sub-reservoir shale separating the MRF injection zone and MR2 allows some pressure communication. The normal hydrostatic gradient in the basal sands of the Domengine Formation provides further proof that the Capay Shale is an effective top seal for the MRF injection zone.

5.2 Observation Wells

"As-build" construction details for pressure/temperature observation wells Piacentine 1-27 and Citizen Green 1 and water saturation observation well Piacentine 2-27 are provided in **Tables 11** through **13** below. As-built schematics for the Piacentine 1-27 and 2-27 wells are provided in **Appendix H**. The locations of the observation wells are shown in **Figures 1** and **2**.

Table 11: General Details for Observation Wells

	Piacentine #1-27	Piacentine #2-27	Citizen Green #1 (Orig. King Island #1-28)
API No.	7720484	7720736	7720688
Surface Location Coordinates (Lat-Long)	38.082389999 121.421970000 (NAD 83)	38.081855418 121.422162206 (NAD 83)	38.082967 121.432646 (NAD 27)
Original Well - Rig Release Date	25-Jul-86	28-Mar-13	27-Jul-05
Most Recent Re-work/Re-drill Program - Rig Release Date	6-Oct-14	NA	6-Mar-12
Surface Elevation (ft MSL)	-6'	-6'	-6'
KB Elevation (ft MSL)	7'	6'	11'
Total Drilled Depth (ft MD)	4900'	4970'	7570'
Completed (Present) Well Depth (ft MD)	4715'	4920'	5366
Perforation Depth Interval (ft MD)	4670' - 4682'	None	5216' - 5222'

Definitions
ft MD = Measured depth below Kelly Bushing in feet
ft MSL = Elevation in feet relative to mean sea level
KB = Kelly Bushing
NA = Not applicable
NAD 83 = North American Datum of 1983
NAD 27 = North American Datum of 1927

Table 12: Casing/Tubing Details for Observation Wells

Piacentine #1-27			
Specifications	**Casing / Tubing**		
	Surface	**Long-String**	**Tubing**
Material	Steel	Steel	Steel
Size (in OD)	8-5/8"	5-1/2"	2-3/8"
Weight (lb/ft)	24#	15.5#	4.7#
Grade	K-55	K-55	J-55
Depth Interval (ft MD)	0 - 627'	0 - 4900'	0 - 4587'

Piacentine #2-27		
Specifications	**Casing / Tubing**	
	Surface	**Long-String**
Material	Steel	Steel
Size (in OD)	9-5/8"	5-1/2"
Weight (lb/ft)	36#	15.5#
Grade	J-55	J-55
Depth Interval (ft MD)	0 - 614'	0 - 4967'

Citizen Green #1			
Specifications	**Casing / Tubing**		
	Surface	**Long-String**	**Tubing**
Material	Steel	Steel	Steel
Size (in OD)	8-5/8"	4-1/2"	2-3/8"
Weight (lb/ft)	24#	11.6#	4.7#
Grade	J-55	N-80	J-55
Depth Interval (ft MD)	0 - 511'	0 - 5513'	0 - 4996'

Definitions
ft MD= Measured depth below Kelly Bushing in feet
in OD = Outside diameter in inches
lb/ft = pounds per foot

Table 13: Packer Details for Observation Wells

Packer Details	**Observation Wells**		
	Piacentine #1-27	**Piacentine #2-27**	**Citizen Green #1**
Type	Retrievable Production	None	None
Name/Model	45A4 R-3		
Setting Depth (ft MD)	4611'		
Type of Annular Fluid	4% KCL with biocide and corrosion inhibitor		

Definitions
ft MD= Measured depth below Kelly Bushing in feet

5.3 Compression Test Overview

The compression test commenced on February 14, 2015 and ended on June 4, 2015, a duration of 110 days. The test was performed in general accordance with the Compression Test Data Acquisition Plan (CTDAP) dated January 12, 2015 (WorleyParsons, 2015a) and in compliance with the Final Underground Injection Control (UIC) Permit for the I/W well (R9UIC-CAS5-FY13-1) issued by the EPA on August 20, 2015 (EPA, 2014; **Appendix I**). The test phases are shown in **Figure 9**.

A table showing daily injection and withdrawal gas volumes, wellhead and reservoir pressures, test phases, well performance tests, logging and pressure/temperature surveys is provided in **Appendix J**.

The compression test consisted of the four phases indicated in **Table 14** below:

Table 14: Compression Test Phases

Phase No.	Phase Description	Duration (Days)	I/W Well Performance Tests / Analyses Performed	Logging and Pressure/Temperature Surveys	Samples Collected
1	Oxygen Depleted Air Bubble Build	80	• 1st, 2nd and 3rd fall-off tests (FOTs) • 1st isochronal test	• 2 BHP&T surveys in Piacentine 1-27 • Temp. logging in Piacentine 1-27 • TMDL logging in Piacentine 1-27 & 2-27	• 1 injection gas sample • 1 withdrawal gas sample
2	Cycle Testing	11	• Cycle tests 1 and 2 • 2nd isochronal test	• BHP&T surveys in Piacentine 1-27 and Citizen Green 1 • TMDL logging in Piacentine 2-27	• 1 injection gas sample • 2 withdrawal gas samples • 2 produced water samples
3	Data Evaluation	5	Preliminary data analysis to decide whether to perform ambient air testing		
4	Ambient Air Injection	10	3rd isochronal test	BHP&T survey in Piacentine 1-27	2 injection air samples
4	Ambient Air Flow Test	4	4th isochronal test	• BHP&T survey in I/W well	• 4 withdrawal air samples • 1 produced water sample • 3 solid/sludge samples

Definitions
FOT = Fall-off Test
BHP&T = Bottomhole pressure and temperature
TMDL = Thermal multi-gate decay log

During the depleted air portion of the test (Phases 1 and 2), 538,809 MMscf of depleted air was injected and 56,314 MMscf was withdrawn. During the ambient air portion of the test (Phase 4), 78,068 MMscf of ambient air was injected and 80,214 MMscf was withdrawn. At the end of the compression test, the approximate volume of air remaining in the reservoir was 480,349 MMscf, which would be oxygen-depleted air theoretically as a greater volume of mostly ambient air was withdrawn than was injected in Phase 4. The oxygen concentration in the final withdrawal gas sample collected at the end of the CTP was 2.0 mole percent[1]. See **Section 5.8** for more details.

5.3.1 *Testing, Logging and Sampling Data Collection*

During each of the four phases of the test, well performance tests were performed (**Table 14** and **Appendix J**). Analyses and simulations of test data provided information on reservoir properties (e.g. flow capacity, permeability, and boundaries), reservoir conditions (e.g. static formation pressure and pressure gradient), reservoir gases (e.g. oxygen, carbon dioxide and methane content) and well performance (e.g. pressure drawdown, air/water production rates and absolute open flow).

During the test, pressure and temperature gradient surveys were conducted several times in the Piacentine 1-27 and once in the Citizen Green 1 and the I/W well (**Table 14** and **Appendix J**). The pressure data were used to track formation pressures in observations wells during the test, to provide pressure gradients for conversion of wellhead to bottomhole pressures, and in the case of the I/W well, to provide bottomhole pressure data at the end of the test that was missing due to malfunction of the permanently installed pressure gauge (see **Section 5.8** for more details).

Temperature survey and logging data were collected to evaluate changes in reservoir temperature due to exothermic oxidation reactions of reservoir minerals, principally pyrite, produced by the injected air (see **Section 5.5.4** for more details). Thermal multi-gate decay (TMDL) logging was performed in the Piacentine 1-27 and 2-27 wells (**Table 14** and **Appendix K**) to evaluate changes in reservoir water saturation, providing information on the depleted air bubble growth rate and lateral expansion (see **Section 5.5.4** for more details).

Laboratory analyses of gas, water and solid/sludge samples during each active phase of the compression test (**Table 14** and **Appendix L**) provided information on reservoir gas and water chemistry changes during the test and injected fluid chemistry required for the EPA UIC Permit. See **Section 5.5.4** for more details.

5.3.2 ***EPA Permit Required Testing, Analyses and Reporting***

Testing and analysis performed to comply with EPA Permit requirements are listed below in **Table 15**:

[1] The 2.0% oxygen content is based on lab analysis. In comparison, the oxygen sensors in the flowline reported the oxygen concentration going to 0.0% at the end of Phase 4 testing.

Table 15: Testing and Sampling Required by EPA UIC Permit

Phase No.	Phase Description	Testing/Analysis	Sampling
	Pre-test	• Geophysical logging of I/W well • Sidewall coring • Discrete depth pressure measurements (RFT) • Initial Step Rate Test / Fall-off Test with water • Reevaluation of Zone of Endangering Influence (ZEI) • Internal mechanical integrity test (MIT) • Annular pressure-temperature analysis	• 1 purged water sample • 1 injection gas sample before start of test
1	Oxygen Depleted Air Bubble Build	• 1st, 2nd and 3rd fall-off tests (FOTs), including plots showing static reservoir pressure over time • Annular pressure-temperature analysis	1 injection gas sample within 5-days of start of test
2	Cycle Testing	Annular pressure-temperature analysis	1 injection gas sample at end of depleted-air testing
4	Ambient Air Injection	Annular pressure-temperature analysis	1 injection gas sample at start of ambient air injection
4	Ambient Air Flow Test	Annular pressure-temperature analysis	1 injection gas sample at end of ambient air injection
	Post-test	External MIT (noise and temperature decay logging)	

A list of the reports submitted by PG&E to the EPA to maintain compliance with the EPA Permit is provided in **Table 16** below:

Table 16: PG&E Submittals to EPA

Report Description	Submittal Date	Reference
Well Completion Report, PG&E CAES Injection/Withdrawal Well and Observation Wells, In Accordance with EPA Form 7520-9 (includes Step Rate Test & Initial Fall Off Test Report)	January 28, 2015	PG&E, 2015a
Submittal of Oxygen-Depleted Air Analytical Results	February 12, 2015	PG&E, 2015b
Revisions to Phase 3 Submittal of the Well Completion Report, including Changes to Appendix A (ZEI Re-evaluation Using Field Data) of Appendix V-6b	February 25, 2015	PG&E, 2015c
Plan to Conduct an External Mechanical Integrity Test	March 18, 2015	PG&E, 2015d
Fall-Off Test Results (1st FOT)	March 18, 2015	PG&E, 2015e
February 2015 Monthly Report for PG&E Test Injection/Withdrawal Well 1 (included annular pressure/temperature changes evaluation and results of 1st FOT)	March 27, 2015	PG&E, 2015f
Cement bond log evaluation in response to EPA request to provide remedial cementing plan	March 31, 2015	PG&E, 2015g
Updated Evaluation of Annular Pressure-Temperature Relationship	April 1, 2015	PG&E, 2015h

Report Description	Submittal Date	Reference
Minor additions to the Phase 3 Submittal of the Well Completion Report (Appendix V-6b, Exhibits 1 – 18)	April 9, 2015	PG&E, 2015i
Responses to EPA Comments on External MIT Plan	April 9, 2015	PG&E, 2015j
Responses to EPA Comments on February 2015 Monthly Report and Updated Evaluation of Annular Pressure Temperature Relationship (revised to include Exhibit 4A: "I/W Test Well Annulus Pressure Calculations based on the change in Water Density as a Function of Temperature")	April 24, 2015	PG&E, 2015k
March 2015 Monthly Report for PG&E Test Injection/Withdrawal Well 1 (included a chart comparing actual and MODFLOW predicted bottomhole pressures relative to the cumulative volume of oxygen-depleted air injected)	April 27, 2015	PG&E, 2015l
Updated Evaluation of Annular Pressure-Temperature Relationship	May 1, 2015	PG&E, 2015m
Submittal of Falloff Test Reports, First and Second Compression Test Falloff Tests Conducted on February 17-18 and April 1-3, 2015	May 4, 2015	PG&E, 2015n
Updated Evaluation of Annular Pressure-Temperature Relationship	May 14, 2015	PG&E, 2015o
Response to Comments on March 2015 Monthly Report	May 19, 2015	PG&E, 2015p
April 2015 Monthly Report for PG&E Test Injection/Withdrawal Well 1	May 27, 2015	PG&E, 2015q
Submittal of Falloff Test Report, Third Compression Test Falloff Test Conducted on May 1-3, 2015	June 2, 2015	PG&E, 2015r
Updated Evaluation of Annular Pressure-Temperature Relationship	June 8, 2015	PG&E, 2015s
May 2015 Monthly Report for PG&E Test Injection/Withdrawal Well 1	June 25, 2015	PG&E, 2015t

The four monthly reports for February to May 2015 included the following continuous monitoring data for the I/W and observation wells and I/W well and test data analyses results:

I/W well:

- Injection rate, daily injection volume, total cumulative volume, wellhead injection pressure, annular pressure, and injection fluid temperature
- Annular pressure-temperature evaluation and pressure exceedances
- Fall-off Test results
- Injection gas sample analytical results
- Static reservoir pressure vs cumulative injected volume

Piacentine 1-27:

- Wellhead tubing and casing annulus pressures and temperatures.

Citizen Green 1:

- Wellhead and calculated bottomhole pressures

5.4 Temporary Site Facility

5.4.1 *Surface Compression/Withdrawal System*

The Temporary Site Facility (TSF) was located on a 650' x 178' (approximately 2.7 acres) pad constructed of road base in a young walnut tree orchard. The TSF equipment was arranged on the pad as shown on **Photo 3** and depicted in the TSF General Arrangement diagram (Stantec Drawing M00-01-001, Rev 0; **Appendix M**).

Photo 3: Temporary Site Facility – Surface Equipment

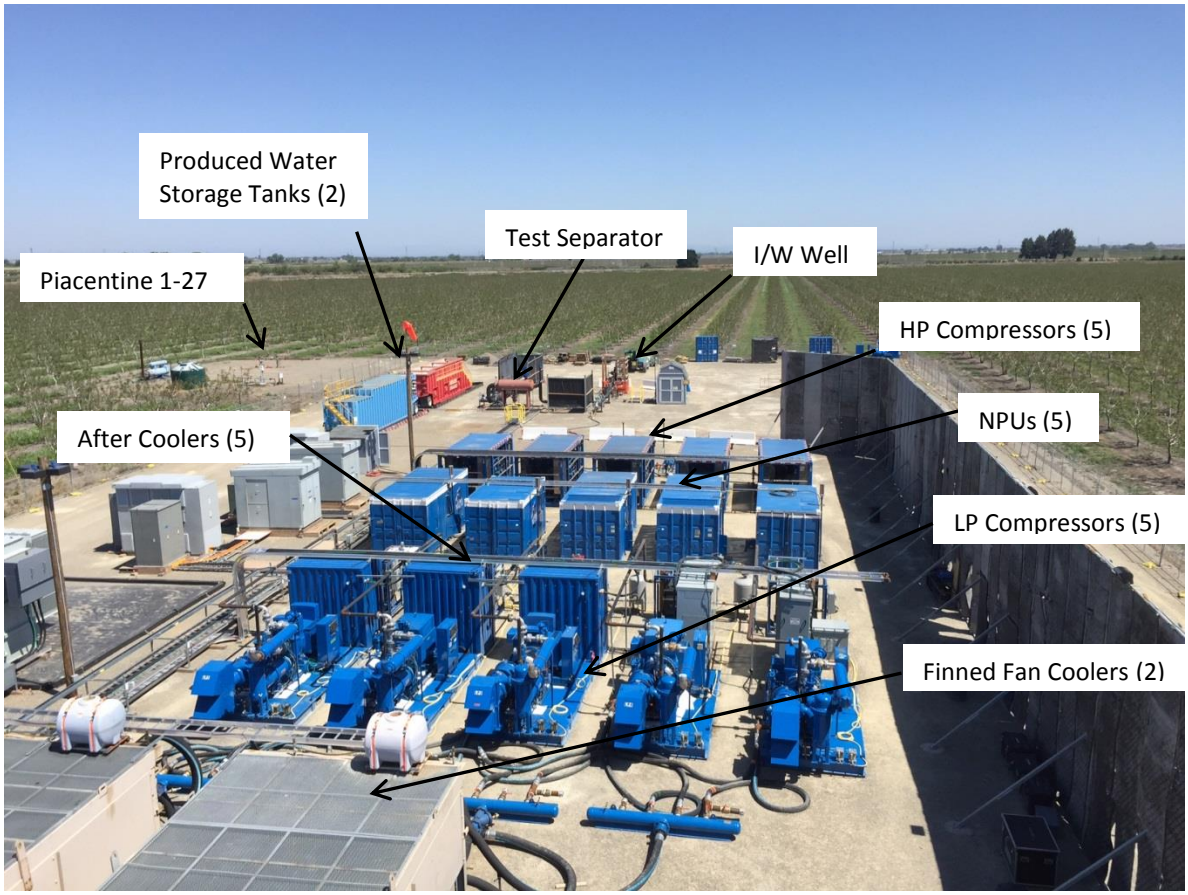

The description and location of the TSF equipment in the General Arrangement diagram is provided in **Table 17**.

Table 17: Temporary Site Facility (TSF) Surface Equipment

TSF Equipment Description	Equipment Identifier (Appendix M)
7 Trailers	1 - 7
5kV switchgear	8
10 MVA Main Transformer (with containment)	9
Finned Fan Coolers A and B	10, 11
LP Compressor No. 2	11
15 kV Breaker	12
Control Building	13
Produced Water Storage Tanks No. 1 and 2 (500 barrels each)	14, 15
2.5 MVA Station Service Transformer No. 1 and 2	16, 17
15 KV Switch	18
480 V Switchgear No. 1 and 2	19, 20
Nitrogen Production Unit (NPU) No. A - E	21 - 24[1]
High Pressure (HP) Compressors No. 1 - 5	25 - 29
Neutral Grounding Resistor	30
480 V Switchboard	31
Trailer Power Distribution	32
27 kV Recloser	33
Test Separator	34
Reducing Station	35
Analyzer Station	36
Metering	37
Cooling Water Pumps A and B	38, 39
LP Compressors No. 1 - 5	40 - 44
After Coolers No. 1 - 5	45 - 45
Flare Stack	

[1] Though Stantec Drawing M00-01-001, Rev 0 (Appendix L) shows 4 NPUs, 5 NPUs were installed.

Each low pressure (LP) compressor was driven by a 1,250 horsepower (hp) electric motor producing a maximum flow of approximately 3,000 standard cubic feet per minute (scfm) at 355 pounds per square inch gage (psig).

The output of the LP Compressors passed through a 1.0 micron coalescing filter, followed by a 0.01 micron coalescing filter, a heater and the membranes in the Nitrogen Production Units (NPUs). The NPUs were provided by GENERON ICS. The compressed air from the LP compressors was delivered to the NPUs where oxygen was removed to less than 5 percent and an “oxygen depleted air” mixture comprising approximately 95 percent nitrogen was produced.

The output of the NPUs was delivered to the high pressure (HP) booster compressors. Each HP compressor unit was an Ariel JGA-4 four-stage reciprocating compressor capable of a maximum flow of 2,000 scfm and driven by a 600 hp electric motor. The output of the HP compressors was delivered to the I/W well.

Withdrawal flow from the I/W well was discharged to a test separator. From the test separator any formation water produced with the withdrawal gas stream was discharged to one of the two 500 barrel (21,000 gallon) produced water storage tanks. The withdrawal gas stream was then discharged to the atmosphere through the vent silencer. The TSF P&IDs showing the TSF process are Stantec drawings P00-02-001 Rev 1 and P00-02-002 Rev 1 (**Appendices N-1** and **N-2**).

5.4.2 *Test Instrumentation*

Specifications for sensors and other instruments to be used for technical data acquisition are summarized below in **Table 18**. The instrument locations, identified by their Tag Numbers, are shown in the P&ID diagrams referenced in the right-most column.

Table 18: Specifications for Gauges, Meters and Sensors

Location	Equipment	Instrument Type	Manufacturer / Model	Accuracy	Operating Limits[1]	Stability	Diagram No. (Instrument located by Tag No.)
I/W Well Downhole (with surface read-out)	Downhole Press/Temp Sensors	Piezoresistive Pressure Transducer	Tendeka SPSRO P/T Quartz Tag No. 00-PT-015	0.02% full scale	500-10,000 psi	<0.02% full scale per year	--
		Platinum Wire RTD	Tendeka SPSRO P/T Quartz Tag No. 00-TT-015	± 045°F	77-350°F	--	
Piacentine 1-27 and Citizen Green 1 Downhole[4]	Suspended Press/Temp Sensors	Hybrid quartz crystal sensor	Metrolog CGM5	± 0.02%	0-15,000 up to 0-30,000 psi	--	--
				± 0.3°F	0-302 °F	--	
I/W Well Wellhead	Press Sensor at tubing head and annulus	Absolute Pressure	Rosemount 3051S2CA4A2A11A1AE5Q4 Tag No. 00-PIT-012 (tubing head) Tag No. 00-PIT-018 (annulus)	± 0.03% of span	0-3,000 psi	± 0.15% of reading for 24 months	P00-02-001-1 (Appendix N-1)
	Temp element and transmitter at tubing head	Thermocouple	Pyromation R1T185L483-(TW)-SL-8HN31 Tag No. 00-TE-002 Rosemount 3144PD1A1E5M5Q4 Tag No. 00-TIT-002	± 0.02% of span	0-120°F (transmitter)	± 0.1% of reading for 24 months	
	Temp element and transmitter at annulus	Thermocouple	Omega SA1-RTD-4W-120 Tag. No. TE-018 Rosemount 648DX1D1I5WASWK1M5Q 4F6B5 Tag No. TIT-018	± 0.06%	-100-500°F (element) 0-120°F (transmitter)	<0.2% per year	
Piacentine 1-27 Wellhead	Press Sensors at tubing head and annulus	Absolute Pressure	Rosemount 3051S2CA4A2A11X5AWA3 WK1I5M5Q4, 701PBKKF Tag No. 00-PIT-016A, 016B	± 0.03% of span	0-3,000 psi	± 0.15% of reading for 24 months	P00-02-002-1 (Appendix N-2)
	Temp element and transmitter at tubing head	Thermocouple	Omega SA1-RTD-4W-120 Tag. No. TE-016A Rosemount 648DX1D1I5WASWK1M5Q 4F6B5 Tag No. TIT-016A	± 0.06%	-100-500°F (element) 0-120°F (transmitter)	<0.2% per year	
	Temp element and transmitter at annulus	Thermocouple	Omega SA1-RTD-4W-120 Tag. No. TE-016B Rosemount 648DX1D1I5WASWK1M5Q	± 0.06%	-100-500°F (element) 0-120°F (transmitter)	<0.2% per year	

Location	Equipment	Instrument Type	Manufacturer / Model	Accuracy	Operating Limits[1]	Stability	Diagram No. (Instrument located by Tag No.)
			4F6B5 Tag No. TIT-016B				
Citizen Green 1 Wellhead	Press Sensor at tubing head	Pressure	Barton Model 202A-2000	0.5% full scale	0 – 2000 psi	--	--
Injection Pipe near I/W Well Manifold	Injection Gas Press/Temp /Flow	Differential Pressure Flow	Rosemount 3051S2CD2A2A11A1AE5Q4 Tag No. 01-FIT-004	± 0.03% of span	0-100 inches water column	± 0.15% of reading for 24 months	P00-02-001-1 (Appendix N-1)
		Absolute Pressure	Rosemount 3051S2CA4A2A11A1AE5Q4 Tag No. 01-PIT-004	± 0.03% of span	0-3,000 psi	± 0.15% of reading for 24 months	
		Thermocouple	Pyromation R1T185L483-(TW)-SL-8HN31 Tag No. 01-TE-004 Rosemount 3144PD1A1EM5Q45 Tag No. 01-TIT-004	± 0.02% of span	0-120°F (transmitter)	± 0.1% of reading for 24 months	
Flow Pipe near Test Separator	Gas to Atmosphere Press/Temp /Flow	Differential Pressure Flow	Rosemount 3051S2CD2A2A11A1AE5Q4 Tag No. 02-FIT-009	± 0.03% of span	0-100 inches water column	± 0.15% of reading for 24 months	P00-02-002-1 (Appendix N-2)
		Absolute Pressure	Rosemount 3051S2CA2A2A11A1AE5Q4 Tag No. 02-PIT-009	± 0.03% of span	0-3,000 psi	± 0.15% of reading for 24 months	
		Thermocouple	Rosemount 0068N21C30A060W44E5XA Tag No. 01-TE-009 Rosemount 3144PD1A1E5M5Q4XA Tag No. 02-TIT-009	± 0.02% of span	0-120°F (transmitter)	± 0.1% of reading for 24 months	
I/W Well Manifold near Wellhead	Hydrocarbon Analyzer 1	Flame Ionization Detector (FID) on slip stream	Baseline Modcon Series 9000 THA Tag No. DAS-AIT-010A	± 1% full scale	1-20,000 ppm	± 1% for 24 hours	P00-02-002-1 (Appendix N-2)
	Hydrocarbon Analyzer 2	IR Detector on slip stream	Hitech Inst. IR600 series Tag No. DAS-AIT-010B	±2.5%	0-100% Methane	±2 %	
	Oxygen Sensor	Zirconia sensor	Sensotec Rapidox 2100ZF Tag No. DAS-AIT-011A, 011B	± 1%	<1 ppm to 100% O_2 10E-4 Torr to 40 Bar 5 to 35°C	± 2% per month	P00-02-002-1 (Appendix N-2)
	Fire and Flame Sensor	IR/UV Sensor	Honeywell FS20X	NA	-40 to +185°F	--	--
Water Tank	Analog Level Transmitter	Piezoresistive pressure sensor	Magtech LT-1	½ to ¼ inch resolution	-400 to 400" H_2O Maximum operating pressure 4,500 psi		--

Footnotes

1. All pressure gauges had a full pressure range of at least 50% greater than the anticipated operating pressure.
2. Mid-test field calibration performed by a mobile calibration service at the end of the bubble building period.
3. Additional mid-test verification of flow performed using a portable strap-on ultrasonic flow meter.
4. Downhole pressure/temperature sensor for two observation wells deployed periodically by slickline.

Definitions

" = inches
°F = degrees Fahrenheit

°C = degrees Celsius
H_2O = water
RTD = Resistance Temperature Detector
FID = Flame Ionization Detector
IR = Infrared
P&ID = Piping and instrumentation diagram
ppm = parts per million
psi = pounds per square inch
-- = Not Applicable

5.4.3 *Data Acquisition System (DAS)*

The DAS for the TSF was engineered, supplied, installed and monitored by the PG&E Applied Technology Solutions (ATS) group. ATS responsibility included calibrating the test instruments, wiring between the TSF PLC and the HP Datalogger and programming the Datalogger that was used to control the gathering and storing of the data. All required data points were collected and stored every 5 seconds for the duration of the TSF operation and testing.

Additionally, the DAS consisted of a Labview based monitoring system with data storage backup for compilation and storage of the required test data. The raw data and daily spreadsheet presentation of the information was available to CAES Project participants both on site and through a remote Dropbox interface.

5.5 Phase 1 – Oxygen-Depleted Air Bubble Build

The test bubble for the compression testing program was built with oxygen-depleted air consisting of approximately 5 percent oxygen and 95 percent nitrogen. Oxygen-depleted air was chosen for the test bubble since the King Island Gas Field still contains native natural gas that is potentially combustible with ambient air for methane concentrations in excess of the lower explosive limit (LEL)[2]. The LEL is defined as the lowest concentration (percentage) of a gas in air capable of producing a flash of fire in the presence of an ignition source (arc, flame, heat). At a concentration in air lower than the LEL, gas mixtures are “too lean” to burn. The reservoir simulation model used in the preliminary compression testing program design (WorleyParsons, 2014a) predicted that the proposed compression testing program should not produce methane in sufficient concentrations to exceed the LEL. Nevertheless, since this field test is the first known test of CAES in a natural gas reservoir, for safety measures, the injected air was chosen to be depleted of oxygen to concentrations below the LEL for the primary 500 MMscf bubble.

An injection sample of the oxygen-depleted air was collected just prior to the start of injection. The composition of the injectate is shown in **Table 19** below.

[2] A LEL of 4% methane was considered appropriate for the operating conditions of the compression test. A threshold of 2% methane, representing 50% of the LEL, was adopted as the trigger for executive action when using ambient air as the injection gas. Additional detail on the LEL determination for the CTP is provided in the WorleyParsons report titled *Compressed Air Energy Storage Test Facility, Air Injection Decision Matrix* (WorleyParsons 2014c).

Table 19: Oxygen-Depleted Air Injectate Composition

Pre-injection Sample - I/W Wellhead		
Collected 2/11/2015 @11:55 am		
Constituent	Mole%	Wt%
Oxygen	3.823%	4.343%
Nitrogen	96.177%	95.657%
Total	100.000%	100.000%
Specific Gravity [air=1] real gas	0.9722	
Compressibility, z	0.9997	

5.5.1 *Test Bubble Development*

Oxygen-depleted air injection was initiated in the I/W well at 1:30 pm on Feb 14, 2015. For the first 10 days, the injection rate was low due to startup issues and staging with the high pressure compression. For the next 30 days, the injection rate reached an average of 6 MMscfd. After the installation of additional equipment and fine tuning existing compression, the injection rate increased to between 9.0 - 9.5 MMscfd for the remainder of the bubble build. The designed bubble size was 500 MMscf. The final bubble size of 493.1 MMscf was achieved on May 4, 2015 after 80 days of injection. The test bubble injection schedule is shown in **Table 20**. Hourly data are provided in **Appendix O**.

Table 20: Compression Test Bubble Build Schedule

PHASE 1 Bubble Build							
Test Day	Week Day	Date	Injected Volume MSCF	Withdrawn Volume MSCF	Bubble Size - Cumulative Net Injection MSCF	I/W Well Bottomhole Pressure PSIA	Comments
0	Sun	2/13/2015	0	0	0	1,895	Start Injection 2/14 at 13:30
1 - 7	Sat - Fri	2/14 - 20/2015	8,152	0	8,152	1,905	Shut-in on 2/17 for 35 hr FOT2
8 - 14	Sat - Fri	2/21 - 27/2015	24,640	0	32,792	1,944	
15 - 21	Sat - Fri	2/28 - 3/6/2015	38,375	0	71,167	1,972	
22 - 28	Sat - Fri	3/7 - 13/2015	42,806	0	113,973	2,001	
29 - 35	Sat - Fri	3/14 - 20/2015	45,257	0	159,230	2,017	
36 - 42	Sat - Fri	3/21 - 27/2015	48,975	0	208,205	2,050	
43 - 49	Sat - Fri	3/28 - 4/3/2015	43,003	0	251,208	2,049	Shut-in on 4/1 for 50 hr FOT3
50 - 56	Sat - Fri	4/4 - 10/2015	67,341	0	318,549	2,095	
57 - 63	Sat - Fri	4/11 - 17/2015	48,120	0	366,669	2,112	
64 - 70	Sat - Fri	4/18 - 24/2015	55,299	0	421,968	2,130	
71 - 77	Sat - Fri	4/25 - 5/1/2015	62,119	0	484,087	2,056	Shut-in on 5/1 for 48 hr FOT4
78	Sat	5/2/2015	0	0	484,087	2,141	Shut-in
79	Sun	5/3/2015	4,734	0	488,821	2,144	
80	Mon	5/4/2015	4,674	423	493,072	2,151	Inject until noon. Pre-test flow 2 hrs at 5 MMscfd
END BUBBLE BUILD - PROCEED TO CYCLING PHASE 2							

Definitions
MSCF = Thousand standard cubic feet
PSIA = Pounds per square inch absolute

5.5.2 *Reservoir Pressure Response*

The reservoir pressures in the I/W well and the two pressure observation wells, Piacentine 1-27 and Citizen Green RD1, increased as a result of the air injection and bubble build. The Piacentine 1-27 and Citizen Green RD1 wellbores at the MRF reservoir level are located 171 ft and 1,980 ft, respectively from the I/W wellbore at the MRF reservoir level. A plot of the measured and estimated bottomhole pressures in these wells as a function of the cumulative net oxygen-depleted air injection is presented by **Figure 10**.

The observed increase in reservoir pressure was in agreement with the pre-testing simulation model predictions. The bottomhole pressure in the I/W well is recorded by a surface readout gauge located in a side pocket at 4,610 ft MD (4,565 ft TVD). The bottomhole pressures in the observation wells are determined based on the recorded tubing pressures and an estimated gas gradient from surface to bottomhole in the wellbore.

Regular pressure gradient surveys were conducted during the compression testing program to validate the gas gradient (**Tables 21** and **22**).

Table 21: Results of Pressure Gradient Surveys for Piacentine 1-27

Piacentine 1-27					
Gradient Survey History - Static Reservoir Pressure					
Prior to and during Compression Testing Program					
Grad Survey Run	Grad Survey Tubing	Grad Survey BHP @ 4674'	Column Weight	Wellbore Gradient	Description
DATE	PSIA	PSIA	PSI	PSI/FT	
2/12/2014	1,703.7	1,897.8	194.1	0.042	Gradient survey
1/26/2015	1,697.7	1,888.9	191.2	0.041	Gradient survey
3/30/2015	1,837.7	2,059.7	222.0	0.047	Run-in for pressure hang
4/4/2015	1,836.2	2,064.4	228.2	0.049	Gradient survey coming out of hole
5/4/2015	1,857.7	2,159.8	302.1	0.065	Run-in for pressure hang
5/9/2015	1,835.1	2,136.3	301.2	0.064	Gradient survey coming out of hole
5/30/2015	1,866.9	2,170.0	303.1	0.065	Gradient survey

Table 22: Results of Pressure Gradient Surveys for Citizen Green 1

Citzen Green RD1					
Gradient Survey History - Static Reservoir Pressure					
Gauge @ 5,219' MD (4,700' TVD)					
Grad Survey Run	Grad Survey Tubing	Grad Survey BHP	Measured Gradient		Description
DATE	PSIA	PSIA	PSI	PSI/FT	
2/12/2014	1,714.7	1,912.2	197.5	0.042	Gradient survey
1/21/2015	1,708.3	1,900.8	192.5	0.041	Gradient survey
5/15/2015	1,895.4	2,108.6	213.2	0.045	Gradient survey

Tables 21 & 22 Definitions
FT = Feet
MD = Measured depth
PSI = Pounds per square inch
PSIA = Pounds per square inch absolute
TVD = True vertical depth

5.5.3 *Pressure Fall-off Testing*

During the Phase 1 bubble build period, a series of pressure fall-off tests were conducted to investigate the expanding bubble size and average reservoir permeability in the bubble area. There were three falloff tests conducted at the beginning, middle and end of the bubble build. Pressure data were recorded by a bottomhole electronic gauge with surface readout capability. The gauge is located inside the tubing at a measured depth (KB) of 4,610 ft, or 4,565 ft TVD. The results are summarized in the **Table 23** below.

Table 23: Results of Fall-off Tests in Injection/Withdrawal Well

–Fall-off Test Results						
Falloff Test Date Description	**Final Rate**	**Fluid Injectate**	**Estimated Effective Permeability md**	**Estimated Bubble Height Feet**	**Flow Capacity kh, md-ft**	**Skin Factor**
10-28-2014 Step Rate Test	-15,840 bbl/day	KCL Water	140.0	31	4,340	+0.62
2-17-2015 Initial Bubble Build	-2.10 mmscfd	Oxygen-Depleted Air	90.5	60	5,431	-1.45
4-1-2015 Mid Bubble Build	-8.52 mmscfd	Oxygen-Depleted Air	238.1	80	19,050	-1.41
5-1-2015 Post Bubble Build	-9.57 mmscfd	Oxygen-Depleted Air	253.0	80	20,237	-1.40

Definitions
bbl = barrel
ft = Feet
kh = Permeability-thickness
md = Milli-Darcy
mmscfd = Million standard cubic feet per day

The log-log diagnostic plots for all three FOTs exhibit a unique pressure derivative behavior (after the infinite acting radial period) which is interpreted to be characteristic of a radial discontinuity. A radial discontinuity is a change in permeability-thickness, viscosity, and/or porosity-compressibility that occurs at a given radius from a well.

Radial discontinuities are almost always associated with fluid injection. In this case, the injected 'air' bubble is distributed radially around the I/W wellbore and the air/water interface appears as a radial discontinuity. The 'air' zone exhibits a relative permeability to gas, gas viscosity, and gas compressibility. The water zone has a relative permeability to water (considering trapped gas), water viscosity and water compressibility. The relative permeability to gas may not equal the

relative permeability to water; however, both viscosity and compressibility are significantly different for air versus water. The result is a change in diffusivity (k/porosity* viscosity* compressibility) and transmissibility (kh/μ) between the two zones which is seen in the current FOT pressure transient behavior.

The distance to the radial discontinuity or extent of the 'air' bubble was made for a simulated test history match using Welltest software. The results of the simulated tests are summarized in **Table 24** and discussed in the FOT reports, which are provided in **Appendix P**. The results show an increasing bubble size consistent with the amount of oxygen-depleted air injection.

Table 24: Results of Simulated Fall-off Tests in Injection/Withdrawal Well

	Cumulative Net Injection	Static Reservoir Presssure	Bubble Radius	
Date	MMscf	PSIA	FOT, ft	Volumetric, ft
14-Feb-2015	0.0	1,893	0.0	0.0
17-Feb-2015	5.0	1,895	72.3	34.4
25-Mar-2015	187.3	2,009	172.2	176.5
1-Apr-2015	245.7	2,031	214.6	201.8
1-May-2015	484.0	2,125	307.0	276.1

Definitions
FOT = Fall-off test
ft = Feet
MMscf = Million cubic feet
PSIA = Pounds per square inch absolute

5.5.4 *Thermal Multi-gate Decay Lithology (TMDL) Logging Results*

Thermal Multi-gate Decay Lithology (TMDL) logging was performed by Halliburton in the Piacentine 1-27 and 2-27 observation wells to obtain information on water saturation (Sw) changes in the injection zone before, during and after building of the depleted air bubble. **Table 25** below provides the dates and compression test phases of the TMDL logging runs:

Table 25: Thermal Multi-gate Decay Lithology (TMDL) Logging Summary

Date	Run No.	Wells	Compression Test Phase	Purpose
September 10, 2014	1	Piacentine 1-27	Pre-compression test	Baseline Sw
October 23, 2014	1	Piacentine 2-27	Pre-compression test	Baseline Sw
April 4, 2015	2	Piacentine 1-27 & 2-27	Mid-bubble build	Mid-bubble build Sw
May 9, 2015	3	Piacentine 2-27	Post-bubble build following Cycle Test 1	Post-bubble build Sw

The TMDL logs were run over the lower portion of the Domengine Formation, the Capay Shale and the Mokelumne River Formation (MRF) injection zone. The raw TMDL logs included gamma ray (GR) and casing collar log (CCL) curves for correlation with open hole logs, and the sigma curves showing the capture cross section of the thermal neutrons emitted by the tool. The raw TMDL logs were processed to derive Sigma-Sw curves. Processing for the TMDL logs run on September 10 and October 23, 2014 and on April 4, 2015 was performed by Digital Formation of Denver, Colorado. Processing for the TMDL log run on May 9, 2015 was performed by Halliburton. All of the raw and processed logs, including a report prepared by Digital Formation describing the processing procedure and interpretation of the results for runs 1 and 2, are provided in **Appendix K**.

The purpose of the TMDL logging was to detect depleted air bubble breakthrough at one or both observation well locations by monitoring changes in Sw in the MRF injection zone. The expectation was that depleted air entering a water saturated permeable layer in the injection zone would result in a decrease in Sw that could be detected with the TMDL log.

The runs 1 and 2 Sigma and Sigma-Sw curves tracked each other well in both wells, suggesting that the depleted air bubble had not reached either well by April 4, 2015. This result was expected for the Piacentine 2-27 due to its greater distance from the I/W well (about 360 ft); however, well testing and volumetric calculations indicated that the bubble should have reached the Piacentine 1-27 by this time due to its closer proximity to the I/W well (about 180 ft away).

Unfortunately, fill above a bridge plug in the Piacentine 1-27 allowed only the top 12 ft of the MRF injection zone to be logged (to the effective total well depth of 4,682 ft), which proved inadequate to evaluate possible bubble breakthrough at this well with the TMDL tool. However, a temperature survey performed in the Piacentine 1-27 on April 4, 2015 showed elevated temperatures starting just above the top of the MRF and increasing rapidly to the total effective TD of the well, which was a significant deviation from the normal temperature gradient established in a temperature survey on February 12, 2015, just prior to the compression test. This temperature anomaly in the MRF injection zone has been interpreted to be the result of exothermic chemical reactions involving injected oxygen and certain formation minerals, especially pyrite.

A more detailed discussion of this phenomenon is provided in JJ&A, 2015. The temperature anomaly detected on April 4, 2014 in the Piacentine 1-27 suggests that the bubble had broken through at this well by April 4; however, it is possible that the breakthrough occurred in more permeable layers beneath the uppermost MRF and that the resultant exothermic heat spread via thermal conduction and/or convection to the upper MRF.

Due to the apparent ineffectiveness of the TMDL tool in the Piacentine 1-27, the third and last run of the TMDL on May 9, 2015 at the end of bubble building (following the 1st cycle test) was performed only in the Piacentine 2-27. The log was run and processed by Halliburton. Tracks 4 and 5 of the processed log (provided in **Appendix K**) provides an overlay of the Sigma and Sigma-

Sw curves from runs 1, 2 and 3. The curves generally track one another with the notable exception of the upper 10 ft of the lower MR-1 sand (4750-4760 ft), where the run 3 Sigma-Sw curve shows significantly lower water saturation, which is consistent with displacement of formation water by injected depleted air. This result is consistent with an Eclipse model simulation that showed reduced water saturation at this time in the two model layers that correspond to the upper 10 ft of the lower MR-1 sand.

5.6 Phase 2 – Oxygen-Depleted Air Cycling

After the bubble was built with the oxygen-depleted air, two sequences of short-term air cycle testing were conducted for the I/W well. The purpose of the air-cycling tests was to evaluate the King Island reservoir's productivity, injectivity, storage capability, oxygen depletion and any chemical reactions during the storage and cycling. The cycle testing schedule was designed to evaluate the reservoir performance under normal well cycling conditions, typical of a commercial CAES plant operation. The short-term test program involved monitoring the oxygen-depleted air flow rates and pressures, obtaining samples, and varying operational procedures over a two week period. Methane and oxygen concentrations of the gas stream were monitored closely during all periods of withdrawal to ensure safety of the surface operations.

5.6.1 *Deliverability Testing*

Isochronal well performance tests were conducted on the I/W well during the air cycle testing phase. The I/W well was flowed at a constant rate for a one hour period, then shut-in for one hour to allow the reservoir pressure to return to stabilized conditions. The well was then flowed at a higher rate for another one hour period. The procedure was repeated to obtain up to four flow periods of equal duration with four shut-in periods of one hour (this is often referred to as a modified isochronal test procedure because the shut-in period duration is equivalent to the flow period duration).

The bottomhole and surface wellhead pressures were evaluated to determine the deliverability of the reservoir and well at various producing pressures including the Absolute Open Flow (AOF) potential of the well which is defined as the rate at which the well will produce against a zero sandface back pressure. The AOF cannot be measure directly due to physical limitations but may be extrapolated from the isochronal tests. The wellhead and sandface AOF test results are valuable in setting maximum producing rates, production forecasting, in designing surface facilities and in determining reservoir problems (such as rate dependent skin factors).

A summary of the isochronal well test results during depleted air cycle testing are presented in **Figures 11** and **12**. The complete analyses are given in **Appendix Q**. The analysis indicates that the AOF potential of the I/W well is high at the sandface with an AOF of 590 MMscfd. The wellhead AOF which is affected by the tubulars and friction is 83 MMscfd. The I/W well showed that the reservoir is capable of excellent deliverability on the order of magnitude required for a

full field CAES development project and the results are useful to support the planned full field flow potential.

5.6.2 *Bubble Performance*

The oxygen-depleted air cycle testing program is summarized in **Table 26** below. The first cycle testing sequence involved a 24 hour schedule of 10-hour withdrawal period flowed by a 14 hour re-injection period. This was repeated for three consecutive 24 hour cycles. The second cycle testing sequence investigated a higher rate over a shorter 5-hour withdrawal period followed by a 19 hour re-injection period. This sequence was also repeated for three consecutive 24 hour cycles. These time periods and rates approach those anticipated for normal air-cycling operations.

Table 26: Oxygen-Depleted Air Cycle Testing Program

PHASE 2 - Oxygen-Depleted Air Cycling										
Test Day	Day	Date	Withdrawal Period HRS	Withdrawal Rate MSCFD	Withdrawal Volume MSCF	Injection Period HRS	Injection Rate MSCFD	Injected Volume MSCF	Bubble Size MSCF	Comments
81	Tues	5/5/2015	4.0	Various	2815	5.0	9.3	1934	492,191	Isochronal Test 1
82	Wed	5/6/2015	10.0	20.9	8,710	13.5	9.6	5,419	488,900	Cycle Program 1
83	Thu	5/7/2015	10.0	22.3	9,288	13.5	9.1	5,101	484,713	
84	Fri	5/8/2015	10.0	21.4	8,914	12.0	9.5	4,757	480,556	
85	Sat	5/9/2015	0.0	0.0	0	8.0	9.6	3,199	483,755	Shut-in at 8:00 for evaluation
86	Sun	5/10/2015	0.0	0.0	0	0.0	0.0	0	483,755	
87	Mon	5/11/2015	0.0	0.0	0	6.0	8.1	2,023	485,778	Start injection at 18:00
88	Tue	5/12/2015	4.0	Various	2,778	14.0	9.4	5,476	488,476	Isochronal Test 2
89	Wed	5/13/2015	5.0	27.9	5,821	17.0	8.6	6,083	488,738	Cycle Program 2
90	Thu	5/14/2015	5.0	40.4	8,421	17.0	9.5	6,742	487,059	
91	Fri	5/15/2015	5.0	43.9	9,144	11.5	9.5	4,536	482,451	Shut-in at 17:00
END OXYGEN-DEPLETED AIR CYCLING - PROCEED TO EVALUATION PHASE 3										

Definitions
HRS = Hours
MSCF = Thousand cubic feet
MSCFD = Thousand cubic feet per day

Pressures, air-flow rates, water rates, oxygen levels and hydrocarbon concentration measurements were monitored closely during the cycle testing. A summary of these data are presented in **Table 27**. The hour by hour DAS data are given in **Appendix O**. Results from the testing are used to history match the numerical reservoir simulation model and to predict performance under ambient air conditions.

Table 27: Compression Test Cycle-Testing Data

PG&E CAES CYCLE TEST DATA						5/16/2015
KING ISLAND GAS FIELD - TEST I/W WELL 1						
	PROGRAM 1				PROGRAM 2	
Parameter	6-May-15	7-May-15	8-May-15	13-May-15	14-May-15	15-May-15
Injection Volume Pre-Flow (Mscf)	**5,137**	**5,068**	**5,160**	**4,973**	**6,732**	**6,689**
Injection Duration (Hrs)	12.5	13.5	12.7	14.5	17.3	17.1
Bubble Size at Start of With. (MMscf)	495.3	491.3	487.6	492.3	493.2	491.5
Withdrawal Start Time	8:02:00	8:00:30	8:00:25	12:00:25	12:00:20	12:01:20
Withdrawal End Time	18:01:00	18:00:20	17:59:55	17:00:35	17:01:30	17:01:25
Withdrawal Duration	9:59:00	9:59:50	9:59:30	5:00:10	5:01:10	5:00:05
Bubble Size at End of With. (MMscf)	486.6	482.1	478.7	486.5	484.8	482.3
Withdrawal Gas Volume (Mscf)	**8,683**	**9,252**	**8,914**	**5,817**	**8,415**	**9,144**
Design Withdrawal Flowrate (Mscfd)	15,000	15,000	15,000	30,000	41,000	45,000
Average Withdrawal Rate (Mscfd)	20,874	22,211	21,411	27,907	40,236	43,879
Withdrawal Water Volume (Gal)	2,993	3,904	3,415	2,482	4,257	5,026
Water Production Start Time	8:50:55	8:43:55	8:36:05	12:26:40	12:32:05	12:16:30
Water Flow Duration	9:10:05	9:16:25	9:23:50	4:33:55	4:29:25	4:44:55
Average Withdrawal Rate (GPM)	5.4	7.0	6.1	9.1	15.8	17.6
Water Rate (Bbl/MMscf)	8.21	10.05	9.12	10.16	12.04	13.09
Starting Bottomhole Pressure (PSIA)	2,154.7	2,147.9	2,126.8	2,133.7	2,133.7	2,152.8
Ending Bottomhole Pressure (PSIA)	2,089.9	2,078.2	2,075.5	2,075.4	2,055.0	2,039.0
Pressure Decline Bottomhole (PSIA)	64.8	69.7	51.3	58.3	78.7	113.8
Starting Wellhead Tubing (PSIA)	1,868	1,864	1,841	1,828	1,842	1,839
Ending Wellhead Tubing (PSIA)	1,706	1,685	1,699	1,797	1,494	1,483
Pressure Decline Wellhead (PSIA)	162.0	179.0	142.0	31.9	348.4	356.3
Starting Annulus (PSIA)	96	73	123	106	116	122
Ending Annulus (PSIA)	316	353	361	347	402	427
Pressure Change Annulus (PSIA)	220	280	238	241	286	305
Piacentine #1-27 Starting Tubing (PSIA)	1,855	1,849	1,841	1,844	1,844	1,841
Piacentine #1-27 Ending Tubing (PSIA)	1,824	1,817	1,813	1,817	1,807	1,803
Pressure Decline Wellhead (PSIA)	31.0	32.0	28.0	26.5	36.8	38.0
Oxygen Content - Start of Test (%)	4.87%	4.88%	4.83%	4.88%	4.76%	4.75%
Oxygen Content - End of Test (%)	4.38%	3.94%	3.29%	4.72%	4.38%	4.04%
Methane Content - Start of Test (%)	0.03%	0.03%	0.02%	0.04%	0.04%	0.05%
Methane Content - End of Test (%)	0.05%	0.08%	0.25%	0.05%	0.04%	0.09%
Hydrocarbon Content - Start of Test (PPM	0	0	0	1	5	3
Hydrocarbon Content - End of Test (PPM)	612	1,942	4,168	294	654	1126

Definitions

Bbl/MMscf = Barrel per million standard cubic feet
Gal = Gallon
GPM = Gallon per minute
Hrs = Hours
Mscf = Thousand standard cubic feet
Mscfd = Thousand standard cubic feet per day
MMscf = Million standard cubic feet
PPM = Parts per million
PSIA = Pounds per square inch absolute

5.6.3 *Reservoir Pressure Response*

The reservoir pressure response in the I/W well and two observation wells during depleted air cycle testing is shown by **Figure 13**. There are three instances during the CTP that an electronic quartz gauge was run in the Piacentine 1-27 observation well to collect bottomhole pressure data concurrent with I/W well bottomhole pressure data (5-second intervals) for the purpose of interference testing. The dates were 1) March 30 to April 4, 2015 (mid-bubble build FOT), 2) April 30 to May 4, 2015 (post bubble build FOT), and 3) May 4 to May 9, 2015 (cycle test program 1).

In all cases, the interference test data showed a high degree of connectivity between the two wells. The bottomhole pressure in the Piacentine 1-27 responsed within 30 to 60 seconds to the rate/pressure changes in the I/W well. It is not clear exactly how this rapid communication occurs since the bottomhole locations of the two wells are 183 feet apart.

5.7 Phase 3 – Data Evaluation

After completion of the compression testing program phases with oxygen-depleted air, withdrawal air and water rates along with measured methane concentrations were analyzed by the PG&E Testing Operations Review Committee (TORC) to determine whether to proceed to the ambient air testing phase. This evaluation period lasted about five days (**Table 28**).

Table 28: Data Evaluation in Consideration of Ambient Air Testing

PHASE 3 - Data Evaluation for Ambient Air Testing										
Test Day	Day	Date	Withdrawal Period HRS	Withdrawal Rate MSCFD	Withdrawal Volume MSCF	Injection Period HRS	Injection Rate MSCFD	Injected Volume MSCF	Bubble Size MSCF	Comments
92	Sat	5/16/2015	0.0	0	0	0.0	0.0	0	482,451	Collect water samples and send air/water samples for analysis
93	Sun	5/17/2015	0.0	0.0	0	0.0	0.0	0	482,451	
94	Mon	5/18/2015	0.0	0.0	0	0.0	0.0	0	482,451	Ambient Air testing approved
95	Tue	5/19/2015	0.0	0.0	0	0.0	0.0	0	482,451	
96	Wed	5/20/2015	0.0	0.0	0	0.0	0.0	0	482,451	
END EVALUATION PERIOD - PROCEED TO AMBIENT AIR TESTING										

Definitions
Hrs = Hours
MSCF = Thousand standard cubic feet
MSCFD = Thousand standard cubic feet per day

Preliminary predictions of hydrocarbon gas production for an ambient air testing program were made using the initial King Island simulation model built in June 2013 (WorleyParsons 2014a). The data from simulation model as well as the field data from the injection/withdrawal testing using oxygen-depleted air were used to evaluate if such testing could be conducted safely using ambient air where the presence of a sufficient oxygen concentration in the withdrawal air mixture could allow combustion if a combustible gas (methane) was present at a concentration in excess of the LEL. The methane concentrations measured during the Phase 2 oxygen-depleted air cycling were less than 0.3 percent.

The simulation model predicted the methane concentration (in mole %) during the proposed ambient air withdrawal period would initially be zero and increase gradually as a function of the cumulative withdrawal air from the well (**Figure 14**).

PG&E management made the decision to approve ambient air testing after conferring with the TORC and key project personnel. The decision to continue to the Ambient Air Testing Phase included the condition that during the withdrawal phase, the I/W well be shut-in immediately and the testing terminated for hydrocarbon or methane concentrations at or above two percent in the produced gas mixture. This shutdown logic was input into the surface equipment control systems prior to the start of ambient air injection to make the shutdown automatic once the threshold hydrocarbon content was exceeded. Initially, shutdown was to be triggered if both hydrocarbon monitors had a reading over 2.0 percent. The shutdown logic was changed so that shutdown was to be triggered if either hydrocarbon monitor registered a single data point above 2.0 percent.

5.7.1 *Sampling Results*

Withdrawal gas samples collected at the wellhead of the I/W well during the Phase 2 air cycle testing were sent to and analyzed by Zalco Laboratories in Bakersfield, California. **Table 29** is a summary of the analysis results from these samples.

Table 29: Analytical Results of I/W Well Gas Samples during Depleted Air Cycle Testing

CAES - Injection/Withdrawal Well - Withdrawal Gas Sample Analytical Results									
			Detected Results - Mole %						Compression Test Phase
Sample ID	Date	Time	Oxygen	Nitrogen	Carbon Dioxide	Methane	Ethane	Total	
I/W Well Withdrawal Gas Sample	05/06/2015	16:32	5.322	94.488	0.140	0.049	< 0.001	100.00	Oxygen-Depleted Air Isochronal Test
I/W Well Withdrawal Gas Sample	05/08/2015	17:20	4.255	94.862	0.526	0.357	< 0.001	100.00	Oxygen-Depleted Air Withdrawal Test 1
I/W Well Withdrawal Gas Sample	05/15/2015	16:42	4.991	94.553	0.365	0.090	< 0.001	100.00	Oxygen-Depleted Air Withdrawal Test 2

5.8 Phase 4 – Ambient Air Testing

The ambient air testing program consisted of injection of an air bubble (78 MMscf) followed by a single withdrawal period. The length of the withdrawal period was designed to produce all of the injected ambient air bubble plus begin to drawdown the remaining oxygen-depleted air bubble as long as the methane concentration in the produced gas mixture stayed below the threshold two percent level.

5.8.1 *Deliverability Testing*

Isochronal well performance tests were conducted for the I/W well after the ambient air bubble was injected. The isochronal testing procedure followed the same one-hour flow and shut-in periods used for the previous isochronal tests during the Phase 2 oxygen-depleted air cycle

testing. The four step rates were 5 - 10 -20 -30 MMscfd each. Isochronal testing was conducted on both May 30 and June 3. The isochronal test on June 3 was necessary because the pressure data being reported by the bottomhole Spartek gauge were suspected of being erroneous so a wireline pressure-temperature gauge (McAnally) was run in the I/W well and hung just above the Spartek gauge. The readings from the wireline gauge showed that the Spartek gauge was not working properly.

The ambient air isochronal well test results are presented along with the depleted air cycle isochronal test results in **Figures 15** and **16** for the wellhead and bottomhole pressure data. The complete analyses are given in **Appendix Q**.

The ambient air data are displayed with the oxygen-depleted air isochronal data and it is clear that the ambient air isochronal data points fall on the same trendline extrapolations as the oxygen-depleted air data points. The high deliverability of the well is confirmed with ambient air isochronal data.

5.8.2 *Withdrawal Testing*

The ambient air injection and withdrawal program is summarized in **Table 30** below.

Table 30: Ambient Air Flow Testing Program

PHASE 4 - Ambient Air Testing										
Test Day	Day	Date	Withdrawal Period HRS	Withdrawal Rate MSCFD	Withdrawal Volume MSCF	Injection Period HRS	Injection Rate MSCFD	Injected Volume MSCF	Bubble Size MSCF	Comments
92	Thurs	5/21/2015	0.0	0	0	11.0	8.8	4051	486,502	Start Phase 4 ambient air injection at 7:00
93	Fri	5/22/2015	0.0	0.0	0	18.0	10.4	7,831	494,333	
94	Sat	5/23/2015	0.0	0.0	0	24.0	10.8	10,770	505,103	
95	Sun	5/24/2015	0.0	0.0	0	24.0	11.0	11,040	516,143	
96	Mon	5/25/2015	0.0	0.0	0	24.0	10.4	10,400	526,543	
97	Tue	5/26/2015	0.0	0.0	0	18.0	10.5	7,880	534,423	
98	Wed	5/27/2015	0.0	0.0	0	18.0	11.1	8,297	542,720	
99	Thu	5/28/2015	0.0	0.0	0	18.0	11.3	8,466	551,186	
100	Fri	5/29/2015	0.0	0.0	0	18.0	11.2	8,402	559,588	
101	Sat	5/30/2015	9.0	Various	8,685	2.0	11.2	931	551,834	Isochronal Test 3; Start constant flow at 19:00
102	Sun	5/31/2015	24.0	30.1	30,052	0.0	0.0	0	521,782	
103	Mon	6/1/2015	23.0	27.6	26,461	0.0	0.0	0	495,321	
104	Tue	6/2/2015	13.0	5.4	2,928	0.0	0.0	0	492,393	
105	Wed	6/3/2015	17.0	13.7	9,734	0.0	0.0	0	482,659	Run wireline gauge to verify bottomhole pressures; Isochronal Test 4
106	Thu	6/4/2015	2.8	20.2	2,354	0.0	0.0	0	480,305	Well SI at 02:47 when hydrocarbon analyzer exceeded shutdown limit of 20,000 ppm
END COMPRESSION TESTING PROGRAM										

Definitions
HRS = Hours
MSCF = Thousand cubic feet
MSCFD = Thousand cubic feet per day

An injection sample of the ambient air was collected just prior to the start of injection. The composition of the air injectate is shown in **Table 31**.

Table 31: Ambient Air Injectate Composition

Ambient Air Sample - I/W Wellhead		
Collected 5/21/2015 @10:15 am		
Constituent	Mole%	Wt%
Oxygen	22.357%	24.745%
Nitrogen	77.601%	75.192%
Carbon Dioxide	0.042%	0.063%
Total	100.000%	100.000%
Specific Gravity [air=1] real gas	0.9980	
Compressibility, z	0.9996	

Pressures, air-flow rates, water rates, oxygen levels and hydrocarbon concentration measurements were monitored closely during the withdrawal testing. These data are presented in **Appendix O** on a hour-by-hour basis. Results from the testing are used to compare to the predicted results of the numerical reservoir simulation model.

Table 32 is a summary of the chromatographic analyses for the ambient air samples collected during the Phase 4 testing. The samples were collected at the wellhead and analyzed by Zalco Laboratories.

Table 32: Analytical Results of I/W Well Gas Samples during Ambient Air Testing

CAES - Injection/Withdrawal Well - Withdrawal Gas Sample Analytical Results									
			Detected Results - Mole %						Compression Test Phase
Sample ID	Date	Time	Oxygen	Nitrogen	Carbon Dioxide	Methane	Ethane	Total	
I/W Well Withdrawal Gas Sample	05/31/2015	0:05	22.110	77.575	0.233	0.082	< 0.001	100.00	Ambient Air Withdrawal Test
I/W Well Withdrawal Gas Sample	06/01/2015	17:17	10.785	85.979	2.416	0.818	0.001	100.00	Ambient Air Withdrawal Test
I/W Well Withdrawal Gas Sample	06/03/2015	17:08	3.502	92.502	2.657	1.336	0.002	100.00	Ambient Air Extended Withdrawal
I/W Well Withdrawal Gas Sample	06/04/2015	9:20	2.047	93.773	2.494	1.685	0.002	100.00	Ambient Air Extended Withdrawal

The methane concentration threshold (2.0 mole percent) was exceeded after 80.2 MMscf of cumulative withdrawal from the I/W well. The methane behavior during withdrawal largely tracked the predicted methane concentrations from the simulation results lending credibility to the model and emphasizing the need to manage and suppress methane production for future CAES operations on a field wide scale.

6. RESERVOIR SIMULATION

A numerical simulation model was built by MHA Petroleum Consultants (Denver, CO) in 2014 and calibrated to the historical King Island reservoir performance. The model was used to predict the I/W Well injection/withdrawal response during the field compression testing program.

Subsequent to that work, and for this report, the model is updated for the observed results of the compression testing program. It is used to simulate the process of air injection into and withdrawal from the reservoir for theoretical full-field development scenarios as documented in **Section 7.0** of this report.

The simulation model covers the gas-productive area of the King Island Gas Field plus the underlying bottom water wherever there is porous and permeable Mokelumne River Formation (MRF) sand. The model domain ends where the MRF is truncated by a subcrop at the edge of the Meganos Channel on all four sides of the field.

The model construction and calibration is described in the June 2014 Report (WorleyParsons, 2014a, pages 25-32). Geologic reports, along with maps, cross-sections and well data including digitized well logs, were used to construct a three-dimensional (3D) geologic (static) model of the King Island Gas Field. The MRF Reservoir was divided into upper and lower units (upper MR1 and lower MR1, respectively) based on correlations across the King Island field area (see **Figure 4**). This interpretation helped establish the structural and stratigraphic relationship of the flow units in the reservoir. The top of the Mokelumne formation structure in the model is shown by **Figure 5**. At the upper MR1 level, the field is interpreted as an anticlinal feature with two structural closures.

The King Island static model was exported from the Petrel software as a series of ASCII grid files (structural framework, porosity, Petrel well connection and well completion files) to create a dynamic simulation model for the dynamic modeling phase of the project. These formatted files are compatible as input to the ECLIPSE simulation software package (Schlumberger).

The ECLIPSE dynamic simulation model consists of 147,983 active gridblocks or cells. Each cell is 50 ft by 50 ft or 0.0574 acres. There are a total of 63 layers. The layers vary in thickness from 4 to 5 ft thick with an average of 4.92 ft in thickness. The dynamic model grid is created using corner-point geometry after importing the static model framework (also corner-point geometry) constructed with the Petrel software. The model grid is shown by **Figure 17**. Two cross-sections (one N-S and one W-E) are made through the entire model grid to illustrate the gridding scheme. The locations of the cross-sections are given in **Figure 17**. The same two cross-sections will be used in future figures in this report to display other model properties and simulation results.

The King Island model is much more than a conceptual model; it is intended to be a replica of the gas reservoir. It is constructed based on the best available geologic maps, cross-sections, information from wireline well logs and core analysis. The gas reservoir is bounded at the top by the Capay Shale, an impermeable cap rock, and on all four sides by the Meganos Channel fill, which consists of impermeable mudstones and shales.

The dynamic model grid cells are populated with porosity, permeability and initial water saturation arrays based on the well log data and estimated petrophysical correlations. Porosity values are sourced from the static model output and are based on the available density-neutron

wireline log information upscaled and distributed stochastically throughout the model area (**Figures 18** and **19**). The gridblock permeabilities are determined using a porosity-permeability transform derived from the Piacentine 2-27 conventional core information and presented by **Figure 8**. The transformed permeabilities are further reduced by a factor of 0.282 to adjust from the laboratory confining stress conditions (250 psi) to the in situ reservoir stress conditions (2,700 psi) for each grid cell. The permeability distribution is shown by **Figures 20** and **21**.

An initial gas water contact (GWC) of -4,783 ft. subsea is used in the dynamic model. For the initial water saturation distribution above the GWC, the model uses the Leverett J-Function[3] option to scale the water-gas capillary pressure (Pc) functions according to the porosity and permeability values in each gridblock. The J-function relationships assign a unique Pc curve and initial water saturation for each simulation cell based on porosity and permeability of that cell. Above the GWC, the gas saturation is the pore space (porosity) not occupied by the initial water saturation.

Water influx models are mathematical models that simulate and predict aquifer performance. When successfully integrated into a reservoir simulator, the net result is a model that effectively simulates performance of a water drive reservoir such as King Island. A Carter-Tracy infinite-acting aquifer is attached to the bottom-most layers of the model grid to simulate the bottomwater drive mechanism for this reservoir (Carter-Tracy is a popular mathematical aquifer model). This analytical aquifer is used to simulate the water influx into the gas-filled pore space known to have occurred during the producing life of the reservoir.

Straight-line relationships are used for the gas-water relative permeability curves in the ECLIPSE model. The initial water saturation endpoints of the relative permeability curves are scaled to the specific initial water saturation assigned to each grid cell by the Leverett J-Function. This is the end-point scaling feature of the ECLIPSE software and the purpose is to make the initial water saturation immobile in all grid cells above the initial GWC.

The minimum or residual gas saturation (S_{gr}) to water displacement in the relative permeability curve is defined using the S_{gr} versus porosity relationship reported by the Gas Research Institute (Katz, 1964).

$$S_{gr} = (-1.2778 \times \text{Porosity, fraction}) + 0.6172$$

This equation is set in the Eclipse model with the only exception that S_{gr} is set to zero for any cell below the original GWC. It was suggested that the inferred residual gas saturation data (1-Sw) from the Piacentine 2-27 core may be compared to the residual gas saturations predicted by the Katz correlation above, however the core data had no resemblance to the Katz correlation. This is likely due to the expansion of the natural gas as the core was depressurized during retrieval.

[3] The Leverett J-Function is a mathematical model for correlating capillary pressure data in unconsolidated sands with similar pore types and wettability but with different permeabilities.

The model is initialized with a reservoir pressure of 2,114.7 psia at the original GWC (-4,783 ft. subsea). This is slightly higher than the current estimated discovery pressure of 2,080 psia based on the initial shut-in tubing pressures of the Moresco A1 and Piacentine 1-27 wells. The Initial Gas-in-Place (GIP) in the model is 14.06 Bscf. Grid displays of the distribution of IGIP are given in **Figures 22** and **23**.

6.1 Model Update

For this report, the initial King Island dynamic simulation model was updated for drilling and completion details of the I/W well 1. Since this model had been successfully calibrated, it was determined that all updates would be made only to the dynamic model. The static model construction was left unchanged (except as noted below) which was reasonable since the I/W well encountered the MRF very close to the structural depths in the original static model. The changes to the dynamic model for this report are:

1. Moved I/W Well wellbore location in model to match directional survey
2. Changed I/W Well completion layers to match gravel pack completion interval depths
3. Changed porosities for respective layers in and around I/W well (approximately 300 ft radius) to match wireline log results
4. Re-calculated layer permeabilities in and around I/W well (300 ft radius) based on King Island porosity-perm transform consistent with revised porosities in step 3

6.2 ECLIPSE Compositional Simulator

The simulations in this study were performed using the ECLIPSE commercial numerical simulator, a Schlumberger software product. ECLIPSE is a three-dimensional (3-D) finite difference black oil simulator used for modelling oil and natural gas hydrocarbon systems. For the King Island reservoir, the model is used in the fully compositional mode (E300) for simulating the injection and withdrawal of air (and oxygen-depleted air). In this mode, the various components of the natural gas (methane, ethane, nitrogen and CO_2) and air (nitrogen and oxygen) are specified in the model with their own properties of viscosity, density and compressibility. The analytical results of a King Island Field natural gas sample collected from the Piacentine 1-27 (**Table 33**), indicates that the gas comprises nearly 92 percent methane and 8 percent nitrogen, with trace amounts of ethane, propane and carbon dioxide.

Table 33: King Island – Native Gas Components in Field and Model

King Island Dynamic Model Compositional PVT			
Original Gas Analysis Based on Piacentine 1-27			
Constituent	Model Name	Mole%	Mole Wt
Methane, C1	WYMF_1	91.7241%	16.04
Ethane, C2	WYMF_2	0.1292%	30.07
Propane		0.0018%	Not in Model
Carbon Dioxide, CO2	WYMF_3	0.0138%	44.01
Nitrogen	WYMF_4	8.1311%	28.01
Oxygen	WYMF_5	0.0000%	32.00
Total		100.0000%	
Specific Gravity [air=1] real gas	0.5890		

Definitions
PVT = Pressure, volume, temperature gas properties
Wt = Weight

6.2.1 *History Match Pre-Compression Testing*

In the previous simulation study in June 2013, the model had been successfully calibrated (history-matched) to the historical production and reservoir pressure performance for the three producing gas wells in the field. After the updates described in **Section 6.1** were applied, it was necessary to re-run the history match case and re-calibrate the updated model as necessary to preserve the original history match. During history-matching, the actual gas production rate is specified for each well in the model and the wells are 'matched' to the reported flowing and static bottomhole pressures and water production rates. The calibration process involved global adjustments to pore volume, variable permeability (horizontal and vertical) and the strength and location of the infinite-acting water aquifers. The global changes to permeability were used to suppress the bottomwater influx and retard water movement toward the gas wells consistent with the timing of the observed water production.

The graphs showing the re-calibrated model history match are presented by **Figures 24** through **32**. The period shown in these graphs is the pre-compression testing period, i.e. from the field discovery and open-up in 1986 up to the start of the compression testing program in February 2015 (the history match of the compression testing program is discussed below). The history matching seeks to establish as best as possible the current reservoir conditions of gas/water saturation and pressure distributions prior to the start of the compression testing program. Another measure of the quality of the history match, as far as water production is concerned, is a comparison of the location of water influx in the reservoir versus the location of water encroachment in the model. This comparison is given by **Figure 33**.

6.2.2 *History Match Compression Testing*

The Eclipse model was also history-matched to the compression testing program Phases 1 through 4 conducted during February 14 to June 5, 2015. The actual injection/withdrawal rate schedule was input into the model for the entire compression testing program (see **Figure 34**). The history match results are shown in **Figures 35** through **40**. These figures show the predicted model response versus the observed field test data for bottomhole pressures in the I/W well and offsetting wells and for the water production and methane concentrations in the withdrawal gas of the I/W Well. The re-calibrated model does an excellent job of matching the observed field test data. The increase in reservoir pressure causes water to flow slowly out of the reservoir back into the underlying aquifer. The predicted rate of efflux during the compression test is provided by **Figure 41**.

A primary benefit of the King Island dynamic model is the ability to predict the movement of the native natural gas (methane) in the reservoir in response to air injection (oxygen-depleted air or ambient air) during the compression testing program. This is important for the safe operation of the field test and to avoid any possibility for explosive conditions in the wellbore and surface equipment due to reaching the LEL for methane in the withdrawal gas. The previous work with the simulation model found that the predicted methane concentration in the withdrawal gas was sensitive to the size of the grid blocks around the I/W Well in the model. As a result, for the history match of the compression testing program, the dynamic model was re-gridded using Local Grid Refinement (LGR) in a 150 ft x 150 ft square area centered around the I/W well. Grid block sizes in this area are 5 ft by 5 ft in x-y dimension, compared to the standard 50 ft by 50 ft gridblock size in the remaining cells of the model. The layering is unchanged. The impact of LGR on the methane concentration for the withdrawals from the I/W Well is shown in **Figure 42**. The predicted methane concentrations are lower for the LGR gridding. This result is believed to be due to less abrupt, more gradual gas saturation changes around the wellbore.

Areal and cross-sectional grid displays from the history-matched model are presented for the following CTP milestone events and model time stamp date:

1. Feb. 14, 2015 Start of Compression Test (**Figures 43** and **44**)
2. Feb. 18, 2015 Fall-off Test 1 beginning of bubble build (**Figures 45** and **46**)
3. April 2, 2015 Fall-off Test 2, mid-point of bubble build (**Figures 47** and **48**)
4. May 2, 2015 Fall-off Test 3, end of bubble build (**Figures 49** and **50**)
5. May 16, 2015 End of Depleted Air Cycling (**Figures 51** through **53**)
6. May 30, 2015 End of Ambient Air Injection (**Figures 54** and **55**)
7. June 5, 2015 End of Compression Testing Program (**Figures 56** and **57**)

The simulation model is subsequently used to make predictions for a full field CAES development project as discussed in **Sections 6.3** and **7.0** below.

6.3 Full Field Development

The King Island site geology determines the storage reservoir's performance characteristics and the suitability for a full scale CAES plant. Since the geology cannot be changed to meet the plant's withdrawal requirements, it is necessary to know if the proposed plant's operational requirements are compatible with the underground air-storage and withdrawal system. The compression testing program confirmed that the King Island site had the necessary geologic conditions for a CAES application. The next step in the reservoir simulation evaluation was to configure the King Island dynamic model to predict the reservoir performance for a theoretical full scale CAES operation. In this investigation, full scale CAES operation for the King Island site is defined as the well development sufficient to support a 300 MW CAES plant generating power for peak demand periods up to 10 hours. In terms of withdrawal rate, the surface requirement for a 300 MW plant is expected to be a total field-wide equivalent deliverability of 1.1 Bscf per day or a volume of 0.458 Bscf.

The conceptual design for the CAES operation includes construction of a number of closely-spaced wells in the field. The wells are used to create a large air bubble in the reservoir. The permeable sands of the MRF, including the gas reservoir and the underlying aquifer, comprise the injection zone that will experience increased pressures as a result of the air injection. As air is injected, the displacement of the native natural gas and water will cause pressures within the water-invaded gas reservoir sands in the uppermost portion of the MRF sands to increase and this pressure increase is expected to be transmitted throughout the reservoir sands relatively rapidly. The increase in pressure will cause water to flow slowly out of the reservoir through the underlying shale and siltstone and into the underlying aquifer sequence. The lateral propagation of pressure will be limited by the lateral extent of the permeable reservoir within the Meganos Channel and underlying aquifer sands at the King Island Gas Field.

For purposes of the full field development (FFD) simulation, the bubble build is projected to start in July 2019. The dynamic model is 'rolled' forward from the end of the compression testing program history match (June 2015) to the start of air injection (July 2019) with the following field performance assumptions:

1) All King Island wells are shut-in during this period with the exception of the Citizen Green RD1 well and the I/W Well. The Citizen Green RD1 well was returned to production on July 8, 2015. It was producing approximately 150 mcfd. In the model, the Citizen Green RD1 well is produced at a specified gas rate of 150 mcfd beginning July 2015 until the start of the FFD bubble build and then shut-in.

2) A small volume of air (50 MMscf) is withdrawn from the I/W Well in September 2015. This activity is planned to reduce the reservoir pressure back to an original pressure level.[4] After this withdrawal, the I/W Well is assumed to be plugged and abandoned.

According to the dynamic model, there is an estimated 3.1 Bscf of native natural gas (composed of 92 percent methane) remaining in the King Island Gas Field at the start of the FFD project. Approximately 1 Bscf is free 'attic' gas located in the east and west structural highs. The remaining native gas is "trapped gas" by the water that encroached into the field area. It is the free 'attic' gas that not only presents a possible safety issue (combustion) but also there are methane concentration limits for the flow stream intake to the air-expansion equipment in the CAES plant.

After accounting for the future field operations to mid-2019, the dynamic model was used to simulate a FFD CAES operational scenario. The design criteria, well plan and operational sequences simulated by the model are presented and discussed in **Section 7.0**. The objectives of the FFD simulations are to demonstrate the suitability of the King Island reservoir for the withdrawal and injection rates associated with a 300 MW CAES plant and to show that the remaining in situ native natural gas in the reservoir may be "pushed aside" such that methane concentrations in the withdrawal streams could meet anticipated equipment and safety design levels on a field wide and individual well basis.

7. CAES REFINED RESERVOIR DEVELOPMENT SCENARIOS

7.1 Design Criteria

The design criteria for the full field CAES plan investigated by the King Island model are shown by **Table 34**. These criteria were established to be a first approximation of what might be developed for a 300 MW CAES plant. Some of the design criteria such as bubble size and well types (horizontal vs. vertical) were settled on after running a number of model sensitivity cases. The optimized FFD case presented in this report has a working bubble size of 9.6 Bscf and utilizes all vertical wells for injection and withdrawal.

[4] A final decision on this small withdrawal had not been made as of the date of this report; regardless, it is insignificant to the FFD modeling results.

Table 34: King Island CAES Full Field Development Design Parameters

Design Criteria	Parameter
CAES Plant Capacity	300 Megawatt
Air Bubble Volume	9.0 to 10.0 Bscf
Working Volume per Withdrawal	0.5 Bscf (5% of Bubble)
Estimated Time Period for Bubble Build	18 months
Field Withdrawal Rate / Plant Intake Rate	1.1 Bscfd
Cycle Withdrawal Period	10 hours maximum
Total Injection Rate	0.5 Bscfd (50% of deliverability)
Number of Wells	As needed to achieve deliverability
Well Locations	Both East and West Structural Areas
Maximum Bottomhole Pressure	3,000 psia
Minimum Bottomhole Flowing Pressure	1,500 psia
Minimum Wellhead Tubing Pressure	850 psia
Maximum Drawdown at Sandface	200 psi
Maximum Methane Concentration - Plant Intake	2.0 percent
Maximum Methane Concentration - Well Stream	4.0 percent

Definitions
Bscf = Billion standard cubic feet
Bscfd = Billion standard cubic feet per day
psi = Pounds per square inch
psia = Pounds per square inch absolute

A 300 MW plant injection/withdrawal schedule, consisting of 10 hours withdrawal followed by 10 hours of injection, was used for a daily 24-hour cycle with two 1-hr transition shut-in periods (see **Table 35**). The injection rate was set at 50 percent of the withdrawal rate based on the original daily injection design criteria (may be higher depending on facility equipment). This cycle is repeated daily for a week in the simulation model then the depleted volume of air is replaced by air injection over the corresponding weekend such that there is no net change in reservoir volume or pressure by the end of a 7-day period, i.e. zero bubble growth.

Table 35: CAES 300 MW Plant Weekly Injection/Withdrawal Schedule

King Island Program 300 MW Plant -Weekly Schedule				
day	Air Rate, mmcfd +prod; -inj	hrs	mmcf	Air, cumulative mmcf
1	1,100.0	10.0	458.33	458.33
	0.0	1.0	0.00	458.33
	(550.0)	12.0	(275.00)	183.33
	0.0	1.0	0.00	183.33
2	1,100.0	10.0	458.33	641.67
	0.0	1.0	0.00	641.67
	(550.0)	12.0	(275.00)	366.67
	0.0	1.0	0.00	366.67
3	1,100.0	10.0	458.33	825.00
	0.0	1.0	0.00	825.00
	(550.0)	12.0	(275.00)	550.00
	0.0	1.0	0.00	550.00
4	1,100.0	10.0	458.33	1,008.33
	0.0	1.0	0.00	1,008.33
	(550.0)	12.0	(275.00)	733.33
	0.0	1.0	0.00	733.33
5	1,100.0	10.0	458.33	1,191.67
	0.0	1.00	0.00	1,191.67
	(550.0)	13.00	(297.92)	893.75
6	(550.0)	24.0	(550.00)	343.75
7	(550.0)	15.0	(343.75)	0.00
	0.0	9.0	0.00	0.00
		168.0	=total hrs	
		50.0	=total withdrawal hrs	
		18.0	=total rest hrs	
		100.0	=total compression hrs	

7.2 Well Plan

The well plan for the full field CAES simulation case is shown by **Figures 58** and **59**. A number of different well plans were investigated with the dynamic model for a variety of vertical and horizontal well combinations. It turned out that while horizontal wells were able to provide higher injectivity and deliverability than vertical wells, they were not as effective as vertical wells in displacing methane away from the wellbore lateral and ended up producing higher methane concentrations during the withdrawal cycles.

The optimized case presented with this report provided the best results in terms of minimizing methane concentration during the initial plant withdrawal cycles. It consists of 29 vertical wells. The wells are distributed between the two structural highs in the field such that 40 percent of the air deliverability is withdrawn and re-injected from the east structural high area and 60 percent is withdrawn and re-injected from the west structural high area. The net effect is to lower methane

concentration in the field withdrawal stream. The wells are drilled and completed in the top 8 - 10 model layers, equivalent to 40 to 50 ft. net reservoir thickness (**Figure 60**).

7.3 Bubble Build

The maximum bottomhole pressure during the bubble build and re-injection periods is designed to be 3,000 psia.[5] Due to the current high reservoir pressure (2080 psia), building an air bubble of 9.2 Bcf requires water to be produced from the King Island reservoir. Without water production, it requires 10 years to build the design bubble size in the model. The project well plan includes four additional aquifer production wells (WAT1 – WAT4) designed to remove water from the reservoir at high rates during the bubble building period. Without the water production, the reservoir pressure will quickly increase above the maximum 3,000 psia bottomhole limit. Although there is water efflux back into the aquifer, it is at a very slow rate (consistent with the rate at which water came into the reservoir under primary production). Supplemental water removal is necessary to build the project air bubble in a reasonable period of time.

The air bubble is built using an 'inside-out' technique where air injection is initiated in two wells (5 MMscfd per well), one well located at the top of each structural high (east and west). As the air bubble increases in size, additional wells are added to both structural areas and air injection increased (5 MMscfd per well) to grow the air bubble radially and push any native gas outward radially from the top of the east and west structures. All wells remain on injection until the end of the bubble build period at injection rates controlled by the simulation model subject to the maximum bottomhole pressure limitation. The bubble build period is summarized by **Figure 61**. It is estimated to require 18 months of elapsed time. A total of 9.2 Bscf of air is injected in addition to the 0.5 Bscf of air injected during the compression testing program for a total bubble size of 9.6 Bscf. Grid displays for the beginning and end of the FFD bubble build are shown by **Figures 62** through **65**. The locations of the cross-sections in **Figure 64** are given by **Figure 59**. **Figure 65** provides a zoomed-in view of two east-west cross-sections in **Figure 64** and shows the range and distribution of the methane mole fraction from 0.01 to less than 0.001 percent.

7.4 Simulated CAES Operations

A base case, 'B', of the simulated CAES full field operations was obtained in an iterative manner to achieve the CAES deliverability/injectivity schedule from the vertical well plan while at the same time minimizing methane concentrations in the withdrawal air.[6] The base case is an optimized case in which group controls in the simulator are used to run the field withdrawal and injection

[5] The fracture gradient based on the I/W Well SRT Instantaneous Shut-in Pressure (ISIP) is 0.808 psi/ft. Applying a safety factor of 20 percent yields a gradient of 0.646 psi/ft and a Maximum Allowable Injection Pressure (MAIP) at the top of the MRF in the I/W Well (4,659 ft TVD) of 3,010 psia.

[6] Of the 29 vertical wells in the optimized base case, 25 wells are used during the CAES withdrawal cycles and 28 wells are used during the CAES re-injection cycles. There is one well, FF11, that is available but never used in the base case.

cycles[7], but manual intervention is made to shut-in wells once they exceed threshold methane concentrations in the withdrawal air.

Specifically, during each air-cycling week, wells with known methane concentration exceedances are shut-in just before methane concentrations reach 4 percent in their withdrawal gas streams and are left shut-in for the remaining weekly withdrawal cycles (these wells are always used for re-injection during the injection cycles). The simulator group control feature then acts to increase the withdrawal rates from the remaining open wells to counterbalance the lost withdrawal rates from the shut-in wells. The goal is to maintain the 1.1 Bscfd inlet plant rate for the remaining weekly cycle while at the same time honoring the given bottomhole and wellhead pressure well constraints.[8] Once the bubble is rebuilt at the end of the each week, the shut-in wells are re-opened for withdrawal and the same process is repeated for the next weekly cycle. Field engineering solutions comparable to this modeling procedure could be implemented during CAES Plant operations to maintain methane concentrations at the CAES plant inlet compatible with surface power generation equipment constraints.

It is worth noting that, due to computational efficiency and runtime limitations, the FFD model was not configured with LGR around any of the model wells. The LGR sensitivity described in **Section 6.2.2** (**Figure 42**) found that saturation changes were more gradual for the use of refined gridding at the I/W Well. It is a reasonable assumption that this result will apply to the vertical wells in the FFD model. Therefore, in a finer gridded model, the predicted methane concentrations during the withdrawal cycles of the 25 wells may increase more gradually and to a lesser extent than the methane predictions presented in this report for the FFD model in its current 50 ft. by 50 ft. gridblock configuration.

The base case demonstrates the feasibility of a CAES operation in a depleted natural gas reservoir such as the King Island Gas Field. The reservoir pressure and average methane concentration in the produced air during the withdrawal/injection cycling of air is shown in **Figure 66** for a two-year operating period. The reservoir pressure decreases with time due to formation water continuing to efflux into the aquifer. The percent methane is below 2 percent for the field-wide average rate. The methane concentration decreases gradually with continued CAES cycle operations. Water production is not significant as it is projected to be less than 300 barrels per day total over the two-year operating period (**Figure 67**). **Figure 68** shows that the none of the individual wells produce over 4 percent methane concentration during the two-year period.

Additional aerial and cross-sectional displays through the model for this base case are presented by **Figures 69** through **75. Figure 75** provides a zoomed-in view of two east-west cross-sections in

[7] The model wells are operated on rate control subject to the bottomhole and surface tubing pressure limitations in **Table 34**. The only pressure limit that is reached for Base Case 'B' is the 3,000 psia limit on injection in some wells.

[8] For Base Case 'B', the early shut-in of key wells with high methane concentrations reduced the 1.1 Bscfd plant inlet rate to 0.99 Bscfd for the last two hours of the last withdrawal day in each air-cycling week. This was not considered to be a critical issue and therefore no model adjustments were made to address it; however, additional wells could be drilled to remedy this type of situation.

Figure 74 and shows the range and distribution of the methane mole fraction from 0.01 to less than 0.001 percent.

Several sensitivity cases were run with the optimized model to investigate what would happen if one or more re-injection cycles were missed or skipped during a week's operational period (for example, if the plant was unable to operate in an injection mode temporarily). The model results showed that there is a delicate balance to keeping the methane away from the wells during a withdrawal cycle. Re-injection is critical to controlling the methane concentrations by well. Only two or three days may be skipped without field re-injection, before methane concentrations begin to increase to unacceptable levels in some wells. If the lost air injection is made up by over-injection, the model predicts that it does help the operations to recover and to bring the methane concentrations back down to previous levels.

8. REFERENCES

EPA, 2014, Final Underground Injection Control (UIC) Permit, Class V Experimental Well, R9UIC-CAS5-FY13-1, Pacific Gas and Electric Company (PG&E), August 20, 2014.

JJ&A, 2015, Evaluation of Geochemical Effects Resulting from Air Injection into a Partially Depleted Gas Reservoir, Pacific Gas and Electric Company, Compressed Air Energy Storage Project, King Island Gas Field, San Joaquin County, California, September 2015.

PG&E, 2014a, Underground Injection Control Permit Application and Technical Attachments, PG&E Compressed Air Energy Storage Project, Compression Testing Program, King Island Gas Field, San Joaquin County, California, revised April 28, 2014.

PG&E, 2014b, Plan to Conduct Step-Rate Test (SRT) and Initial Fall-Off Test (FOT), In Accordance with EPA Underground Injection Control (UIC) Permit No. R9UIC-CA5-FY13-1, September 25, 2015.

PG&E, 2015a, Well Completion Report, PG&E CAES Injection/Withdrawal Well and Observation Wells, In Accordance with EPA Form 7520-9, January 28, 2015.

PG&E, 2015b, Submittal of Oxygen-Depleted Air Analytical Results Permit No. R9UIC-CA5-FY13-1, PG&E Test Injection/Withdrawal Well 1, King Island, San Joaquin County, California, February 12, 2015.

PG&E, 2015c, Submittal of Revisions to Phase 3 Submittal of the Well Completion Report, Permit No. R9UIC-CA5-FY13-1, PG&E Test Injection/Withdrawal Well 1, King Island, San Joaquin County, California, February 25, 2015.

PG&E, 2015d, Submittal of Plan to Conduct an External Mechanical Integrity Test, Permit No. R9UIC-CA5-FY13-1, PG&E Test Injection/Withdrawal Well 1, King Island, San Joaquin County, California, March 18, 2015.

PG&E, 2015e, Submittal of Fall-Off Test Results, Permit No. R9UIC-CA5-FY13-1, PG&E Test Injection/Withdrawal Well 1, King Island, San Joaquin County, California, March 18, 2015.

PG&E, 2015f, February 2015 Monthly Report for PG&E Test Injection/Withdrawal Well 1, Permit No. R9UIC-CA5-FY13-1, King Island, San Joaquin County, California, March 27, 2015.

PG&E, 2015g, Request to Provide Remedial Cementing Plan, PG&E Test Injection/Withdrawal Well 1, Permit No. R9UIC-CA5-FY13-1, King Island, San Joaquin County, California, March 31, 2015.

PG&E, 2015h, Updated Evaluation of Annular Pressure-Temperature Relationship, PG&E Test Injection/Withdrawal Well 1, Permit No. R9UIC-CA5-FY13-1, King Island, San Joaquin County, California, April 1, 2015.

PG&E, 2015i, Submittal of Appendix V-6b, Exhibits 1 - 18, to Phase 3 Submittal of the Well Completion Report, Permit No. R9UIC-CA5-FY13-1, PG&E Test Injection/Withdrawal Well 1, King Island, San Joaquin County, California, April 9, 2015.

PG&E, 2015j, Responses to EPA Comments on External MIT Plan, PG&E Test Injection/Withdrawal Well 1, Permit No. R9UIC-CA5-FY13-1, King Island, San Joaquin County, California, April 9, 2015.

PG&E, 2015k, February 2015 Monthly Report and Updated Evaluation of Annular Pressure Temperature Relationship, PG&E Test Injection/Withdrawal Well 1, Permit No. R9UIC-CA5-FY13-1, King Island, San Joaquin County, California, April 24, 2015.

PG&E, 2015l, March 2015 Monthly Report for PG&E Test Injection/Withdrawal Well 1, Permit No. R9UIC-CA5-FY13-1, King Island, San Joaquin County, California, April 27, 2015.

PG&E, 2015m, Updated Evaluation of Annular Pressure-Temperature Relationship, PG&E Test Injection/Withdrawal Well 1, Permit No. R9UIC-CA5-FY13-1, King Island, San Joaquin County, California, May 1, 2015.

PG&E, 2015n, Submittal of Falloff Test Reports, First and Second Compression Test Falloff Tests Conducted on February 17-18 and April 1-3, 2015, PG&E Test Injection/Withdrawal Well 1, Permit No. R9UIC-CA5-FY13-1, King Island, San Joaquin County, California, May 4, 2015.

PG&E, 2015o, Updated Evaluation of Annular Pressure-Temperature Relationship, PG&E Test Injection/Withdrawal Well 1, Permit No. R9UIC-CA5-FY13-1, King Island, San Joaquin County, California, May 14, 2015.

PG&E, 2015p, Response to Comments on March 2015 Monthly Report, PG&E Test Injection/Withdrawal Well 1, Permit No. R9UIC-CA5-FY13-1, King Island, San Joaquin County, California, May 19, 2015.

PG&E, 2015q, April 2015 Monthly Report for PG&E Test Injection/Withdrawal Well 1, Permit No. R9UIC-CA5-FY13-1, King Island, San Joaquin County, California, May 27, 2015.

PG&E, 2015r, Submittal of Falloff Test Report, Third Compression Test Falloff Test Conducted on May 1-3, 2015, PG&E Test Injection/Withdrawal Well 1, Permit No. R9UIC-CA5-FY13-1, King Island, San Joaquin County, California, June 2, 2015.

PG&E, 2015s, Updated Evaluation of Annular Pressure-Temperature Relationship, PG&E Test Injection/Withdrawal Well 1, Permit No. R9UIC-CA5-FY13-1, King Island, San Joaquin County, California, June 8, 2015.

PG&E, 2015t, May 2015 Monthly Report for PG&E Test Injection/Withdrawal Well 1, Permit No. R9UIC-CA5-FY13-1, King Island, San Joaquin County, California, June 25, 2015.

WorleyParsons, 2014a, Preliminary Reservoir Characterization and Testing for Compressed Air Energy Storage, Document No. PGCS-1-LI-022-017, June 4, 2014.

WorleyParsons, 2014b, Compressed Air Energy Storage Energy Conversion Facility Air Transmission System Conceptual Design and Cost Estimate, Document No. PGCS-1-LI-027-0001, September 29, 2014.

WorleyParsons, 2014c, Compressed Air Energy Storage Test Facility, Air Injection Decision Matrix, Document No. PGCS-1-LI-073-004, July 11, 2014.

WorleyParsons, 2015a, Compression Test Data Acquisition Plan, PG&E Compressed Air Energy Storage Project, King Island Gas Field, San Joaquin County, California, Document No. PGCS-1-L1-022-0019, January 12, 2015.

FIGURES

Final Technical Memorandum for Compressed Air Energy Storage
Reservoir Characterization & Full Field Development Model
King Island Gas Field, San Joaquin County, CA
9/25/2015

FIGURE 1

KING ISLAND
RESERVOIR AND WELL LOCATIONS

SECTION 27, TOWNSHIP 3 NORTH, RANGE 5 EAST

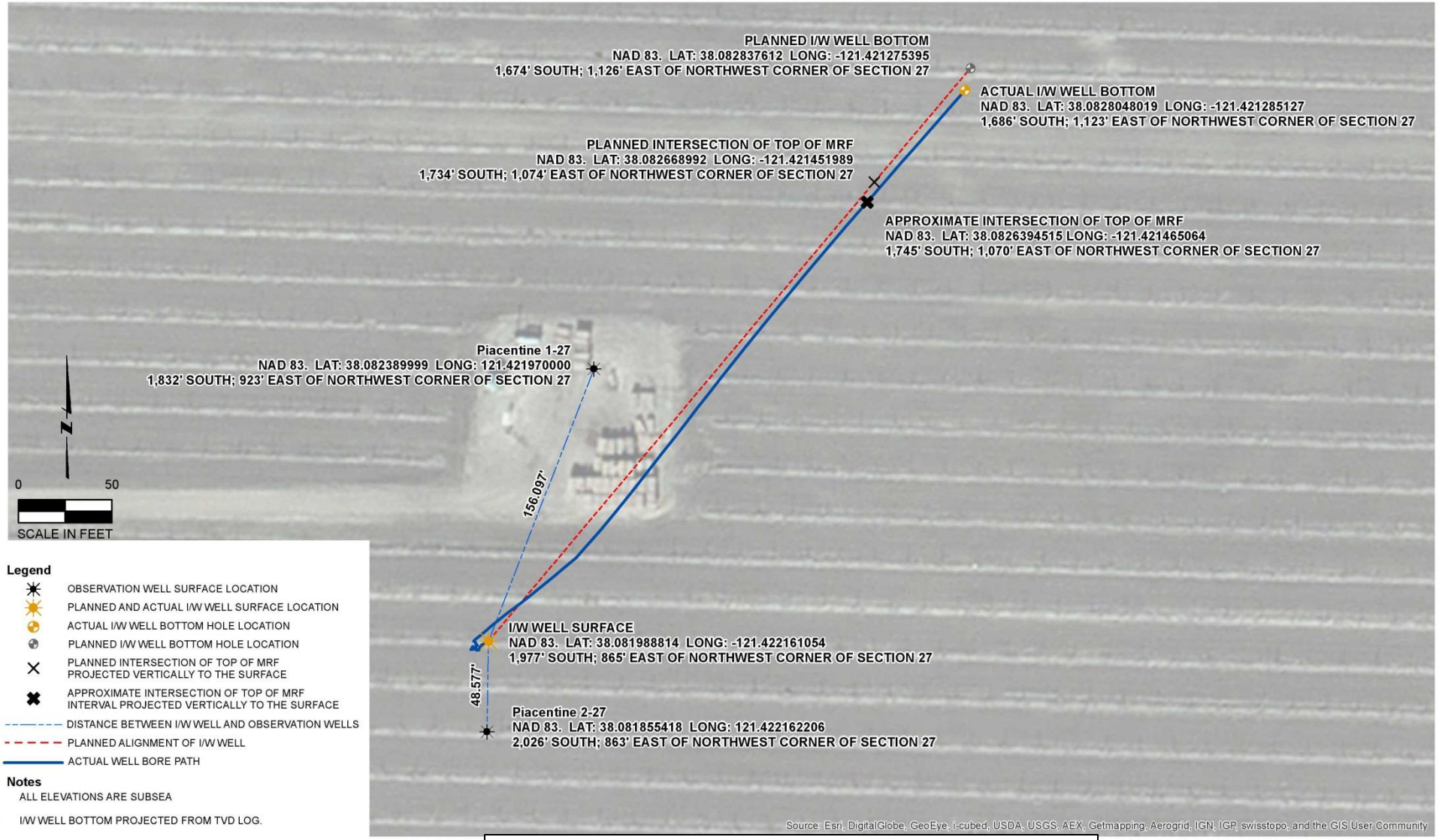

Legend

- OBSERVATION WELL SURFACE LOCATION
- PLANNED AND ACTUAL I/W WELL SURFACE LOCATION
- ACTUAL I/W WELL BOTTOM HOLE LOCATION
- PLANNED I/W WELL BOTTOM HOLE LOCATION
- PLANNED INTERSECTION OF TOP OF MRF PROJECTED VERTICALLY TO THE SURFACE
- APPROXIMATE INTERSECTION OF TOP OF MRF INTERVAL PROJECTED VERTICALLY TO THE SURFACE
- DISTANCE BETWEEN I/W WELL AND OBSERVATION WELLS
- PLANNED ALIGNMENT OF I/W WELL
- ACTUAL WELL BORE PATH

Notes

ALL ELEVATIONS ARE SUBSEA

I/W WELL BOTTOM PROJECTED FROM TVD LOG.

I/W WELL BORE PATH PROVIDED FROM TVD LOG.

I/W INJECTION/WITHDRAWAL
MRF MOKELUMNE RIVER FORMATION
TVD TRUE VERTICAL DEPTH
UIC UNDERGROUND INJECTION CONTROL

FIGURE PREPARED BY: JACOBSON, JAMES & ASSOCIATES, INC.

Path: J:\GIS\WPPGE_CAES\Appendix II-2 I/W Well Location.mxd

Final Technical Memorandum for Compressed Air Energy Storage Reservoir Characterization & Full Field Development Model
King Island Gas Field, San Joaquin County, CA
9/25/2015

FIGURE 2

PLANNED AND ACTUAL I/W AND OBSERVATION WELL COORDINATES AND ACTUAL WELL BORE PATH

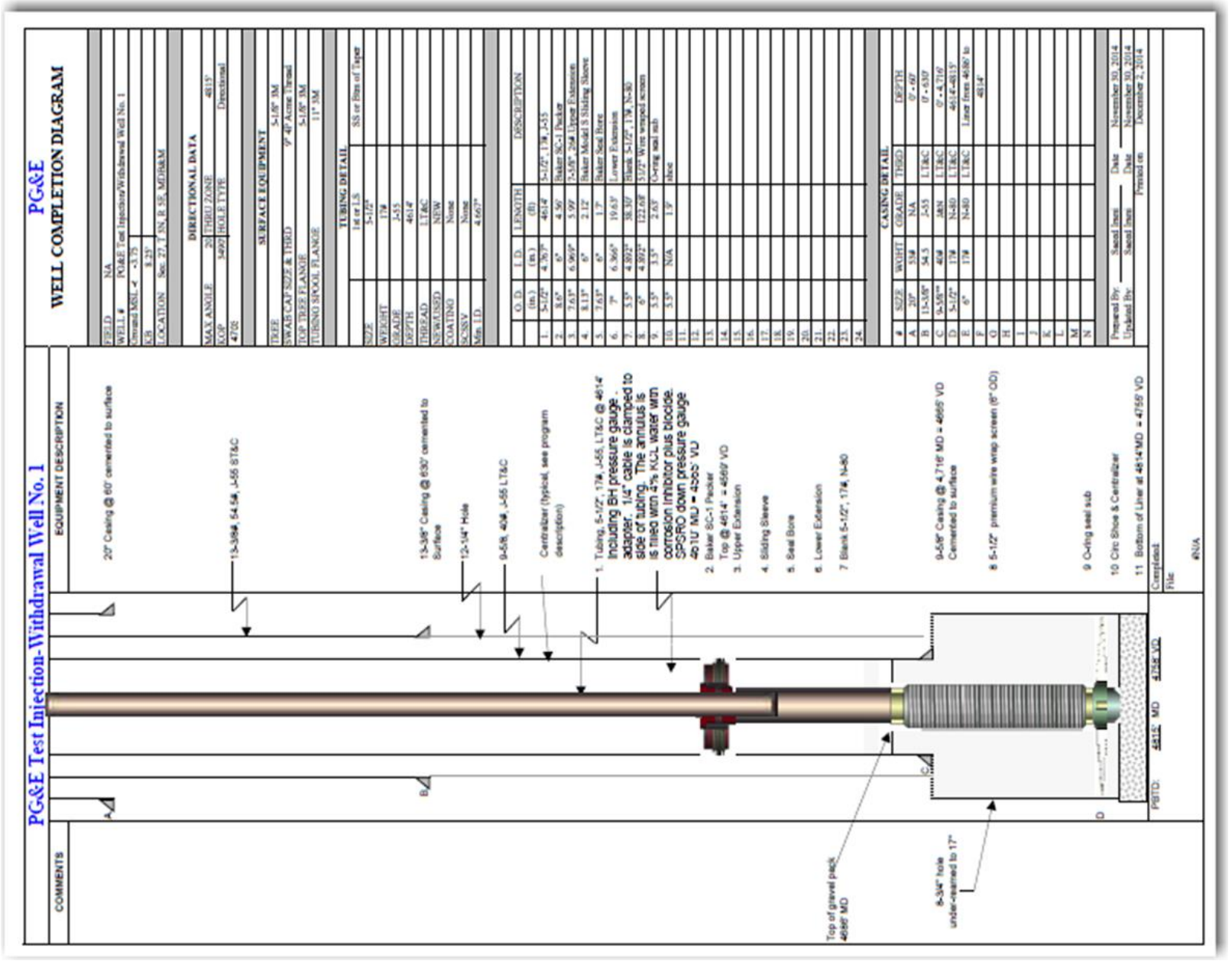

Final Technical Memorandum
for Compressed Air Energy Storage
Reservoir Characterization & Full Field Development Model
King Island Gas Field, San Joaquin County, CA
9/25/2015

Figure 3

Injection/Withdrawal Well 1

Wellbore Diagram

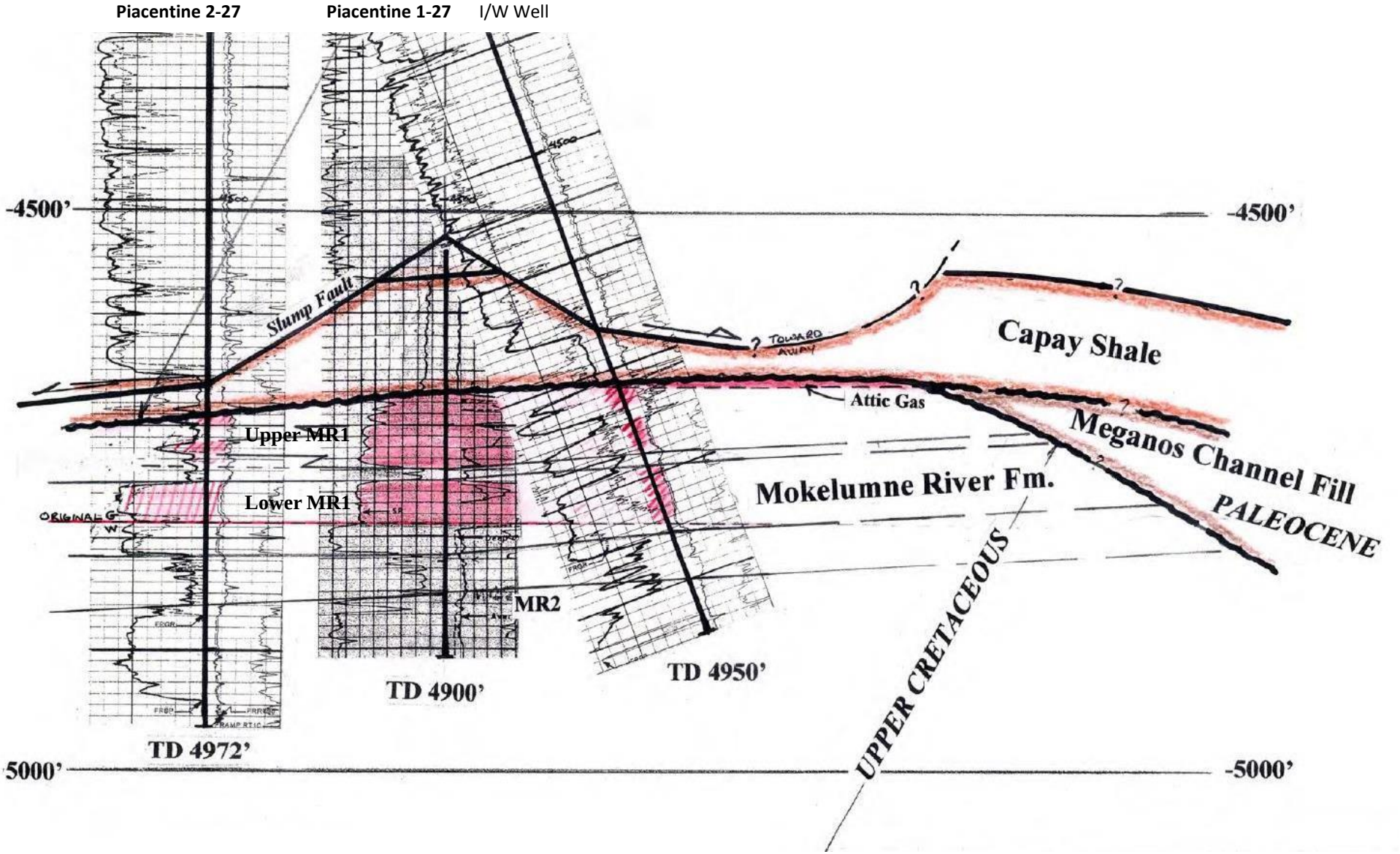

Final Technical Memorandum
for Compressed Air Energy Storage
Reservoir Characterization & Full Field Development Model
King Island Gas Field, San Joaquin County, CA
9/25/2015

Figure 4

Geological Structure Cross-Section Across East Lobe

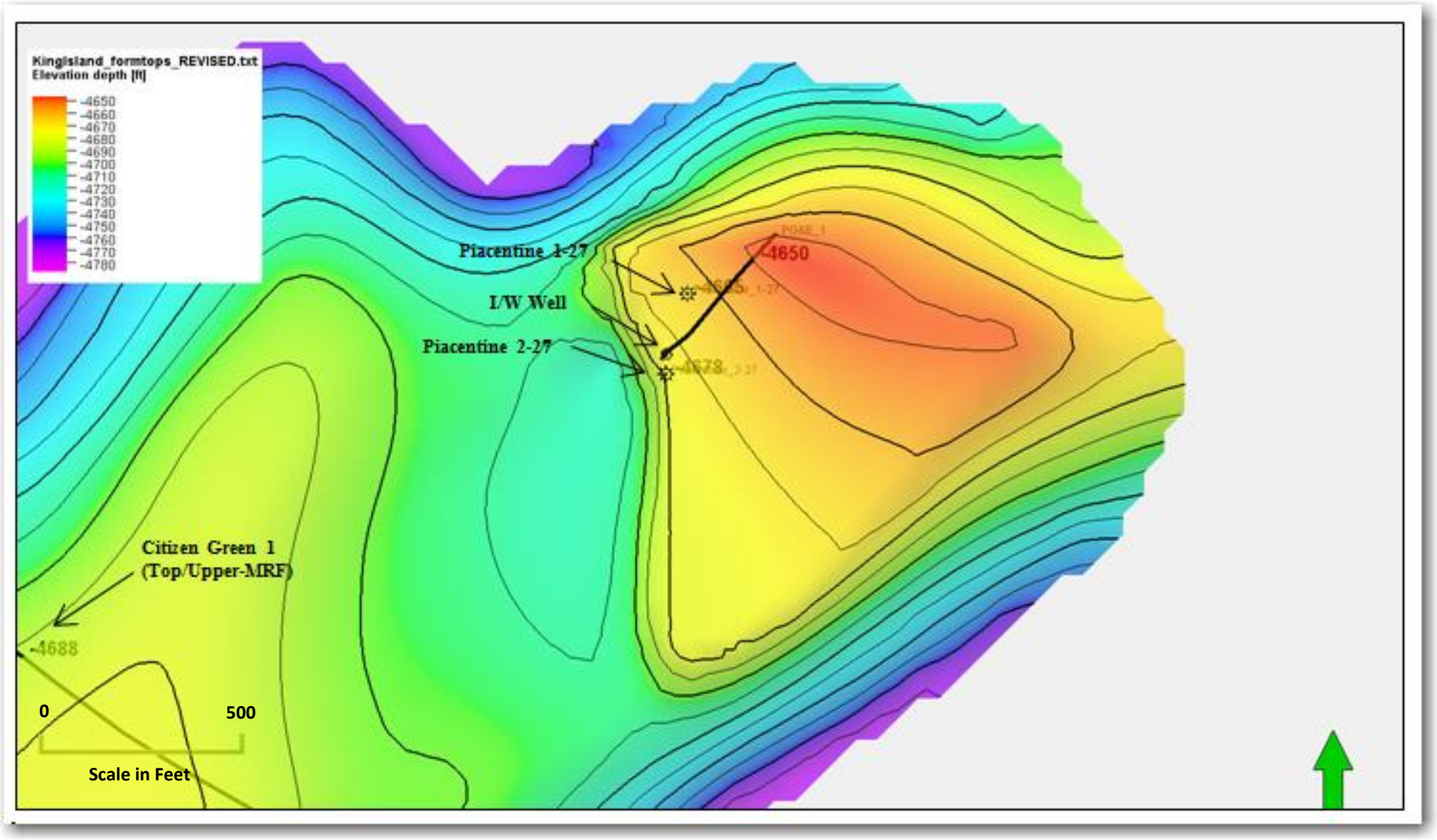

Final Technical Memorandum
for Compressed Air Energy Storage
Reservoir Characterization & Full Field Development Model
King Island Gas Field, San Joaquin County, CA
9/25/2015

Figure 5

Structure Map of Top Upper MR1

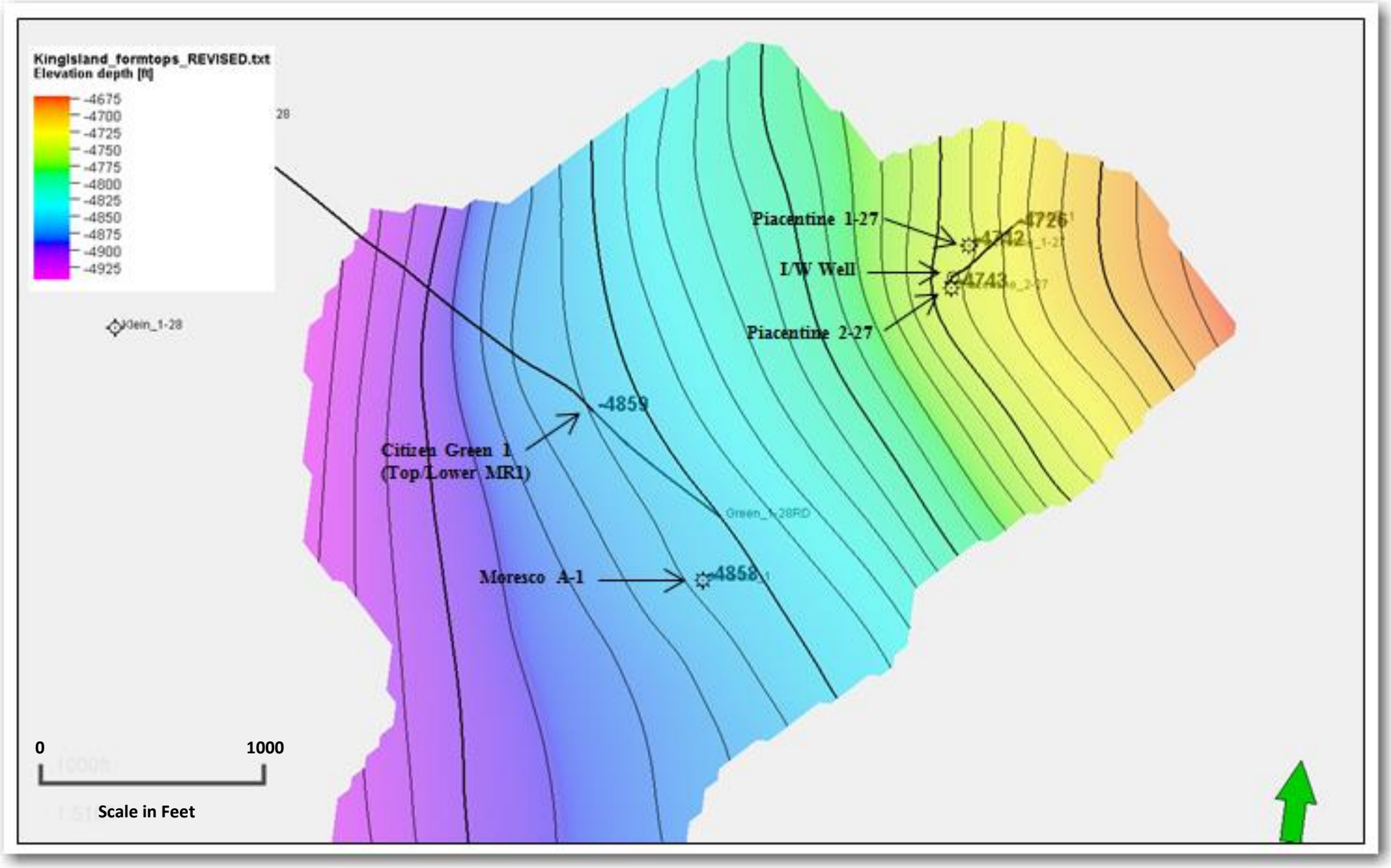

Final Technical Memorandum
for Compressed Air Energy Storage
Reservoir Characterization & Full Field Development Model
King Island Gas Field, San Joaquin County, CA
9/25/2015

Figure 6

Structure Map of Top Lower MR1

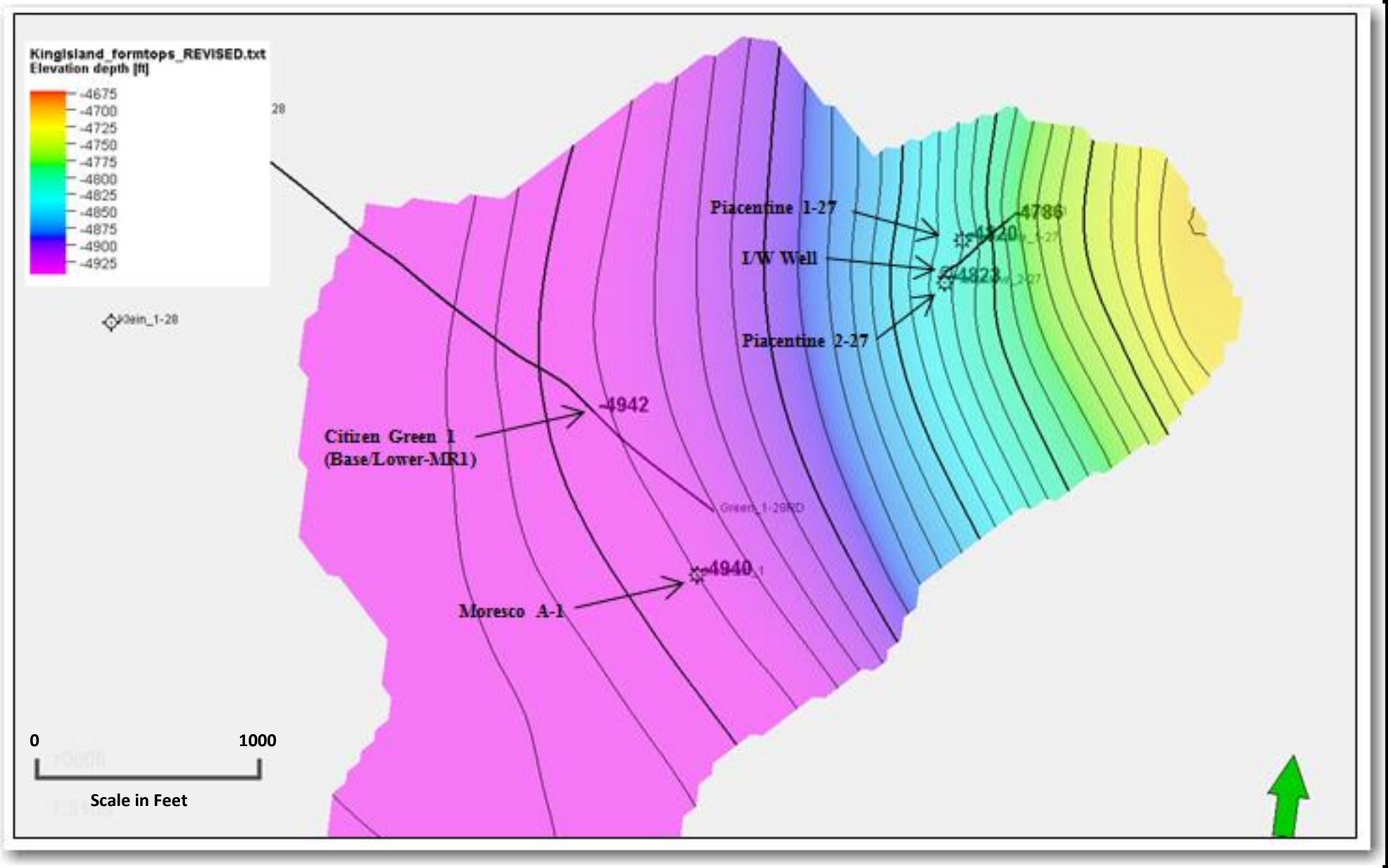

Final Technical Memorandum
for Compressed Air Energy Storage
Reservoir Characterization & Full Field Development Model
King Island Gas Field, San Joaquin County, CA
9/25/2015

Figure 7

Structure Map of Base Lower MR1

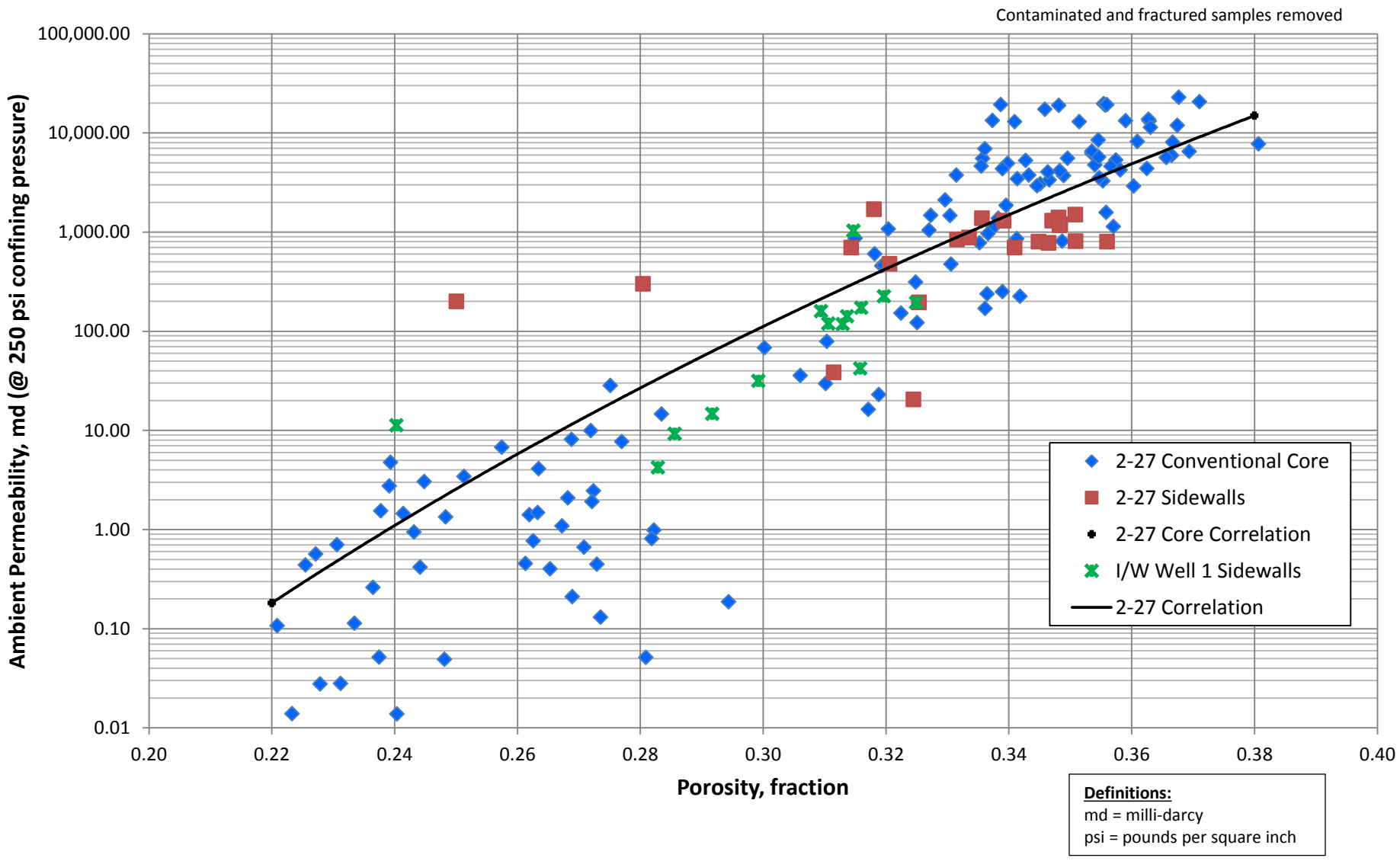

Final Technical Memorandum
for Compressed Air Energy Storage
Reservoir Characterization & Full Field Development Model
King Island Gas Field, San Joaquin County, CA
9/25/2015

Figure 8

Piacentine 2-27 and I/W Well Core Results

Porosity vs. Permeability

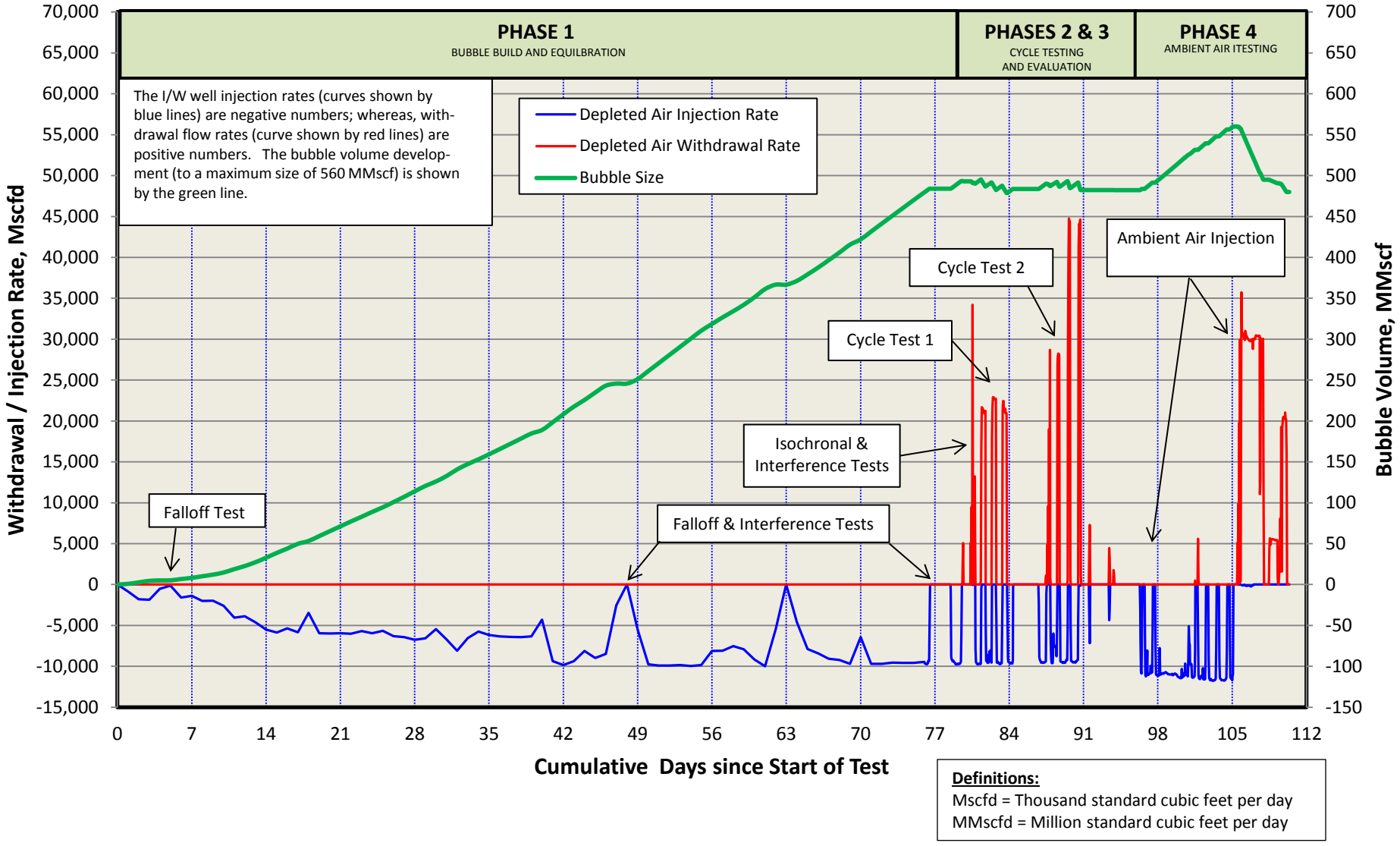

Definitions:
Mscfd = Thousand standard cubic feet per day
MMscfd = Million standard cubic feet per day

Final Technical Memorandum
for Compressed Air Energy Storage
Reservoir Characterization & Full Field Development Model
King Island Gas Field, San Joaquin County, CA
9/25/2015

Figure 9

King Island Gas Field

Compression Testing Program

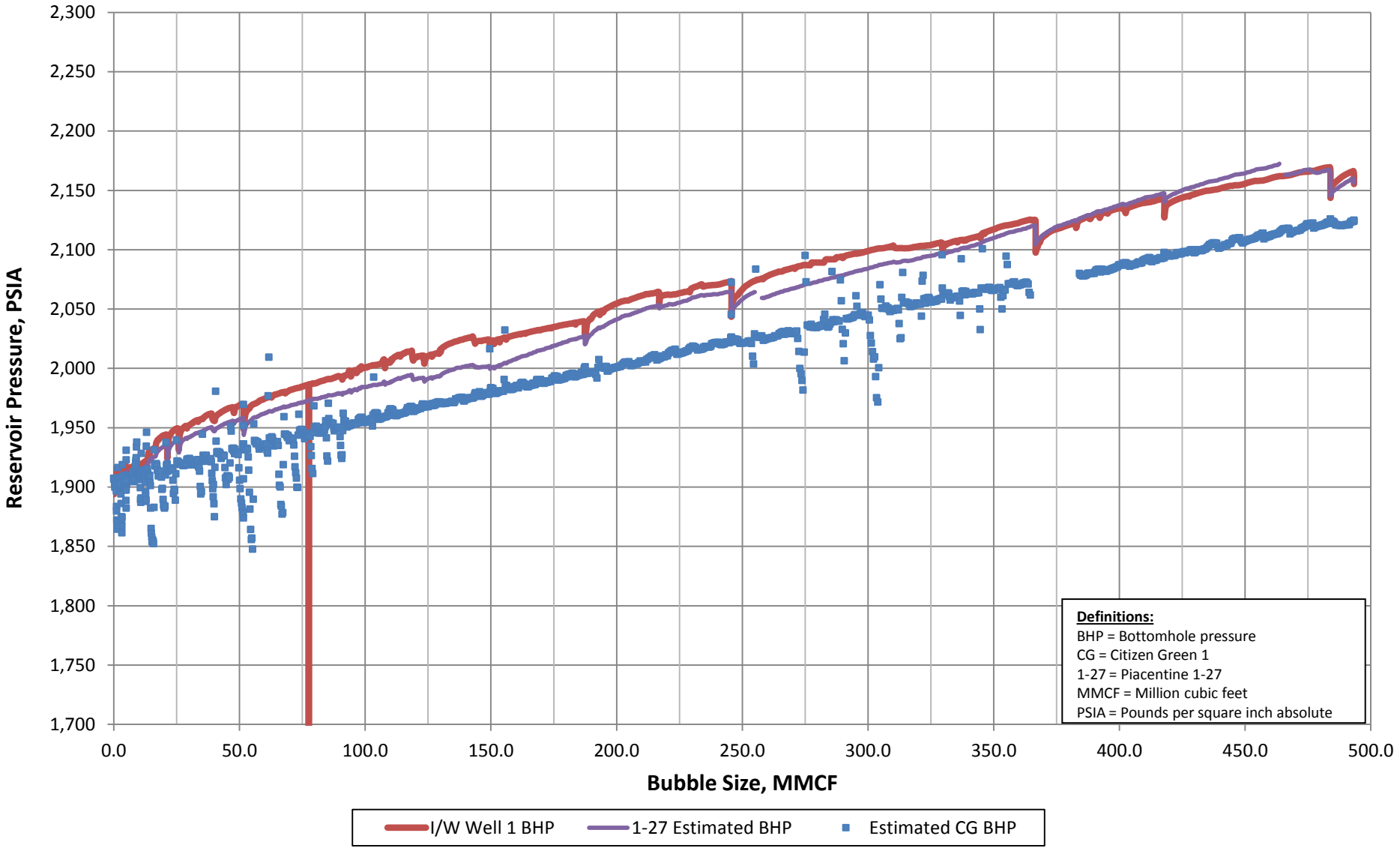

Final Technical Memorandum
for Compressed Air Energy Storage
Reservoir Characterization & Full Field Development Model
King Island Gas Field, San Joaquin County, CA
9/25/2015

Figure 10

Reservoir Pressure Response vs. Bubble Build Volume

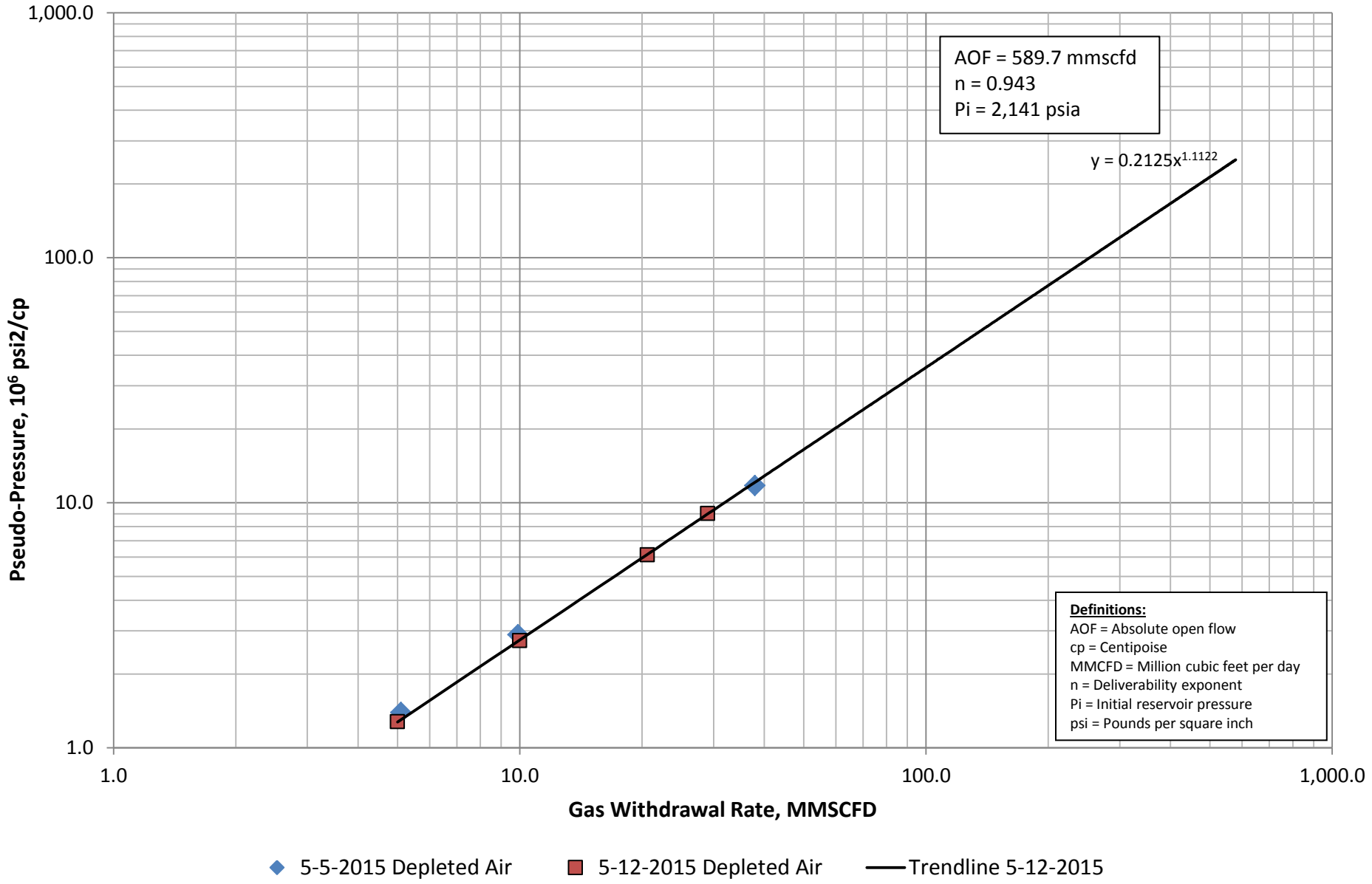

Final Technical Memorandum
for Compressed Air Energy Storage
Reservoir Characterization & Full Field Development Model
King Island Gas Field, San Joaquin County, CA
9/25/2015

Figure 11

Results of Isochronal Tests in I/W Well During Depleted Air Cycle Testing Bottomhole Absolute Open Flow Plot

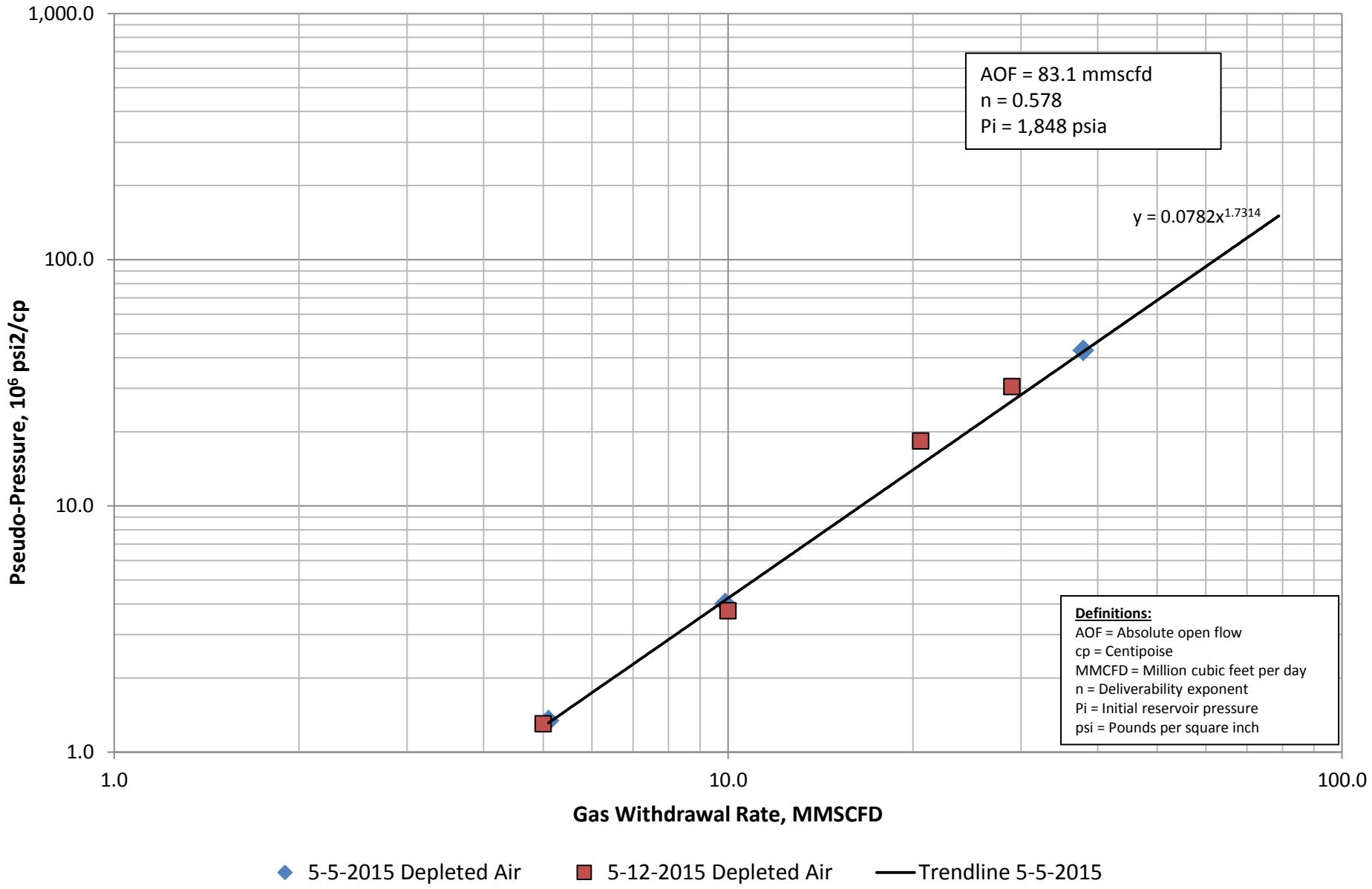

Final Technical Memorandum
for Compressed Air Energy Storage
Reservoir Characterization & Full Field Development Model
King Island Gas Field, San Joaquin County, CA
9/25/2015

Figure 12

Results of Isochronal Tests in I/W Well During Depleted Air Cycle Testing Wellhead Absolute Open Flow Plot

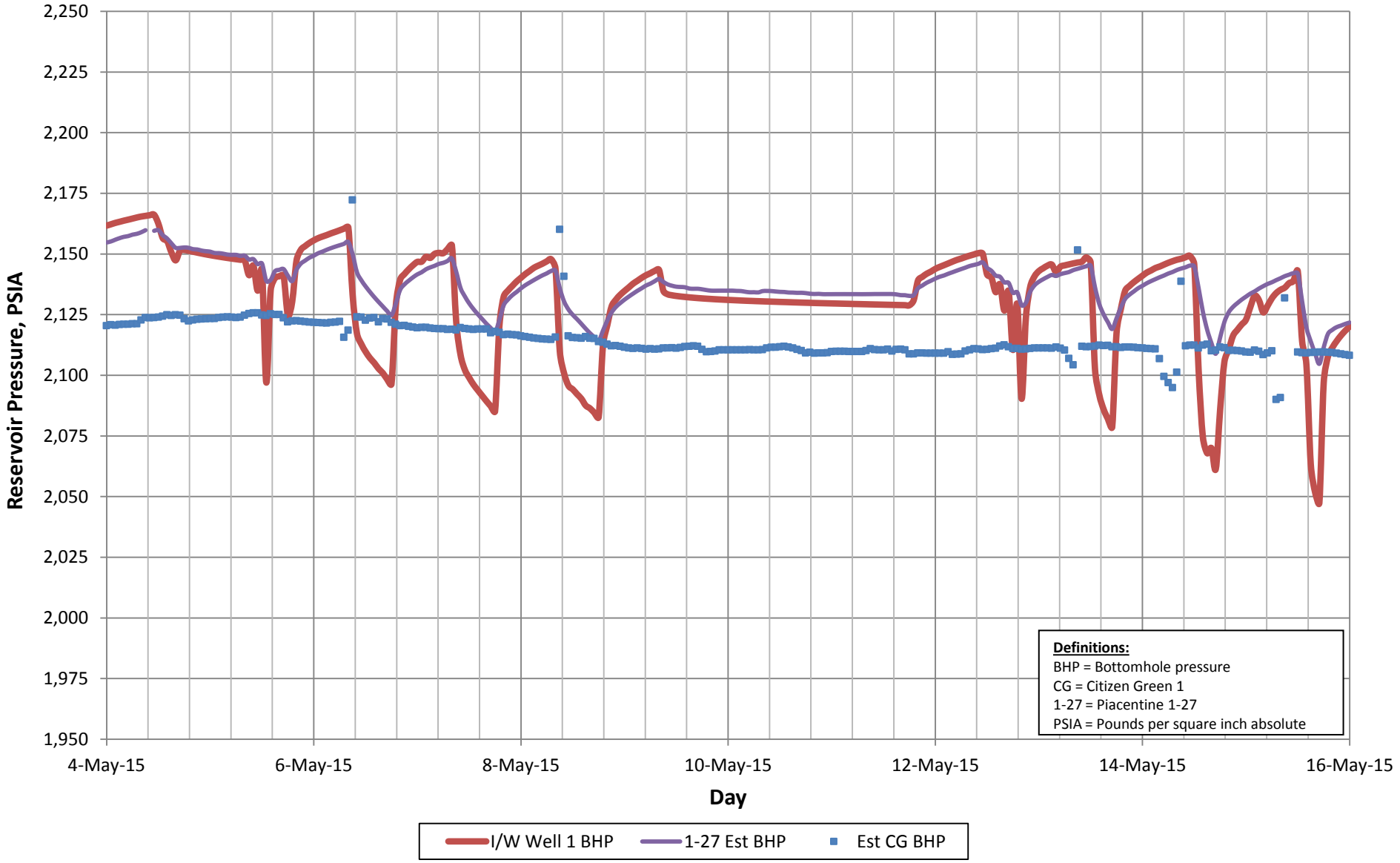

Final Technical Memorandum
for Compressed Air Energy Storage
Reservoir Characterization & Full Field Development Model
King Island Gas Field, San Joaquin County, CA
9/25/2015

Figure 13

Reservoir Pressure Response During Depleted Air Cycle Testing

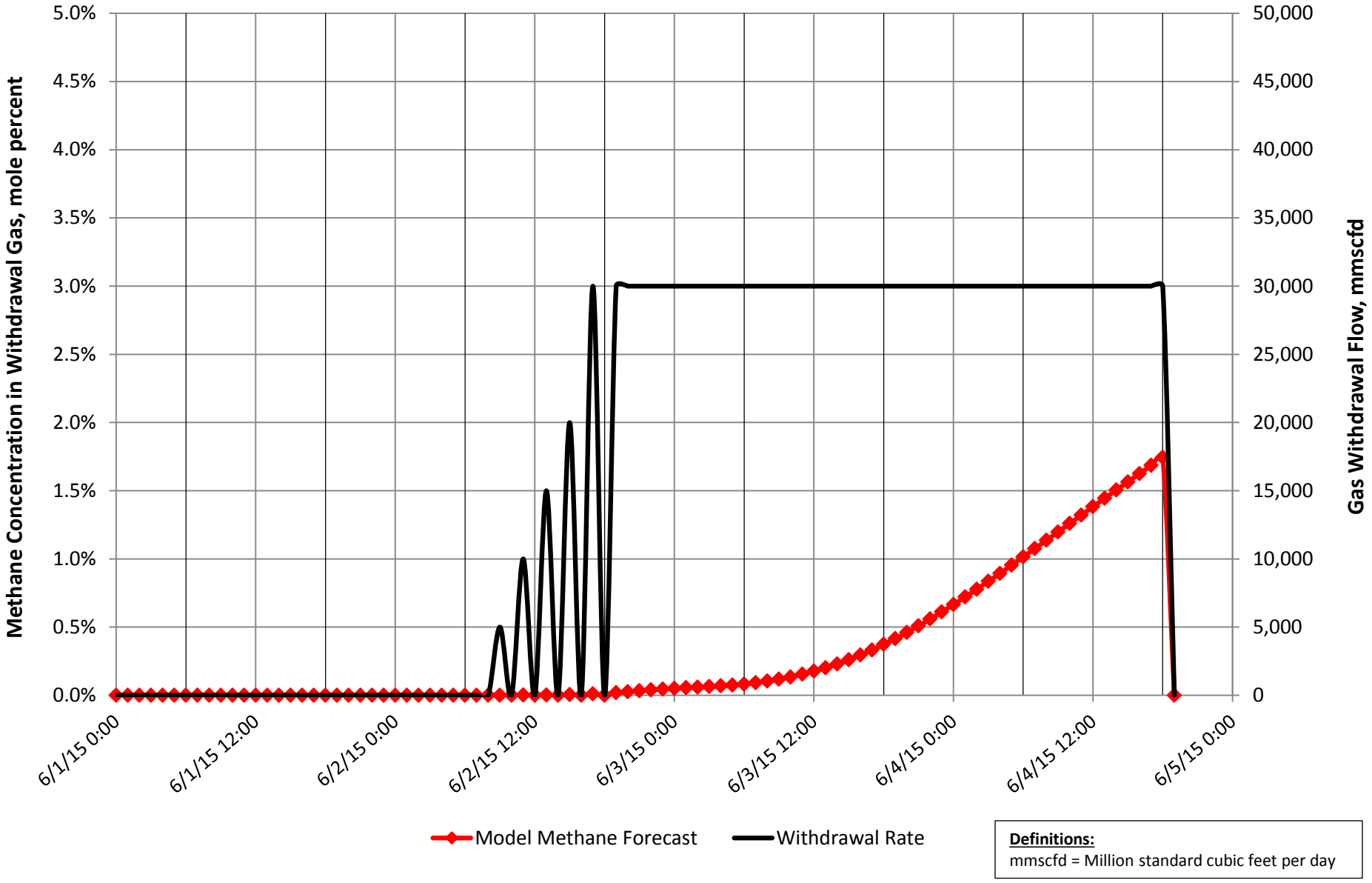

Final Technical Memorandum
for Compressed Air Energy Storage
Reservoir Characterization & Full Field Development Model
King Island Gas Field, San Joaquin County, CA
9/25/2015

Figure 14

King Island Model Forecast of Methane Concentration During Ambient Air Flow Testing

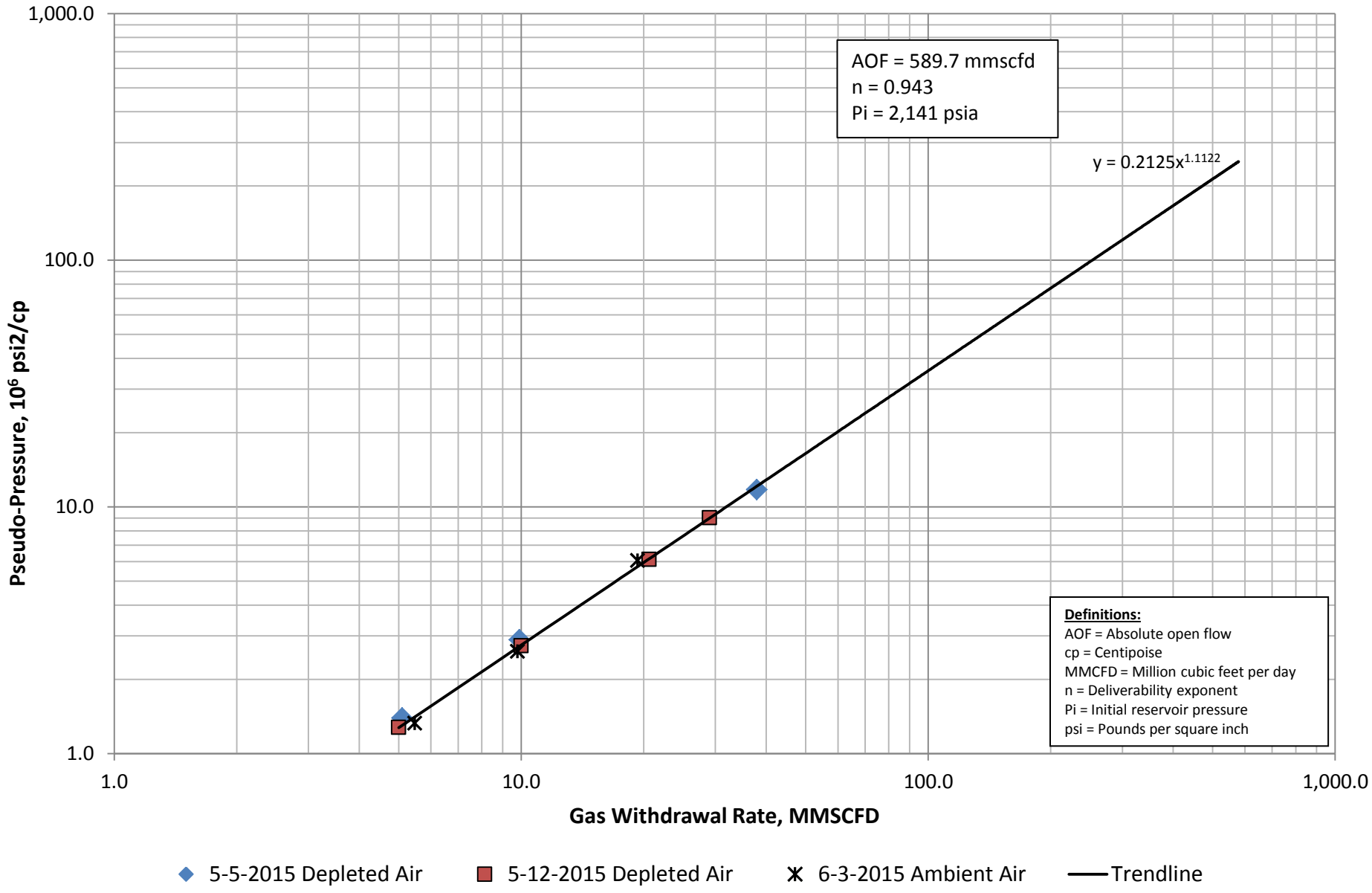

Final Technical Memorandum
for Compressed Air Energy Storage
Reservoir Characterization & Full Field Development Model
King Island Gas Field, San Joaquin County, CA
9/25/2015

Figure 15

Results of Isochronal Tests in I/W Well During Depleted Air Cycle Testing and Ambient Air Flow Testing - Bottomhole Absolute Open Flow Plot

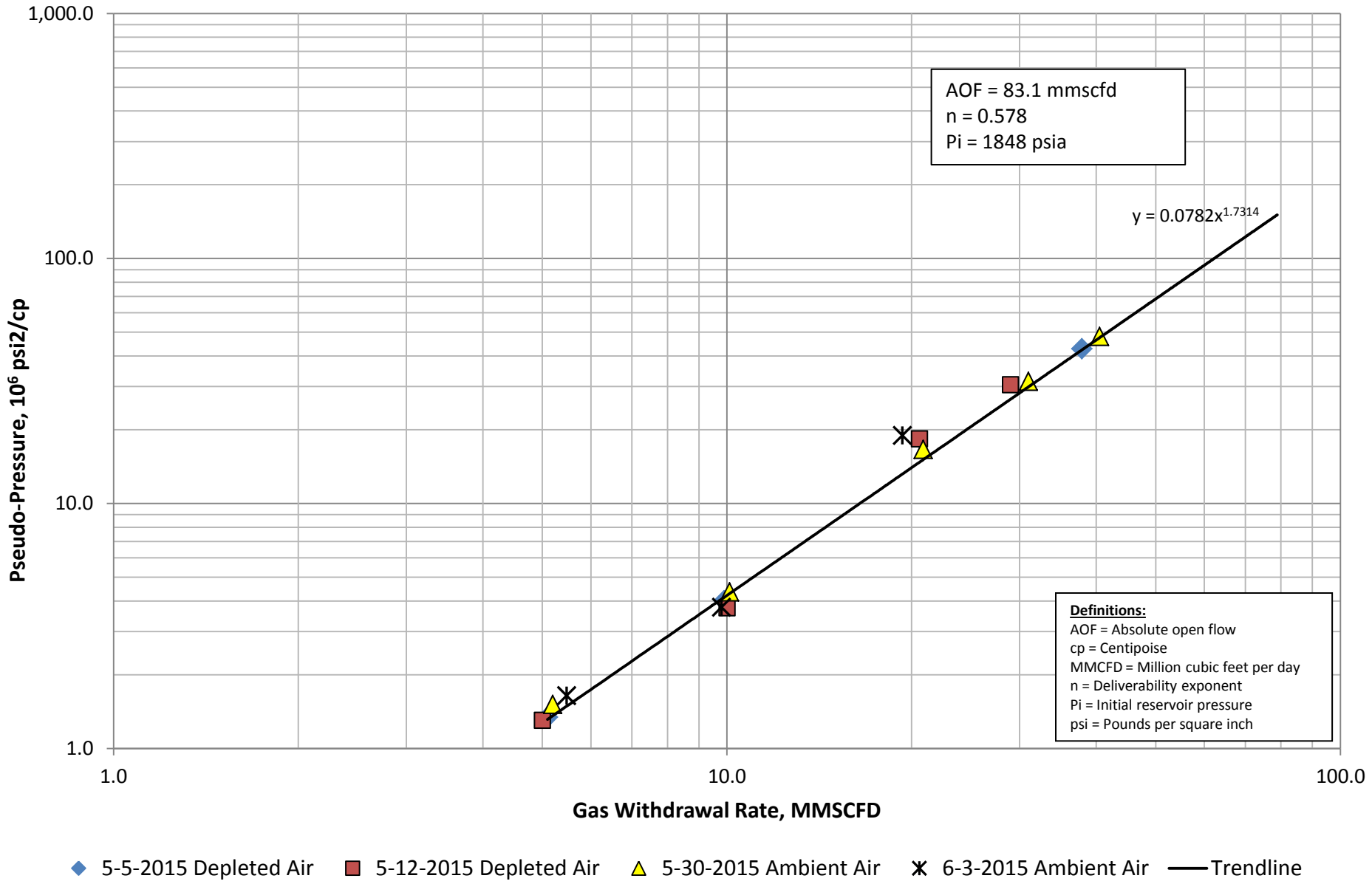

Final Technical Memorandum
for Compressed Air Energy Storage
Reservoir Characterization & Full Field Development Model
King Island Gas Field, San Joaquin County, CA
9/25/2015

Figure 16

Results of Isochronal Tests in I/W Well During Depleted Air Cycle Testing and Ambient Air Flow Testing - Wellhead Absolute Open Flow Plot

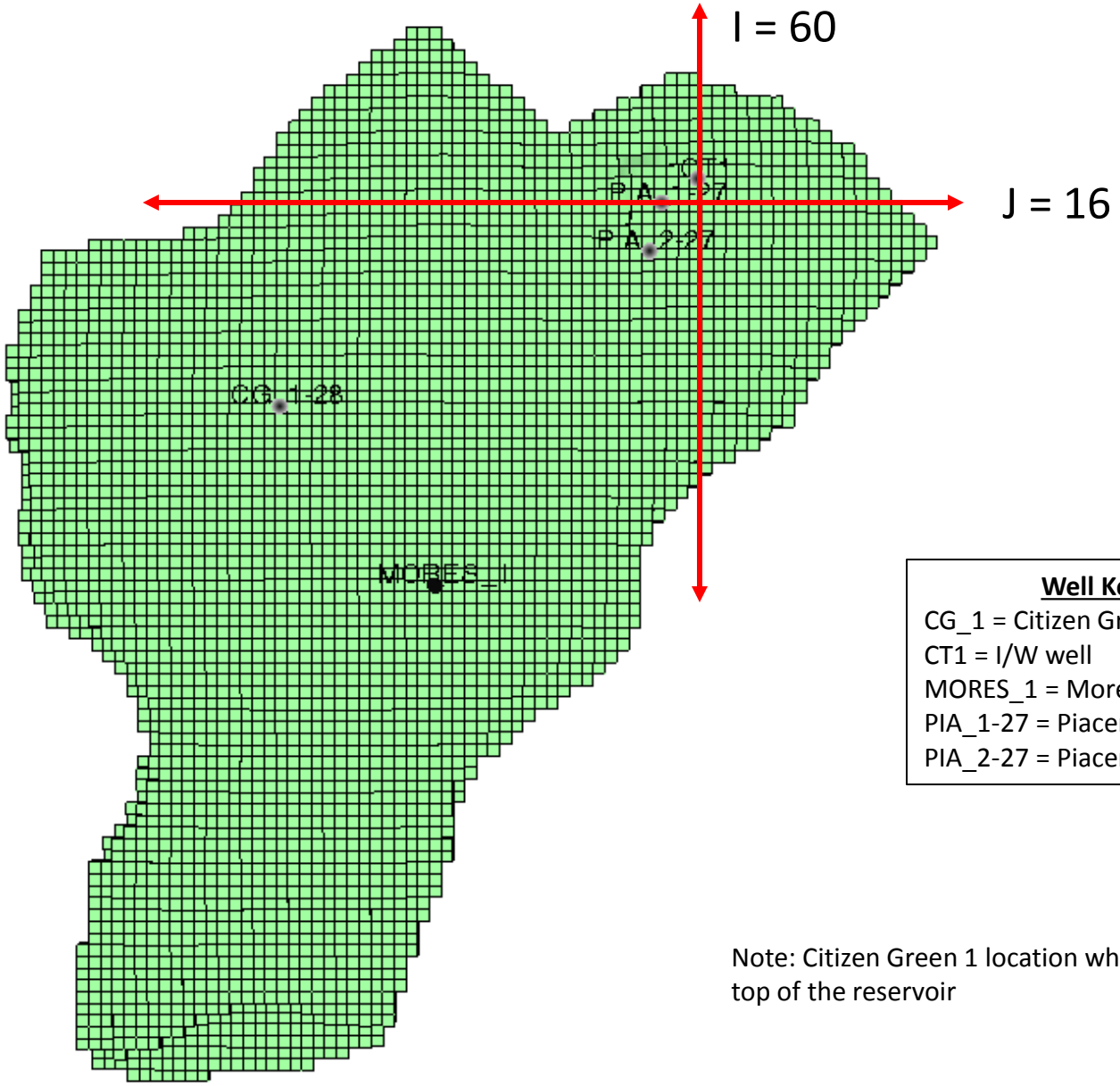

Well Key

CG_1 = Citizen Green 1
CT1 = I/W well
MORES_1 = Moresco A1
PIA_1-27 = Piacentine 1-27
PIA_2-27 = Piacentine 2-27

Note: Citizen Green 1 location where the well bore intersects the top of the reservoir

Final Technical Memorandum
for Compressed Air Energy Storage
Reservoir Characterization & Full Field Development Model
King Island Gas Field, San Joaquin County, CA
9/25/2015

Figure 17

Grid Display

Cross-Section Locations

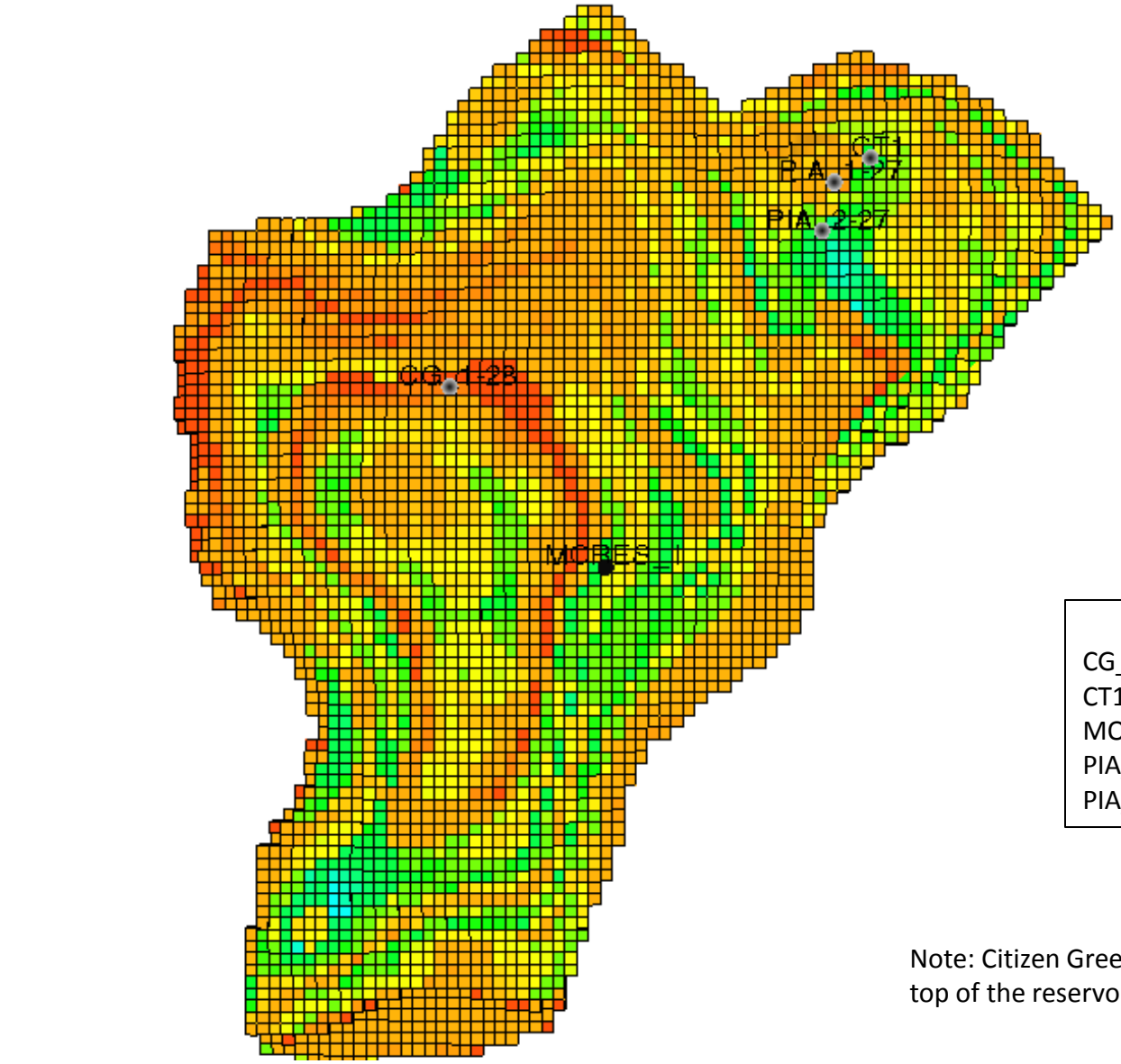

Well Key

CG_1 = Citizen Green 1
CT1 = I/W well
MORES_1 = Moresco A1
PIA_1-27 = Piacentine 1-27
PIA_2-27 = Piacentine 2-27

Note: Citizen Green 1 location where the well bore intersects the top of the reservoir

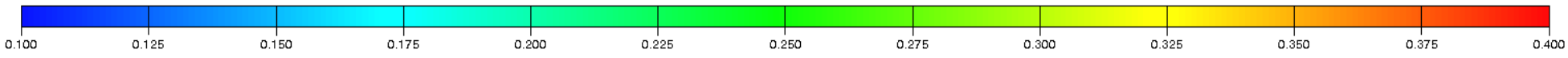

Final Technical Memorandum
for Compressed Air Energy Storage
Reservoir Characterization & Full Field Development Model
King Island Gas Field, San Joaquin County, CA
9/25/2015

Figure 18

Porosity

Aerial

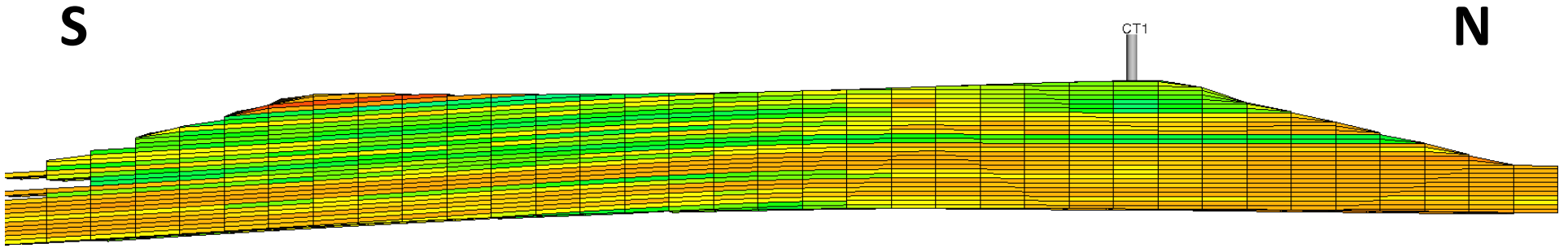

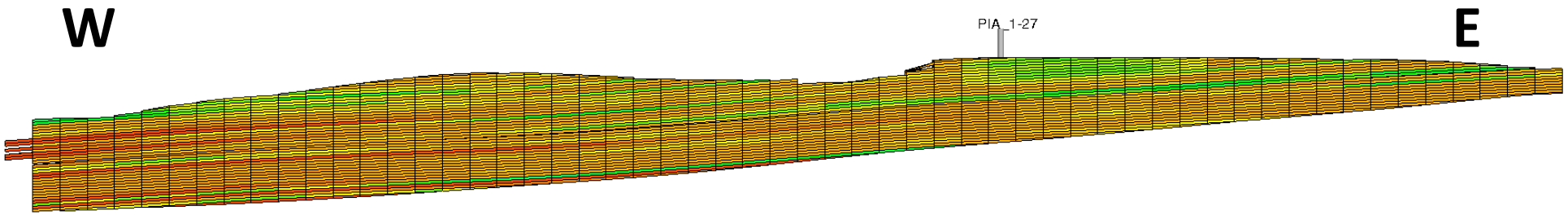

Well Key

CT1 = I/W well

PIA_1-27 = Piacentine 1-27

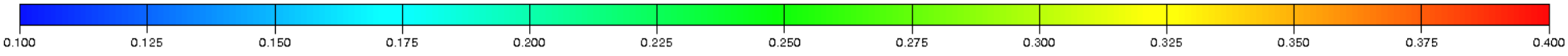

Final Technical Memorandum
for Compressed Air Energy Storage
Reservoir Characterization & Full Field Development Model
King Island Gas Field, San Joaquin County, CA
9/25/2015

Figure 19

Porosity

Cross-Section

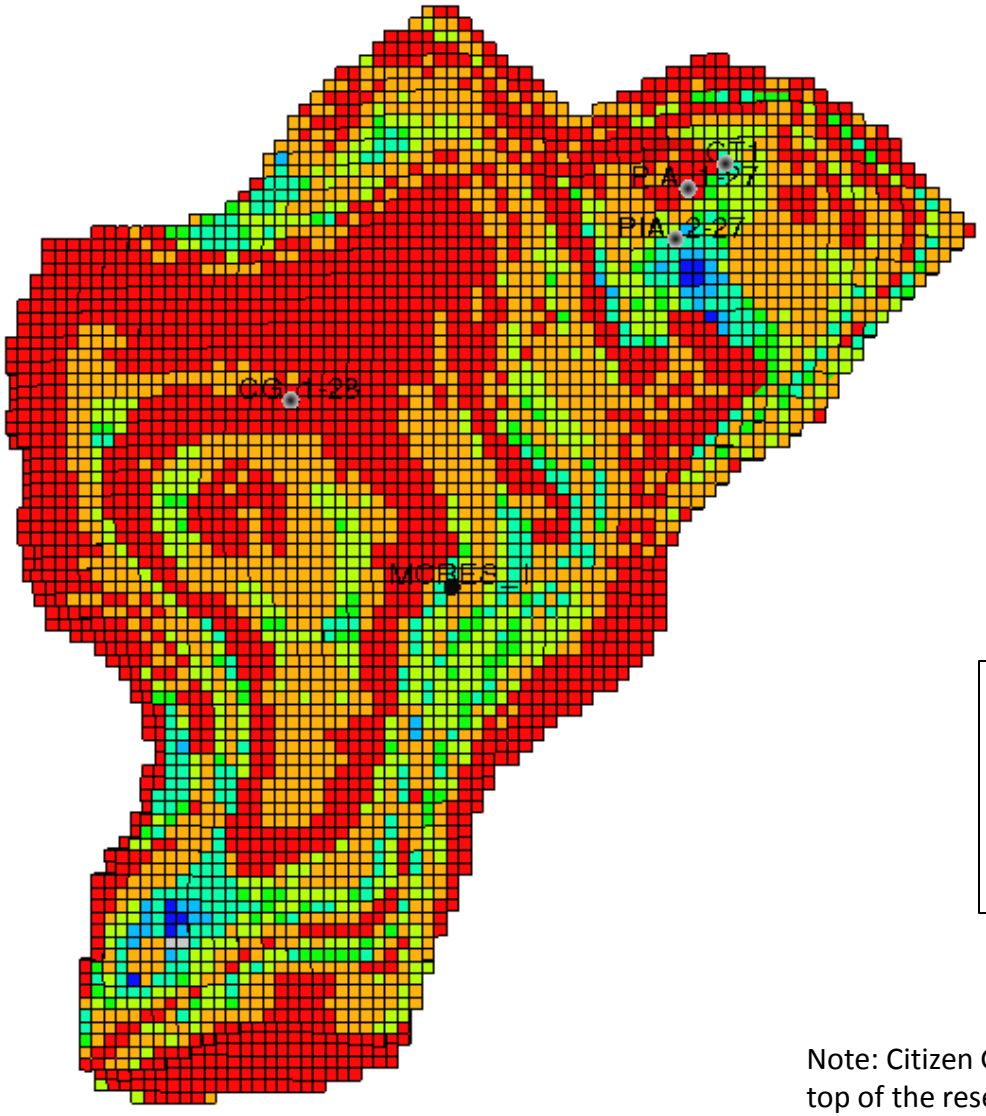

Well Key

CG_1 = Citizen Green 1
CT1 = I/W Well
MORES_1 = Moresco A1
PIA_1-27 = Piacentine 1-27
PIA_2-27 = Piacentine 2-27

Note: Citizen Green 1 location where the well bore intersects the top of the reservoir

Final Technical Memorandum
for Compressed Air Energy Storage
Reservoir Characterization & Full Field Development Model
King Island Gas Field, San Joaquin County, CA
9/25/2015

Figure 20

Permeability

Aerial

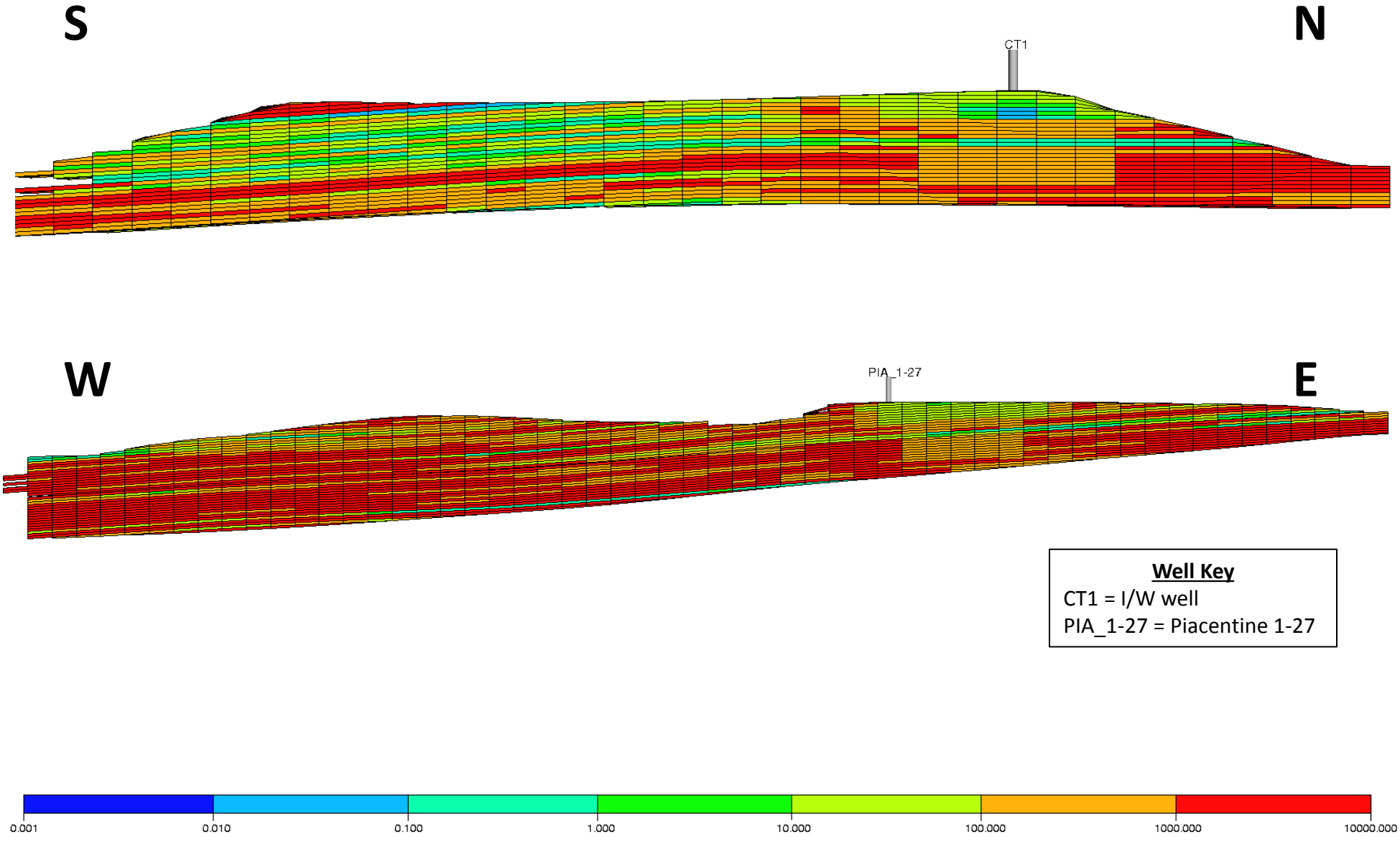

Final Technical Memorandum
for Compressed Air Energy Storage
Reservoir Characterization & Full Field Development Model
King Island Gas Field, San Joaquin County, CA
9/25/2015

Figure 21

Permeability

Cross-Section

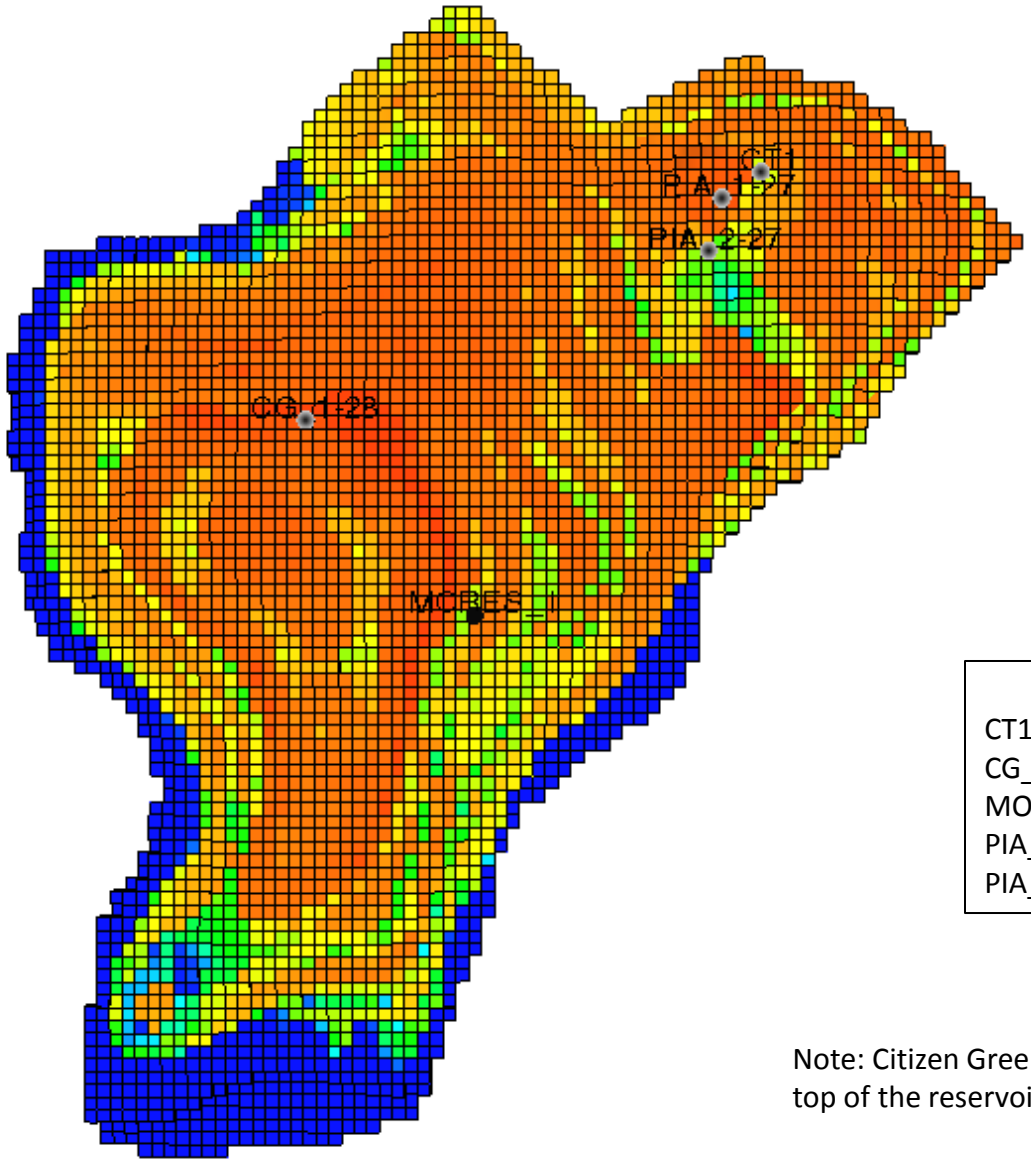

Well Key

CT1 = I/W well
CG_1 = Citizen Green 1
MORES_1 = Moresco A1
PIA_1-27 = Piacentine 1-27
PIA_2-27 = Piacentine 2-27

Note: Citizen Green 1 location where the well bore intersects the top of the reservoir

Final Technical Memorandum
for Compressed Air Energy Storage
Reservoir Characterization & Full Field Development Model
King Island Gas Field, San Joaquin County, CA
9/25/2015

Figure 22

King Island Gas Field
Initial Gas-in-Place - Aerial
Gas Saturation

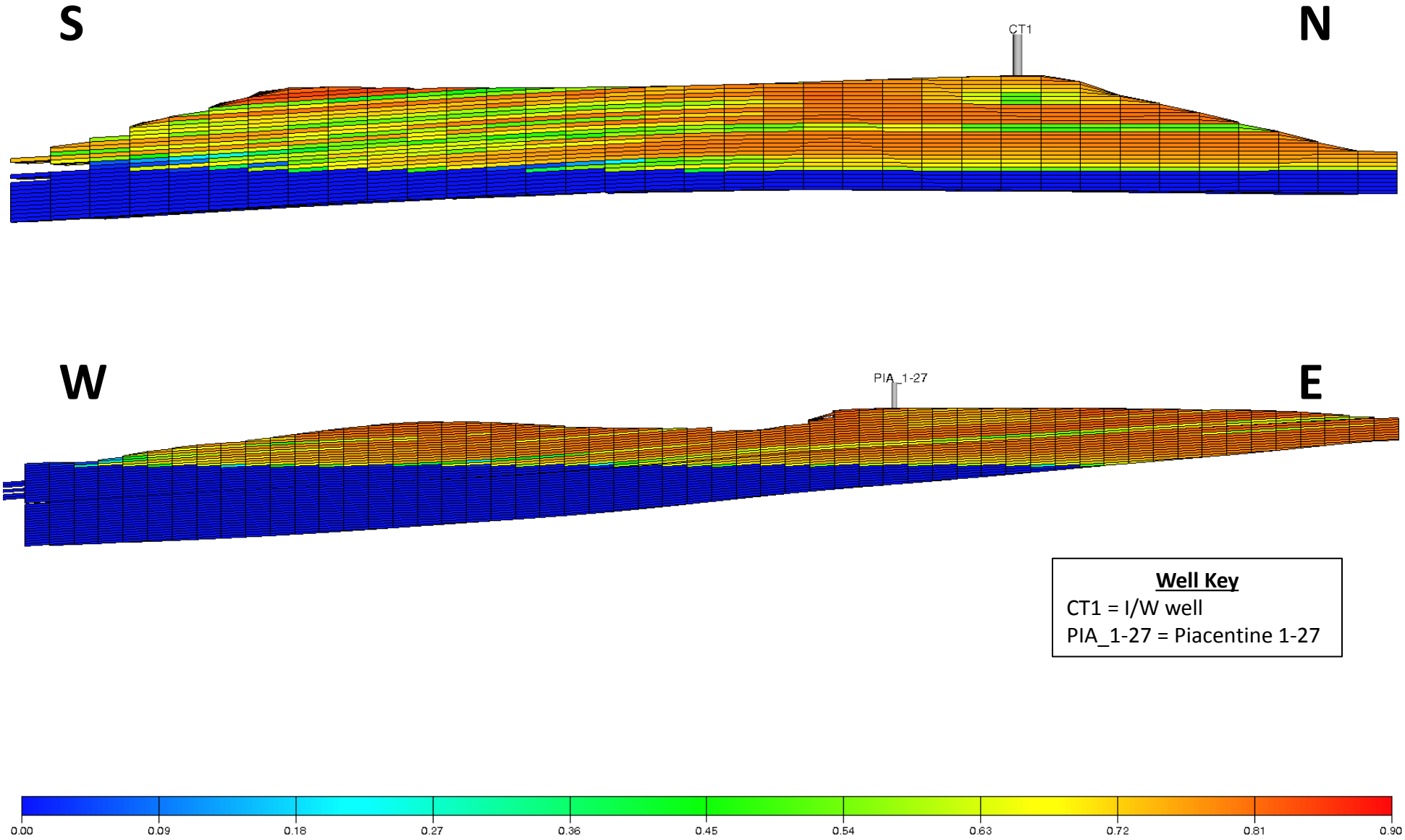

Final Technical Memorandum
for Compressed Air Energy Storage
Reservoir Characterization & Full Field Development Model
King Island Gas Field, San Joaquin County, CA
9/25/2015

Figure 23

Initial Gas-in-Place – Cross-Section

Gas Saturation

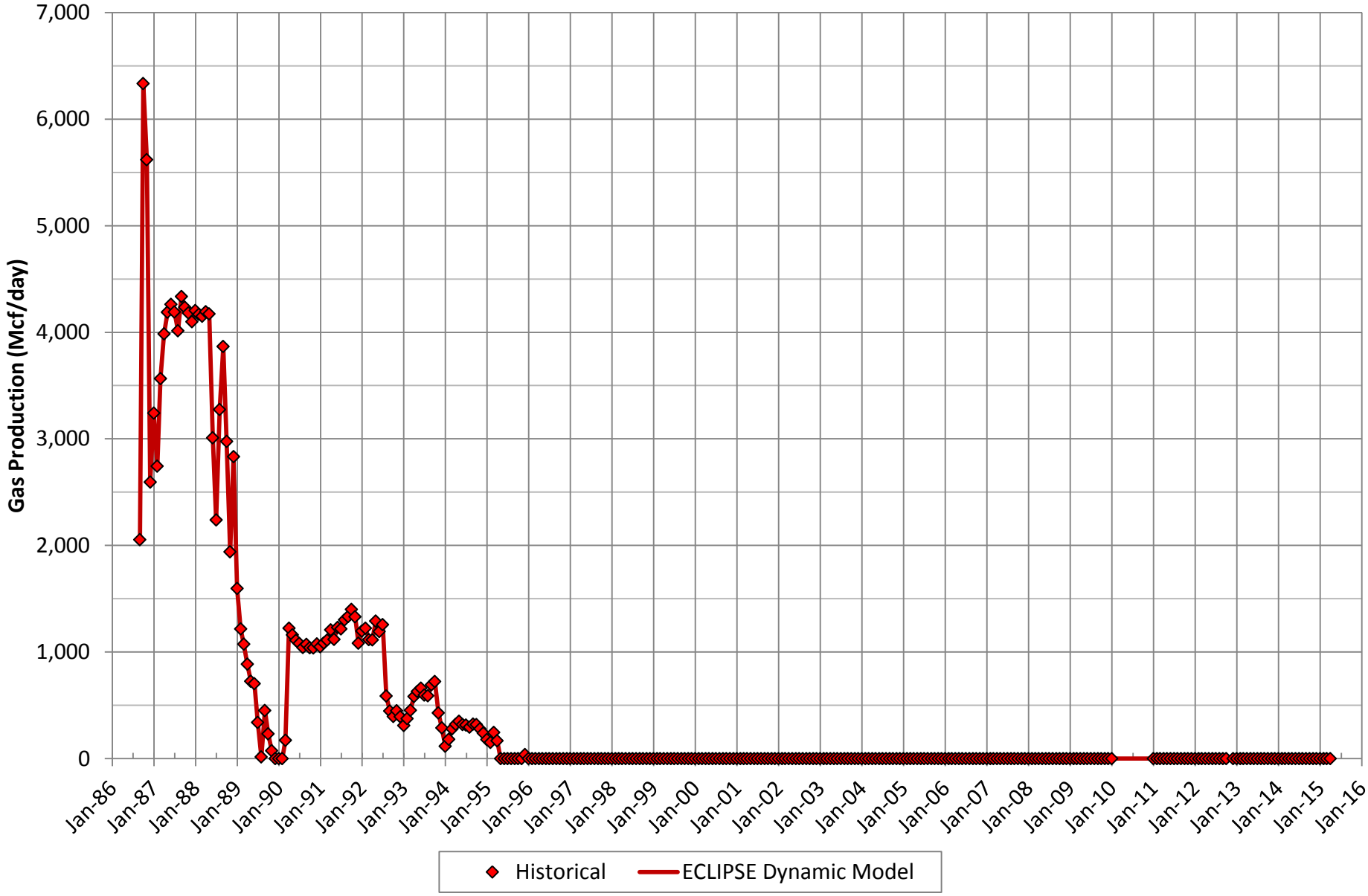

Mcf = Thousand cubic feet

Final Technical Memorandum
for Compressed Air Energy Storage
Reservoir Characterization & Full Field Development Model
King Island Gas Field, San Joaquin County, CA
9/25/2015

Figure 24

Moresco A1 History Match

Gas Production

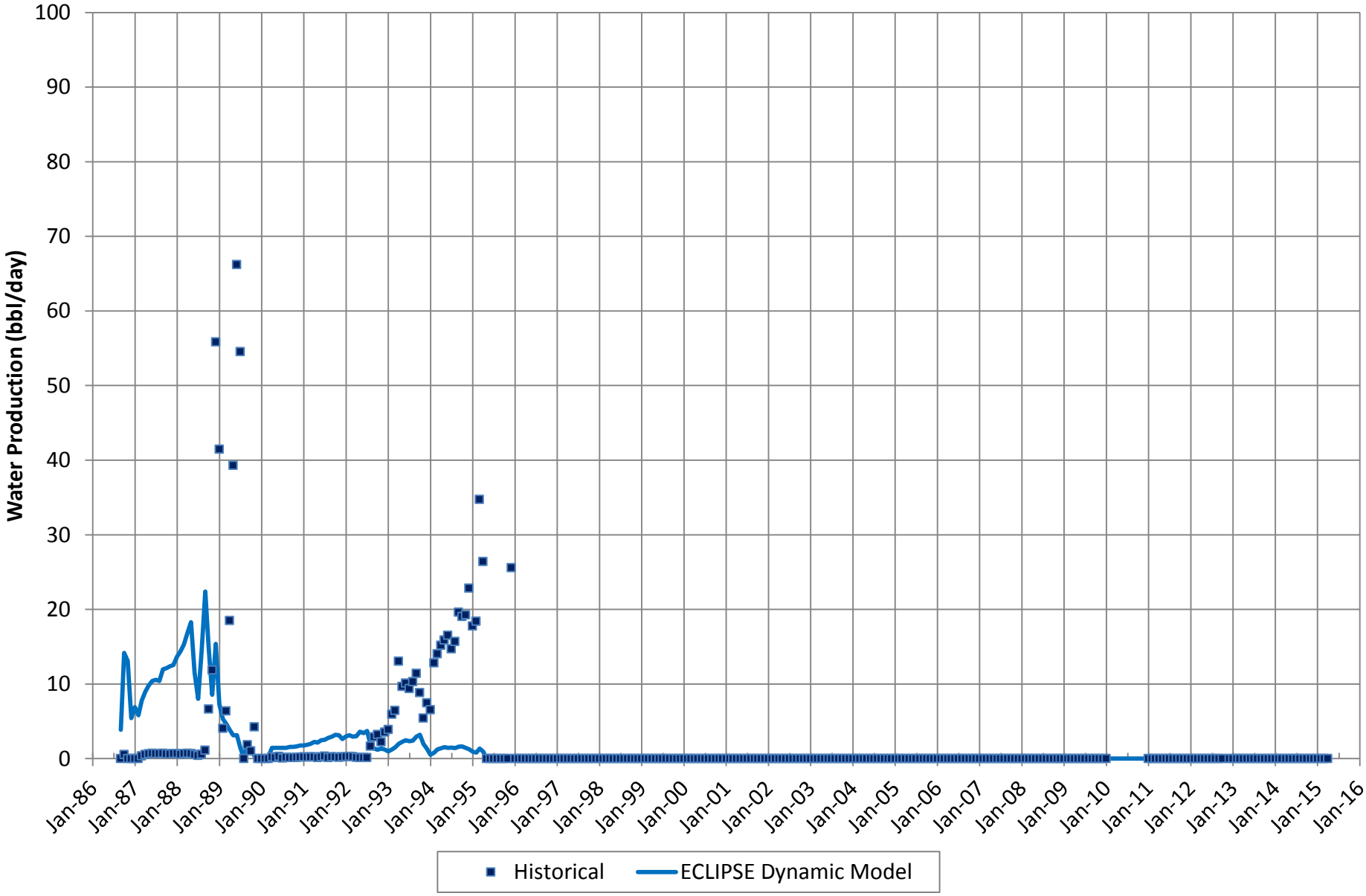

bbls = barrels

Final Technical Memorandum
for Compressed Air Energy Storage
Reservoir Characterization & Full Field Development Model
King Island Gas Field, San Joaquin County, CA
9/25/2015

Figure 25

Moresco A1 History Match

Water Production

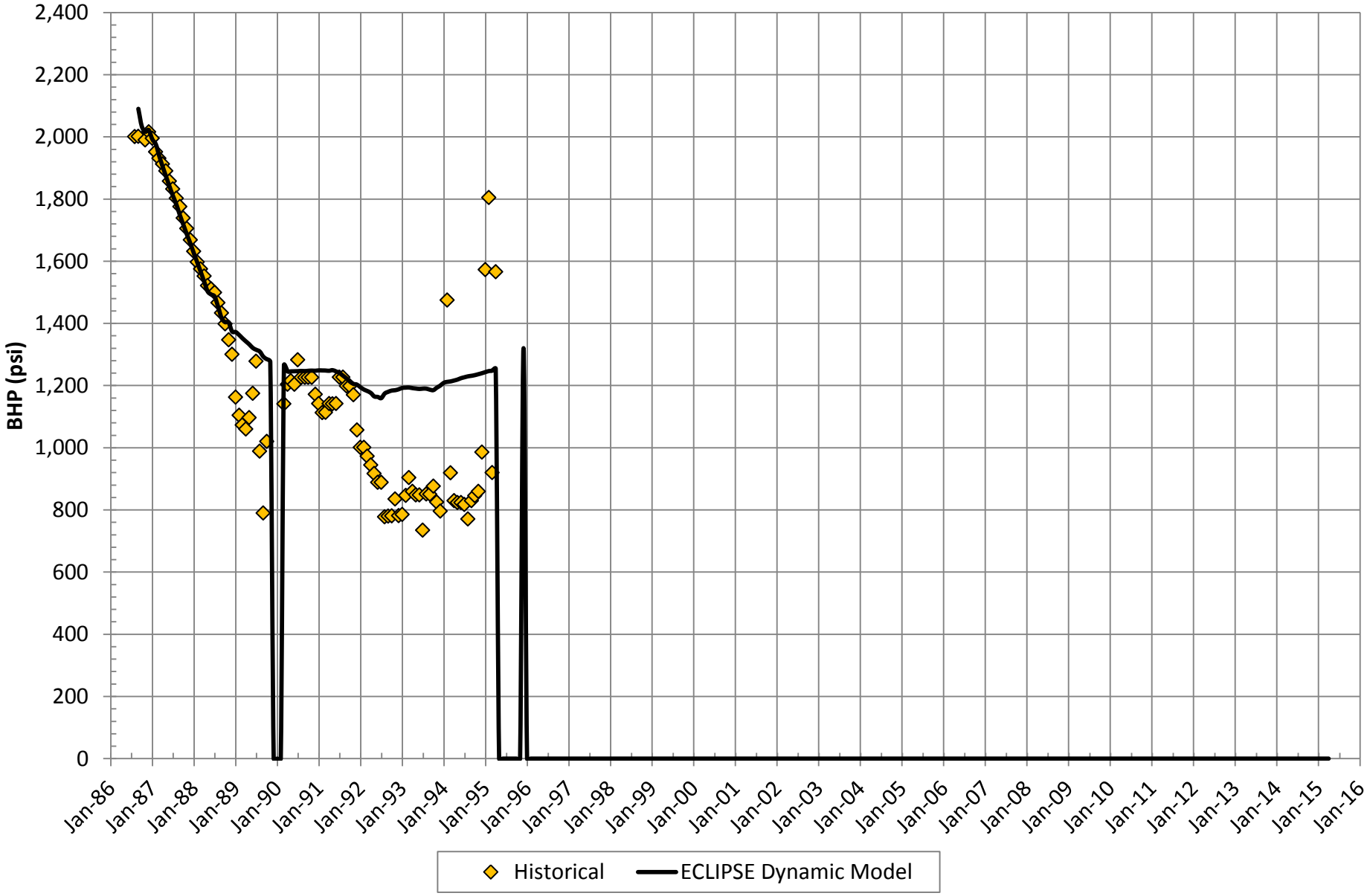

BHP = Bottom hole pressure
psi = Pounds per square inch

Final Technical Memorandum
for Compressed Air Energy Storage
Reservoir Characterization & Full Field Development Model
King Island Gas Field, San Joaquin County, CA
9/25/2015

Figure 26

Moresco A1 History Match

BHP

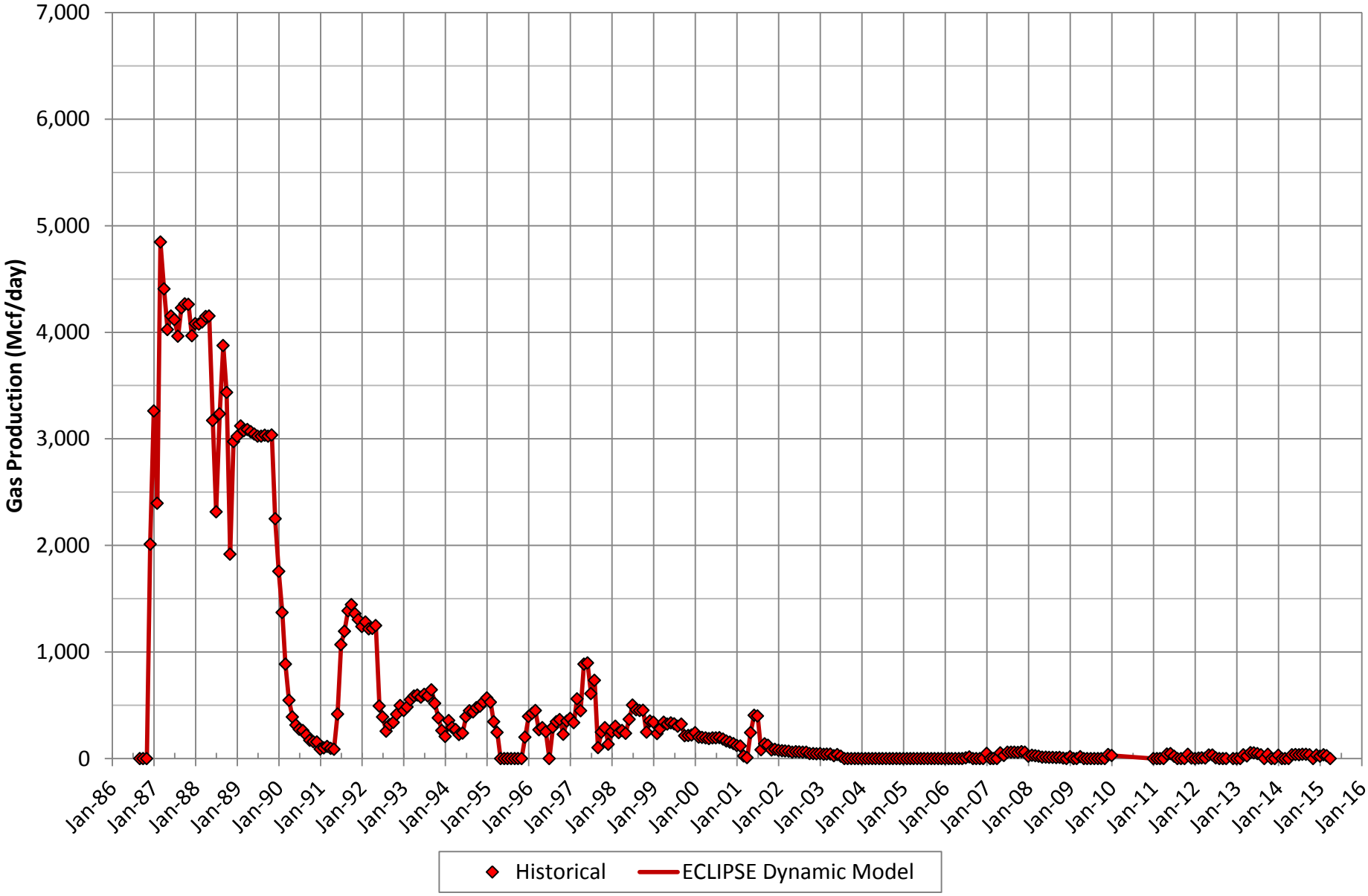

Mcf = Thousand cubic feet

Final Technical Memorandum
for Compressed Air Energy Storage
Reservoir Characterization & Full Field Development Model
King Island Gas Field, San Joaquin County, CA
9/25/2015

Figure 27

Piacentine 1-27 History Match

Gas Production

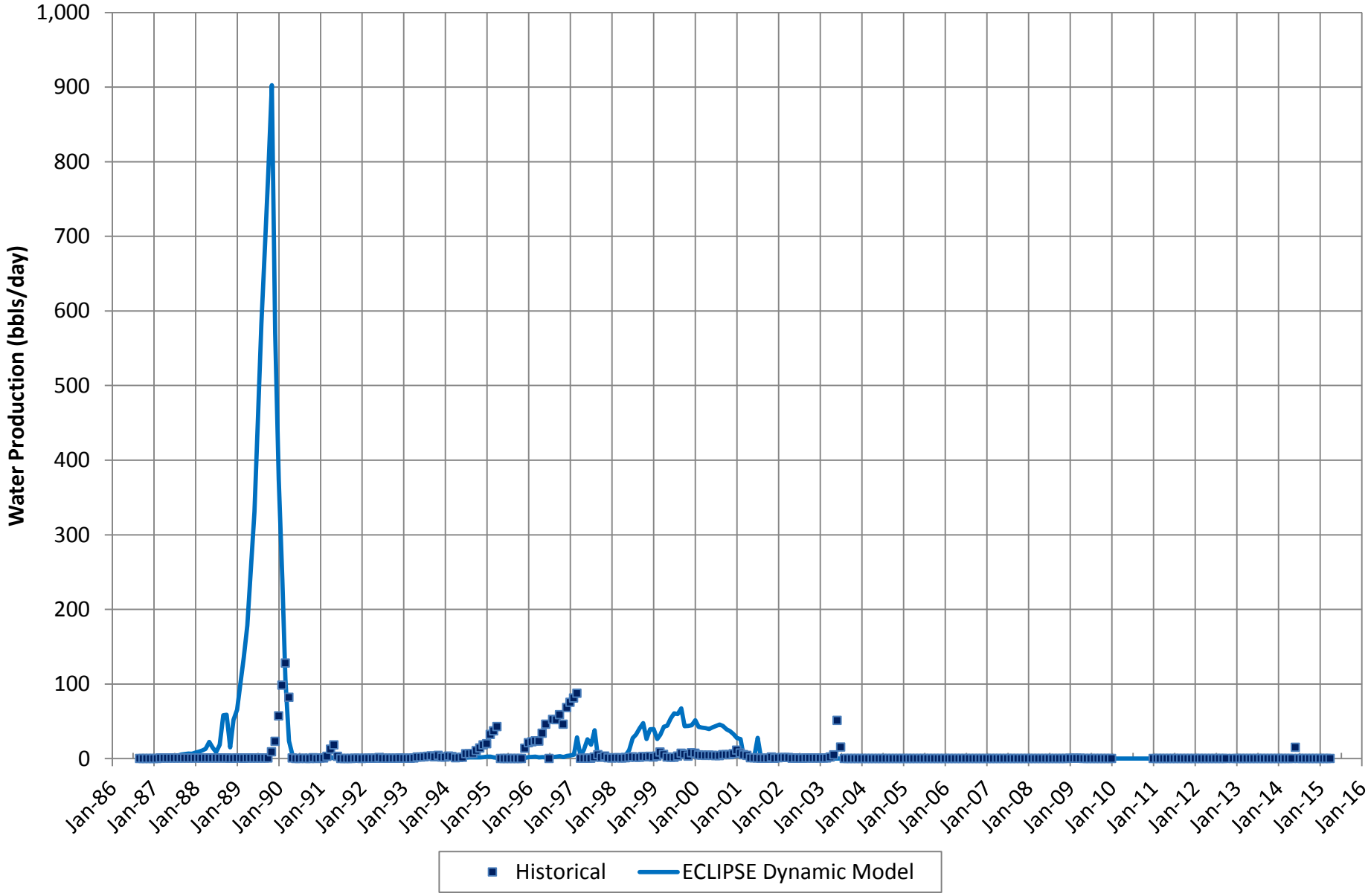

bbls = barrels

Final Technical Memorandum
for Compressed Air Energy Storage
Reservoir Characterization & Full Field Development Model
King Island Gas Field, San Joaquin County, CA
9/25/2015

Figure 28

Piacentine 1-27 History Match
Water Production

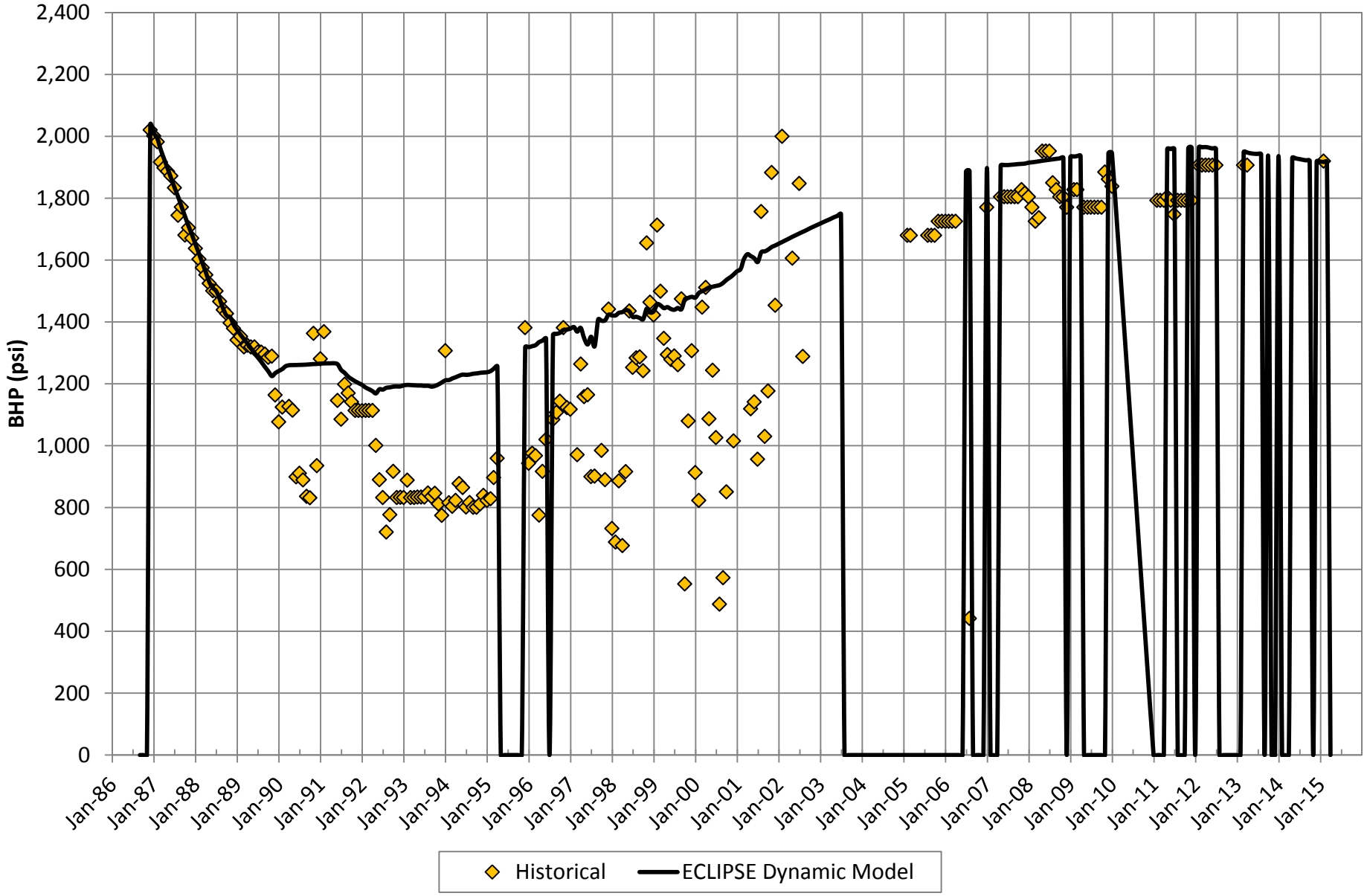

BHP = Bottom hole pressure
psi = Pounds per square inch

Final Technical Memorandum
for Compressed Air Energy Storage
Reservoir Characterization & Full Field Development Model
King Island Gas Field, San Joaquin County, CA
9/25/2015

Figure 29

Piacentine 1-27 History Match

BHP

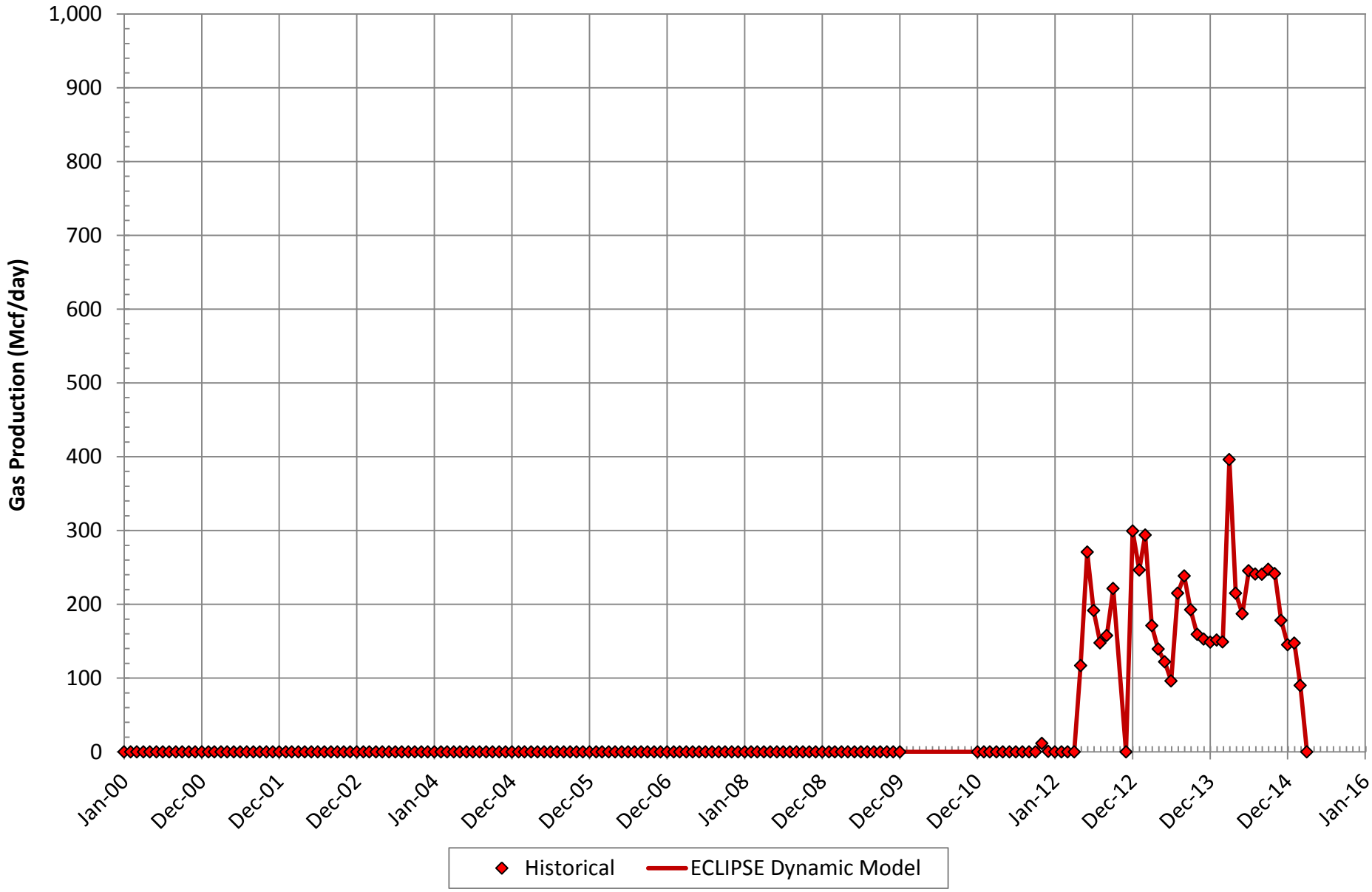

Mcf = Thousand cubic feet

Final Technical Memorandum
for Compressed Air Energy Storage
Reservoir Characterization & Full Field Development Model
King Island Gas Field, San Joaquin County, CA
9/25/2015

Figure 30

Citizen Green RD1 History Match

Gas Production

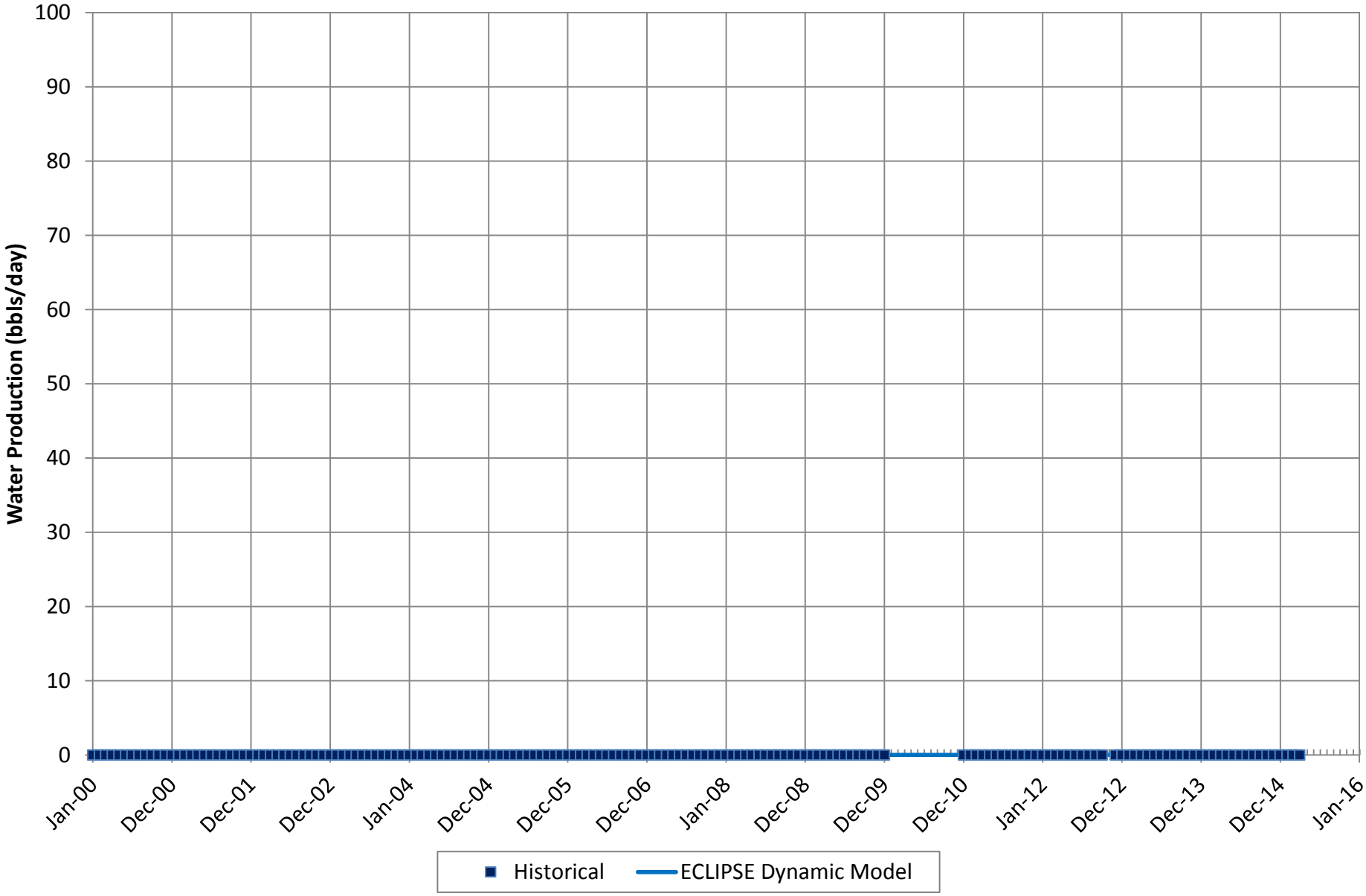

bbls = barrels

Final Technical Memorandum
for Compressed Air Energy Storage
Reservoir Characterization & Full Field Development Model
King Island Gas Field, San Joaquin County, CA
9/25/2015

Figure 31

Citizen Green RD1 History Match
Water Production

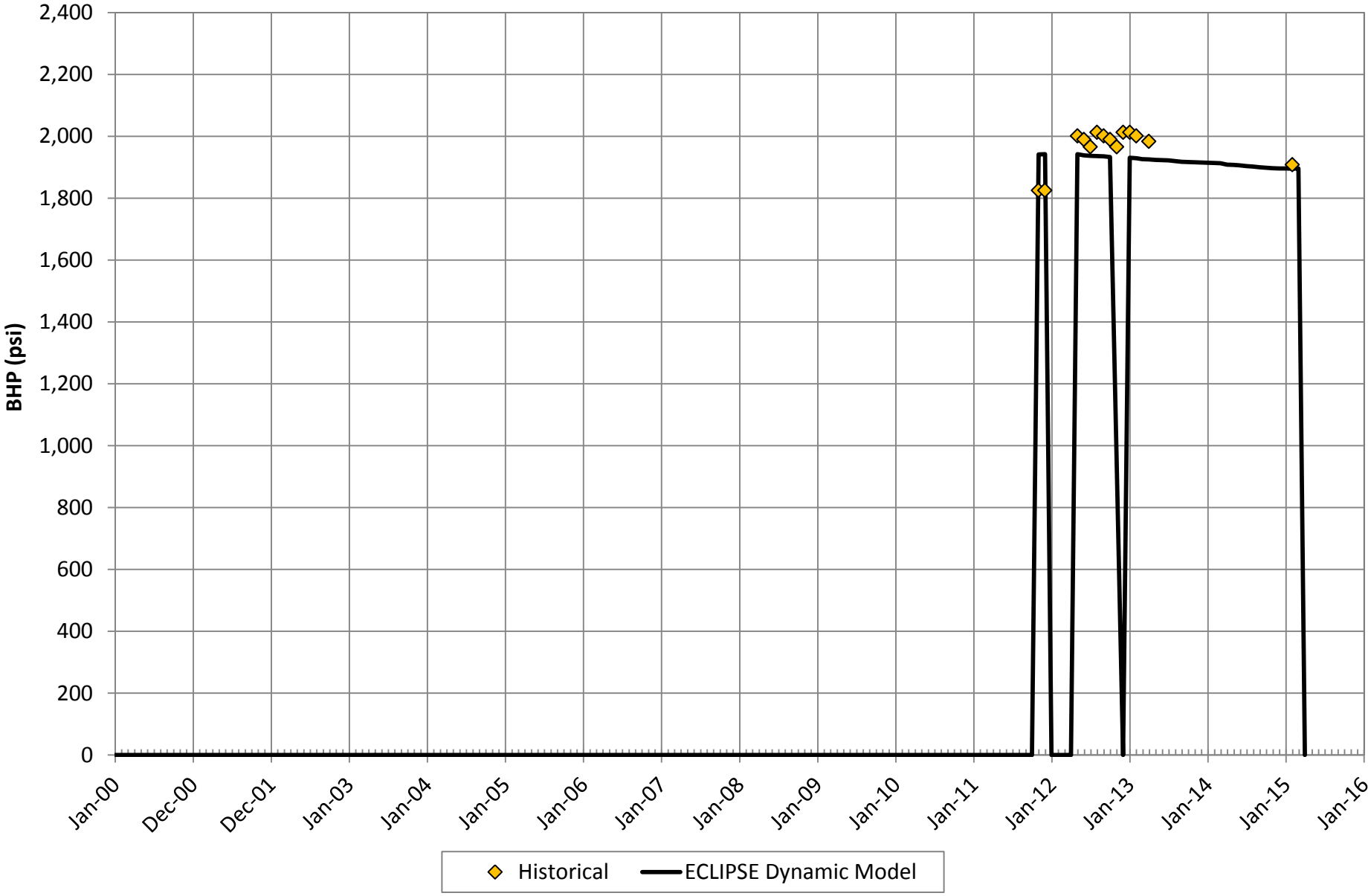

BHP = Bottom hole pressure
psi = Pounds per square inch

Final Technical Memorandum
for Compressed Air Energy Storage
Reservoir Characterization & Full Field Development Model
King Island Gas Field, San Joaquin County, CA
9/25/2015

Figure 32

Citizen Green RD1 History Match

BHP

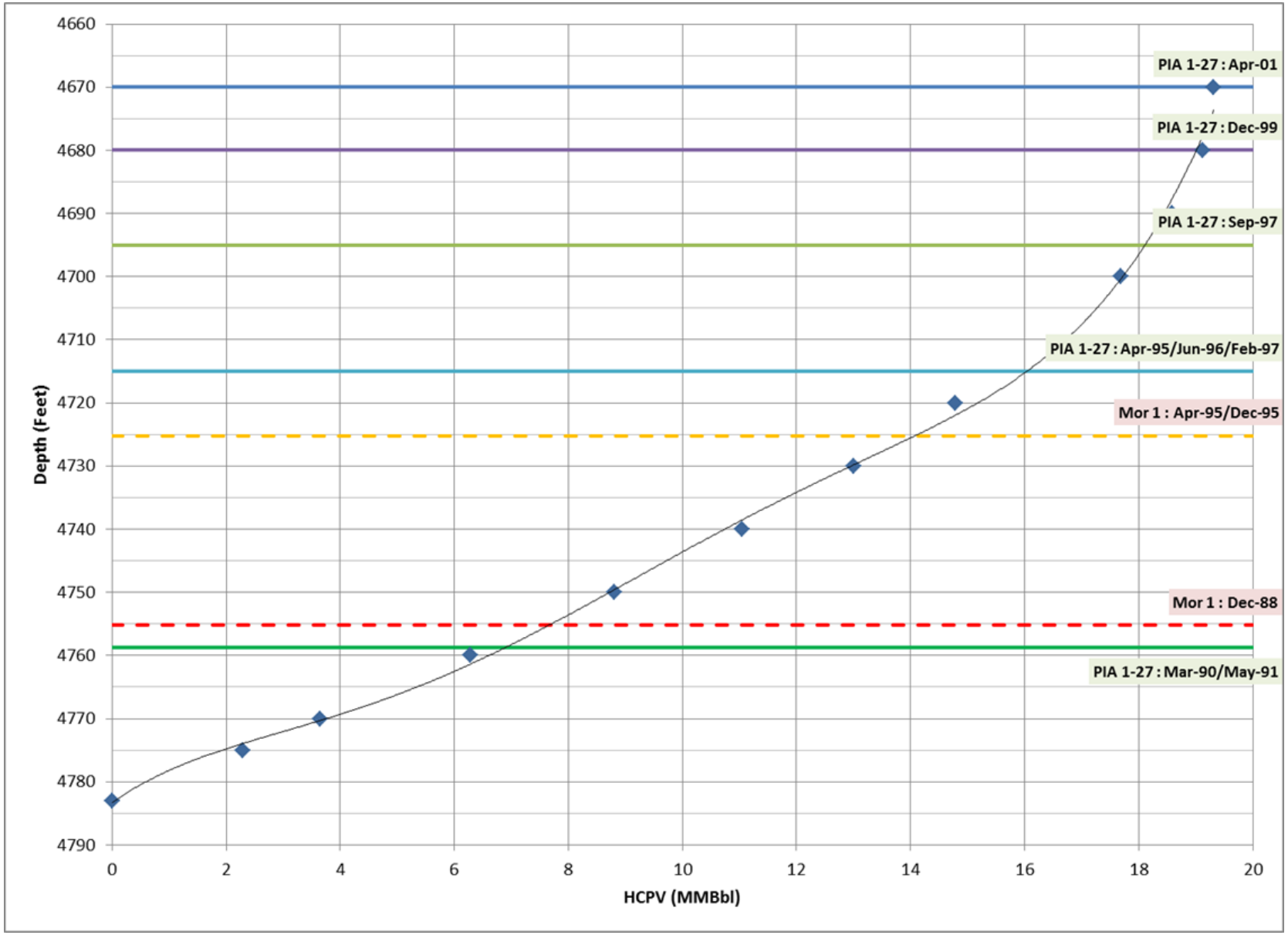

Horizontal lines represent the depths and times at which the wells were impacted by water.

HCPV = Hydrocarbon Pore Volume
MMBbl = Million Barrels
Mor 1 = Moresco A1
PIA 1-27 = Piacentine 1-27

Final Technical Memorandum
for Compressed Air Energy Storage
Reservoir Characterization & Full Field Development Model
King Island Gas Field, San Joaquin County, CA
9/25/2015

Figure 33

King Island HCPV vs. Depth
Used to Define Strength and Volume of Aquifer Influx

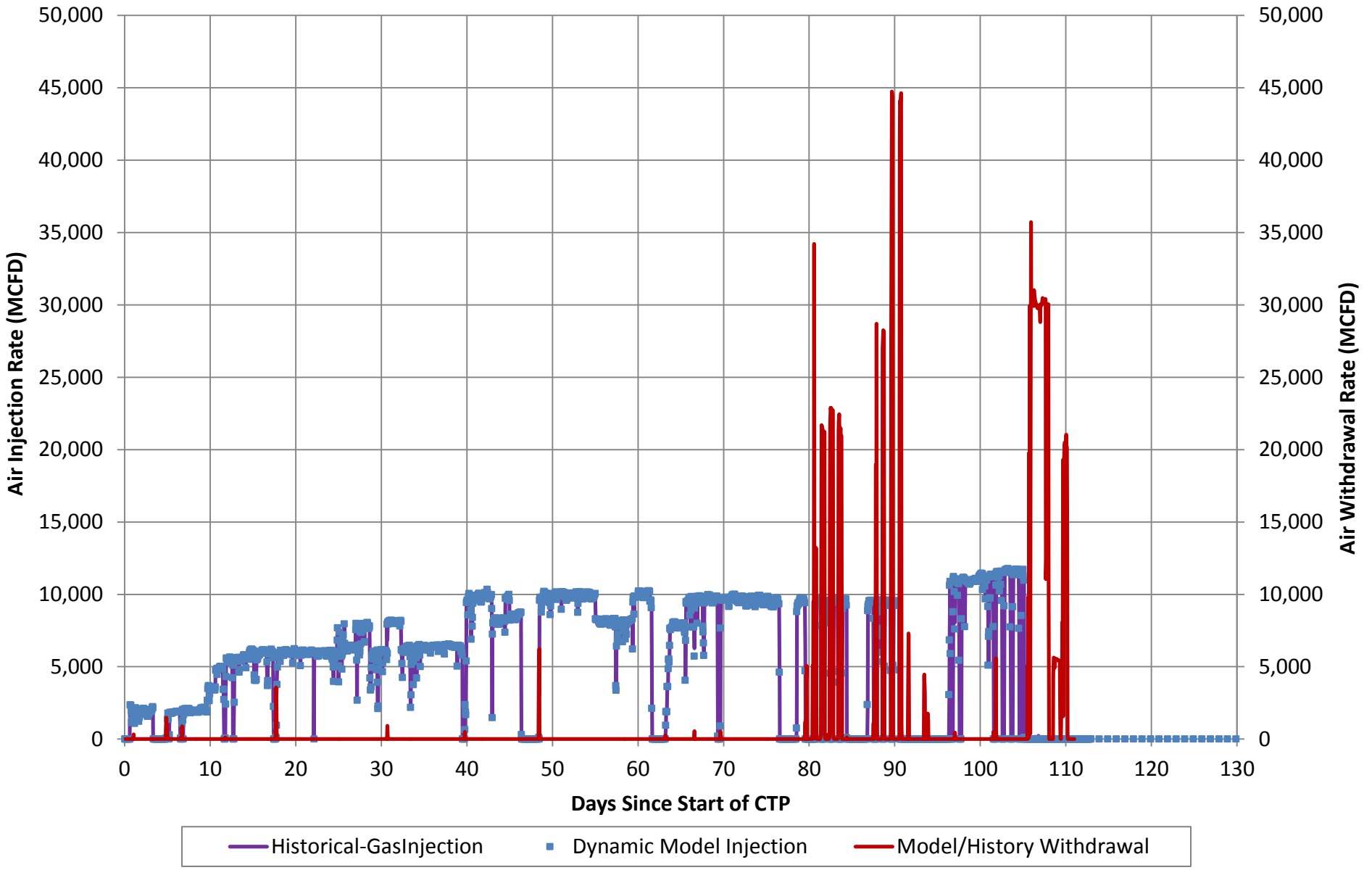

CTP = Compression Test Program
Mcf = Thousand cubic feet

Final Technical Memorandum
for Compressed Air Energy Storage
Reservoir Characterization & Full Field Development Model
King Island Gas Field, San Joaquin County, CA
9/25/2015

Figure 34

Compression Testing History Match
I/W Well Gas Production/Injection

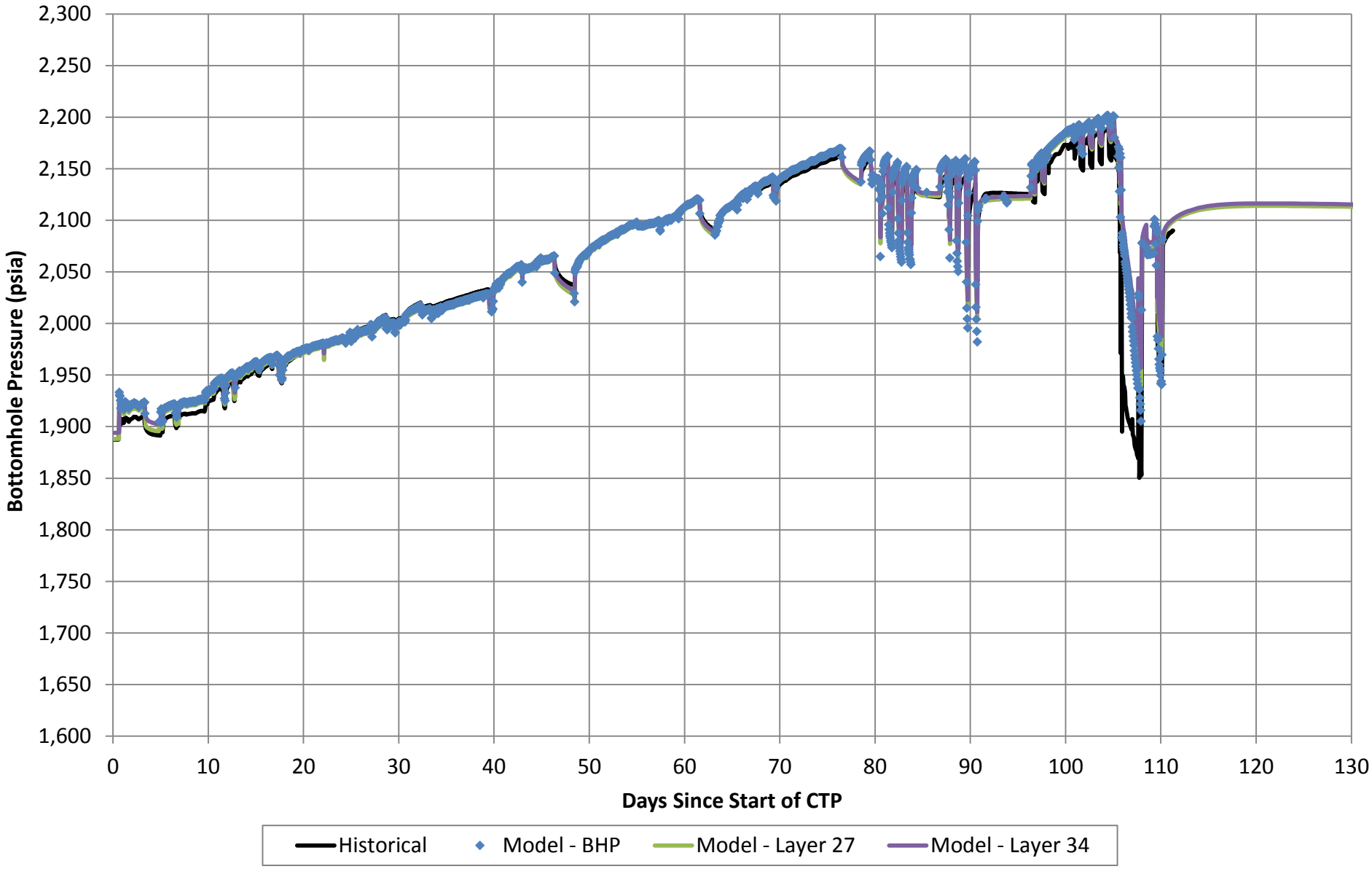

BHP = Bottom hole pressure
CTP = Compression Test Program
psia = Pounds per square inch atmospheric

Final Technical Memorandum
for Compressed Air Energy Storage
Reservoir Characterization & Full Field Development Model
King Island Gas Field, San Joaquin County, CA
9/25/2015

Figure 35

Compression Test History Match

BHP – I/W Well

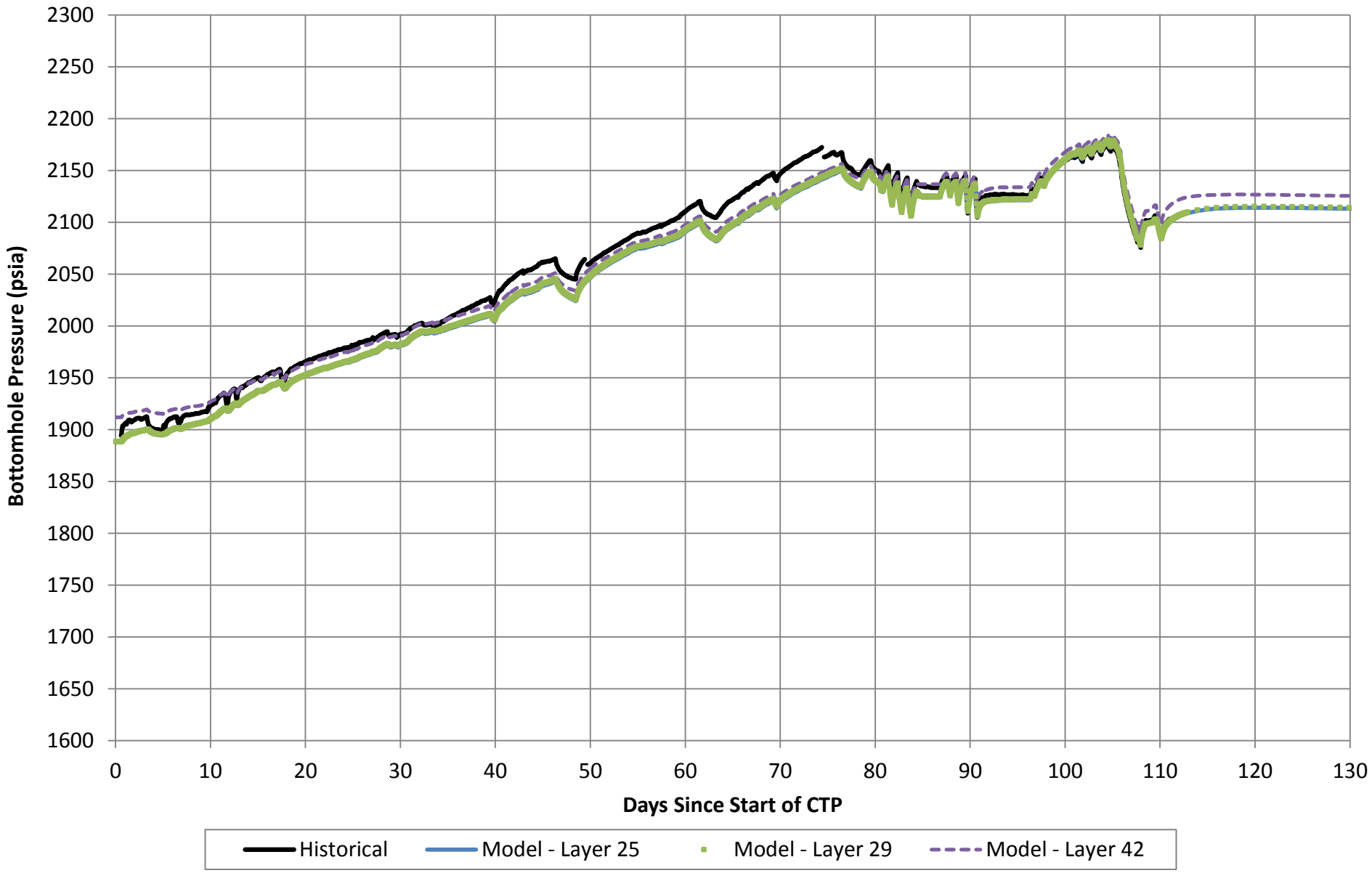

BHP = Bottom hole pressure
CTP = Compression Test Program
psia = Pounds per square inch atmospheric

Final Technical Memorandum
for Compressed Air Energy Storage
Reservoir Characterization & Full Field Development Model
King Island Gas Field, San Joaquin County, CA
9/25/2015

Figure 36

Compression Test History Match

BHP – Piacentine 1-27

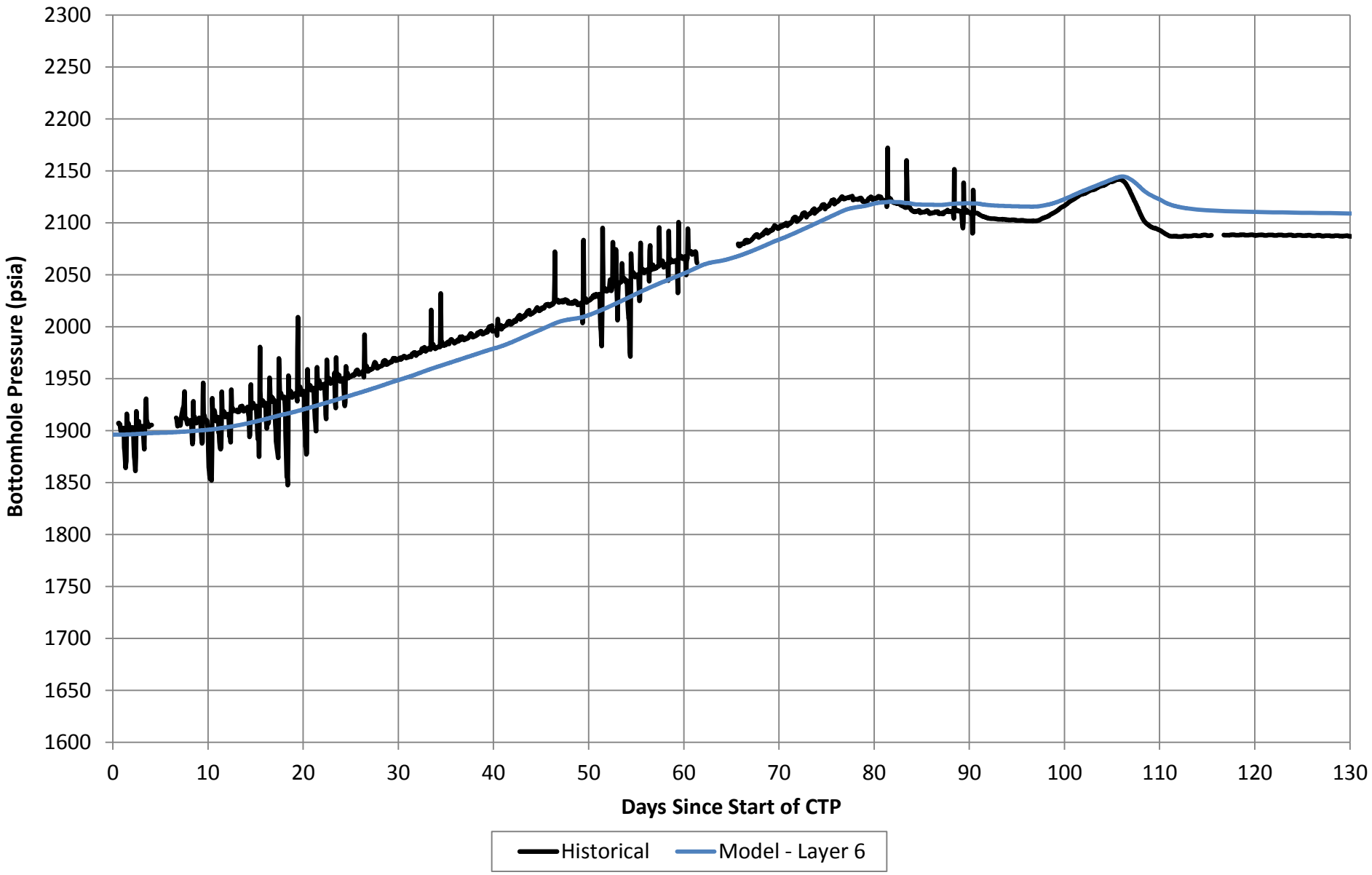

BHP = Bottom Hole Pressure
CTP = Compression Test Program
psia = pounds per square inch atmospheric

Final Technical Memorandum
for Compressed Air Energy Storage
Reservoir Characterization & Full Field Development Model
King Island Gas Field, San Joaquin County, CA
9/25/2015

Figure 37

Compression Test History Match

BHP – Citizen Green RD1

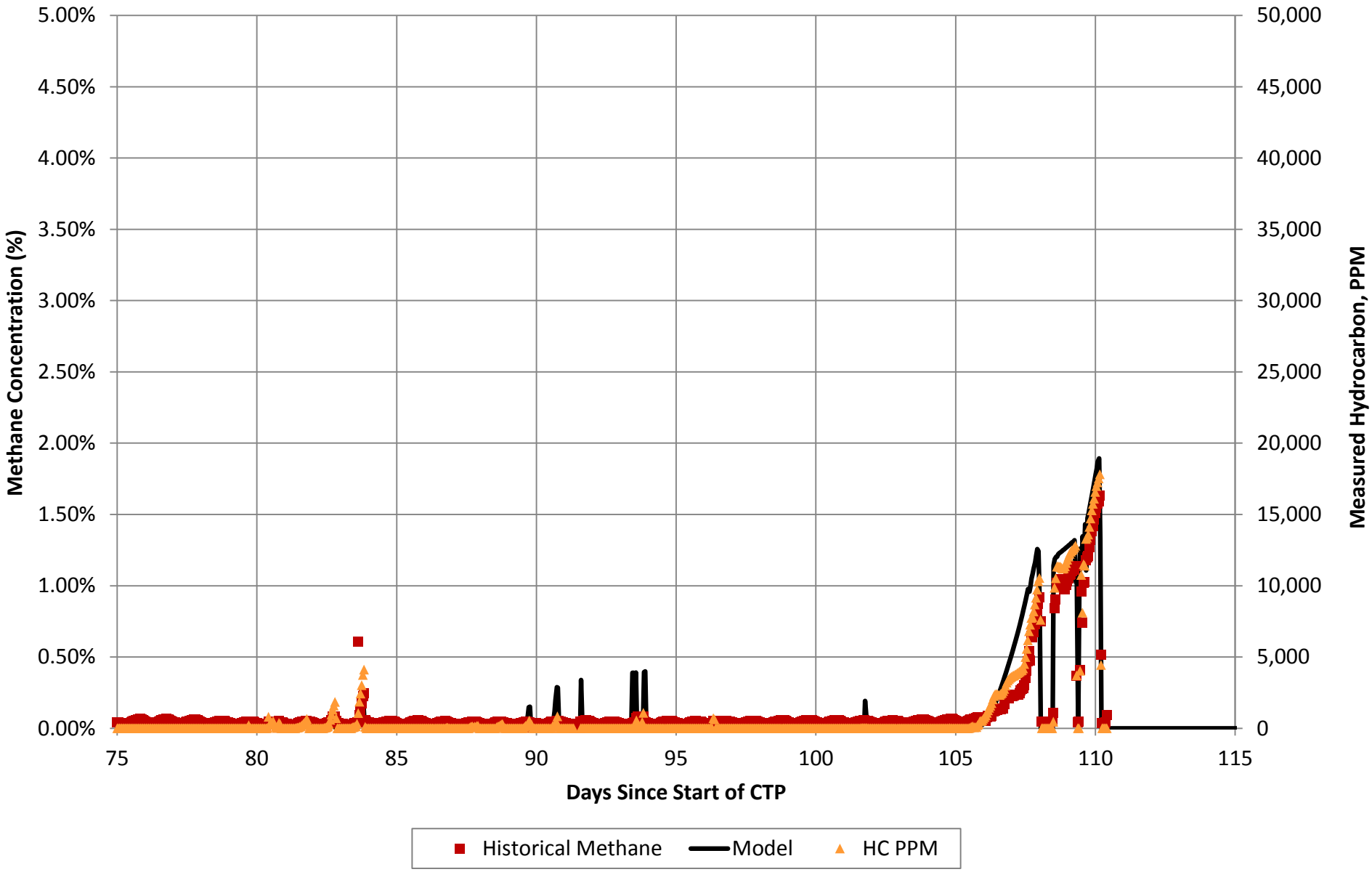

BHP = Bottom Hole Pressure
CTP = Compression Test Program
HC = Hydrocarbons
PPM = Parts per million

Final Technical Memorandum
for Compressed Air Energy Storage
Reservoir Characterization & Full Field Development Model
King Island Gas Field, San Joaquin County, CA
9/25/2015

Figure 38

Compression Test History Match
I/W Well
% Methane in Withdrawal Stream

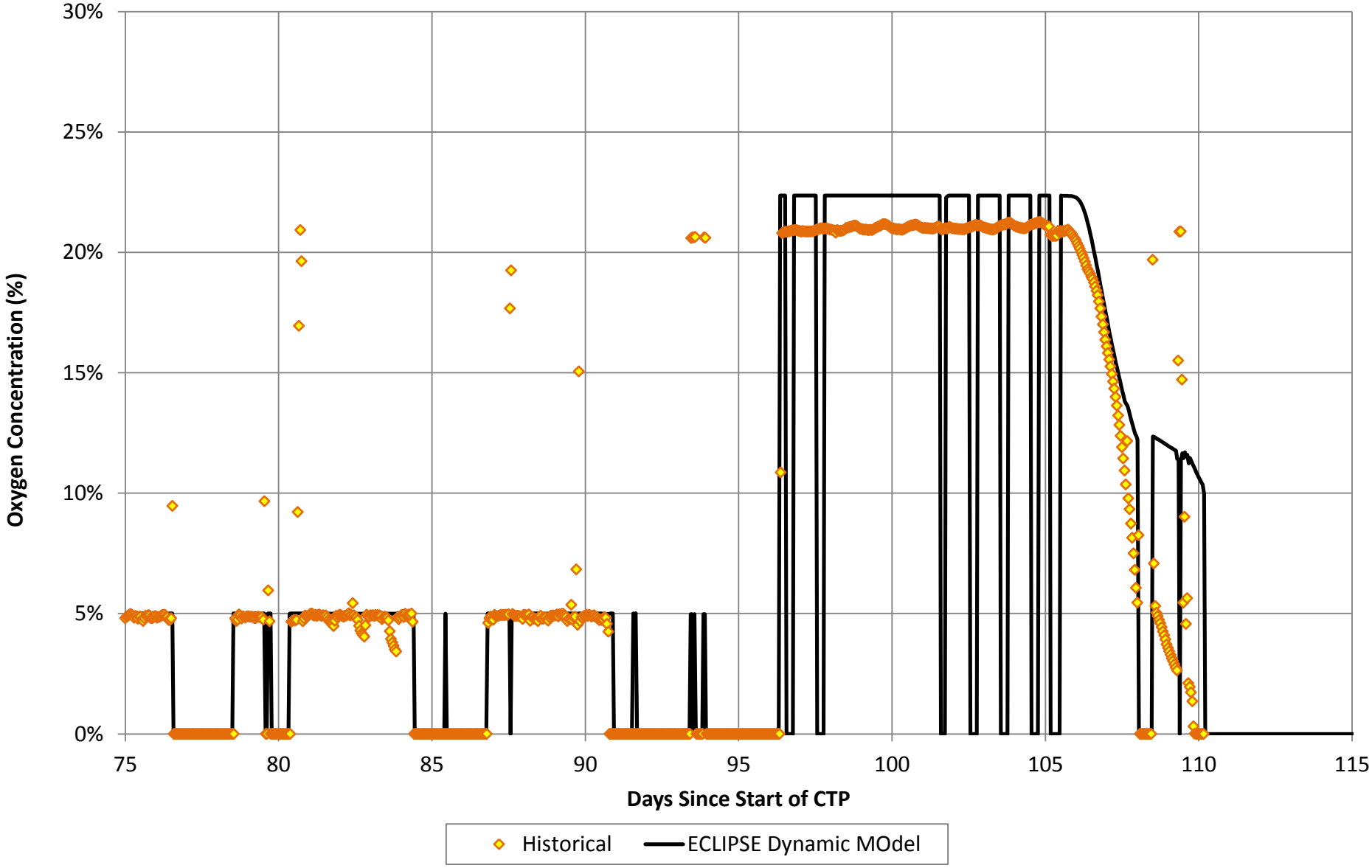

CTP = Compression Test Program

Final Technical Memorandum
for Compressed Air Energy Storage
Reservoir Characterization & Full Field Development Model
King Island Gas Field, San Joaquin County, CA
9/25/2015

Figure 39

Compression Test History Match
I/W Well
% Oxygen in Withdrawal Stream

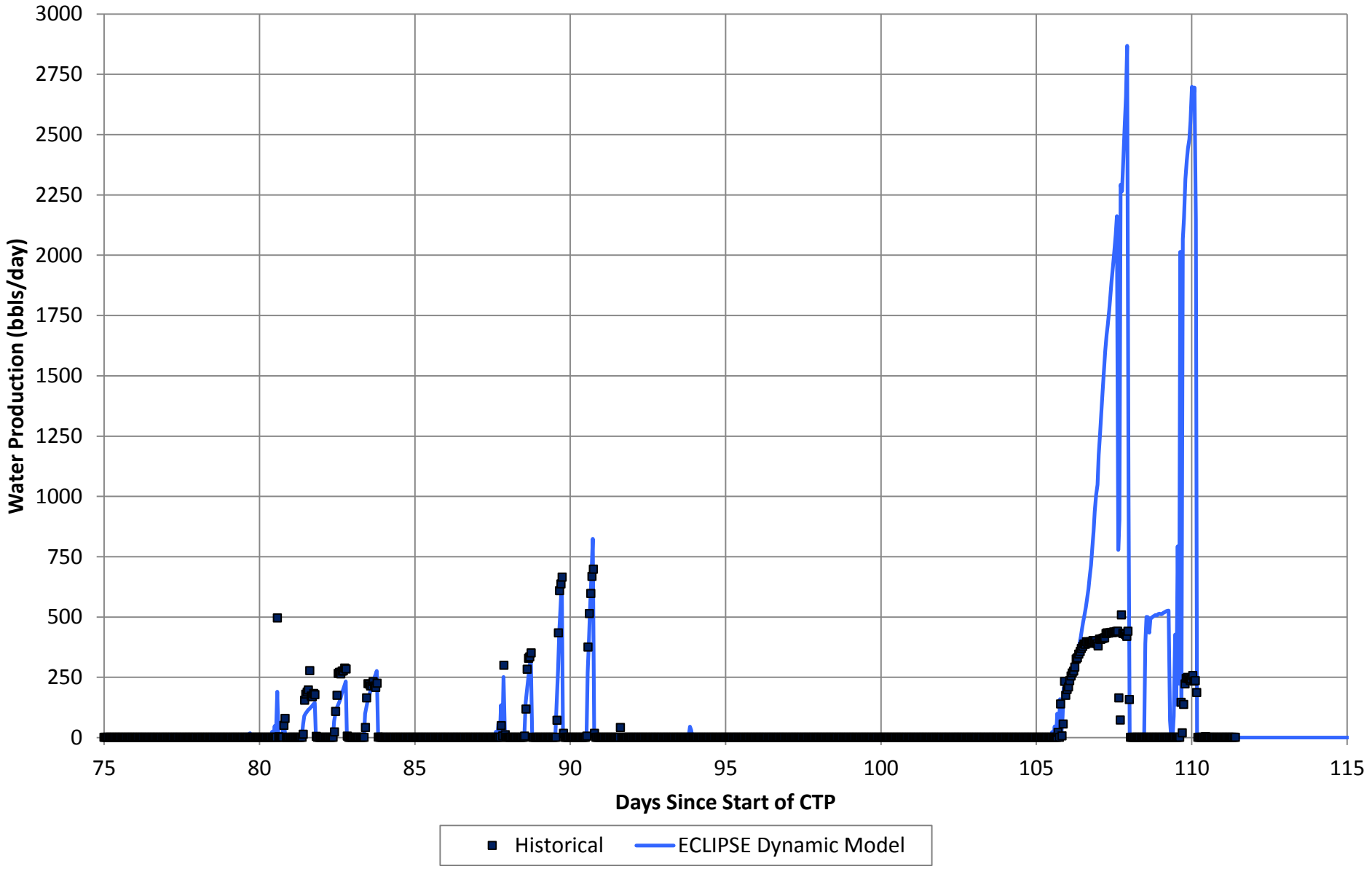

bbls = barrels
CTP = Compression Test Program

Final Technical Memorandum
for Compressed Air Energy Storage
Reservoir Characterization & Full Field Development Model
King Island Gas Field, San Joaquin County, CA
9/25/2015

Figure 40

Compression Test History Match
I/W Well
Water Production

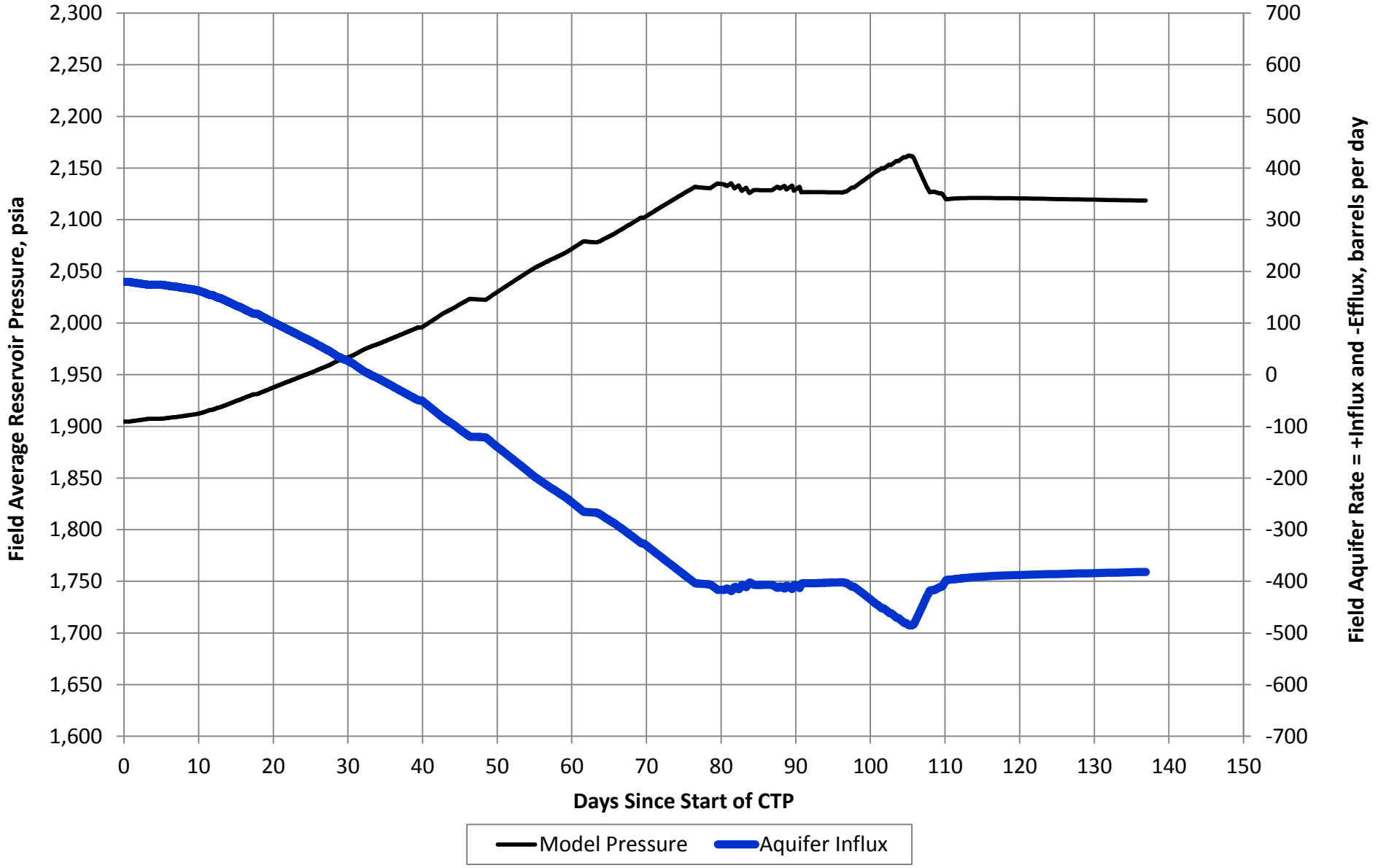

CTP = Compression Test Program
psia = Pounds per square inch atmospheric
SI = Shut-in

Final Technical Memorandum
for Compressed Air Energy Storage
Reservoir Characterization & Full Field Development Model
King Island Gas Field, San Joaquin County, CA
9/25/2015

Figure 41

Reservoir Pressure Response and Aquifer Influx / Efflux During King Island Compression Testing and SI Period

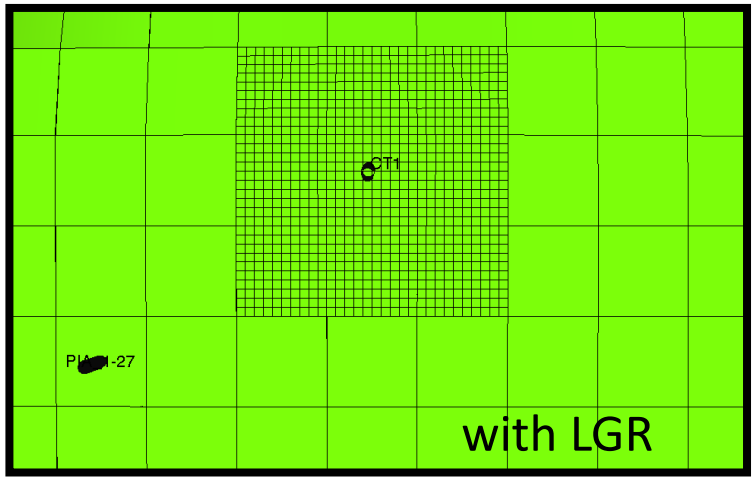

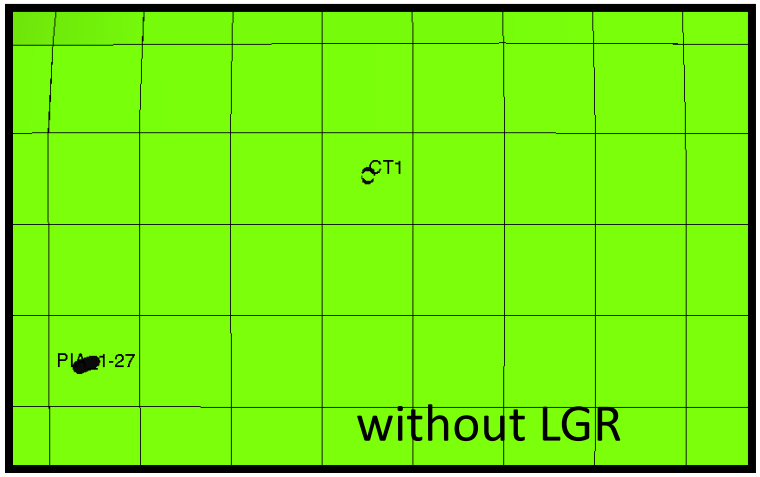

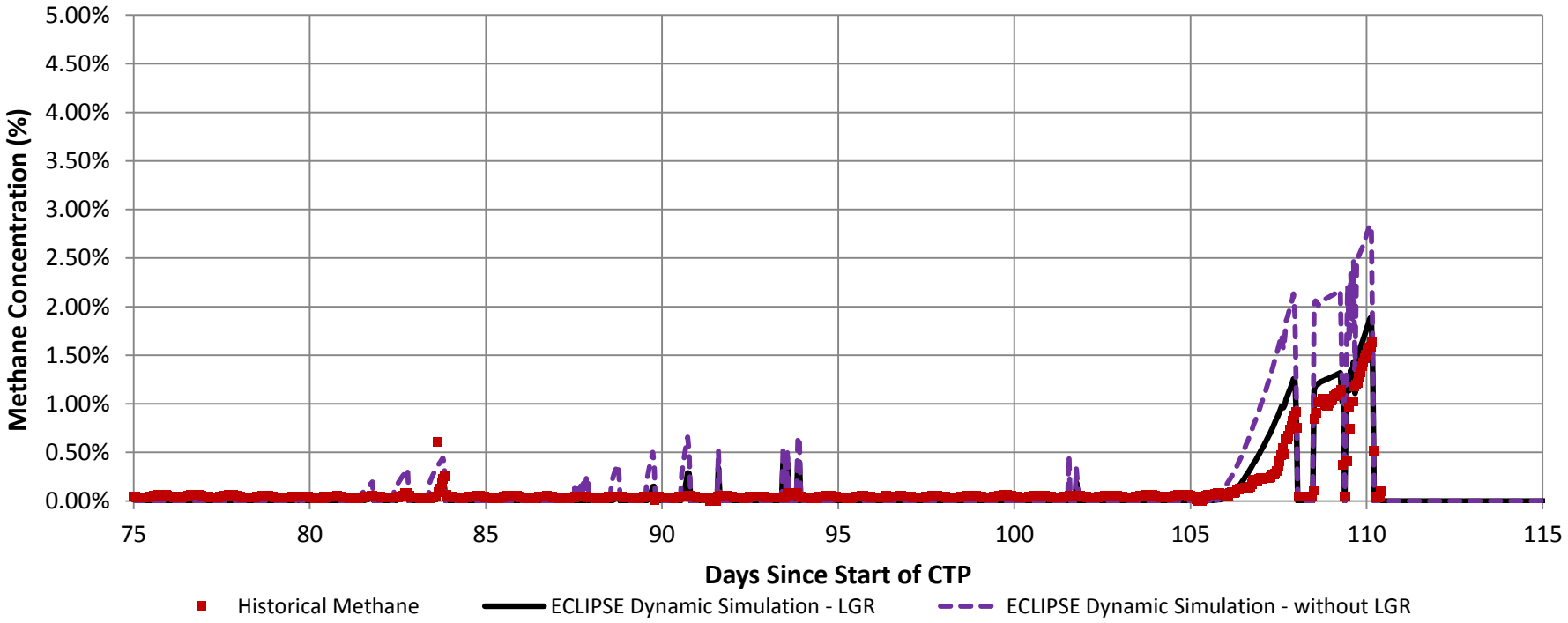

CTP = Compression Test Program
LGR = Local Grid Refinement
CT1 = I/W well

Final Technical Memorandum
for Compressed Air Energy Storage
Reservoir Characterization & Full Field Development Model
King Island Gas Field, San Joaquin County, CA
9/25/2015

Figure 42

LGR vs. No LGR

Methane Concentration

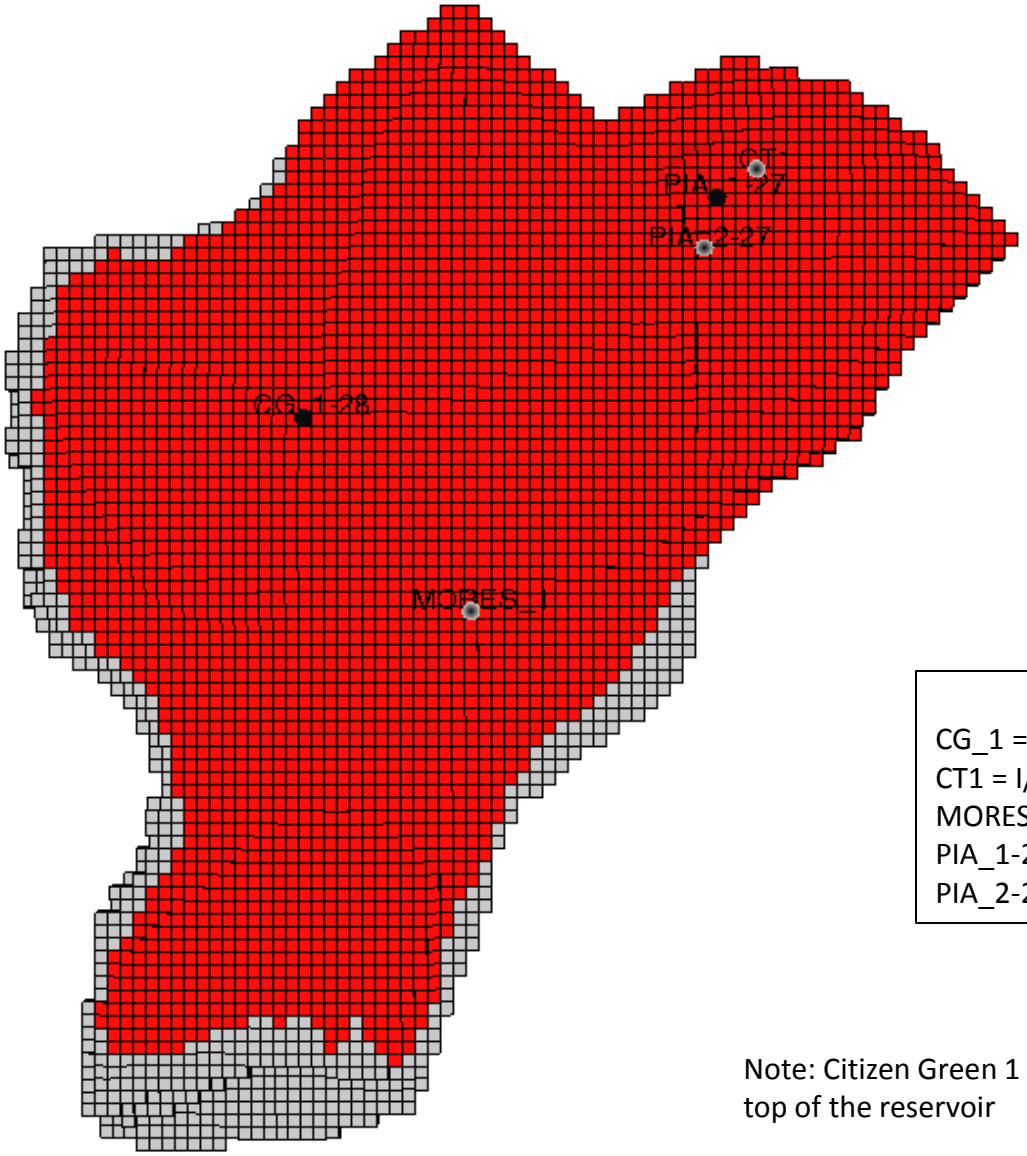

Well Key

CG_1 = Citizen Green 1
CT1 = I/W well
MORES_1 = Moresco A1
PIA_1-27 = Piacentine 1-27
PIA_2-27 = Piacentine 2-27

Note: Citizen Green 1 location where the well bore intersects the top of the reservoir

Feb 14, 2015

Final Technical Memorandum
for Compressed Air Energy Storage
Reservoir Characterization & Full Field Development Model
King Island Gas Field, San Joaquin County, CA
9/25/2015

Figure 43

Compression Testing Bubble Build (Beginning)

Methane Composition Mole Fraction

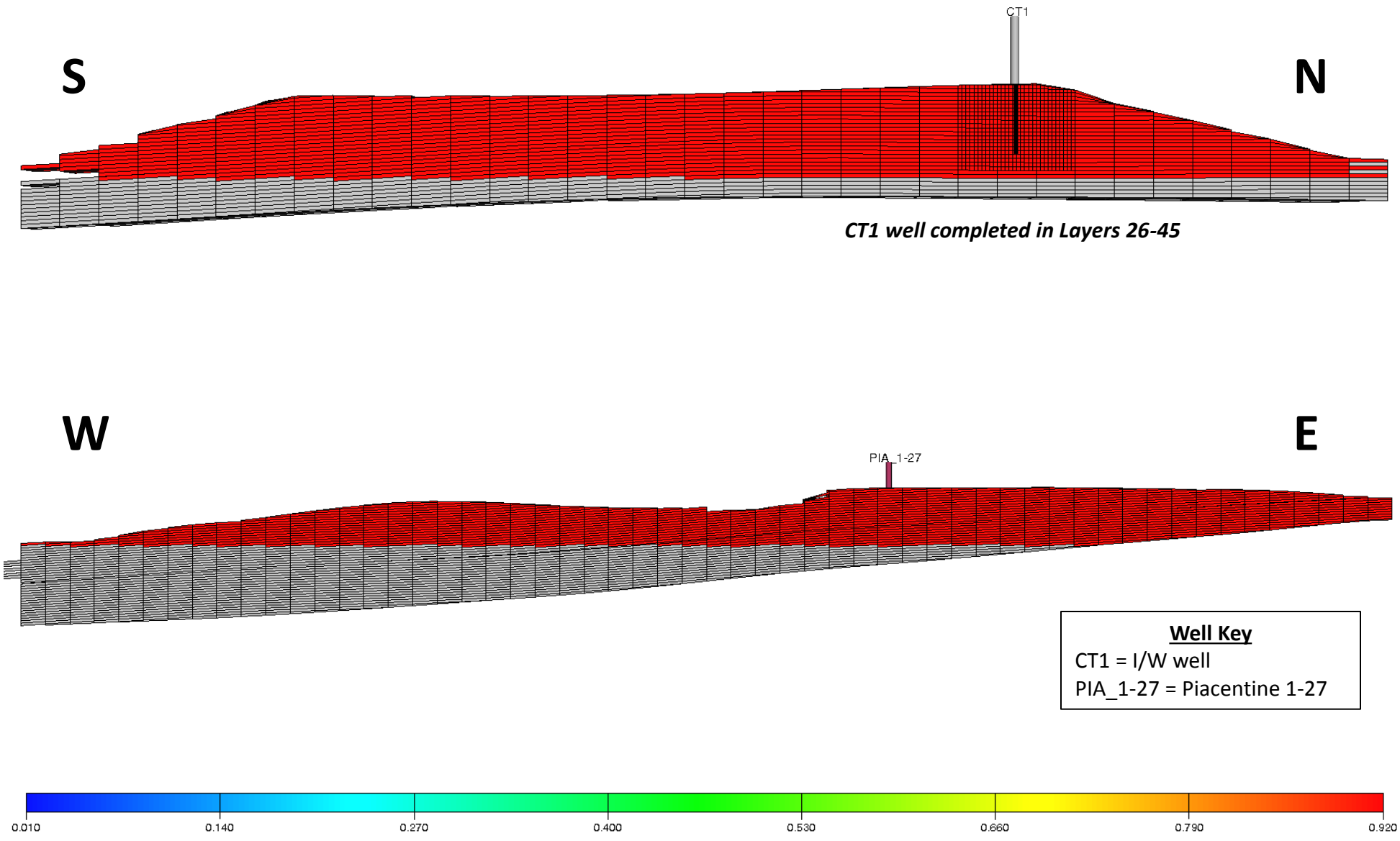

Feb 14, 2015

Final Technical Memorandum
for Compressed Air Energy Storage
Reservoir Characterization & Full Field Development Model
King Island Gas Field, San Joaquin County, CA
9/25/2015

Figure 44

Compression Testing Bubble Build (Beginning) – Cross-Section

Methane Composition Mole Fraction

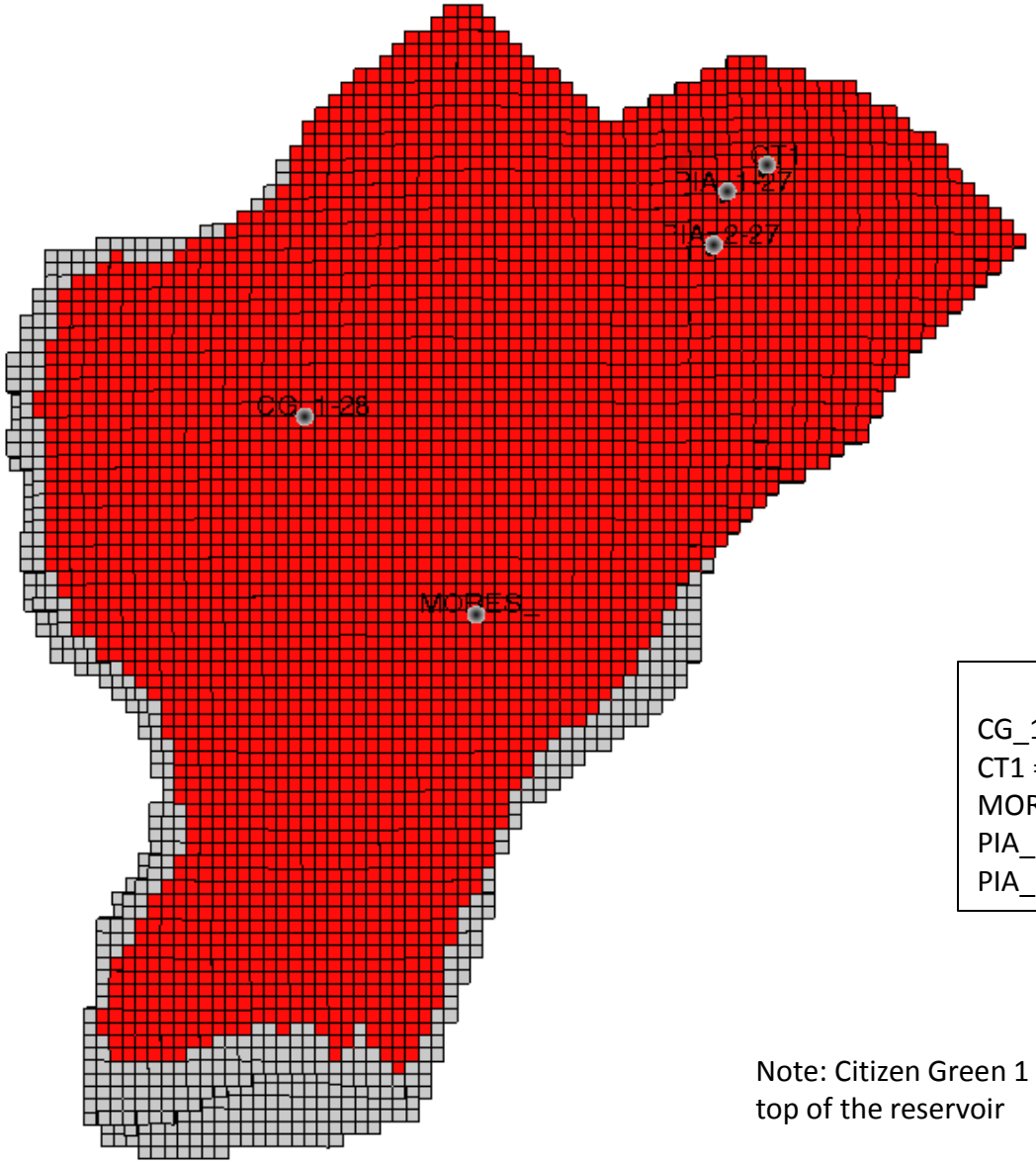

Well Key

CG_1 = Citizen Green 1
CT1 = I/W well
MORES_1 = Moresco A1
PIA_1-27 = Piacentine 1-27
PIA_2-27 = Piacentine 2-27

Note: Citizen Green 1 location where the well bore intersects the top of the reservoir

Feb 18, 2015
1st Fall-off Test

Final Technical Memorandum
for Compressed Air Energy Storage
Reservoir Characterization & Full Field Development Model
King Island Gas Field, San Joaquin County, CA
9/25/2015

Figure 45

Compression Testing Bubble Build (Beginning)

Methane Composition Mole Fraction

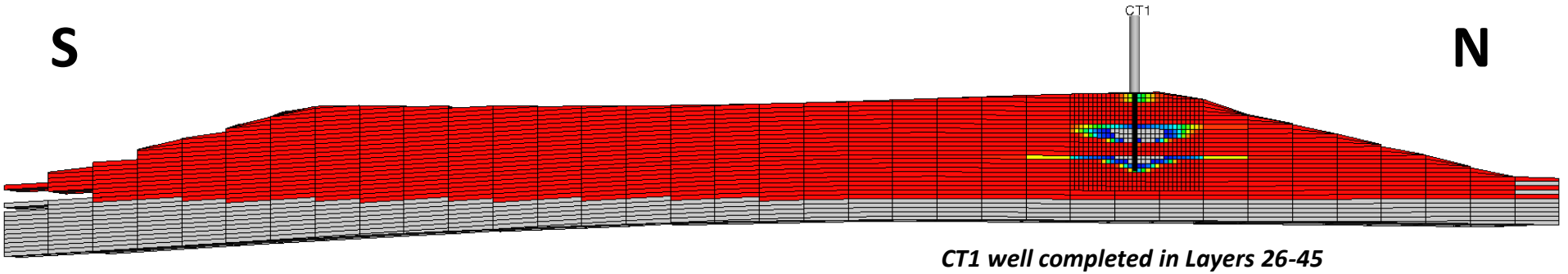

CT1 well completed in Layers 26-45

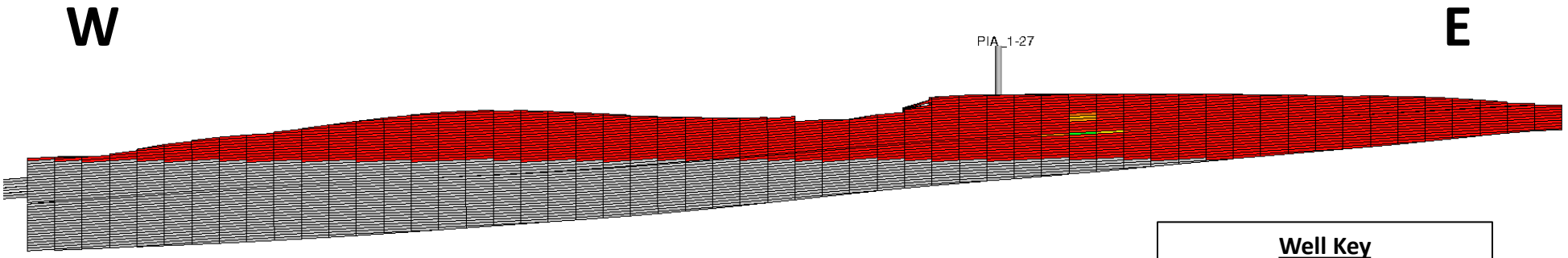

Well Key

CT1 = I/W well

PIA_1-27 = Piacentine 1-27

Feb 18, 2015

1st Fall-off Test

Final Technical Memorandum
for Compressed Air Energy Storage
Reservoir Characterization & Full Field Development Model
King Island Gas Field, San Joaquin County, CA
9/25/2015

Figure 46

Compression Testing Bubble Build (Beginning) – Cross-Section

Methane Composition Mole Fraction

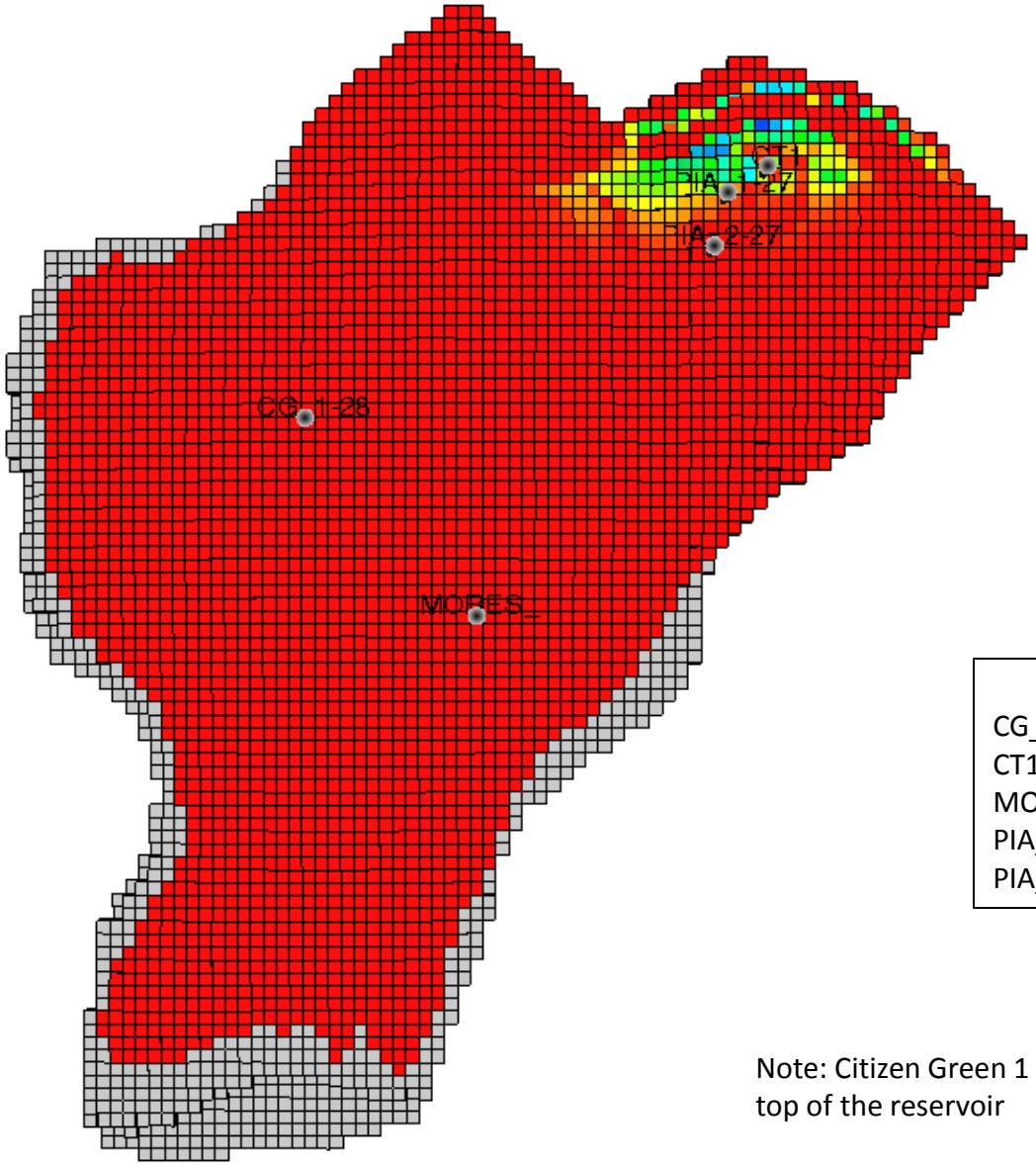

Well Key

CG_1 = Citizen Green 1
CT1 = I/W well
MORES_1 = Moresco A1
PIA_1-27 = Piacentine 1-27
PIA_2-27 = Piacentine 2-27

Note: Citizen Green 1 location where the well bore intersects the top of the reservoir

April 2, 2015
2nd Fall-off Test

Final Technical Memorandum
for Compressed Air Energy Storage
Reservoir Characterization & Full Field Development Model
King Island Gas Field, San Joaquin County, CA
9/25/2015

Figure 47

Compression Testing Bubble Build (Middle)

Methane Composition Mole Fraction

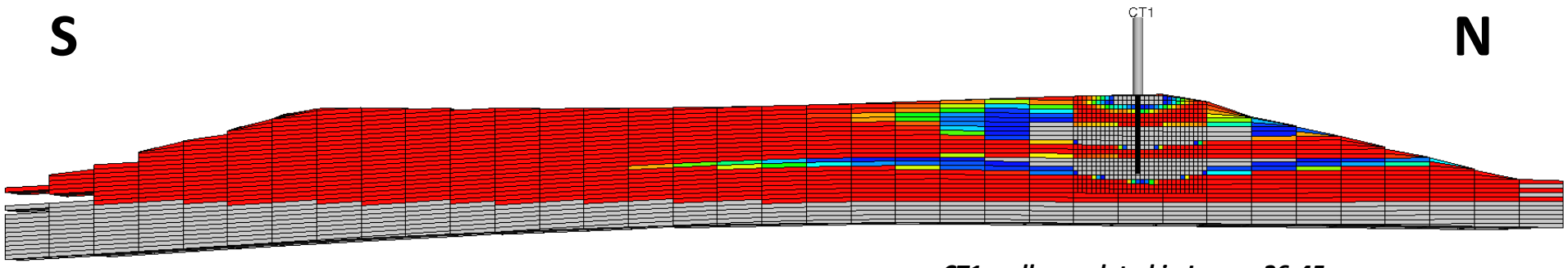

CT1 well completed in Layers 26-45

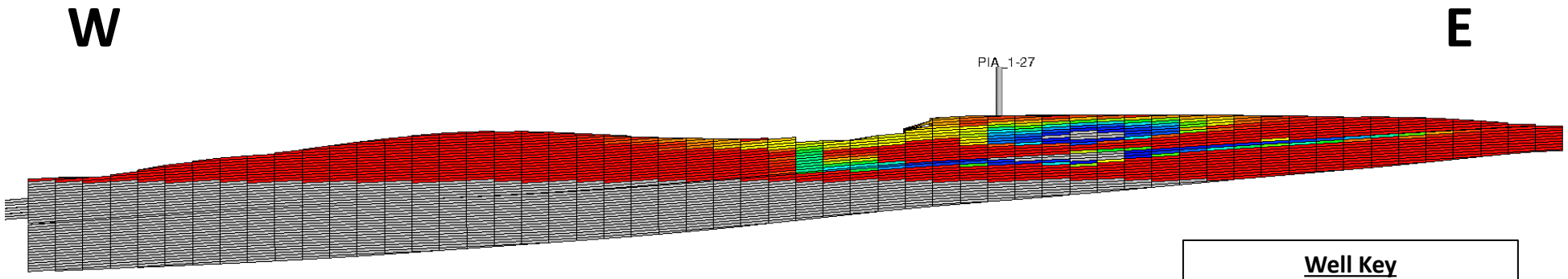

Well Key
CT1 = I/W well
PIA_1-27 = Piacentine 1-27

April 2, 2015
2nd Fall-off Test

Final Technical Memorandum
for Compressed Air Energy Storage
Reservoir Characterization & Full Field Development Model
King Island Gas Field, San Joaquin County, CA
9/25/2015

Figure 48

Compression Testing Bubble Build (Middle) – Cross-Section
Methane Composition Mole Fraction

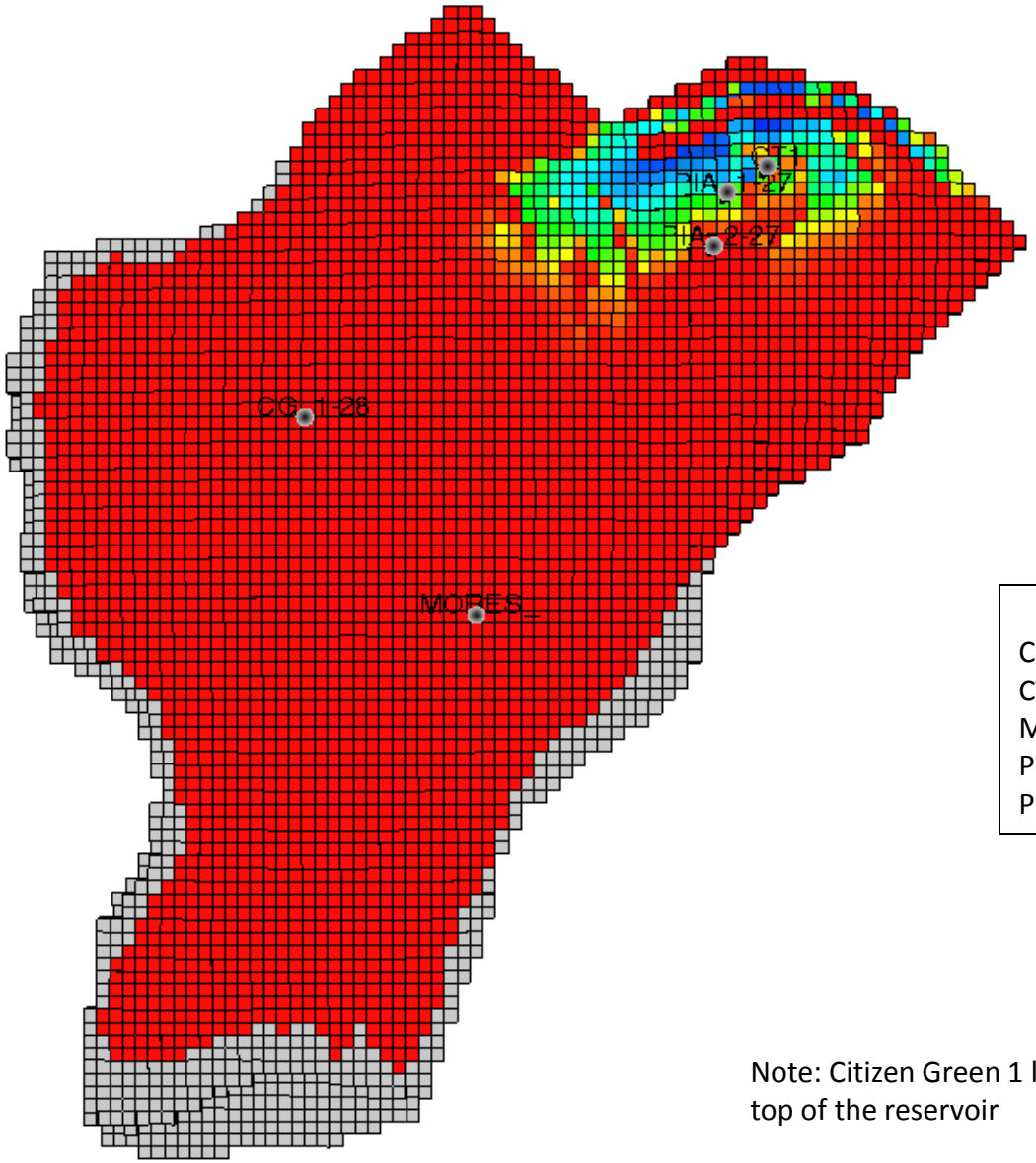

Well Key

CG_1 = Citizen Green 1
CT1 = I/W well
MORES_1 = Moresco A1
PIA_1-27 = Piacentine 1-27
PIA_2-27 = Piacentine 2-27

Note: Citizen Green 1 location where the well bore intersects the top of the reservoir

May 2, 2015
3rd Fall-off Test

Final Technical Memorandum
for Compressed Air Energy Storage
Reservoir Characterization & Full Field Development Model
King Island Gas Field, San Joaquin County, CA
9/25/2015

Figure 49

Compression Testing Bubble Build (End)

Methane Composition Mole Fraction

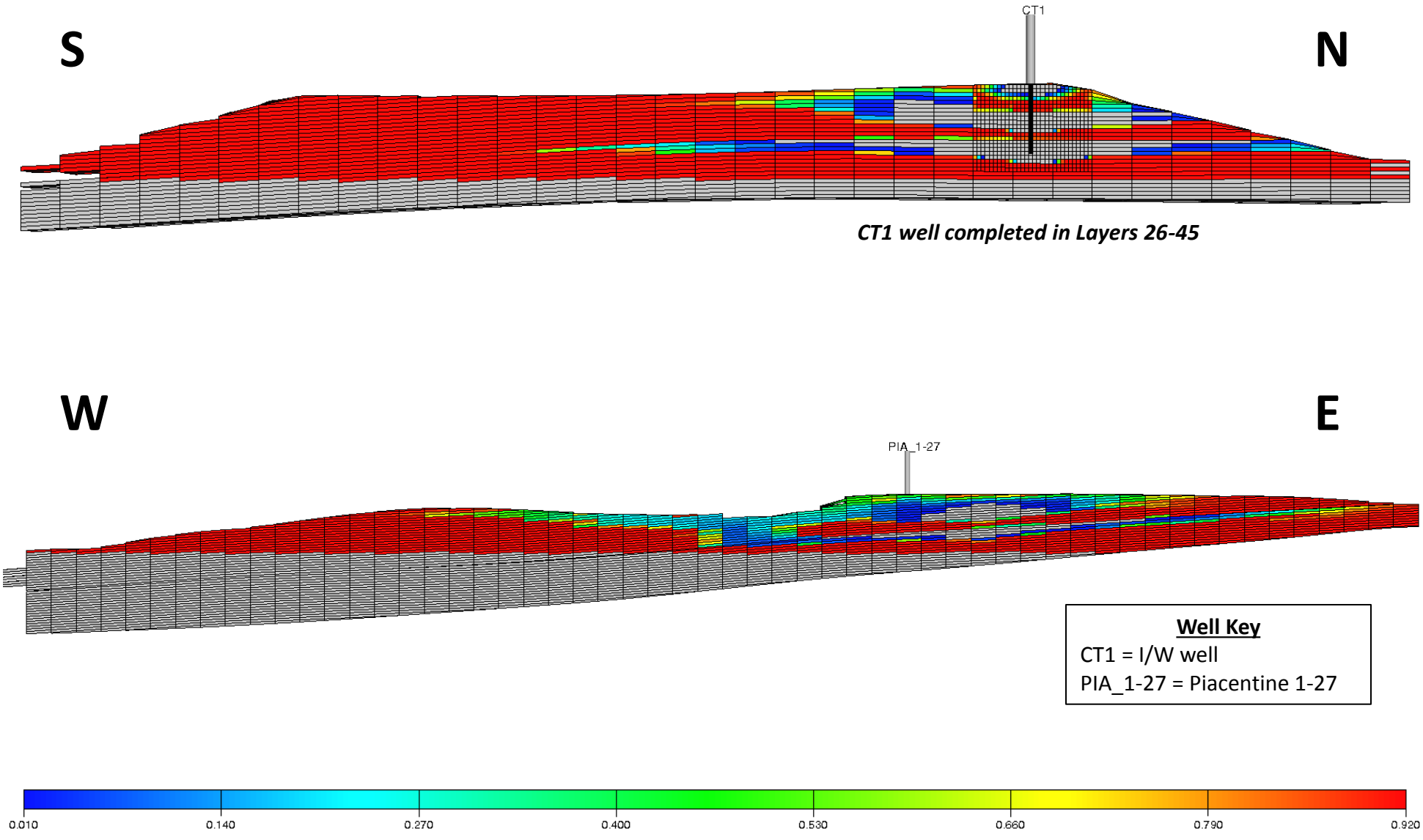

May 2, 2015
3rd Fall-off Test

Final Technical Memorandum
for Compressed Air Energy Storage
Reservoir Characterization & Full Field Development Model
King Island Gas Field, San Joaquin County, CA
9/25/2015

Figure 50

Compression Testing Bubble Build (End) – Cross-Section

Methane Composition Mole Fraction

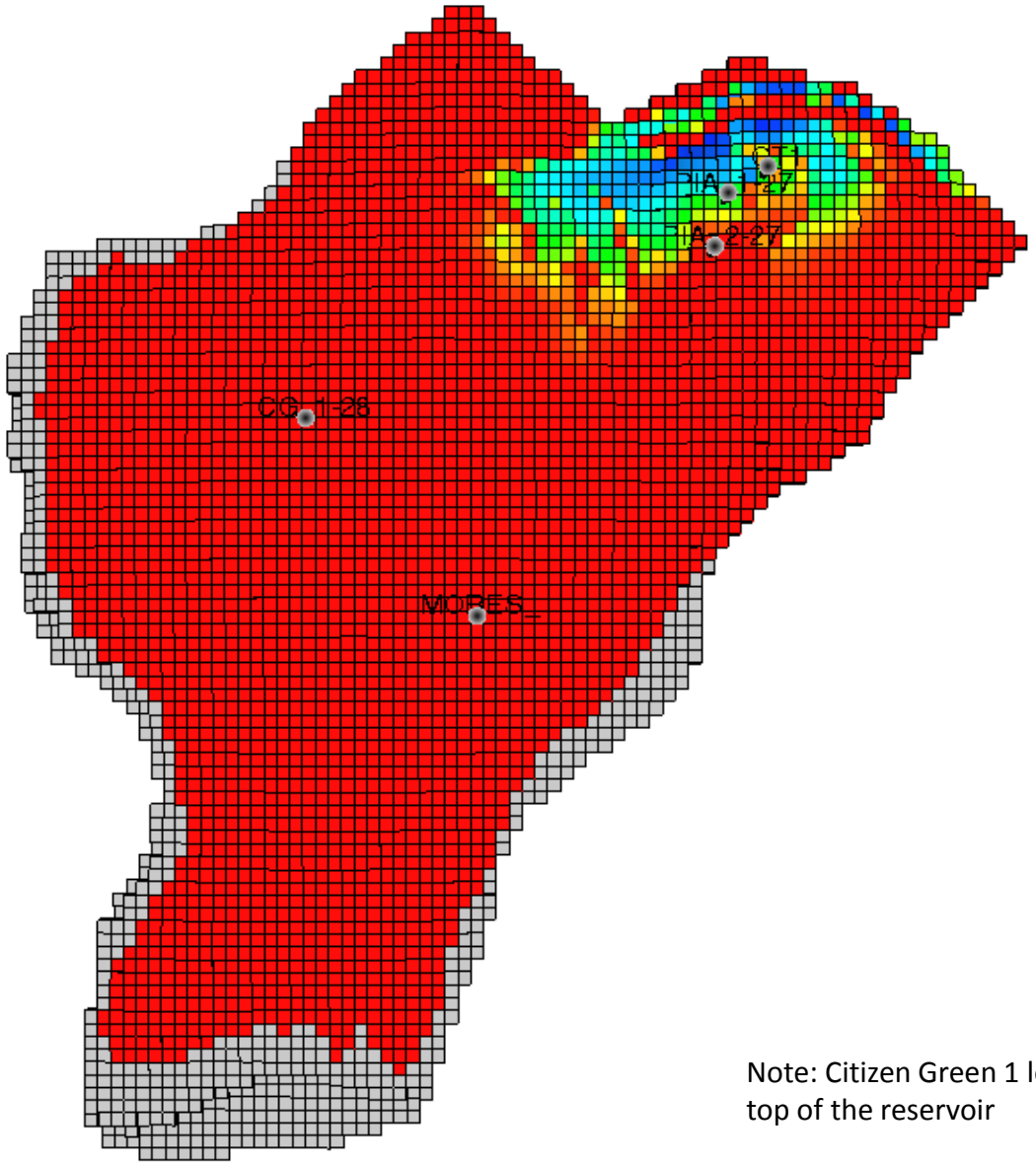

Well Key

CG_1 = Citizen Green 1
CT1 = I/W well
MORES_1 = Moresco A1
PIA_1-27 = Piacentine 1-27
PIA_2-27 = Piacentine 2-27

Note: Citizen Green 1 location where the well bore intersects the top of the reservoir

May 16, 2015
End of depleted air cycling

Final Technical Memorandum
for Compressed Air Energy Storage
Reservoir Characterization & Full Field Development Model
King Island Gas Field, San Joaquin County, CA
9/25/2015

Figure 51

Compression Testing Program (End)

Methane Composition Mole Fraction

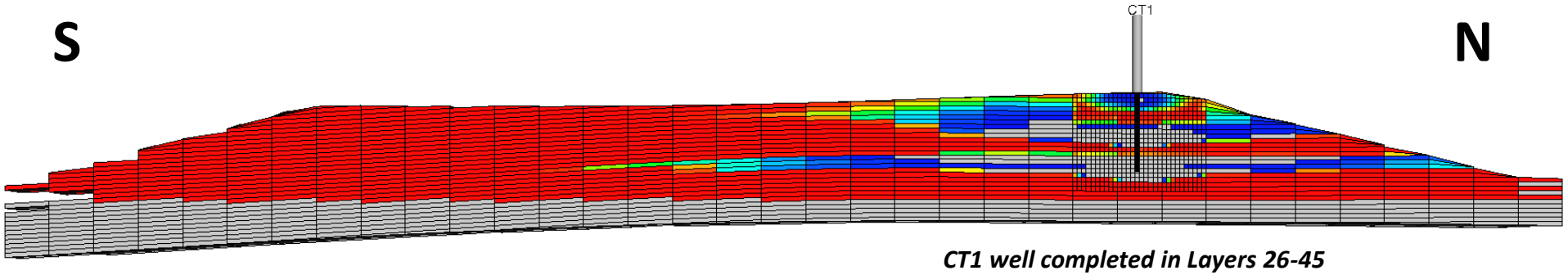

CT1 well completed in Layers 26-45

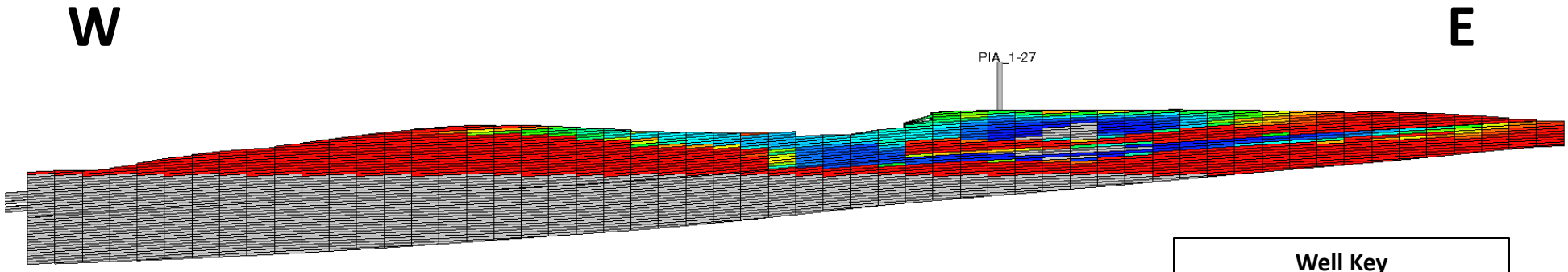

Well Key
CT1 = I/W well
PIA_1-27 = Piacentine 1-27

May 16, 2015
End of depleted air cycling

Final Technical Memorandum
for Compressed Air Energy Storage
Reservoir Characterization & Full Field Development Model
King Island Gas Field, San Joaquin County, CA
9/25/2015

Figure 52

Compression Testing Program (End) – Cross-Section

Methane Composition Mole Fraction

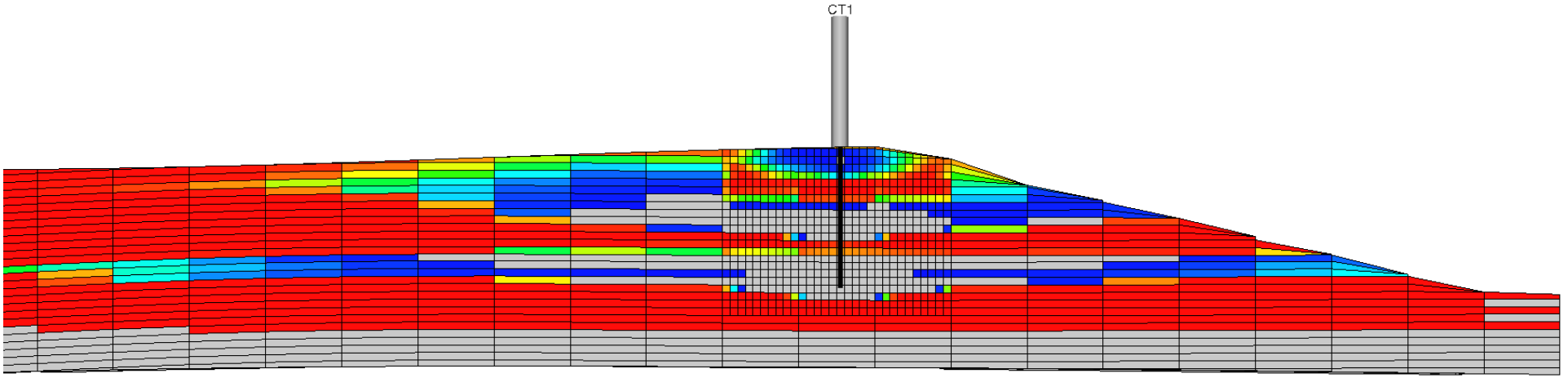

CT1 well completed in Layers 26-45

Well Key
CT1 = I/W well

May 16, 2015
End of depleted air cycling

Final Technical Memorandum
for Compressed Air Energy Storage
Reservoir Characterization & Full Field Development Model
King Island Gas Field, San Joaquin County, CA
9/25/2015

Figure 53

Compression Testing Program (End) – Zoom CT1

Methane Composition Mole Fraction

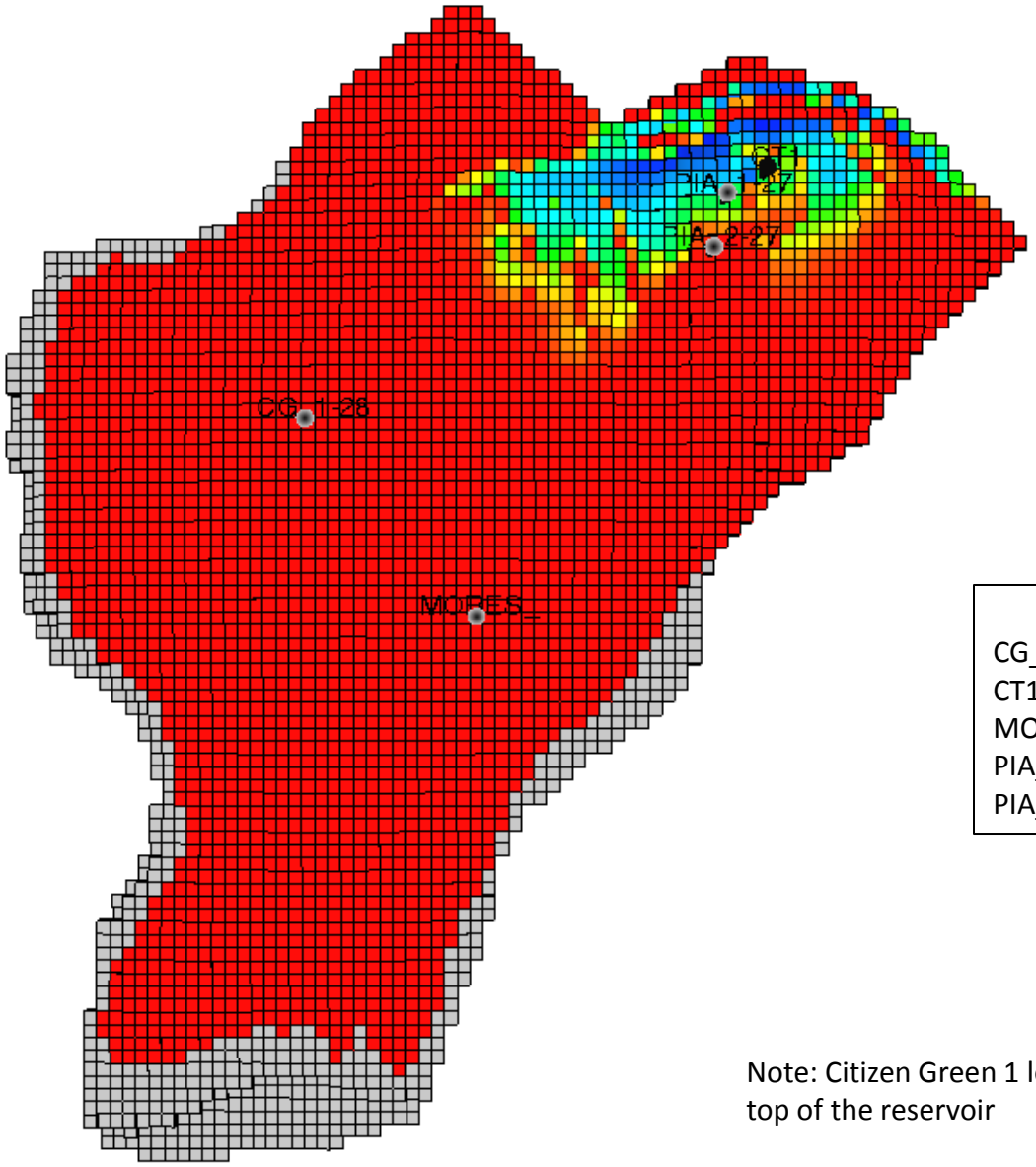

Well Key

CG_1 = Citizen Green 1
CT1 = I/W well
MORES_1 = Moresco A1
PIA_1-27 = Piacentine 1-27
PIA_2-27 = Piacentine 2-27

Note: Citizen Green 1 location where the well bore intersects the top of the reservoir

May 30, 2015
Ambient Air Injection

Final Technical Memorandum
for Compressed Air Energy Storage
Reservoir Characterization & Full Field Development Model
King Island Gas Field, San Joaquin County, CA
9/25/2015

Figure 54

Compression Testing Program
End of Ambient Air Injection
Methane Composition Mole Fraction

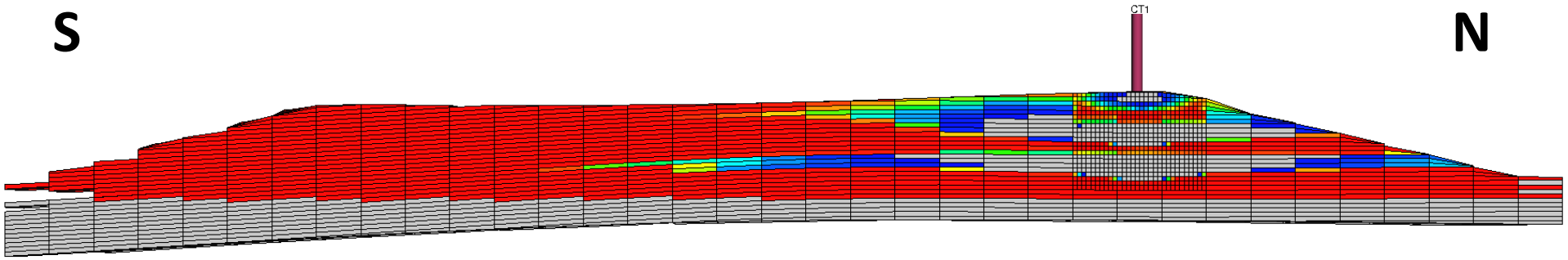

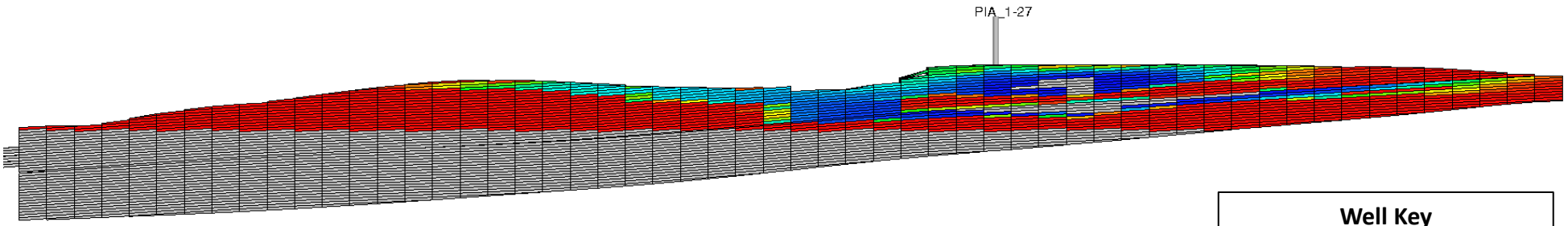

Well Key
CT1 = I/W well
PIA_1-27 = Piacentine 1-27

May 30, 2015
Ambient Air Injection

Final Technical Memorandum
for Compressed Air Energy Storage
Reservoir Characterization & Full Field Development Model
King Island Gas Field, San Joaquin County, CA
9/25/2015

Figure 55

Compression Testing Program
End of Ambient Air Injection – Cross-Section
Methane Composition Mole Fraction

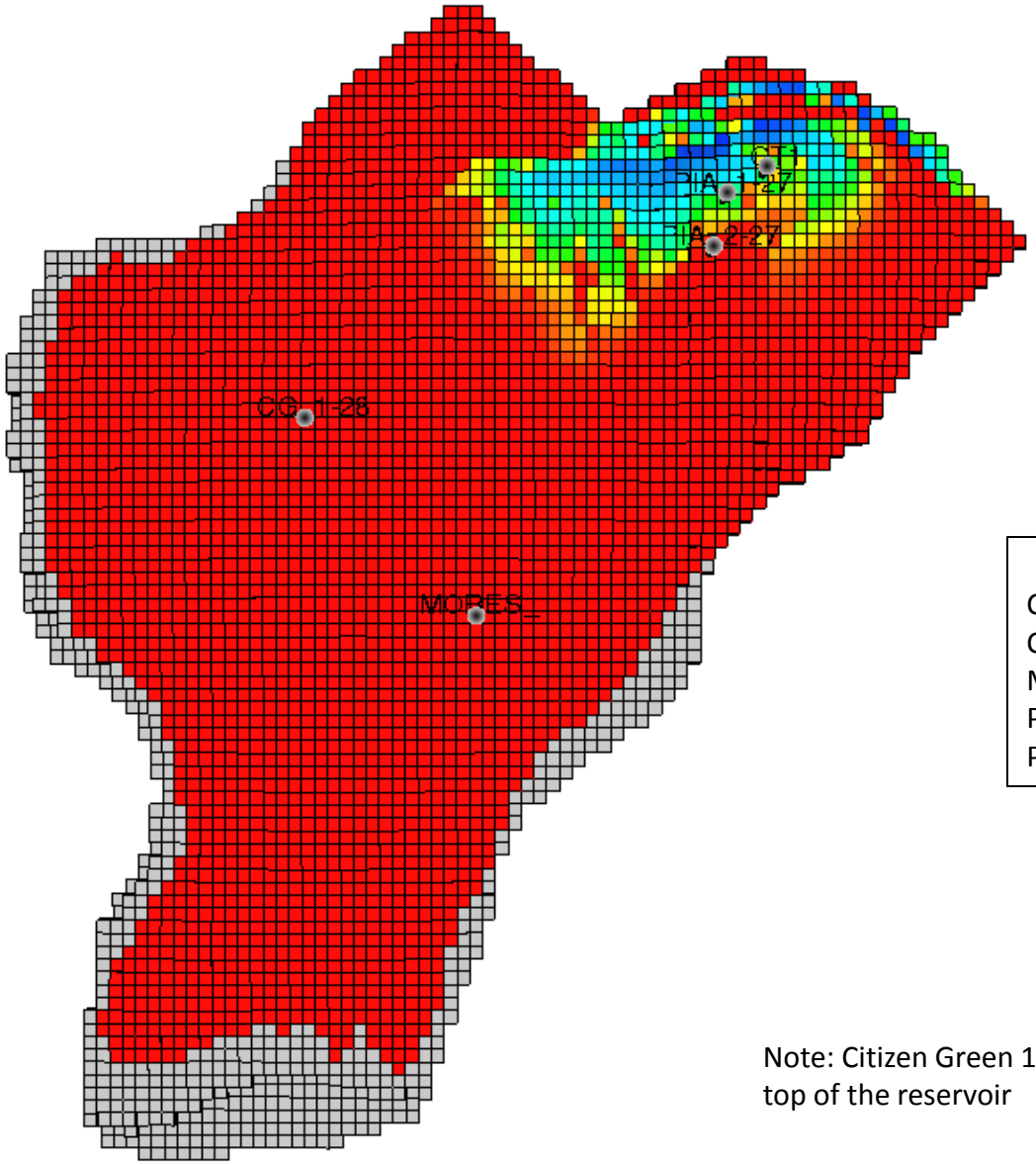

Well Key

CG_1 = Citizen Green 1
CT1 = I/W well
MORES_1 = Moresco A1
PIA_1-27 = Piacentine 1-27
PIA_2-27 = Piacentine 2-27

Note: Citizen Green 1 location where the well bore intersects the top of the reservoir

June 5, 2015

Final Technical Memorandum
for Compressed Air Energy Storage
Reservoir Characterization & Full Field Development Model
King Island Gas Field, San Joaquin County, CA
9/25/2015

Figure 56

Compression Testing Program (End)

Methane Composition Mole Fraction

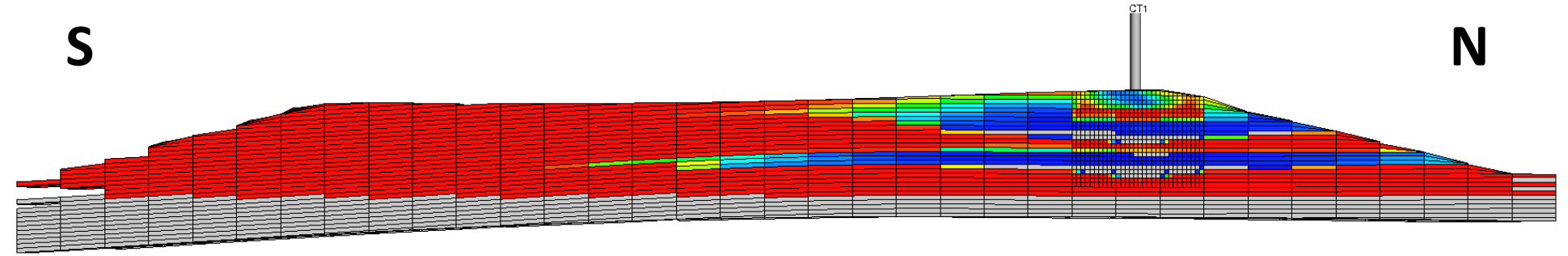

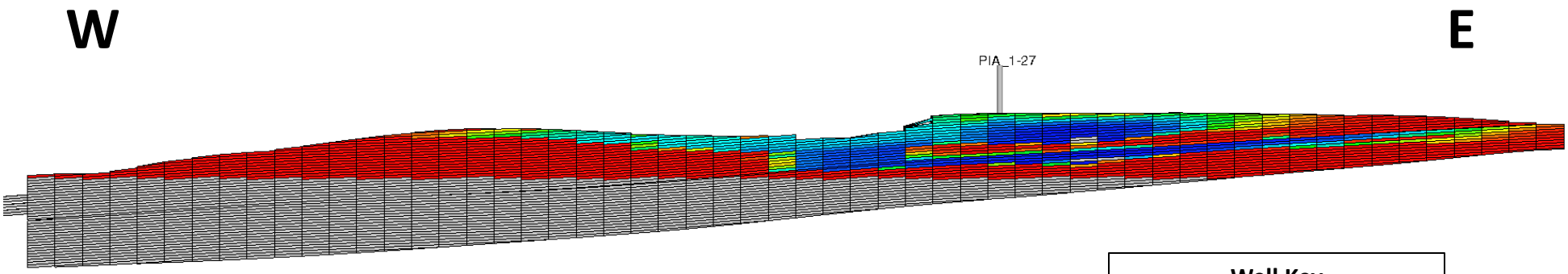

Well Key

CT1 = I/W well

PIA_1-27 = Piacentine 1-27

June 5, 2015

Final Technical Memorandum
for Compressed Air Energy Storage
Reservoir Characterization & Full Field Development Model
King Island Gas Field, San Joaquin County, CA
9/25/2015

Figure 57

Compression Testing Program (End) – Cross-Section

Methane Composition Mole Fraction

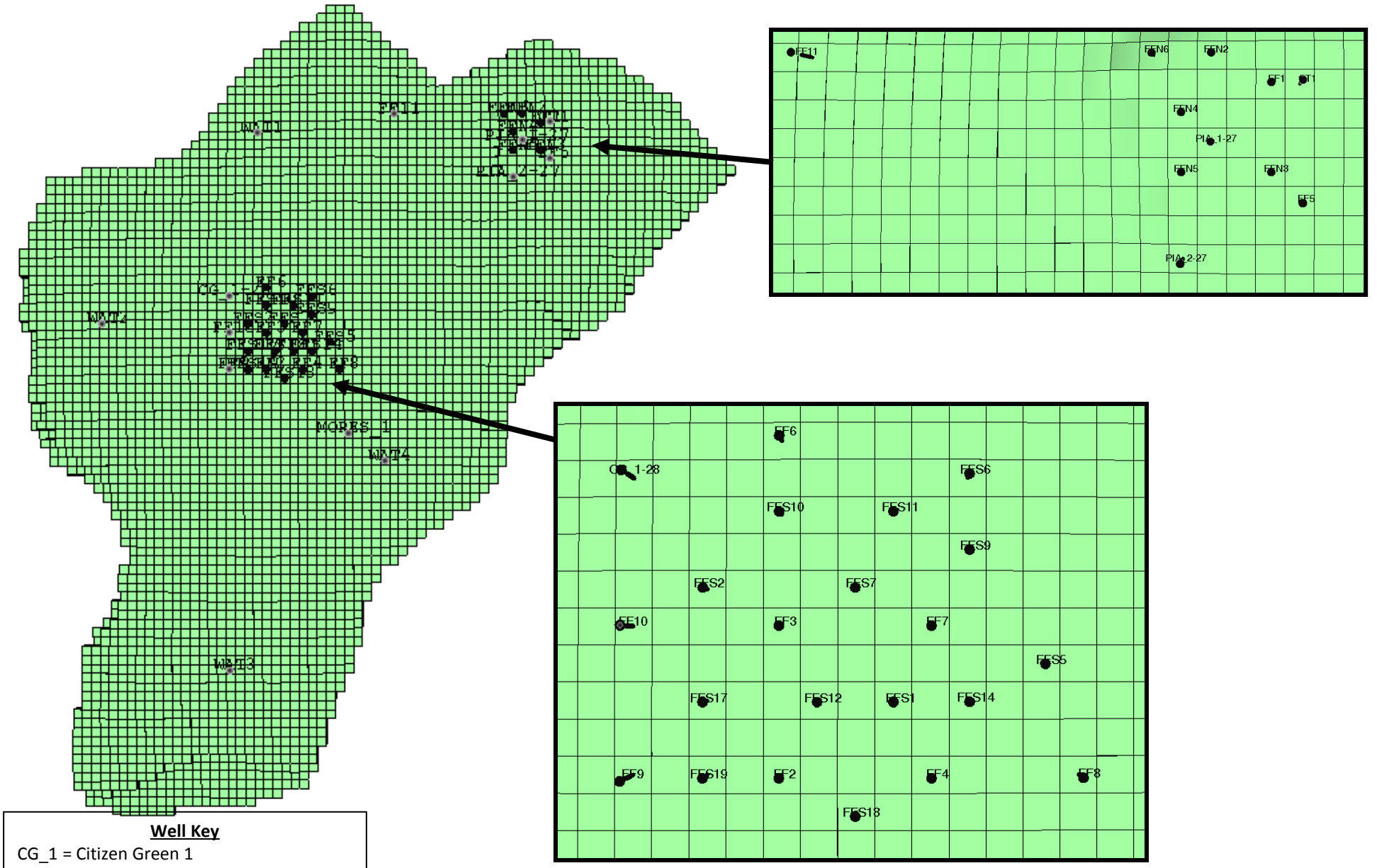

Well Key

CG_1 = Citizen Green 1
CT1 = I/W well
FF; FFN and FFS = Simulated full field development wells ; north and south
MORES_1 = Moresco A1
PIA_1-27 = Piacentine 1-27
PIA_2-27 = Piacentine 2-27
WAT = Water production wells

Final Technical Memorandum
for Compressed Air Energy Storage
Reservoir Characterization & Full Field Development Model
King Island Gas Field, San Joaquin County, CA
9/25/2015

Figure 58

CAES Full Field Well Plan

Aerial View

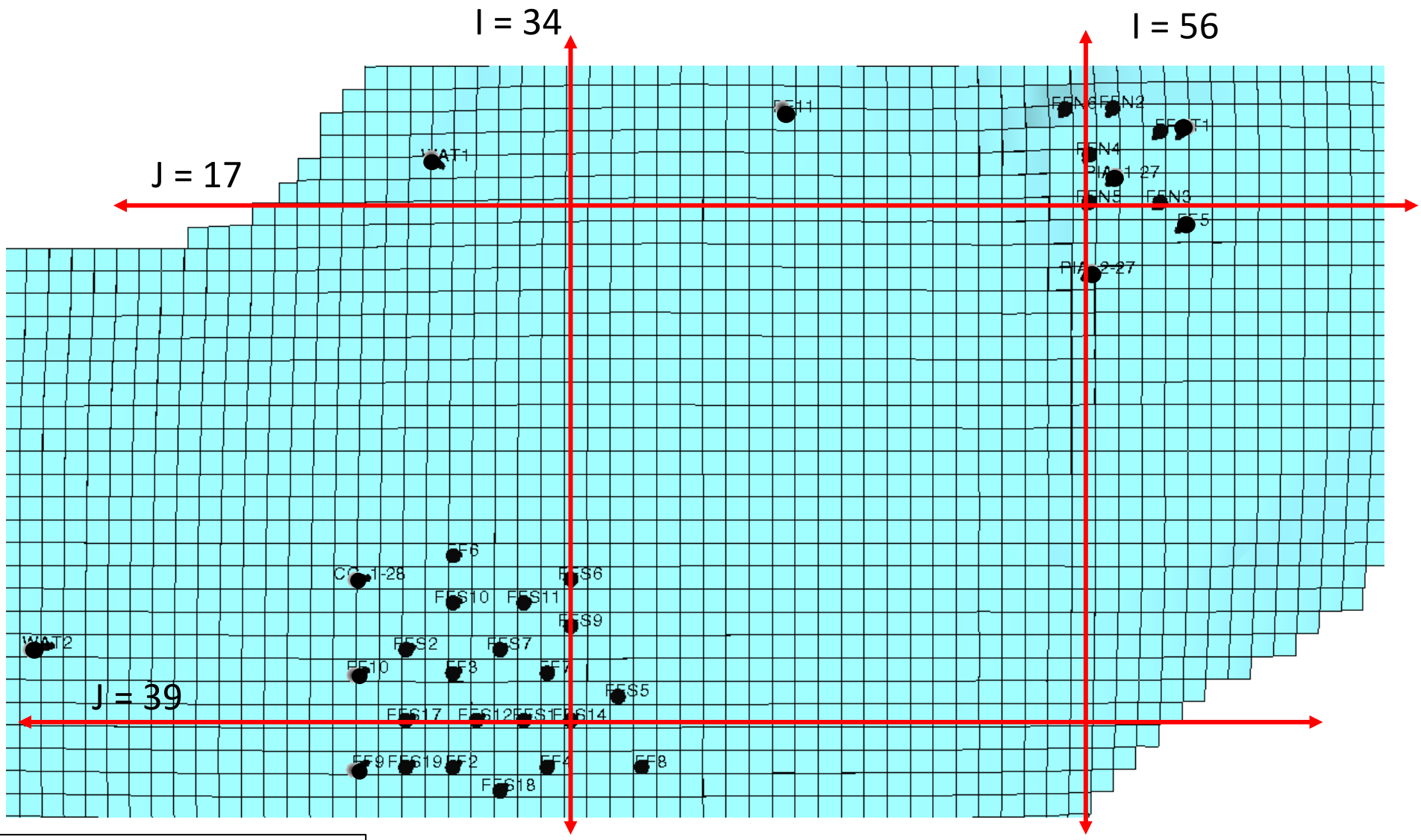

Well Key

CG_1 = Citizen Green 1
CT1 = I/W well
FF; FFN and FFS = Simulated full field development wells ; north and south
MORES_1 = Moresco A1
PIA_1-27 = Piacentine 1-27
PIA_2-27 = Piacentine 2-27
WAT = Water production wells

Final Technical Memorandum
for Compressed Air Energy Storage
Reservoir Characterization & Full Field Development Model
King Island Gas Field, San Joaquin County, CA
9/25/2015

Figure 59

CAES Full Field Well Plan

Cross-Sections

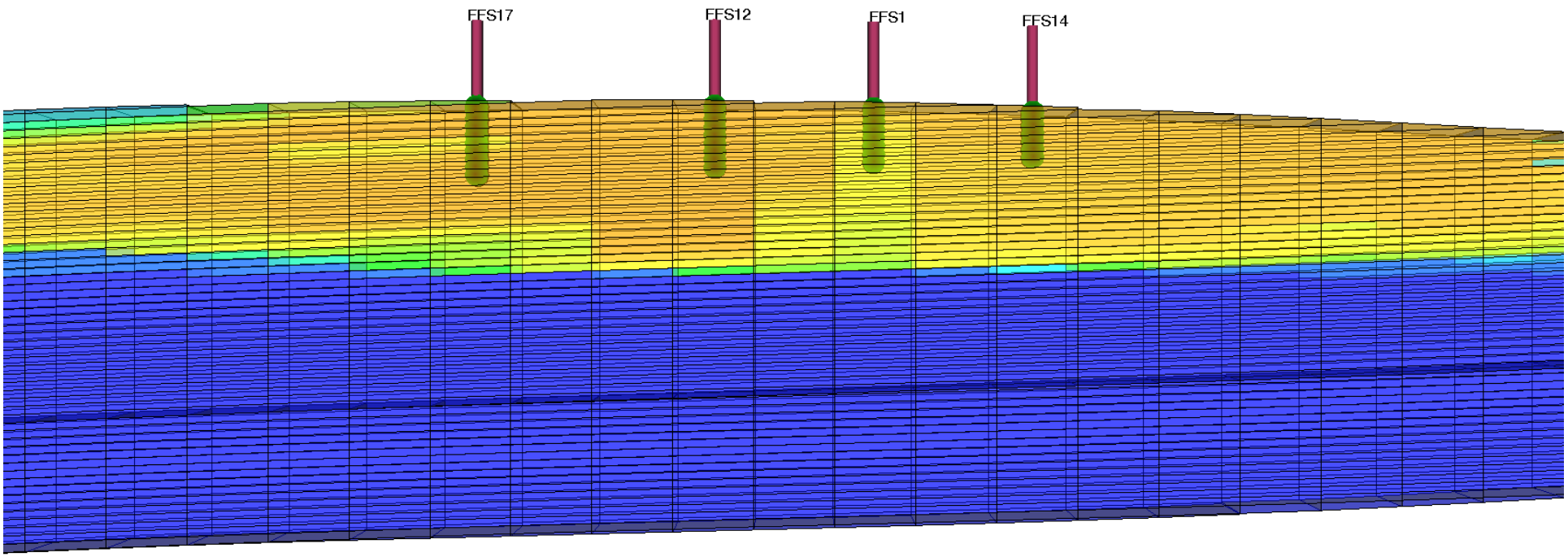

Completion Intervals = 40 – 50 feet

Well Key
FFS = Simulated full field development wells, south

Final Technical Memorandum
for Compressed Air Energy Storage
Reservoir Characterization & Full Field Development Model
King Island Gas Field, San Joaquin County, CA
9/25/2015

Figure 60

CAES Full Field Well Plan

Completion Interval - Cross-Section

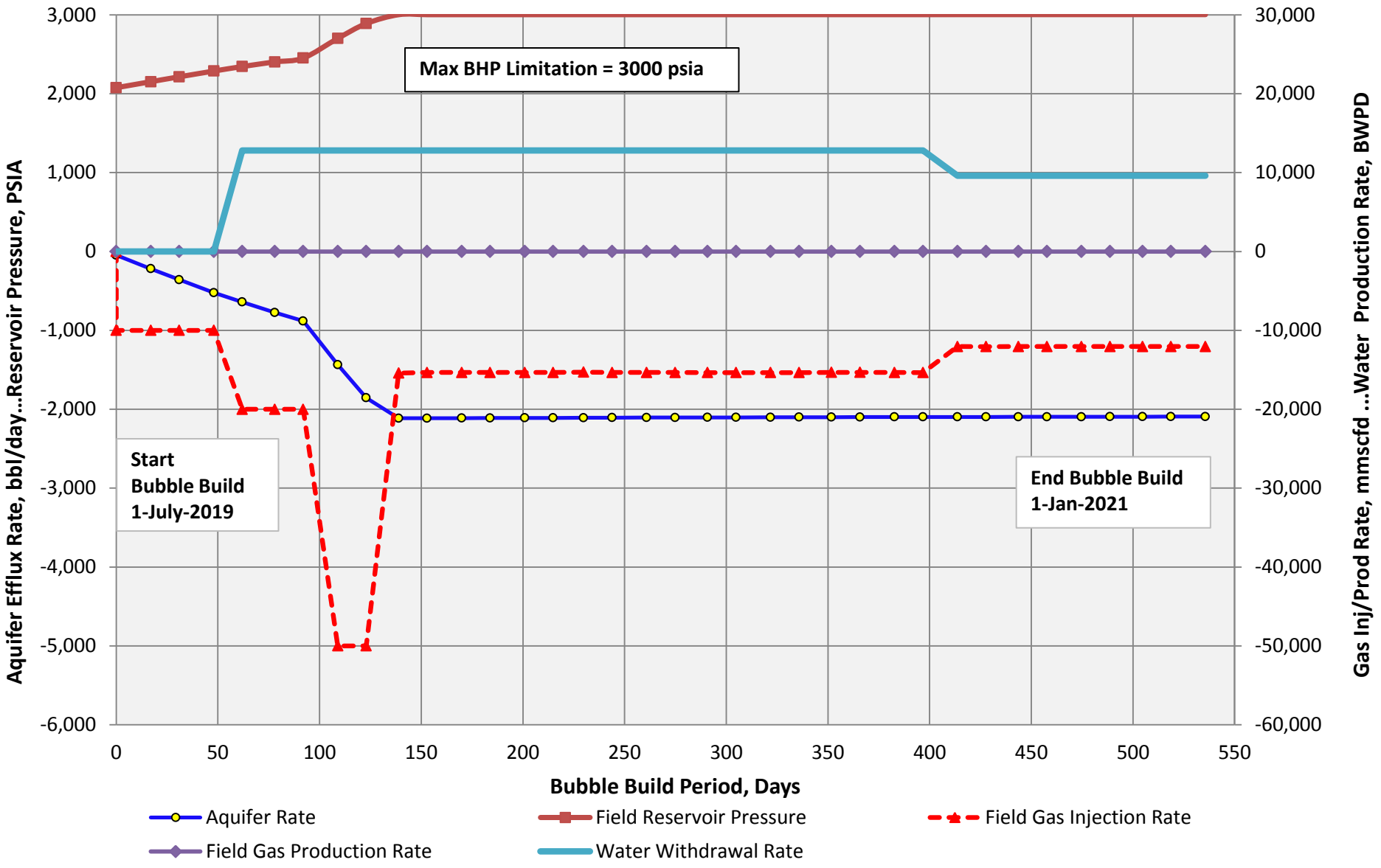

BHP = Bottom hole pressure
mmscf/d = Million standard cubic feet per day
PSIA = Pounds per square inch absolute

Final Technical Memorandum
for Compressed Air Energy Storage
Reservoir Characterization & Full Field Development Model
King Island Gas Field, San Joaquin County, CA
9/25/2015

Figure 61

King Island Full Field CAES Simulation
Bubble Build Period

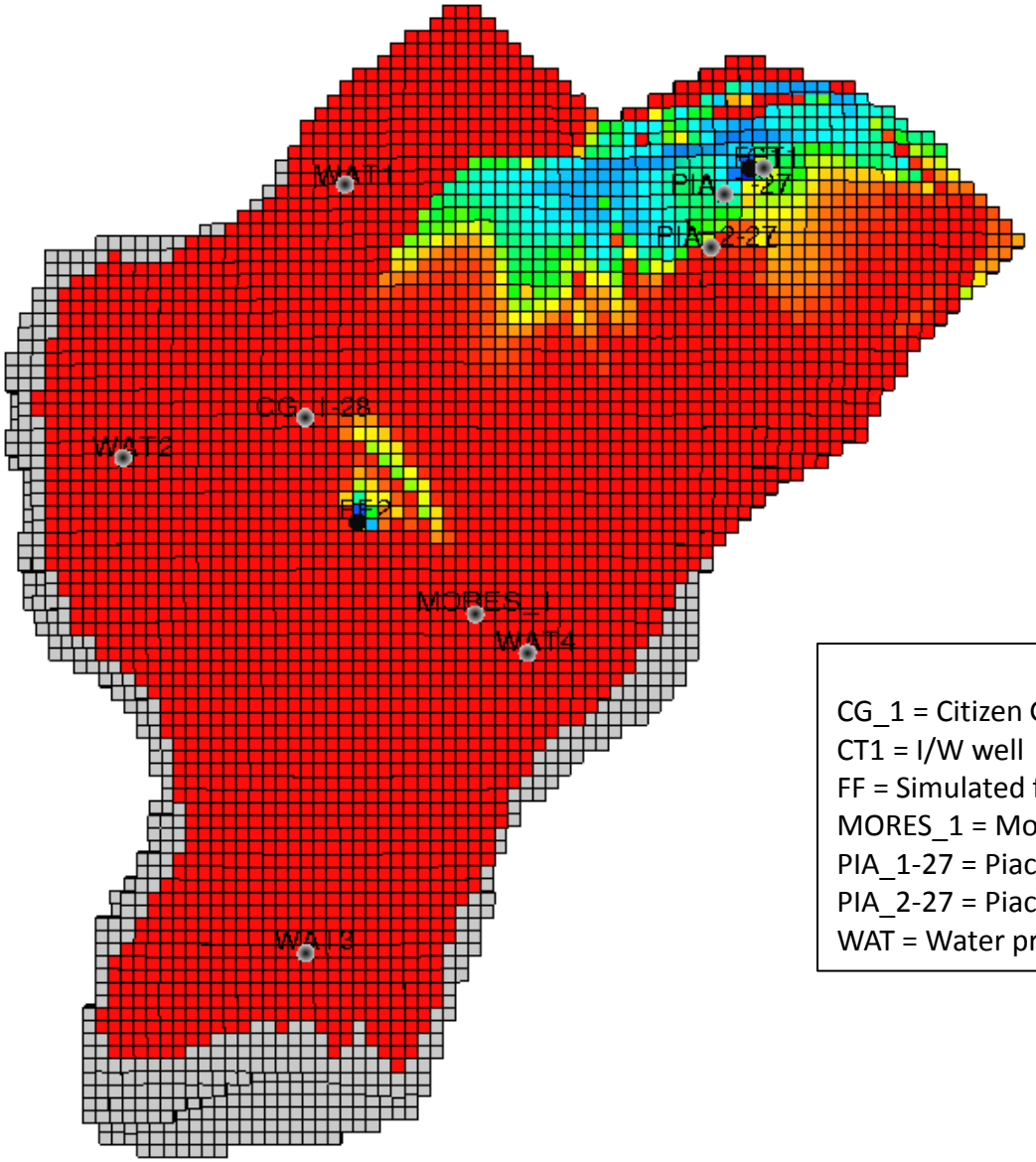

Well Key

CG_1 = Citizen Green 1
CT1 = I/W well
FF = Simulated full field development wells
MORES_1 = Moresco A1
PIA_1-27 = Piacentine 1-27
PIA_2-27 = Piacentine 2-27
WAT = Water production wells

July 1, 2019

Final Technical Memorandum
for Compressed Air Energy Storage
Reservoir Characterization & Full Field Development Model
King Island Gas Field, San Joaquin County, CA
9/25/2015

Figure 62

CAES Full Field Well Plan
Beginning of Bubble Build
Methane Composition Mole Fraction

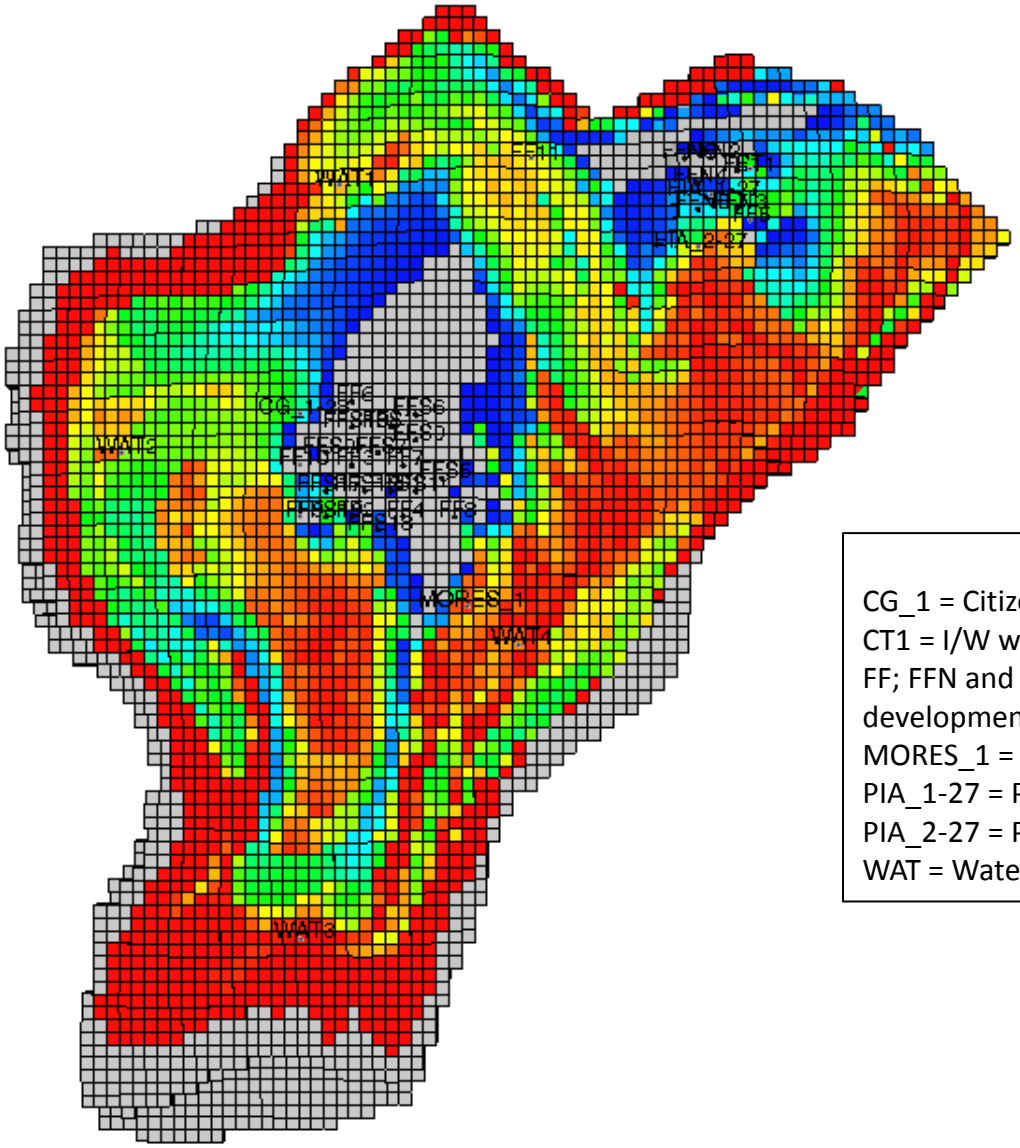

Well Key

CG_1 = Citizen Green 1
CT1 = I/W well
FF; FFN and FFS = Simulated full field development wells; north and south
MORES_1 = Moresco A1
PIA_1-27 = Piacentine 1-27
PIA_2-27 = Piacentine 2-27
WAT = Water production wells

January 1, 2021

Final Technical Memorandum
for Compressed Air Energy Storage
Reservoir Characterization & Full Field Development Model
King Island Gas Field, San Joaquin County, CA
9/25/2015

Figure 63

CAES Full Field Well Plan
End of Bubble Build
Methane Composition Mole Fraction

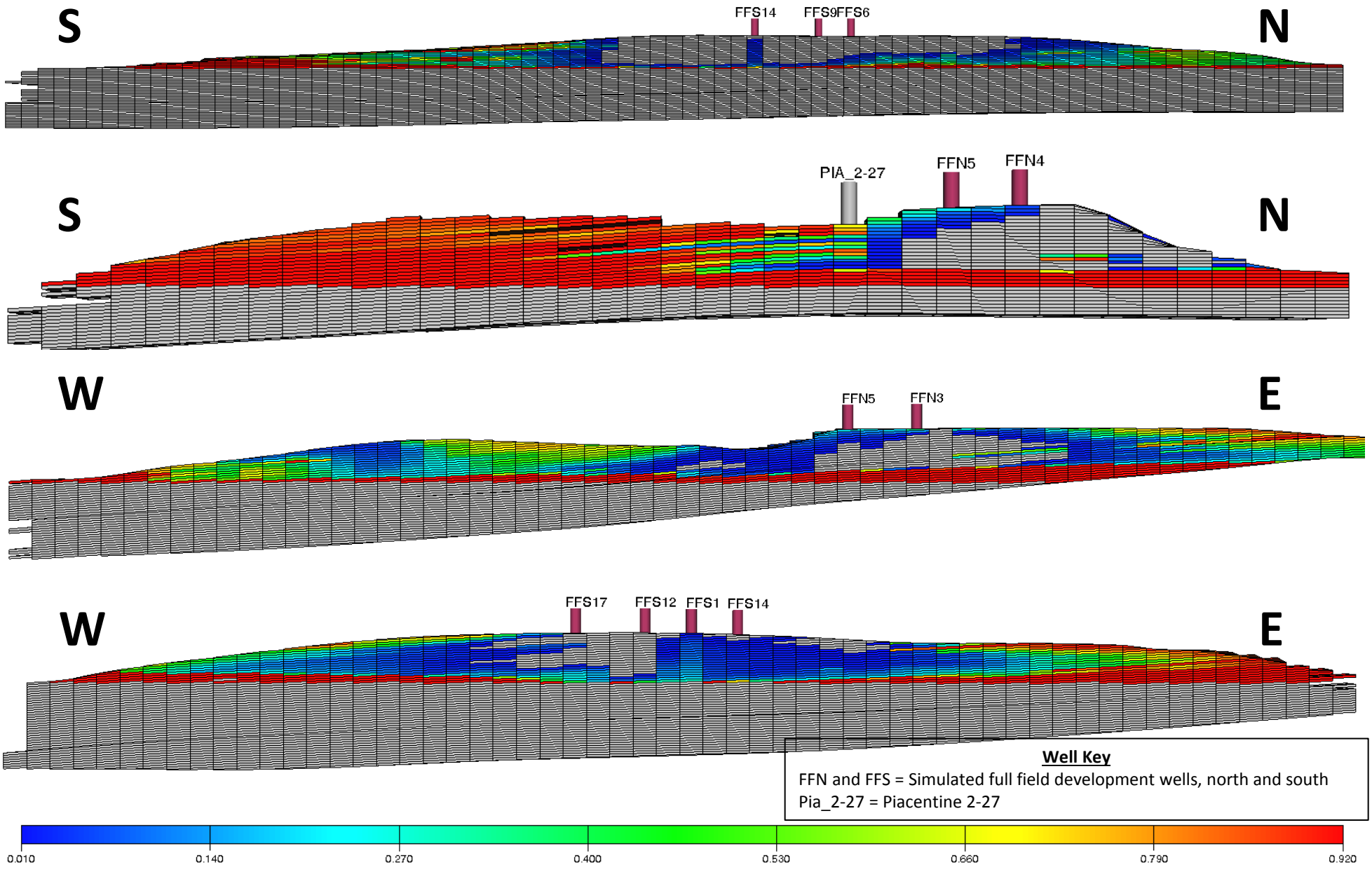

January 1, 2021

Final Technical Memorandum
for Compressed Air Energy Storage
Reservoir Characterization & Full Field Development Model
King Island Gas Field, San Joaquin County, CA
9/25/2015

Figure 64

CAES Full Field Well Plan
End of Bubble Build – Cross Section Views
Methane Composition Mole Fraction

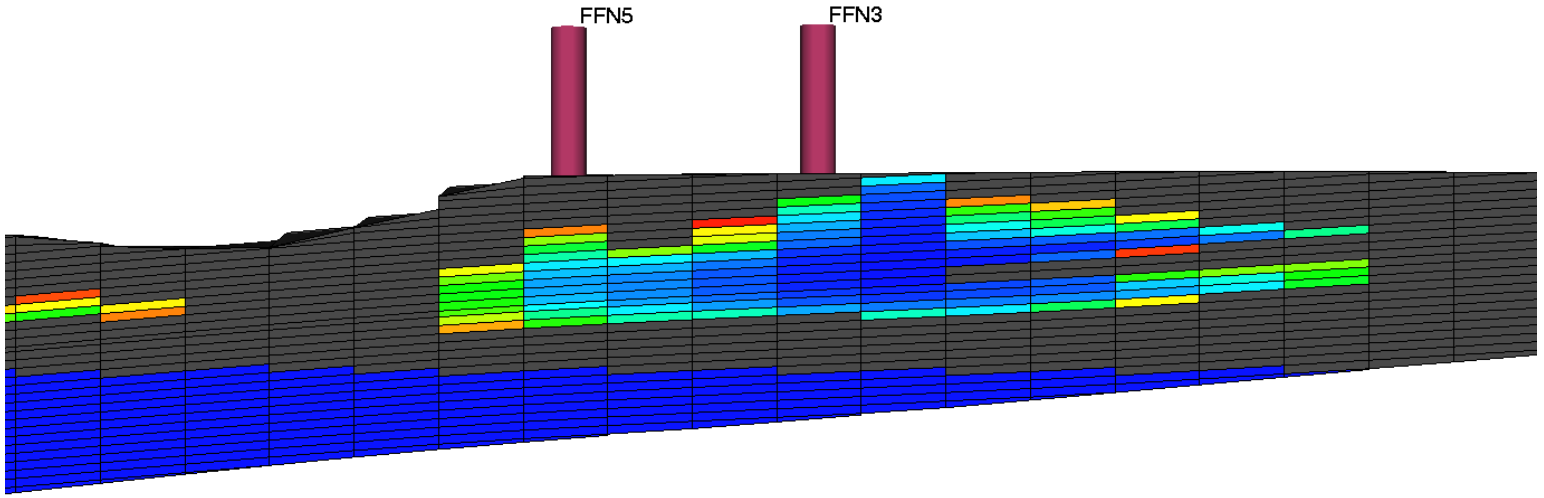

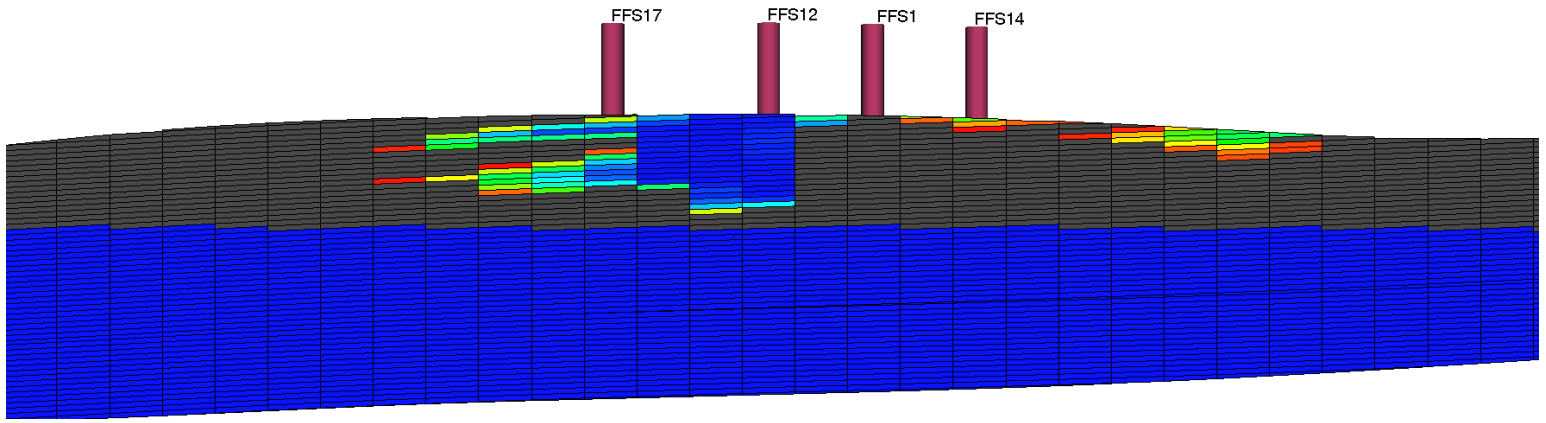

Methane Composition Mole Fraction Range 0.00 to 0.01 Displayed

January 1, 2021

Final Technical Memorandum
for Compressed Air Energy Storage
Reservoir Characterization & Full Field Development Model
King Island Gas Field, San Joaquin County, CA
9/25/2015

Figure 65

CAES Full Field Well Plan End of Bubble Build

Cross Section View Zoom

Methane Composition Within Air Bubble

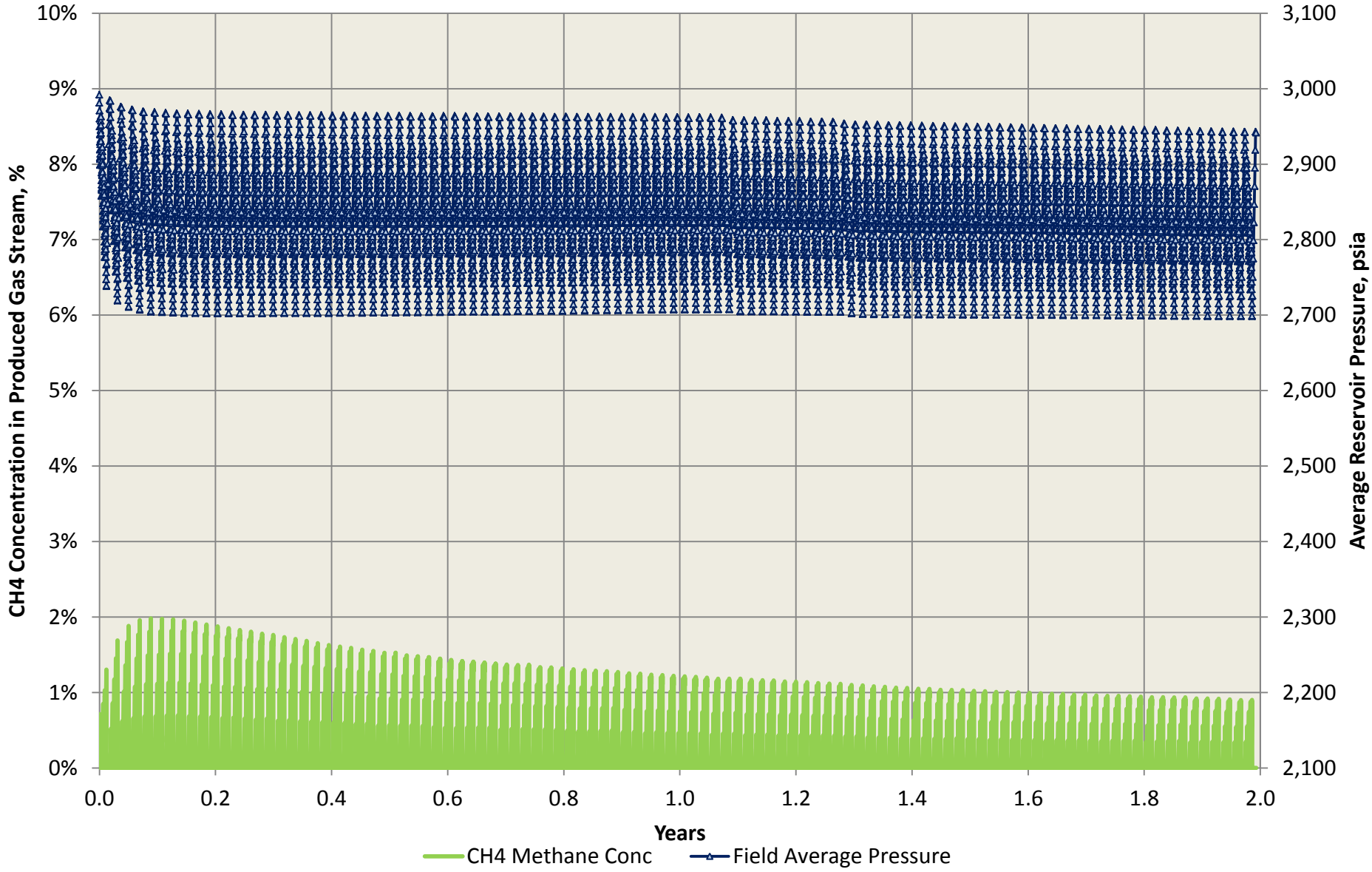

CH4 = Methane
psia = Pounds per square inch absolute

Final Technical Memorandum
for Compressed Air Energy Storage
Reservoir Characterization & Full Field Development Model
King Island Gas Field, San Joaquin County, CA
9/25/2015

Figure 66

CAES Full Field Development - B

Field Methane Concentration in Produced Gas Stream, and Field Average Pressure

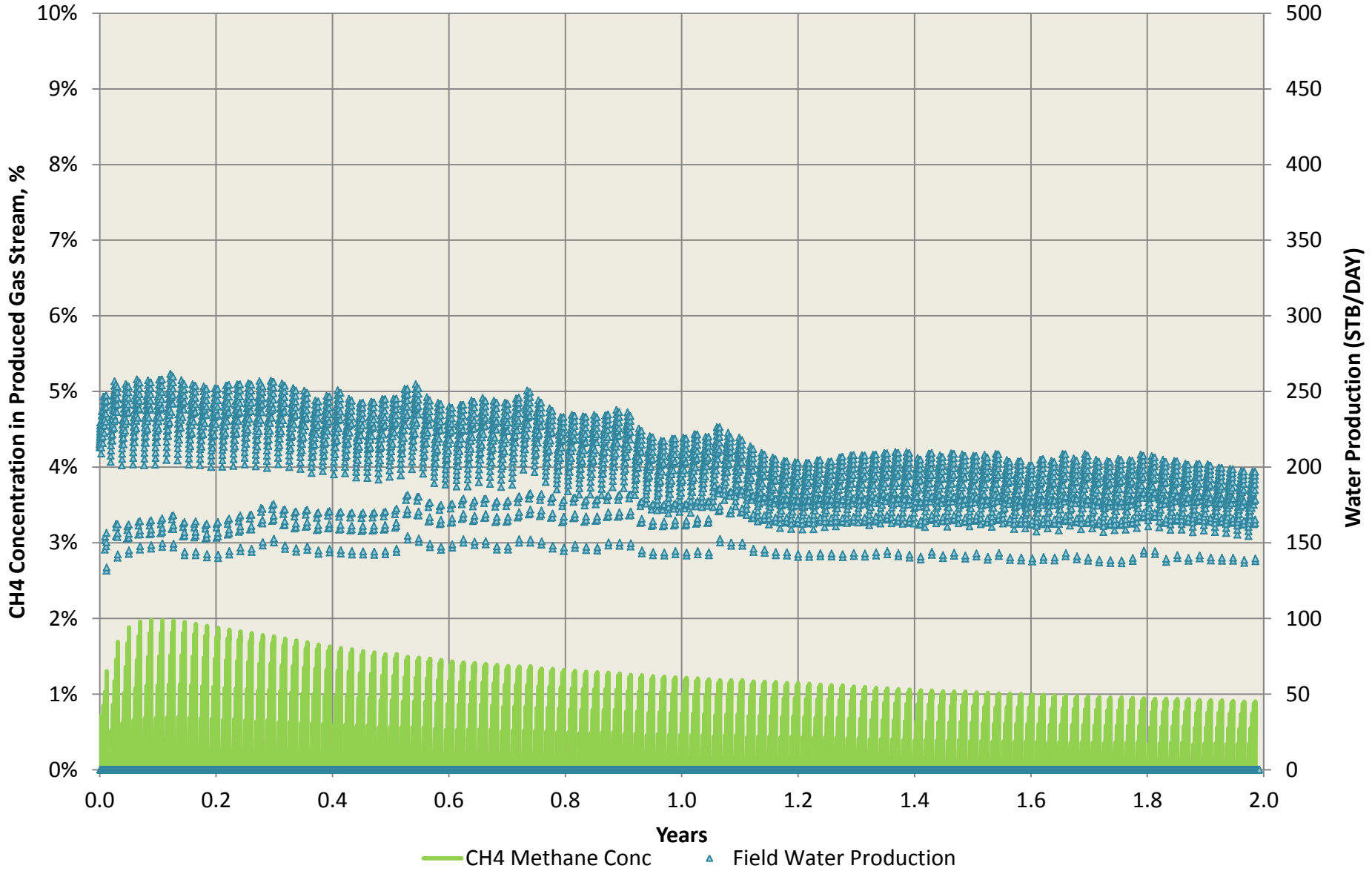

CH4 = Methane
STB = Stock tank barrels

Final Technical Memorandum
for Compressed Air Energy Storage
Reservoir Characterization & Full Field Development Model
King Island Gas Field, San Joaquin County, CA
9/25/2015

Figure 67

CAES Full Field Development - B

Field Methane Concentration in Produced Gas Stream, and Field Water Production

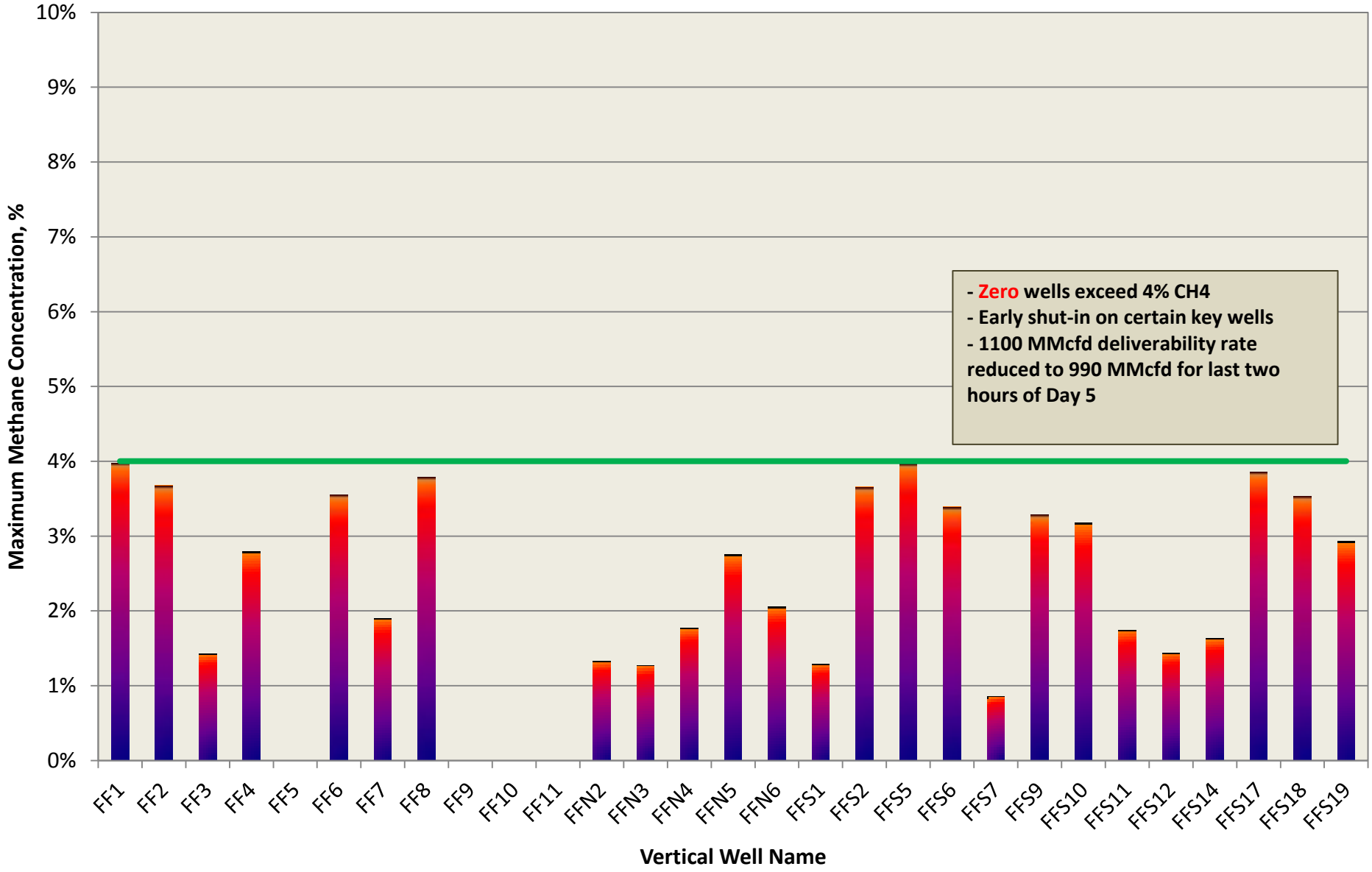

Well Key

FF; FFN and FFS = Simulated full field development wells; north and south

Final Technical Memorandum
for Compressed Air Energy Storage
Reservoir Characterization & Full Field Development Model
King Island Gas Field, San Joaquin County, CA
9/25/2015

Figure 68

CAES Full Field Development - B
Maximum Methane Concentration
During first 2-years of Operation

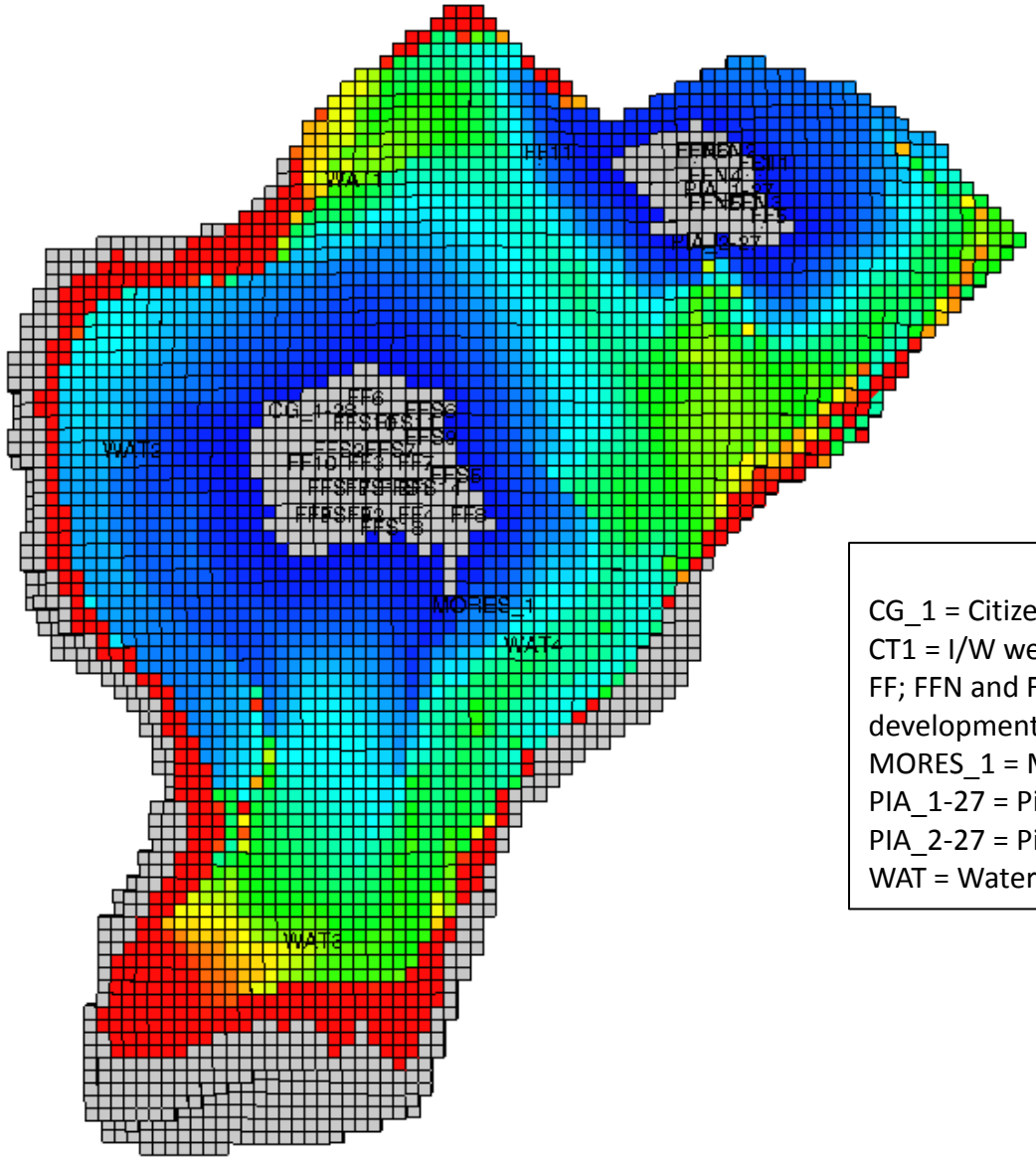

Well Key

CG_1 = Citizen Green 1
CT1 = I/W well
FF; FFN and FFS = Simulated full field development wells; north and south
MORES_1 = Moresco A1
PIA_1-27 = Piacentine 1-27
PIA_2-27 = Piacentine 2-27
WAT = Water production wells

January 7, 2022

Final Technical Memorandum
for Compressed Air Energy Storage
Reservoir Characterization & Full Field Development Model
King Island Gas Field, San Joaquin County, CA
9/25/2015

Figure 69

CAES Full Field Development - B
Aerial View
Methane Composition Mole Fraction, 1-7-2022

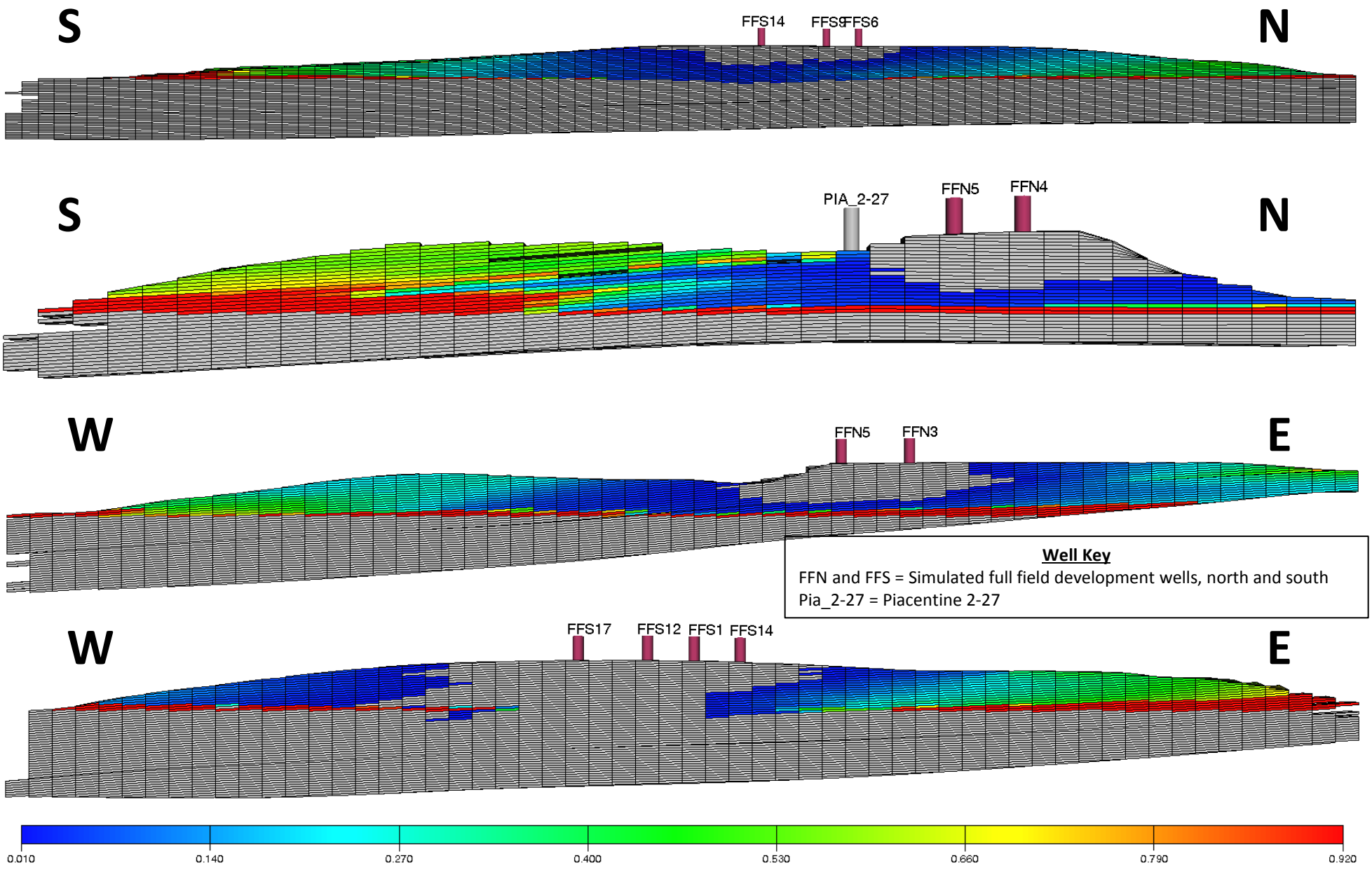

January 7, 2022

Final Technical Memorandum
for Compressed Air Energy Storage
Reservoir Characterization & Full Field Development Model
King Island Gas Field, San Joaquin County, CA
9/25/2015

Figure 70

CAES Full Field Development - B
Cross-Section Views
Methane Composition Mole Fraction, 1-7-2022

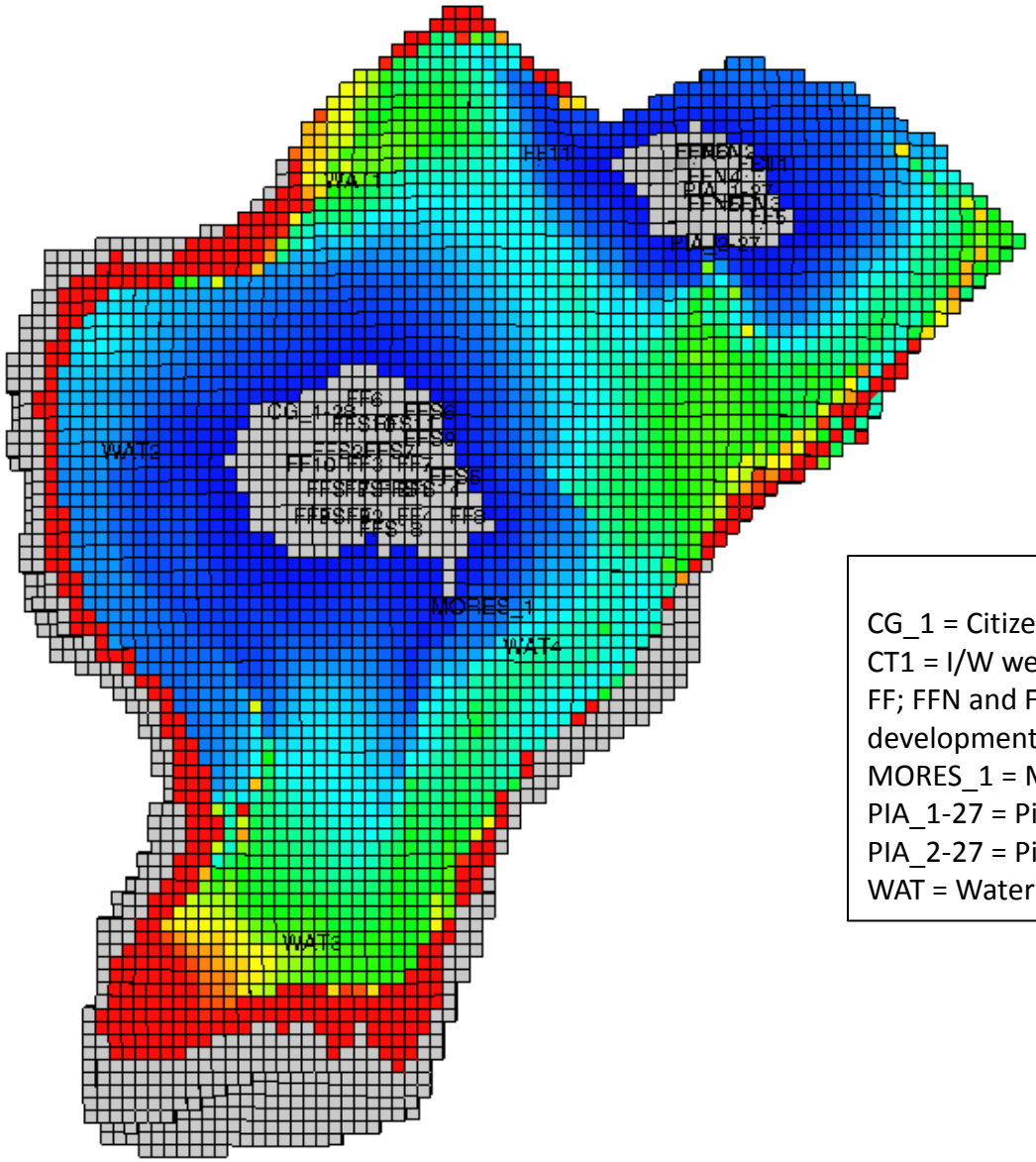

Well Key

CG_1 = Citizen Green 1
CT1 = I/W well
FF; FFN and FFS = Simulated full field development wells; north and south
MORES_1 = Moresco A1
PIA_1-27 = Piacentine 1-27
PIA_2-27 = Piacentine 2-27
WAT = Water production wells

March 11, 2022

Final Technical Memorandum
for Compressed Air Energy Storage
Reservoir Characterization & Full Field Development Model
King Island Gas Field, San Joaquin County, CA
9/25/2015

Figure 71

CAES Full Field Development - B
Aerial View
Methane Composition Mole Fraction, 3-11-2022

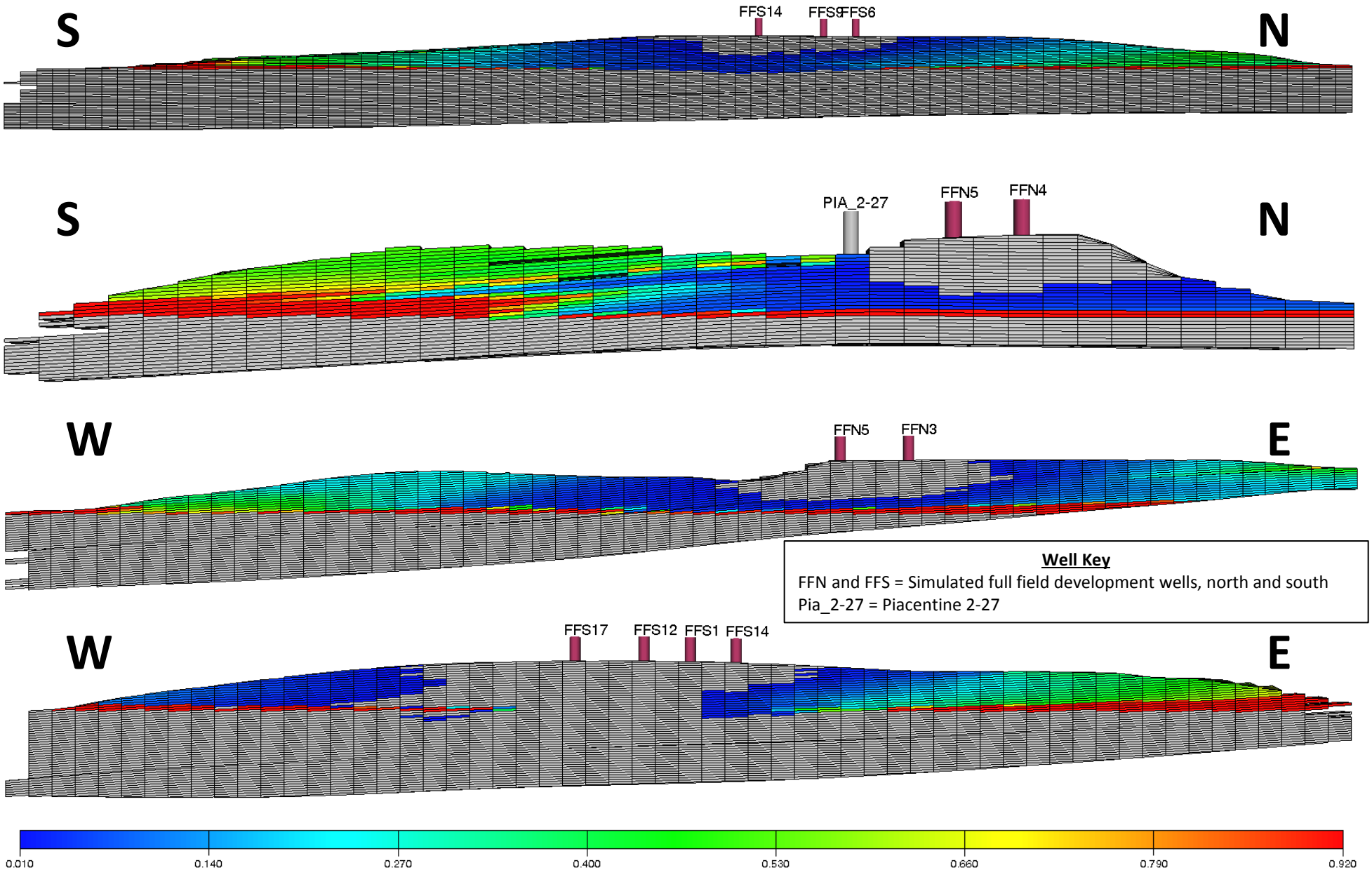

March 11, 2022

Final Technical Memorandum
for Compressed Air Energy Storage
Reservoir Characterization & Full Field Development Model
King Island Gas Field, San Joaquin County, CA
9/25/2015

Figure 72

CAES Full Field Development - B
Cross-Section Views
Methane Composition Mole Fraction, 3-11-2022

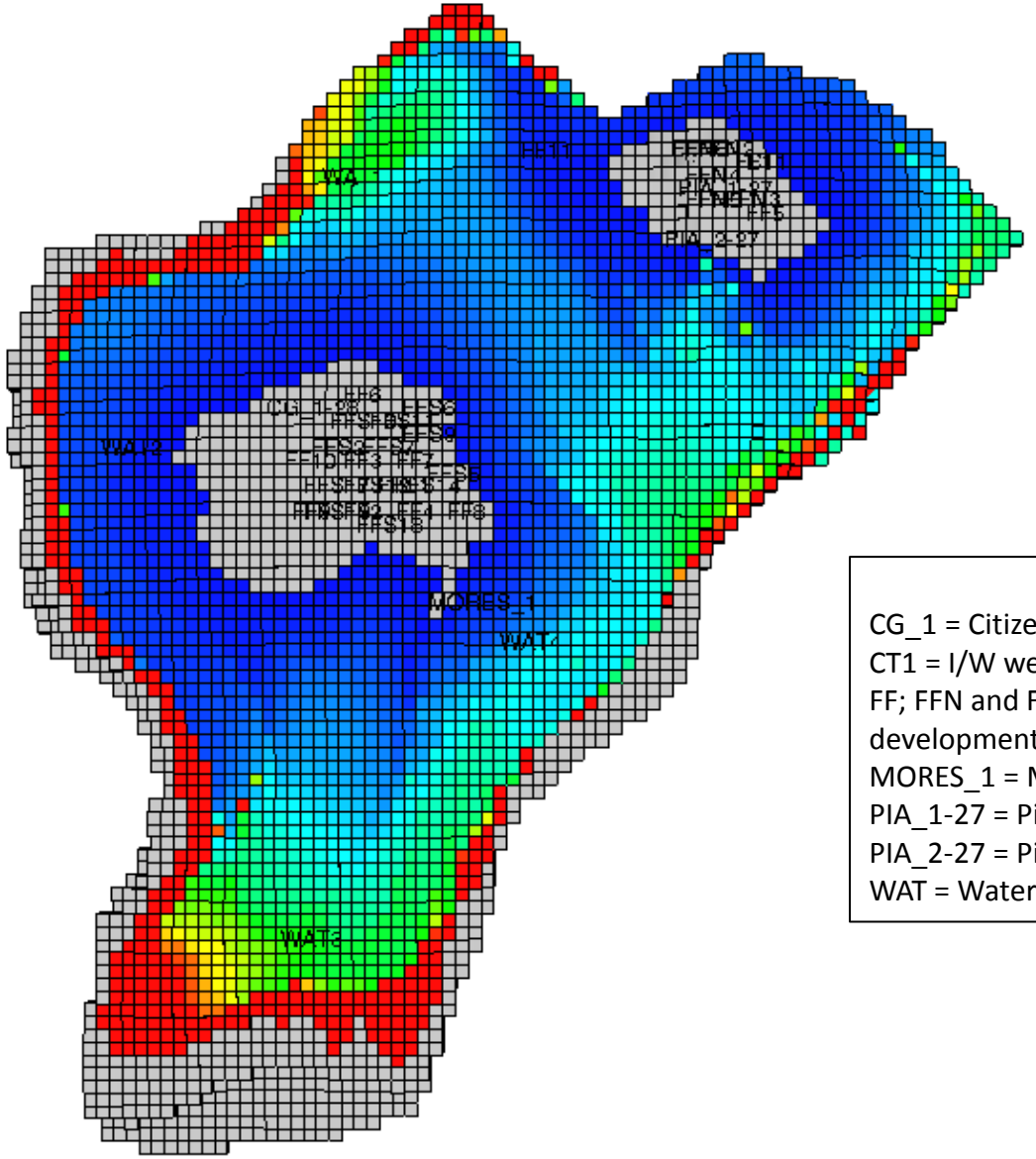

Well Key

CG_1 = Citizen Green 1
CT1 = I/W well
FF; FFN and FFS = Simulated full field development wells; north and south
MORES_1 = Moresco A1
PIA_1-27 = Piacentine 1-27
PIA_2-27 = Piacentine 2-27
WAT = Water production wells

December 23, 2022

Final Technical Memorandum
for Compressed Air Energy Storage
Reservoir Characterization & Full Field Development Model
King Island Gas Field, San Joaquin County, CA
9/25/2015

Figure 73

CAES Full Field Development - B
Aerial View
Methane Composition Mole Fraction, 12-23-2022

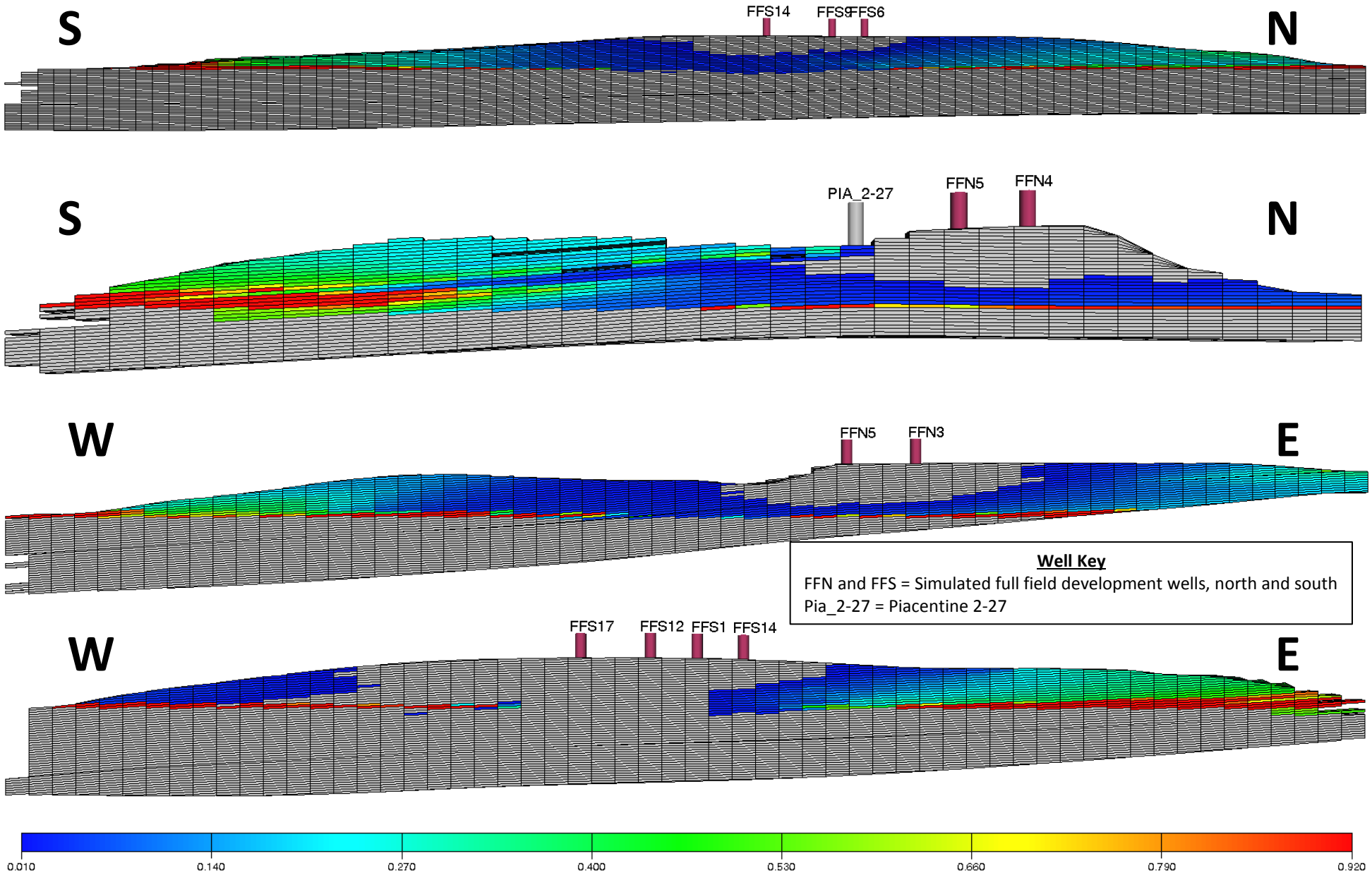

December 23, 2022

Final Technical Memorandum
for Compressed Air Energy Storage
Reservoir Characterization & Full Field Development Model
King Island Gas Field, San Joaquin County, CA
9/25/2015

Figure 74

CAES Full Field Development - B
Cross-Section Views
Methane Composition Mole Fraction, 12-23-2022

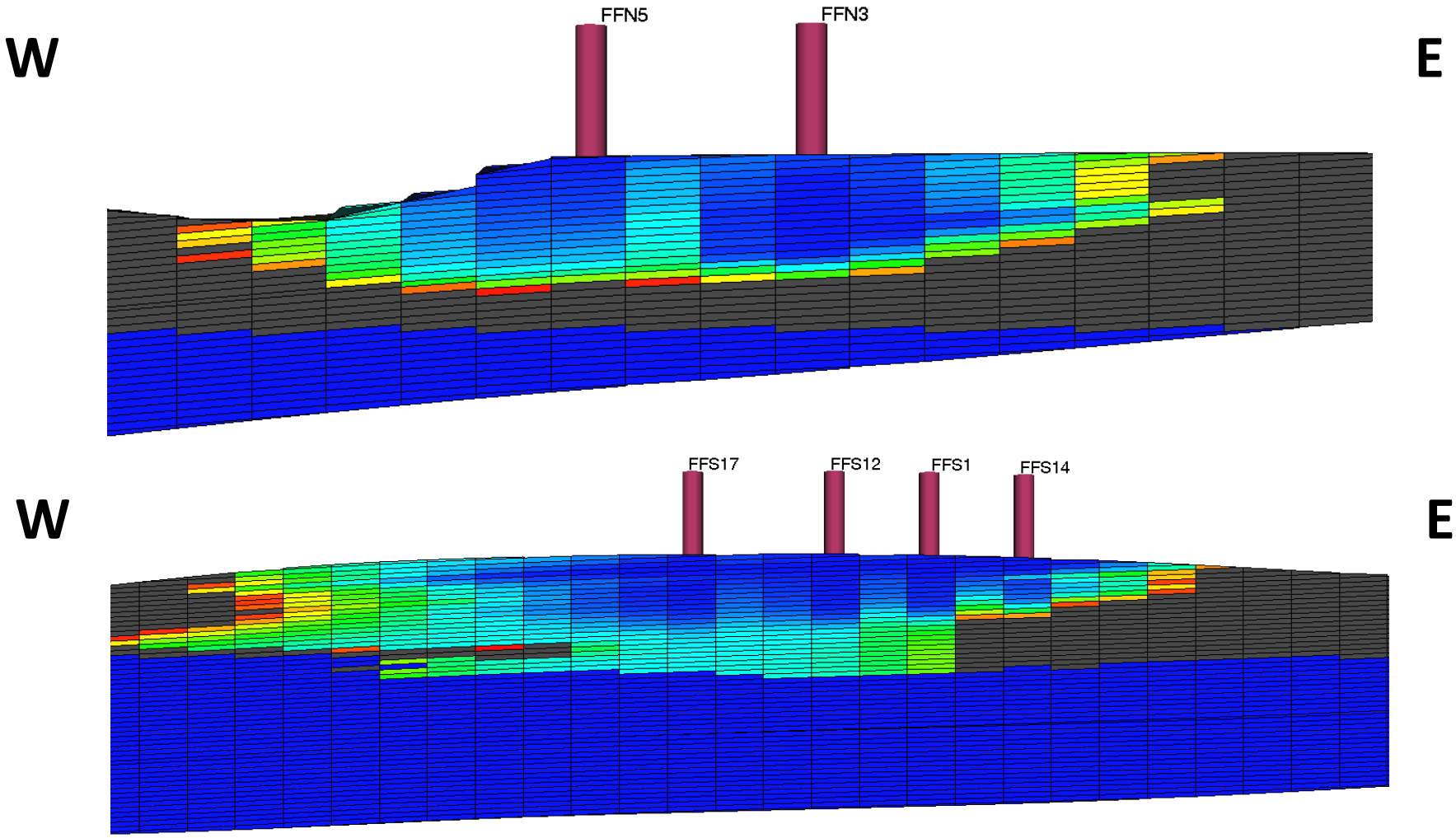

Methane Composition Mole Fraction Range 0.00 to 0.01 Displayed

December 23, 2022

Final Technical Memorandum
for Compressed Air Energy Storage
Reservoir Characterization & Full Field Development Model
King Island Gas Field, San Joaquin County, CA
9/25/2015

Figure 75

CAES Full Field Development - B
Cross-Section View Zoom
Methane Composition Within Air Bubble, 12-23-2022

A602: Flammability Characteristics of Combustible Cases and Vapors

Bulletin 627

BUREAU OF MINES

FLAMMABILITY CHARACTERISTICS OF COMBUSTIBLE GASES AND VAPORS

By Michael G. Zabetakis

MASTER

DISTRIBUTION OF THIS DOCUMENT IS UNLIMITED

DISCLAIMER

This report was prepared as an account of work sponsored by an agency of the United States Government. Neither the United States Government nor any agency Thereof, nor any of their employees, makes any warranty, express or implied, or assumes any legal liability or responsibility for the accuracy, completeness, or usefulness of any information, apparatus, product, or process disclosed, or represents that its use would not infringe privately owned rights. Reference herein to any specific commercial product, process, or service by trade name, trademark, manufacturer, or otherwise does not necessarily constitute or imply its endorsement, recommendation, or favoring by the United States Government or any agency thereof. The views and opinions of authors expressed herein do not necessarily state or reflect those of the United States Government or any agency thereof.

DISCLAIMER

Portions of this document may be illegible in electronic image products. Images are produced from the best available original document.

This publication has been cataloged as follows:

Zabetakis, Michael George, 1924—

Flammability characteristics of combustible gases and vapors. [Washington] U.S. Dept of the Interior, Bureau of Mines [1965]

121 p. illus., tables. (U.S. Bureau of Mines. Bulletin 627)

Includes bibliography.

1. Combustion gases. 2. Gases. 3. Vapors. I. Title. II. Title: Combustible gases. (Series)

TN23.U4 no. 627 622.06173

U.S. Dept. of the Int. Library.

For sale by the Superintendent of Documents, U.S. Government Printing Office
Washington, D.C., 20402 - Price 75 cents

CONTENTS

	Page
Abstract	1
Introduction	1
Definitions and theory	2
Limits of flammability	2
Ignition	3
Formation of flammable mixtures	4
Presentation of data	9
Deflagration and detonation processes	15
Deflagration	15
Detonation	16
Blast pressure	16
Preventive measures	18
Inerting	18
Flame arrestors and relief diaphragms	18
Flammability characteristics	20
Paraffin hydrocarbons	20
Limits in air	20
Limits in other atmospheres	27
Autoignition	32
Burning rate	42
Unsaturated hydrocarbons	47
Limits in air	47
Limits in other atmospheres	50
Autoignition	50
Burning rate	51
Stability	51
Acetylenic hydrocarbons	53
Limits in air	53
Limits in other atmospheres	55
Autoignition	56
Burning rate	56
Stability	57
Aromatic hydrocarbons	59
Limits in air	59
Flammability characteristics—Continued	Page
Aromatic hydrocarbons—Continued	
Limits in other atmospheres	60
Autoignition	62
Burning rate	62
Alicyclic hydrocarbons	63
Limits in air	63
Limits in other atmospheres	64
Alcohols	65
Limits in air	65
Limits in other atmospheres	66
Autoignition	67
Burning rate	68
Ethers	69
Limits in air	69
Limits in other atmospheres	69
Autoignition	70
Esters	70
Aldehydes and ketones	73
Sulfur compounds	74
Fuels and fuel blends	74
Ammonia and related compounds	74
Boron hydrides	82
Gasolines, diesel and jet fuels	82
Hydrogen	89
Hydraulic fluids and engine oils	95
Miscellaneous	97
Acknowledgments	106
Bibliography	107
Appendix A.—Summary limits of flammability	114
Appendix B.—Stoichiometric composition	117
Appendix C.—Heat contents of gases	118
Appendix D.—Definitions of principal symbols	119
Subject index	120

ILLUSTRATIONS

Fig.		Page
1.	Ignitibility curve and limits of flammability for methane-air mixtures at atmospheric pressure and 26° C	2
2.	Effect of temperature on limits of flammability of a combustible vapor in air at a constant initial pressure	3
3.	Time delay before ignition of NPN in air at 1,000 psig in the temperature range from 150° to 210° C	5
4.	Logarithm of time delay before ignition of NPN in air at 1,000 psig initial pressure	6
5.	Simplified mixer	7
6.	Composition of gas in chamber 2, figure 5 (instantaneous mixing)	7
7.	Composition of gas in chamber 2, figure 5 (delayed mixing)	7
8.	Variation in lower limits of flammability of various combustibles in air as a function of droplet diameter	7
9.	Flammability diagram for the system methane-oxygen-nitrogen at atmospheric pressure and 26° C	9
10.	Flammability diagram for the system methane-oxygen-nitrogen at atmospheric pressure and 26° C	10
11.	Effect of initial temperature on limits of flammability of a combustible vapor-inert-air system at atmospheric pressure	11
12.	Effect of initial pressure on limits of flammability of JP-4 in air at 26° C	11

Fig. Page

13. Effect of temperature and pressure on limits of flammability of a combustible vapor in a specified oxident 12
14. Flammability diagram for the system gasoline vapor-water vapor-air at 70° F and at 212° F and atmospheric pressure 13
15. Pressure produced by ignition of a 9.6 volume-percent methane-air mixture in a 9-liter cylinder 15
16. Detonation velocity, V; static pressure, P_s; and reflected pressure, P_r, developed by a detonation wave propagating through hydrogen-oxygen mixtures in a cylindrical tube at atmospheric pressure and 18° C 16
17. Pressure variation following ignition of a flammable mixture in unprotected and protected enclosures 18
18. Pressure produced by ignition of a flammable mixture in a vented oven 19
19. Effect of molecular weight on lower limits of flammability of paraffin hydrocarbons at 25° C 20
20. Effect of temperature on lower limit of flammability of methane in air at atmospheric pressure 22
21. Effect of temperature on lower limits of flammability of 10 paraffin hydrocarbons in air at atmospheric pressure 23
22. Effect of temperature on lower limits of flammability of 10 paraffin hydrocarbons in air at atmospheric pressure by weight 24
23. Effect of temperature on $L_t/L_{25°}$ ratio of paraffin hydrocarbons in air at atmospheric pressure 25
24. Effect of temperature on $U_t/U_{25°}$ ratio of paraffin hydrocarbons in air at atmospheric pressure in the absence of cool flames 26
25. Effect of pressure on limits of flammability of pentane, hexane, and heptane in air at 26° C 26
26. Effect of pressure on limits of flammability of natural gas in air at 28° C 27
27. Effect of pressure on lower temperature limits of flammability of pentane, hexane, heptane, and octane in air 28
28. Limits of flammability of various methane-inert gas-air mixtures at 25° C and atmospheric pressure 29
29. Limits of flammability of ethane-carbon dioxide-air and ethane-nitrogen-air mixtures at 25° C and atmospheric pressure 30
30. Limits of flammability of propane-carbon dioxide-air and propane-nitrogen-air mixtures at 25° C and atmospheric pressure 31
31. Limits of flammability of butane-carbon dioxide-air and butane-nitrogen-air mixtures at 25° C and atmospheric pressure 32
32. Limits of flammability of various n-pentane-inert gas-air mixtures at 25° C and atmospheric pressure 33
33. Limits of flammability of various n-hexane-inert gas-air mixtures at 25° C and atmospheric pressure 34
34. Limits of flammability of n-heptane-water vapor-air mixtures at 100° and 200° C and atmospheric pressure 35
35. Approximate limits of flammability of higher paraffin hydrocarbons (C_nH_{2n+2}, $n \geq 5$) in carbon dioxide-air and nitrogen-air mixtures at 25° C and atmospheric pressure 36
36. Effect of pressure upon limits of flammability of natural gas-nitrogen-air mixtures at 26° C 37
37. Effect of pressure on limits of flammability of ethane-carbon dioxide-air mixtures at 26° C 38
38. Effect of pressure on limits of flammability of ethane-nitrogen-air mixtures at 26° C 39
39. Effect of pressure on limits of flammability of propane-carbon dioxide-air mixtures 40
40. Effect of pressure on limits of flammability of propane-nitrogen-air mixtures 41
41. Effect of pressure on minimum oxygen requirements for flame propagation through natural gas-nitrogen-air, ethane-nitrogen-air, and propane-nitrogen-air mixtures at 26° C 42
42. Low-temperature limit of flammability of decane-air, dodecane-air, and decane-dodecane-air mixtures
43. Minimum autoignition temperatures of paraffin hydrocarbons in air as a function of average carbon chain length 44
44. Burning velocities of methane-, ethane-, propane-, and n-heptane vapor-air mixtures at atmospheric pressure and room temperature 45
45. Burning velocities of methane-, ethane-, and propane-oxygen mixtures at atmospheric pressure and room temperature 46
46. Variation in burning velocity of stoichiometric methane-air and propane-air mixtures with pressure at 26° C 47
47. Variation in burning velocity of stoichiometric methane- and ethylene-oxygen mixtures with pressure at 26° C 48
48. Effect of temperature on burning velocities of four paraffin hydrocarbons in air at atmospheric pressure 49
49. Detonation velocities of methane-air mixtures at atmospheric pressure 49
50. Detonation velocities of methane-, ethane-, propane-, butane-, and hexane-oxygen mixtures at atmospheric pressure 49
51. Detonation velocities of n-heptane vapor in WFNA (white fuming nitric acid)-nitrogen gas mixtures at atmospheric pressure and 400° K 50
52. Relation between liquid-burning rate (large-pool diameter) and ratio of net heat of combustion to sensible heat of vaporization 50
53. Effect of temperature on lower limit of flammability of ethylene in air at atmospheric pressure 50
54. Limits of flammability of ethylene-carbon dioxide-air and ethylene-nitrogen-air mixtures at atmospheric pressure and 26° C 50
55. Limits of flammability of propylene-carbon dioxide-air and propylene-nitrogen-air mixtures at atmospheric pressure and 26° C 51
56. Limits of flammability of isobutylene-carbon dioxide-air and isobutylene-nitrogen-air mixtures at atmospheric pressure and 26° C 52
57. Limits of flammability of isobutylene-water vapor-oxygen mixtures at 150° C and atmospheric pressure 53
58. Limits of flammability of butene-1-carbon dioxide-air and butene-1-nitrogen-air mixtures at atmospheric pressure and 26° C 54
59. Limits of flammability of 3 methyl butene-1-carbon dioxide-air and 3 methyl-butene-1-nitrogen-air mixtures at atmospheric pressure and 26° C 54

Fig. Page
60. Limits of flammability of butadiene-carbon dioxide-air and butadiene-nitrogen-air mixtures at atmospheric pressure and 26° C 55
61. Effect of tube diameter on initial pressure requirements for propagation of deflagration and detonation through acetylene gas 56
62. Range of flammable mixtures for methylacetylene-propadiene-propylene system at 120° C and at 50 and 100 psig 57
63. Quenched limits of flammability of acetylene-carbon dioxide-air and acetylene-nitrogen-air mixtures at atmospheric pressure and 26° C obtained in a 2-inch tube 58
64. Minimum autoignition temperatures of acetylene-air and acetylene-oxygen mixtures at atmospheric and elevated pressures 58
65. Burning velocity of acetylene-air mixtures at atmospheric pressure and room temperature 59
66. Maximum L/D ratio required for transition of a deflagration to a detonation in acetylene vapor at 60° F and from 10 to 70 psia 59
67. Final-to-initial pressure ratios developed by acetylene with detonation initiation at various points along a tube 60
68. Limits of flammability of benzene-methyl bromide-air mixtures at 25° C and benzene-carbon dioxide-air and benzene-nitrogen-air mixtures at 25° and 150° C and atmospheric pressure 61
69. Limits of flammability of H_2O_2-C_6H_4·$(CH_3)_2$-H_2O at 154° C and 1 atmosphere pressure 62
70. Limits of flammability of 90-weight-percent H_2O_2-C_6H_4·$(CH_3)_2$-HCOOH at 154° C and 1 atmosphere pressure 63
71. Minimum autoignition temperatures of aromatic hydrocarbons in air as a function of correlation parameter L_{ave} 64
72. Limits of flammability of cyclopropane-carbon dioxide-air, cyclopropane-nitrogen-air, and cyclopropane-helium-air mixtures at 25° C and atmospheric pressure 65
73. Limits of flammability of cyclopropane-helium-oxygen and cyclopropane-nitrous oxide-oxygen mixtures at 25° C and atmospheric pressure 66
74. Limits of flammability of cyclopropane-helium-nitrous oxide mixtures at 25° C and atmospheric pressure 66
75. Limits of flammability of methyl alcohol-carbon dioxide-air and methyl alcohol-nitrogen-air mixtures at 25° C and atmospheric pressure 66
76. Limits of Flammability of methyl alcohol-water vapor-air mixtures at 100°, 200°, and 400° C and atmospheric pressure 67
77. Limits of flammability of ethyl alcohol-carbon dioxide-air and ethyl alcohol-nitrogen-air mixtures at 25° C and atmospheric pressure 68
78. Limits of flammability of ethyl alcohol-water vapor-air mixtures at 100° C and atmospheric pressure 68
79. Limits of flammability of *tert*-butyl alcohol-water vapor-air mixtures at 150° C and atmospheric pressure 68
80. Limits of flammability of *tert*-butyl alcohol-carbon dioxide-oxygen mixtures at 150° C and atmospheric pressure 68
81. Limits of flammability of 2-ethylbutanol-nitrogen-oxygen mixtures at 150° C and atmospheric pressure 69
82. Limits of flammability of dimethyl ether-carbon dioxide-air and dimethyl ether-nitrogen-air mixtures at 25° C and atmospheric pressure 69
83. Limits of flammability of diethyl ether-carbon dioxide-air and diethyl ether-nitrogen-air mixtures at 25° C and atmospheric pressure 69
84. Limits of flammability of diethyl ether-helium-oxygen and diethyl ether-nitrous oxide-oxygen mixtures at 25° C and atmospheric pressure 70
85. Limits of flammability of diethyl ether-nitrous oxide-helium mixtures at 25° C and atmospheric pressure 70
86. Limits of flammability of methyl formate-carbon dioxide-air and methyl formate-nitrogen-air mixtures 71
87. Limits of flammability of isobutyl formate-carbon dioxide-air and isobutyl formate-nitrogen-air mixtures 72
88. Limits of flammability of methyl acetate-carbon dioxide-air and methyl acetate-nitrogen-air mixtures 72
89. Effect of temperature on lower limits of flammability of MEK-toluene mixtures in air at atmospheric pressure 73
90. Effect of temperature on lower limits of flammability of THF-toluene mixtures in air at atmospheric pressure 74
91. Effect of liquid composition on lower limits of flammability of MEK-toluene mixtures in air at 30° and 200° C 75
92. Effect of liquid composition on lower limits of flammability of THF-toluene mixtures in air at 30° and 200° C 76
93. Limits of flammability of acetone-carbon dioxide-air and acetone-nitrogen-air mixtures 77
94. Limits of flammability of methyl ethyl ketone (MEK)-chlorobromomethane (CBM)-air, MEK-carbon dioxide-air and MEK-nitrogen-air mixtures at 25° C and atmospheric pressure 78
95. Limits of flammability of carbon disulfide-carbon dioxide-air, carbon dioxide-nitrogen-air mixtures at 25° C and atmospheric pressure, and carbon disulfide-water vapor-air at 100° C and atmospheric pressure 79
96. Limits of flammability of hydrogen sulfide-carbon dioxide-air mixtures at 25° C and atmospheric pressure 79
97. Limits of flammability of ethyl mercaptan-F-12-air and ethyl mercaptan-F-22-air mixtures at atmospheric pressure and 27° C 79
98. Limits of flammability of ammonia, UDMH, MMH, and hydrazine at atmospheric pressure in saturated and near-saturated vapor-air mixtures 80
99. Flammable mixture compositions of hydrazine-heptane-air at 125° C and approximately atmospheric pressure 81
100. Minimum spontaneous ignition temperatures of liquid hydrazine, MMH, and UDMH at an initial temperature of 25° C in contact with NO_2*-air mixtures at 740±10 mm Hg as a function of NO_2* concentration 82
101. Minimum spontaneous ignition temperatures of liquid hydrazine at various initial temperatures in NO_2*-air mixtures at 740±10 mm Hg as a function of NO_2* concentration 83

Fig. Page
102. Minimum spontaneous ignition temperatures of liquid MMH at various initial temperatures in NO_2*-air mixtures at 740±10 mm Hg as a function of NO_2* concentration 84
103. Minimum spontaneous ignition temperatures of liquid UDMH at various initial temperatures in NO_2*-air mixtures at 740±10 mm Hg as a function of NO_2* concentration 85
104. Minimum spontaneous ignition temperatures of 0.05 cc of liquid UDMH in He-O_2-NO_2* atmospheres at 1 atmosphere for various He/O_2 ratios 86
105. Minimum spontaneous ignition temperatures of 0.05 cc of liquid UDMH in NO_2*-air mixtures at 15 and 45 psia as a function of NO_2* concentration 87
106. Minimum spontaneous ignition temperatures of vaporized UDMH-air mixtures in contact with 100 pct NO_2* at 25° C and 740±10 mm Hg as a function of UDMH concentration in air 87
107. Limits of flammability of diborane-ethane-air mixtures at laboratory temperatures and 300 mm Hg initial pressure 88
108. ASTM distillation curves for, *A*, aviation gasoline, grade 100/130; *B*, aviation gasoline, grade 115/145; *C*, aviation jet fuel, grade JP–1; *D*, aviation jet fuel, grade JP–3; and, *E*, aviation jet fuel, grade JP–4 88
109. Limits of flammability of aviation gasoline, grades 115/145 vapor-carbon dioxide-air and 115/145 vapor-nitrogen-air, at 27° C and atmospheric pressure 88
110. Limits of flammability of JP–4 vapor-carbon dioxide-air and JP–4 vapor-nitrogen-air mixtures at 27° C and atmospheric pressure 88
111. Limits of flammability of hydrogen-carbon dioxide-air and hydrogen-nitrogen-air mixtures at 25° C and atmospheric pressure 89
112. Limits of flammability of H_2-NO-N_2O at approximately 28° C and 1 atmosphere 90
113. Limits of flammability of H_2-N_2O-air at approximately 28° C and 1 atmosphere 91
114. Limits of flammability of H_2-NO-air at approximately 28° C and 1 atmosphere 92
115. Rate of vaporization of liquid hydrogen from paraffin in a 2.8-inch Dewar flask: Initial liquid depth—6.7 inches 93
116. Theoretical liquid regression rates following spillage of liquid hydrogen onto, *A*, an average soil; *B*, moist sandy soil; and *C*, dry sandy soil 93
117. Theoretical decrease in liquid hydrogen level following spillage onto, *A*, dry sandy soil; *B*, moist sandy soil; and *C*, an average soil 94
118. Extent of flammable mixtures and height of visible cloud formed after rapid spillage of 3 liters of liquid hydrogen on a dry macadam surface in a quiescent air atmosphere at 15° C 94
119. Motion picture sequence of visible clouds and flames resulting from rapid spillage of 7.8 liters of liquid hydrogen on a gravel surface at 18° C 95
120. Maximum flame height and width produced by ignition of vapor-air mixtures formed by sudden spillage of 2.8 to 89 liters of liquid hydrogen 96
121. Burning rates of liquid hydrogen and of liquid methane at the boiling points in 6-inch-Pyrex Dewar flasks 96
122. Variation in minimum autoignition temperature with pressure of commercial phosphate ester and mineral oil lubricants in air in a 450-cc-stainless steel bomb 98
123. Logarithm of initial pressure-AIT ratio of seven fluids in air for various reciprocal temperatures 99
124. Variation in T_f/T_i of air with V_i/V_f and with P_f/P_i in an adiabatic compression process 100
125. Variation in air temperature with P_f/P_i in an adiabatic compression process for five initial air temperatures 101
126. Limits of flammability of carbon monoxide-carbon dioxide-air and carbon monoxide-nitrogen-air mixtures at atmospheric pressure and 26° C 102
127. Lower limits of flammability of NPN vapor-air mixtures over the pressure range from 0 to 1,000 psig at 75°, 125°, 150° and 170° C 102
128. Flammable NPN vapor-air mixtures formed over the pressure range from 0 to 1,000 psig at 50° and 125° C 103
129. Variation of explosion pressure following spontaneous ignition with NPN concentration 104
130. Minimum spontaneous ignition and decomposition temperatures of *n*-propyl nitrate in air as a function of pressure 104
131. Flammability of trichloroethylene-air mixtures 105

TABLES

Page
1. Conditions of failure of peak overpressure-sensitive elements 17
2. Properties of paraffin hydrocarbons 21
3. Upper flammability limits of methane-air mixtures at 15 psig 24
4. Lower temperature limits and autoignition temperatures of paraffin hydrocarbons at atmospheric pressure 25
5. Limits of flammability of methane in chlorine 27
6. Limits of flammability of ethane in chlorine 28
7. Properties of unsaturated hydrocarbons 48
8. Limits of flammability of unsaturated hydrocarbons at atmospheric pressure and room temperature, in volume-percent combustible vapor 52
9. Minimum autoignition temperatures of unsaturated hydrocarbons at atmospheric pressure 52
10. Heats of formation of unsaturated hydrocarbons at 25° C 53
11. Properties of selected aromatic hydrocarbons 60

Page

12. Properties of selected alicyclic hydrocarbons ---- 64
13. Properties of selected simple alcohols ---- 67
14. Properties of selected ethers ---- 70
15. Properties of selected esters ---- 71
16. Properties of selected aldehydes and ketones ---- 73
17. Properties of selected sulfur compounds ---- 74
18. Properties of selected fuels and fuel blends ---- 77
19. Limits of flammability of ammonia at room temperature and near atmospheric pressure ---- 78
20. Autoignition temperature values of various fuels in air at 1 atmosphere ---- 88
21. Limits of flammability of hydrogen in various oxidants at 25° C and atmospheric pressure ---- 89

A–1. Summary of limits of flammability, lower temperature limits, and minimum autoignition temperatures of individual gases and vapors in air at atmospheric pressure ---- 114

FLAMMABILITY CHARACTERISTICS OF COMBUSTIBLE GASES AND VAPORS

by

Michael G. Zabetakis [1]

Abstract

THIS is a summary of the available limit of flammability, autoignition, and burning-rate data for more than 200 combustible gases and vapors in air and other oxidants, as well as of empirical rules and graphs that can be used to predict similar data for thousands of other combustibles under a variety of environmental conditions. Specific data are presented on the paraffinic, unsaturated, aromatic, and alicyclic hydrocarbons, alcohols, ethers, aldehydes, ketones, and sulfur compounds, and an assortment of fuels, fuel blends, hydraulic fluids, engine oils, and miscellaneous combustible gases and vapors.

Introduction

Prevention of unwanted fires and gas explosion disasters requires a knowledge of flammability characteristics (limits of flammability, ignition requirements, and burning rates) of pertinent combustible gases and vapors likely to be encountered under various conditions of use (or misuse). Available data may not always be adequate for use in a particular application since they may have been obtained at a lower temperature and pressure than is encountered in practice. For example, the quantity of air that is required to decrease the combustible vapor concentration to a safe level in a particular process carried out at 200 °C should be based on flammability data obtained at this temperature. When these are not available, suitable approximations can be made to permit a realistic evaluation of the hazards associated with the process being considered; such approximations can serve as the basis for designing suitable safety devices for the protection of personnel and equipment.

The purpose of this bulletin is to present a general review of the subject of flammability, and to supply select experimental data and empirical rules on the flammability characteristics of various families of combustible gases and vapors in air and other oxidizing atmospheres. It contains what are believed to be the latest and most reliable data for more than 200 combustibles of interest to those concerned with the prevention of disastrous gas explosions. In addition, the empirical rules and graphs presented here can be used to predict similar data for other combustibles under a variety of conditions. This bulletin supplements Bureau bulletins (*40*)[2] and other publications (*158*).

Basic knowledge of combustion is desirable for a thorough understanding of the material, which can be found in numerous publications (*69*, *199*, *202*). Therefore, only those aspects required for an understanding of flammability are considered here; even these are considered from a fairly elementary viewpoint.

[1] Physical chemist, project coordinator, Gas Explosions, Explosives Research Center, Bureau of Mines, Pittsburgh, Pa.

[2] Italicized numbers in parentheses refer to items in the bibliography at the end of this report.

Work on manuscript completed May 1964.

DEFINITIONS AND THEORY

LIMITS OF FLAMMABILITY

A combustible gas-air mixture can be burned over a wide range of concentrations—when either subjected to elevated temperatures or exposed to a catalytic surface at ordinary temperatures. However, homogeneous combustible gas-air mixtures are flammable, that is, they can propagate flame freely within a limited range of compositions. For example, trace amounts of methane in air can be readily oxidized on a heated surface, but a flame will propagate from an ignition source at ambient temperatures and pressures only if the surrounding mixture contains at least 5 but less than 15 volume-percent methane. The more dilute mixture is known as the lower limit, or combustible-lean limit, mixture; the more concentrated mixture is known as the upper limit, or combustible-rich limit, mixture. In practice, the limits of flammability of a particular system of gases are affected by the temperature, pressure, direction of flame propagation, gravitational field strength, and surroundings. The limits are obtained experimentally by determining the limiting mixture compositions between flammable and nonflammable mixtures (*244*). That is,

$$L_{T,P}=1/2[C_{gn}+C_{1f}], \quad (1)$$

and

$$U_{T,P}=1/2[C_{gf}+C_{1n}], \quad (2)$$

where $L_{T,P}$ and $U_{T,P}$ are the lower and upper limits of flammability, respectively, at a specified temperature and pressure, C_{gn} and C_{1n} are the greatest and least concentrations of fuel in oxidant that are nonflammable, and C_{1f} and C_{gf} are the least and greatest concentrations of fuel in oxidant that are flammable. The rate at which a flame propagates through a flammable mixture depends on a number of factors including temperature, pressure, and mixture composition. It is a minimum at the limits of flammability and a maximum at near stoichiometric mixtures (*130*).

The Bureau of Mines has adopted a standard apparatus for limit-of-flammability determinations (*40*). Originally designed for use at atmospheric pressure and room temperature, it was later modified for use at reduced pressures by incorporating a spark-gap ignitor in the base of the 2-inch, glass, flame-propagation tube. This modification introduced a difficulty that was not immediately apparent, as the spark energy was not always adequate for use in limit-of-flammability determinations. Figure 1 illustrates the effect of mixture composition on the electrical spark energy requirements for

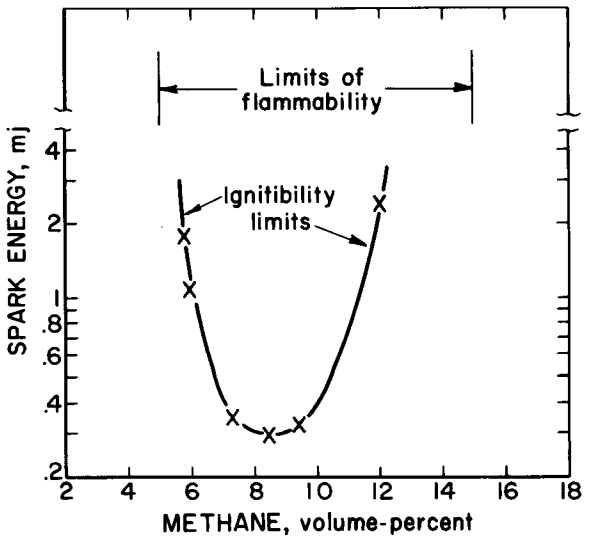

FIGURE 1.—Ignitibility Curve and Limits of Flammability for Methane-Air Mixtures at Atmospheric Pressure and 26° C.

ignition of methane-air mixtures (*75*). For example, a 0.2-millijoule (mj) spark is inadequate to ignite even a stoichiometric mixture at atmospheric pressure and 26° C; a 1-mj spark can ignite mixtures containing between 6 and 11.5 volume-percent methane, etc. Such limit-mixture compositions that depend on the ignition source strength may be defined as limits of ignitibility or more simply ignitibility limits; they are thus indicative of the igniting ability of the energy source. Limit mixtures that are essentially independent of the ignition source strength and that give a measure of the ability of a flame to propagate away from the ignition source may be defined as limits of flammability. Considerably greater spark energies are required to establish limits of flammability than are required for limits of ignitibility (*218*); further, more energy is usually required to establish the upper limit than is required to establish the lower limit. In general, when the source strength is adequate, mixtures just outside the range of flammable compositions yield flame caps when ignited. These flame caps propagate only a short distance from the ignition source in a uniform mixture. The reason for this may be seen in figure 2 which shows the effect of temperature on limits of flammability at a constant initial pressure. As the temperature is increased, the lower limit decreases and the upper limit increases. Thus, since a localized energy source elevates the temperature of nearby gases, even a nonflammable mixture can propagate flame a short distance from the

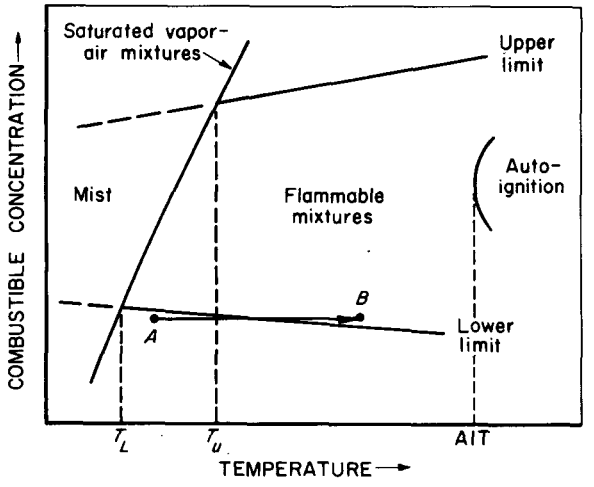

FIGURE 2.—Effect of Temperature on Limits of Flammability of a Combustible Vapor in Air at a Constant Initial Pressure.

source. That is, a nonflammable mixture (for example, composition-temperature point *A*, fig. 2) may become flammable for a time, if its temperature is elevated sufficiently (composition-temperature point *B*).

Flammable mixtures considered in figure 2 fall in one of three regions. The first is left of the saturated vapor-air mixtures curve, in the region labeled "Mist". Such mixtures consist of droplets suspended in a vapor-air mixture; they are discussed in greater detail in the section on formation of flammable mixtures. The second lies along the curve for saturated vapor-air mixtures; the last and most common region lies to the right of this curve. Compositions in the second and third regions make up the saturated and unsaturated flammable mixtures of a combustible-oxidant system at a specified pressure.

In practice, complications may arise when flame propagation and flammability limit determinations are made in small tubes. Since heat is transferred to the tube walls from the flame front by radiation, conduction, and convection, a flame may be quenched by the surrounding walls. Accordingly, limit determinations must be made in apparatus of such a size that wall quenching is minimized. A 2-inch-ID vertical tube is suitable for use with the paraffin hydrocarbons (methane, ethane, etc.) at atmospheric pressure and room temperature. However, such a tube is neither satisfactory under these conditions for many halogenated and other compounds nor for paraffin hydrocarbons at very low temperatures and pressures (*197*, *244*).

Because of the many difficulties associated with choosing suitable apparatus, it is not surprising to find that the very existence of the limits of flammability has been questioned. After a thorough study, Linnett and Simpson concluded that while fundamental limits may exist there is no experimental evidence to indicate that such limits have been measured (*132*). In a more recent publication, Mullins reached the same conclusion (*154*). Accordingly, the limits of flammability obtained in an apparatus of suitable size and with a satisfactory ignition source should not be termed fundamental or absolute limits until the existence of such limits has been established. However, as long as experimentally determined limits are obtained under conditions similar to those found in practice, they may be used to design installations that are safe and to assess potential gas-explosion hazards.

Industrially, heterogeneous single-phase (gas) and multi-phase (gas, liquid, and solid) flammable mixtures are probably even more important than homogeneous gas mixtures. Unfortunately, our knowledge of such mixtures is rather limited. It is important to recognize, however, that heterogeneous mixtures can ignite at concentrations that would normally be nonflammable if the mixture were homogeneous. For example, 1 liter of methane can form a flammable mixture with air near the top of a 100-liter container, although a nonflammable (1.0 volume-percent) mixture would result if complete mixing occurred at room temperature. This is an important concept, since layering can occur with any combustible gas or vapor in both stationary and flowing mixtures. Roberts, Pursall, and Sellers (*176–180*) have presented an excellent series of review articles on the layering and dispersion of methane in coal mines.

The subject of flammable sprays, mists, and foams is well-documented (*5*, *18*, *22*, *27*, *76*, *205*, *215*, *245*). Again, where such heterogeneous mixtures exist, flame propagation can occur at so-called average concentrations well below the lower limit of flammability (*86*); thus, the term "average" may be meaningless when used to define mixture composition in heterogeneous systems.

IGNITION

Lewis and von Elbe (*130*). Mullins (*153*, *154*), and Belles and Swett (*156*) have prepared excellent reviews of the processes associated with spark-ignition and spontaneous-ignition of a flammable mixture. In general, many flammable mixtures can be ignited by sparks having a relatively small energy content (1 to 100 mj) but a large power density (greater than 1 megawatt/cm^3). However, when the source energy is diffuse, as in a sheet discharge, even the total energy requirements for ignition

may be extremely large (*79, 82, 85, 123, 181, 228*). There is still much to be learned in this field, however, since electrical discharges are not normally as well defined in practice as they are in the laboratory.

When a flammable mixture is heated to an elevated temperature, a reaction is initiated that may proceed with sufficient rapidity to ignite the mixture. The time that elapses between the instant the mixture temperature is raised and that in which a flame appears is loosely called the time lag or time delay before ignition. In general, this time delay decreases as the temperature increases. According to Semenov (*193*), these quantities are related by the expression

$$\log \tau = \frac{0.22E}{T} + B, \qquad (3)$$

where τ is the time delay before ignition in seconds; E is an apparent activation energy for the rate controlling reaction in calories per mole; T is the absolute temperature, expressed in degrees, Kelvin; and B is a constant. Two types of ignition temperature data are found in the current literature. In the first, the effect of temperature on time delay is considered for delays of less than 1 second (*127, 153*). Such data are applicable to systems in which the contact time between the heated surface and a flowing flammable mixture is very short; they are not satisfactory when the contact time is indefinite. Further, equation (3) is of little help, because it gives only the time delay for a range of temperatures at which autoignition occurs; if the temperature is reduced sufficiently, ignition does not occur. From the standpoint of safety, it is the lowest temperature at which ignition can occur that is of interest. This is called the minimum spontaneous-ignition, or autoignition, temperature (AIT) and is determined in a uniformly heated apparatus that is sufficiently large to minimize wall quenching effects (*194, 237*). Figures 3 and 4 illustrate typical autoignition-temperature data. In figure 3 the minimum autoignition-temperature or AIT value for *n*-propyl nitrate is 170° C at an initial pressure of 1,000 psig (*243*). Data in this figure may be used to construct a log τ versus $\frac{1}{T}$ plot such as that in figure 4. Such graphs illustrate the applicability of equation (3) to autoignition temperature data. The equation of the broken line in figure 4 is

$$\log \tau = \frac{12.3 \times 10^3}{T} - 25.1. \qquad (4)$$

In this specific case, equation (4) is applicable only in the temperature range from 170° to 195° C; another equation must be used for data at higher temperatures. The solid lines in figure 4 define an 8 C° band that includes the experimental points in the temperature range from 170° to 195° C.

FORMATION OF FLAMMABLE MIXTURES

In practice, heterogeneous mixtures are always formed when two gases or vapors are first brought together. Before discussing the formation of such mixtures in detail, a simplified mixer such as that shown in figure 5 will be considered briefly. This mixer consists of chambers 1 and 2 containing gases A and B, respectively; chamber 2, which contains a stirrer, is separated from chamber 1 and piston 3 by a partition with a small hole, H. At time t_o, a force F applied to piston 3 drives gas A into chamber 2 at a constant rate. If gas A is distributed instantaneously throughout chamber 2 as soon as it passes through H, a composition diagram such as that given in figure 6 results; the (uniform) piston motion starts at t_o and stops at t_F. However, if a time interval Δt is required to distribute a samll volume from chamber 1 throughout chamber 2, then at any instant between t_o and $t_F + \Delta t$, a variety of mixture compositions exists in chamber 2. This situation is represented schematically in figure 7. The interval of time during which heterogeneous gas mixtures would exist in the second case is determined in part by the rate at which gas A is added to chamber 2, by the size of the two chambers, and by the efficiency of the stirrer.

In practice, flammable mixtures may form either by accident or design. When they are formed by accident, it is usually desirable to reduce the combustible concentration quickly by adding enough air or inert gas to produce nonflammable mixtures. Under certain conditions, it may be possible to increase the combustible concentration so as to produce a nonflammable mixture. Such procedures are discussed in greater detail in the following section.

Flammable mixtures are encountered in production of many chemicals and in certain physical operations. These include gasfreeing a tank containing a combustible gas (*232*), drying plastic-wire coating, and recovering solvent from a solvent-air mixture. When layering can occur, as in drying operations, it is not enough to add air at such a rate that the overall mixture composition is below the lower limit of flammability (assuming that uniform mixtures result). Special precautions must be taken to assure the rapid formation of nonflammable mixtures (*235*). When a batch

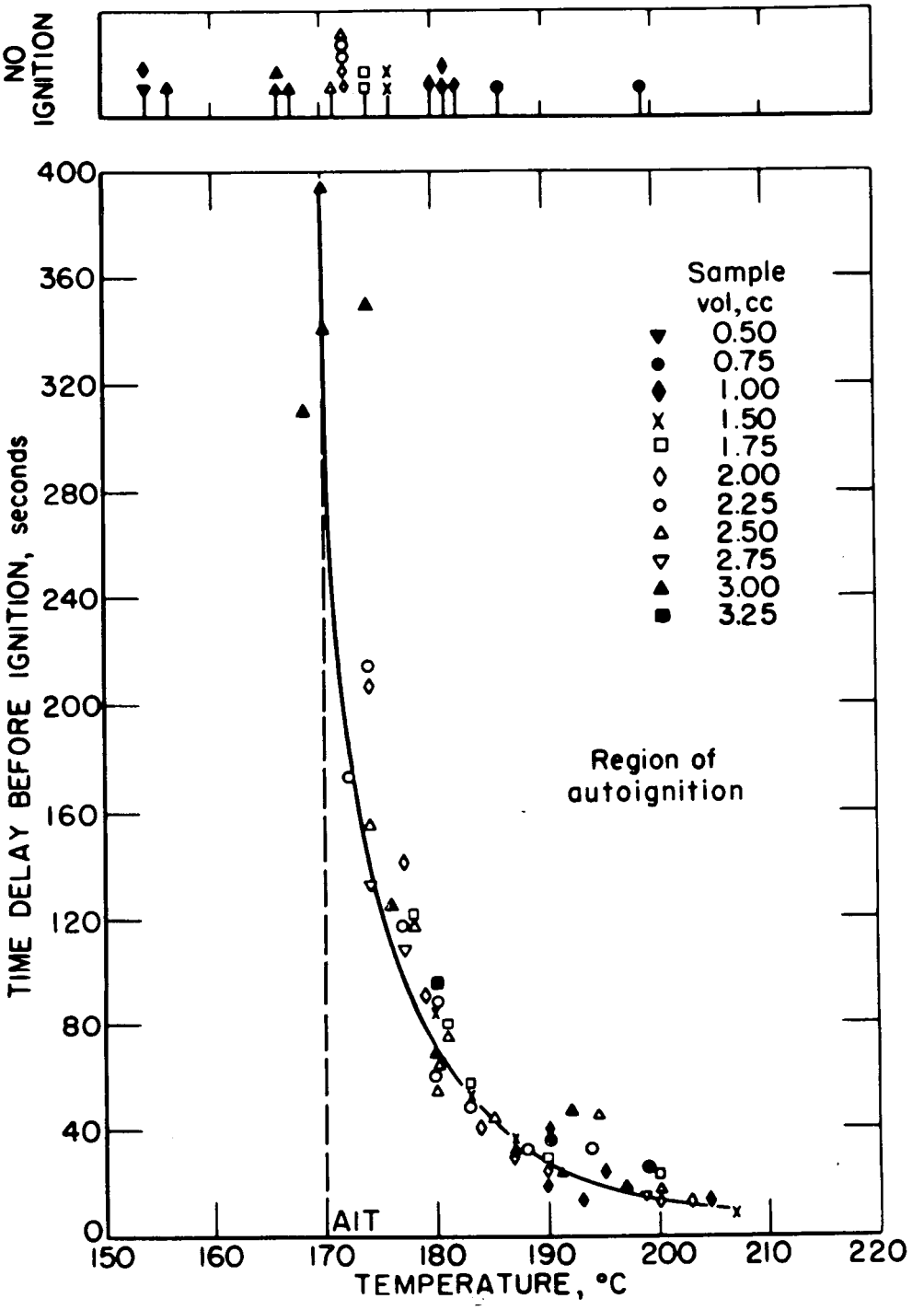

FIGURE 3.—Time Delay Before Ignition of NPN in Air at 1,000 Psig in the Temperature Range From 150° to 210° C. (1–33 apparatus; type-347, stainless steel test chamber.)

process is involved, an added precaution must be taken; a constituent at a partial pressure near its vapor pressure value may condense when it is momentarily compressed by addition of other gases or vapors. Accordingly, mixtures that are initially above the upper limit of flammability may become flammable. A similar effect must be considered when mixtures are sampled with equipment that is cooler than the original sample; if vapor condenses in the

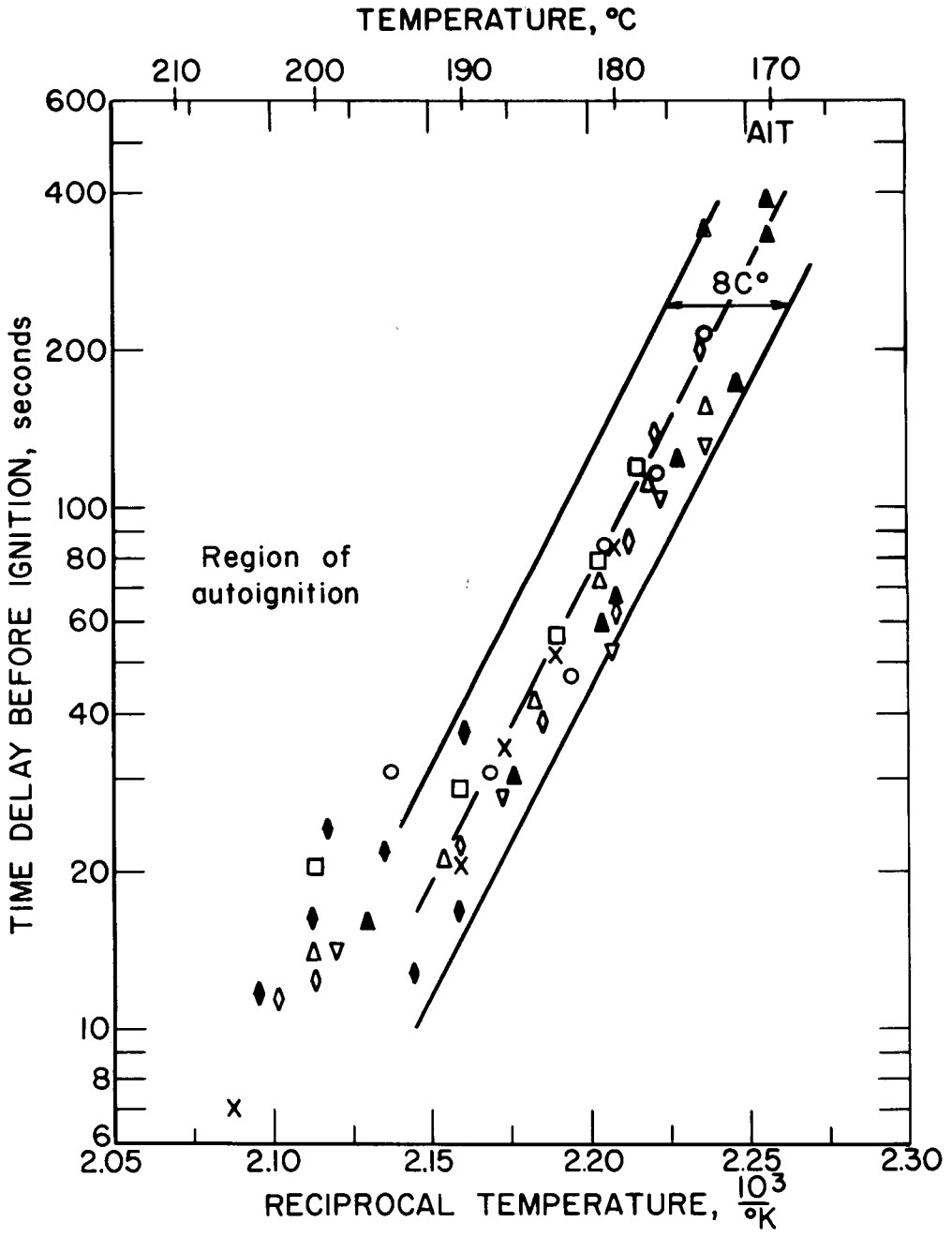

FIGURE 4.—Logarithm of Time Delay Before Ignition of NPN in Air at 1,000 Psig Initial Pressure. (Data from figure 3.)

sampling line, the test sample will not yield accurate data. A flammable mixture sampled in this manner may appear to be nonflammable and thus create a hazardous situation (*236*).

A flammable mixture can also form at temperatures below the flash point of the liquid combustible either if the latter is sprayed into the air, or if a mist or foam forms. With fine mists and sprays (particle sizes below 10 microns), the combustible concentration at the lower limit is about the same as that in uniform vapor-air mixtures (*17*, *18*, *22*, *24*, *76*, *245*). However, as the droplet diameter increases, the lower limit appears to decrease. In studying this problem, Burgoyne found that coarse droplets tend to fall towards the flame front in an

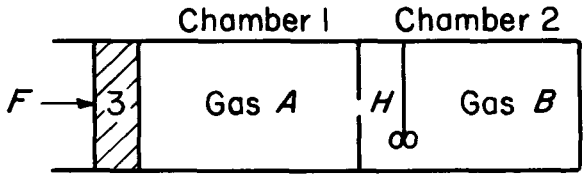

Figure 5.-Simplified mixer.

FIGURE 5.—Simplified Mixer.

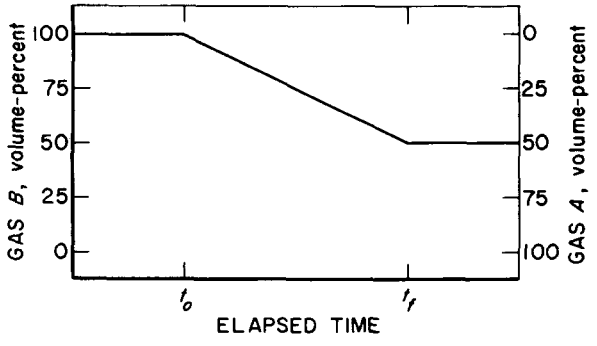

FIGURE 6.—Composition of Gas in Chamber 2, Figure 5 (Instantaneous Mixing).

upward propagating flame, and as a result the concentration at the flame front actually approaches the value found in lower limit mixtures

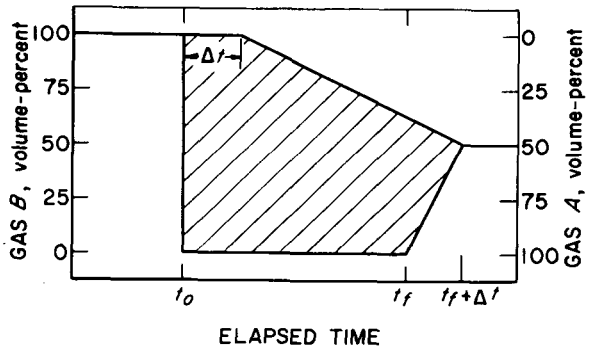

FIGURE 7.—Composition of Gas in Chamber 2, Figure 5 (Delayed Mixing).

of fine droplets and vapors (*24*). With sprays, the motion of the droplets also affects the limit composition, so that the resultant behavior is rather complex. The effect of mist and spray droplet size on the apparent lower limit is illustrated in figure 8. Kerosine vapor and mist data were obtained by Zabetakis and Rosen (*245*); tetralin mist data, by Burgoyne and Cohen (*24*); kerosine spray data, by Anson (*5*); and the methylene bistearamide data, by Browning, Tyler, and Krall (*18*).

Flammable mist-vapor-air mixtures may occur as the foam on a flammable liquid collapses. Thus, when ignited, many foams can propagate flame. Bartkowiak, Lambiris, and Zabetakis found that the pressure rise ΔP pro-

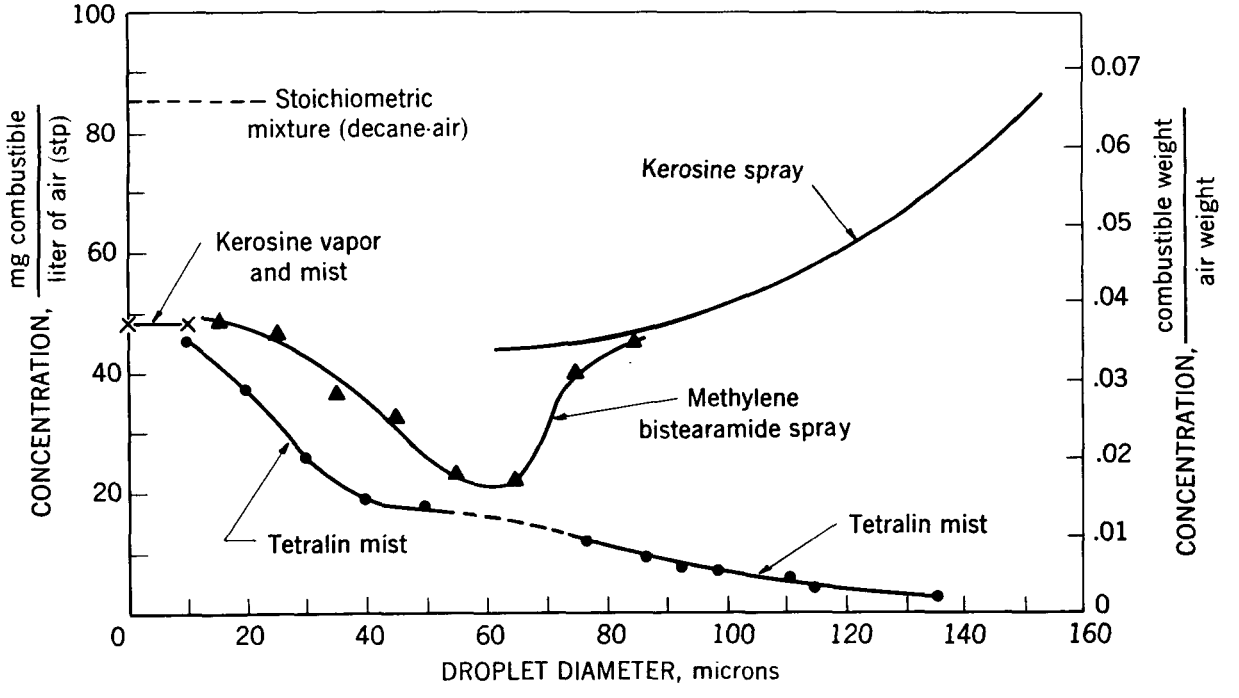

FIGURE 8.—Variation in Lower Limits of Flammability of Various Combustibles in Air as a Function of Droplet Diameter.

duced in an enclosure by the complete combustion of a layer of foam of thickness h_f is proportional to h_f and inversely proportional to h_a, the height of the air space above the liquid before foaming (*7*). That is

$$\Delta P \propto \frac{h_f}{h_a}. \tag{5}$$

Pressures in excess of 30 psi were produced by the ignition of foams in small containers.

Thomas found that an additional hazard could arise from production of foams by oxygen-enriched air at reduced pressures (*215*). Air can become oxygen-enriched as the pressure is reduced, because oxygen is more soluble than nitrogen in most liquids (*83*). Thus the presence of foams on combustible liquids are a potential explosion hazard.

A flammable foam can also form on nonflammable liquid if the foam is generated by a flammable gas mixture instead of air. Burgoyne and Steel, who studied this problem, found that the flammability of methane-air mixtures in water-base foams was affected by both the wetness of the foam and the bubble size (*28*).

PRESENTATION OF DATA

Limit-of-flammability data that have been obtained at a specified temperature and pressure with a particular combustible-oxidant-inert system may be presented on either a triangular or a rectangular plot. For example, figure 9 shows a triangular flammability diagram for the system methane-oxygen-nitrogen. This method of presentation is frequently used because all mixture components are included in the diagram. However, as the sum of all mixture compositions at any point on the triangular plot is constant (100 pct) the diagram can be simplified by use of a rectangular plot (*244*). For example, the flammable area of figure 9 may be presented as illustrated in figure 10. As noted, the oxygen concentration at any point is obtained by subtracting the methane and nitrogen concentrations at the point of interest from 100 as follows:

$$\text{Pct } O_2 = 100 \text{ pct} - \text{pct } CH_4 - \text{pct } N_2. \quad (6)$$

With either type of presentation, addition of methane, oxygen, or nitrogen to a particular mixture results in formation of a series of mixtures that fall along the line between the composition point (for example, *M*1 in figures 9 and 10) and the vertices of the bounding triangle. For example, addition of methane ($+CH_4$) to mixture *M*1 yields initially all mixture compositions between *M*1 and C (100 pct CH_4). After a homogeneous mixture is produced, a new mixture composition point, such as *M*2, is obtained. Similarly, if oxygen is added ($+O_2$) to the mixture represented by point *M*1, all compositions between *M*1 and O (100 pct O_2) are obtained initially; if nitrogen is added, all compositions between *M*1 and N (100 pct N_2) are obtained initially. If more than one gas is added to *M*1, for example, methane and oxygen, the resultant composition point may be obtained by considering that the mixing process

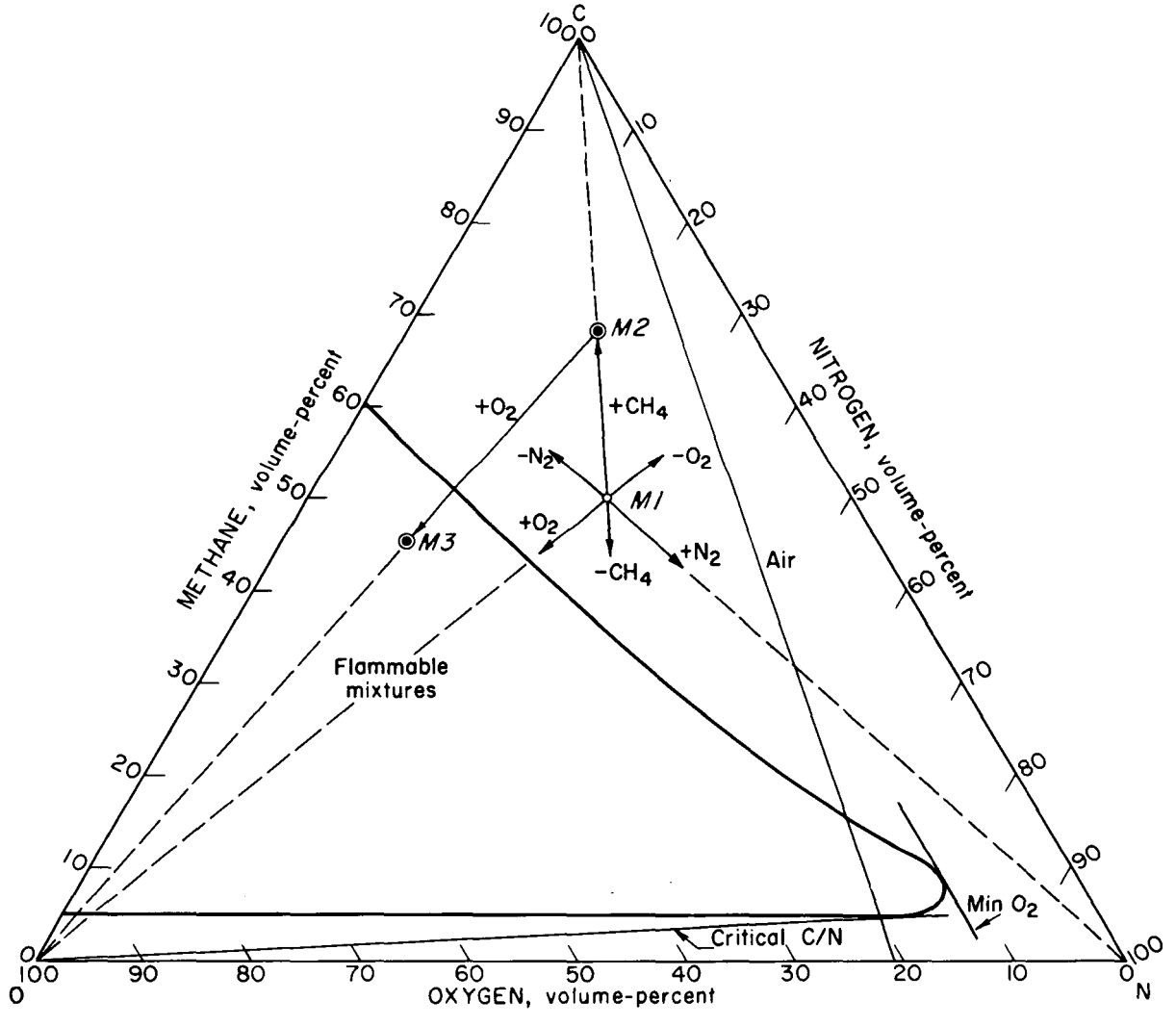

FIGURE 9.—Flammability Diagram for the System Methane-Oxygen-Nitrogen at Atmospheric Pressure and 26° C.

761-928 O-65—2

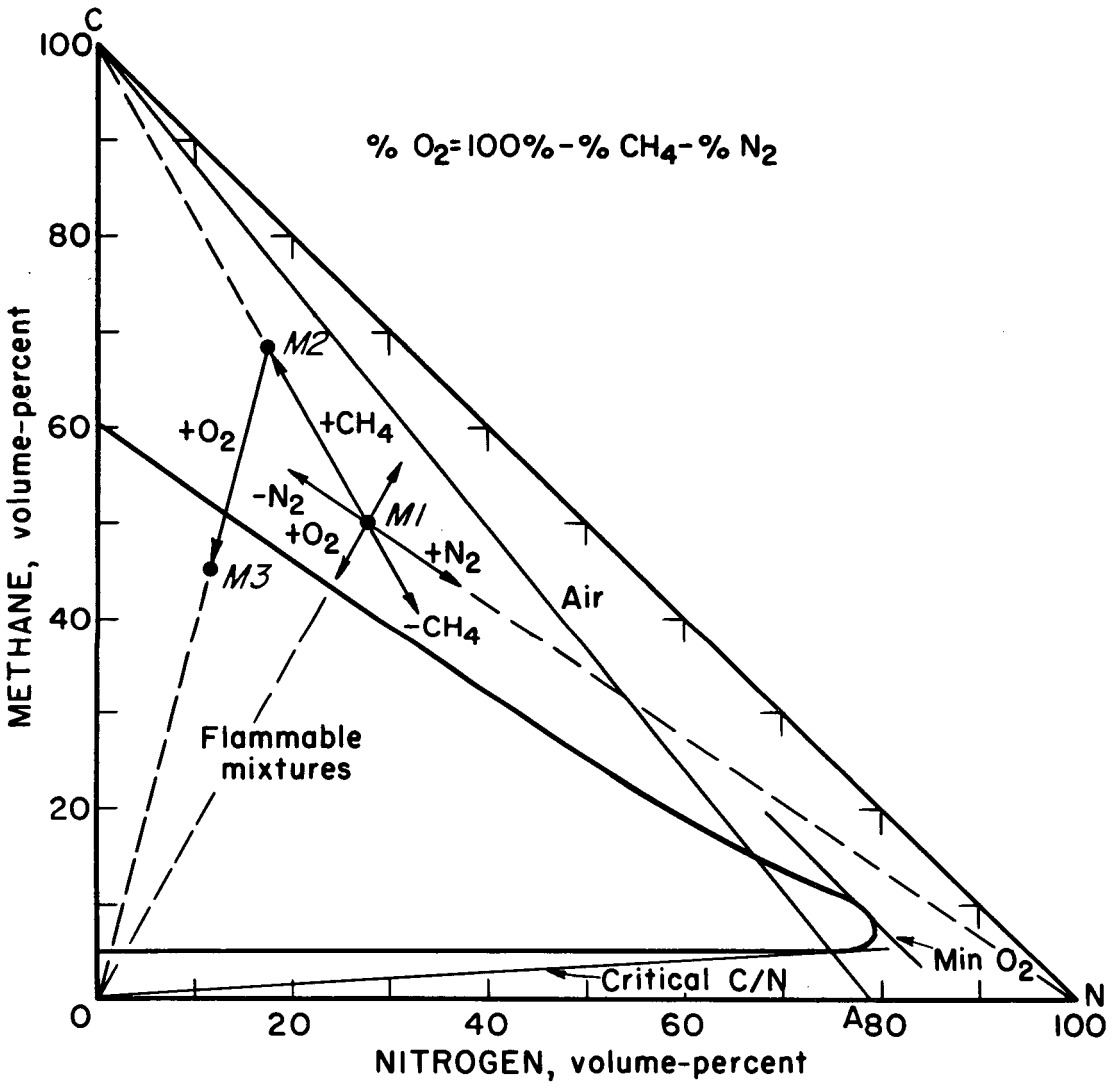

FIGURE 10.—Flammability Diagram for the System Methane-Oxygen-Nitrogen at Atmospheric Pressure and 26° C. (Data from fig. 9).

occurs in two steps. First, the methane is added to *M*1 and the gases are mixed thoroughly to give *M*2. Oxygen is then added to *M*2 with mixing to give a new (flammable) mixture, *M*3. If the methane and oxygen were added to a fixed volume at constant pressure, some of *M*1 and then of *M*2 would escape and mix with the surrounding atmosphere. In many instances this is an important consideration because the resulting mixtures may be flammable. For example, even if an inert gas is added to a constant-volume tank filled with methane, flammable mixtures can form outside the tank as the displaced methane escapes into the atmosphere. If the methane is not dissipated quickly, a dangerous situation can arise.

When a mixture component is removed by condensation or absorption, the corresponding composition point (for example, *M*1 in figures 9 and 10) shifts away from the vertices C, O, and N along the extensions to the lines *M*1—C, *M*1—O and *M*1—N, indicated in figures 9 and 10 by the minus signs. The final composition is determined by the percentage of each component removed from the initial mixture.

Mixtures with constant oxygen-to-nitrogen ratio (as in air), are obtained in figures 9 and 10 by joining the apex, C, with the appropriate mixture composition along the baseline, ON. Thus, the Air line, C*A*, (fig. 10) is formed by joining C with the mixture *A* (21 percent O_2 +79 percent N_2). Using this latter point, *A*, one can readily determine the mixture compositions that are formed when mixture *M*1 is displaced from an enclosure and mixed with air. Initially, all mixture compositions between *M*1

and A would form. Since these would pass through the flammable mixture zone, a hazardous condition would be created. Similarly, if pure combustible CH_4 were dumped into the atmosphere (air), all mixtures between C and A would form. These would include the flammable mixtures along CA so that a hazardous condition would again be created, unless the combustible were dissipated quickly.

Mixtures with constant oxidant content are obtained by constructing straight lines parallel to zero oxidant line; such mixtures also have a constant combustible-plus-inert content. One particular constant oxidant line is of special importance—the minimum constant oxidant line that is tangent to the flammability diagram or, in some cases, the one that passes through the extreme upper-limit-of-flammability value. This line gives the minimum oxidant (air, oxygen, chlorine, etc.) concentration needed to support combustion of a particular combustible at a specified temperature and pressure. In figures 9 and 10, the tangent line gives the minimum oxygen value (Min O_2, 12 volume-percent) required for flame propagation through methane-oxygen-nitrogen mixtures at 26° C and 1 atmosphere.

Another important construction line is that which gives the maximum nonflammable combustible-to-inert ratio (critical C/N). Mixtures along and below this line form nonflammable mixtures upon addition of oxidant. The critical C/N ratio is the slope of the tangent line from the origin (Figs. 9 and 10), 100 percent oxidant, to the lean side of the flammable mixtures curve. The reciprocal of this slope gives the minimum ratio of inert-to-combustible at which nonflammable mixtures form upon addition of oxidant. It is of interest in fire extinguishing.

An increase in temperature or pressure usually widens the flammable range of a particular combustible-oxidant system. The effect of temperature is shown in figure 11; two flammable areas, T_1 and T_2, are defined for a combustible-inert-oxidant system at constant pressure. The effect of temperature on the limits of flammability of a combustible in a specified oxidant was previously shown in figure 2. This type of graph is especially useful since it gives the vapor pressure of the combustible, the lower and upper temperature limits of flammability (T_L and T_U), the flammable region for a range of temperatures, and the autoignition temperature (AIT). Nearly 20 of these graphs were presented by Van Dolah and coworkers for a group of combustibles used in flight vehicles (*218*).

The lower temperature limit, T_L, is essentially the flash point of a combustible, in which upward propagation of flame is used; in general, it is somewhat lower than the flash point, in which

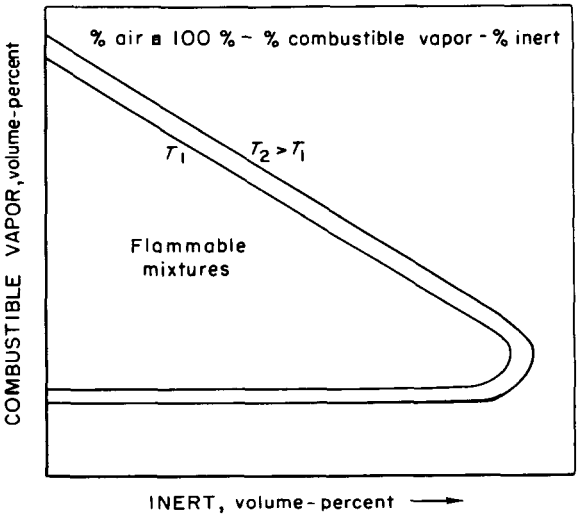

FIGURE 11.—Effect of Initial Temperature on Limits of Flammability of a Combustible Vapor-Inert-Air System at Atmospheric Pressure.

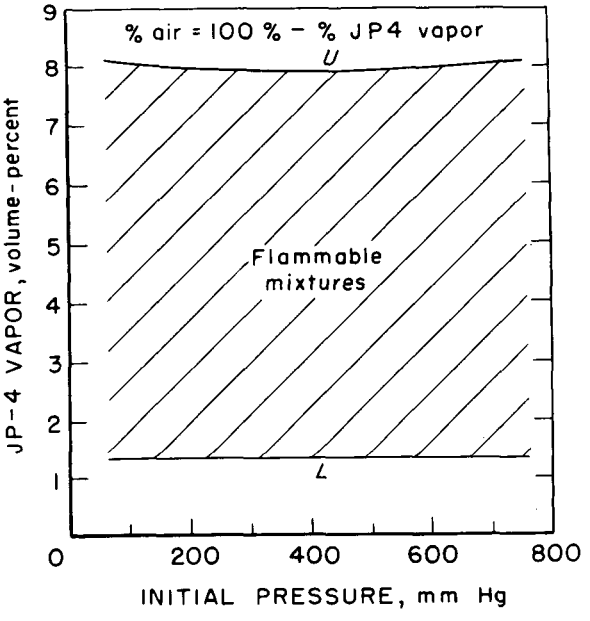

FIGURE 12.—Effect of Initial Pressure on Limits of Flammability of JP-4 (Jet Fuel Vapor) in Air at 26° C.

downward propagation of flame is used. Since T_L is the intersection of the lower-limit and vapor-pressure curves, a relationship can be developed between T_L, or the flash point, and the constants defining the vapor pressure of a combustible liquid. An excellent summary of such relationships has been presented by Mullins for simple fuels and fuel blends (*154*).

At constant temperature, the flammable range of a combustible in a specified oxidant can be represented as in figure 12. Here the flammable range of JP–4 vapor-air mixtures is given

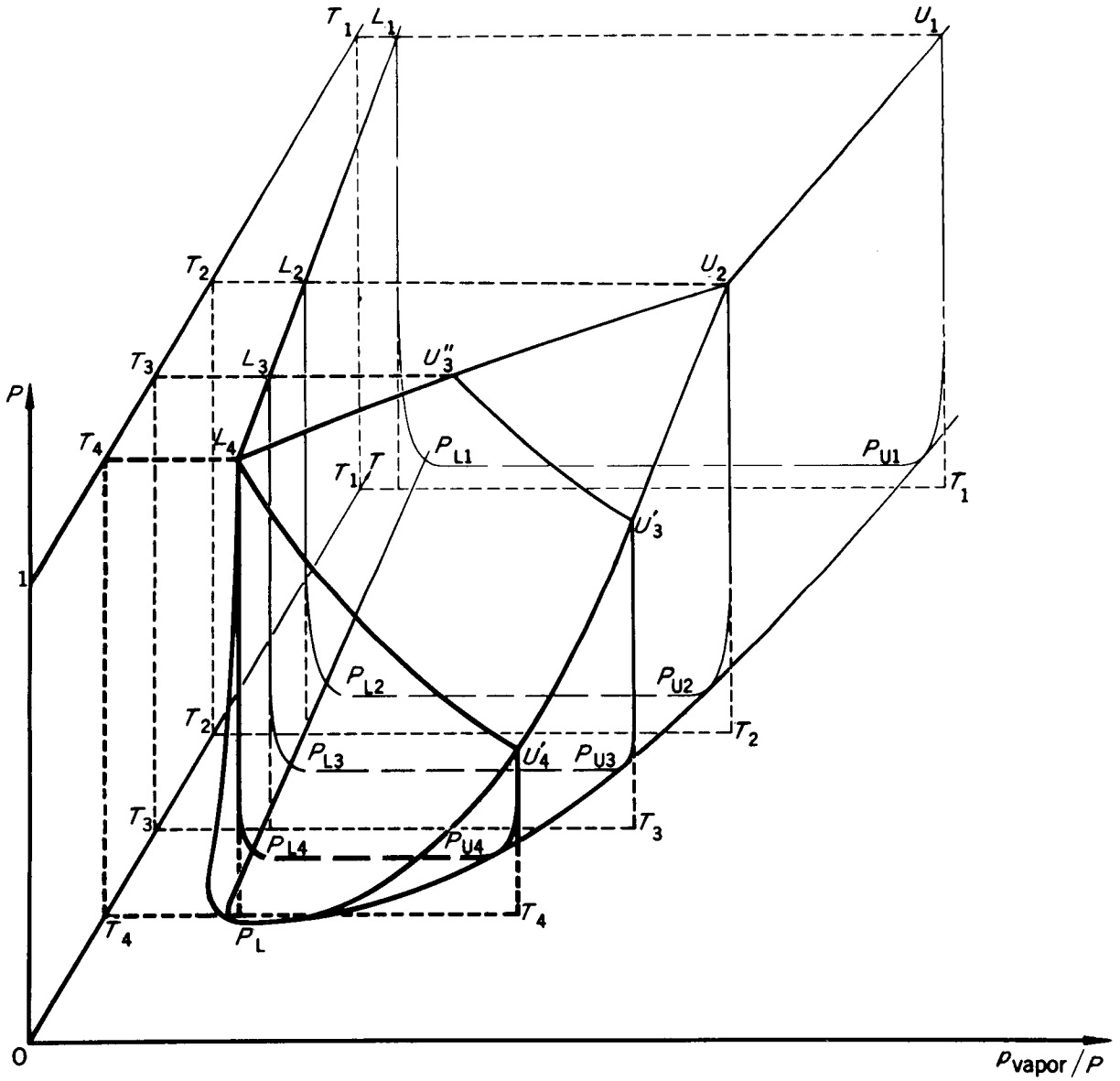

FIGURE 13.—Effect of Temperature and Pressure on Limits of Flammability of a Combustible Vapor in a Specified Oxidant.

as a function of pressure (*241*). A more generalized flammability diagram of a particular combustible-oxidant system can be presented in a three dimensional plot of temperature, pressure, and combustible content—as illustrated in figure 13 (*244*). Here, composition is given as the ratio of partial pressure of the combustible vapor, p_{VAPOR}, to the total pressure, P. For any value of P, the limits of flammability are given as a function of the temperature. For example, at 1 atmosphere ($P=1$), the flammable range is bounded by the lower limit curve $L_1L_2L_3L_4$, and the upper limit curve U_1U_2; all mixtures along the vapor pressure curve $L_4U_3''U_2$ are flammable. The flammable range is the same as that depicted in figure 2. At constant temperature (for example, T_1), the flammable range is bounded by the lower limit curve L_1P_{L1} and the upper limit curve U_1P_{U1}; the broken curve $P_{L1}P_{U1}$ represents the low pressure (quenched) limit. The flammable range is the same as that depicted in figure 12. A similar range is defined at temperatures T_2, T_3, and T_4 which are less than T_1. However, at T_3 and T_4 the upper limit curves intersect the vapor pressure curves, so that no upper limits are found above U_3' and U_4'. In other words, all compositions along $U_3'U_3''$ and $U_4'L_4$ are flammable. The curve

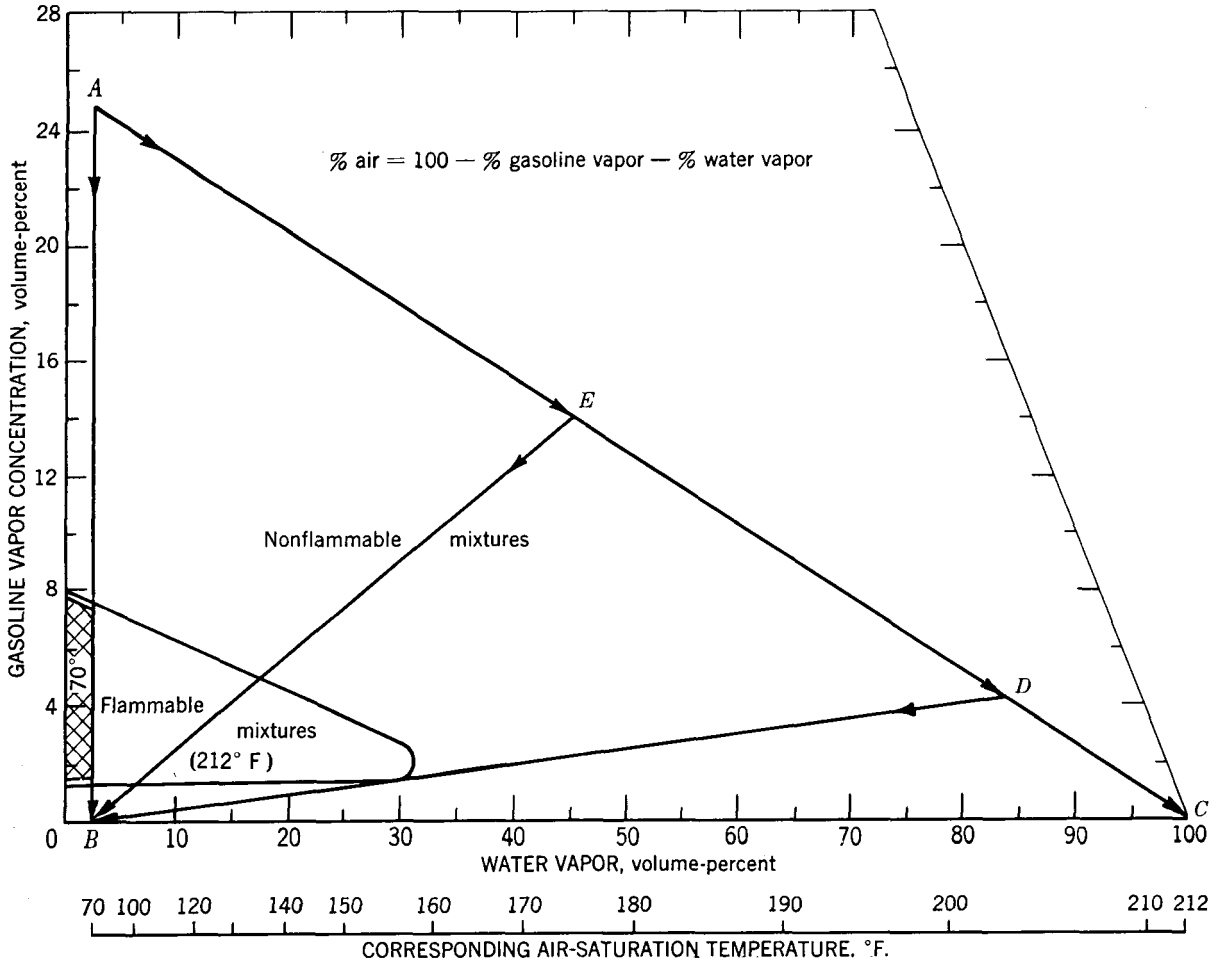

FIGURE 14.—Flammability Diagram for the System Gasoline Vapor-Water Vapor-Air at 70° F (21° C) and at 212° F (100° C) and Atmospheric Pressure.

$L_4P_LU_4'U_3'U_2$ defines the range of limit mixtures which are saturated with fuel vapor. Further, since L_4 is the saturated lower limit mixture at one atmosphere, T_4 is the flash point.

Some of the points considered in this and the previous section are illustrated in figure 14 (*232*). This is the flammability diagram for the system gasoline vapor-water vapor-air at 70° F (21° C) and 212° F (100 °C) and atmospheric pressure. The air saturation temperature, that is, the temperature at which saturated air contains the quantity of water given on the water vapor axis, is also included. For precise work, a much larger graph or an enlargement of the region from 0 to 8 percent gasoline vapor and from 0 to 30 percent water vapor would be used. However, figure 14 is adequate here. If water vapor is added to a particular mixture A, all mixture compositions between A and pure water vapor will form as noted (if the temperature is at least 212° F), and the composition point will shift towards the 100-percent-water-vapor point. If water vapor is removed by condensation or absorbtion, the composition point will move along the extension to the line drawn from A to the 100-percent-water-vapor point. The same applies to the other components, air and gasoline, as indicated earlier. Moreover, if more than one component is involved, the final composition point can be found by considering the effect of each component separately.

Figure 14 is of special interest since it can be used to evaluate the hazards associated with a gas-freeing operation. For example, mixture A represents a saturated gasoline vapor-air-water vapor mixture at 70° F. A more volatile gasoline than the one used here would give a saturated mixture with more gasoline vapor and less air in a closed tank; a less volatile gasoline would give less gasoline vapor and more air. In any event, if a continuous supply of air saturated with water vapor is added to a tank containing mixture A, all compositions

between A and B (air plus water vapor) will be formed until all the gasoline vapor is flushed from the tank, and mixture B alone remains. If steam is used to flush mixture A from the tank, all compositions between A and C will form until all the gasoline vapor has been flushed from the tank and only steam remains (at 212° F or higher). If the tank is permitted to cool, the steam will condense and air will be drawn into the tank giving mixtures along C–B. At 70° F, only air plus a small amount of water vapor will remain.

If hot water and water vapor at 175° F are used to flush mixture A from the tank, the mixture composition can only shift along AC to E. Mixtures between A and E that are flushed from the tank mix with air to give mixtures between points along AE and B. Again, as the water vapor in these mixtures condenses outside the tank, the composition of the resultant mixtures will shift away from the 100-percent-water-vapor point, C. The mixture in the tank will remain at E unless air is used to flush the tank, in which case mixture compositons between E and B will form. Again, if the water vapor within the tank condenses, the mixture composition will shift away from C. In any event, at this temperature (175° F), the addition of air to mixture E will lead to formation of flammable mixtures. Thus, mixture A cannot be flushed from a tank without forming flammable mixtures, unless steam or some other inert vapor or gas is used.

DEFLAGRATION AND DETONATION PROCESSES

Once a flammable mixture is ignited, the resulting flame, if not extinguished, will either attach itself to the ignition source or propagate from it. If it propagates from the source, the propagation rate will be either subsonic (deflagration) or supersonic (detonation) relative to the unburned gas. If it is subsonic, the pressure will equalize at the speed of sound throughout the enclosure in which combustion is taking place so that the pressure drop across the flame (reaction) front will be relatively small. If the rate is supersonic, the rate of pressure equalization will be less than the propagation rate and there will be an appreciable pressure drop across the flame front. Moreover, with most combustible-air mixtures, at ordinary temperatures, the ratio of the peak-to-initial pressure within the enclosure will seldom exceed about 8:1 in the former, but may be more than 40:1 in the latter case. The pressure buildup is especially great when detonation follows a large pressure rise due to deflagration. The distance required for a deflagration to transit to a detonation depends on the flammable mixture, temperature, pressure, the enclosure, and the ignition source. With a sufficiently powerful ignition source, detonation may occur immediately upon ignition, even in the open. However, the ignition energy required to initiate a detonation is usually many orders of magnitude greater than that required to initiate a deflagration (*32*, *249*).

DEFLAGRATION

Where a deflagration occurs in a spherical enclosure of volume V with central ignition, the approximate pressure rise ΔP at any instant t after ignition is given by the expressions:

$$\Delta P = K P_1 \frac{S_u^3 t^3}{V} \leq P_m, \tag{7}$$

and

$$P_m = P_1 \frac{n_b T_b}{n_1 T_1} = P_1 \frac{\overline{M}_1 T_b}{\overline{M}_b T_1}, \tag{8}$$

where K is a constant, S_u is the burning velocity, P_1 is the initial pressure, P_m is the maximum pressure, T_1 is the initial temperature, n_1 is the number of moles of gas in the initial mixture, n_b is the number of moles of gas in the burned gases, $\overline{M}_1$ is the average molecular weight of the initial mixture, $\overline{M}_b$ is the average molecular weight of the burned gases, and T_b is the final (adiabatic) temperature of the products. With other enclosures, or with noncentral ignition, the flame front is disturbed by the walls before combustion is completed, so that calculated pressure cannot be expected to approximate actual pressure. Even with spherical enclosures, the flame front is not actually spherical, so that the walls tend to disturb the flame before combustion is complete (*118*, *130*). A graph of the pressure developed by the combustion of a stoichiometric methane-air mixture (central ignition) in a 19.7 cm diameter, 9-liter cylinder is given in figure 15. The calculated pressure for a 9-liter sphere is included for comparison; K in equation (7) was evaluated from the experimental curve at 70 milliseconds. The calculated curve follows the experimental curve closely about 75 milliseconds, when the latter curve has a break. This suggests that the flame front was affected by the cylinder walls in such a way that the rate of pressure rise decreased, and the experimental curve fell below the calculated curve. Further, since the combustion gases were being cooled, the maximum

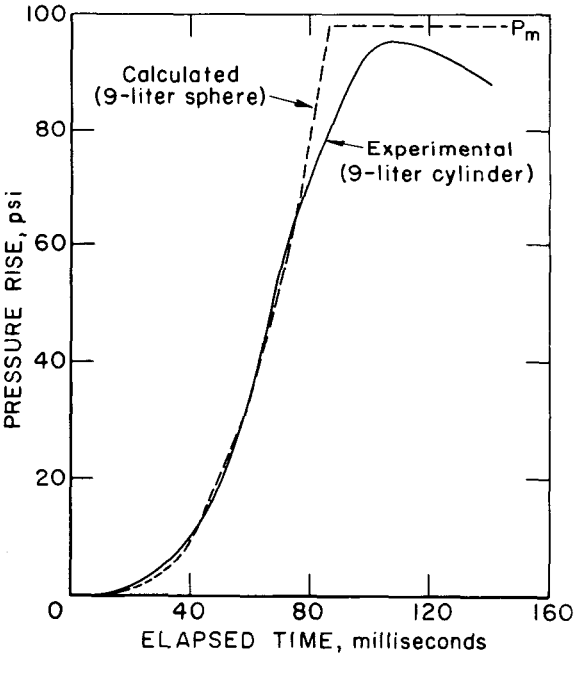

FIGURE 15.—Pressure Produced by Ignition of a 9.6 Volume-Percent Methane-Air Mixture in a 9-Liter Cylinder (Experimental).

pressure fell below the calculated value. The minimum elapsed time (in milliseconds) required to reach the maximum pressure appears to be about 75 $\sqrt[3]{V}$ for the paraffin hydrocarbons and fuel blends such as gasoline; V is the volume in cubic feet in this case.

DETONATION

Wolfson and Dunn (*52, 230*) have expressed the pressure ratio P_2/P_1 across a detonation front as

$$\frac{P_2}{P_1}=\frac{1}{\gamma_2+1}(\gamma_1 M_1^2+1), \qquad (9)$$

where γ_2 is the specific heat ratio of the burned gases, γ_1 is the specific heat ratio of the initial mixture, and M_1 is the Mach number of the detonation wave with respect to the initial mixture. M_1 is given in terms of the temperatures T and molecular weights W of the initial and final mixtures by the expression:

$$\frac{(\gamma_1 M_1^2+1)^2}{\gamma_1 M_1^2}=\frac{(\gamma_2+1)^2 T_2 W_1}{\gamma_2 T_1 W_2}. \qquad (10)$$

Wolfson and Dunn have developed generalized charts that simplify the operations involved in obtaining the pressure ratio as well as the density and temperature/molecular weight ratios across the detonation wave and the energy release in the detonation wave.

Many investigators have measured and calculated detonation and reflected pressures resulting from detonation waves (*54, 57, 204*). Figure 16 from the data of Stoner and Bleakney (*204*) gives the detonation velocity, the static or detonation pressure, and the reflected pressure developed by a detonation wave propagating through hydrogen-oxygen mixtures at atmospheric pressure and 18° C.

BLAST PRESSURE

The pressures produced by a deflagration or a detonation are often sufficient to demolish an enclosure (reactor, building, etc.). As noted, a deflagration can produce pressure rises in excess of 8:1, and pressure rises of 40:1 (reflected pressure) can accompany a detonation. As ordinary structures can be demolished by pressure differentials of 2 or 3 psi, it is not surprising

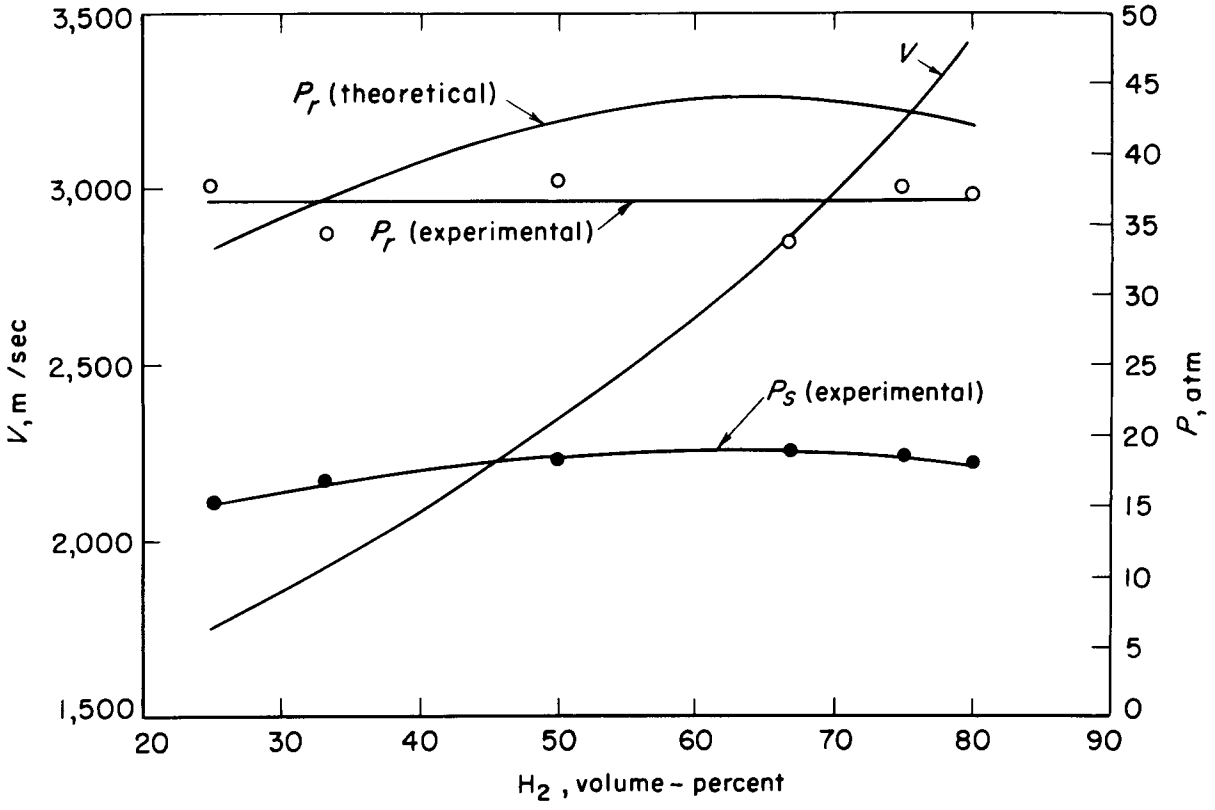

FIGURE 16.—Detonation Velocity, V; Static Pressure, P_s; and Reflected Pressure, P_r, Developed by a Detonation Wave Propagating Through Hydrogen-Oxygen Mixtures in a Cylindrical Tube at Atmospheric Pressure and 18° C.

that even reinforced concrete structures have been completely demolished by explosions of near-limit flammable mixtures.

Jacobs and coworkers have studied the damage potential of detonation waves in great detail (*91, 170*). They have considered the principles involved in rupturing of pipes and vessels by detonations and the relevance of engineering and metallurgical data to explosions. More recently, Randall and Ginsburg (*171*) have investigated bursting of tubular specimens at ordinary and reduced temperatures. They found that the detonation pressure required to burst such specimens was, in general, slightly higher than the corresponding static-bursting pressure. Ductility of the test specimen appeared to have little effect on the bursting pressure, but ductility increased the strength of pipes containing notches or other stress raisers.

When a detonation causes an enclosure to fail, a shock wave may propagate outward at a rate determined by characteristics of the medium through which it is transmitted, and the available energy. If the shock velocity, V, is known, the resulting overpressure, $(P-P_o)$, is given by the expression (*204*)

$$P-P_o=P_o\left[\frac{2\gamma}{\gamma-1}\right]\left[\frac{V}{a}-1\right], \qquad (11)$$

where γ is the ratio of specific heats, and a is the velocity of sound in the medium through which the shock wave passes. The approximate damage potential can be assessed from the data in table 1 (*217*).

In conducting experiments in which blast pressures may be generated, special precautions must be taken to protect the personnel and equipment from blast and missiles. Browne, Hileman, and Weger (*16*) have reviewed the design criteria for suitable barricades. Other authors have considered the design of suitable laboratories and structures to prevent fragment damage to surrounding areas (*44, 174, 203, 220*).

TABLE 1.—*Conditions of failure of peak overpressure-sensitive elements* (217)

Structural element	Failure	Approximate incident blast overpressure (psi)
Glass windows, large and small.	Usually shattering, occasional frame failure.	0. 5–1. 0
Corrugated asbestos siding.	Shattering.	1. 0–2. 0
Corrugated steel or aluminum paneling.	Connection failure, followed by buckling.	1. 0–2. 0
Wood siding panels, standard house construction.	Usually failure occurs at main connections, allowing a whole panel to be blown in.	1. 0–2. 0
Concrete or cinder-block wall panels, 8 or 12 inches thick (not reinforced).	Shattering of the wall.	2. 0–3. 0
Brick wall panel, 8 or 12 inches thick (not reinforced).	Shearing and flexure failures.	7. 0–8. 0

PREVENTIVE MEASURES

INERTING

In principle, a gas explosion hazard can be eliminated by removing either all flammable mixtures or all ignition sources (*23*, *240*). However, this is not always practical, as many industrial operations require the presence of flammable mixtures, and actual or potential ignition sources. Accordingly special precautions must be taken to minimize the damage that would result if an accidental ignition were to occur. One such precaution involves the use of explosive actuators which attempt to add inert material at such a rate that an explosive reaction is quenched before structural damage occurs (*70*, *72*). Figure 17 shows how the pressure varies with and without such protection. In the latter case, the pressure rise is approximately a cubic function of time, as noted earlier. In the former case, inert is added when the pressure or the rate of pressure rise exceeds a predetermined value. This occurs at the time t_i in figure 17 when the explosive actuators function to add the inert. As noted, the pressure increases momentarily above the value found in the unprotected case and then falls rapidly as the combustion reaction is quenched by the inert.

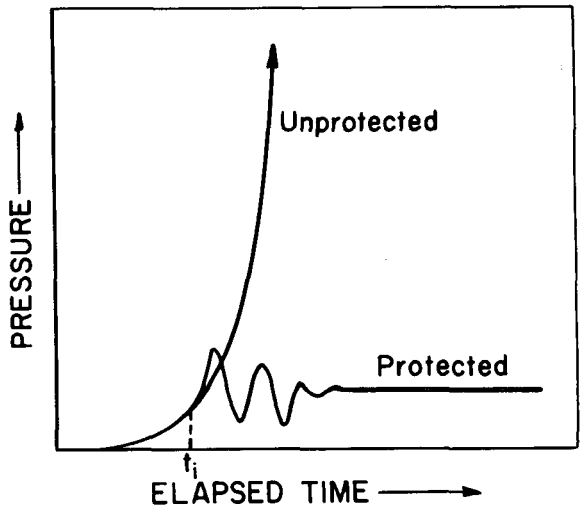

FIGURE 17.—Pressure Variation Following Ignition of a Flammable Mixture in Unprotected and Protected Enclosures.

FLAME ARRESTORS AND RELIEF DIAPHRAGMS

Inert atmospheres must be used when not even a small explosive reaction can be tolerated. However, when the ignition of a flammable mixture would create little hazard if the burning mixture were vented, flame arrestors and relief diaphragms could be used effectively. The design of such systems is determined by the size and strength of the confining vessels, ducts, etc.

In recent studies of the efficiency of wire gauze and perforated block arrestors (*161*, *162*), Palmer found the velocity of approach of the flame to be the major factor in determining whether flame passed through an arrestor. For these two types of arrestors, he found the critical approach velocity to be

$$V' = \frac{1.75k(T_h - T_o)}{m^{0.9}Q/x_o}, \qquad (12)$$

and

$$V = \frac{9.6kA't(T_h - T_o)}{d^2Q/x_o}, \qquad (13)$$

where k is the thermal conductivity of the gas; m is the mesh width; T_h is the mean bulk temperature of the flame gases through the arrestor; T_o is the initial temperature of the arrestor; Q is the heat lost by unit area of flame; x_o is the thickness of the flame propagating at the burning velocity, S; d is the diameter of an aperture; A' is the area of a hole in unit area of the arrestor face; and t is the arrestor thickness.

Equations (12) and (13) can be used to determine the mesh width or aperture diameter needed to stop a flame having a particular approach velocity. In practice, application of these equations assumes a knowledge of the flame speed in the system of interest. Some useful data have been made available by Palmer and Rasbash and Rogowski (*172*, *173*), as well as by Jost (*118*) and Lewis and von Elbe (*130*).

Tube bundles also may be used in place of wire screens. Scott found that these permit increased aperture diameters for a given approach velocity (*192*).

In practice, it may be desirable to install pressure relief vents to limit damage to duct systems where flame may propagate. Rasbash and Rogowski (*173*) found that with propane- and pentane-air mixtures, the maximum pressure P_M (pounds per square inch) developed in an open-ended duct, having a cross section of 1 ft^2 is:

$$P_M=0.07\frac{L}{D}, \text{ and } 6\leq\frac{L}{D}\leq 48, \qquad (14)$$

where $\frac{L}{D}$ is the ratio of duct length to diameter. However, the presence of an obstacle (bend, constriction, etc.) in the path of escaping gases increased the pressure due to resistance to fluid flow by the obstacle. Location of a relief vent near the ignition source decreased the maximum pressure as well as the flame speed. For values of K (cross-section area of duct/area of vent) greater than 1, these authors found

$$0.8K\leq P_M\leq 1.8K, \qquad (15)$$

where $2\leq K\leq 32$, and $6\leq\frac{L}{D}\leq 30$. To keep the pressure at a minimum either many small vents or a continuous slot was recommended rather than a few large vents. In addition, vents should be located at positions where ignition is likely to occur and should open before the flame has traveled more than 2 feet.

When possible, relief vents should be used with flame arrestors. The vents tend not only to reduce the pressure within a system following ignition but also to reduce the flame speed, thus making all arrestors more effective. Unfortunately, in certain large applications (for example, drying ovens), it is difficult to use flame arrestors effectively. In such cases, greater reliance must be placed on the proper functioning of relief vents. Simmonds and Cubbage (*42*, *43*, *195*) have investigated the design of effective vents for industrial ovens. They found two peaks in the pressure records obtained during the venting of cubical ovens (fig. 18). The first peak, P_1; the oven volume, V; the factor, K; and the weight per unit area (lb/ft^2) of relief, w, were related as follows for a 25 percent town gas [3]-air mixture:

$$P_1V^{1/3}=1.18kw+1.57. \qquad (16)$$

More generally,

$$P_1V^{1/3}=S_o(0.3Kw+0.4), \qquad (17)$$

where S_o is the burning velocity of the mixture at the oven temperature.

The first pressure pulse was ascribed to the release and motion of the relief vent following ignition; the second pulse, to continued burning at an increased rate. The second pulse represents the pressure drop across the vent, and it is thus proportional to K. For small values of K it was found that

$$P_2=K. \qquad (18)$$

As with ducts, larger pressures were obtained when obstructions were placed in the oven.

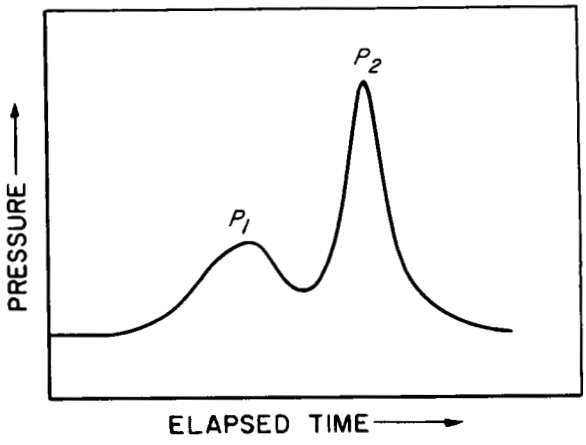

FIGURE 18.—Pressure Produced by Ignition of a Flammable Mixture in a Vented Oven.

In designing explosion reliefs for ovens, Simmonds and Cubbage pointed out that (1) the reliefs should be constructed in such a way that they do not form dangerous missiles if an explosion occurs; (2) the weight of the relief must be small so that it opens before the pressure builds up to a dangerous level; (3) the areas and positions of relief openings must be such that the explosion pressure is not excessive; (4) sufficient free space must be utilized around the oven to permit satisfactory operation of the relief and minimize risk of burns to personnel; and (5) oven doors should be fastened securely so that they do not open in the event of an explosion.

Burgoyne and Wilson have presented the results of an experimental study of pentane vapor-air explosions in vessels of 60- and 200-cubic-foot volume (*30*). They found the rates of pressure rise greater than could be predicted from laminar burning velocity data, so that the effect of a relief area in lowering the peak pressure was less than expected. All experiments were conducted at an initial pressure of 1 atmosphere. Vent data for use at higher initial pressures are summarized in an article by Block (*10*); a code for designing pressure relief systems has been proposed in this article. Other authors have considered the effects of temperature and characteristics of the flammable mixture on vent requirements (*14*, *35*, *38*, *45*, *46*, *134*, *145*, *168*, *221*).

[3] Town gas contained approximately 52 pct hydrogen, 17 pct carbon monoxide, 15 pct methane; the balance was other hydrocarbons, 3 pct; nitrogen, 9 pct; carbon dioxide, 3 pct; and oxygen.

FLAMMABILITY CHARACTERISTICS

The flammability data (limits of flammability, flash point, ignition temperature and burning velocity) of the various chemical families exhibit many similarities. Accordingly, the data presented here are grouped under the various commercially important families, blends, and miscellaneous combustibles.

PARAFFIN HYDROCARBONS (C_nH_{2n+2})

Limits in Air

Lower and upper limits of flammability at 25° C (or at the temperature noted) and 1 atmosphere (L_{25} and U_{25}) for many members of the paraffin hydrocarbon series are given in table 2, together with the molecular weight, M, vapor specific gravity, sp gr, stoichiometric composition in air, C_{st} (appendix B) and heat of combustion, ΔH_c (*183*). At room temperature and atmospheric or reduced pressure, the lower limits of flammability of most of this series fall in the range from 45 to 50 mg combustible vapor per liter of air at standard conditions, that is, 0° C and 760 mm Hg (0.045 to 0.050 oz combustible vapor per cubic foot of air) (*247*). This is illustrated in figure 19 in which some lower limits of flammability are plotted against molecular weight; except for methane, ethane, and propane all limit values fall in a band between concentrations of approximately 45 and 50 mg/lr.

The following expression may be used to convert from a lower limit L in volume-percent of vapor in the vapor-air mixture to one in milligrams of combustible, per liter of air at standard conditions:

$$L\left(\frac{\text{mg}}{\text{l}}\right)=\frac{L\ (\text{vol pct})}{[100-L\ (\text{vol pct})]\left[\text{sp vol}\ \frac{\text{l}}{\text{mg}}\right]}, \quad (19)$$

specific volume being volume of combustible vapor per milligram of combustible. At standard conditions (0° C and 760 mm Hg) this is about $22.414/1{,}000M$, where M is the molecular

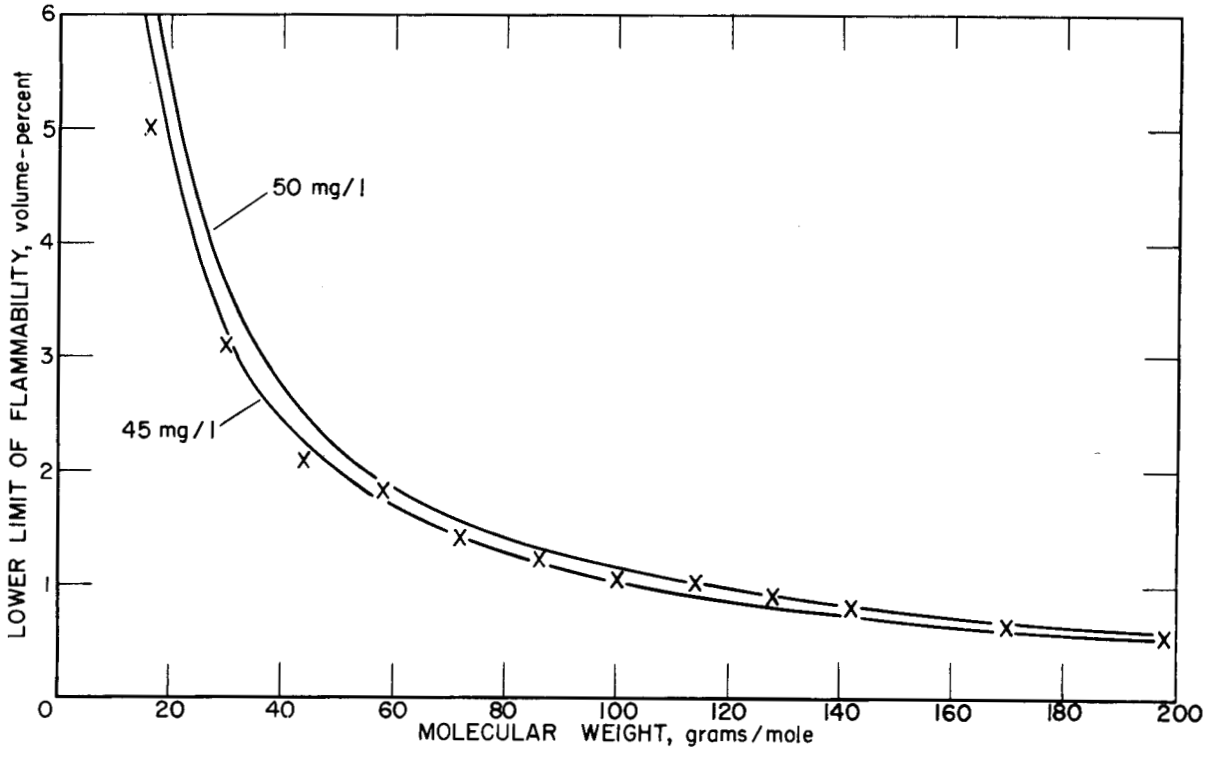

FIGURE 19.—Effect of Molecular Weight on Lower Limits of Flammability of Paraffin Hydrocarbons at 25° C.

TABLE 2.—*Properties of paraffin hydrocarbons*

Combustible	Formula	M	Sp gr (Air=1)	C_{st} in air (vol pct)	Net ΔH_c $\left(\frac{\text{Kcal}}{\text{mole}}\right)$	Lower limit in air				Upper limit in air			
						L_{25} (vol pct)	$\frac{L_{25}}{C_{st}}$	$L\left(\frac{\text{mg}}{\text{l}}\right)$	Ref.	U_{25} (vol pct)	$\frac{U_{25}}{C_{st}}$	$U\left(\frac{\text{mg}}{\text{l}}\right)$	Ref.
Methane	CH_4	16.04	0.55	9.48	191.8	5.0	0.53	38	(40)	15.0	1.6	126	(40)
Ethane	C_2H_6	30.07	1.04	5.65	341.3	3.0	.53	41	(40)	12.4	2.2	190	(41)
Propane	C_3H_8	44.09	1.52	4.02	488.5	2.1	.52	42	(115)	9.5	2.4	210	(41)
n-Butane	C_4H_{10}	58.12	2.01	3.12	635.4	1.8	.58	48	(115)	8.4	2.7	240	(41)
n-Pentane	C_5H_{12}	72.15	2.49	2.55	782.0	1.4	.55	46	(40)	7.8	3.1	270	(40)
n-Hexane	C_6H_{14}	86.17	2.98	2.16	928.9	1.2	.56	47	(246)	7.4	3.4	310	(40)
n-Heptane	C_7H_{16}	100.20	3.46	1.87	1075.8	1.05	.56	47	(246)	6.7	3.6	320	(40)
n-Octane	C_8H_{18}	114.23	3.94	1.65	1222.8	.95	.58	49	(246)				
n-Nonane	C_9H_{20}	128.25	4.43	1.47	1369.7	[1] .85	.58	49	(246)				
n-Decane	$C_{10}H_{22}$	142.28	4.91	1.33	1516.6	[2] .75	.56	48	(246)	[3] 5.6	4.2	380	
n-Undecane	$C_{11}H_{24}$	156.30	5.40	1.22	1663.6	.68	.56	48	(4)				
n-Dodecane	$C_{12}H_{26}$	170.33	5.88	1.12	1810.5	.60	.54	46	(4)				
n-Tridecane	$C_{13}H_{28}$	184.36	6.37	1.04	1957.4	.55	.53	46	(4)				
n-Tetradecane	$C_{14}H_{30}$	198.38	6.85	.97	2104.3	.50	.52	44	(4)				
n-Pentadecane	$C_{15}H_{32}$	212.41	7.33	.90	2251.2	.46	.51	46	(4)				
n-Hexadecane	$C_{16}H_{34}$	226.44	7.82	.85	2398.2	.43	.51	44	(4)				

[1] t=43° C.
[2] t=53° C.
[3] t=86° C.

[4] Calculated value extrapolated to 25° C at Explosives Res. Center, Federal Bureau of Mines.

weight of the combustible. Since L (vol pct) of most members of this series is much less than 100 percent, the lower limit can be expressed as

$$L\left(\frac{\text{mg}}{\text{l}}\right)\approx 0.45ML \text{ (vol pct)}. \qquad (20)$$

At any specified temperature, the ratio of the lower limit to the amount of combustible needed for complete combustion, C_{st}, also is approximately constant. This was first noted by Jones (*95*) and later by Lloyd (*133*), who found that for paraffin hydrocarbons at about 25° C,

$$L_{25°}\approx 0.55C_{st}. \qquad (21)$$

For the complete combustion of the paraffin hydrocarbons, we have:

$$C_nH_{2n+2}+(1.5n+0.5)O_2\rightarrow nCO_2+(n+1)H_2O, \qquad (22)$$

so that in air

$$C_{st}=\frac{100}{1+4.773(1.5n+0.5)} \text{ vol pct}, \qquad (23)$$

where 4.773 is the reciprocal of 0.2095, the molar concentration of oxygen in dry air. The values of C_{st} (appendix B) are included in table 2. By weight these become

$$C_{st}=\frac{1{,}000[12.01n+1.008(2n+2)]}{22.414\times 4.773(1.5n+0.5)}\frac{\text{mg}}{\text{l}}, \qquad (24)$$

or

$$C_{st}=9.34\left[\frac{14.03n+2.02}{1.5n+0.5}\right]\frac{\text{mg}}{\text{l}}. \qquad (25)$$

Thus,

$$C_{st}\approx 87 \text{ mg/l}, \qquad n\geq 4. \qquad (26)$$

Combining this equation with equation (21), we have

$$L_{25°}(\text{mg/l})\approx 48 \text{ mg/l}, \qquad (27)$$

for paraffin hydrocarbons, except methane, ethane, and propane. Substitution of this value into equation (20) gives

$$L_{25°}(\text{vol pct})\approx\frac{107}{M}. \qquad (28)$$

The following expression may be used to convert a lower limit value in volume-percent to a fuel-air (weight) ratio:

$$L(F/A)=\frac{M}{28.96}\left[\frac{L \text{ (vol pct)}}{100-L \text{ (vol pct)}}\right]. \qquad (29)$$

The reciprocal expression gives the air-fuel (weight) ratio:

$$L(A/F)=\frac{28.96}{M}\left[\frac{100}{L \text{ (vol pct)}}-1\right]. \qquad (30)$$

As noted, the lower limits given in figure 19 were determined at room temperature and atmospheric or reduced pressure. Lower limits vary with temperature as shown for methane in figure 20. The limit values obtained with upward propagation of flame (*21*) fall fairly close to a straight line that passes through the lower limit value at 25° C and the flame temperature (1,225° C). This is in accordance with the White criterion that the flame temperature is constant at the lower limit (*222*). The data obtained by White with downward propagation of flame fall along a line parallel to the line through the limit values obtained with upward propagation. Taking the value 1,300° C as

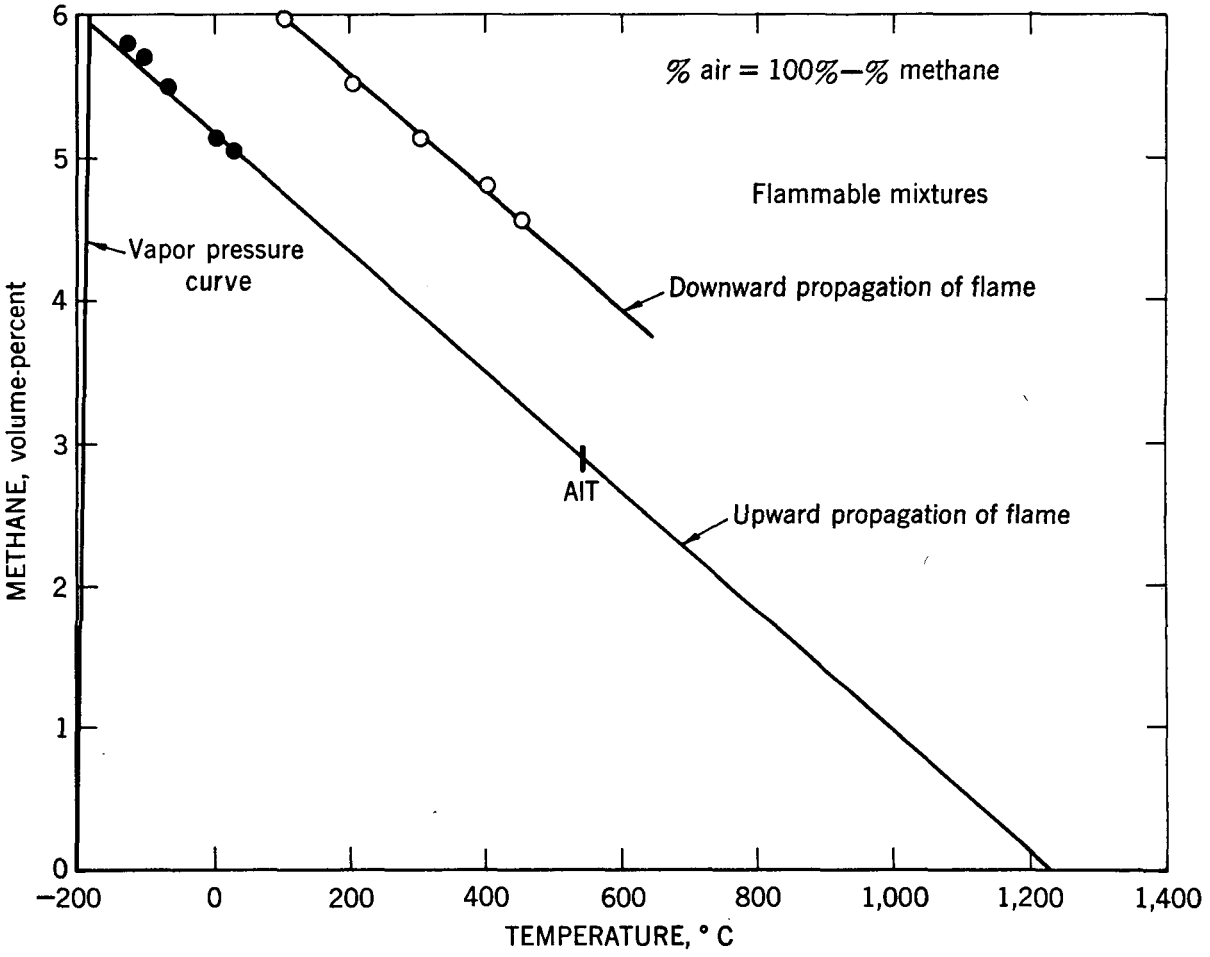

FIGURE 20.—Effect of Temperature on Lower Limit of Flammability of Methane in Air at Atmospheric Pressure.

the approximate flame temperature for the paraffin hydrocarbon series (*55*), and using the lower limit values at room temperature in table 2, the limits of the first 10 paraffin hydrocarbons are represented as in figures 21 and 22. Figure 21 gives the lower limits in volume-percent and figure 22 in milligrams per liter. By weight, the lower limits of most members of this series again fall in a fairly narrow band ("higher hydrocarbons" region). Individual adiabatic flame temperatures can be determined for lower limit mixtures using the data in table 2 and appendix C (*55*).

The straight lines of figures 21 and 22 are given by:

$$L_t = L_{25°} - \frac{L_{25°}}{(1{,}300° - 25°)}(t - 25°), \qquad (31)$$

or

$$\frac{L_t}{L_{25°}} = 1 - 0.000784(t - 25°). \qquad (32)$$

They are described in more general terms by a plot of $L_t/L_{25°}$ against the temperature (fig. 23, solid line).

These data are also correlated fairly well with the modified Burgess-Wheeler Law suggested by Zabetakis, Lambiris, and Scott (*242*):

$$L_t = L_{25°} - \frac{0.75}{\Delta H_c}(t - 25°), \qquad (33)$$

where t is the temperature in °C and ΔH_c is the net heat of combustion in kilocalories per mole. Then,

$$\frac{L_t}{L_{25°}} = 1 - \frac{0.75}{L_{25°} \cdot \Delta H_c}(t - 25°). \qquad (34)$$

Substituting the value 1,040 for $L_{25} \cdot \Delta H_c$ obtained by Spakowski (*201*), we have

$$\frac{L_t}{L_{25°}} = 1 - 0.000721(t - 25°), \qquad (35)$$

which is also given in figure 23 for a limited temperature range with the broken line.

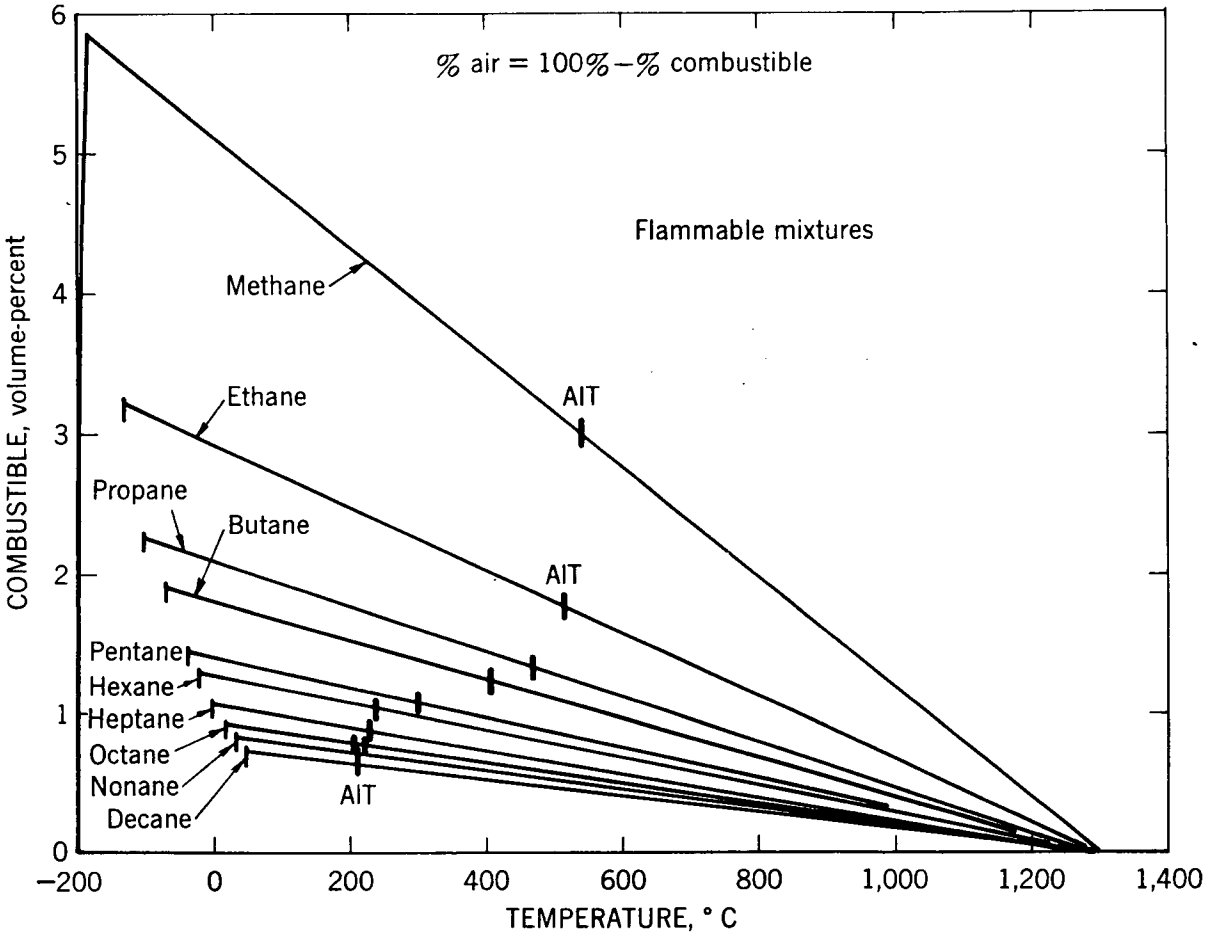

FIGURE 21.—Effect of Temperature on Lower Limits of Flammability of 10 Paraffin Hydrocarbons in Air at Atmospheric Pressure.

Only the lower limit at 25° C and atmospheric pressure is needed to use figure 23. For example, assuming a constant flame temperature, the ratio $L_t/L_{25°}$ at 600° C is 0.55. The calculated lower limit of methane at 600° C therefore is 5.0×0.55, or 2.75 volume-percent. The same value can be obtained directly from figure 21. From the modified Burgess-Wheeler Law curve, $L_t/L_{25°}=0.585$ at 600° C, so that $L_{600°}=2.92$ volume-percent.

Limit-of-flammability measurements are complicated by surface and vapor-phase reactions that occur at temperatures above the autoignition temperature. For example, Burgoyne and Hirsch (*25*) have shown that methane-air mixtures containing up to 5 percent methane burn readily at 1,000° C. Experiments were conducted with mixtures containing as little as 0.5 percent methane; figure 20 predicts that a flame would not propagate through such a mixture.

Flammability experiments at elevated temperatures indicate that in the absence of cool flames (*87*, *88*), the upper limit also increases linearly with temperature. The effect of temperature appears to be fairly well correlated by the modified Burgess-Wheeler law:

$$U_t=U_{25°}+\frac{0.75}{\Delta H_c}(t-25°). \qquad (36)$$

If we assume that the heat release at the upper limit is equal to that at the lower limit, then

$$\frac{U_t}{U_{25°}}=1+0.000721(t-25°). \qquad (37)$$

A plot of $U_t/U_{25°}$ against temperature (fig. 24) was used to compare recent experimental values of Rolingson and coworkers (*182*) for methane-air mixtures at 15 psig with those predicted by the modified Burgess-Wheeler law. The experimental and calculated upper limits are given in table 3 together with the difference, $U_{calc}-U_{exper}$. In each case, the difference is less than

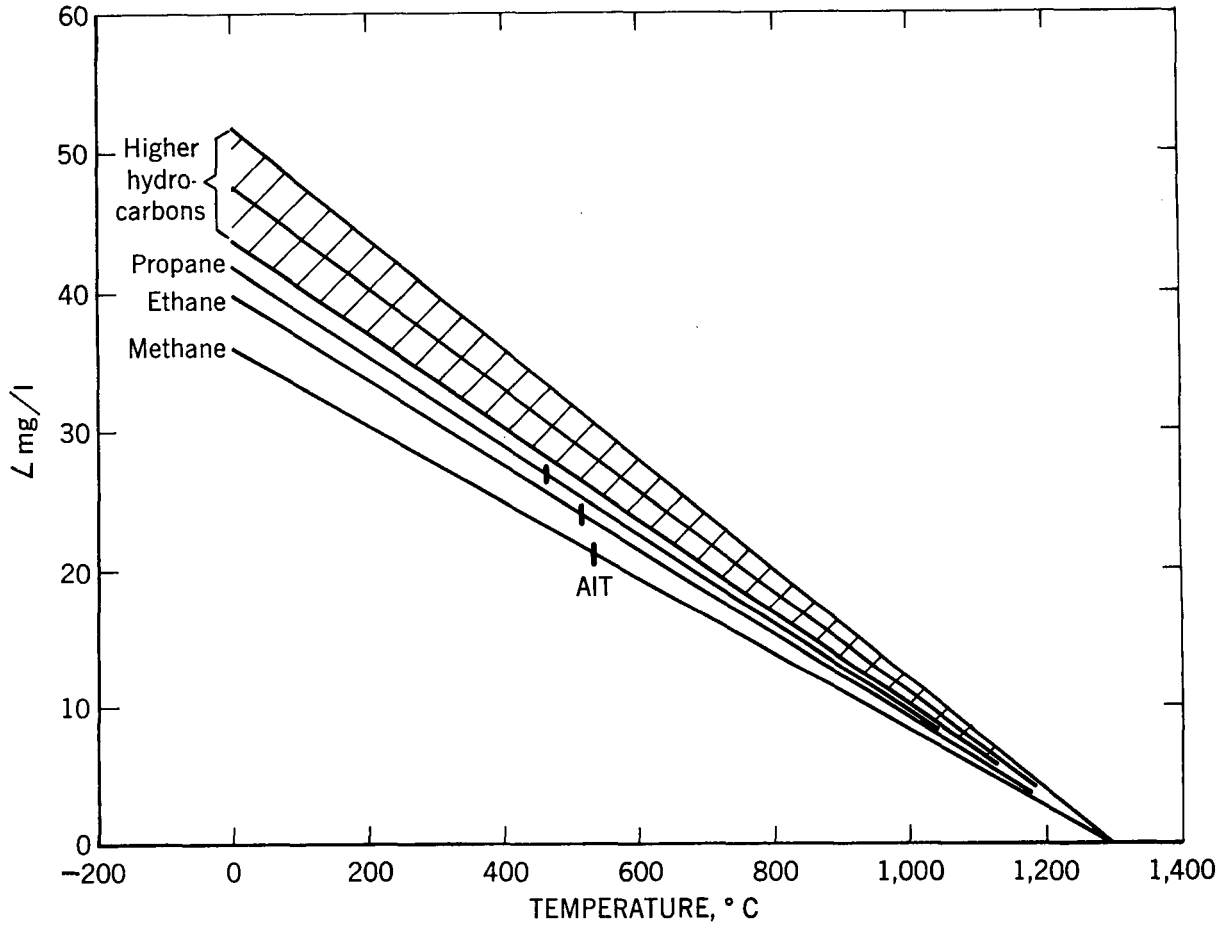

FIGURE 22.—Effect of Temperature on Lower Limits of Flammability of 10 Paraffin Hydrocarbons in Air at Atmospheric Pressure by Weight.

4 percent of the experimental value, which is approximately within the limit of experimental error. Earlier experiments of White (*222*) at temperatures to 400° C, with downward flame propagation, also are represented quite adequately by equation (37). For example, White found that the upper limit of pentane in air (downward propagation) increased linearly from 4.50 volume-percent at about 17° C to 5.35 volume-percent at 300° C. The ratio of 5.35: 4.50 is 1.17, which compares quite well with $U_{300°}/U_{25°} \approx 1.20$ obtained from figure 24.

Given the vapor pressure curve and the lower limit of flammability, the lower temperature limit or approximate flash point of a combustible can be calculated from either equation (32) or (35) (*218*). Approximate flash points were obtained previously, using only the vapor pressure curve and the lower limit at ordinary or elevated temperatures (*154*). The values obtained with this procedure are somewhat low because the lower limit at any temperature above the flash point is less than at the flash point. The lower temperature limits of paraffin hydrocarbon at atmospheric pressure are given in table 4.

TABLE 3.—*Upper flammability limits, U, of methane-air mixtures at 15 psig*

Temperature (° C)	U_{exper}[1] (vol percent)	U_{calc} (vol percent)	U_{calc}-U_{exper} (vol percent)
25	15. 5	15. 5	0
100	16. 3	16. 4	. 1
200	17. 0	17. 5	. 5
300	17. 9	18. 6	. 7

[1] (*182*).

Moderate changes in pressure do not ordinarily affect the limits of flammability of the paraffins in air, as shown in figure 25 for pentane, hexane, and heptane in air (*241*) in a range from 75 to 760 mm Hg. The lower limits

TABLE 4.—*Lower temperature limits and autoignition temperatures of paraffin hydrocarbons at atmospheric pressure*

	Lower temperature limit In air			Autoignition temperature					
				In air			In oxygen		
	° C	° F	Ref.	° C	° F	Ref.	° C	° F	Ref.
Methane	−187	−305	[1]	537	999	(*158*)			
Ethane	−130	−202	[1]	515	959	(*237*)	506	943	(*94*)
Propane	−102	−152	[1]	466	871	(*158*)			
n-Butane	−72	−96	[1]	405	761	(*237*)	283	542	(*191*)
Isobutane	−81	−114	[1]	462	864	(*158*)	319	606	(*94*)
n-Pentane	−48	−54	[1]	258	496	(*194*)	258	496	(*144*)
n-Hexane	−26	−15	(*159*)	223	433	(*194*)	225	437	(*94*)
n-Heptane	−4	25	(*159*)	223	433	(*237*)	209	408	(*94*)
n-Octane	13	56	(*159*)	220	428	(*237*)	208	406	(*191*)
n-Nonane	31	88	(*159*)	206	403	(*237*)			
n-Decane	46	115	(*159*)	208	406	(*237*)	202	396	(*94*)
n-Dodecane	74	165	(*159*)	204	399	(*237*)			
n-Hexadecane	126	259	[1]	205	401	(*237*)			

[1] Caculated value.

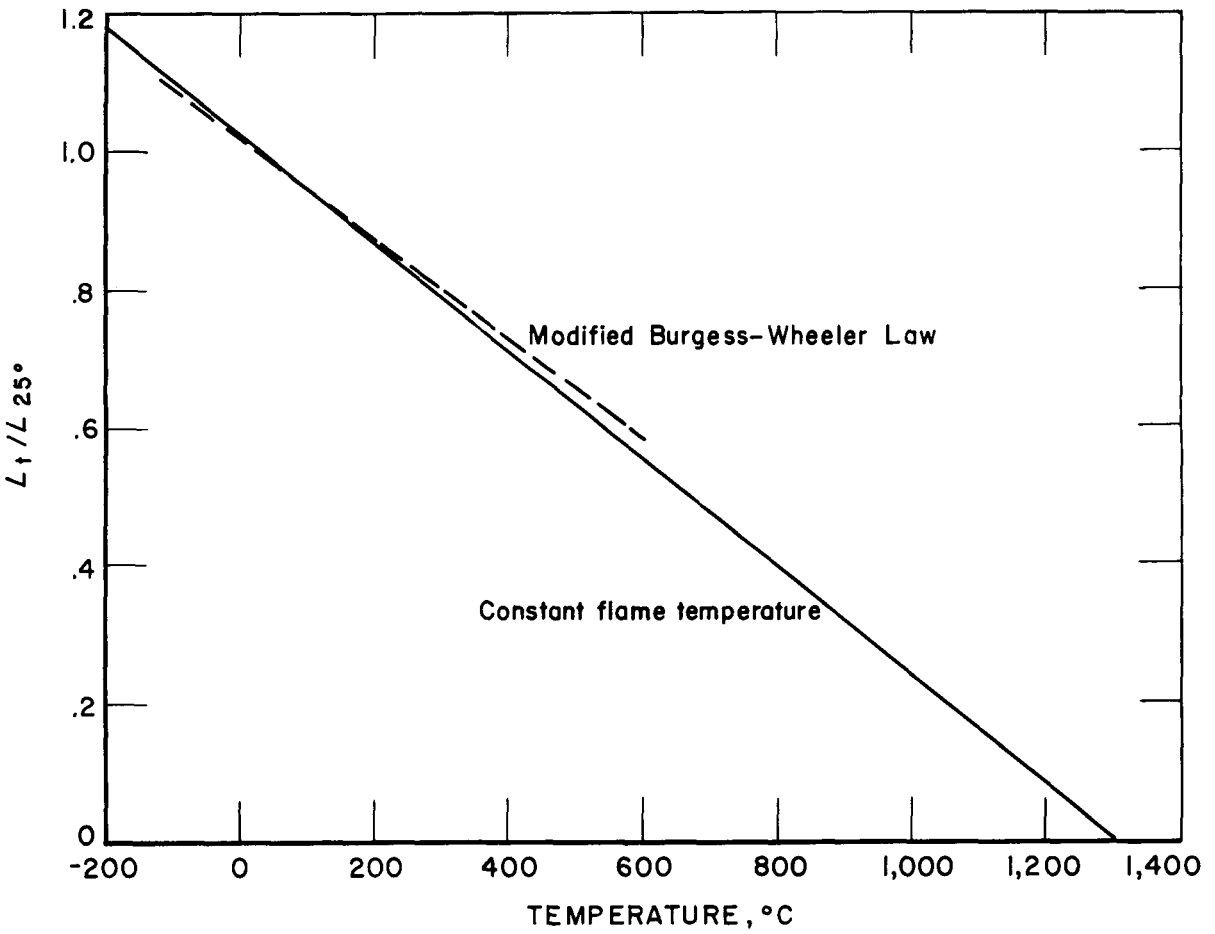

FIGURE 23.—Effect of Temperature on $L_t/L_{25°}$ Ratio of Paraffin Hydrocarbons in Air at Atmospheric Pressure.

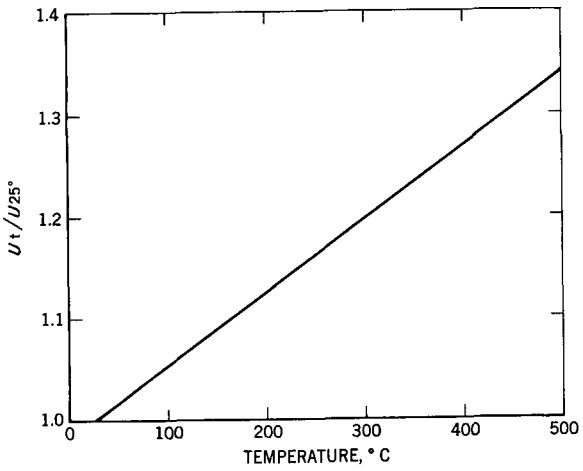

FIGURE 24.—Effect of Temperature on $U_t/U_{25°}$ Ratio of Paraffin Hydrocarbons in Air at Atmospheric Pressure in the Absence of Cool Flames.

coincide, but the upper limits, by weight, increase with increasing molecular weight.

By volume, at atmospheric pressure and 25° C, Spakowski (*201*) found that the upper and lower limits were related by the expression:

$$U_{25°}=7.1L_{25°}^{0.56}. \quad (38)$$

However, the data presented here are correlated more precisely by a somewhat simpler expression:

$$U_{25°}=6.5\sqrt{L_{25°}}. \quad (39)$$

Neither expression is applicable when cool flames are obtained. Substitution of equation (21) for $L_{25°}$ into equation (39) gives

$$U_{25°}=4.8\sqrt{C_{st}}. \quad (40)$$

The limits of flammability of natural gas (85–95 pct methane and 15–5 pct ethane) have been determined over an extended pressure range by Jones and coworkers (*78, 105*). They are given in figure 26 for pressures from 1 to 680 atmospheres (10,000 psig). An analysis of these data shows the limits vary linearly with the logarithm of the initial pressure. That is,

$$L \text{ (vol pct)}=4.9-0.71 \log P \text{ (atm)}, \quad (41)$$

and

$$U \text{ (vol pct)}=14.1+20.4 \log P \text{ (atm)}, \quad (42)$$

with a standard error of estimate of 0.53 vol pct for L and 1.51 vol pct for U.

Although the limits of flammability are not affected significantly by moderate changes in pressure, the temperature limits are pressure dependent. As the total pressure is lowered, the partial pressure of the combustible must also be lowered to maintain a constant combustible concentration. The effect of pressure on the lower temperature limit of the normal paraffins pentane, hexane, heptane, and octane in air, for pressures from 0.2 to 2 atmospheres,

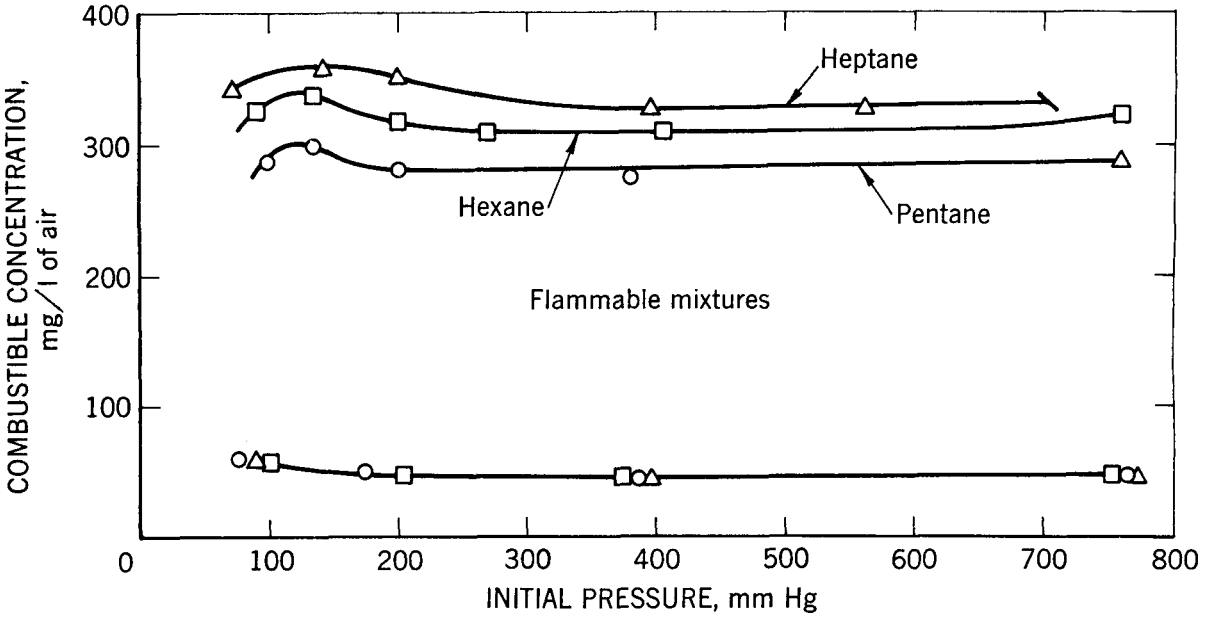

FIGURE 25.—Effect of Pressure on Limits of Flammability of Pentane, Hexane, and Heptane in Air at 26° C.

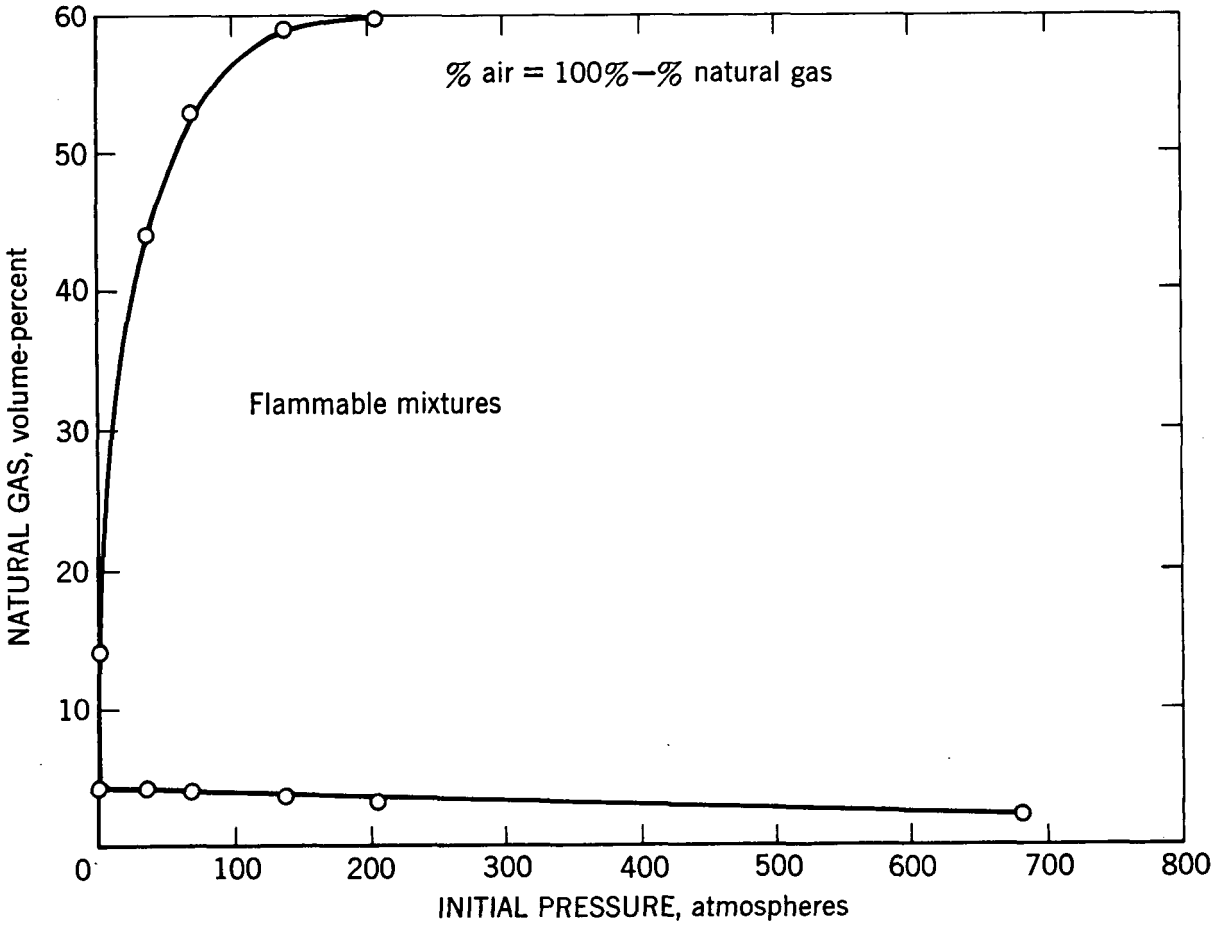

FIGURE 26.—Effect of Pressure on Limits of Flammability of Natural Gas in Air at 28° C.

is shown in figure 27. The temperature limits were calculated from the $L_{25°}$ values, the vapor pressure curves, and the data of figure 23.

Limits in Other Atmospheres

Limits of flammability of some paraffin hydrocarbons have been determined in oxygen, chlorine, and oxides of nitrogen, as well as in mixtures of air and various inerts. The lower limits in oxygen and in a wide variety of oxygen-nitrogen mixtures are essentially the same as those in air at the same temperature and pressure (fig. 10). Limit-of-flammability measurements by Bartkowiak and Zabetakis for methane and ethane in chlorine at 1, 7.8, and 14.6 atmospheres, ranging from 25° to 200° C, are summarized in tables 5 and 6 (*8*).

Coward and Jones (*40*) have presented graphically the limits of flammability of the first six members of the paraffin series in air containing various inerts, based on a representation found useful in some mining applications and treating inert gas or vapor as part of the atmosphere with which the combustible is mixed. The composition of a point on such a diagram, except one that represents only combustible and air, cannot be read directly. Instead, one must determine the composition of the atmosphere, add the combustible content, and then compute the total mixture com-

TABLE 5.—*Limits of flammability of methane in chlorine*

(volume-percent)

Pressure, psig	Limits	Temperature, ° C		
		25	100	200
0	Lower	5.6	3.6	0.6
	Upper	70	66	--------
100	Lower	--------	2.4	.6
	Upper	72	76	77
200	Lower	--------	--------	--------
	Upper	73	72	75

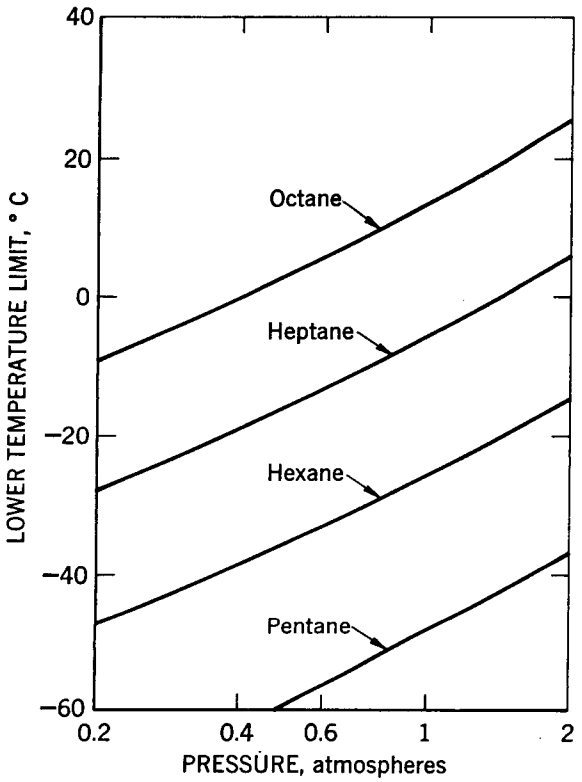

FIGURE 27.—Effect of Pressure on Lower Temperature Limits of Flammability of Pentane, Hexane, Heptane, and Octane in Air.

TABLE 6.—*Limits of flammability of ethane in chlorine*

(volume-percent)

Pressure, psig	Limits	Temperature, ° C		
		25	100	200
0	Lower	6. 1	2. 5	2. 5
	Upper	58	58	
100	Lower	3. 5	1. 0	1. 0
	Upper	63	75	82
200	Lower			
	Upper	66	73	76

position. This has been done for methane through hexane (figs. 28–33). Compositions are determined directly from the abscissas (inert concentration) and ordinates (combustible concentration); the air in any mixture is the difference between 100 percent and the sum of inert and combustible. Data of Burgoyne and Williams-Leir for methane-methyl bromide (MeBr)-air and methane-carbon tetrachloride-air mixtures are included in figure 28 (*29*). Unfortunately, the methane-methyl bromide-air data were obtained in a 1⅞-inch tube. Although satisfactory for methane and other hydrocarbons, this tube is apparently not satisfactory for many of the halogenated hydrocarbons. Thus a recent industrial explosion involving methyl bromide prompted Hill to reconsider the flammability of methyl bromide in air (*84*). He found that methyl bromide was not only flammable in air but that it formed flammable mixtures at 1 atmosphere with a wider variety of concentrations than Jones had reported (*96*). This would suggest that there is no justification for the assumption that Jones' flammability data for methyl bromide were influenced by the presence of mercury vapor (*196*). Hill's limit values at atmospheric pressure are included in figure 28 and are used to form the approximate, broken, flammability curves for the methane-methyl bromide-air system.

Data of Moran and Bertschy for pentane-perfluoropropane-air, pentane-sulfur hexafluoride-air and pentane-perfluoromethane-air mixtures are included in figure 32 (*147*). Data by Burgoyne and Williams-Leir for hexane-methyl bromide-air and hexane-Freon-12 [4] (F–12; CF_2Cl_2)-air mixtures have been included in figure 33. These data were all obtained in 1⅞-inch-diameter tubes. An investigation of flammability of hexane-methyl bromide-air mixtures in a 4-inch tube indicated that an increase in tube size (from 1⅞-inches to 4-inches-ID) resulted in a narrowing of the flammable range; the upper limit decreased from 7.5 to 5.7 volume-percent *n*-hexane vapor in air while the lower limit remained constant. The amount of methyl bromide required for extinction decreased from 7.05 volume-percent in the 1⅞-inch tube to 6.0 volume-percent in the 4-inch tube. However, again this is not in line with the results obtained by Hill with methyl bromide-air mixtures (*84*). Accordingly, while the data obtained in approximately 2-inch tubes were used to construct figure 33, the Hill data, obtained in a larger apparatus, are also used to form the approximate, broken, flammability curves for the hexane-methyl bromide-air system.

The limits of flammability diagrams for the system *n*-heptane-water vapor-air at 100° and 200° C (fig. 34) show the effects of temperature on a system that produces both normal and cool flames at atmospheric pressure (*192*). Interestingly enough, the minimum oxygen requirement for flame propagation (Min O_2) at 200° C is the same for the cool and normal flame regions in this instance. Further, the decrease in minimum oxygen requirements

[4] Trade names are used for identification only; this does not imply endorsement by the Bureau of Mines.

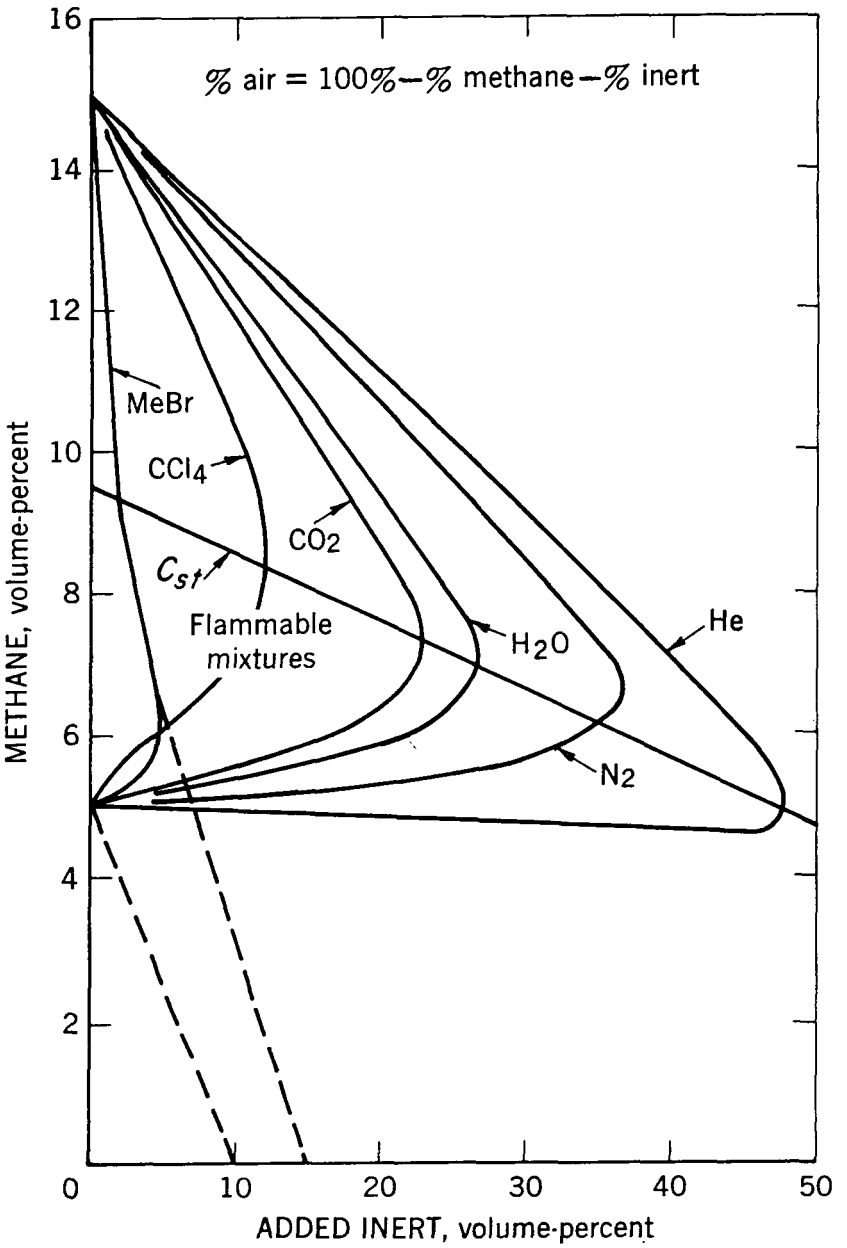

FIGURE 28.—Limits of Flammability of Various Methane-Inert Gas-Air Mixtures at 25° C and Atmospheric Pressure.

(from 13.5±0.3 volume-percent at 100° C to 12.8±0.3 volume-percent at 200° C) is within the range predicted by the modified Burgess-Wheeler law (equation 35 and fig. 23). However, the available data are too meager at present to permit a realistic evaluation of the validity of this law.

Inspection of the limit-of-flammability curves in figures 28 to 33 reveals that except for methane and ethane, the minimum amounts of carbon dioxide and nitrogen required for flame extinction (peak values) at 25° C and atmospheric pressure are about 28 and 42 volume-percent, respectively. The ratio of these values is approximately inversely proportional to the ratio of their heat capacities at the temperature at which combustion occurs. Accordingly, generalized flammability diagrams of the type given in figure 35 can be constructed for the higher hydrocarbons, ignoring the presence of cool flames. Such diagrams do not appear to be applicable to the halogenated hydrocarbons

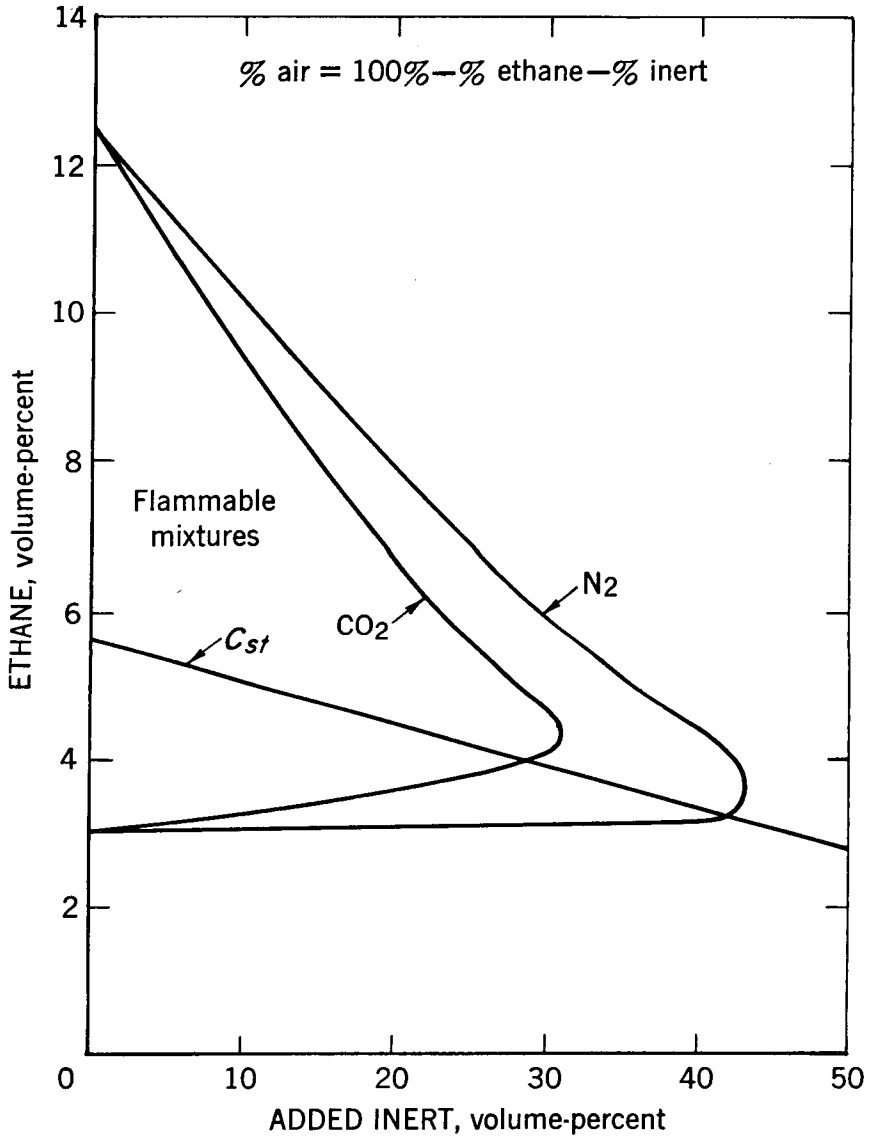

FIGURE 29.—Limits of Flammability of Ethane-Carbon Dioxide-Air and Ethane-Nitrogen-Air Mixtures at 25° C and Atmospheric Pressure.

since these materials tend to decompose even in flames of limit-mixture composition and, as noted, may themselves propagate flame. Coleman (*37*) has found that the ratios of the peak values of a halogenated hydrocarbon are not constant but are proportional to the heats of combustion of the combustibles to which the halogenated hydrocarbon is added.

Few data are available for the effects of pressure on the limits of flammability of combustible-inert-air mixtures. One such set of data is summarized in figure 36, which gives the limits of flammability of natural gas (85 pct methane+15 pct ethane) nitrogen-air at 26° C and 0, 500, 1,000 and 2,000 psig (*105*). Similar data are given for ethane-carbon dioxide-air (fig. 37) and ethane-nitrogen-air (fig. 38) (*121*), and for propane-carbon dioxide-air (fig. 39) and propane-nitrogen-air (fig. 40) (*122*). Minimum oxygen requirements for flame propagation (min O_2) through natural gas-nitrogen-air, ethane-nitrogen-air, and propane-nitrogen-air at atmospheric and elevated pressures and 26° C are summarized in figure 41. The minimum O_2 values in volume-percent are related to pressure as follows:

for natural gas:

$$\text{Min. } O_2 = 13.98 - 1.68 \log P; \qquad (43)$$

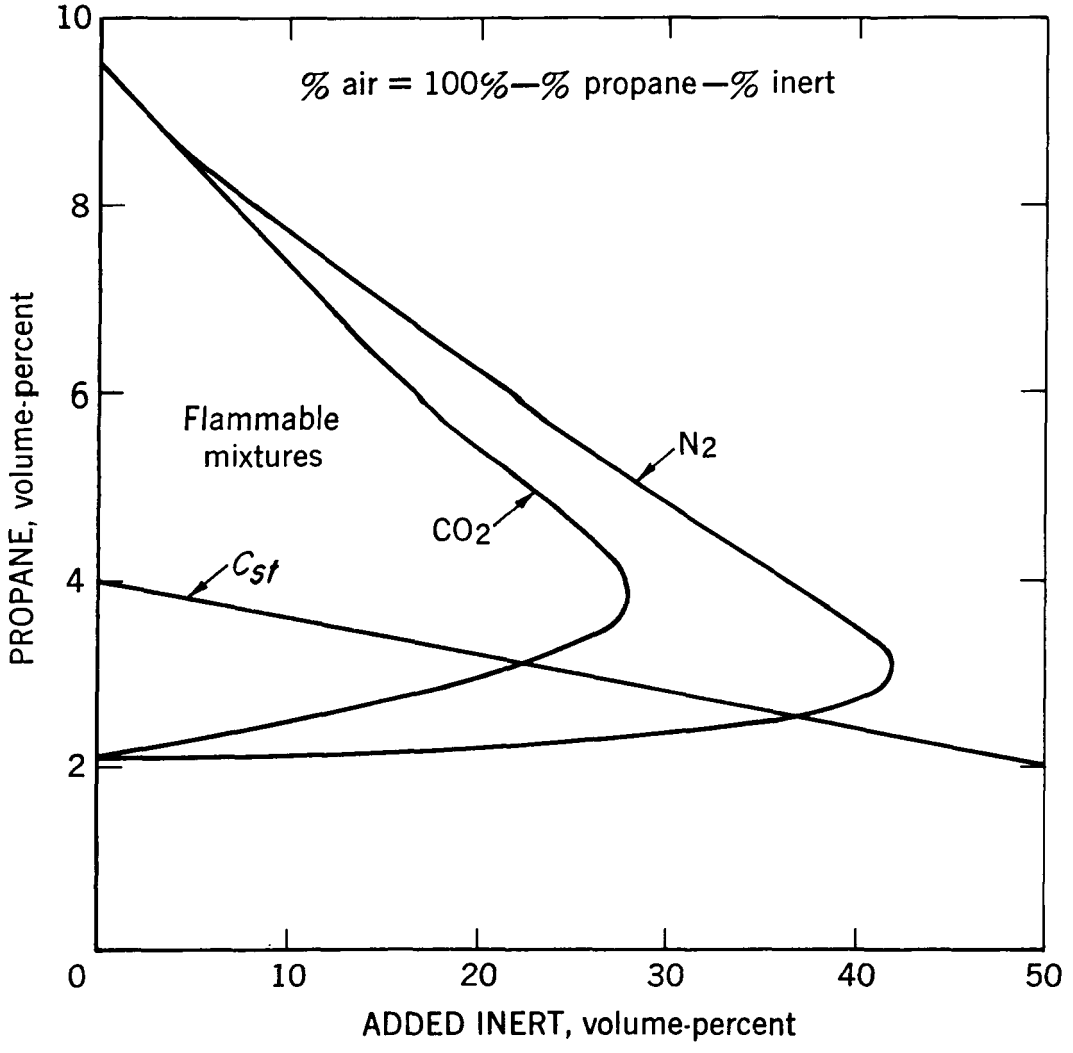

FIGURE 30.—Limits of Flammability of Propane-Carbon Dioxide-Air and Propane-Nitrogen-Air Mixtures at 25° C and Atmospheric Pressure.

for ethane:

$$\text{Min. } O_2 = 12.60 - 1.36 \log P; \text{ and} \quad (44)$$

for propane:

$$\text{Min. } O_2 = 13.29 - 1.52 \log P; \quad (45)$$

where P is the initial pressure in psia.

The lower limit of flammability of any mixture of the paraffin hydrocarbons can be calculated by Le Chatelier's law (*40, 129, 235*):

$$L = \frac{100}{\sum_{i=1}^{n} \frac{C_i}{L_i}}, \quad \sum_{i=1}^{n} C_i = 100 \quad (46)$$

where C_i and L_i are the percentage composition and lower limit, respectively, of the i^{th} combustible in the mixture. For example, a mixture containing 80 volume-percent methane, 15 volume-percent ethane and 5 volume-percent propane has a lower limit in air at 25° C and atmospheric pressure of:

$$L_{25°} = \frac{100}{\frac{80}{5.0} + \frac{15}{3.0} + \frac{5}{2.1}} = 4.3 \text{ vol pct.} \quad (47)$$

Liquid mixtures can be treated in the same way if the relative escaping tendencies of the various components are known. Since the paraffin hydrocarbons obey Raoult's law (*143*), the partial pressure of each component can be calculated as follows:

$$p_i = p_o N_i \quad (48)$$

where p_i is the vapor pressure of the i^{th} com-

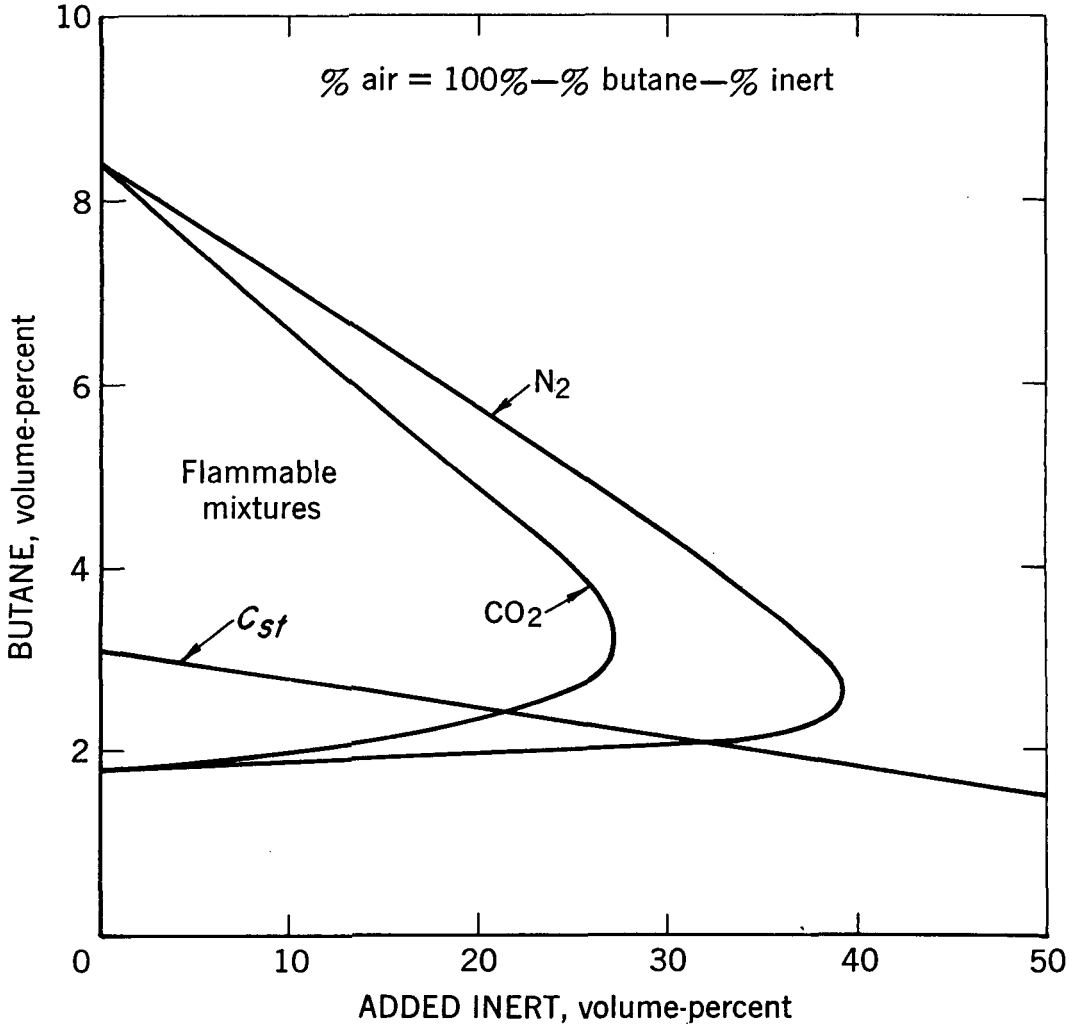

FIGURE 31.—Limits of Flammability of Butane-Carbon Dioxide-Air and Butane-Nitrogen-Air Mixtures at 25° C and Atmospheric Pressure.

ponent in the blend, p_o is the vapor pressure of the pure component and N_i is its mole fraction in the solution. This procedure has been used to calculate the lower temperature limits of decane-dodecane blends in air (fig. 42). The vapor pressures of decane and dodecane and the calculated low temperature limits are given by solid lines and four experimental values by circles.

Autoignition

Two types of autoignition data are obtained depending upon whether the objective is to cause or to prevent the ignition of a combustible in air. The first type are usually obtained at high temperatures, where the ignition delay is relatively short. Typical of these are the data of Mullins (*153*), Brokaw and Jackson (*15*, *90*), Ashman and Büchler (*6*), and Kuchta, Lambiris, and Zabetakis (*127*). These are not normally used for safety purposes, unless there is some assurance that the contact time of combustible and air is less than the ignition delay at the temperature of the hot zone. The minimum autoignition temperature (AIT) is usually the quantity of interest in safety work, especially when combustible and air can remain in contact for an indefinite period.

Some AIT values for paraffin hydrocarbons in air obtained by Setchkin in a 1-liter spherical Pyrex flask (*194*) and by Zabetakis, Furno, and Jones in a 200 cc Pyrex Erlenmeyer flask (*237*) are given in table 4. Interestingly enough, experiments conducted in these and other flasks generally indicate that flask shape and size are important in determining the AIT. The AIT data obtained in the 200 cc flask may

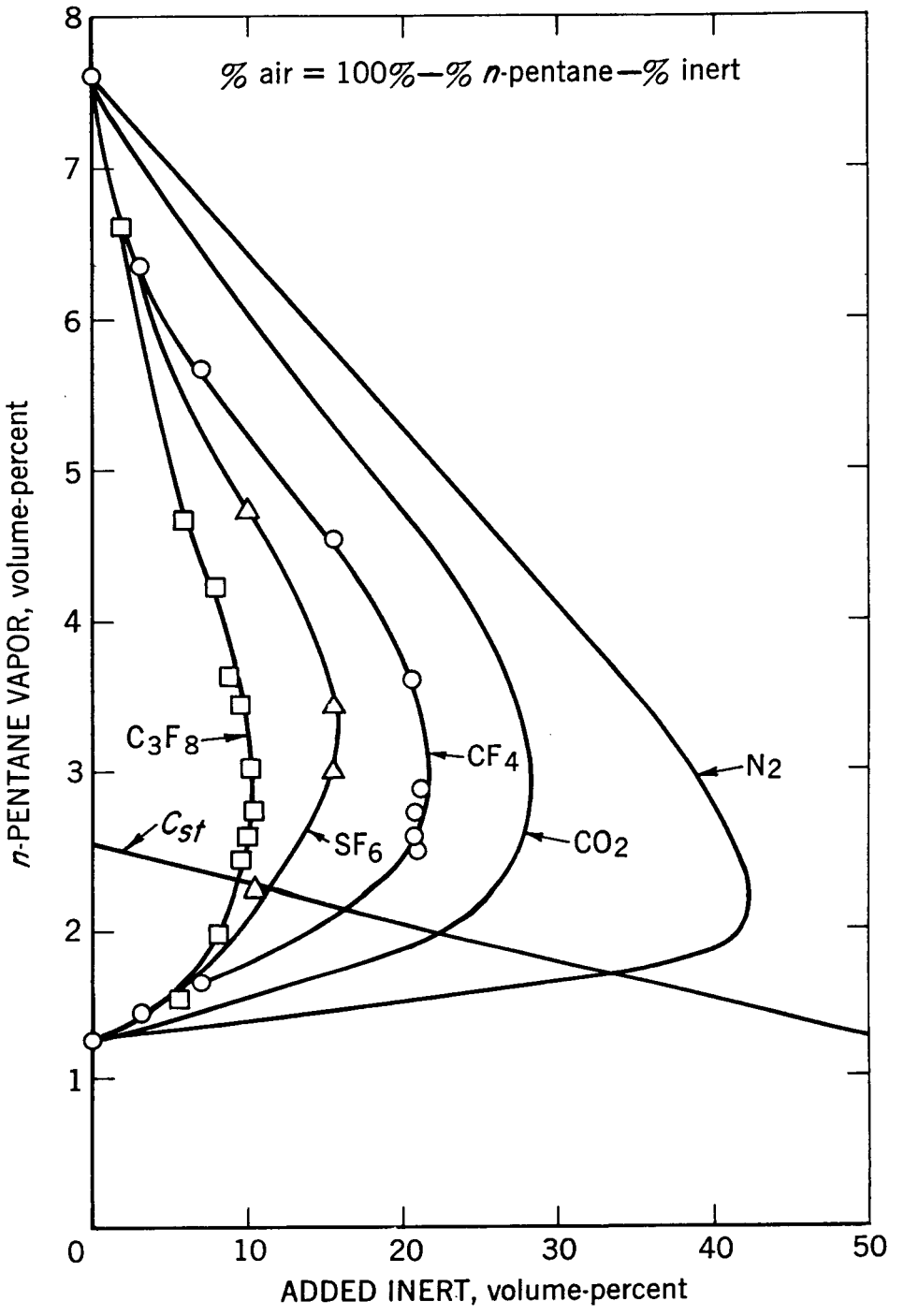

FIGURE 32.—Limits of Flammability of Various *n*-Pentane-Inert Gas-Air Mixtures at 25° C and Atmospheric Pressure.

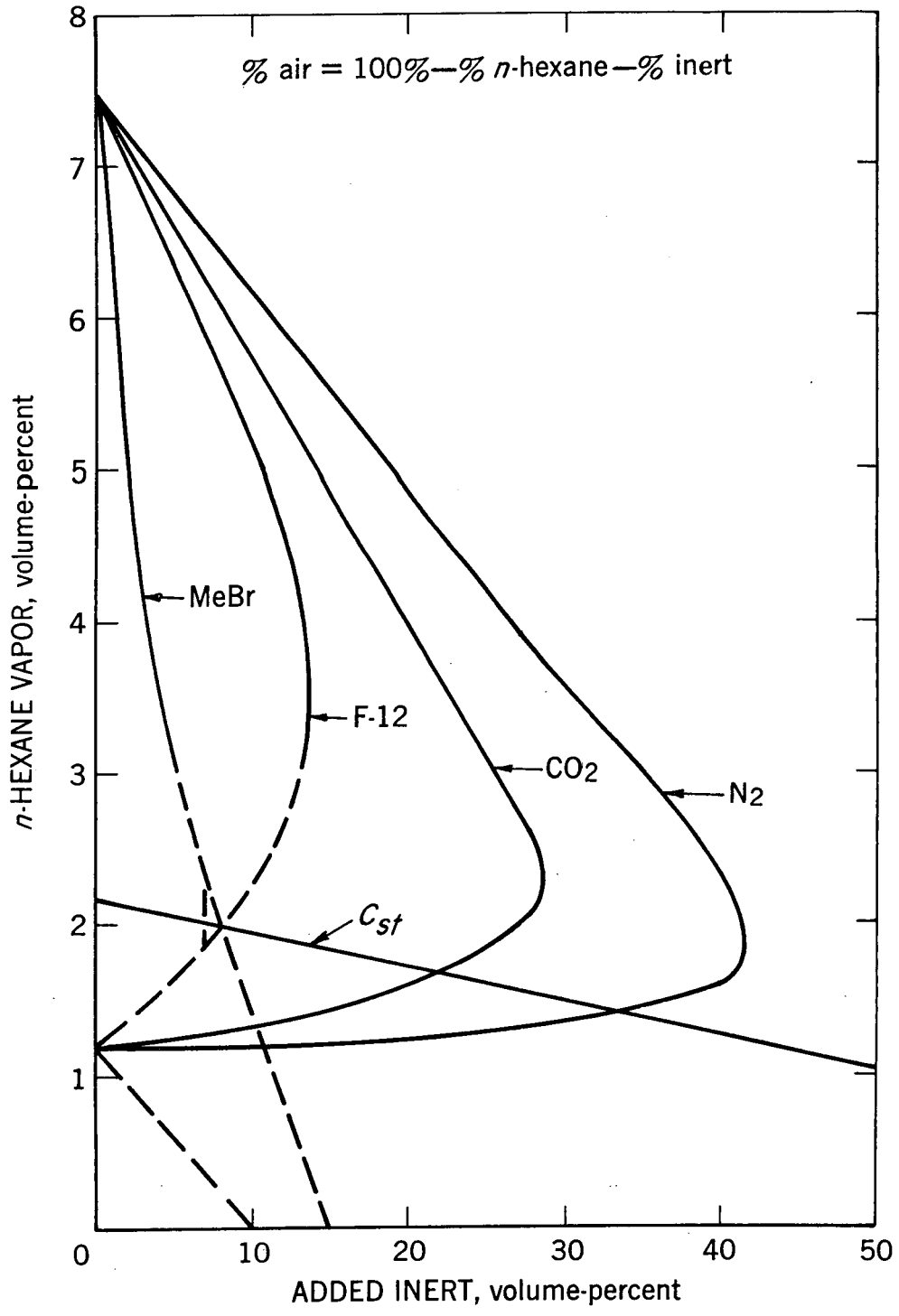

FIGURE 33.—Limits of Flammability of Various *n*-Hexane-Inert Gas-Air Mixtures at 25° C and Atmospheric Pressure.

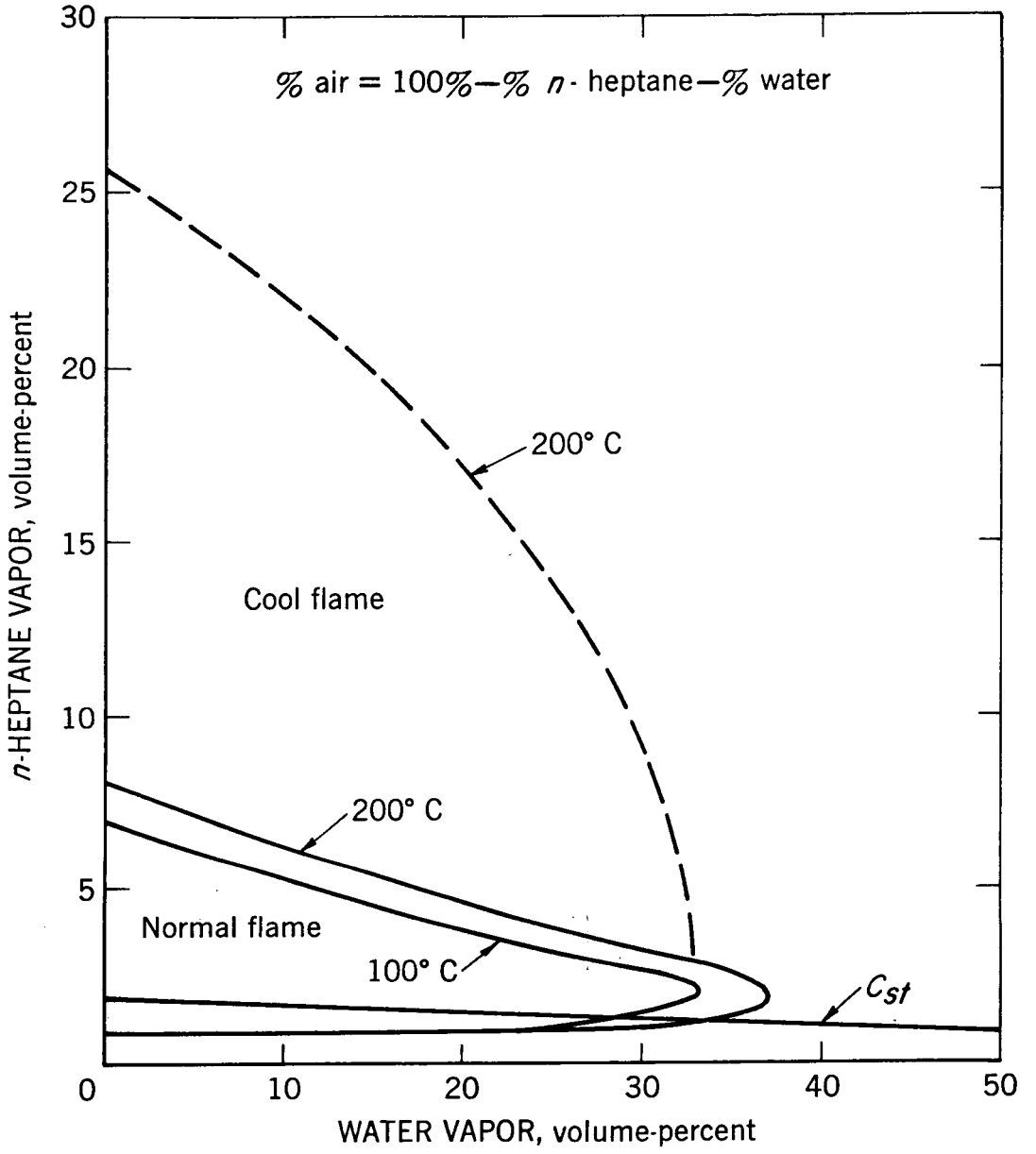

FIGURE 34.—Limits of Flammability of *n*-Heptane-Water Vapor-Air Mixtures at 100° and 200° C and Atmospheric Pressure.

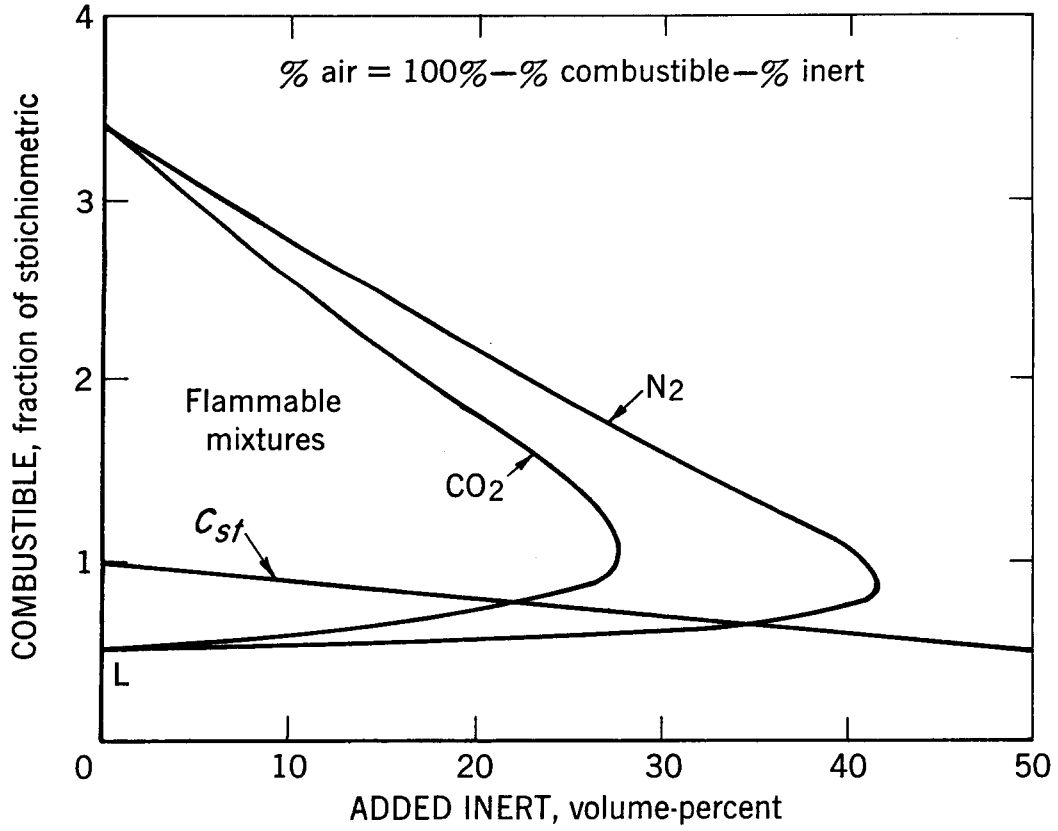

FIGURE 35.—Approximate Limits of Flammability of Higher Paraffin Hydrocarbons (C_nH_{2n+2}, $n \geq 5$) in Carbon Dioxide-Air and Nitrogen-Air Mixtures at 25° C and Atmospheric Pressure.

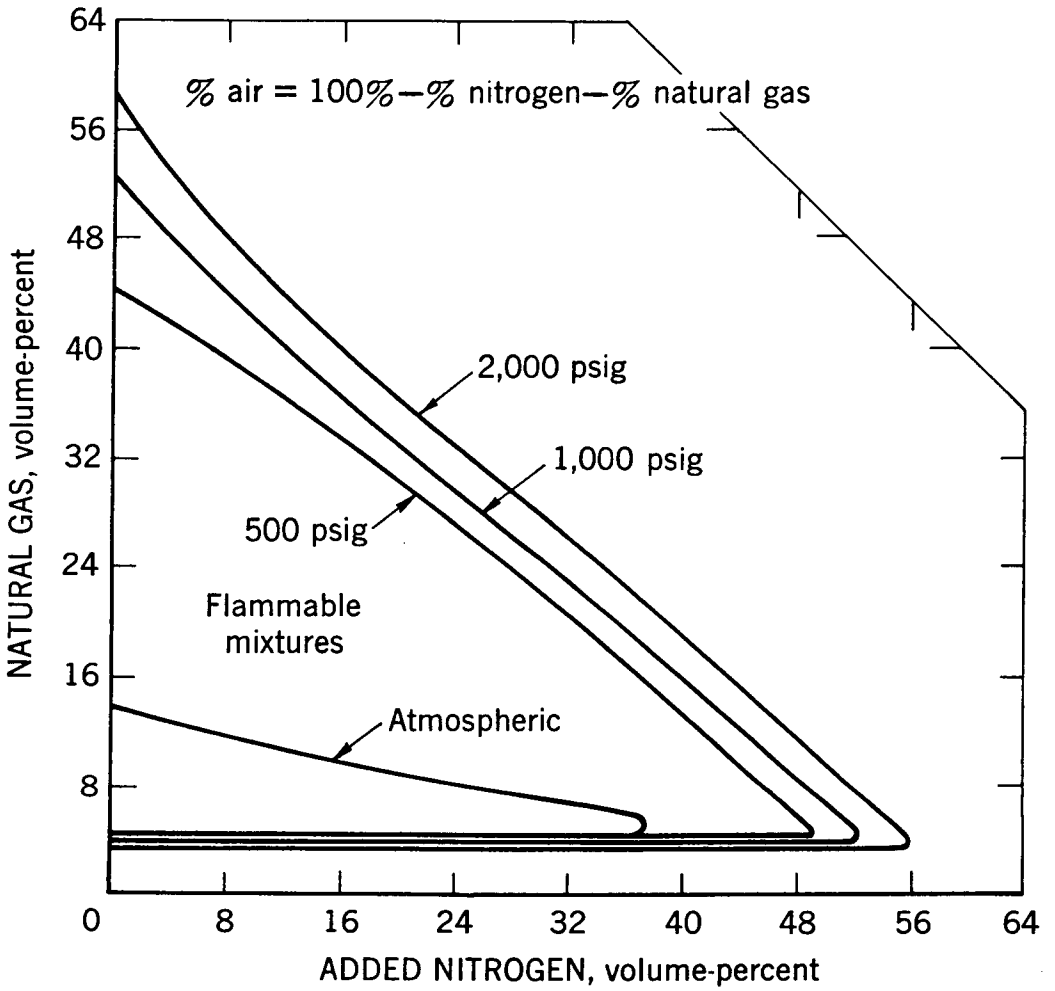

FIGURE 36.—Effect of Pressure on Limits of Flammability of Natural Gas-Nitrogen-Air Mixtures at 26° C.

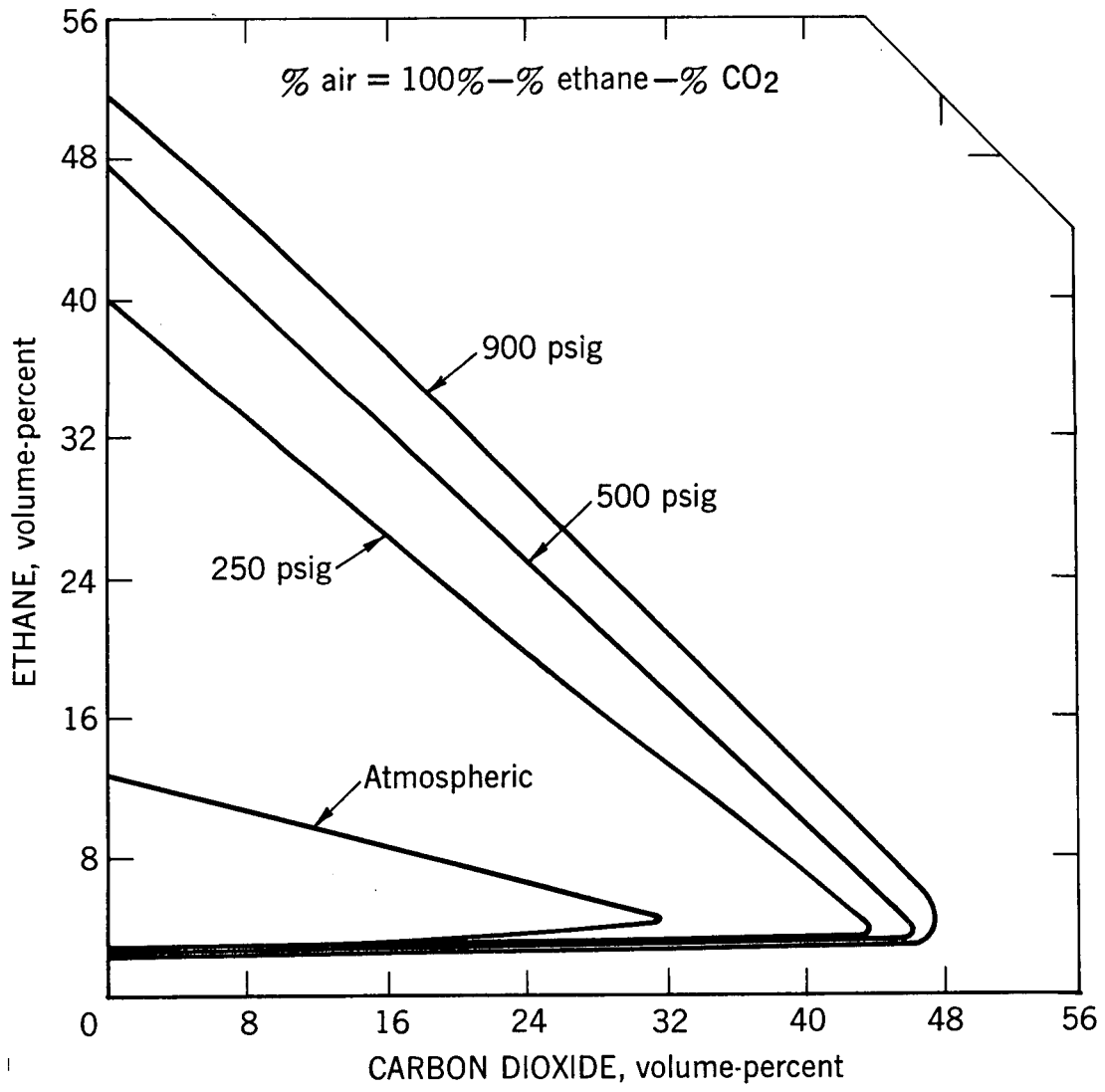

FIGURE 37.—Effect of Pressure on Limits of Flammability of Ethane-Carbon Dioxide-Air Mixtures at 26° C.

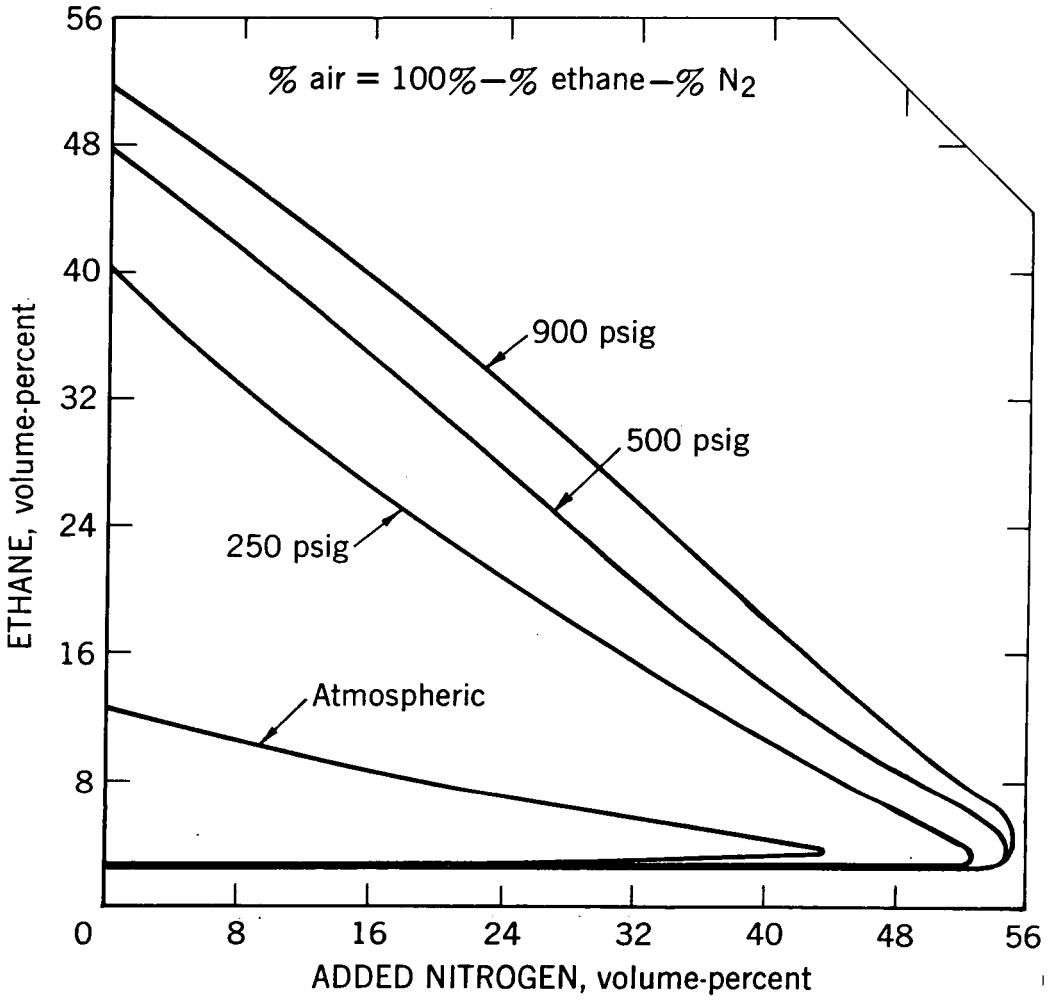

FIGURE 38.—Effect of Pressure on Limits of Flammability of Ethane-Nitrogen-Air Mixtures at 26° C.

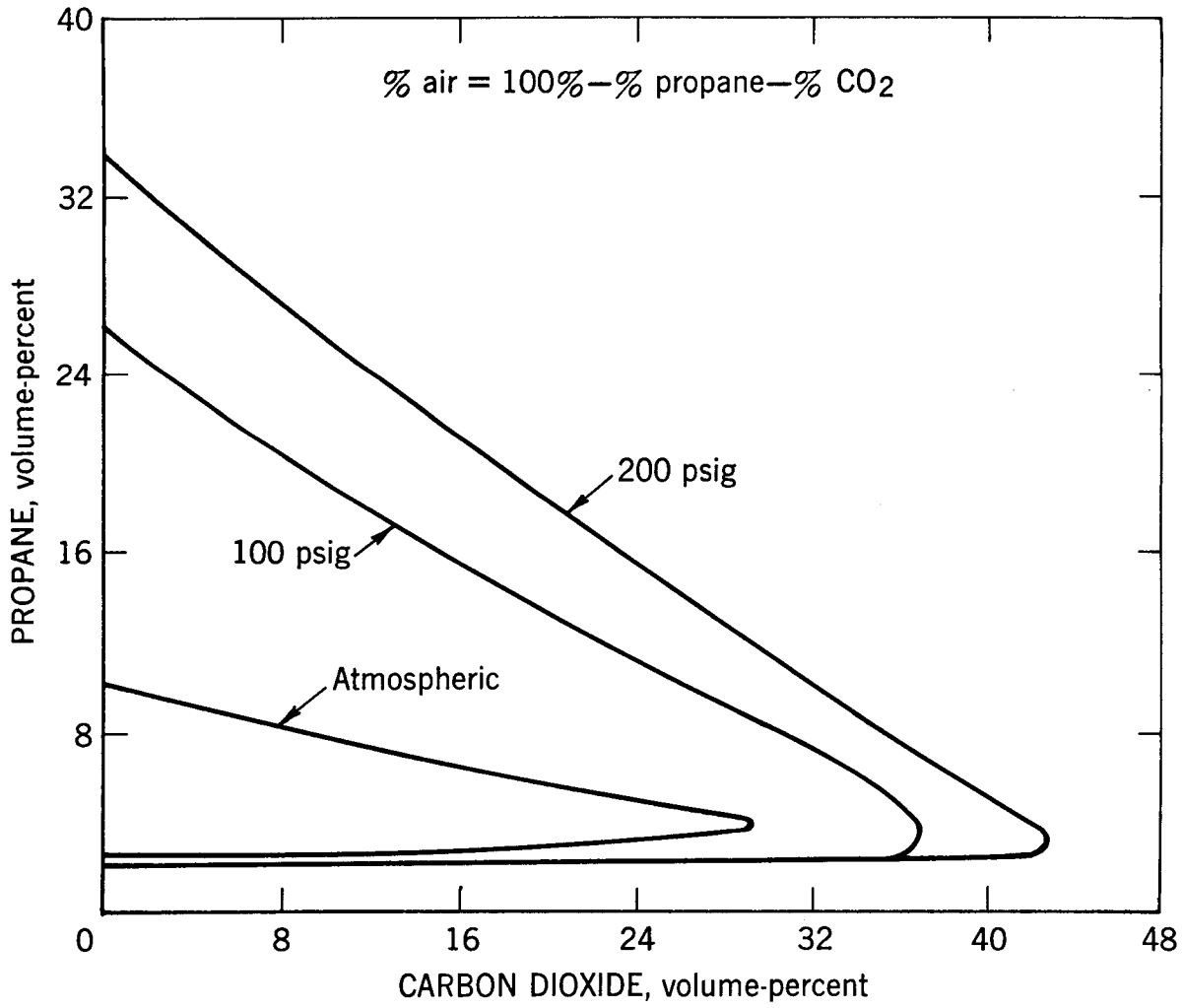

FIGURE 39.—Effect of Pressure on Limits of Flammability of Propane-Carbon Dioxide-Air Mixtures.

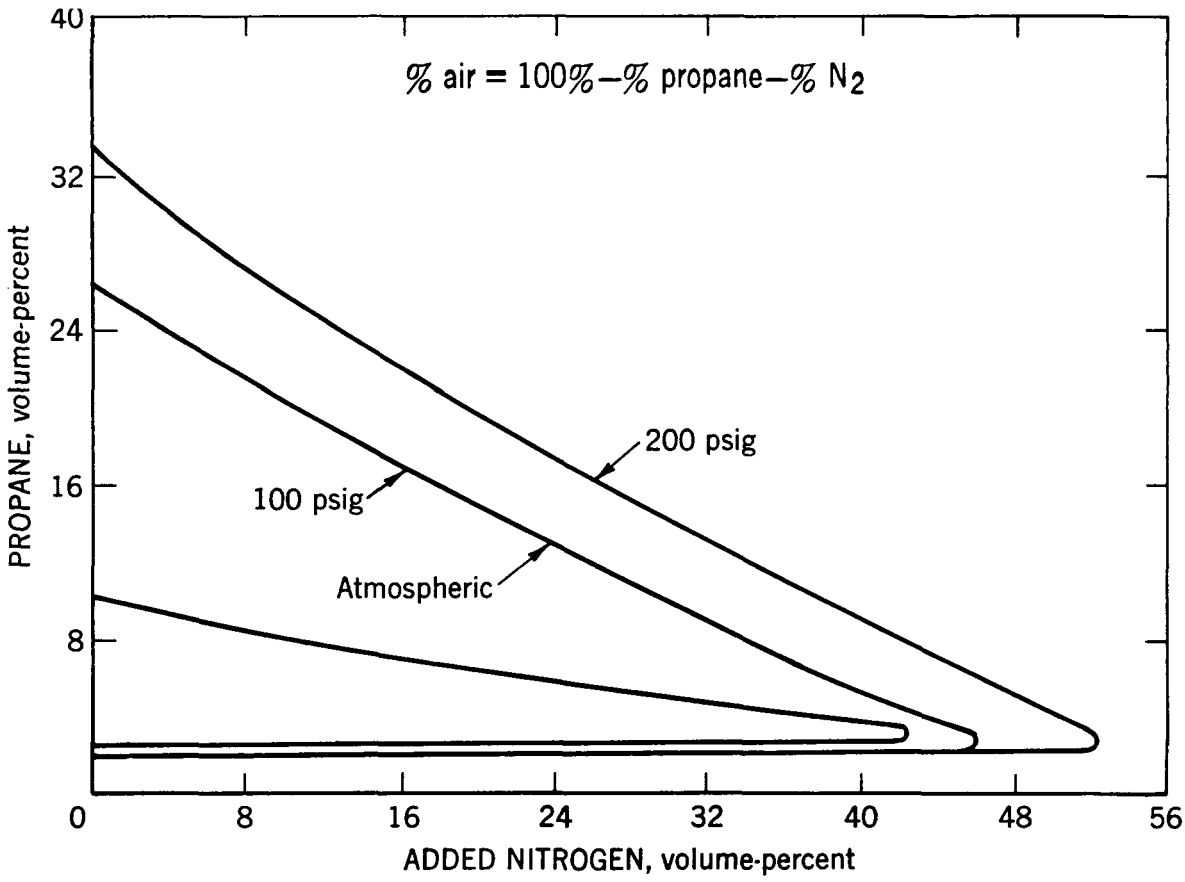

FIGURE 40.—Effect of Pressure on Limits of Flammability of Propane-Nitrogen-Air Mixtures.

be correlated with molecular structure by plotting them against the average carbon chain length defined as

$$L_{ave}=\frac{2\sum_{i}^{n} g_i N_i}{M(M-1)}, \qquad (49)$$

where g_i is the number of possible chains each containing N_i carbon atoms and M is the number of methyl (—CH_3) groups. For example, n-nonane and 2,2,3,3-tetramethyl pentane each have 9 carbon atoms, but the former has 2 methyl groups and the latter has 6. The former has only one chain of 9 carbon atoms with a methyl group on each end, and the latter has a maximum of 4 chains with 3 carbon atoms, 8 chains with 4 carbon atoms, and 3 chains with 5 carbon atoms. Thus, *n*-nonane has an average chain length of 9 and 2,2,3,3-tetramethyl pentane has an average of 3.9. The more highly branched a combustible is, the higher its ignition temperature will be. Minimum autoignition temperatures of 20 paraffins were plotted as ordinate against the average chain length as abscissa (fig. 43). The data fall into two regions—a high-temperature region in which the AIT is greater than 400° C and a low temperature region in which the AIT is less than 300° C. These regions coincide with those of Mulcahy who found that oxidation proceeds by one of two different mechanisms (*152*), and by Frank, Blackham, and Swarts (*60*). The AIT values of combustibles in the first region are normally much more sensitive to the oxygen concentration of the oxidizing atmosphere and to the spray injection pressure than are the combustibles in the second region. Unfortunately, the available consistent AIT data about the effects of oxygen concentration and injection pressure are too meager to permit a detailed comparison.

The physical processes (*206*) and reactions that lead to autoignition are of interest in any detailed study of this ignition process. Salooja (*184*), Terao (*207*), Affens, Johnson and Carhart (*1*, *2*), and others have studied the autoignition of various hydrocarbons in an effort to determine the mechanisms that lead to the ignition reaction.

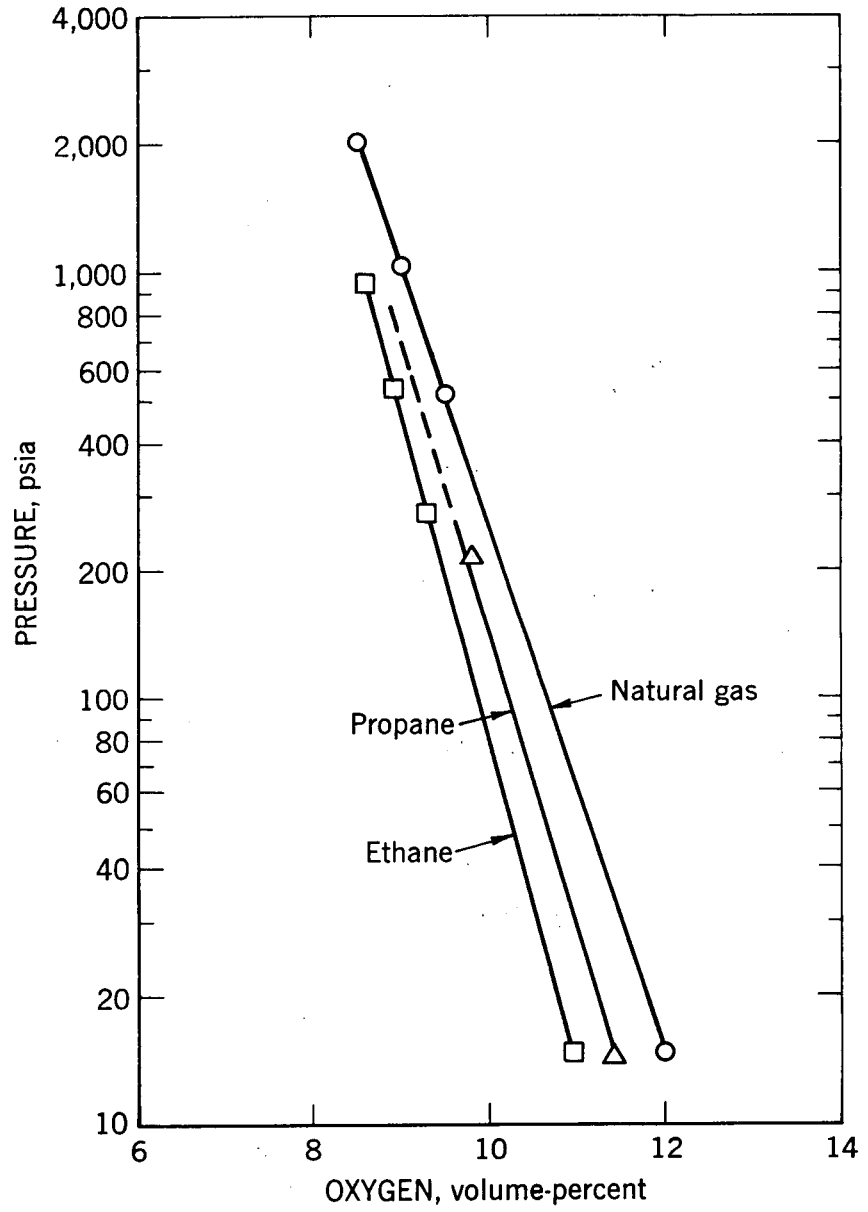

FIGURE 41.—Effect of Pressure on Minimum Oxygen Requirements for Flame Propagation Through Natural Gas-Nitrogen-Air, Ethane-Nitrogen-Air, and Propane-Nitrogen-Air Mixtures at 26° C.

An increase in pressure generally decreases the AIT of a combustible in a given oxidant. For example, the AIT of a natural gas in air decreased from 530° C at 1 atmosphere to 240° C at 610 atmospheres (9,000 psig) (*78*). The AIT's of several hydrocarbons were found to obey Semenov's equation over a limited pressure range (*248*):

$$\log \frac{P}{T} = \frac{A}{T} + B \qquad (50)$$

where T is the AIT at an initial pressure P, and A and B are constants. Accordingly, the AIT values obtained at atmospheric pressure should not be used to assess ignition hazards at high pressures.

Burning Rate

The burning velocities, S_u, of various hydrocarbons have been measured by numerous investigators in air and other oxidants (*68, 131*). At one atmosphere and 26° C, the burning

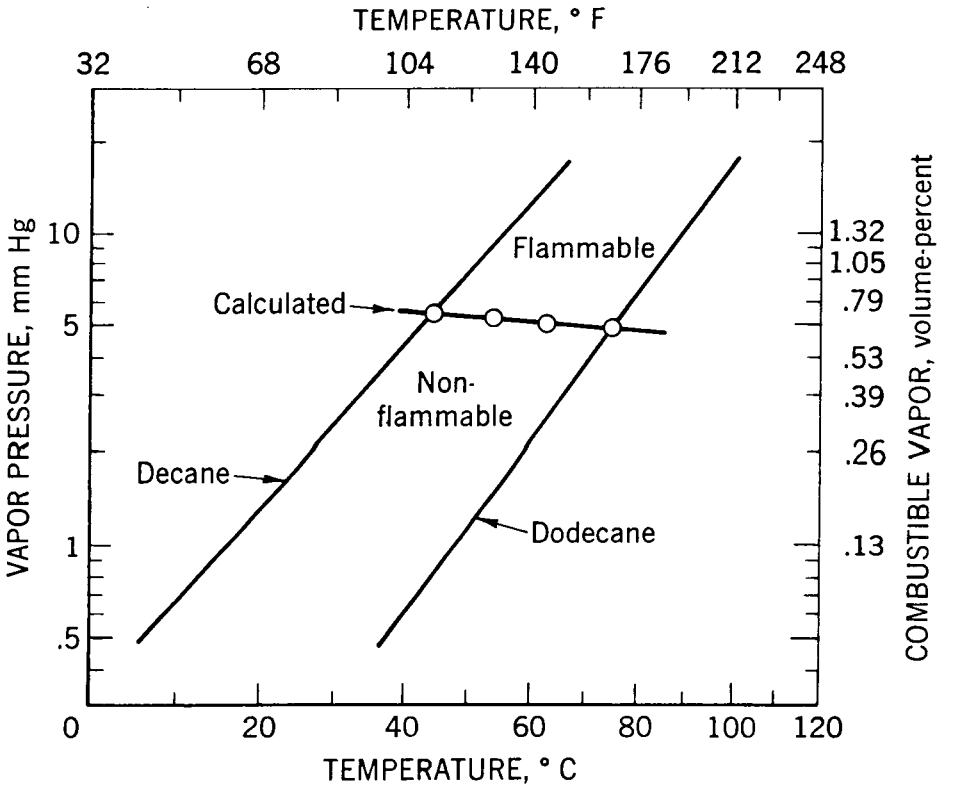

FIGURE 42.—Low-Temperature Limit of Flammability of Decane-Air, Dodecane-Air and Decane-Dodecane-Air Mixtures (Experimental Points 0).

velocities of paraffin hydrocarbons in air range from a few centimeters a second near the limits to about 45 cm/sec near the stoichiometric mixture composition; much higher values are obtained with paraffin hydrocarbon-oxygen mixtures. Figure 44 gives results obtained by Gibbs and Calcote for four paraffin hydrocarbon-air mixtures at atmospheric pressure and room temperature (*68*). The data are expressed in terms of the stoichiometric composition, C_{st}; burning velocities are given for the composition range from 0.7 to 1.4 C_{st}. These authors have presented similar data for combustibles at 25° and 100° C. Figure 45 gives results obtained by Singer, Grumer, and Cook for three paraffin hydrocarbon-oxygen mixtures at atmospheric pressure and room temperature in the range from 0.3 to 1.4 C_{st} (*198*). Burning velocities range from a low of 125 cm/sec to a high of 425 cm/sec; these values are considerably greater than those obtained in air. A change in either temperature or pressure will alter S_u for a particular mixture. For example, Agnew and Graiff (*3*) found that an increase in pressure causes S_u of stoichiometric methane-air and propane-air mixtures to decrease in the pressure range from 0.5 to 20 atmospheres (fig. 46); S_u of stoichiometric methane-oxygen mixtures, however, increased in the pressure range from 0.2 to 2 atmospheres (fig. 47). The effect of temperature is more consistent. For a given pressure and mixture composition, an increase in temperature raises S_u. In general:

$$S_u = A + BT^n \qquad (51)$$

where A and B are constants, T is the temperature and n is a constant for a particular mixture composition. Dugger, Heimel, and Weast (*50, 51, 81*) obtained a value of 2.0 for n for some of the paraffin hydrocarbons (fig. 48). The burning velocity of the stoichiometric methane-air and methane-oxygen mixtures given in figures 44 and 45 do not agree with the values given in figures 46 to 48 but, in each case, the burning velocity data are internally consistent.

The actual flame speed relative to a fixed observer may be much greater than S_u since the burned gases, if not vented, will expand and impart a motion to the flame zone. If detonation occurs, the reaction speed increases markedly. For example, figure 49 gives the Kogarko data on velocities with which a detonation wave propagates through various methane-air mixtures at atmospheric pressure in a 30.5 cm-diameter pipe (*125*). Similar results have been obtained by Gerstein, Carlson, and Hill at low pressures with natural gas-air mixtures (*67*).

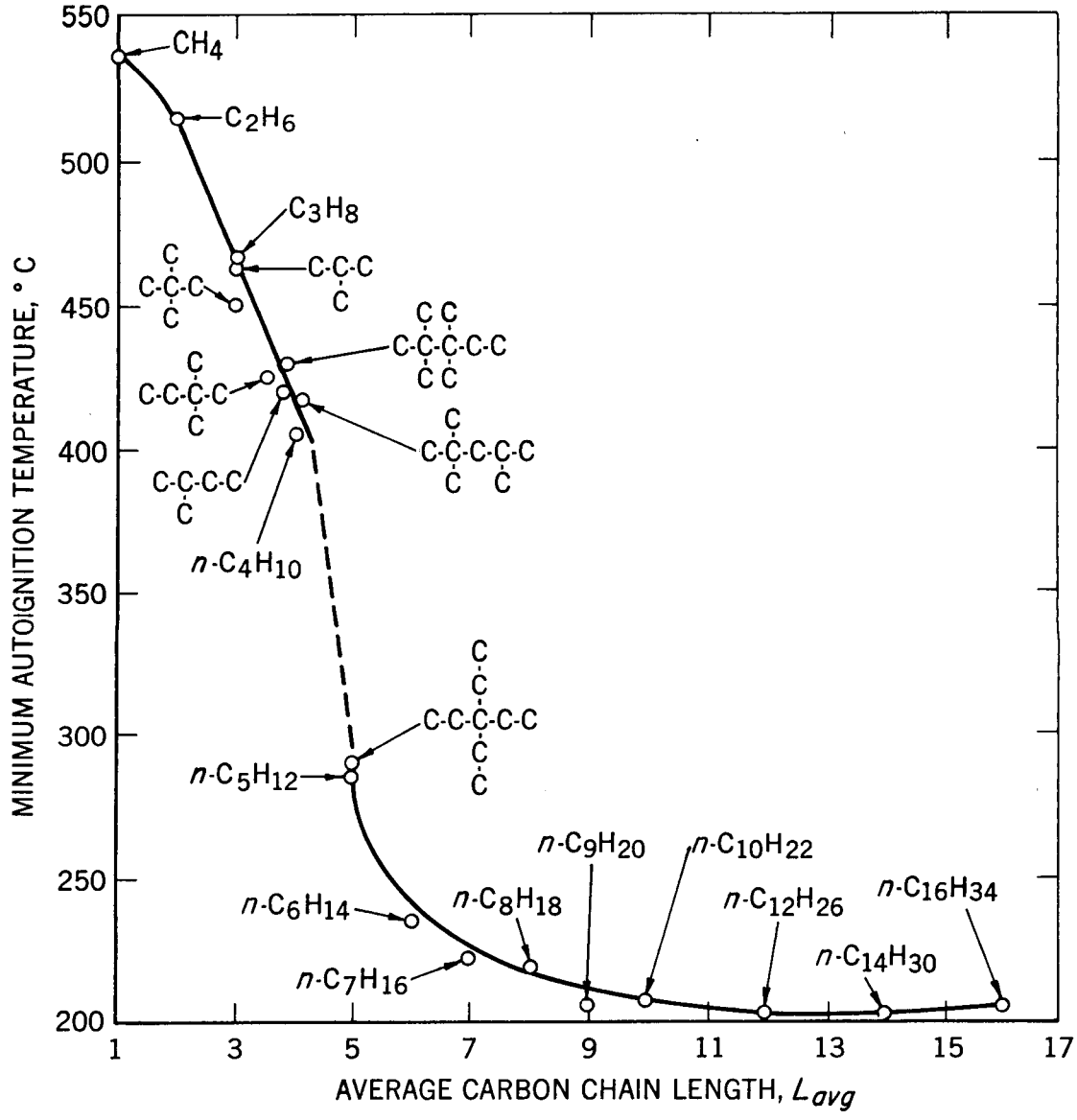

FIGURE 43.—Minimum Autoignition Temperatures of Paraffin Hydrocarbons in Air as a Function of Average Carbon Chain Length.

In each case, powerful initiators were required to obtain a detonation in relatively large pipes. The energy requirements for ignition are reduced if oxygen is used as the oxidant in place of air. Further, the detonation velocity increases as the oxygen content of the atmosphere is increased. Detonation velocities obtained by Morrison for methane, ethane, propane, butane, and hexane in oxygen are given in figure 50 (*150*); similar data obtained by Wayman and Potter are given in figure 51 for *n*-heptane-nitrogen-white fuming nitric acid vapors (*219*). Of principal interest here is the magnitude of the detonation velocity; even in air, this velocity is so great that pressure waves are not sent out ahead of the detonation front. Thus, pressure detectors that are useful in explosion prevention with deflagration waves are useless with detonations.

With liquid fuels, the burning rate depends in part on the rate of vaporization and on the pool size. Burgess, Strasser, and Grumer (*20*) have shown that the liquid regression rate v is given by

$$v=v_\infty(1-e^{-Kd}), \qquad (52)$$

where v_∞ is the value of v in large pools, K is a constant, and d is the pool diameter. They

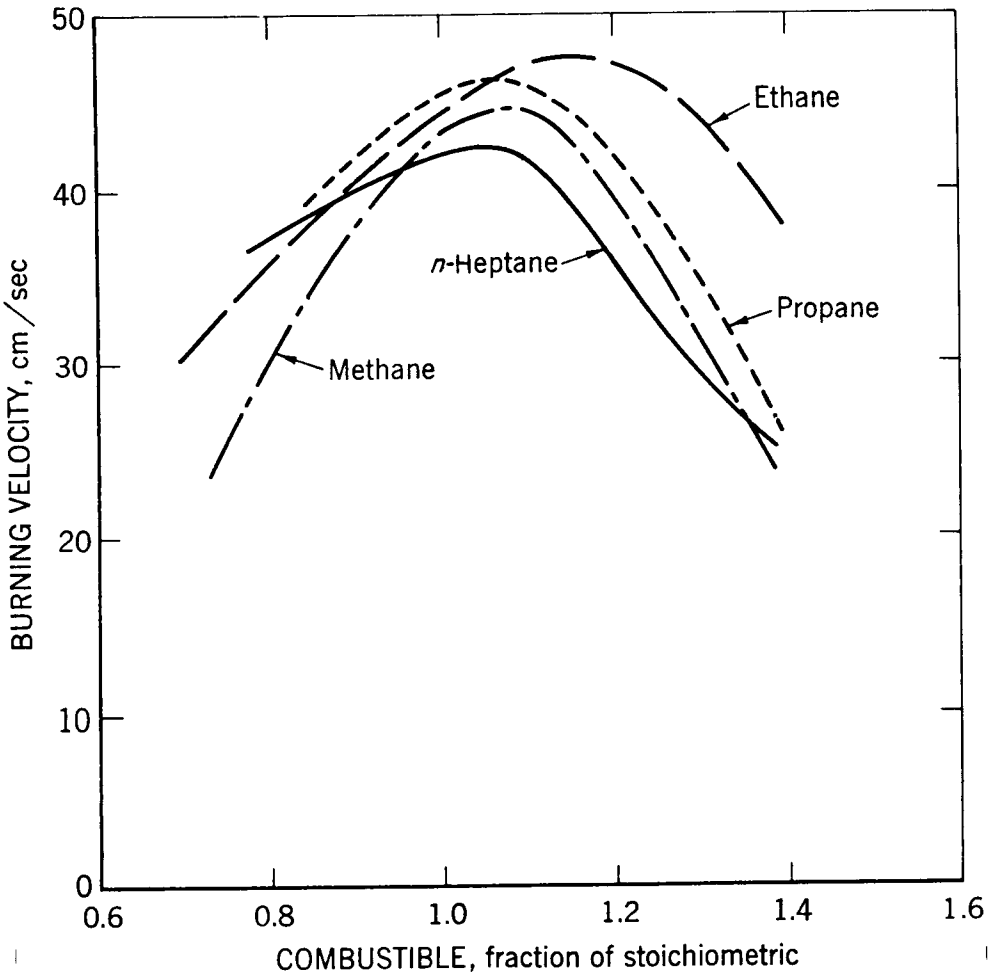

FIGURE 44.—Burning Velocities of Methane-, Ethane-, Propane-, and *n*-Heptane Vapor-Air Mixtures at Atmospheric Pressure and Room Temperature.

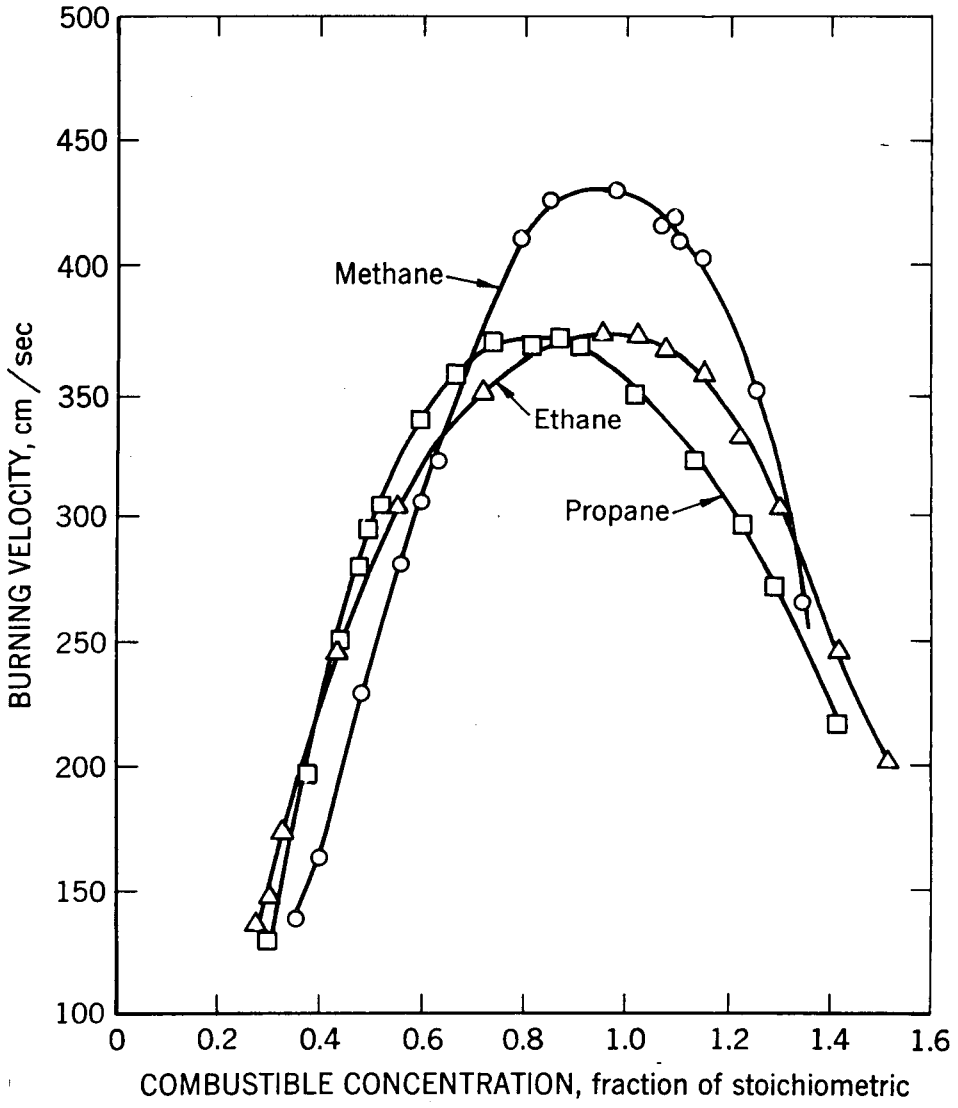

FIGURE 45.—Burning Velocities of Methane-, Ethane-, and Propane-Oxygen Mixtures at Atmospheric Pressure and Room Temperature.

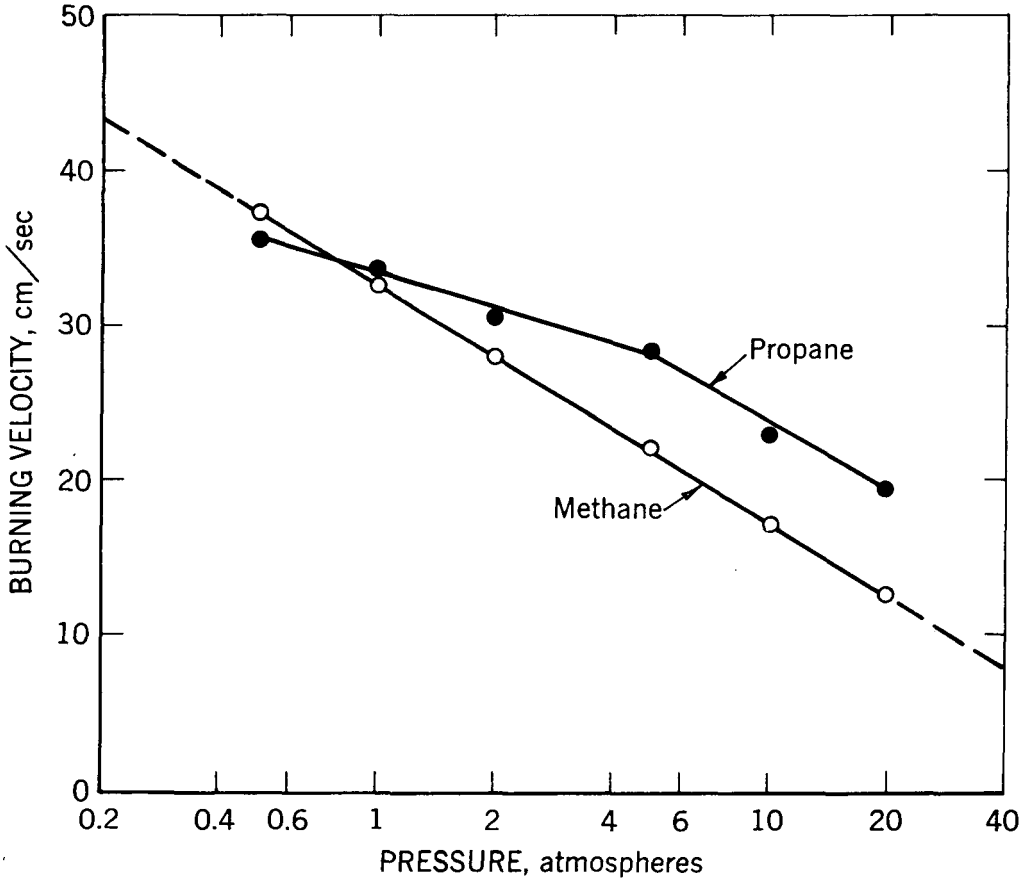

FIGURE 46.—Variation in Burning Velocity of Stoichiometric Methane-Air and Propane-Air Mixtures With Pressure at 26° C.

expressed v_∞ as:

$$v_\infty = 0.0076 \left(\frac{\text{net heat of combustion, } \Delta H_c}{\text{sensible heat of vaporization, } \Delta H_r} \right) \text{ cm/min.} \quad (53)$$

Figure 52 gives a summary of the v_∞ values for a number of combustibles, including several paraffin hydrocarbons (*21*). Of special significance here is that $\Delta H_c/\Delta H_r$ is nearly constant (about 100) for the paraffin hydrocarbons, so that their linear burning rates in large pools are all about ¾ cm per minute.

UNSATURATED HYDROCARBONS

(C_nH_{2n}, C_nH_{2n-2})

Limits in Air

The molecular weight, specific gravity, and other properties of the hydrocarbons considered here are included in table 7. At room temperature and atmospheric pressure, the lower limits of flammability of the olefins (C_nH_{2n}) excluding ethylene fall in the range from 46 to 48 mg combustible vapor per liter of air (0.046 to 0.048 oz combustible vapor per cubic foot of air).

The effect of temperature on the lower limit of flammability of ethylene in air at atmospheric pressure, assuming a constant limit flame temperature, is shown by the curve labeled "Upward propagation of flame" in figure 53. Unfortunately, only downward flame propagation data are available over an extended temperature range (*222*); these are included in figure 53. As in the case of similar data obtained with methane, these define a straight line parallel to the "Constant flame temperature," "Upward propagation of flame" line. Again, the modified Burgess-Wheeler law, equation (33), gives a variation in lower limit with temperature that is close to that given by the "Constant flame temperature" line, so that either could be used at temperatures below the AIT of ethylene (490° C). Moreover, as the limit flame temperatures of olefins are not too

TABLE 7.—*Properties of unsaturated hydrocarbons*

Combustible	Formula	M	Sp gr (Air=1)	C_{st} in air (vol pct)	Net ΔH_c $\left(\frac{\text{Kcal}}{\text{mole}}\right)$	Lower limit in air				Upper limit in air			
						L_{25} (vol pct)	$\frac{L_{25}}{C_{st}}$	$\left(\frac{\text{mg}}{\text{l}}\right)$	Ref.	U_{25} (vol pct)	$\frac{U_{25}}{C_{st}}$	$\left(\frac{\text{mg}}{\text{l}}\right)$	Ref.
Ethylene	C_2H_4	28.05	0.97	6.53	316.2	2.7	0.41	35	(115)	36	5.5	700	(26)
Propylene	C_3H_6	42.08	1.45	4.45	460.4	2.4	.54	46	(101)	11	2.5	210	(40)
Butene-1	C_4H_8	56.10	1.94	3.37	607.7	1.7	.50	44	(1)	9.7	2.9	270	(1)
cis-Butene-2	C_4H_8	56.10	1.94	3.37	606.0	1.8	.53	46	(40)	9.7	2.9	270	(40)
Isobutylene	C_4H_8	56.10	1.94	3.37	604.1	1.8	.53	46	(40)	9.6	2.8	260	(26)
3-Methyl-butene-1	C_5H_{10}	70.13	2.42	2.72	752.3	1.5	.55	48	(40)	9.1	3.3	310	(40)
Propadiene	C_3H_4	40.06	1.38	4.97	443.7	2.6	.53	48	(2)				
1,3-Butadiene	C_4H_6	54.09	1.87	3.67	576.3	2.0	.54	49	(108)	12	3.3	320	(26)

[1] Figures compiled at Explosive Res. Center, Federal Bureau of Mines.
[2] Calculated value.

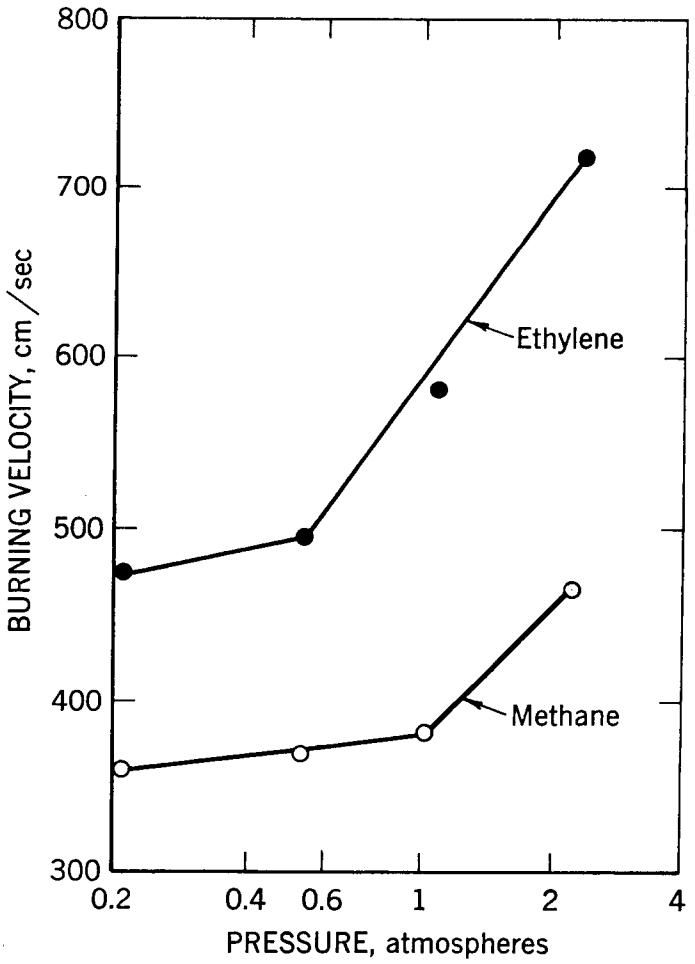

FIGURE 47.—Variation in Burning Velocity of Stoichiometric Methane- and Ethylene-Oxygen Mixtures With Pressure at 26°C.

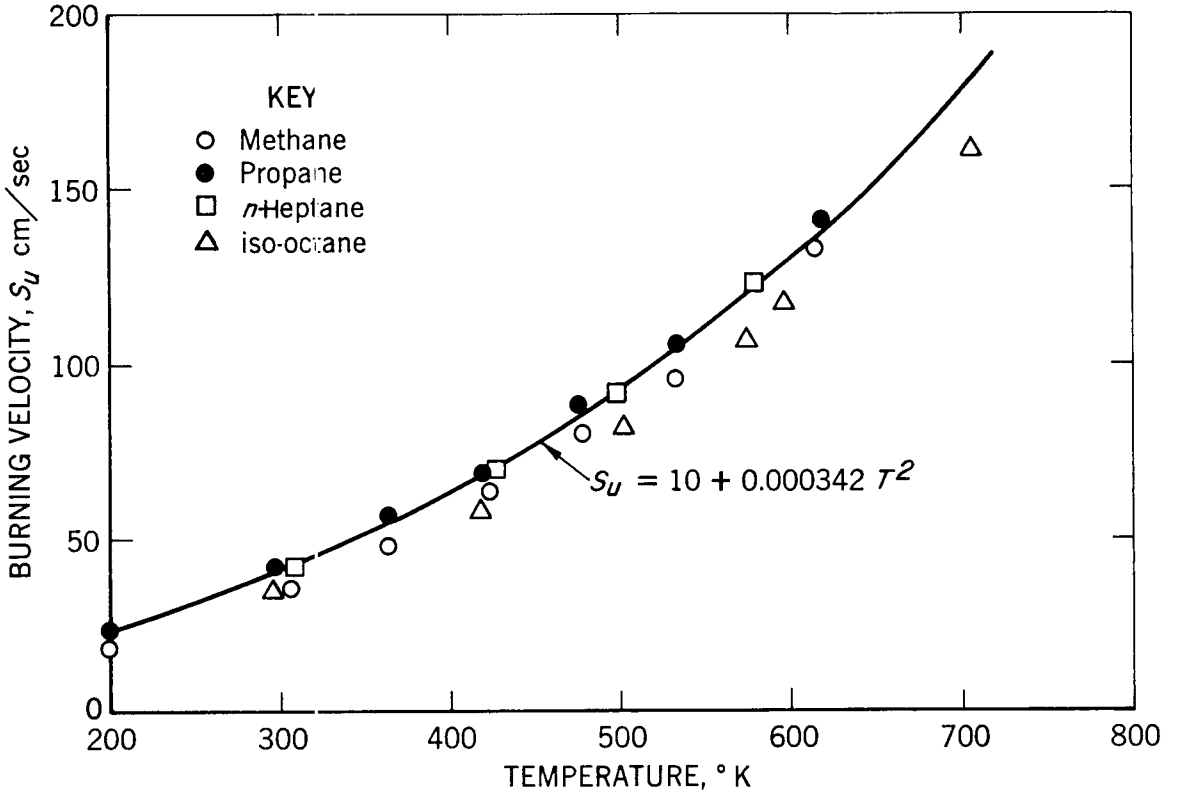

FIGURE 48.—Effect of Temperature on Burning Velocities of Four Paraffin Hydrocarbons in Air at Atmospheric Pressure.

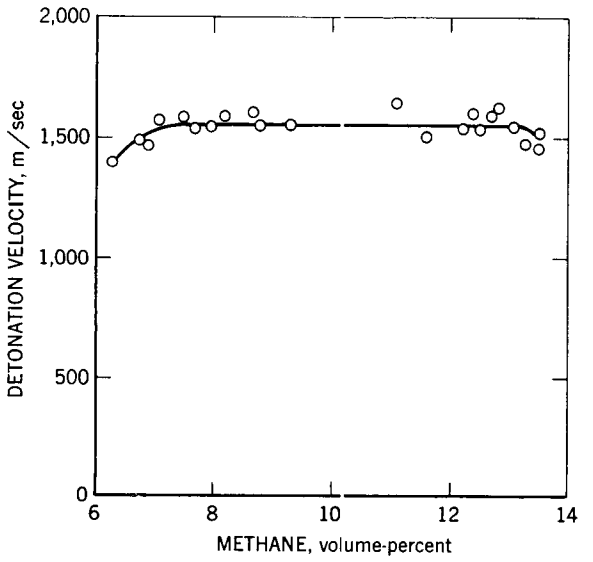

FIGURE 49.—Detonation Velocities of Methane-Air Mixtures at Atmospheric Pressure. (Initiator: 50–70 grams of amatol explosive. Pipe diameter: 30.5 cm.)

different from those of paraffin hydrocarbons, the generalized graph for $L_u/L_{25}°$ (fig. 23) can be used for these unsaturated hydrocarbons.

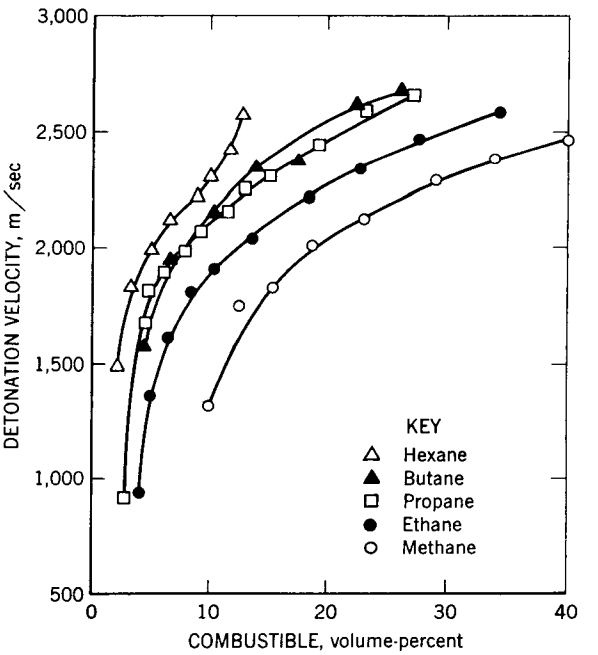

FIGURE 50.—Detonation Velocities of Methane-, Ethane-, Propane-, Butane-, and Hexane-Oxygen Mixtures at Atmospheric Pressure.

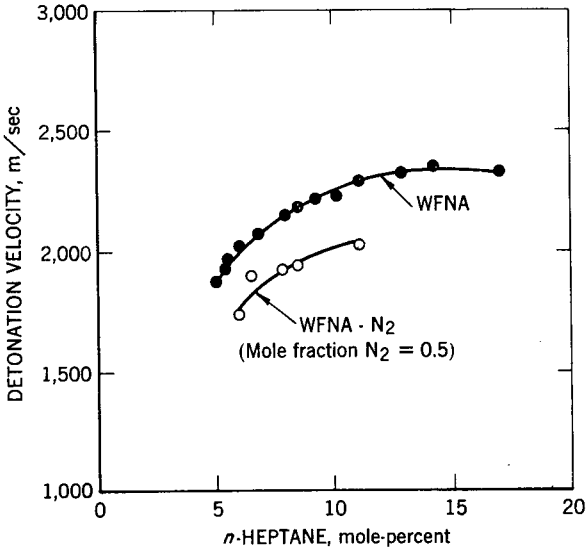

FIGURE 51.—Detonation Velocities of *n*-Heptane Vapor in WFNA (White Fuming Nitric Acid)-Nitrogen Gas Mixtures at Atmospheric Pressure and 400° K.

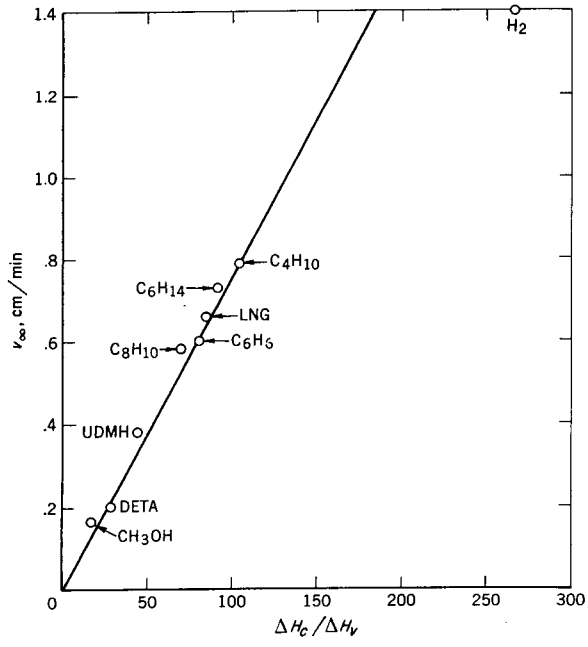

FIGURE 52.—Relation Between Liquid-Burning Rate (Large-Pool Diameter) and Ratio of Net Heat of Combustion to Sensible Heat of Vaporization.

Limits in Other Atmospheres

The limits of flammability of ethylene, propylene, isobutylene, butene-1, 3 methyl butene-1, and butadiene in various inert-air atmospheres have been determined by Jones and coworkers

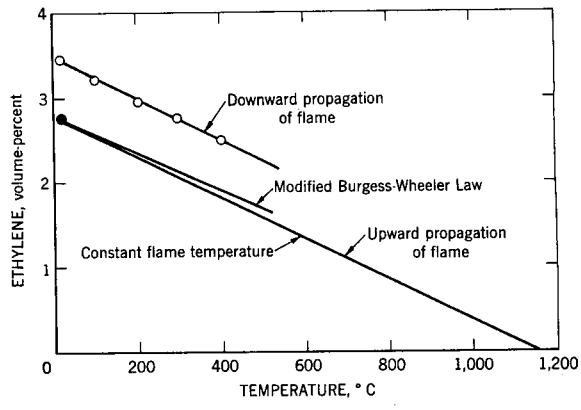

FIGURE 53.—Effect of Temperature on Lower Limit of Flammability of Ethylene in Air at Atmospheric Pressure.

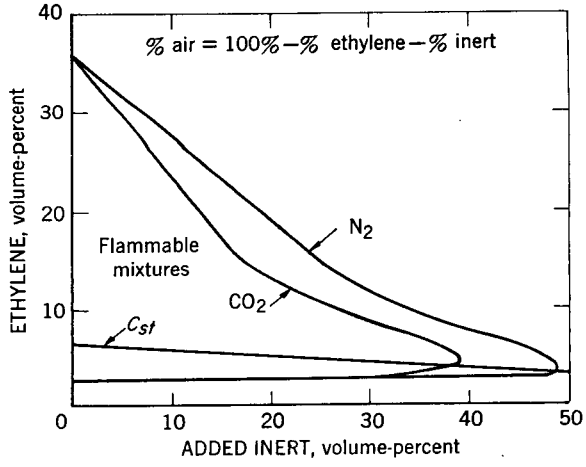

FIGURE 54.—Limits of Flammability of Ethylene-Carbon Dioxide-Air and Ethylene-Nitrogen-Air Mixtures at Atmospheric Pressure and 26° C.

(*100*, *101*, *103*), (figs. 54–60). The first two figures are modifications of the limit-of-flammability diagrams given in (*40*); the third is essentially the same as that given in the earlier publication but includes the experimental points. The other curves were constructed from original, unpublished data obtained at the Explosives Res. Center, Federal Bureau of Mines.

Other limit-of-flammability determinations have been made in oxygen and nitrous oxide. These data are included in table 8 (*40*, *100*, *106*).

Autoignition

There have been few determinations of AIT's of the unsaturated hydrocarbons in air or other oxidants; the available data (*94*, *116*, *191*) are summarized in table 9.

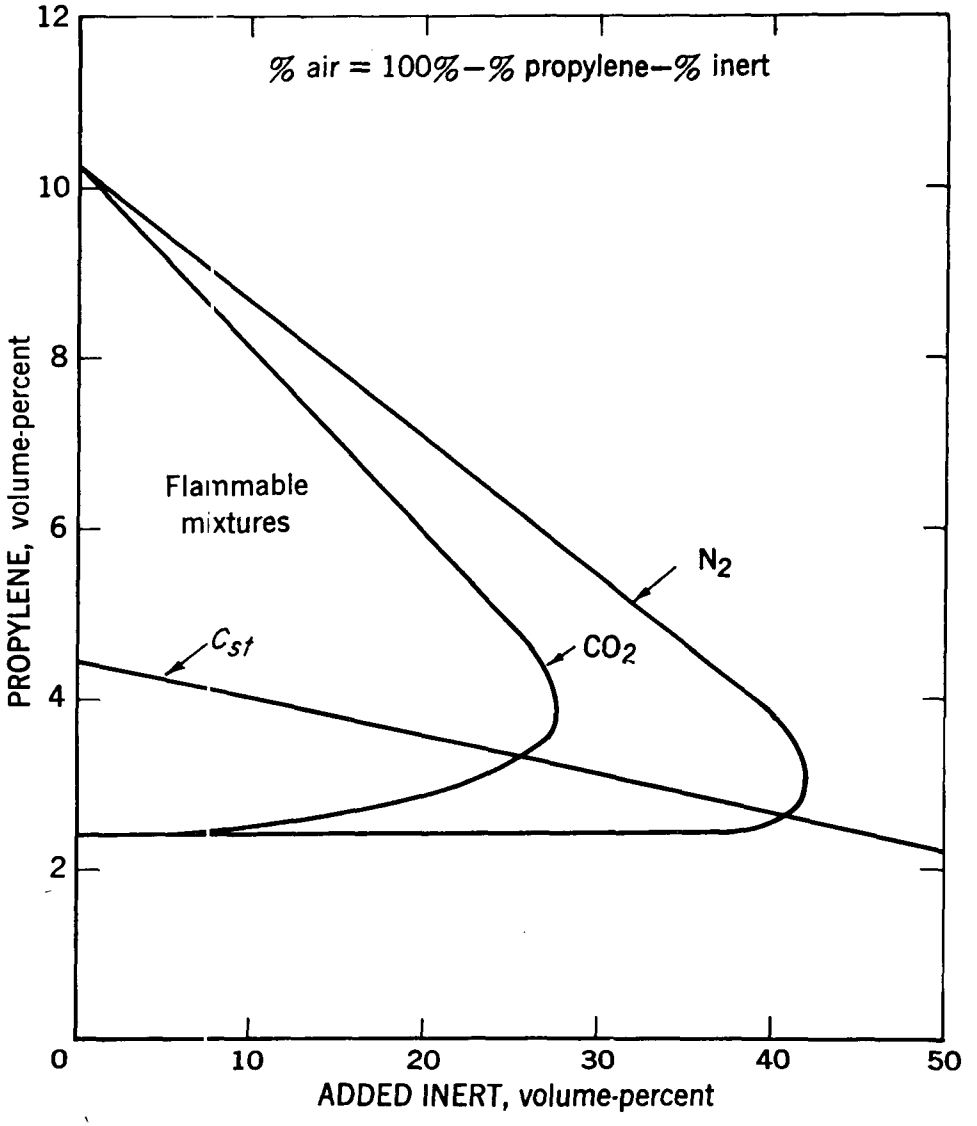

FIGURE 55.—Limits of Flammability of Propylene-Carbon Dioxide-Air and Propylene-Nitrogen-Air Mixtures at Atmospheric Pressure and 26° C.

Burning Rate

The burning velocity of ethylene has been determined in air, oxygen, and oxygen-nitrogen atmospheres by numerous investigators (*3*, *47*, *49*, *68*, *131*). In general, it is higher than the burning velocities of the paraffin hydrocarbons under the same conditions (fig. 47). Similar results are to be expected for other unsaturated hydrocarbons, although the available data are rather meager.

Stability

Many unsaturated hydrocarbon vapors can propagate flame in the absence of air at elevated temperatures and pressures; that is, they have no upper limit of flammability. These combustibles have positive heats of formation, ΔH_f (table 10) and would therefore liberate heat if decomposed to the elements carbon and hydrogen. Even more heat would be liberated if gases with a negative heat of formation—for example, methane—form from the elements. In practice, a mixture of products results upon decomposition of such combustibles. For example, a propagating decomposition reaction can be initiated in pure ethylene in a 2-inch-ID tube at 23° C and pressures as low as 750 psig, using 2 grams of guncotton. A reaction can be initiated at 21° C and pressures as low as 975 psig with 1 gram of guncotton. The decomposition products are

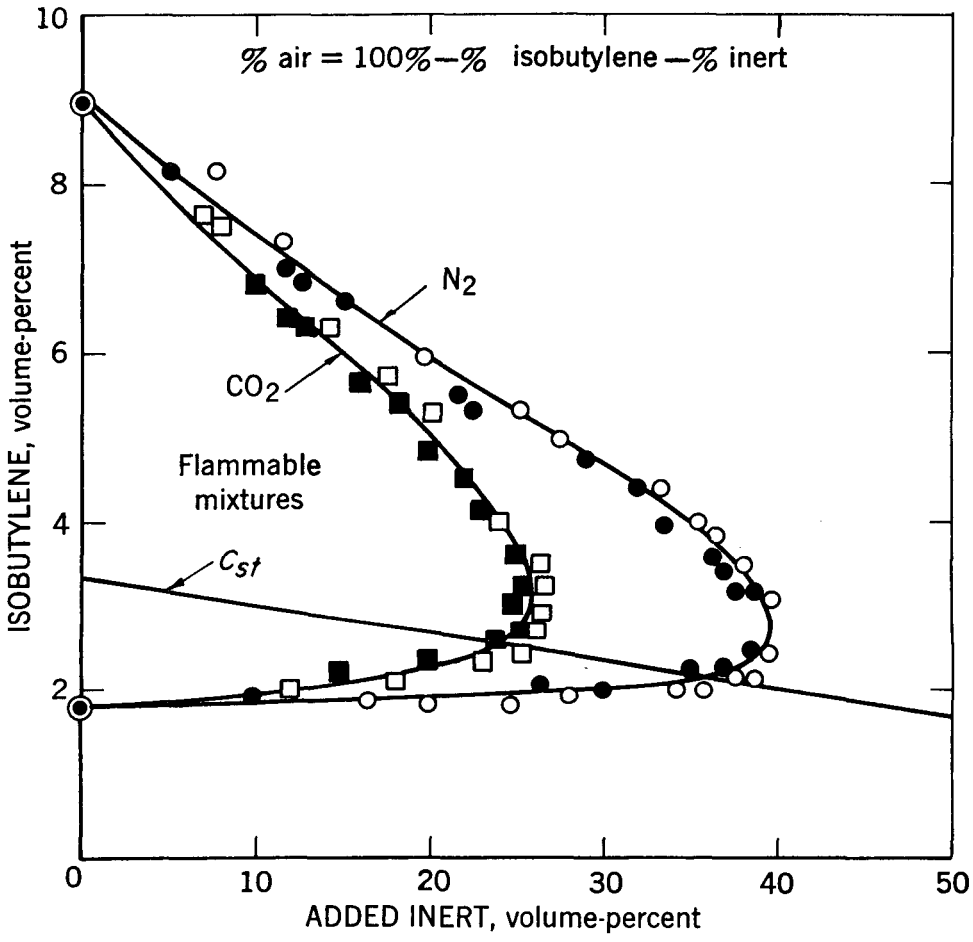

FIGURE 56.—Limits of Flammability of Isobutylene-Carbon Dioxide-Air and Isobutylene-Nitrogen-Air Mixtures at Atmospheric Pressure and 26° C.

TABLE 8.—*Limits of flammability of unsaturated hydrocarbons at atmospheric pressure and room temperature, in volume-percent combustible vapor*

(*L*=lower limit; *U*=upper limit)

Combustible	In air		In oxygen		In nitrous oxide	
	L	*U*	*L*	*U*	*L*	*U*
Ethylene	2.7	36	2.9	80	1.9	40
Propylene	2.0	11	2.1	53	1.4	29
Butene-1	1.6	10	1.7	58	-----	-----
Butene-2	1.7	9.7	1.7	55	-----	-----

primarily carbon, methane, and hydrogen; approximately 30 Kcal are released per mole of ethylene decomposed. Propylene yielded similar products following explosive decomposition during compression to 4,860 atmospheres (34).

TABLE 9.—*Minimum autoignition temperatures of unsaturated hydrocarbons at atmospheric pressure*

Combustible	Autoignition temperature					
	In air			In oxygen		
	° C	° F	Ref.	° C	° F	Ref.
Ethylene	490	914	(*116*)	485	905	(*116*)
Propylene	458	856	(*94*)	423	793	(1)
Butene-1	384	723	(1)	310	590	(1)
Butene-2	324	615	(1)	-----	-----	-----
1,3-Butadiene	418	784	(*191*)	335	635	(*191*)

[1] Figures compiled by Explosives Res. Center, Federal Bureau of Mines.

Propadiene and butadiene also decompose readily under the action of powerful ignitors. Propadiene vapor has been decomposed in a

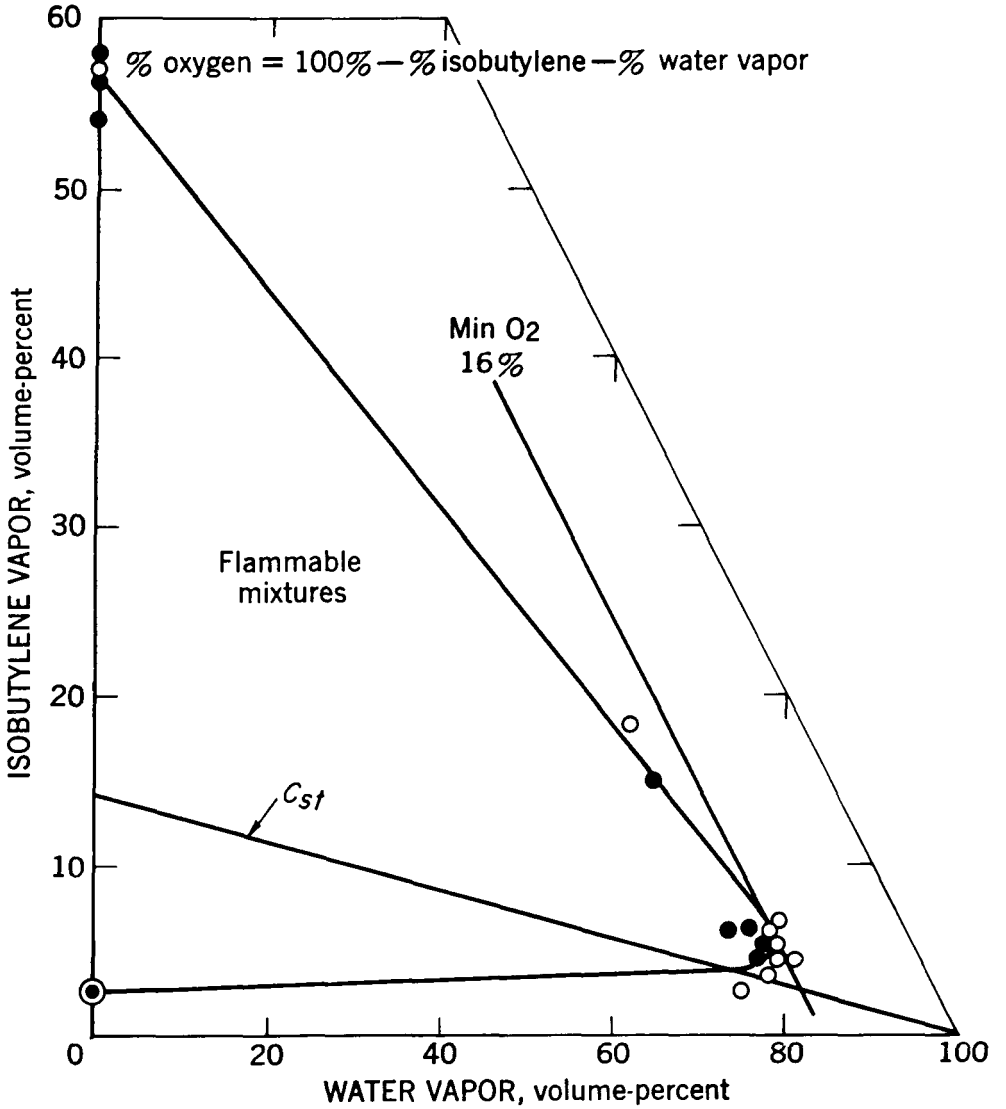

FIGURE 57.—Limits of Flammability of Isobutylene-Water Vapor-Oxygen Mixtures at 150° C and Atmosperic Pressure.

2-inch tube at 120° C and 50 psig using a platinum wire ignitor. Decomposition of butadiene in an industrial accident resulted in a "popcorn" polymer; the reaction was apparently initiated by an unstable peroxide (*4*).

TABLE 10.—*Heats of formation (Kcal/mole) of unsaturated hydrocarbons at 25° C.*

Combustible:	ΔH_f[1]
Acetylene	54. 2
Propadiene	45. 9
Methylacetylene	44, 3
1-3, Butadiene	26. 8
Ethylene	12. 5
Propylene	4. 9
1-Butene	. 3

[1] Refs. (*124, 185*).

ACETYLENIC HYDROCARBONS (C_nH_{2n-2})

Limits in Air

Acetylene forms flammable mixtures in air at atmospheric pressure and 25° C, in a range from 2.5 to 100 volume-percent acetylene. Quenched and apparatus limited upper limits have been obtained in 1-, and 2-, and 3-inch-diameter tubes (*40*), but pure acetylene can propagate flame at atmospheric pressure in tubes with diameters of at least 5 inches. Sargent has summarized available data on initial pressure requirements for deflagration and

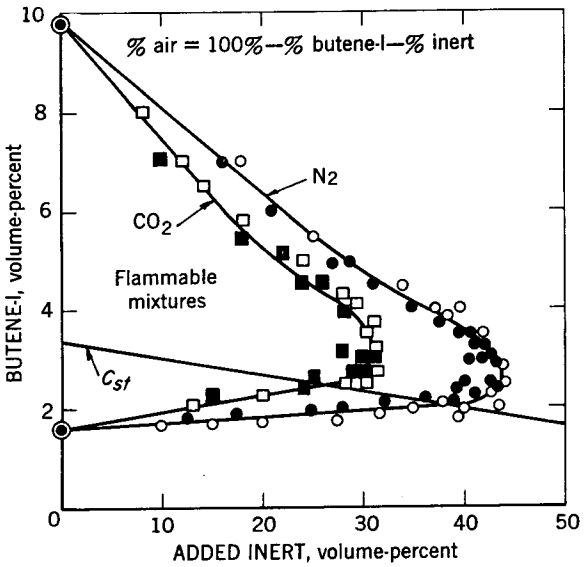

FIGURE 58.—Limits of Flammability of Butene-1-Carbon Dioxide-Air and Butene-1-Nitrogen-Air Mixtures at Atmospheric Pressure and 26° C.

detonation through acetylene in horizontal tubes of about .02 to 6 inches ID at 60° F. (*89, 185*). His curves are given in figure 61, which also includes an experimental point from the data of Jones and coworkers obtained in a vertical 2-inch-diameter tube. The existence of this point, at a pressure below that given by Sargent's curve for a 2-inch tube, indicates that this curve should be used only for horizontal systems. The point labeled "Industrial explosion" was reported by Miller and Penny (*144*) and presumably refers to a deflagration. The third experimental point is discussed, along with the detonation curve, in the section on stability.

The effect of temperature on the lower limit of flammability was determined by White in a 2.5-cm tube with downward propagation of flame (*222*). Although the actual limit values are not satisfactory for our purposes, they can be used to check the applicability of the $L_t/L_{25}°$ ratio data presented in figure 23. The White ratio of lower limits at 300° and 20° C. is 2.19/2.90=0.76; the corresponding ratio from

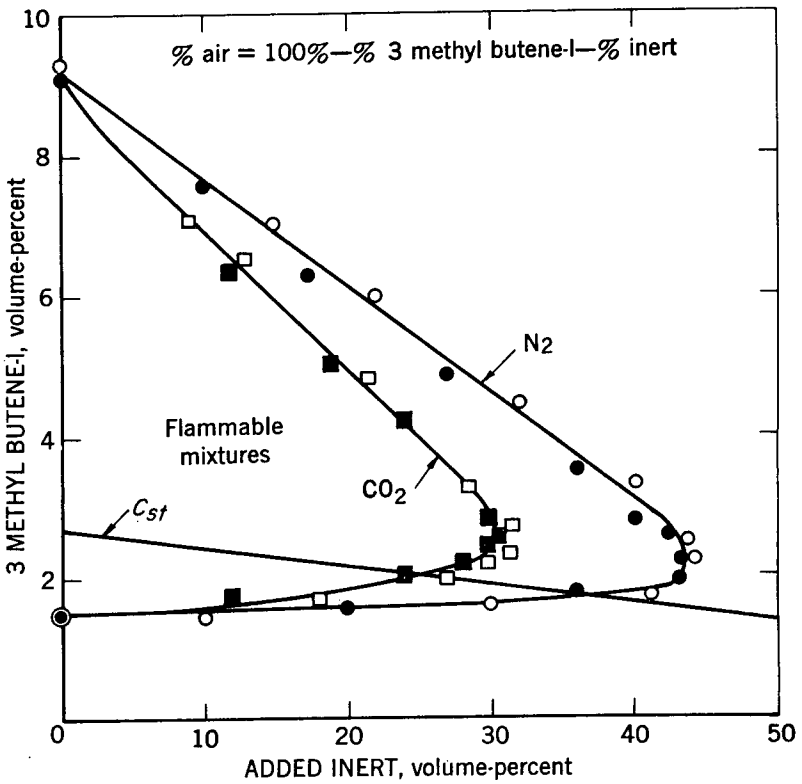

FIGURE 59.—Limits of Flammability of 3 Methyl Butene-1-Carbon Dioxide-Air and 3 Methyl-Butene-1-Nitrogen-Air Mixtures at Atmospheric Pressure and 26° C.

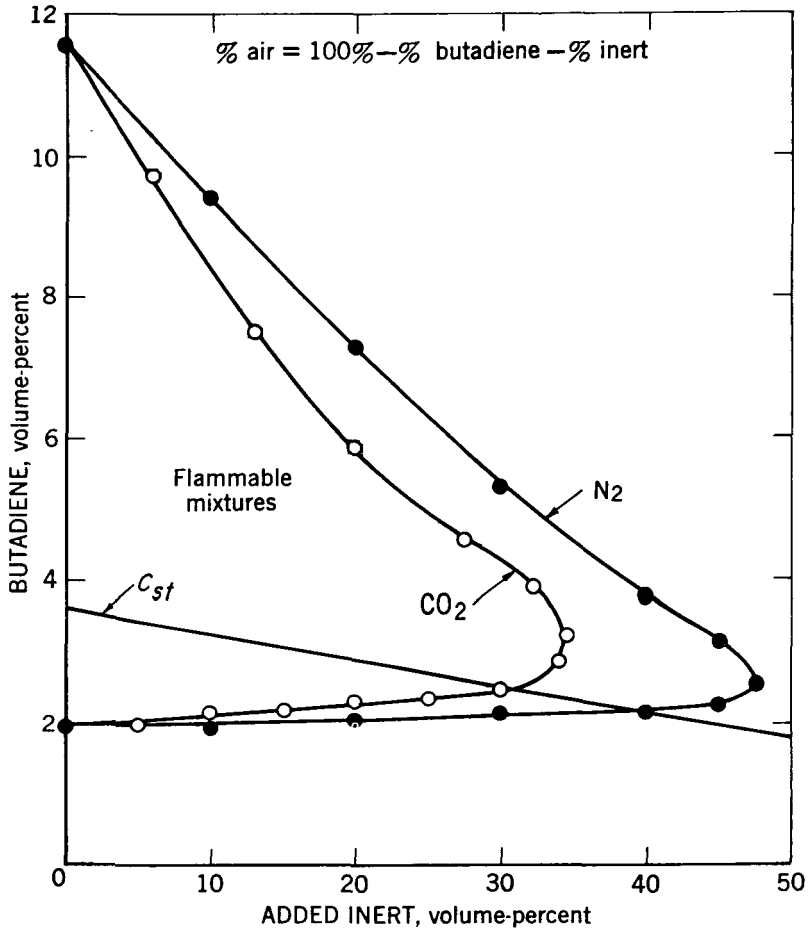

FIGURE 60.—Limits of Flammability of Butadiene-Carbon Dioxide-Air and Butadiene-Nitrogen-Air Mixtures at Atmospheric Pressure and 26° C.

"Constant flame temperature" curve in figure 23 is 0.78. Accordingly, this figure should be satisfactory for use with acetylene at temperatures in the range from 20° to 300° C.

The lower limit of flammability of methylacetylene (propyne) in air at atmospheric pressure is 1.7 volume-percent, equal to 0.34 C_{st} which compares favorably with the value for acetylene (0.32 C_{st}). Upper limit investigations have been conducted by Fitzgerald (*59*) in a 2-inch tube at 20° and 120° C to determine the low-pressure limits or lowest pressures at which a flame will propagate through methylacetylene vapor at these temperatures. He found these to be 50 and 30 psig at 20° and 120° C, respectively. In a 4-inch tube, Hall and Straker (*77*) obtained a low-pressure limit of 43 psig at 20° C. This indicates that the upper limit of flammability of methylacetylene in air is probably less than 100 percent at 20° C and 1 atmosphere.

The quantities of propylene required to prevent flame propagation through methylacetylene-propadiene-propylene mixtures at 120° C and 50 and 100 psig have been determined in 1-, 2-, 4-, and 12-inch tubes (fig. 62), and at 120° C and 100 psig in a 24-inch sphere. As noted, the propylene requirements are strongly affected by temperature, pressure, and container size. As the tube diameter increases, the quantity of propylene required to prevent flame propagation increases; this effect is less pronounced in the larger vessels (diameter greater than 4 inches) than in the smaller vessels (diameter less than 4 inches). The results obtained in the 24-inch sphere were similar to those in the 12-inch tube.

Limits in Other Atmospheres

Gliwitzky (*71*), and Jones and coworkers determined the effects of carbon dioxide and

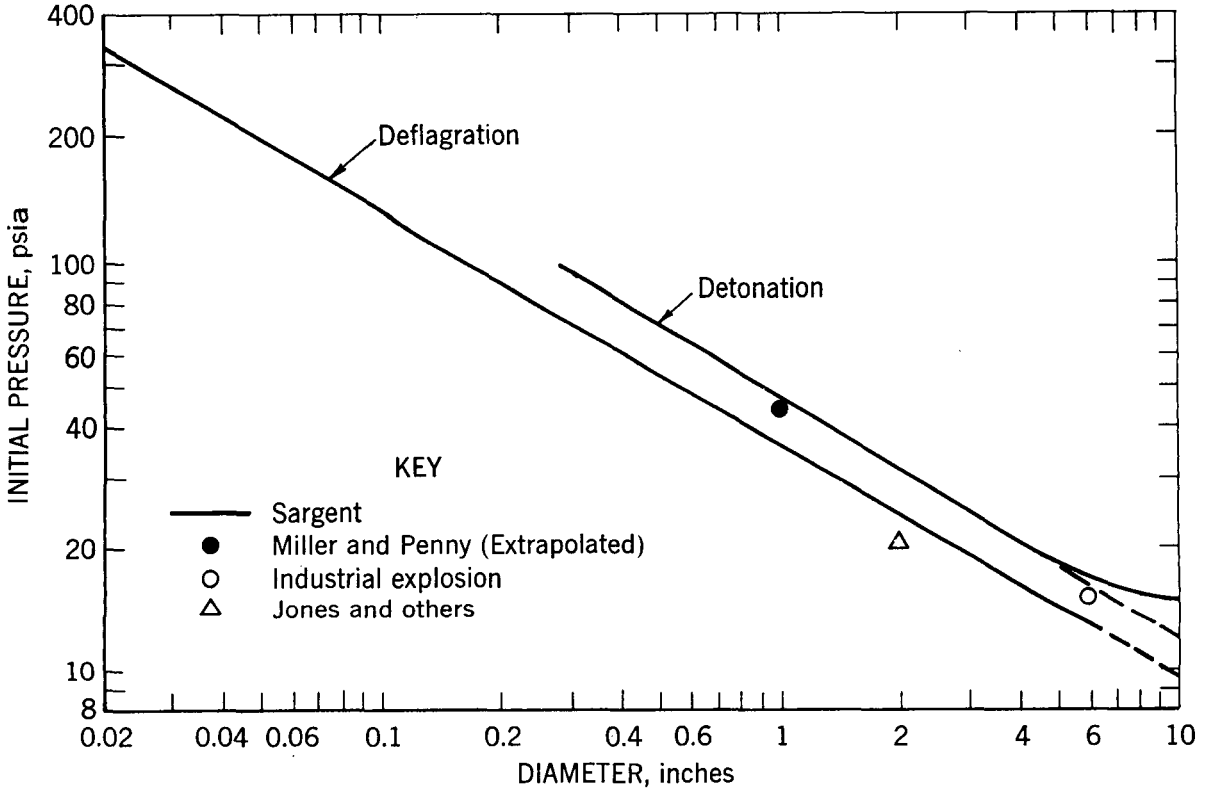

FIGURE 61.—Effect of Tube Diameter on Initial Pressure Requirements for Propagation of Deflagration and Detonation Through Acetylene Gas.

nitrogen on the limits of acetylene in air at atmospheric pressure and room temperature. Unfortunately, all measurements were made in tubes that were too narrow to give actual upper limit data. Nevertheless, the resulting quenched-limit data are summarized in figure 63, because they show the relative effects of adding two inert diluents to acetylene-air mixtures in a 2-inch-ID tube.

Autoignition

A summary of available autoignition temperature data for acetylene, acetylene-air, and acetylene-oxygen mixtures in clean systems is given in figure 64. They are based on measurements by Jones and Miller (*110*), by Jones and Kennedy in quartz tubes (*99*), and by Miller and Penny in a 0.5-inch steel pipe, 15 inches long (*144*). Jones and Miller found minimum autoignition temperatures of 305° and 296° C for a variety of acetylene-air and acetylene-oxygen mixtures, respectively, at atmospheric pressure. Miller and Penny report little variation in the autoignition temperature of acetylene in a clean pipe at 4 to 26 atmospheres initial pressure. However, the presence of 1 gram of powdered rust, scale, kieselguhr, alumina, silica gel, or charcoal lowered the pipe temperature required for ignition to a 280° to 300° C range. The presence of 1 gram of potassium hydroxide lowered the pipe temperature still further to 170° C. The impact of a 0.25-inch steel ball falling from a height of 15 inches against a fragment of copper acetylide produced a hot spot that ignited the surrounding gaseous acetylene at room temperature and 3 atmospheres.

Burning Rate

The burning velocity data for acetylene in air obtained by Manton and Milliken at 1 atmosphere and room temperature are given in figure 65 (*138*). The burning velocity ranges from a low of a few centimeters per second near the lower limit to a high of about 160 cm/sec on the rich side of the stoichiometric composition. Parker and Wolfhard (*164*) have found considerable variation in the burning velocity of acetylene in various oxidants. The burning velocities in stoichiometric mixtures with oxygen, nitrous oxide, nitric oxide, and nitrogen tetroxide were found to be 900, 160, 87, and 135 cm/sec, respectively; for comparison, the burning velocity in a stoichiometric acetylene-air mixture (fig. 65) is 130 cm/sec.

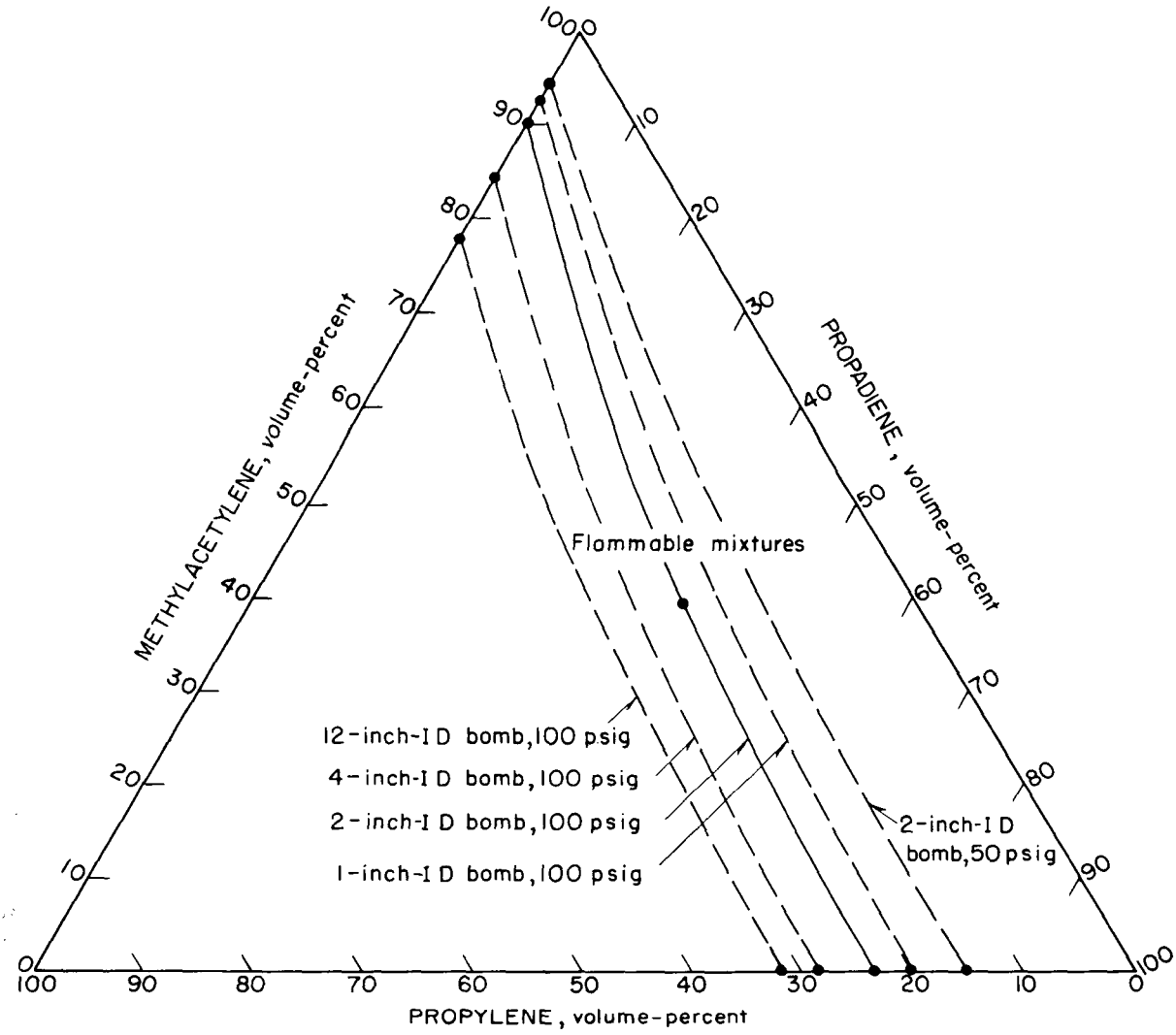

FIGURE 62.—Range of Flammable Mixtures for Methylacetylene-Propadiene-Propylene System at 120° C and at 50 and 100 Psig.

The burning velocities of acetylene-air mixtures were found to be independent of pressure between 0.1 and 1.0 atmosphere (*138*). Similarly, Agnew and Graiff (*3*) and Parker and Wolfhard (*164*) found the burning velocities of stoichiometric acetylene-oxygen and acetylene-nitrous oxide mixtures were independent of pressure between approximately 0.5 and 2 atmospheres and 0.03 and 1 atmosphere, respectively. The burning velocities of stoichiometric acetylene-nitric oxide and acetylene-nitrogen tetroxide mixtures increased slightly over this pressure range 0.03 to 1 atmosphere (*164*).

Stability

As noted, acetylene can propagate flame in the absence of air (*39, 165*). The pressures required for propagation at subsonic (deflagration) and supersonic rates (detonation) into the unburned gas are given for a range of pipe diameters in figure 61 (*185*). Deflagration is discussed briefly under Limits of Flammability; detonation is discussed in this section.

The curve labeled "Detonation" in figure 61 gives the minimum pressure required for propagation of a detonation, once initiated, in tubes of 0.3 to 10 inches diameter. In practice, a detonation may be initiated directly from a deflagration that has propagated through a rather ill-defined distance, known as the predetonation or run-up distance. This distance depends on temperature, pressure, tube diameter, condition of tube walls, and on ignition-source strength. For example, using a fused platinum wire ignitor, Miller and Penny

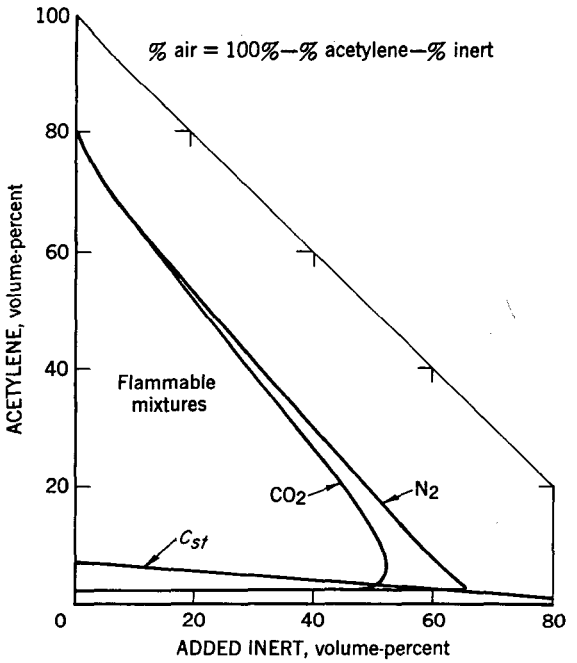

FIGURE 63.—Quenched Limits of Flammability of Acetylene-Carbon Dioxide-Air and Acetylene-Nitrogen-Air Mixtures at Atmospheric Pressure and 26° C, Obtained in a 2-Inch Tube.

(*144*) found the predetonation distance for acetylene in a 1-inch tube to be 30 feet at 51.4 psia, 22 feet at 55.9 psia, 12 feet at 73.5 psia, and 2.8 to 3.2 feet at 294 psia initial pressure. Extrapolation of these data yields the point in figure 61 for a very large predetonation distance. This point (44 psia and 1-inch diameter) lies fairly close to the detonation curve established by Sargent (*185*). The maximum lenth-to-diameter ratios (L/D) given by Sargent for establishing detonation in acetylene is plotted against intial pressure in figure 66. In tubes, having a diameter greater than those given along the top of the figure and having powerful ignitors, the L/D ratio will be less than that given by the curve. Nevertheless, this figure should be of use in giving the outer bound of L/D and the approximate quenching diameter; a better value for the quenching diameter can be obtained directly from figure 61.

Although predetonation distances are difficult to measure and experimental data often exhibit much scatter, they are of interest in safety work because they can be used to evaluate the maximum pressures likely to occur in a system due to cascading or pressure piling. This phenomenon presents a special problem because the final pressure achieved in a detona-

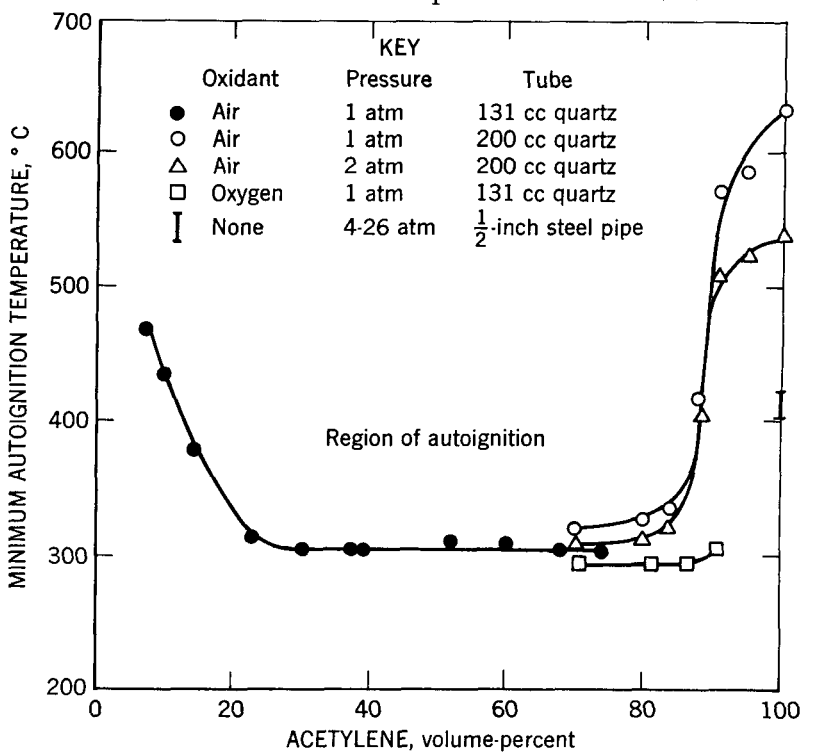

FIGURE 64—Minimum Autoignition Temperatures of Acetylene-Air and Acetylene-oxygen mixtures at atmospheric and elevated pressures.

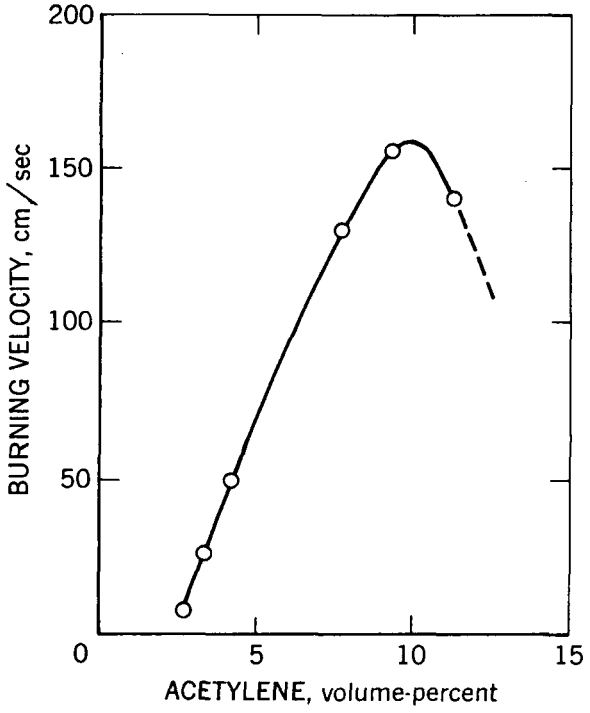

FIGURE 65.—Burning Velocity of Acetylene-Air Mixtures at Atmospheric Pressure and Room Temperature.

tion depends on the initial pressure at the onset of detonation. For example, the maximum pressure to be expected from the deflagration of acetylene at moderate pressures is about 11 times the initial pressure (*144*); the maximum to be expected from a detonation is about 50 times the initial pressure. As the pressure equalizes at the speed of sound in a deflagration, the maximum initial pressure to be expected upon transition from deflagration to a detonation is approximately 11 times the fraction of acetylene that has been burned times the initial precombustion pressure. Fifty times this pressure is the approximate maximum pressure that would be obtained when a detonation occurs. To illustrate this, Sargent has plotted the final-to-initial pressure ratio (P_f/P_i) against the predetonation distance-to-tube length for acetylene. A similar graph is given in figure 67. To use this graph, the maximum predetonation distance to be expected must first be determined from figure 66. This distance divided by the tube length gives the maximum final-to-initial pressure ratio.

AROMATIC HYDROCARBONS (C_nH_{2n-6})

Limits in Air

The combustibles considered in this section are listed in table 11, with pertinent properties. At atmospheric pressure and room temperature, the lower limits of flammability of the aromatic hydrocarbons are approximately 50 ± 2 mg/l (0.050 ± 0.002 oz combustible vapor per cubic foot of air).

The lower limit of toluene was determined by Zabetakis and coworkers in air at 30°,

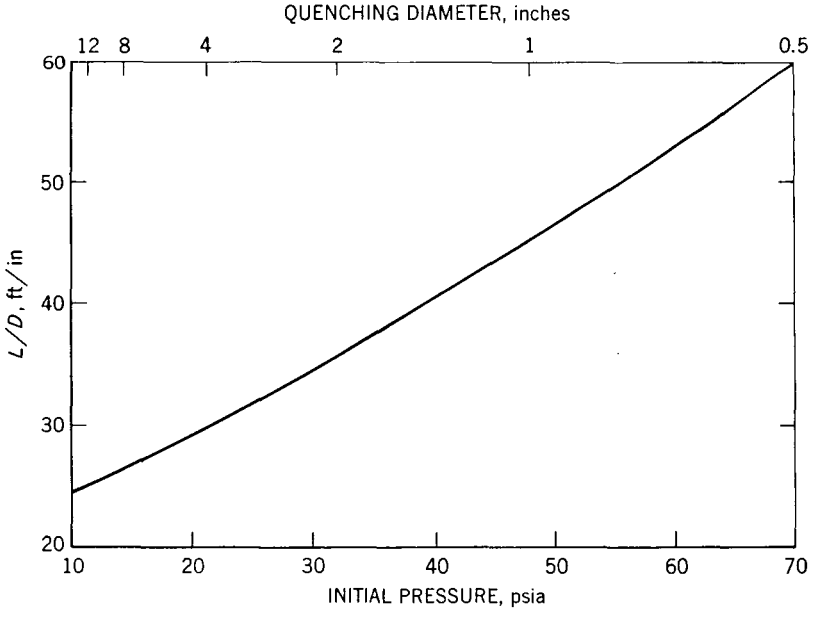

FIGURE 66.—Maximum L/D ratio Required for Transition of a Deflagration to a Detonation in Acetylene Vapor at 60° F and from 10 to 70 Psia.

TABLE 11.—*Properties of selected aromatic hydrocarbons*

Combustible	Formula	M	Sp gr (Air=1)	C_{st} in air (vol pct)	net ΔH_c $\left(\frac{\text{Kcal}}{\text{mole}}\right)$	Lower limit in air [1]			Upper limit in air [1]		
						L_{100} (vol pct)	$\frac{L_{100}}{C_{st}}$	L $\left(\frac{\text{mg}}{\text{l}}\right)$	U_{100} (vol pct)	$\frac{U_{100}}{C_{st}}$	U $\left(\frac{\text{mg}}{\text{l}}\right)$
Benzene	C_6H_6	78.11	2.69	2.72	757.5	1.3	0.48	47	7.9	2.9	300
Toluene	C_7H_8	92.13	3.18	2.27	901.5	1.2	.53	50	7.1	3.1	310
Ethyl benzene	C_8H_{10}	106.16	3.67	1.96	1048.5	1.0	.51	48	6.7	3.4	340
o-Xylene	C_8H_{10}	106.16	3.67	1.96	1045.9	1.1	.56	53	6.4	3.3	320
m-Xylene	C_8H_{10}	106.16	3.67	1.96	1045.5	1.1	.56	53	6.4	3.3	320
p-Xylene	C_8H_{10}	106.16	3.67	1.96	1045.7	1.1	.56	53	6.6	3.4	340
Cumene	C_9H_{12}	120.19	4.15	1.72	1194.2	.88	.51	48	6.5	3.8	370
p-Cymene	$C_{10}H_{14}$	134.21	4.63	1.53	1341.8	.85	.56	51	6.5	3.6	350

[1] Ref. (247).

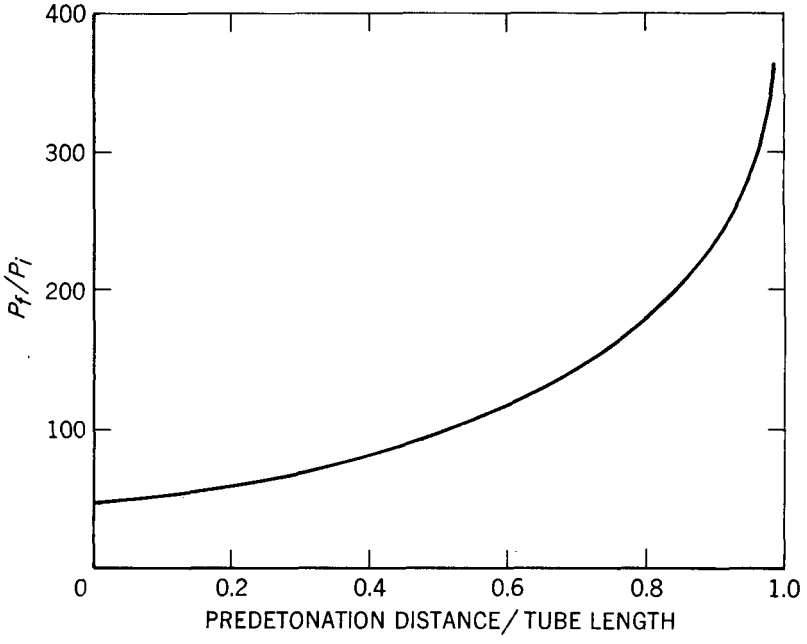

FIGURE 67.—Final-to-Initial Pressure Ratios Developed by Acetylene With Detonation Initiation at Various Points Along a Tube.

100°, and 200° C (*235*, *247*); the variation in lower limit with temperature is given by equations (31) and (33) derived for paraffin hydrocarbons, and the corresponding curves of figure 23. For example, $L_{200° C}/L_{30° C}$ was found to be 1.07/1.24 or 0.86; the ratio predicted by the curve in figure 23 is 0.87.

The upper limits of the aromatics considered here at 100° C are included in table 11 (*247*). These were obtained at atmospheric pressure in a 2-inch-diameter tube, open at one end. Butler and Webb obtained upper limit data on a commercial grade cumene (93.3 pct cumene) in air at elevated temperatures and atmospheric and elevated pressures in a closed bomb (*31*). Their values range from 8.8 percent cumene (80° C and atmospheric pressure) to 10.8 percent cumene (146° C and 100 psig pressure).

Limits in Other Atmospheres

The limits of flammability obtained by Burgoyne (*29*) and by Jones (*40*) for benzene-carbon dioxide-air and benzene-nitrogen-air mixtures at atmospheric pressure and 25° C are given in figure 68; similar data are given for the last two mixtures at atmospheric pressure and 150° C. The inerting requirements at 25° C are approximately the same as those of *n*-hexane (fig. 33). Again, it should be noted

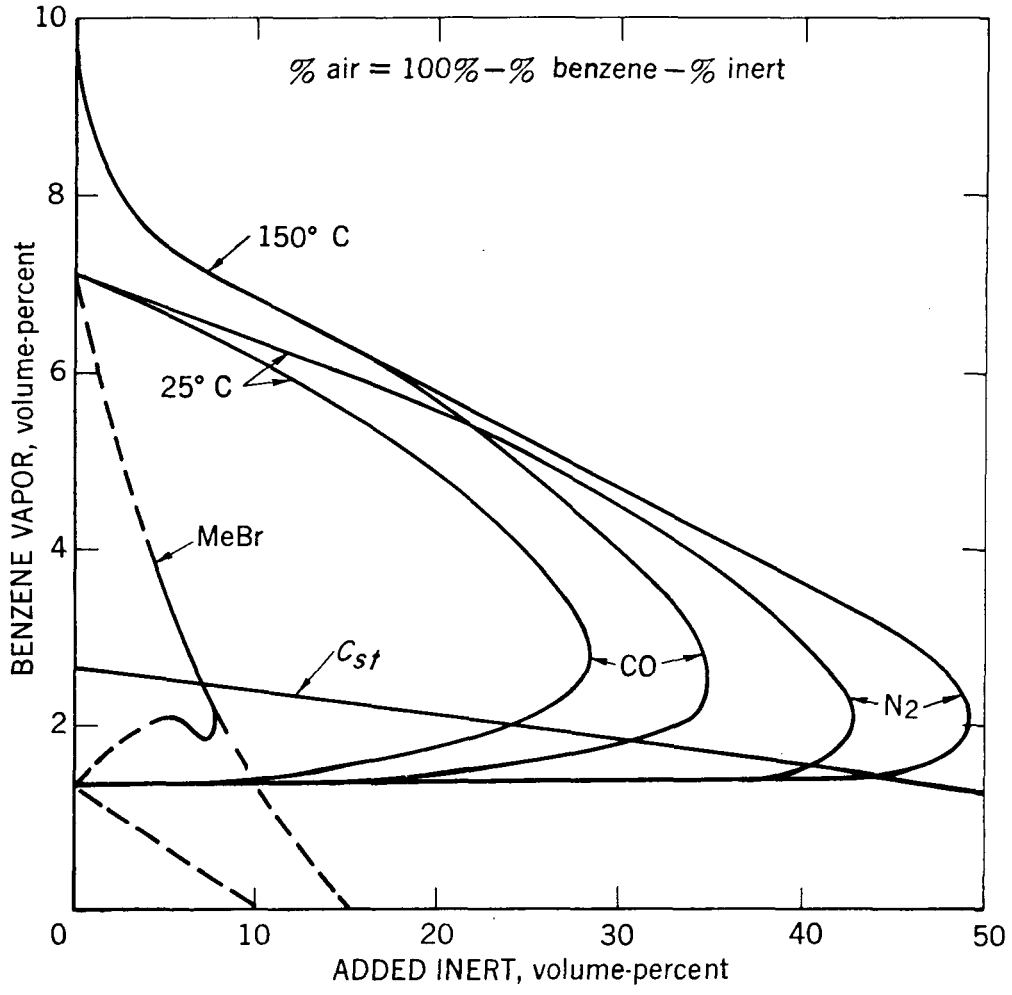

FIGURE 68.—Limits of Flammability of Benzene-Methyl Bromide-Air Mixtures at 25° C and Benzene-Carbon Dioxide-Air and Benzene-Nitrogen-Air Mixtures at 25° and 150° C and Atmospheric Pressure.

that the methyl bromide data are not consistent with those obtained by Hill (compare figs. 28 and 33). These latter data (*84*) were used to construct the approximate (broken) flammability curves for the benzene-methyl bromide-air system.

The decrease in the minimum oxygen requirements for flame propagation (from 14.2 ± 0.3 volume-percent at 25° C to 13.1 ± 0.3 volume-percent at 150° in a carbon dioxide-air atmosphere; from 11.4 ± 0.3 volume-percent at 25° C to 10.1 ± 0.3 volume-percent at 150° in a nitrogen-air atmosphere) is within the range predicted by the modified Burgess-Wheeler law (equation (35), fig. 23).

The limits of flammability of orthoxylene ($C_6H_4 \cdot (CH_3)_2$)-water-hydrogen peroxide mixtures were determined at 154° C and 1 atmosphere presssure by Martindill, Lang, and Zabetakis (*140*). The data are presented in a triangular plot in figure 69; compositions are expressed in mole-percent as in the original presentation. This system has no lower limit mixtures, as a flame can be initiated in hydrogen peroxide vapors (*186*). As a 90-weight-percent hydrogen peroxide was actually used to obtain these flammability data, all compositions were calculated to yield values based on a 100-percent hydrogen peroxide content. This could be done here because only three components are considered. Where four components are considered, the flammability data can be presented in a three-dimensional plot; if two of the components appear in fixed proportions, a triangular plot can be used with the two components (for example, 90-weight-percent hydrogen peroxide) considered as a single component. Such a plot is presented in figure 70 for 90-weight-percent hydrogen peroxide-orthoxylene-formic acid (HCOOH) at 154° C and 1 atmosphere. This was considered to be a plane in a regular tetrahedron in the original article and is there-

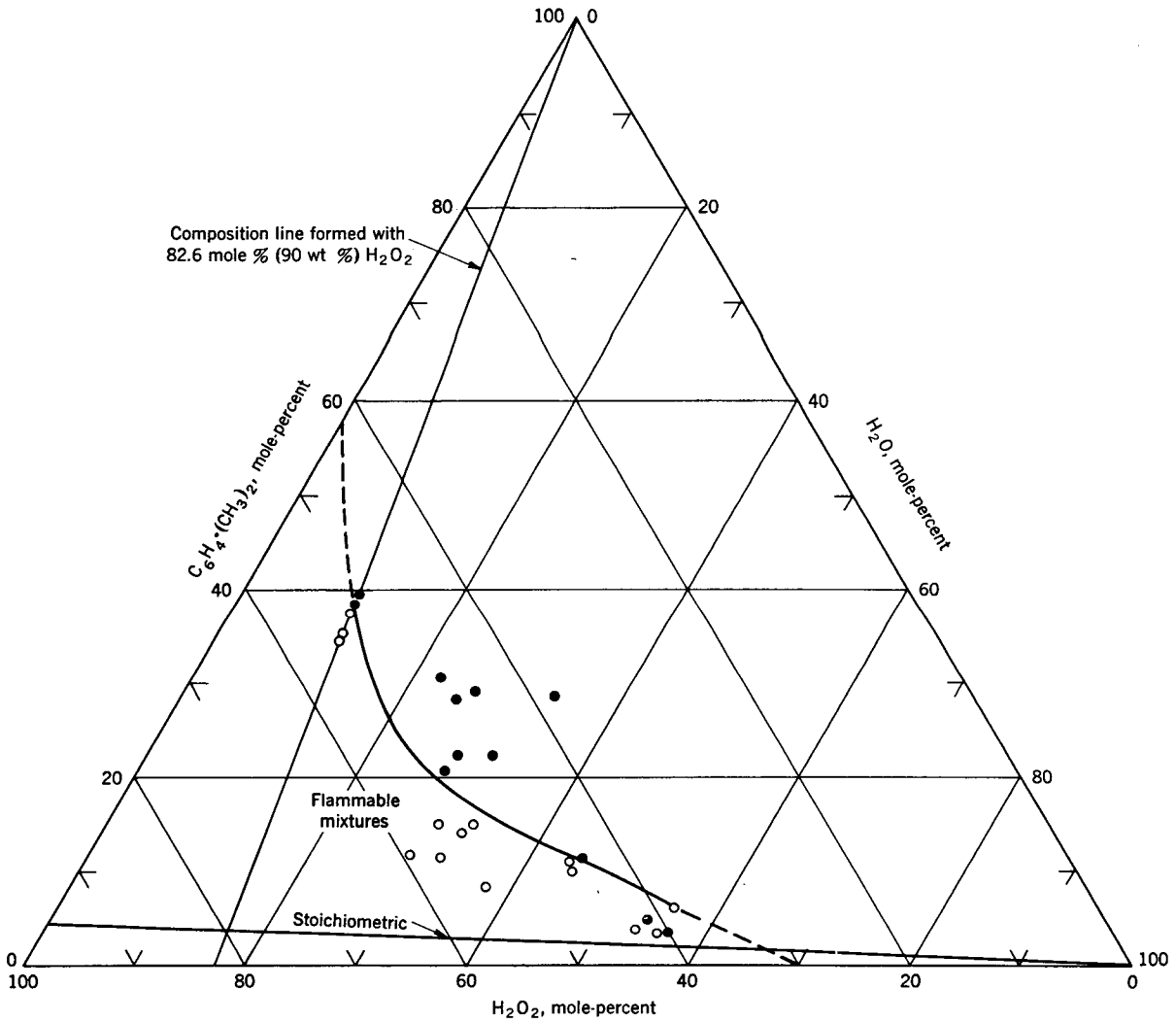

FIGURE 69.—Limits of Flammability of H_2O_2-$C_6H_4\cdot(CH_3)_2$-H_2O at 154° C and 1 Atmosphere Pressure.

fore not a regular triangle. As before, only an upper limit curve is given because 90-weight-percent hydrogen peroxide is flammable. In addition, a calculated curve based on Le Chatelier's rule is given, as is the upper limit curve obtained with decomposed hydrogen peroxide. Decomposition of the peroxide lowers the upper limit appreciably and yields a system which has a lower limit of flammability (not determined in this study).

Autoignition

The minimum autoignition temperatures of a series of aromatic hydrocarbons in air at atmospheric pressure are given in figure 71 as a function of the correlation parameter L_{ave}. This parameter was determined by use of equation (*49*), treating the benzene ring as a $-CH_3$ group (*241*). When the benzene ring contains two side groups, L_{ave} is determined first for the side group that yields the largest average value and to this is added ½, ⅓, or ¼ of the average chain length of the second side group; (½, ⅓, and ¼ correspond to the ortho-, meta-, and para-positions, respectively). The data again fall into high- and low-temperature regions (fig. 43).

Burning Rate

Burning rates and detonation velocities of benzene in air and oxygen appear to be approximately the same as those of the higher paraffin hydrocarbons. For example, the results of Golovina and Fyodorov (*211*) show that the maximum burning velocities of benzene in nitrogen-oxygen mixtures range from about

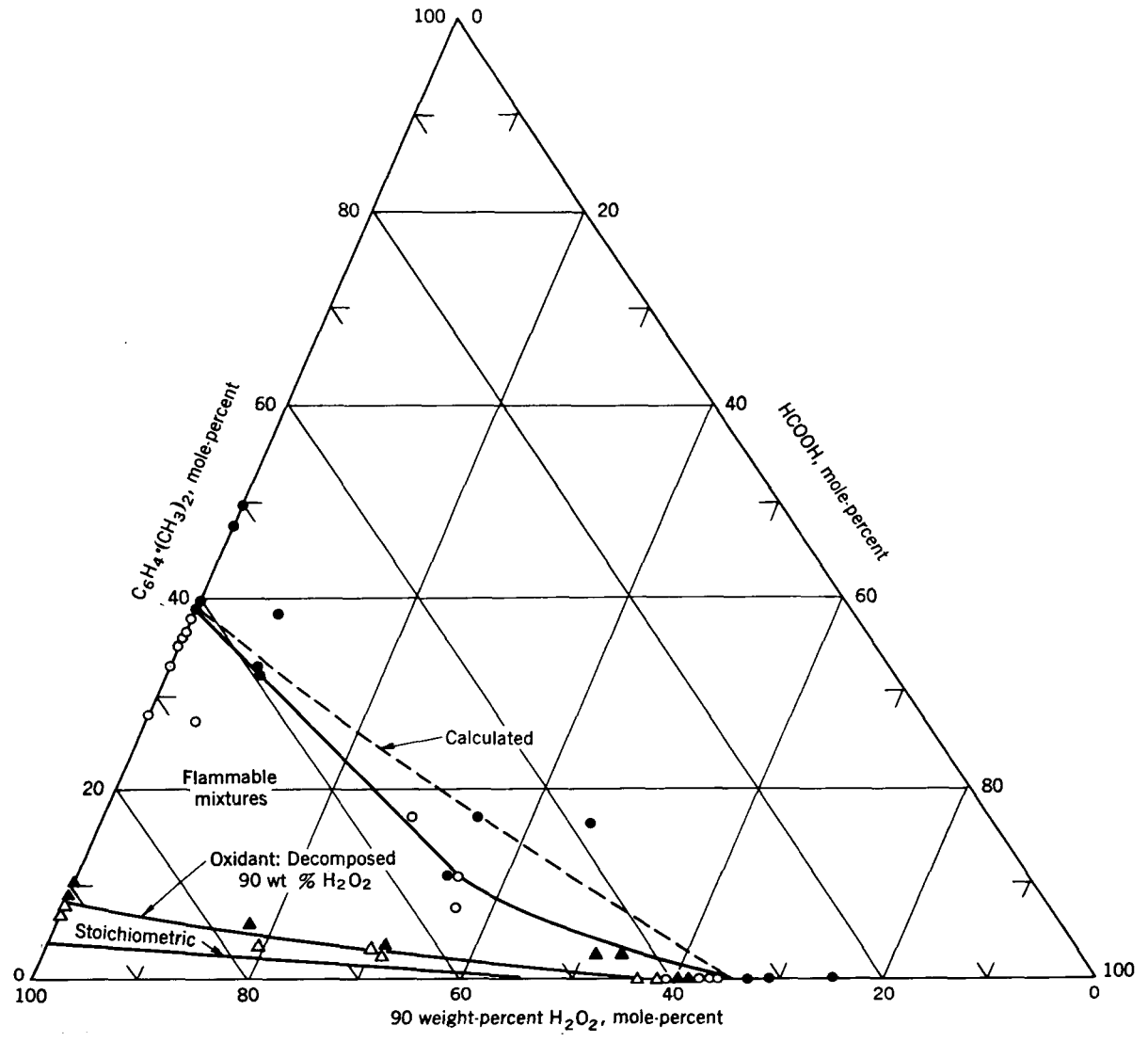

FIGURE 70.—Limits of Flammability of 90-Weight-Percent H_2O_2-$C_6H_4\cdot(CH_3)_2$-HCOOH at 154° C and 1 Atmosphere Pressure.

295 cm/sec in oxygen to 45 cm/sec in air; the maximum burning velocities of hexane in various nitrogen-oxygen mixtures range from about 260 cm/sec in oxygen to 40 cm/sec in air. Similarly, Fraser (*61*) found the maximum detonation velocities of benzene and *n*-octane in oxygen to be 2,510 and 2,540 m/sec, respectively.

ALICYCLIC HYDROCARBONS (C_nH_{2n})

Limits in Air

A summary of the pertinent properties of some of the members of the series is given in table 12. The lower limits of flammability in air at atmospheric pressure and room temperature fall in the range from 48±3mg/l (.048 ±.003 oz combustible per cubic foot of air). By volume, this is equivalent to approximately 0.55 C_{st}, which is the same as for paraffin hydrocarbons. The ratio of the upper limit to C_{st} appears to increase with molecular weight.

According to Jones (*40*), the lower limit of cyclohexane in air at atmospheric pressure and 26° C determined in a 2.0-inch tube is 1.26 volume-percent. Under the same conditions, Burgoyne and Neale (*26*) found the lower limit to be 1.34 volume-percent, using a 2.5-inch tube. Matson and Dufour (*141*) found the

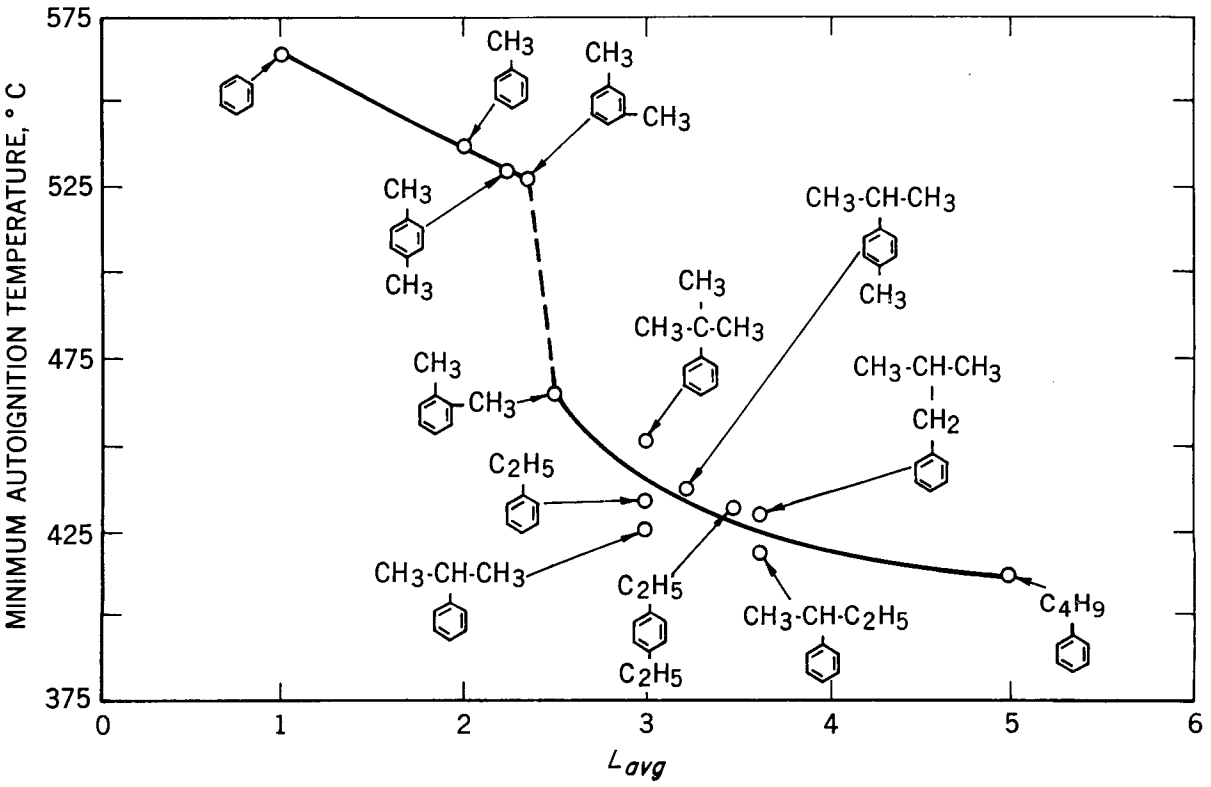

FIGURE 71.—Minimum Autoignition Temperatures of Aromatic Hydrocarbons in Air as a Function of Correlation Parameter L_{ave}.

TABLE 12.—*Properties of selected alicyclic hydrocarbons*

Combustible	Formula	M	Sp gr (Air=1)	C_{st} in air (vol pct)	Net ΔH_c $\left(\frac{\text{kcal}}{\text{mole}}\right)$	Lower limit in air				Upper limit in air			
						L_{25} (vol pct)	$\frac{L_{25}}{C_{st}}$	$L\left(\frac{\text{mg}}{\text{l}}\right)$	Ref.	U_{25} (vol pct)	$\frac{U_{25}}{C_{st}}$	$U\left(\frac{\text{mg}}{\text{l}}\right)$	Ref.
Cyclopropane	C_3H_6	42.08	1.45	4.45	465	2.4	0.54	46	(107)	10.4	2.3	220	(107)
Cyclobutane	C_4H_8	56.10	1.94	3.37	[1] 600	1.8	.56	46	[1]				
Cyclopentane	C_5H_{10}	70.13	2.42	2.72	740.8	1.5	.55	48	[1]				
Cyclohexane	C_6H_{12}	84.16	2.91	2.27	881.7	1.3	.57	49	(40)	7.8	3.4	320	(40)
Ethylcyclobutane	C_6H_{12}	84.16	2.91	2.27	[1] 880	1.2	.53	46	(40)	7.7	3.4	310	(40)
Cycloheptane	C_7H_{14}	98.18	3.39	1.96	[1] 1024	1.1	.56	49	[1]	6.7	3.4	310	[1]
Methylcheylhexane	C_7H_{14}	98.18	3.39	1.96	1026.0	1.1	.56	49	(40)	6.7	3.4	310	[1]
Ethylcyclopentane	C_7H_{14}	98.18	3.39	1.96	1032.6	1.1	.56	49	(40)	[2] 6.7	3.4	310	(40)
Ethylcylcohexane	C_8H_{16}	112.21	1.71	1.71	1173.7	[3] 95	.56	48	(40)	[3] 6.6	3.9	350	(40)

[1] Calculated value.
[2] P=0.5 atm.
[3] t=130° C.

lower limit to be 1.12 volume-percent at 21° C in a 12-inch diameter chamber about 15 inches long; however, there is evidence that they did not use the same criteria of flammability as did the other authors; only one observation window was provided at the top of a rather squatty chamber, whereas with the glass tubes used by Jones and by Burgoyne and Neale the flame could be observed along the entire tube. Accordingly, the data of Jones and of Burgoyne and Neale are used here.

Limits in Other Atmospheres

The limits of flammability of cyclopropane-carbon dioxide-air, cyclopropane-nitrogen-air, and cyclopropane-helium-air mixtures at 25° C and atmospheric pressure are given in figure

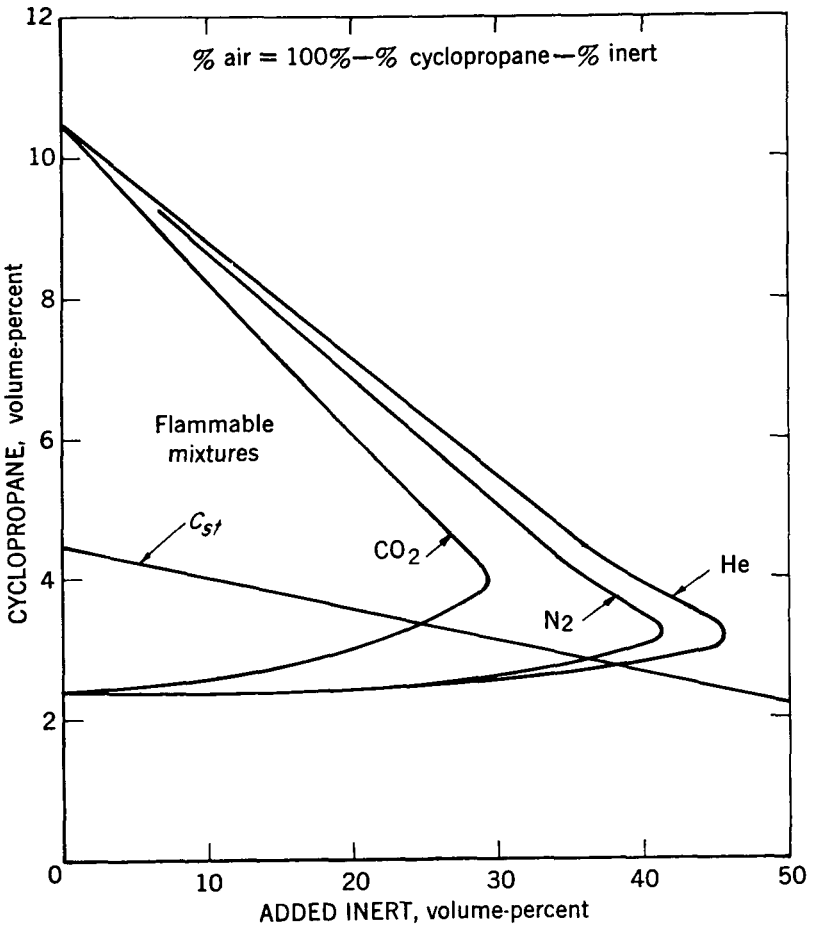

FIGURE 72.—Limits of Flammability of Cyclopropane-Carbon Dioxide-Air, Cyclopropane-Nitrogen-Air, and Cyclopropane-Helium-Air Mixtures at 25° C and Atmospheric Pressure.

72 (*106*). The first two curves are similar to those obtained with paraffin hydrocarbons (fig. 35).

The limits of flammability of cyclopropane-helium-oxygen and cyclopropane-nitrous oxide-oxygen mixtures at 25° C and atmospheric pressure are given in figure 73 (*106*). The latter curve differs from the former, as both additives are oxidants (oxygen and nitrous oxide).

The limits of flammability of cyclopropane-helium-nitrous oxide mixtures at 25° C and atmospheric pressure are given in figure 74 (*106*). Here the minimum oxidant concentration (nitrous oxide) required for flame propagation is approximately twice the corresponding concentration of oxygen in the systems cyclopropane-helium-air (fig. 72) and cyclopropane-helium-oxygen (fig. 73).

ALCOHOLS ($C_nH_{2n+1}OH$)

Limits in Air

The alcohols considered here are listed in table 13 together with $L_{25°}$ and $U_{25°}$. The ratios $L_{25°}/C_{st}$ are approximately 0.5. However, the L (mg/l) values decrease with increase in molecular weight. If L^* is taken to be the weight of combustible material (exclusive of the oxygen in the molecule) per liter of air, then for the simple alcohols:

$$L^*=L\frac{M-16}{M}. \qquad (54)$$

This equation gives the values listed in parentheses in the mg/l column; these are in fair agreement with the values obtained for the

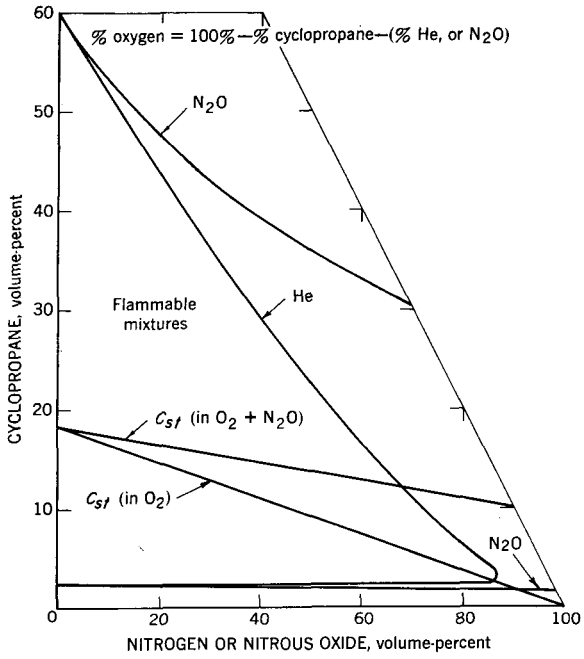

FIGURE 73.—Limits of Flammability of Cyclopropane-Helium-Oxygen and Cyclopropane-Nitrous Oxide-Oxygen Mixtures at 25° C and Atmospheric Pressure.

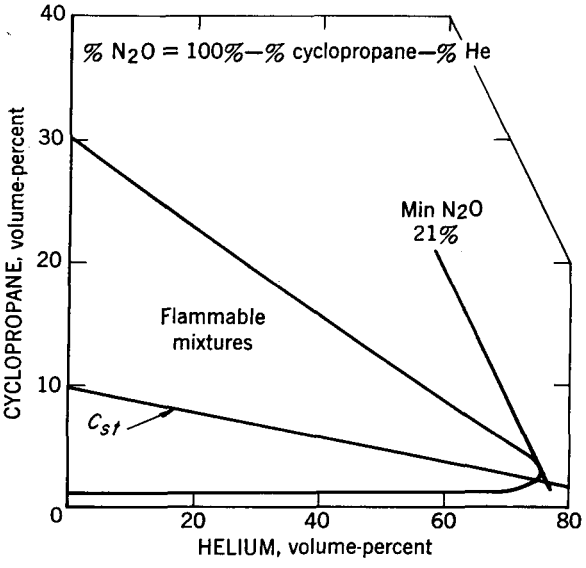

FIGURE 74.—Limits of Flammability of Cyclopropane-Helium-Nitrous Oxide Mixtures at 25° C and Atmospheric Pressure.

saturated hydrocarbons. Approximate L (mg/l) values can be obtained from the higher hydrocarbon values given in figure 22 by multiplying these by the ratio $M/(M-16)$. Further, figure 19 can be used to obtain L^* and L values in volume-percent. For example, at 25° C, L^* is about 47 mg/l from figure 22; the corresponding $L^*_{25°}$ from figure 19 for ethyl alcohol (M=46) is 2.2 volume-percent. Then, from equation (54), L is 3.4 volume-percent; the measured value is 3.3 volume-percent.

The lower limits of methyl alcohol have been determined by Scott and coworkers at 25°, 100°, and 200° C (*192*). The values at these three temperatures are 6.7, 6.5, and 5.9 volume-percent, respectively. The calculated values obtained from the modified Burgess-Wheeler law (fig. 23) at 100° and 200° C are 6.4 and 5.8 volume-percent, respectively.

Limits in Other Atmospheres

The limits of flammability of methyl alcohol-carbon dioxide-air and methyl alcohol-nitrogen-air mixtures at atmospheric pressure and 25° and 50° C are given in figure 75; flammability determinations on mixtures containing more than 15 percent methyl alcohol vapor were conducted at 50° C. The maximum amounts of carbon dioxide and nitrogen required to prevent flame propagation in these mixtures

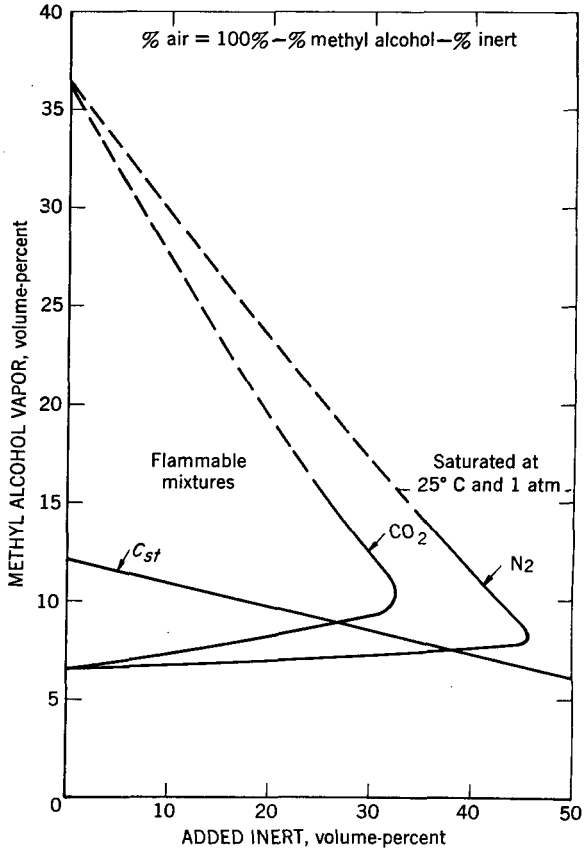

FIGURE 75.—Limits of Flammability of Methyl Alcohol-Carbon Dioxide-Air and Methyl Alcohol-Nitrogen-Air Mixtures at 25° C and Atmospheric Pressure. (Broken curve at 50° C and atmospheric pressure.)

TABLE 13.—*Properties of selected simple alcohols*

Combustible	Formula	M	Sp gr (Air=1)	C_{st} in air (vol pct)	Net ΔH_c $\left(\frac{Kcal}{mole}\right)$	Lower limit in air				Upper limit in air			
						L_{25} (vol pct)	$\frac{L_{25}}{C_{st}}$	$\left(\frac{mg}{l}\right)$	Ref.	U_{25} (vol pct)	$\frac{U_{25}}{C_{st}}$	$\left(\frac{mg}{l}\right)$	Ref.
Methyl alcohol	CH_3OH	32.04	1.11	12.25	159	6.7	0.55	103 / [1] 52	(40)	[2] 36	2.9	810 / [1] 405	(225)
Ethyl alcohol	C_2H_5OH	46.07	1.59	6.53	306	3.3	.50	70 / [1] 46	(40)	[2] 19	2.9	480 / [1] 310	(226)
n-Propyl alcohol	C_3H_7OH	60.09	2.07	4.45	448	[3] 2.2	.49	60 / [1] 44	(40)	[3] 14	3.2	420 / [1] 310	(40)
n-Butyl alcohol	C_4H_9OH	74.12	2.56	3.37	596	[4] 1.7	.50	57 / [1] 45	(5)	[4] 12			(5)
pri-n-Amyl alcohol	$C_5H_{11}OH$	88.15	3.04	2.72	742	[4] 1.4	.51	56 / [1] 46	(5)	[4] 10			
n-Hexyl alcohol	$C_6H_{13}OH$	102.17	3.53	2.27	[6] 888	1.2	.53	55 / [1] 46	(4)				

[1] $L^* = L\frac{M-16}{M}$.
[2] $t = 60°$.
[3] At saturation temperature.
[4] $t = 100°$ C.
[5] Figures compiled by Explosives Res. Center, Federal Bureau of Mines.
[6] Calculated value.

were compared with the corresponding maxima for paraffin hydrocarbons (figs. 28–35); it was found that appreciably more inert is required to make mixtures containing methyl alcohol nonflammable. Conversely, methyl alcohol requires less oxygen to form flammable mixtures, at a given temperature and pressure, than paraffin hydrocarbons do. This may be due in part to the oxygen of the alcohol molecule. For the simple alcohols, we have:

$$C_nH_{2n+1}OH + 1.5nO_2 \rightarrow nCO_2 + (n+1)H_2O. \quad (55)$$

Thus, the ratio of oxygen required for complete combustion of an alcohol to that for complete combustion of the corresponding paraffin, equation (22), is:

$$R_{O_2} = \frac{3n}{3n+1}. \quad (56)$$

When $n=1$, this ratio is 0.75. The corresponding ratios of the experimental minimum oxygen values from figures 75 and 28 are 0.82 with carbon dioxide and 0.85 with nitrogen as inert.

The limits of flammability of methyl alcohol-water vapor-air were obtained by Scott (*192*) in a 2-inch-ID cylindrical tube at 100° and 200° C and in a 4.9-liter cylindrical bomb at 400° C and 1 atmosphere (fig. 76). Similar data were obtained by Dvorak and Reiser in a 2.2-liter apparatus at 100° C (*53*).

The limits of flammability of ethyl alcohol-carbon dioxide-air and ethyl alcohol-nitrogen-air mixtures were obtained at 25° C and atmospheric, or one-half atmosphere, pressure as noted (fig. 77). Additional flammability data obtained for ethyl alcohol at 100° C and 1 atmosphere are given in figure 78. Flammability data for the systems *tert*-butyl alcohol-carbon dioxide-oxygen and 2-ethylbutanol-nitrogen-oxygen are given in figures 79–81.

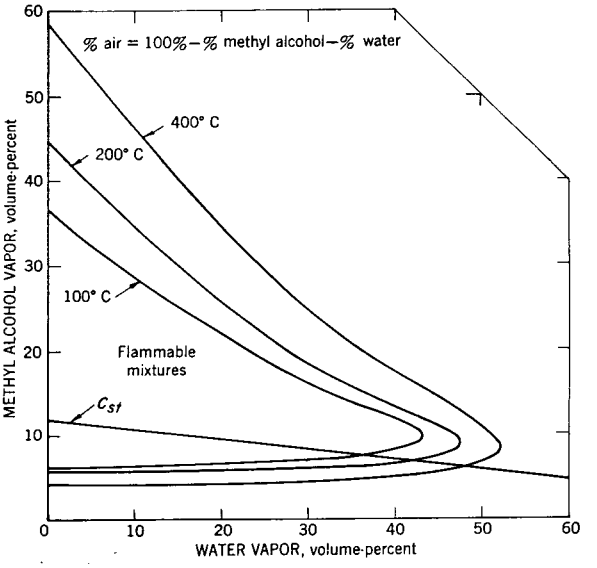

FIGURE 76.—Limits of Flammability of Methyl Alcohol-Water Vapor-Air Mixtures at 100°, 200°, and 400° C and Atmospheric Pressure.

Autoignition

The minimum autoignition temperatures in air and oxygen of a number of alcohols at atmospheric pressure are given in appendix A. Comparison of these values with those of the corresponding paraffins (methyl alcohol and methane; ethyl alcohol and ethane, etc.), shows that the AIT values of the alcohols are generally lower.

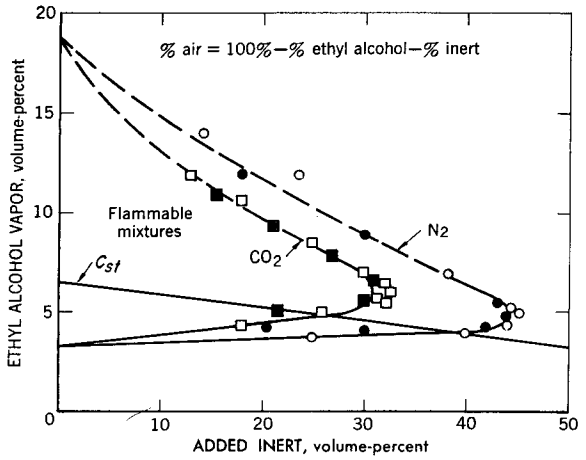

FIGURE 77.—Limits of Flammability of Ethyl Alcohol-Carbon Dioxide-Air and Ethyl Alcohol-Nitrogen-Air Mixtures at 25° C and Atmospheric Pressure. (Broken curves at one-half atmosphere.)

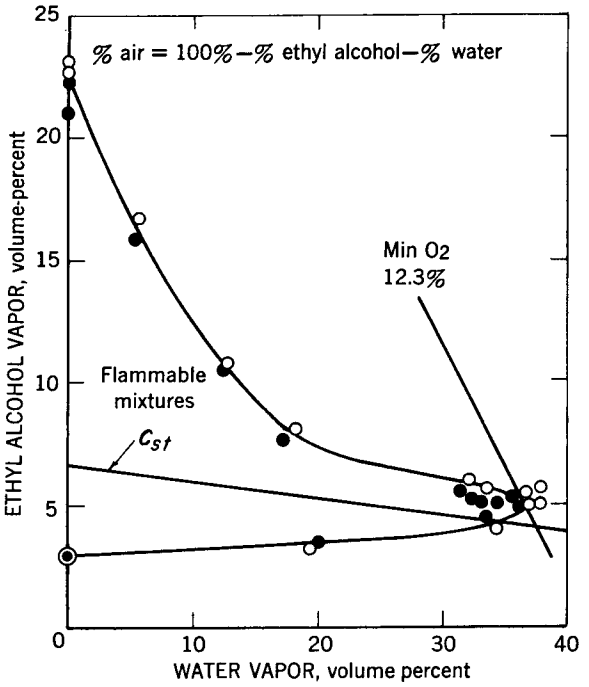

FIGURE 78.—Limits of Flammability of Ethyl Alcohol-Water Vapor-Air Mixtures at 100° C and Atmospheric Pressure.

Burning Rate

The burning velocities of methyl and isopropyl alcohol in air were determined by Gibbs and Calcote for a range of mixture compositions at 25° C; the maximum burning velocities were found to be 50.4 and 41.4 cm/sec, respectively (*68*). These investigators also obtained the burning velocities of methyl and *n*-propyl alcohol at 100° C; the maximum values were 72.2 and 64.8 cm/sec, respectively. These values

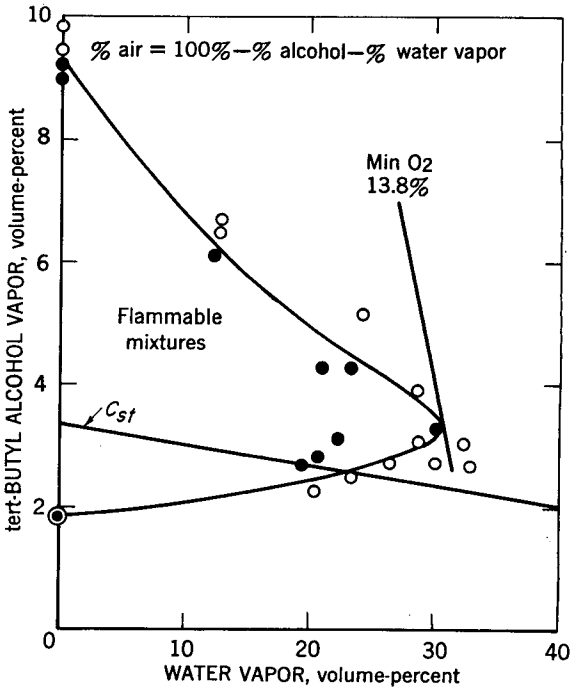

FIGURE 79.—Limits of Flammability of *tert*-Butyl Alcohol-Water Vapor-Air Mixtures at 150° C and Atmospheric Pressure.

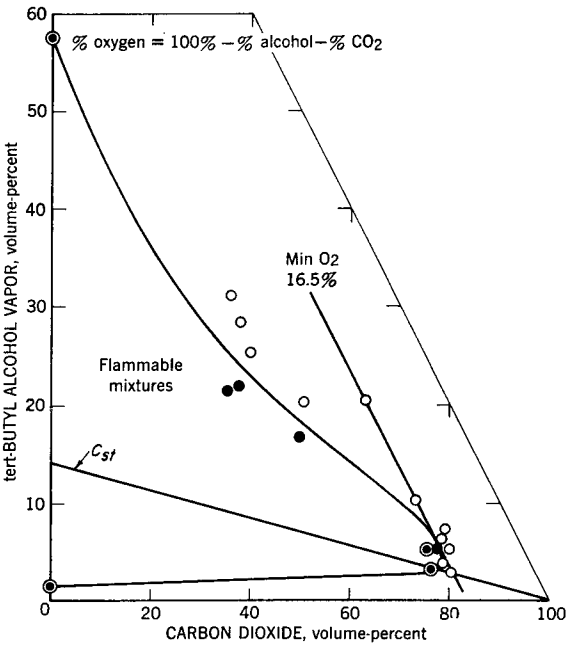

FIGURE 80.—Limits of Flammability of *tert*-Butyl Alcohol-Carbon Dioxide-Oxygen Mixtures at 150° C and Atmospheric Pressure.

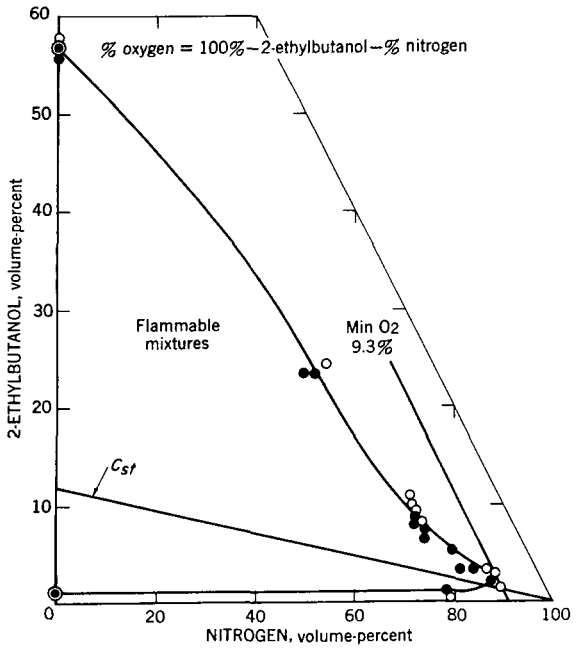

FIGURE 81.—Limits of Flammability of 2-Ethylbutanol-Nitrogen-Oxygen Mixtures at 150° C and Atmospheric Pressure.

are in fair agreement with the corresponding values of the paraffin hydrocarbons.

The methyl alcohol liquid-burning rate obtained from equation (53) is in fair agreement with that obtained experimentally (fig. 52). The relatively low $\Delta H_c/\Delta H_v$ ratios for the alcohols indicates that they should be characterized by low-burning rates in large pools.

ETHERS ($C_nH_{2n+1}OC_mH_{2m+1}$)

Limits in Air

The properties of a few common ethers are listed in table 14. Unfortunately, the limits data show appreciable scatter, so it is difficult to establish any general rules with the given data. However, as a first approximation, the L_{25}/C_{st} is about 0.5 for the simple ethers.

Limits in Other Atmospheres

Because of the importance of ethers as anesthetics, limits of flammability were determined in several atmospheres. The limits of the systems dimethyl ether-Freon-12 (CCl_2F_2)-air, dimethyl ether-carbon dioxide-air, and dimethyl ether-nitrogen-air obtained by Jones and coworkers are given in figure 82 (*114*); the limits of the systems diethyl ether-carbon dioxide-air and diethyl ether-nitrogen-air are given in figure 83 (*26, 106, 108*), Cool flames exist above the upper limit as noted; the upper

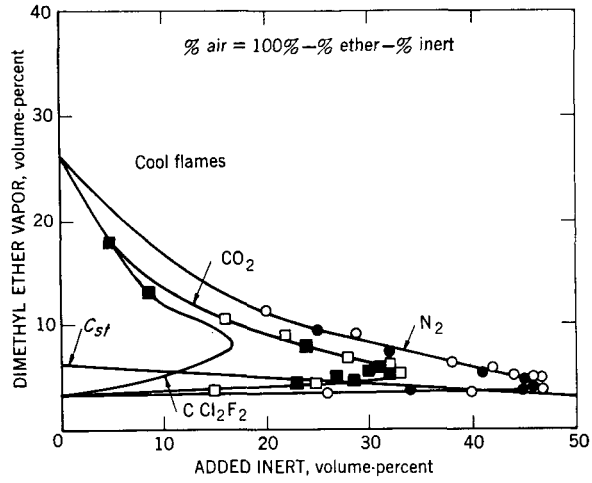

FIGURE 82.—Limits of Flammability of Dimethyl Ether-Carbon Dioxide-Air and Dimethyl Ether-Nitrogen-Air Mixtures at 25° C and Atmospheric Pressure.

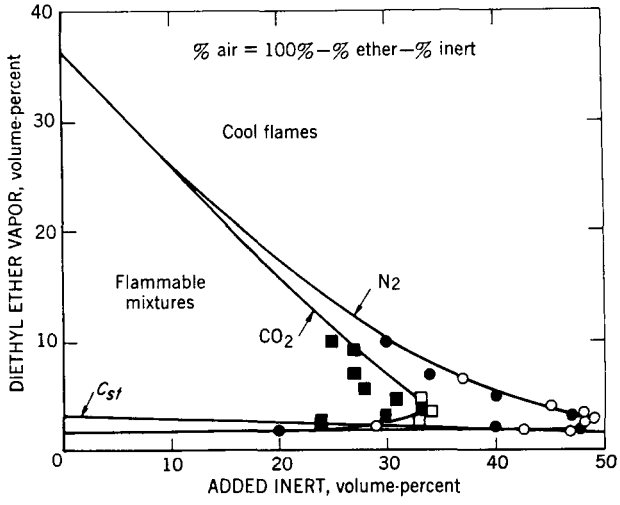

FIGURE 83.—Limits of Flammability of Diethyl Ether-Carbon Dioxide-Air and Diethyl Ether-Nitrogen-Air Mixtures at 25° C and Atmospheric Pressure.

limit of the cool flame region in air is 48.4 volume-percent, according to Burgoyne and Neale (*26*). The limits of the systems diethyl ether-helium-oxygen and diethyl ether-nitrous oxide-oxygen are given in figure 84 and the limits of diethyl ether-helium-nitrous oxide are given in figure 85 (*106*). Again, as with the alcohols, more inert is needed to assure the formation of nonflammable mixtures than is needed for the corresponding paraffin hydrocarbons. Also, cool flames are encountered at lower temperatures and pressures.

Comparison of curves in figures 84 and 85 shows that the minimum oxidant requirement for the formation of flammable diethyl ether-helium-oxidant mixtures is approximately twice

TABLE 14.—*Properties of selected ethers*

Combustible	Formula	M	Sp gr (Air=1)	C_{st} in air (vol pct)	Net ΔH_c $\left(\frac{\text{Kcal}}{\text{mole}}\right)$	Lower limit in air				Upper limit in air			
						L_{25} (vol pct)	$\frac{L_{25}}{C_{st}}$	L $\left(\frac{\text{mg}}{\text{l}}\right)$	Ref.	U_{25} (vol pct)	$\frac{U_{25}}{C_{st}}$	U $\left(\frac{\text{mg}}{\text{l}}\right)$	Ref.
Dimethyl ether	CH_3OCH_3	46.07	1.59	6.53	316	3.4	0.52	72 / [1] 47	*114*	27	4.1	760	(*114*)
Diethyl ether	$C_2H_5OC_2H_5$	74.12	2.56	3.37	605	1.9	.56	64 / [1] 50	(*40*)	[2] 36	11	1,880	(*40*)
Ethyl propyl ether	$C_2H_5OC_3H_7$	88.15	3.28	2.72	[3] 750	1.7	.62	68 / [1] 56	(*26*)	[4] 9	3.3	390	(*26*)
Di-i-propyl ether	$C_3H_7OC_3H_7$	102.17	3.53	2.27	[5] 900	1.4	.57	60 / [1] 51	(*40*)	7.9	3.5	290	(*40*)
Divinyl ether	$C_2H_3OC_2H_3$	70.09	2.42	4.02	[3] 1,770	1.7	.42	54 / [1] 42	(*97*)	27	6.7	1,160	(*97*)

[1] $L^*=L\frac{M-16}{M}$.
[2] Cool flames: $U_{25}=53$ vol pct.
[3] Calculated value.
[4] Cool flames: $U_{25}>16$ vol pct.
[5] Ref. (*155*).

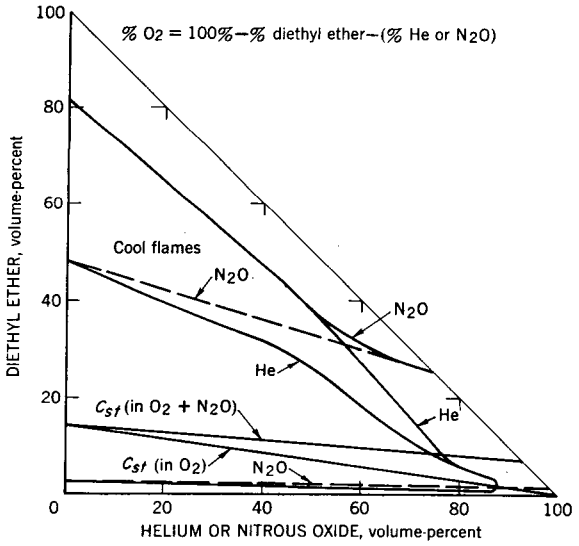

FIGURE 84.—Limits of Flammability of Diethyl Ether-Helium-Oxygen and Diethyl Ether-Nitrous Oxide-Oxygen Mixtures at 25° C and Atmospheric Pressure.

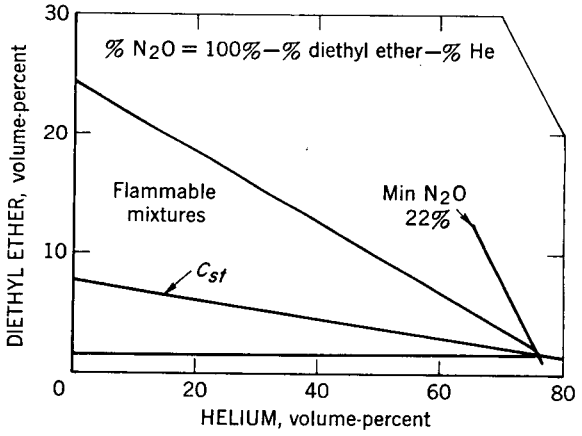

FIGURE 85.—Limits of Flammability of Diethyl Ether-Nitrous Oxide-Helium Mixtures at 25° C and Atmospheric Pressure.

as great with nitrous oxide as with oxygen. However, if 1 mole of nitrous oxide furnishes one-half mole of oxygen during combustion, then the minimum oxygen contents in the two cases are nearly equal. Unfortunately, the available data are too meager to permit a more detailed comparison.

Autoignition

In general, ethers are readily ignited by hot surfaces. These combustibles usually have a lower ignition temperature in air and in oxygen than do the corresponding paraffins and alcohols. The available autoignition temperature data are included in appendix A.

Since the ethers tend to form peroxides under a variety of conditions, they may appear to be unstable at room temperature (*233*).

ESTERS ($C_nH_{2n-1}OOC_mH_{2m+1}$)

The properties of several esters are listed in table 15. The ratio of the lower limit at 25° C to the stoichiometric concentration is about 0.55 for many of these compounds. This is the same ratio as in equation (21) for paraffin hydrocarbons. The lower limit values expressed in terms of the weight of combustible per liter of air (see section about alcohols) are listed in parentheses under L(mg/l). These are larger than the corresponding values for the hydrocarbons and alcohols. The inert requirements and minimum oxygen requirements for the first member of the series, methyl formate, are nearly the same as for methyl alcohol and dimethyl ether (figs. 76, 82, 86). This is not

TABLE 15.—*Properties of selected esters*

Combustible	Formula	M	Sp. gr. (Air=1)	C_{st} in air (vol pct)	Net ΔH_c $\left(\frac{\text{Kcal}}{\text{mole}}\right)$	Lower limit in air				Upper limit in air			
						L_{25} (vol pct)	$\frac{L_{25}}{C_{st}}$	$\left(\frac{L}{\frac{\text{mg}}{1}}\right)$	Ref.	U_{25} (vol pct)	$\frac{U_{25}}{C_{st}}$	$\left(\frac{U}{\frac{\text{mg}}{1}}\right)$	Ref.
Methyl formate	$HCOOCH_3$	60.05	2.07	9.48	219	5.0	0.53	142 / [1] 66	(111)	23.0	2.4	800	(111)
Ethyl formate	$HCOOC_2H_5$	74.08	2.56	5.65	367	2.8	.50	95 / [1] 54	(40)	16.0	2.8	630	(40)
n-Butyl formate	$HCOOC_4H_9$	102.13	3.53	3.12	[2] 650	1.7	.54	79 / [1] 50	(40)	8.2	2.6	410	(40)
Methyl acetate	CH_3COOCH_3	74.08	2.56	5.65	358	3.2	.57	106 / [1] 60	(40)	16.0	2.8	630	(40)
Ethyl acetate	$CH_3COOC_2H_5$	88.10	3.04	4.02	504	2.2	.55	88 / [1] 56	(40)	11.0	2.7	510	(175)
n-Propyl acetate	$CH_3COOC_3H_7$	102.13	3.53	3.12	[2] 650	1.8	.58	83 / [1] 57	(40)	[3] 8.0	2.6	400	(40)
n-Butyl acetate	$CH_3COOC_4H_9$	116.16	4.01	2.55	----------	[4] 1.4	.55	73 / [1] 53	([5])	[4] 8.0	3.1	450	([5])
n-Amyl acetate	$CH_3COOC_5H_{11}$	130.18	4.50	2.16	----------	[4] 1.0	.51	65 / [1] 49	([5])	[4] 7.1	3.3	440	([5])
Methyl propionate	$C_2H_5COOCH_3$	88.10	3.04	4.02	----------	2.4	.60	97 / [1] 62	(40)	13.0	[6] 3.2	580	(40)
Ethyl propionate	$C_2H_5COOC_2H_5$	102.13	3.53	3.12	[2] 650	1.8	.58	83 / [1] 57	(40)	11.0	[6] 3.5	510	(40)

[1] $L^* = L\frac{M-32}{M}$.
[2] Calculated value.
[3] t=90° C.
[4] t=100° C.
[5] Figures compiled by Explosives Res. Center, Federal Bureau of Mines.
[6] P=0.5 atm.

true of the other members for which data compiled at the Explosives Research Center are available—isobutyl formate and methyl acetate (figs. 87, 88). Accordingly, it is rather difficult to make additional generalizations for this series.

The autoignition temperatures of many esters in air and oxygen at atmospheric pressure are given in appendix A. In general, the AIT values of the esters are lower than are those of the corresponding paraffins.

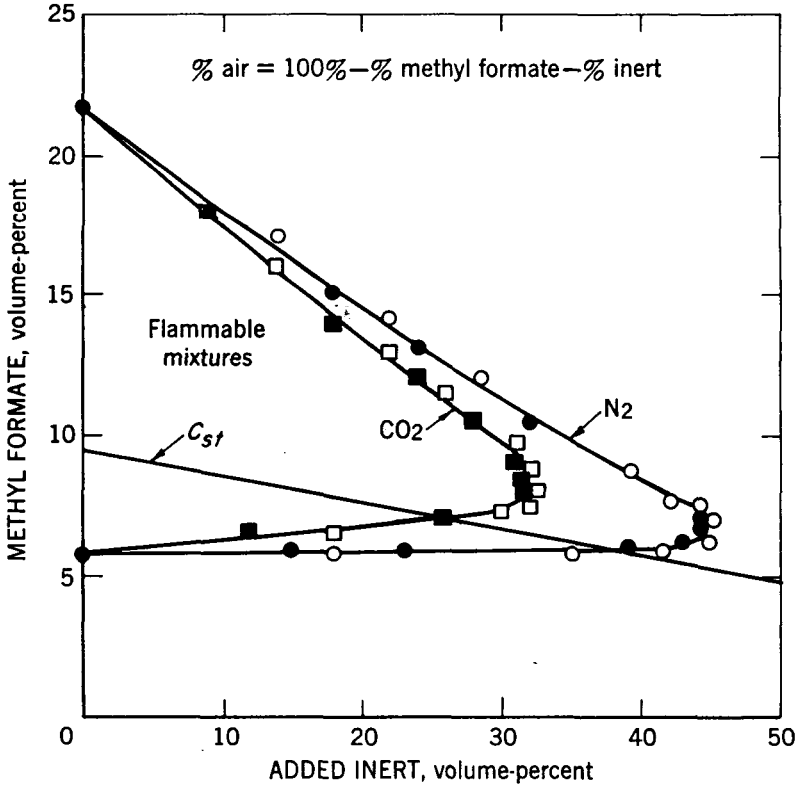

FIGURE 86.—Limits of Flammability of Methyl Formate-Carbon Dioxide-Air and Methyl Formate-Nitrogen-Air Mixtures.

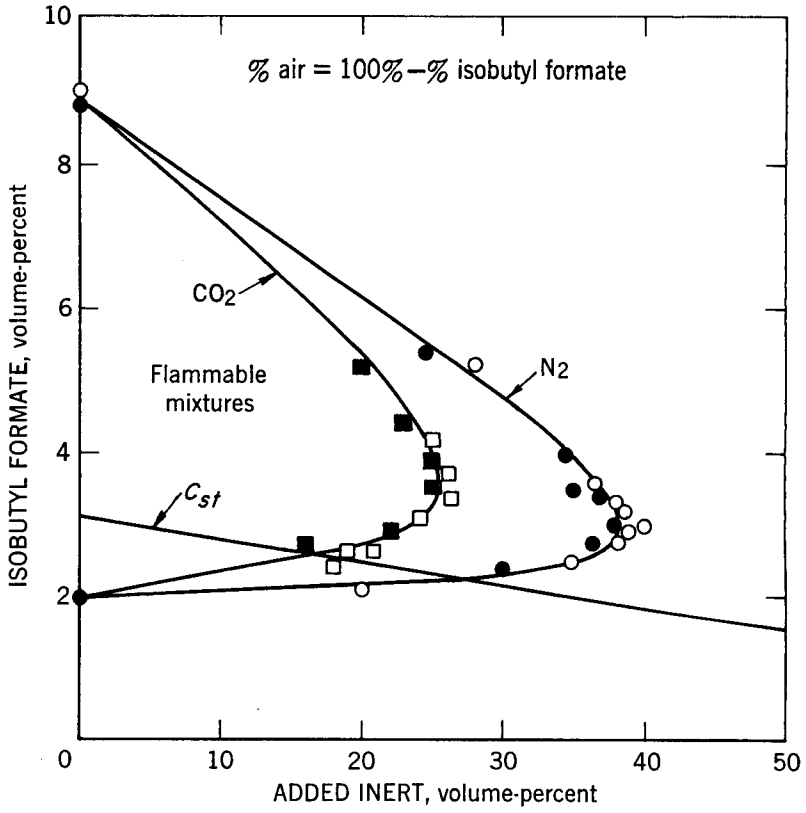

FIGURE 87.—Limits of Flammability of Isobutyl Formate-Carbon Dioxide-Air and Isobutyl Formate-Nitrogen-Air Mixtures.

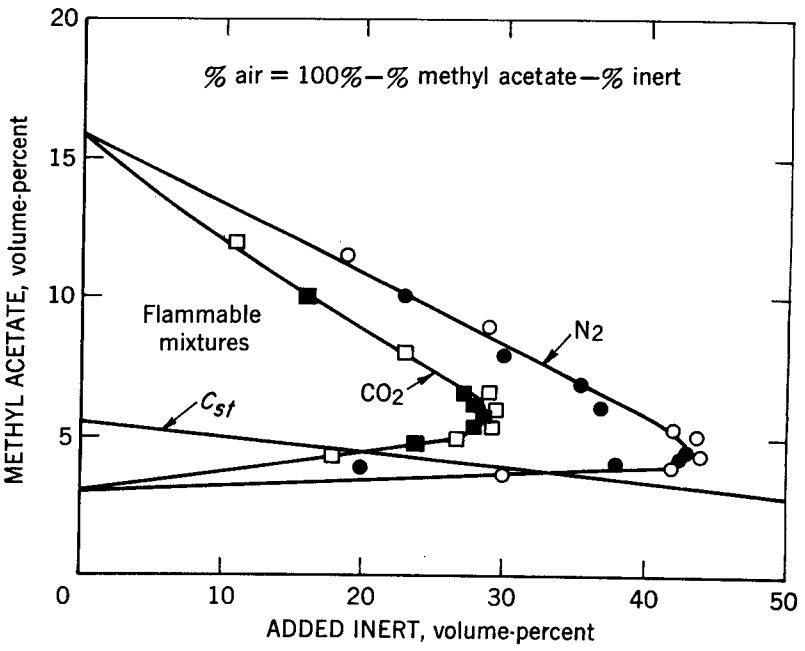

FIGURE 88.—Limits of Flammability of Methyl Acetate-Carbon Dioxide-Air and Methyl Acetate-Nitrogen-Air Mixtures.

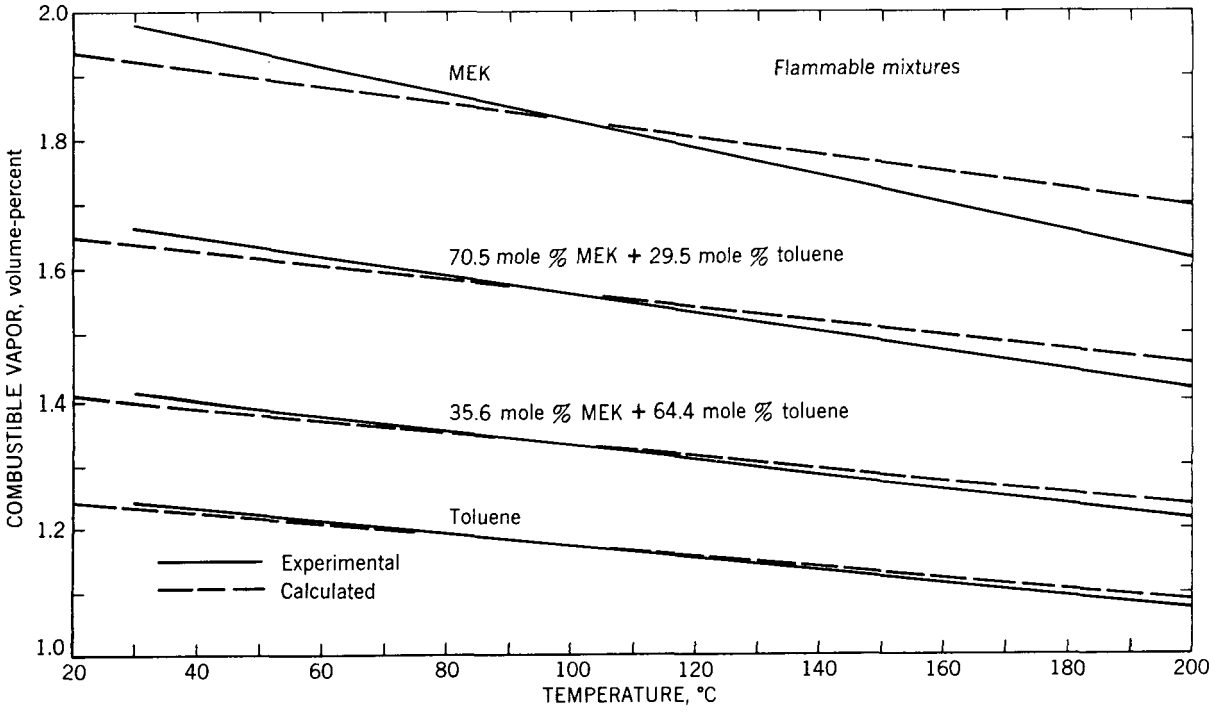

FIGURE 89.—Effect of Temperature on Lower Limits of Flammability of MEK-Toluene Mixtures in Air at Atmospheric Pressure.

ALDEHYDES AND KETONES ($C_n H_{2n}O$)

Properties of some aldehydes and ketones are given in table 16. The ratio of the lower limit at 25° C in air to the stoichiometric composition is approximately 0.5.

Zabetakis, Cooper, and Furno found that the lower limits of methyl ethyl ketone (MEK) and MEK-toluene mixtures vary linearly with temperature between room temperature and 200° C (*235*). A summary of these data is given in figure 89; broken curves in this figure were obtained from the modified Burgess-Wheeler law, equation (33), taking the lower limit at 100° C as the reference value. Similar data were obtained for tetrahydrofuran (THF) and THF-toluene mixtures (fig. 90). In addition, it was shown that the systems MEK-toluene and THF-toluene obey Le Chatelier's law, equation (46). Calculated and experimental values for the preceding systems in air are given in figures 91 and 92.

The limits of the systems acetone-carbon dioxide-air, acetone-nitrogen-air, MEK-chlorobromomethane (CBM)-air, MEK-carbon dioxide-air, and MEK-nitrogen-air are given in figures 93 and 94. The data in these figures were obtained by Jones and coworkers (*238*).

TABLE 16.—*Properties of selected aldehydes and ketones*

Combustible	Formula	M	Sp gr (Air=1)	C_{st} in air (vol pct)	Net ΔH_c $\left(\frac{\text{Kcal}}{\text{mole}}\right)$	Lower limit in air				Upper limit in air			
						L_{25} (vol pct)	$\frac{L_{25}}{C_{st}}$	$\left(\frac{L}{\text{mg}/\text{l}}\right)$	Ref.	U_{25} (vol pct)	$\frac{U_{25}}{C_{st}}$	$\left(\frac{U}{\text{mg}/\text{l}}\right)$	Ref.
Acetaldehyde	CH_3CHO	44.05	1.52	7.73	264	4.0	0.52	82	(*223*)	[1] 36	4.7	1,100	(*26*)
Propionaldehyde	C_2H_5CHO	58.08	2.01	4.97	409	2.9	.59	77	(*26*)	[2] 14	2.8	420	(*26*)
Paraldehyde	$(CH_3CHO)_3$	132.16	4.56	2.72		1.3	.48	78	(*40*)				
Acetone	CH_3COCH_3	58.08	2.01	4.97	403	2.6	.52	70	(*98*)	13	2.6	390	(*98*)
Methyl ethyl ketone	$CH_3COC_2H_5$	72.10	2.49	3.67	548	1.9	.52	62	(*235*)	10	2.7	350	(*223*)
Methyl prepyl ketone	$CH_3COC_3H_7$	86.13	2.97	2.90	692	1.6	.55	63	(*40*)	8.2	2.8	340	(*40*)
Diethyl ketone	$C_2H_5COC_2H_5$	86.13	2.97	2.90	692	1.6	.55	63	[3]				
Methyl butyl ketone	$CH_3COC_4H_9$	100.16	3.46	2.40	840	[4] 1.4	.58	64	(*40*)	[5] 8.0	3.3	390	(*40*)

[1] Cool flames: U_{25}=60 vol pct.
[2] Cool flames: U_{25}=17 vol pct.
[3] Calculated value.
[4] t=50° C.
[5] t=100° C.

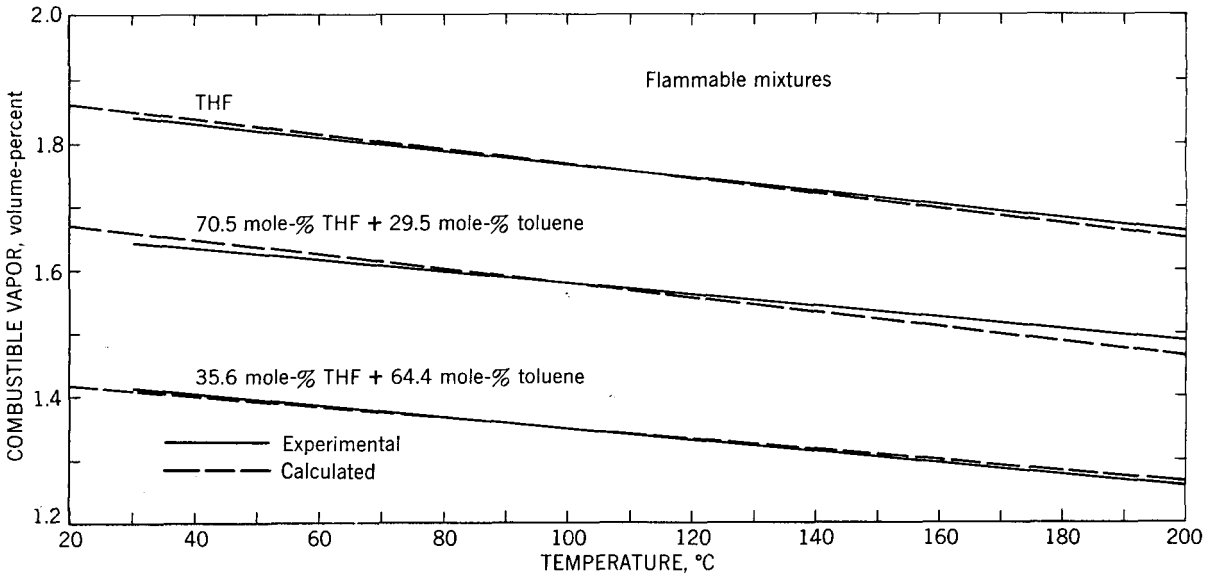

FIGURE 90.—Effect of Temperature on Lower Limits of Flammability of THF-Toluene Mixtures in Air at Atmospheric Pressure.

The autoignition temperatures of various aldehydes and ketones in oxygen and air at atmospheric pressure are given in appendix A. In general, the AIT values are lower than those of the corresponding paraffins.

SULFUR COMPOUNDS

The pertinent properties of sulfur compounds are given in table 17. In general, they have wide flammable ranges and relatively low ignition temperatures (appendix A).

Flammability diagrams are given for carbon disulfide mixed with carbon dioxide-air, water vapor-air (*239*) and nitrogen-air (fig. 95); hydrogen sulfide-carbon dioxide-air (fig. 96); and ethyl mercaptan with chlorodifluoromethane and dichlorodifluoromethane in air (*117*) (fig. 97). Figure 95 is interesting in that it shows not only the wide flammable range of carbon disulfide in air but also the large quantities of inert required to prevent the formation of flammable mixtures.

FUELS AND FUEL BLENDS

Fuels used for propulsion, not covered in other sections, are considered here (table 18).

Ammonia and Related Compounds

This series includes ammonia (NH_3), hydrazine (N_2H_4), monomethylhydrazine ($N_2H_3 \cdot CH_3$) and unsymmetrical dimethylhydrazine ($N_2H_2 \cdot (CH_3)_2$).

Ammonia forms flammable mixtures with air and other oxidants in a variety of concentrations, as noted in table 19. White (*225*) and more recently, Buckley and Husa, (*19*) reported that, as with hydrocarbons, an increase in either temperature or pressure tends to widen the flammable range. Further, White found that the lower limit flame temperature remains essentially constant with increase in initial temperature.

TABLE 17.—*Properties of selected sulfur compounds*

Combustible	Formula	M	Sp gr (Air=1)	C_{st} in air (vol pct)	Net ΔH_c $\left(\frac{\text{Kcal}}{\text{mole}}\right)$	Lower limit in air				Upper limit in air			
						L_{25} (vol pct)	$\frac{L_{25}}{C_{st}}$	$\left(\frac{L}{\frac{\text{mg}}{\text{l}}}\right)$	Ref.	U_{25} (vol pct)	$\frac{U_{25}}{C_{st}}$	$\left(\frac{U}{\frac{\text{mg}}{\text{l}}}\right)$	Ref.
Hydrogen sulfide	H_2S	34.08	1.18	12.25	145	4.0	0.33	63	(1)	44	3.6	1,190	(1)
Carbon disulfide	CS_2	76.13	2.63	6.53	252	1.3	.20	45	(*239*)	50	7.7	3,400	(*225*)
Methyl mercaptan	CH_3SH	48.10	1.66	6.53	276	3.9	.60	87	(1)	22	3.4	600	(1)
Ethyl mercaptan	C_2H_5SH	62.13	2.15	4.45	492	2.8	.63	80	(*104*)	18	4.4	610	(*104*)
Dimethyl sulfide	CH_3SCH_3	62.13	2.15	4.45	----------	2.2	.50	62	(1)	20	4.5	690	(1)

[1] Figures compiled at Explosives Res. Center, Federal Bureau of Mines.

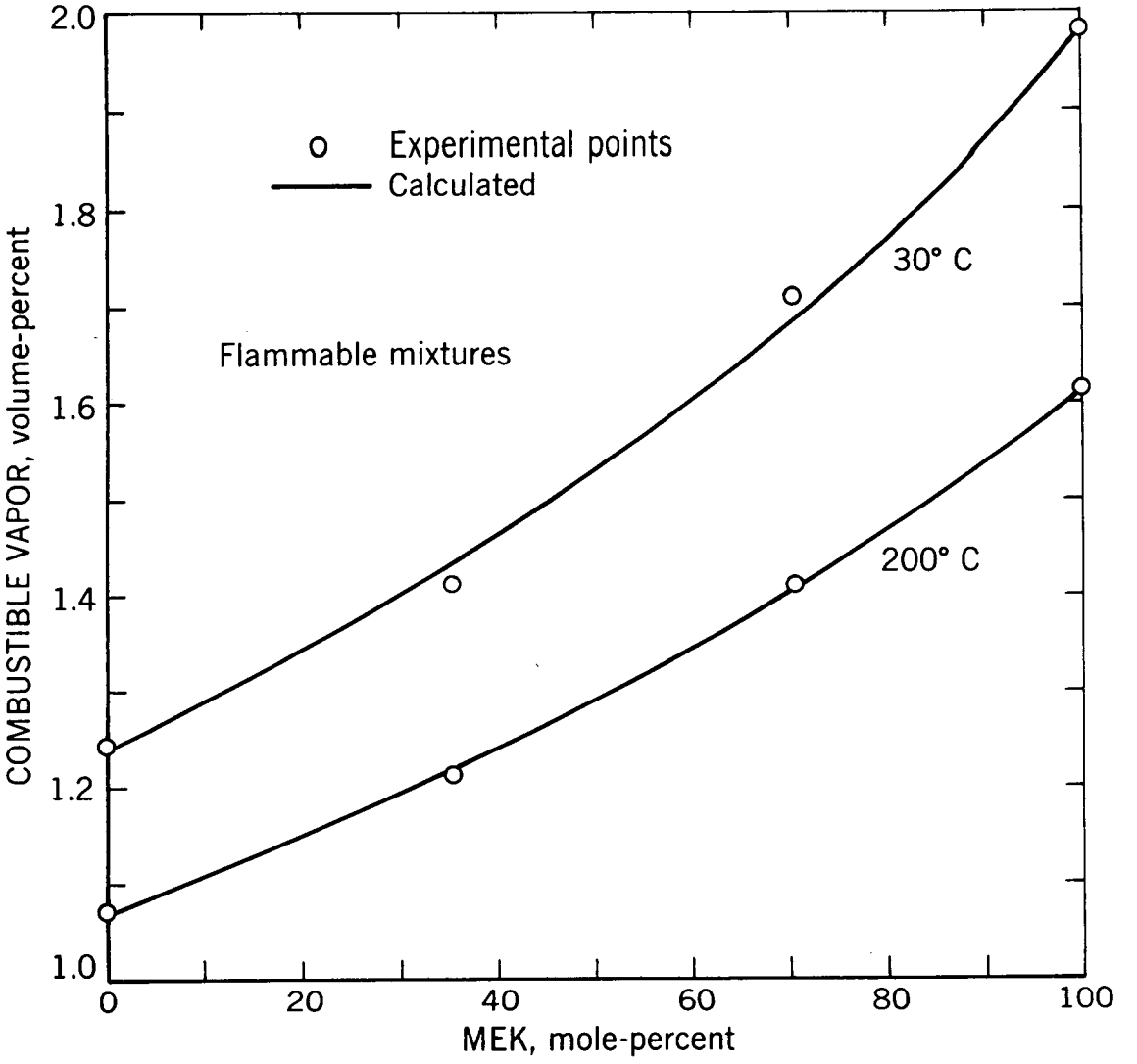

FIGURE 91.—Effect of Liquid Composition on Lower Limits of Flammability of MEK-Toluene Mixtures in Air at 30° and 200° C.

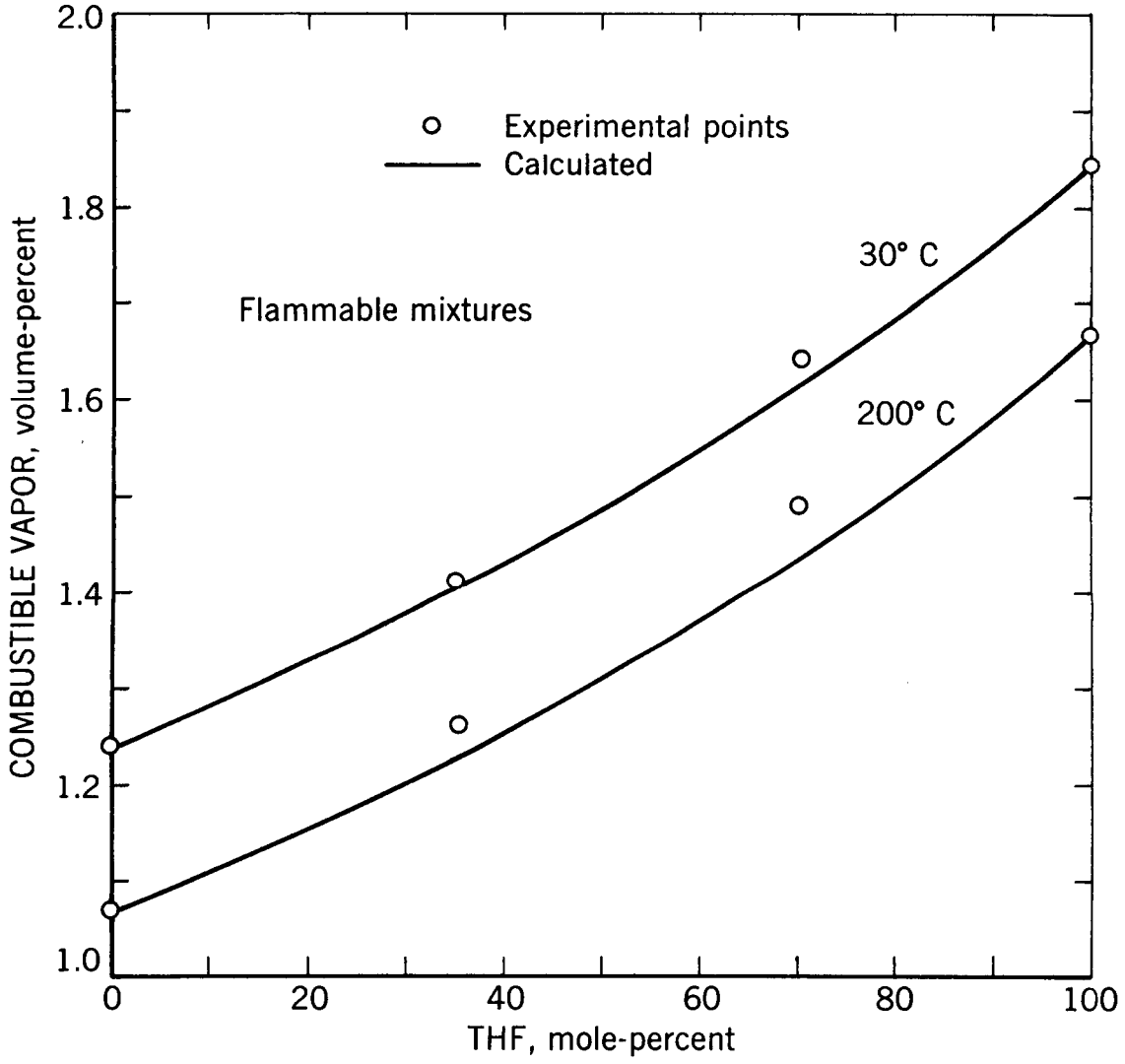

FIGURE 92.—Effect of Liquid Composition on Lower Limits of Flammability of THF-Toluene Mixtures in Air at 30° and 200° C.

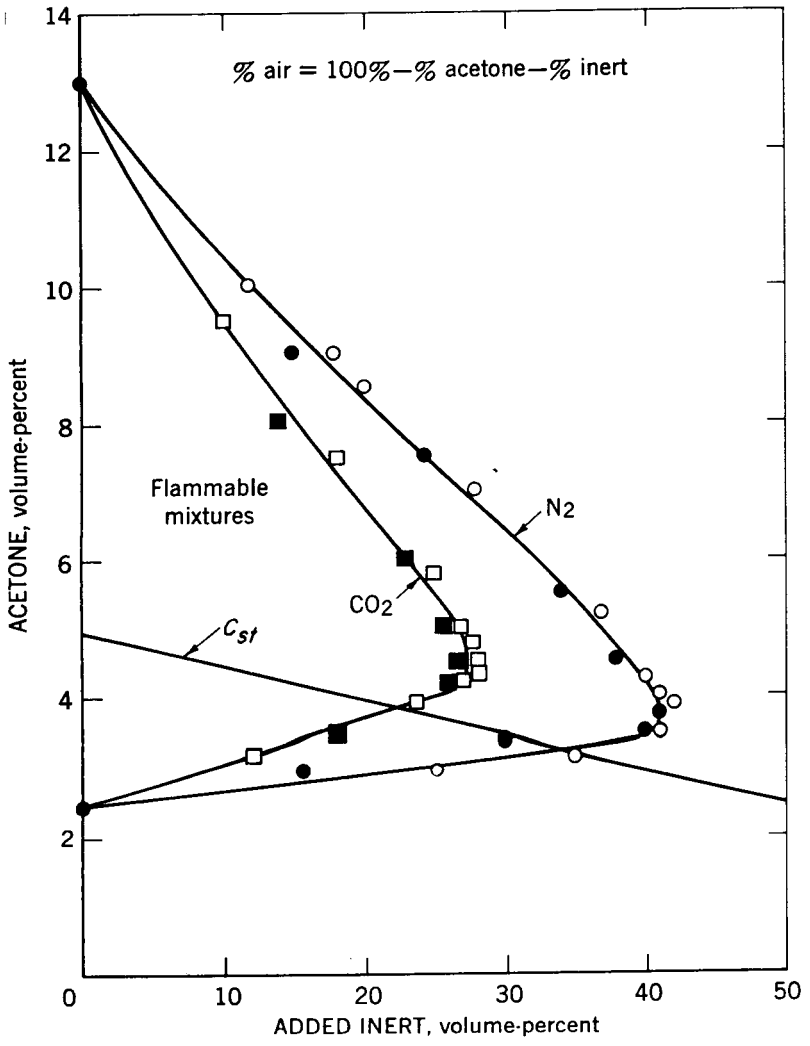

FIGURE 93.—Limits of Flammability of Acetone-Carbon Dioxide-Air and Acetone-Nitrogen-Air Mixtures.

TABLE 18.—*Properties of selected fuels and fuel blends*

Combustible	Formula	M	Sp gr (Air=1)	C_{st} in air (vol pct)	Net ΔH_c $\left(\frac{\text{Kcal}}{\text{mole}}\right)$	Lower limit in air				Upper limit in air			
						L_{25} (vol pct)	$\frac{L_{25}}{C_{st}}$	$\left(\frac{\text{mg}}{\text{l}}\right)$	Ref.	U_{25} (vol pct)	$\frac{U_{25}}{C_{st}}$	$\left(\frac{\text{mg}}{\text{l}}\right)$	Ref.
Ammonia	NH_3	17.03	0.59	21.83		15	0.69	134	(167)	28	1.3	300	(182)
Hydrazine	N_2H_4	32.05	1.11	17.32		4.7	.27	70	(188)	100	5.8		(218)
Monomethyl hydrazine	$N_2H_3CH_3$	46.07	1.59	7.73		4	.52	86	(218)				
Unsymmetrical dimethylhydrazine.	$N_2H_2(CH_3)_2$	60.10	2.08	4.97		2	.40	55	(166)	95	19.1		(218)
Diborane	B_2H_6	27.69	.96	6.53	478	.8	.12	10	(163)	88	13.5		(163)
Tetraborane	B_4H_{10}	53.36	1.84	3.67		.4	.11	10	(1)				
Pentaborane	B_5H_9	63.17	2.18	3.37	1030	.42	.12	12					
Decaborane	$B_{10}H_{14}$	122.31	4.23	1.87		.2	.11	11	(1)				
Aviation gasoline 100/130						1.3			(241)	7.1			(241)
Aviation gasoline 115/145						1.2			(241)	7.1			(241)
Aviation jet fuel JP-1								[2] 48	(241)			[2] 380	(241)
Aviation jet fuel JP-3						1.4			(241)	8			(241)
Aviation jet fuel JP-4						1.3		48	(241)	8		330	(241)
Aviation jet fuel JP-6								[3] 46	(127)			[2] 290	(127)
Hydrogen	H_2	2.016	.07	29.53	57.8	4.0	.14	3.7	(40)	75	2.54	270	(224)

[1] Calculated value.
[2] t=150° C.
[3] t=100° C.

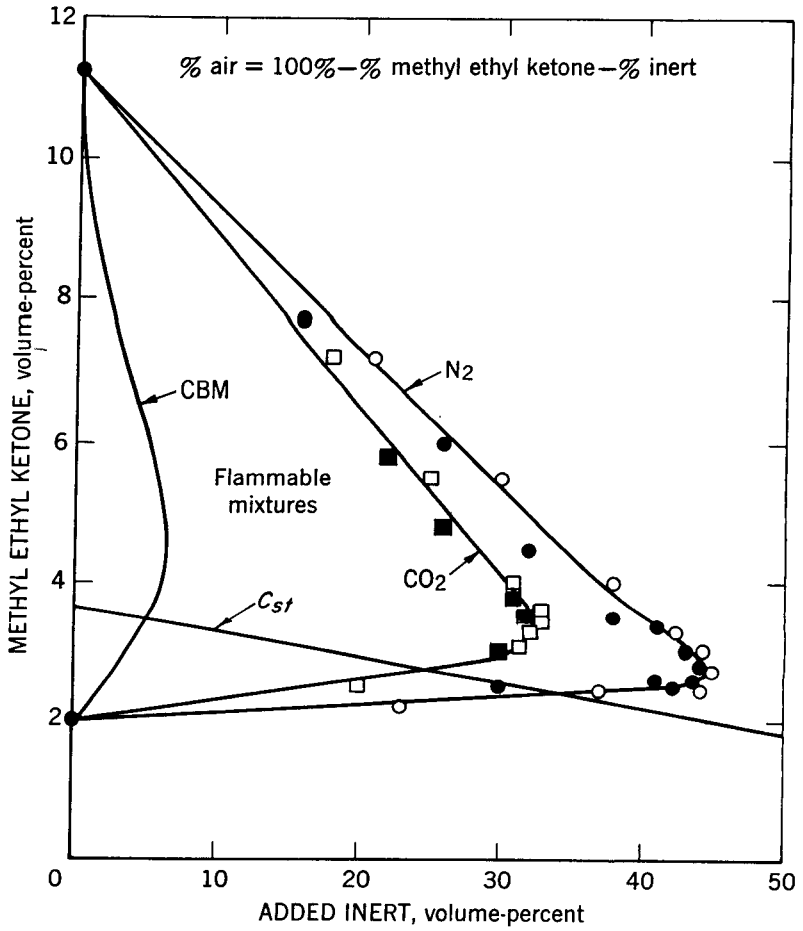

FIGURE 94.—Limits of Flammability of Methyl Ethyl Ketone (MEK) - Chlorobromemethane (CBM)-Air, MEK-Carbon Dioxide Dioxide-Air and MEK-Nitrogen-Air Mixtures at 25° C and Atmospheric Pressure.

TABLE 19.—*Limits of flammability of ammonia at room temperature and near atmospheric pressure*

Oxidant	C_{st}	L	U	Ref.
Air	21. 8	15	28	(*167, 182*)
Oxygen	57. 1	15	79	(*225*)
Nitrous oxide	40. 0	2. 2	72	(*109*)

Hydrazine vapor burns in the absence of an oxidizer, so that it has no upper limit and can therefore be used as a monopropellant. The decomposition flame yields hydrogen, nitrogen, and ammonia (*64, 73*). However, hydrazine vapor can be rendered nonflammable by addition of stable diluents or inhibitors. The amount of diluent required at any temperature and pressure appears to be governed in part by the ignition source strength. With a 0.25-inch spark gap and a 15,000-volt, 60-ma-luminous-tube transformer as the energy source, Furno, Martindill, and Zabetakis (*63*) found that the following quantities of hydrocarbon vapor were needed to inhibit flame propagation in a 1¼-inch glass tube [5] at 125° C and atmospheric pressure: 39.8 pct benzene; 35.0 pct toluene; 27.3 pct *m*-xylene; 23.8 pct cumene; 21.0 pct *n*-heptane. On this same basis, 95.3 pct air is needed to prevent flame propagation (*188*); this corresponds to a lower limit of flammability of 4.7 pct hydrazine vapor. The flammable range in air at atmospheric pressure is presented graphically in figure 98, which also gives the flammable ranges of monomethylhydrazine, unsymmetrical dimethylhydrazine, and ammonia for comparison (*218*). The flammability diagram for the system hydrazine-*n*-heptane-air at 125° C and atmospheric pressure is given in figure 99. These data were also obtained in a 1¼-inch glass tube.

A summary of the autoignition temperature data obtained by Perlee, Imhof, and Zabetakis (*166*) for hydrazine, MMH, and UDMH in air and nitrogen dioxide (actually, the equilibrium

[5] Comparable results were partially obtained in a 2-inch tube.

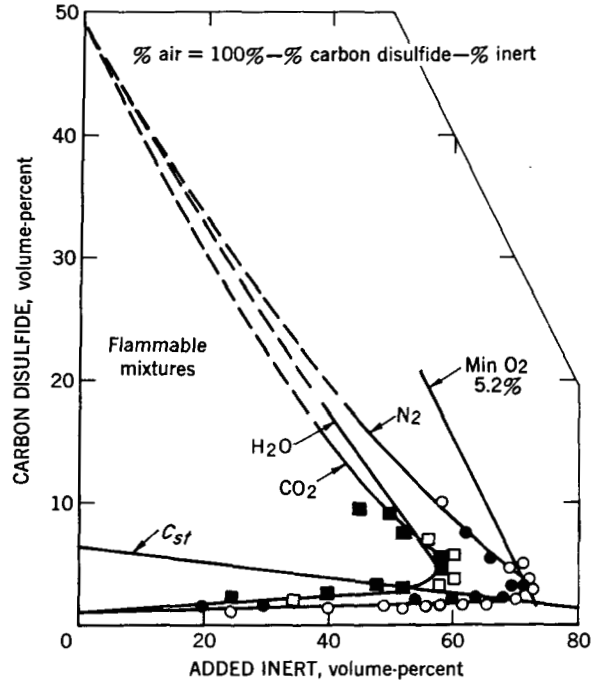

FIGURE 95.—Limits of Flammability of Carbon Disulfide-Carbon Dioxide-Air, Carbon Dioxide-Nitrogen-Air Mixtures at 25° C and Atmospheric Pressure, and Carbon Disulfide-Water Vapor-Air at 100° C and Atmospheric Pressure.

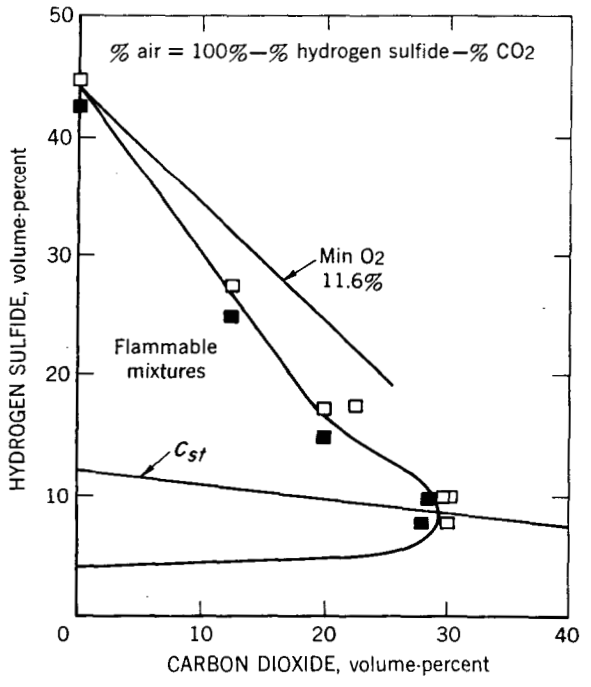

FIGURE 96.—Limits of Flammability of Hydrogen Sulfide-Carbon Dioxide-Air Mixtures at 25° C and Atmospheric Pressure.

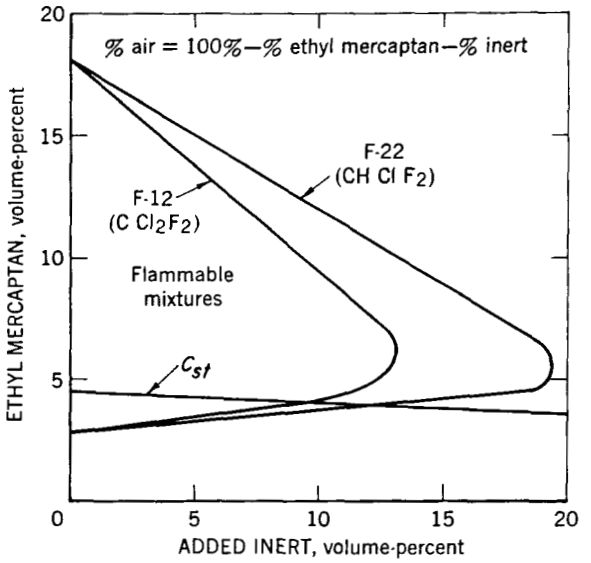

FIGURE 97.—Limits of Flammability of Ethyl Mercaptan-F-12-Air and Ethyl Mercaptan-F-22-Air Mixtures at Atmospheric Pressure and 27° C.

mixture $NO_2^* \rightleftharpoons NO_2 + N_2O_4$) is given in figure 100; short horizontal lines indicate the uncertainty in NO_2^* concentrations. These materials may ignite spontaneously at room temperature with relatively small NO_2^* concentrations in the air; at 25° C, liquid UDMH ignites in NO_2^*-air atmospheres that contain more than about 8 volume-percent NO_2^*; MMH and hydrazine ignite in atmospheres that contain more than about 11 and 14 volume-percent NO_2^*, respectively. In general, even smaller concentrations of NO_2^* produce spontaneous ignition of these combustibles at higher initial combustible liquid temperatures. The effect of the hydrazine liquid temperature on the spontaneous ignition temperature in NO_2^*-air atmospheres is illustrated in figure 101. Similar data are given in figures 102 and 103 for MMH and UDMH; there is an apparent anomaly in the data obtained with MMH at 36°, 55°, and 67° C.

The use of various helium-oxygen atmospheres in place of air results in the spontaneous ignition temperature curves given in figure 104 for UDMH. Comparison of curve *B* of this set with curve *A* of figure 100 indicates that the spontaneous ignition temperature of UDMH in NO_2^*-He-O_2 atmospheres is the same as that obtained in NO_2^*-air atmospheres.

Ignition temperature data obtained with UDMH in NO_2^*-air mixtures at 15 and 45 psia are summarized in figure 105. These indicate that although the spontaneous ignition temperature of UDMH in air is not affected ap-

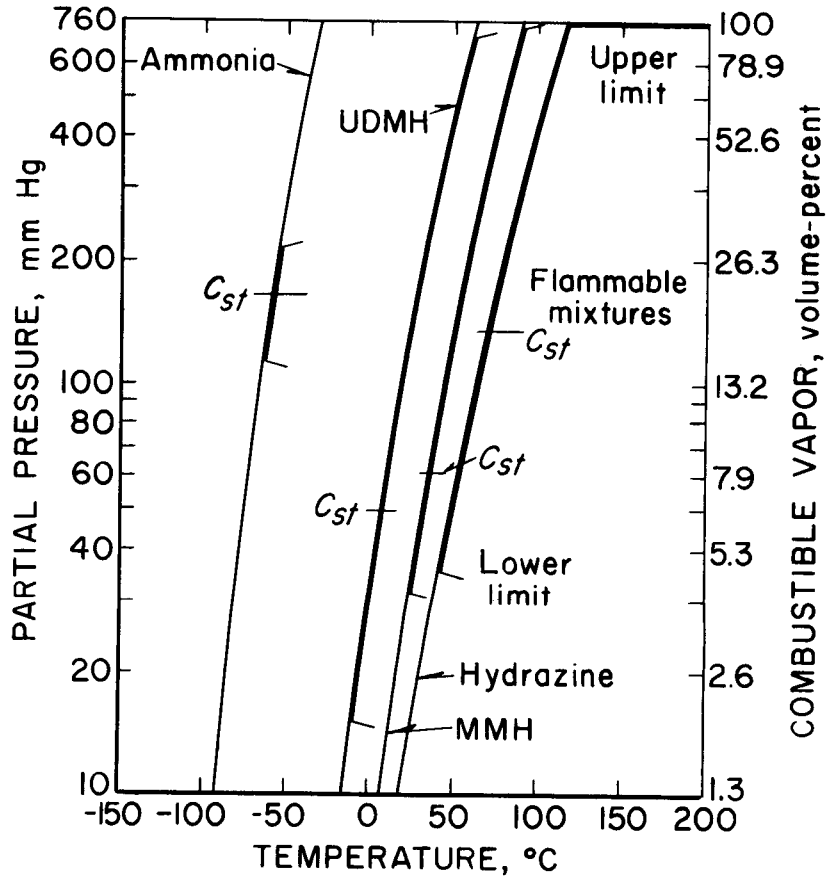

FIGURE 98.—Limits of Flammability of Ammonia, UDMH, MMH, and Hydrazine at Atmospheric Pressure in Saturated and Near-Saturated Vapor-Air Mixtures.

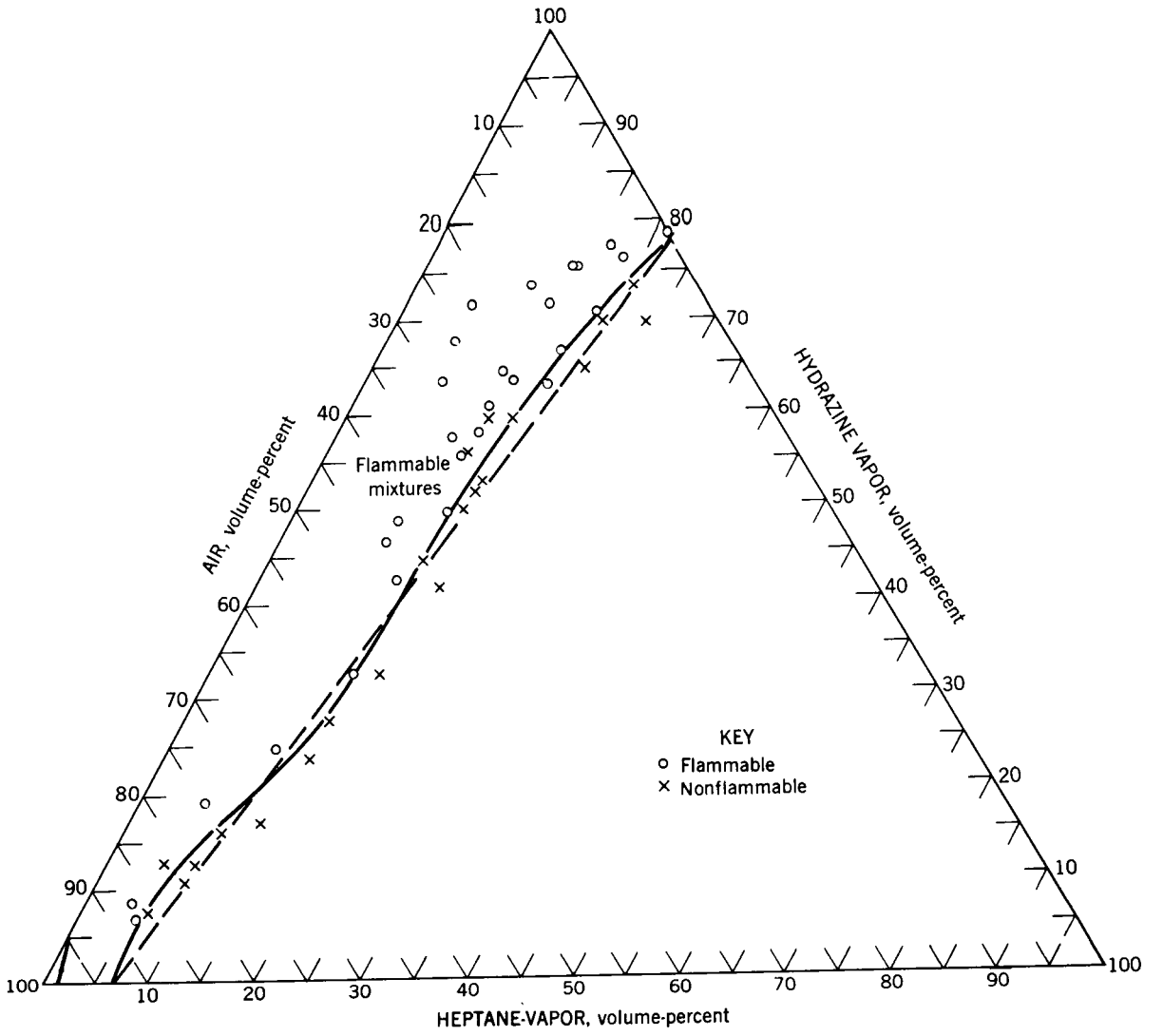

FIGURE 99.—Flammable Mixture Compositions of Hydrazine-Heptane-Air at 125° C and Approximately Atmospheric Pressure.

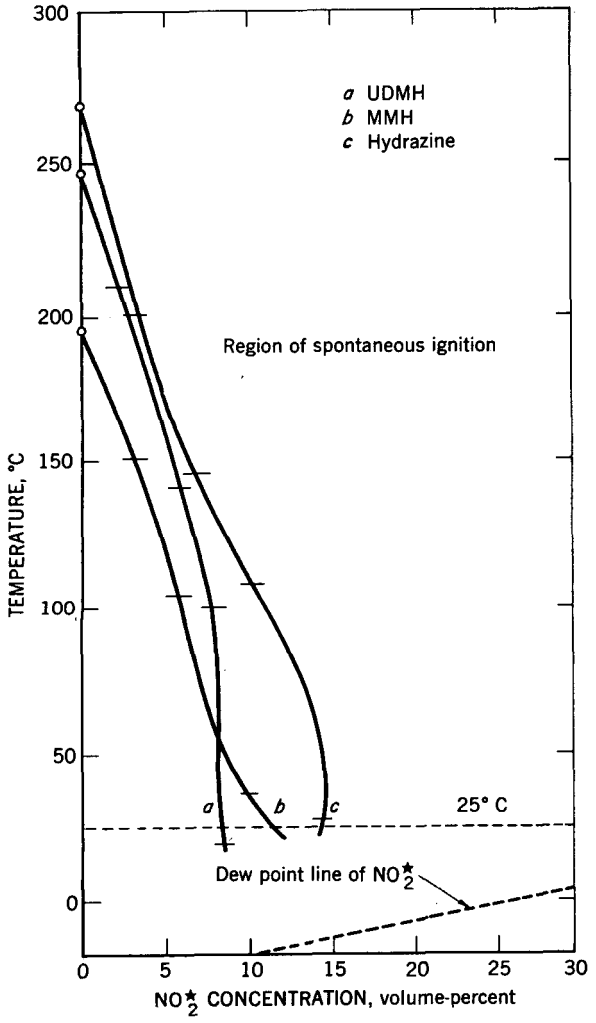

FIGURE 100.—Minimum Spontaneous Ignition Temperatures of Liquid Hydrazine, MMH, and UDMH at an Initial Temperature of 25° C in Contact With NO_2*-Air Mixtures at 740 ± 10 mm Hg as a Function of NO_2* Concentration.

preciably by this pressure change, it is affected in a range of NO_2*-air mixtures.

The data presented in figures 100 to 105 were obtained with liquid fuel in contact with vaporized NO_2^* in air. Similar data obtained with vaporized UDMH-air in contact with NO_2^* are given in figure 106. This figure indicates that UDMH-air mixtures that contain more than 9 volume-percent UDMH will ignite spontaneously on contact with NO_2^*; UDMH-air mixtures that contain more than approximately 2 volume-percent UDMH can be ignited by an ignition source under the same conditions (*166*).

Boron Hydrides

This series includes diborane (B_2H_6), tetraborane (B_4H_{10}), pentaborane (B_5H_9), and decaborane ($B_{10}H_{14}$). However, reliable upper and lower limit data are available only on the first member of this series at the present time. These were obtained by Parker and Wolfhard (*163*) who determined the limits of flammability of diborane in air in a 5-cm-diameter tube at an initial pressure of 300 mm Hg; this combustible forms flammable mixtures in air in the range from 0.8 to 87.5 volume-percent. A pale blue flame propagated throughout the tube at the upper limit; luminous flames were not visible above 79 volume-percent. Limit of flammability curves for the system diborane-ethane-air are presented in rectangular coordinates in figure 107. Except for the slight dip to the ethane-axis (zero diborane) in the area in which ethane forms flammable mixtures in air, these curves are rather similar to those obtained with other combustible-oxidant-inert systems. Burning velocities in excess of 500 cm/sec were measured in this same study for fuel-rich diborane-air mixtures.

Berl and Renich have prepared a summary report about boron hydrides (*9*). It includes data obtained by these and other authors; they found the lower limit of pentaborane in air to be 0.42 volume-percent.

The autoignition temperature of diborane in air is apparently quite low. Price obtained a value of 135° C at 16.1 mm Hg (*169*); that of pentaborane is 30° C at about 8 mm Hg (*9*).

Gasolines, Diesel and Jet Fuels

Fuels considered in this section are blends that contain a wide variety of hydrocarbons and additives. Accordingly, their flammability characteristics are governed by the method used to extract a vapor sample as well as by the history of the liquid. For example, since the lower limit of flammability, expressed in volume-percent, is inversely proportional to the molecular weight of the combustible vapor, equation (28), the first vapors to come from a blend, such as gasoline, give a higher lower limit value than the completely vaporized sample. Conversely, the heavy fractions or residue give a smaller lower limit value. For this reason, there is some disagreement about the limits of flammability of blends such as gasoline and the diesel and jet fuels. These fuels are, in general, characterized by a wide distillation range; the ASTM distillation curves

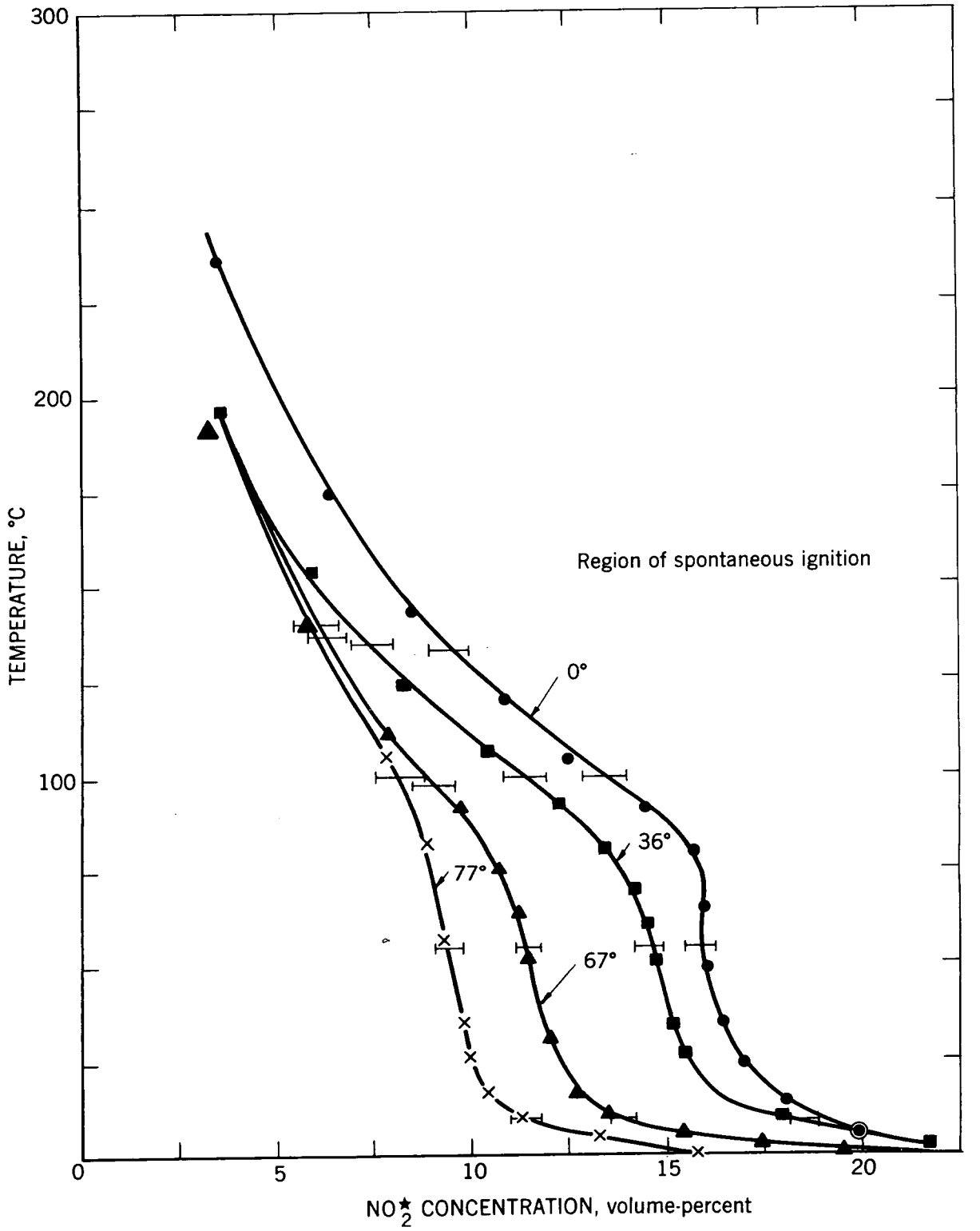

FIGURE 101.—Minimum Spontaneous Ignition Temperatures of Liquid Hydrazine at Various Initial Temperatures in NO_2*-Air Mixtures at 740±10 mm Hg as a Function of NO_2* Concentration.

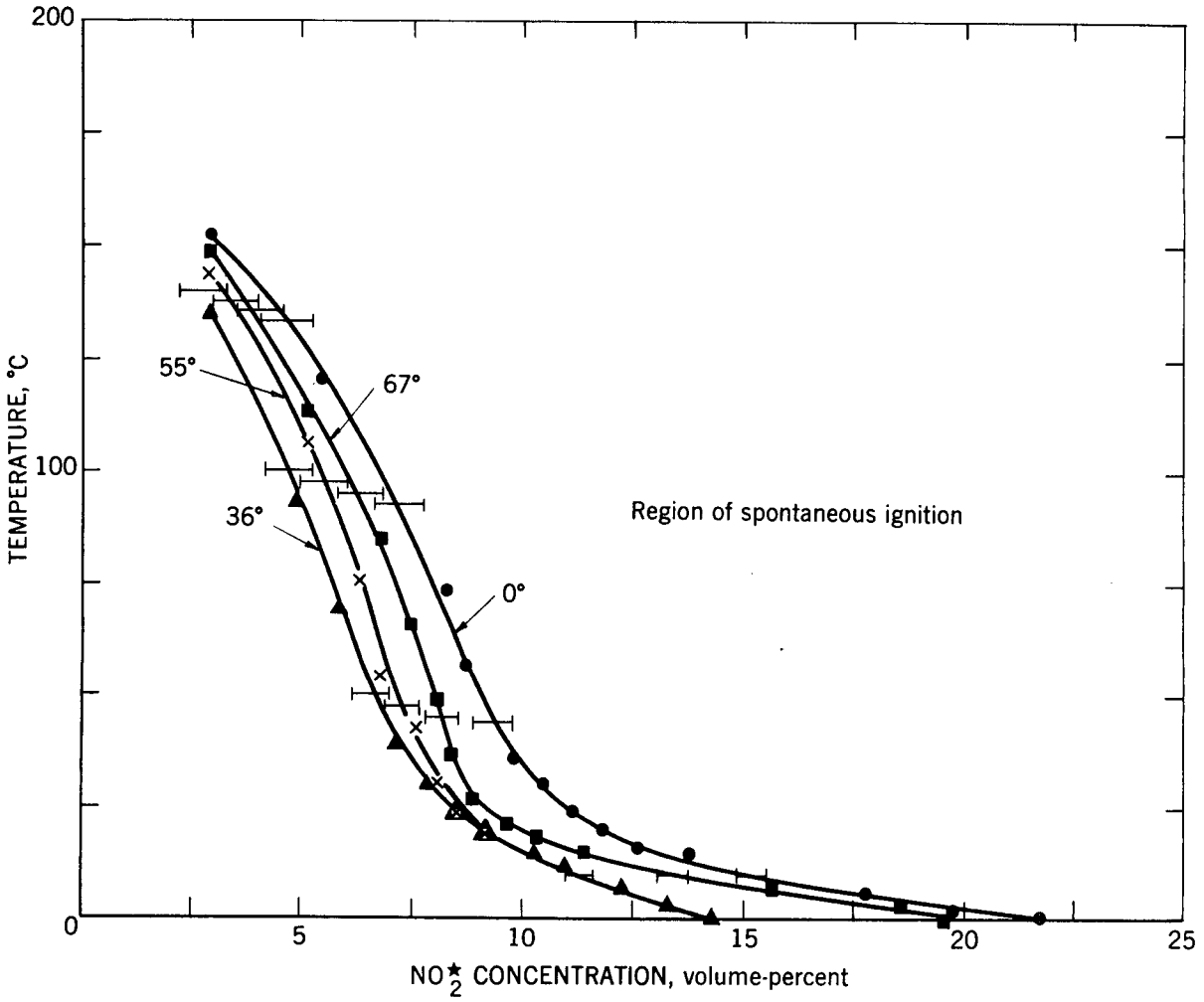

FIGURE 102.—Minimum Spontaneous Ignition Temperatures of Liquid MMH at Various Initial Temperatures in NO_2*-Air Mixtures at 740 ± 10 mm Hg as a Function of NO_2* Concentration.

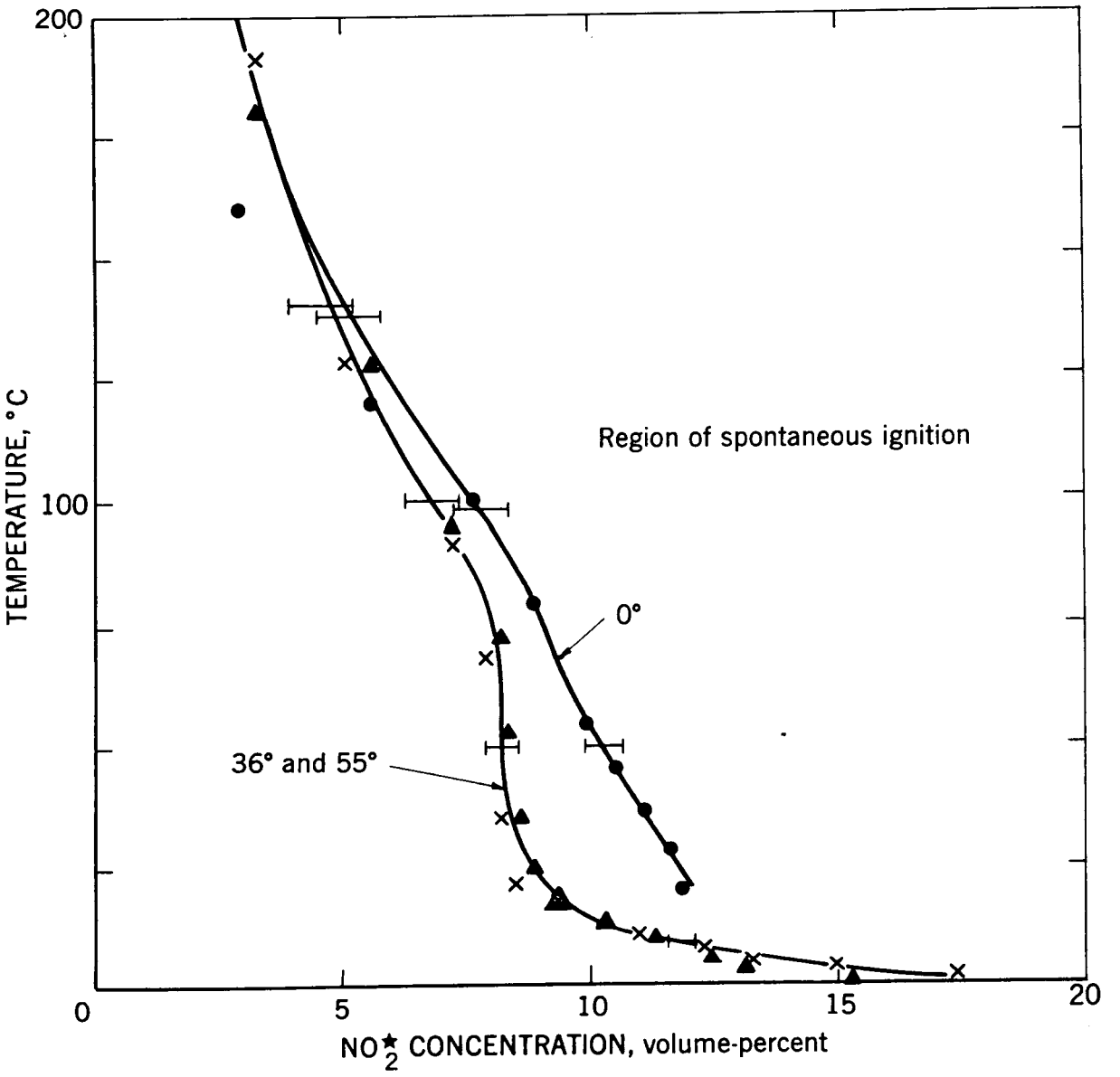

FIGURE 103.—Minimum Spontaneous Ignition Temperatures of Liquid UDMH at Various Initial Temperatures in NO_2*-Air Mixtures at 740±10 mm Hg as a Function of NO_2* Concentration.

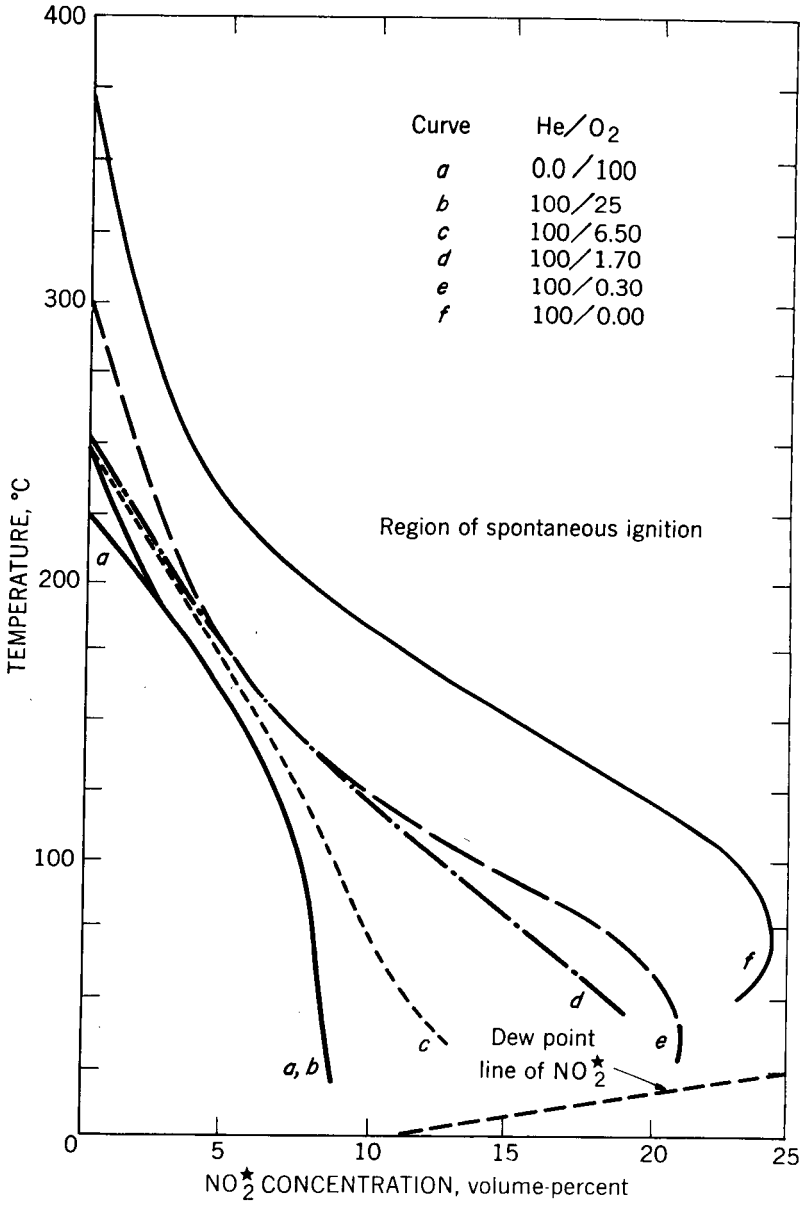

FIGURE 104.—Minimum Spontaneous Ignition Temperatures of 0.05 cc of Liquid UDMH in $He-O_2-NO_2$* Atmospheres at 1 Atmosphere for Various He/O_2 Ratios.

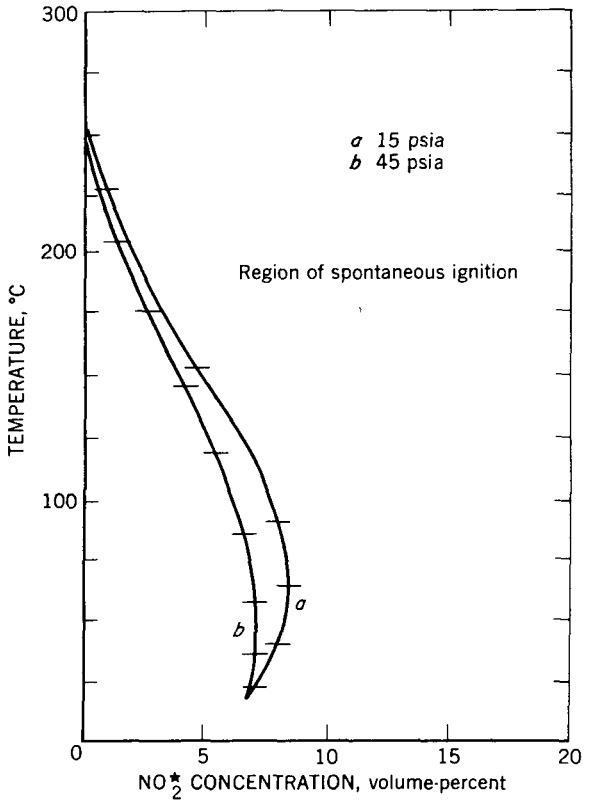

FIGURE 105.—Minimum Spontaneous Ignition Temperatures of 0.05 cc of Liquid UDMH in NO_2*-Air Mixtures at 15 and 45 Psia as a Function of NO_2* Concentration.

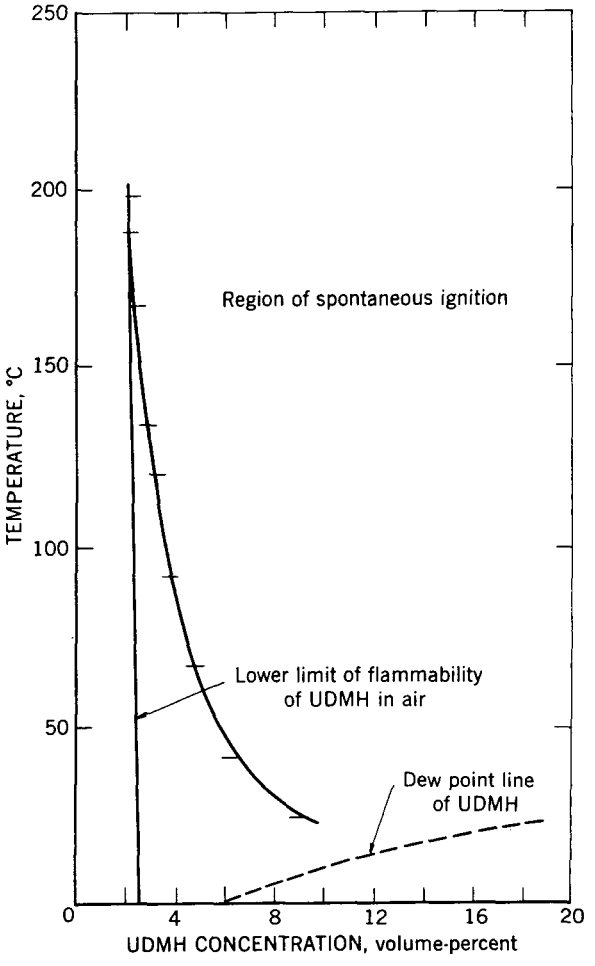

FIGURE 106.—Minimum Spontaneous Ignition Temperatures of Vaporized UDMH-Air Mixtures in Contact With 100 pct NO_2^* at 25° C and 740±10 mm Hg as a Function of UDMH Concentration in Air.

of two gasolines and three jet fuels considered here are given in figure 108. Unfortunately, such curves give only an approximate measure of the volatile constituents in the liquid blend. Even relatively nonvolatile high-flashpoint oils may liberate flammable vapors at such a slow rate that the closed vapor space above the liquid may be made flammable at reduced temperatures. Gasolines can produce flammable saturated vapor-air mixture at temperatures below −65° C (*241*), although the flash points of such fuels are considered to be about −45° C (*158*). An apparent discrepancy thus exists if flashpoint data are used to predict the lowest temperature at which flammable mixtures can be formed in a closed vapor space above a blend in long-term storage.

As noted earlier, the limits of flammability of hydrocarbon fuels are not strongly dependent on molecular weight when the limits are expressed by weight. However, since results measured by a volume are perhaps more widely used than those measured by weight, typical flammability curves are presented by volume for the light fractions from aviation gasoline, grade 115/145 (fig. 109), and aviation jet fuel, grade JP–4 (fig. 110). Combustible vapor-air-carbon dioxide and vapor-air-nitrogen mixtures at about 25° C and atmospheric pressure are considered for each. Similar data are given in figure 14 for the gasoline vapor-air-water vapor system at 21° and 100° C; the effect of pressure on limits of flammability of volatile constituents of JP–4 vapor in air are discussed in connection with figure 12.

Minimum autoignition temperatures of gasolines and jet fuels considered here are given in compilations by Zabetakis, Kuchta, and coworkers (*126*, *237*). These data are included in table 20.

Setchkin (*194*) determined the AIT values of four diesel fuels with cetane numbers of 41, 55, 60 and 68. These data are included in table 20. Johnson, Crellin, and Carhart (*92*, *93*) obtained values that were larger than those obtained by Setchkin, using a smaller apparatus.

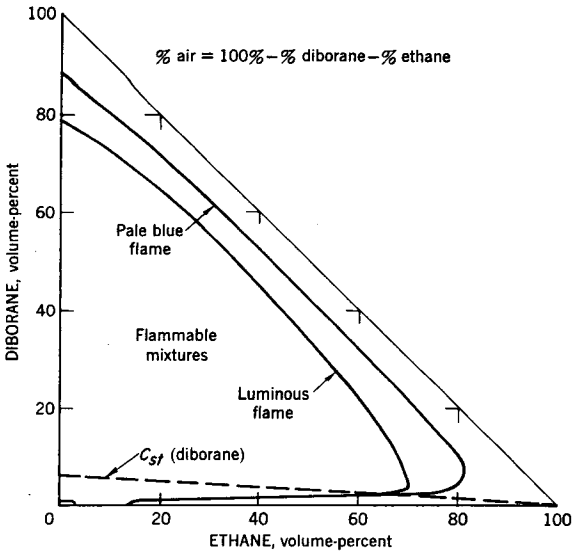

FIGURE 107.—Limits of Flammability of Diborane-Ethane-Air Mixtures at Laboratory Temperatures and 300 mm Hg Initial Pressure.

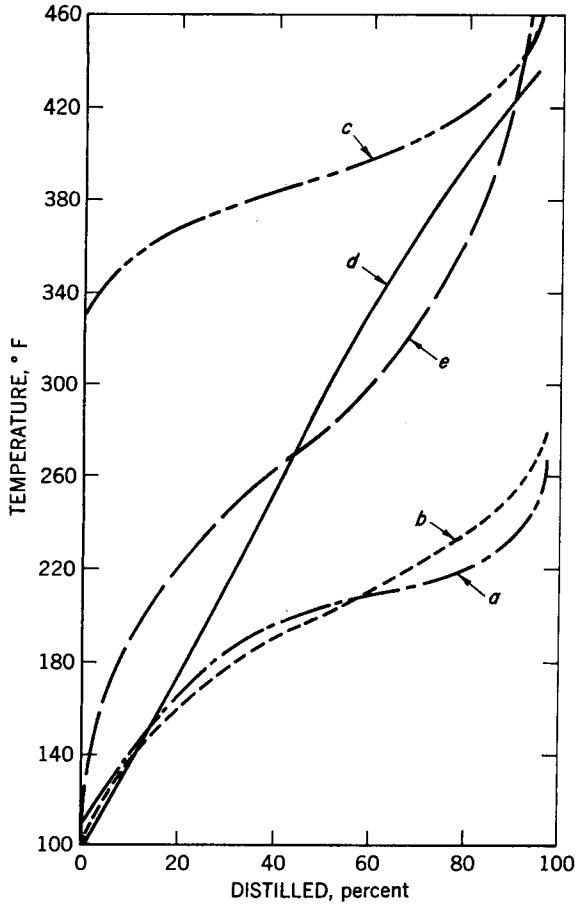

FIGURE 108.—ASTM Distillation Curves for, *A*, Aviation Gasoline, Grade 100/130; *B*, Aviation Gasoline, Grade 115/145; *C*, Aviation Jet Fuel, Grade JP–1; *D*, Aviation Jet Fuel, Grade JP–3; and *E*, Aviation Jet Fuel, Grade JP–4.

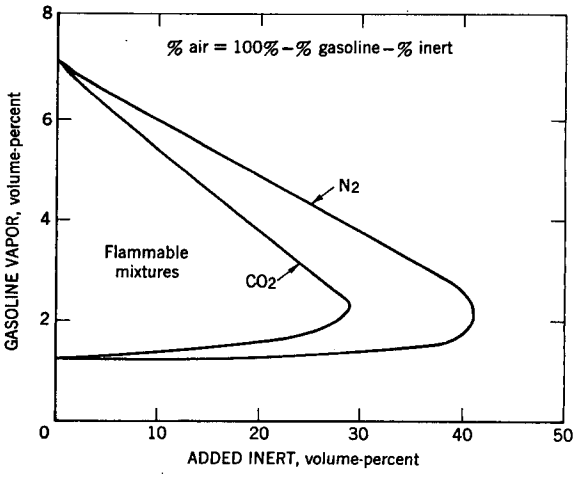

FIGURE 109.—Limits of Flammability of Aviation Gasoline, Grades 115/145 Vapor-Carbon Dioxide-Air and 115/145 Vapor-Nitrogen-Air, at 27° C and Atmospheric Pressure.

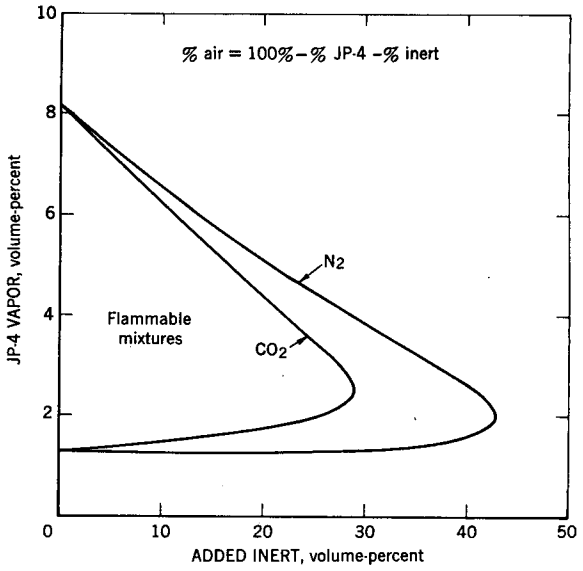

FIGURE 110.—Limits of Flammability of JP–4 Vapor-Carbon Dioxide-Air and JP–4 Vapor-Nitrogen-Air Mixtures at 27° C and Atmospheric Pressure.

TABLE 20.—*Autoignition temperature values of various fuels in air at 1 atmosphere*

Fuel:	*AIT*, °C
Aviation gasoline:	
100/130	440
115/145	471
Aviation jet fuel:	
JP–1	228
JP–3	238
JP–4	242
JP–6	232
Diesel fuel:	
41 cetane	233
55 cetane	230
60 cetane	225
68 cetane	226

Burning velocities of the fuels considered here are in the same range as those of the hydrocarbons considered earlier. Values for various fuels have been tabulated by Barnett and Hibbard (*156*).

Hydrogen

Numerous flammability characteristics studies have been conducted with hydrogen in recent years. Drell and Belles have prepared an excellent survey of these characteristics (*48*). This survey includes all but the most recent work of interest.

The low pressure limits of flame propagation for stoichiometric hydrogen-air mixtures are somewhat lower than those for stoichiometric ethylene-air mixtures (*197*) in cylindrical tubes. In the range from 6 to 130 mm Hg, the limit for stoichiometric hydrogen-air mixtures is given by the expression:

$$\log P = 3.19 - 1.19 \log D, \qquad (57)$$

where P is the low-pressure limit in millimeters of Hg, and D is the tube diameter in millimeters.

Hydrogen forms flammable mixtures at ambient temperatures and pressures with oxygen, air, chlorine, and the oxides of nitrogen. Limits of flammability in these oxidants at approximately 25° C and 1 atmosphere are listed in table 21.

TABLE 21.—*Limits of flammability of hydrogen in various oxidants at 25° C and atmospheric pressure*

Oxidant	L_{25}	U_{25}	Ref.
Oxygen	4.0	95	(*40*)
Air	4.0	75	(*40*)
Chlorine	4.1	89	(*216, 128*)
N_2O	3.0	84	(*189*)
NO	6.6	66	(*189*)

Flammability diagrams of the systems hydrogen-air-carbon dioxide and hydrogen-air-nitrogen obtained by Jones and Perrott (*112*) are given in figure 111. Lines that establish minimum oxygen values for each system are also included. Note that although the minimum value occurs near the "nose" of the hydrogen-air-nitrogen curve, the corresponding value occurs at the upper limit of the hydrogen-air-carbon dioxide curve.

Flammability diagrams obtained by Scott, Van Dolah, and Zabetakis for the systems hydrogen-nitric oxide-nitrous oxide, hydrogen-nitrous oxide-air, and hydrogen-nitric oxide-air are given in figures 112–114 (*189*). Upper limit

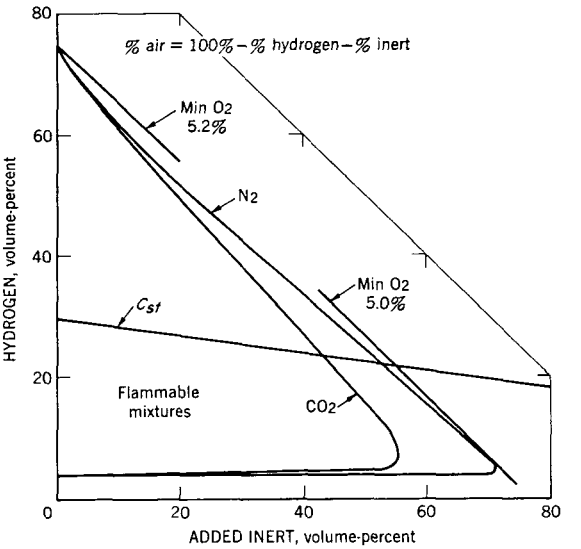

FIGURE 111.—Limits of Flammability of Hydrogen-Carbon Dioxide-Air and Hydrogen-Nitrogen-Air Mixtures at 25° C and Atmospheric Pressure.

curves were found to deviate from the results obtained from the Le Chatelier law, broken curves; additional data are given in the original article.

The burning velocity of hydrogen in air at 25° C and one atmosphere range from a low of a few centimeters per second to 325 cm/sec (*68*). When liquefied, it vaporizes and burns in air at a rate that is determined by the rate at which heat enters the liquid. Heat is abstracted from the surroundings and, where a flame exists, from the flame itself. Figure 115 gives the results obtained from vaporizing liquid hydrogen from paraffin cast in a Dewar flask; experimental points were obtained from gas evolution measurements. The solid curve (theoretical) was obtained by Zabetakis and Burgess by assuming the heat influx rate to be conduction limited (*234*); the initial flash vaporization rates are probably film- and nucleate boiling-limited. The theoretical liquid regression rates following spillage of liquid hydrogen onto three soils are presented in figure 116, the corresponding decrease in liquid level is given in figure 117. Because of its low temperature, the vaporized hydrogen forms a vapor trail as it leaves the liquid. However, the position of this trail or visible cloud does not necessarily coincide with that of the flammable zones formed above the liquid pool. This is illustrated in figure 118, in which the positions of the flammable zones and visible clouds are defined in a height-elapsed time graph. Two flammable zones are defined here. These are also seen in the motion picture sequence (fig. 119) of the visible clouds and

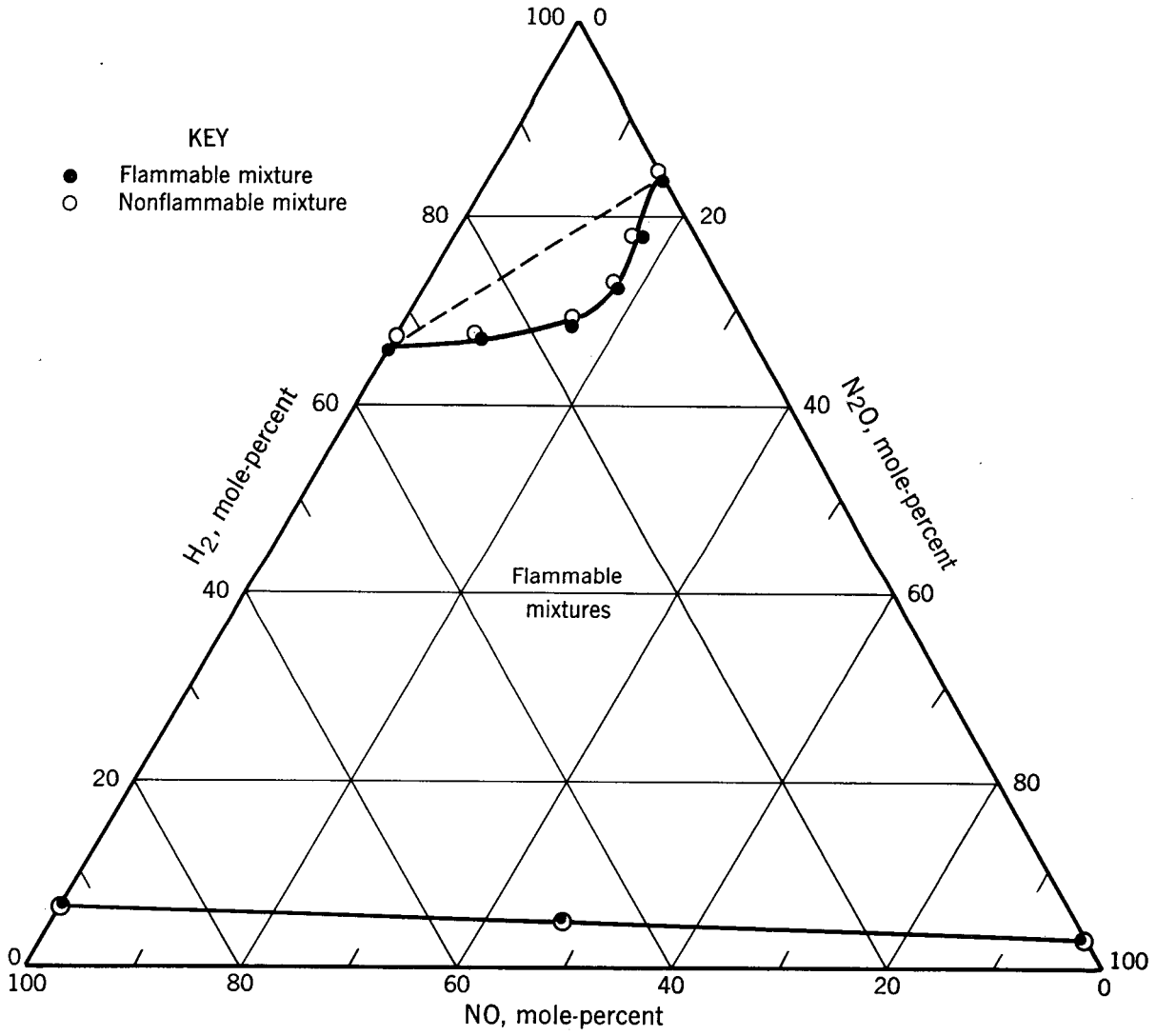

FIGURE 112.—Limits of Flammability of H_2-NO-N_2O at Approximately 28° C and 1 Atmosphere.

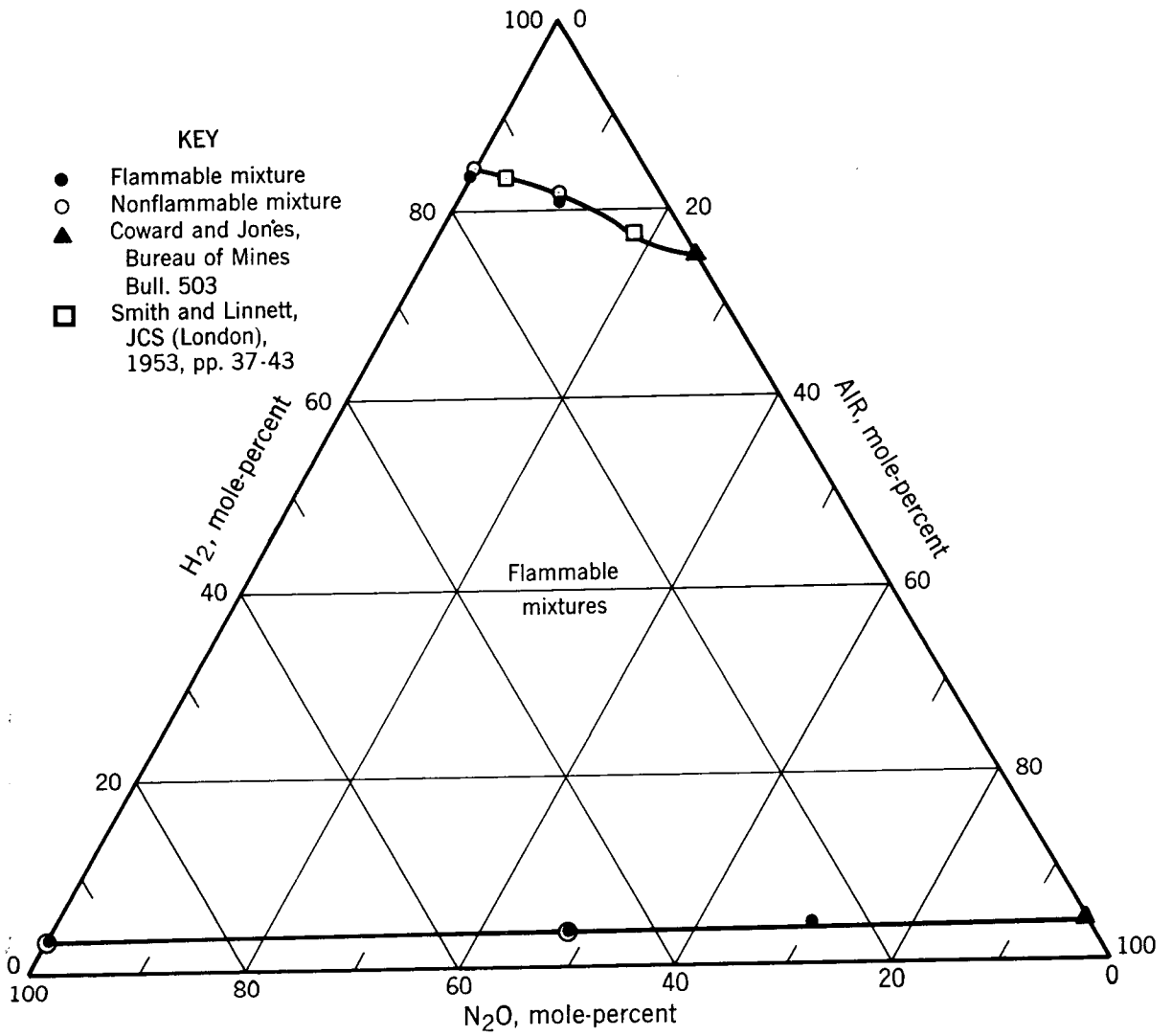

FIGURE 113.—Limits of Flammability of H_2-N_2O-Air at Approximately 28° C and 1 Atmosphere.

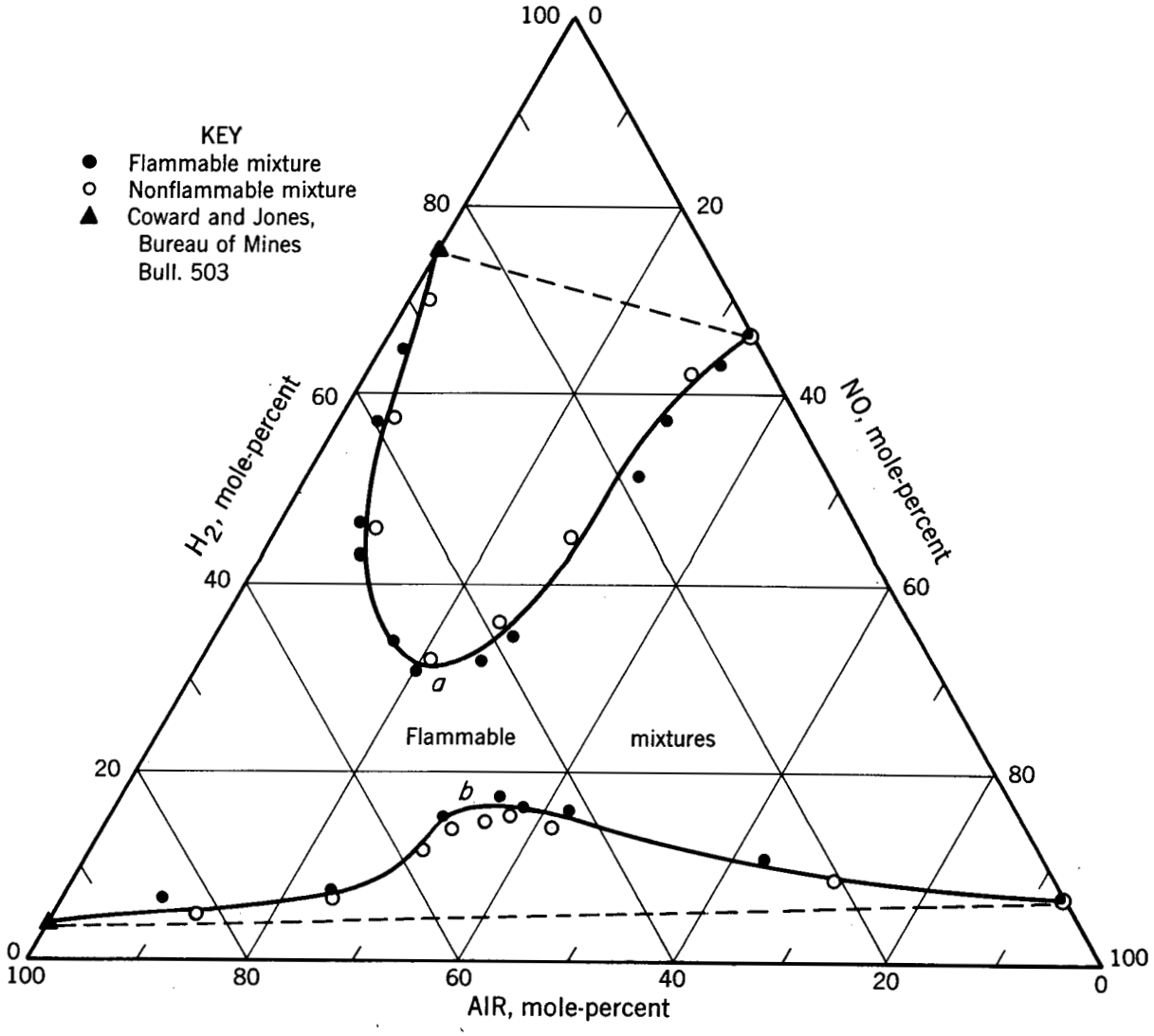

FIGURE 114.—Limits of Flammability of H_2-NO-Air at Approximately 28° C and 1 Atmosphere.

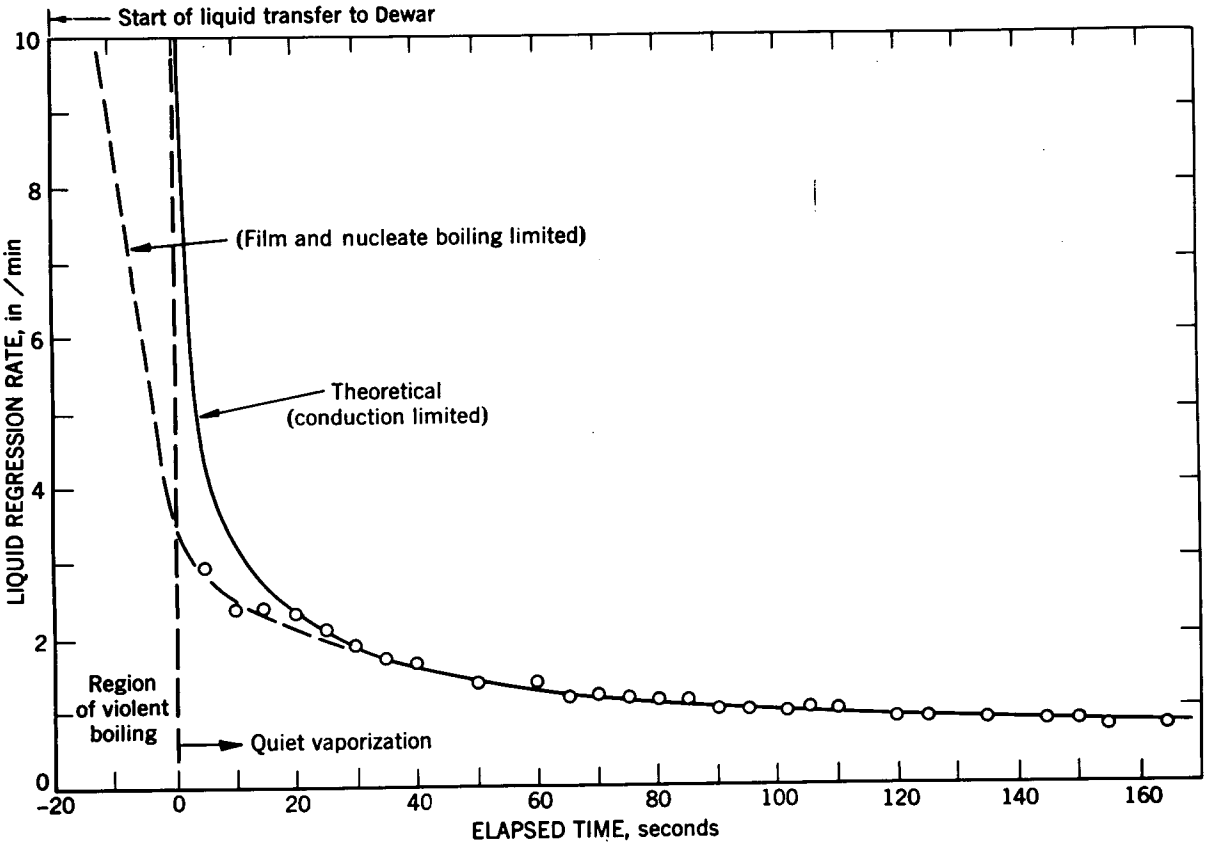

FIGURE 115.—Rate of Vaporization of Liquid Hydrogen From Paraffin in a 2.8-Inch Dewar Flask: Initial Liquid Depth—6.7 Inches.

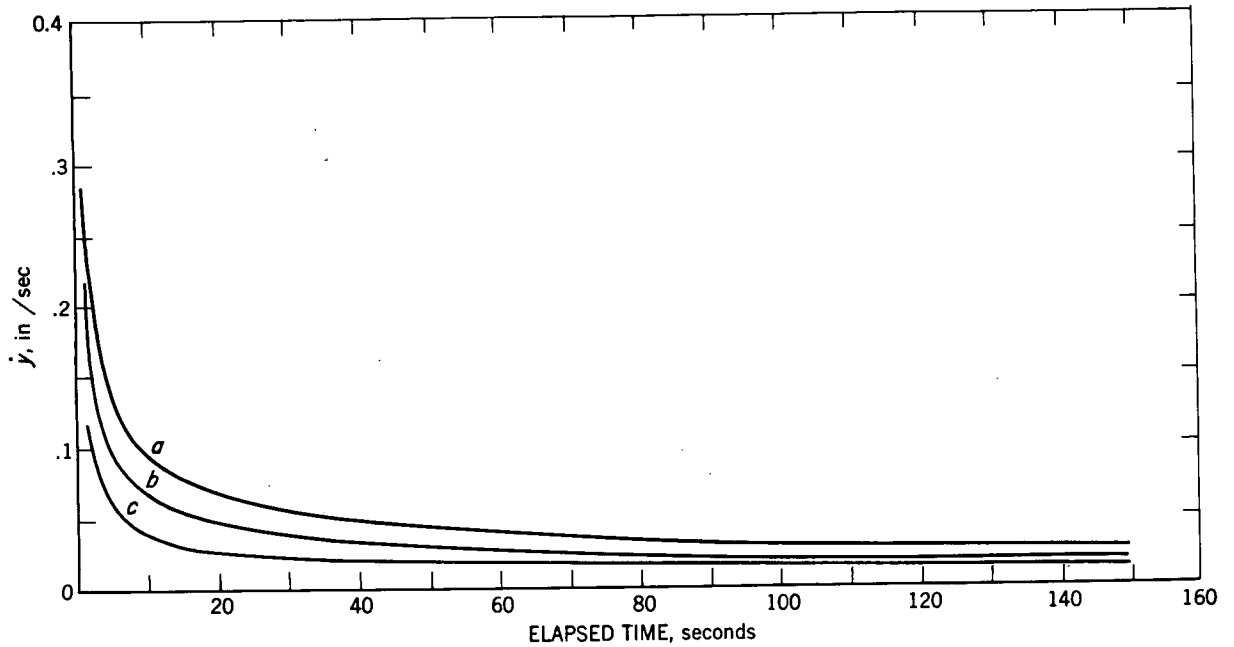

FIGURE 116.—Theoretical Liquid Regression Rates Following Spillage of Liquid Hydrogen Onto, *A*, an Average Soil; *B*, Moist Sandy Soil (8 Pct. Moisture); and *C*, Dry Sandy Soil.

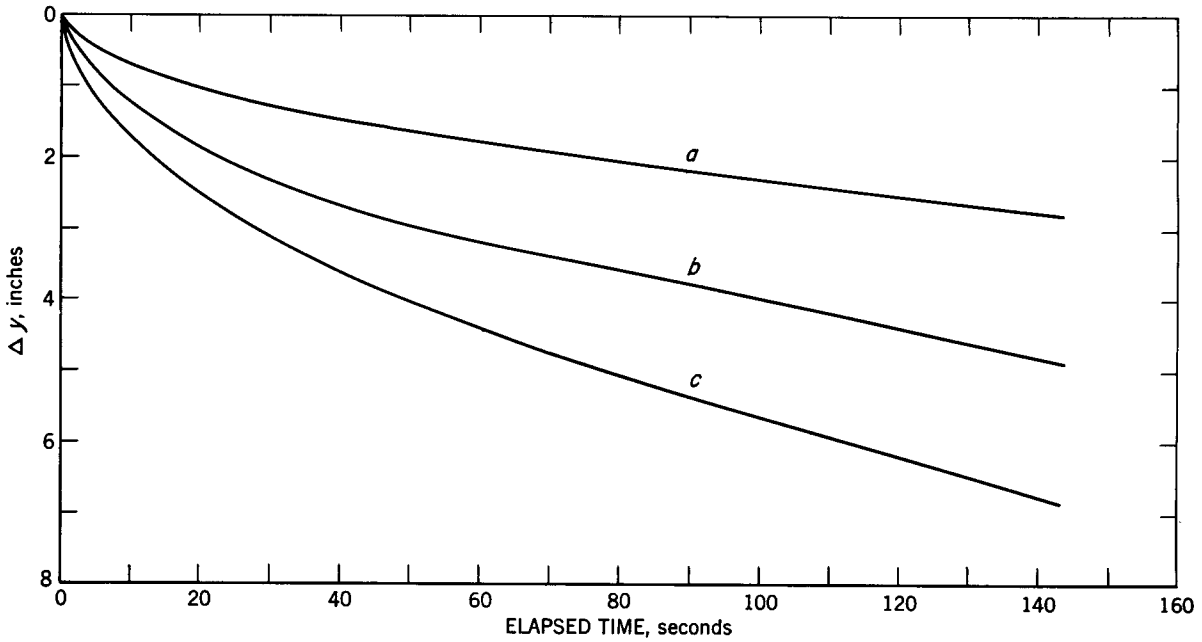

FIGURE 117.—Theoretical Decrease in Liquid Hydrogen Level Following Spillage Onto, *A*, Dry Sandy Soil; *B*, Moist Sandy Soil (8 Pct. Moisture); and *C*, and Average Soil.

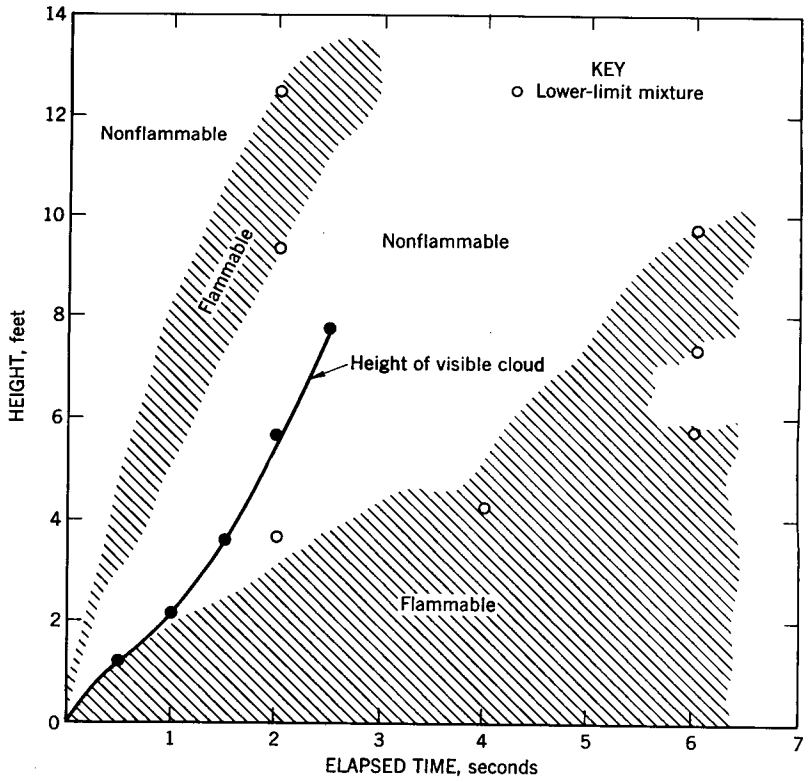

FIGURE 118.—Extent of Flammable Mixtures and Height of Visible Cloud Formed After Rapid Spillage of 3 Liters of Liquid Hydrogen on a Dry Macadam Surface in a Quiescent Air Atmosphere at 15° C.

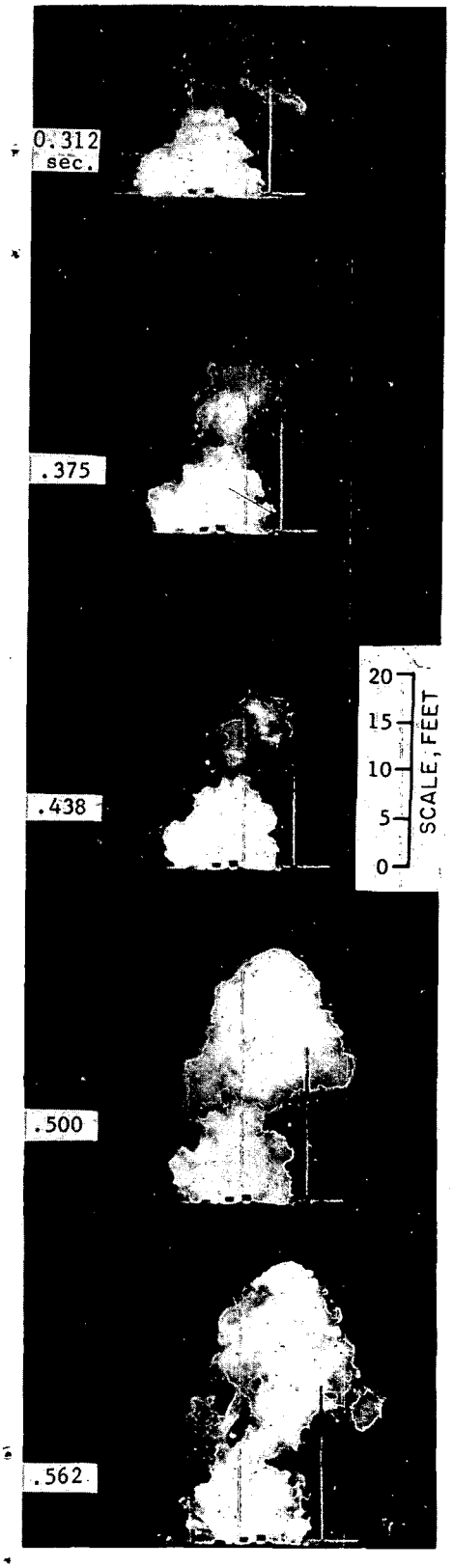

flames that resulted following spillage of 7.8 liters of liquid hydrogen and subsequent ignition of vapors above the spill area. The height and width of fireballs that resulted from ignition of vapors produced by rapid vaporization of about 3 to 90 liters of liquid hydrogen are given in figure 120. The data are represented fairly well by the equation

$$H_{max}=W_{max}=7\sqrt{V_l}\text{ feet}=17.8\sqrt{M}\text{ feet}, \quad (56)$$

where H_{max} and W_{max} are the maximum flame height and width, respectively, V_l is the volume of liquid hydrogen in liters, and M is the mass of this volume in pounds.

The burning rate of a 6-inch pool of liquid hydrogen in air is given as the regression of the liquid level in figure 121; burning rate data for liquid methane are included for comparison. An extrapolated value of burning rate for large pools of liquid hydrogen is included in figure 52.

Approximate quantity-distance relationships can be established for the storage of liquid hydrogen near inhabited buildings and other storage sites if certain assumptions are made (*33*, *160*, *234*). Additional work is required to establish such distances for very large quantities of liquid.

The detonation velocity and the static and reflected pressures developed by a detonation wave propagating through hydrogen-oxygen mixtures are given in figure 16. The predetonation distance in horizontal pipes is reportedly proportional to the square root of the pipe diameter (*229*); this is presumably applicable to results obtained with a mild ignition source, since a shock front can establish a detonation at essentially zero runup distance. Numerous investigators have examined this and related problems in recent years (*11–13*, *65*, *135–137*, *151*).

HYDRAULIC FLUIDS AND ENGINE OILS

Both mineral oil derived and synthetic hydraulic fluids and engine oils are presently in common use (*148*). These materials are often used at elevated temperatures and pressures and contain additives designed to improve stability, viscosity, load-bearing characteristics, etc. Such additives affect flammability characteristics of the base fluid. However, the base

FIGURE 119.—Motion Picture Sequence (16 Frames per Second) of Visible Clouds and Flames Resulting From Rapid Spillage of 7.8 Liters of Liquid Hydrogen on a Gravel Surface at 18° C. Ignition Source: 20 Inches Above Gravel.

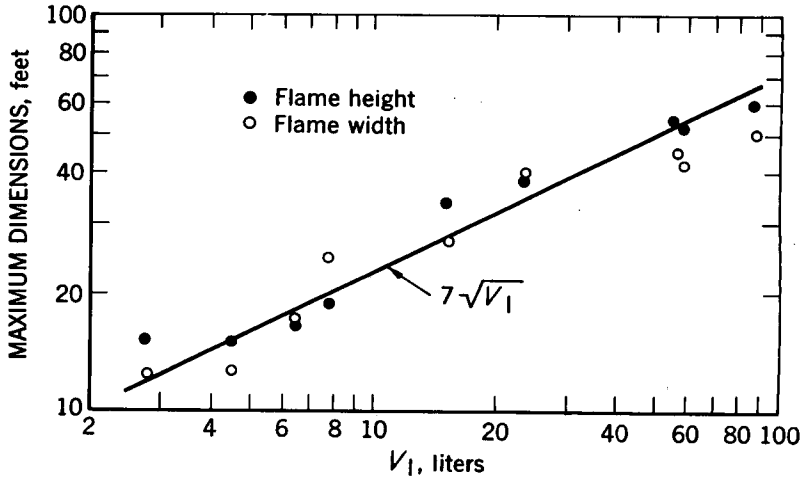

FIGURE 120.—Maximum flame height and width produced by ignition of vapor-air mixtures formed by sudden spillage of 2.8 to 89 liters of liquid hydrogen (V_l).

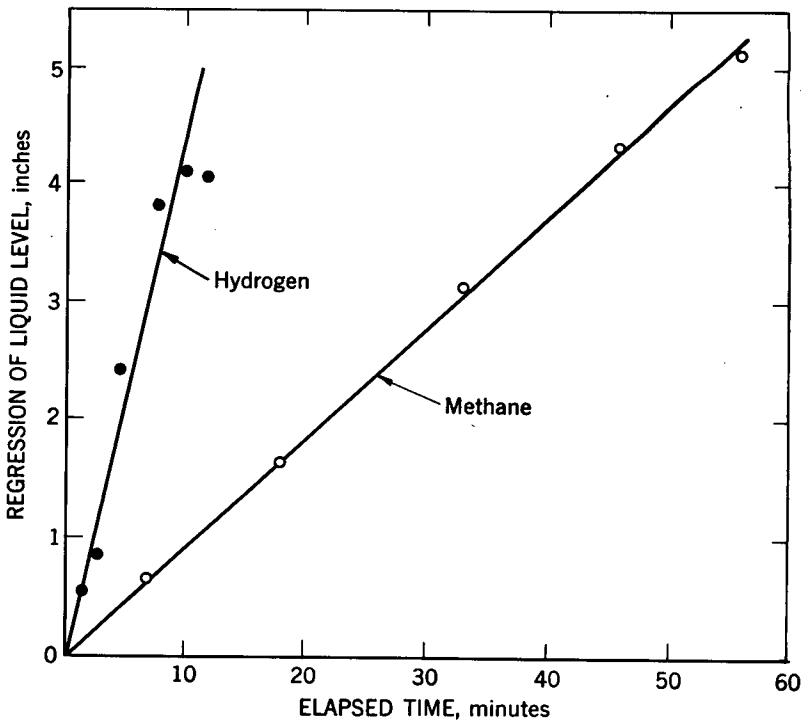

FIGURE 121.—Burning rates of liquid hydrogen and of liquid methane at the boiling points in 6-inch-Pyrex Dewar flasks.

fluid generally plays a predominant role in determining limits of flammability and ignition temperature of a particular fluid. For example, many of the oil-based fluids have lower limits of flammability that fall in the ranges given in figure 22 for paraffin hydrocarbons. Further, those that have minimum autoignition temperatures in the lower temperature ranges considered in fiugres 43 and 71 are not affected appreciably by oxygen concentration of the atmosphere and by ambient and fluid-injection pressures; those that have minimum autoignition temperatures in the higher temperature ranges do not follow these generalizations (*237*). Since these fluids are designed for use at elevated temperatures and pressures, they are normally made up of high-molecular weight matetials. Accordingly, they are flammable at ordinary temperatures and pressures as mists and foams. Burgoyne and his coworkers (*27*) found that lubricating-oil mists were flammable in air but not in carbon dioxide-air mixtures that contained about 28 volume-percent carbon dioxide (fig. 35). At elevated temperatures, the oil vapors cracked and produced acetylene and hydrogen, which affected the flammability of the resultant mixture; the vapors are often unstable at elevated temperatures. Chiantella, Affens, and Johnson have determined the effect of elevated temperatures on the stability and ignition properties of three commercial triaryl phosphate fluids (*36*).

Zabetakis, Scott, and Kennedy have determined the effect of pressure on the autoignition temperatures of commercial lubricants (*248*). Figure 122 gives the minimum autoignition temperatures for four commercial phosphate ester-base fluids (curves 1–4) and three mineral oils (curves 5–7). In each case, the minimum autoignition temperature was found to decrease with increase in pressure over most of the pressure range considered. A plot of the logarithm of the initial pressure to temperature ratio versus the reciprocal of the temperature is given for curves 1 to 7 in figure 123. The resultant curves are linear over a limited temperature range.

The ratio of the final temperature attained by air in an adiabatic compression process to the initial temperature is given in figure 124 as a function of both the final-to-initial pressure ratio and initial-to-final volume ratio. If a lubricating oil is exposed to high temperatures during a compression process, autoignition may occur if the residence or contact time is adequate. Such high temperatures do occur in practice and have been known to cause disastrous explosions (*58*, *146*, *149*, *227*, *231*). The curves in figure 125 show that in the compression pressure range 1 to 10 atmospheres (initial pressure=1 atmosphere), a wide range of ambient temperatures can lead to the autoignition of a mineral oil lubricant (curve 5) if sufficient vapor or mist is in the system. In the same pressure range, only elevated initial temperatures could lead to the autoignition of a phosphate ester (curve 4). If the initial pressure is increased to 10 atmospheres, autoignition can occur at lower air-intake temperatures in every case (*248*).

MISCELLANEOUS

The flammability characteristics of a number of miscellaneous combustibles not considered elsewhere, are discussed in this section. These include carbon monoxide, *n*-propyl nitrate, and the halogenated hydrocarbons. The properties of these and a great variety of other materials are included in Appendix A.

The limits of flammability of the systems carbon monoxide-carbon dioxide-air and carbon monoxide-nitrogen-air are presented in figure 126. These curves were constructed from the flammability data obtained by Jones in a 2-inch vertical glass tube with upward flame propagation (*112*); other representations may be found in the original reference and in the compilation prepared by Coward and Jones (*40*).

Materials that are oxidized or decomposed readily may yield erratic flammability data under certain conditions. This effect is illustrated in figure 127 which summarizes the lower-limits data obtained by Zabetakis, Mason and Van Dolah with *n*-propyl nitrate (NPN) in air at various temperatures and pressures (*243*). An increase in temperature from 75° to 125° C is accompanied by a decrease in the lower-limit values; a further increase in temperature to 150° C results in a further lowering of the lower limit at pressures below 100 psig, but not at the higher pressures. An increase in the temperature to 170° C results in an apparent increase in the lower-limit value because of the slow oxidation of NPN. A complete flammability diagram has been constructed for the NPN vapor system in figure 128; a single lower limit curve and two upper limit curves are given here to show the effect of pressure on the flammable range of a vapor-air system.

The spontaneous ignition of NPN in air was considered earlier at 1,000 psig (figs. 3, 4). The explosion pressures obtained at this initial pressure in air and in a 10-volume-percent oxygen +90-volume-percent nitrogen atmosphere at various NPN concentrations are presented in figure 129. A summary of the minimum spontaneous ignition and decomposition temperatures obtained with NPN in air and nitrogen respectively are given in figure 130. The data given in this figure exhibit a behavior that is typical of that found with other combustibles

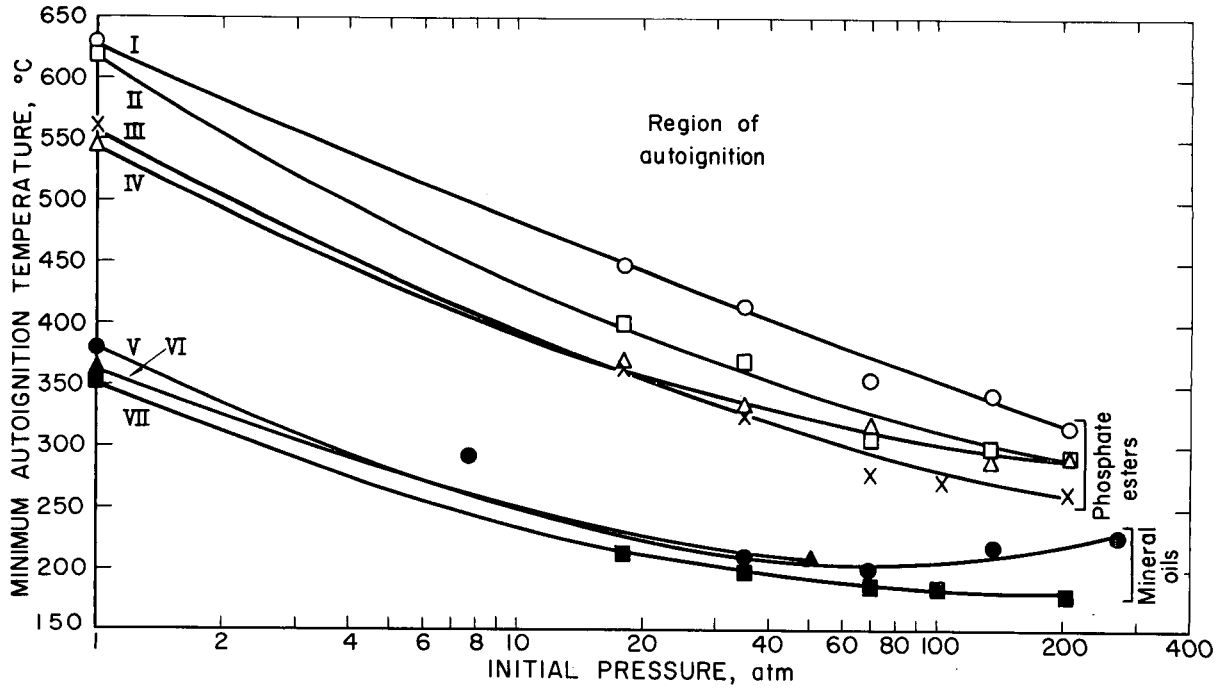

FIGURE 122.—Variation in Minimum Autoignition Temperature With Pressure of Commercial Phosphate Ester and Mineral Oil Lubricants in Air in a 450-cc-Stainless Steel Bomb.

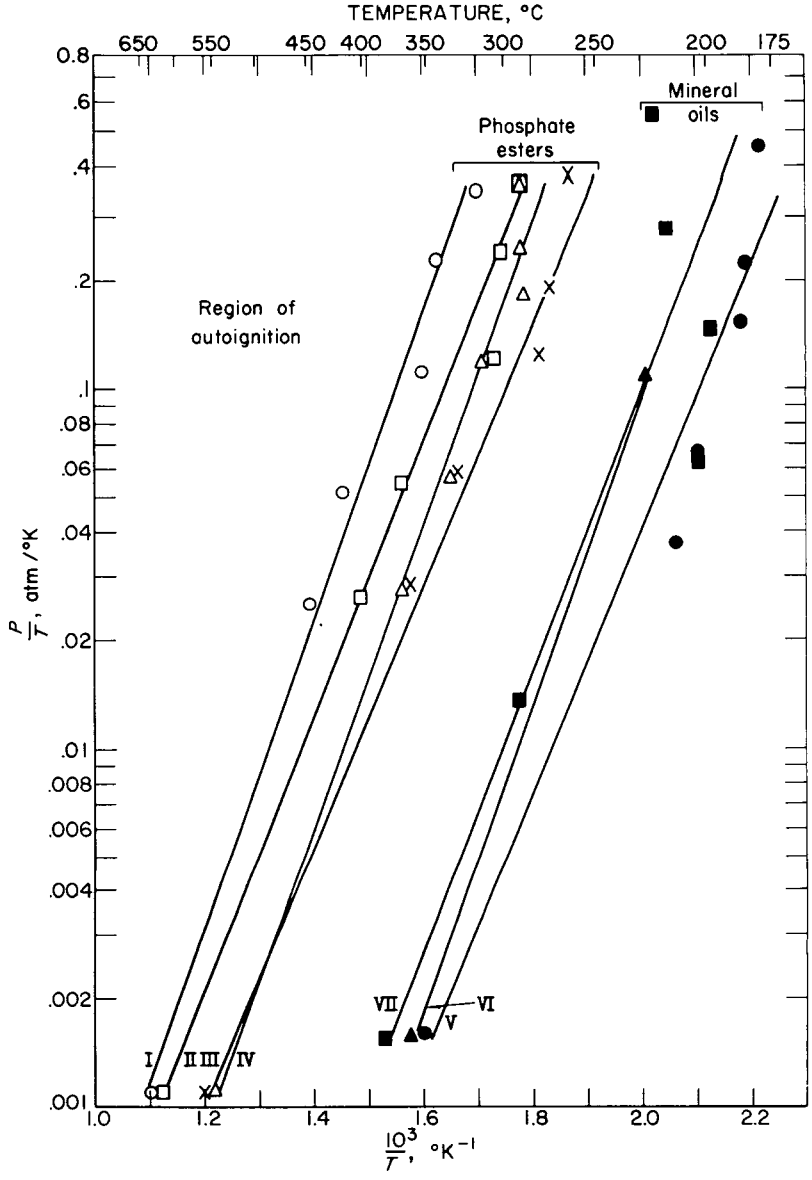

FIGURE 123.—Logarithm of Initial Pressure–AIT Ratio of Seven Fluids in Air for Various Reciprocal Temperatures. Data from Figure 122.

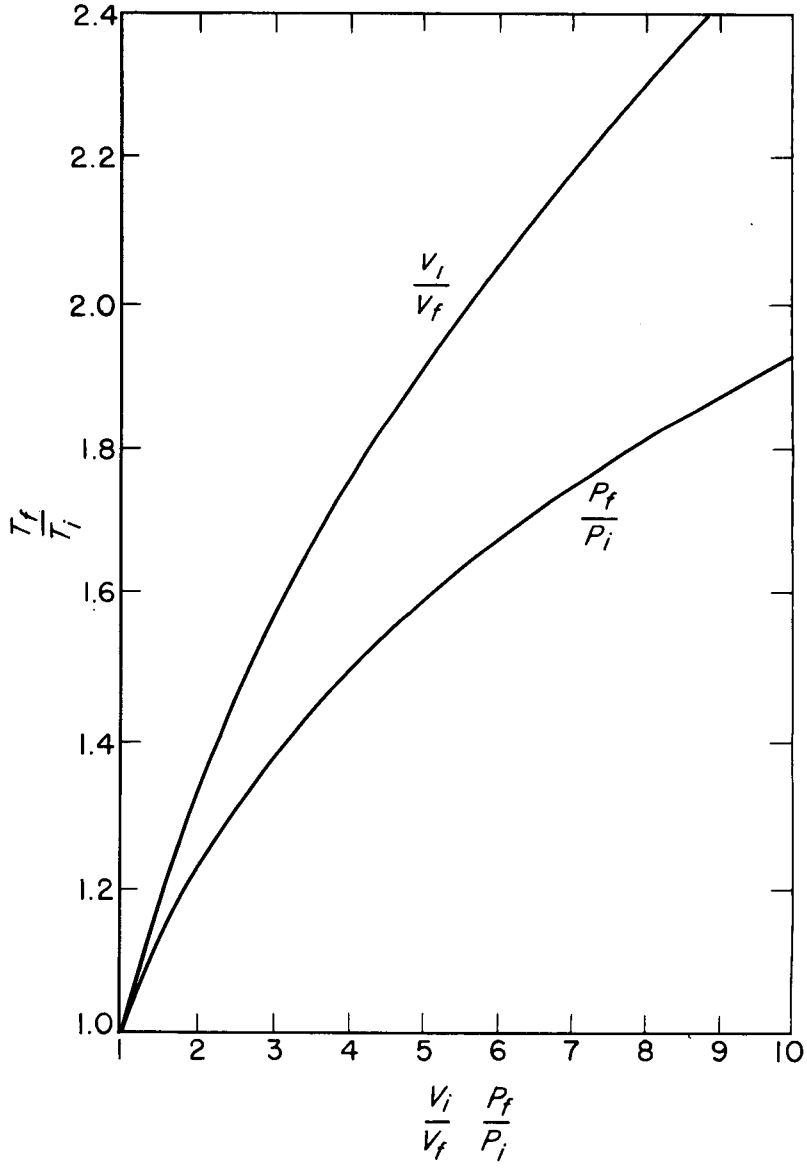

FIGURE 124.—Variation in T_f/T_i of Air With V_i/V_f and With P_f/P_i in an Adiabatic Compression Process.

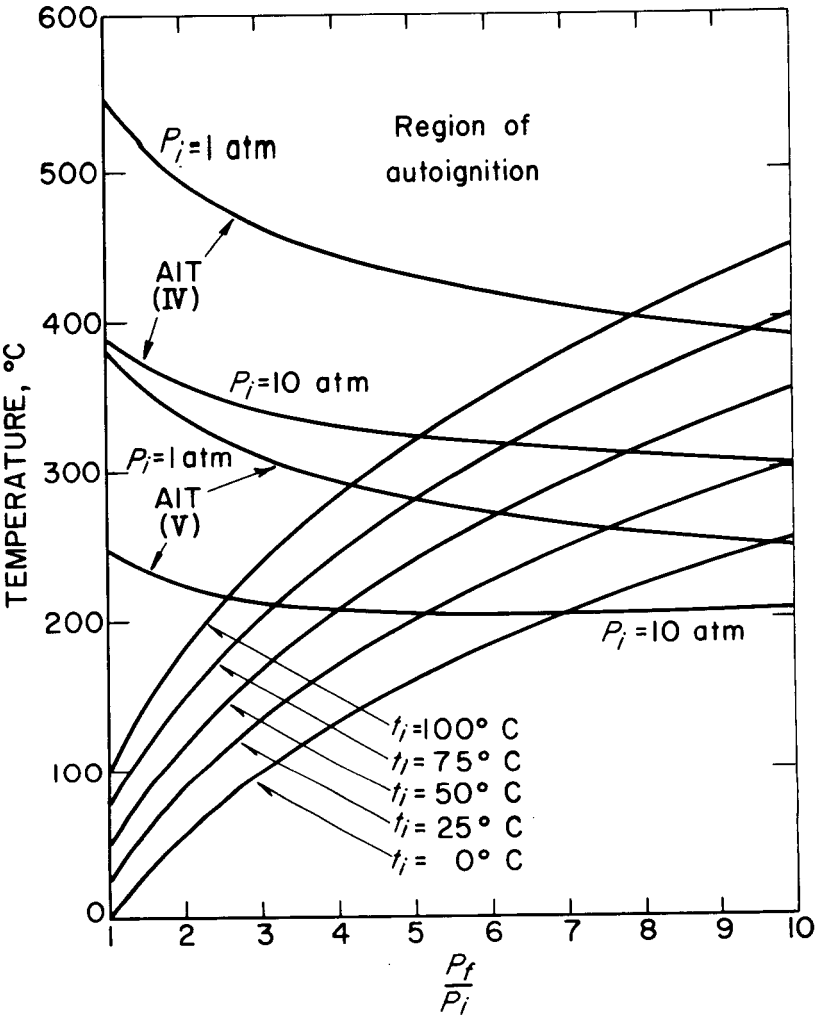

FIGURE 125.—Variation In Air Temperature With P_f/P_i in an Adiabatic Compression Process for Five Initial Air Temperatures (0°, 25°, 50°, 75°, and 100° C). Regions of autoignition for lubricants IV and V at P_f/P_i Between 1 and 10 Atmosphere and P_i of Between 1 and 10 Atmospheres.

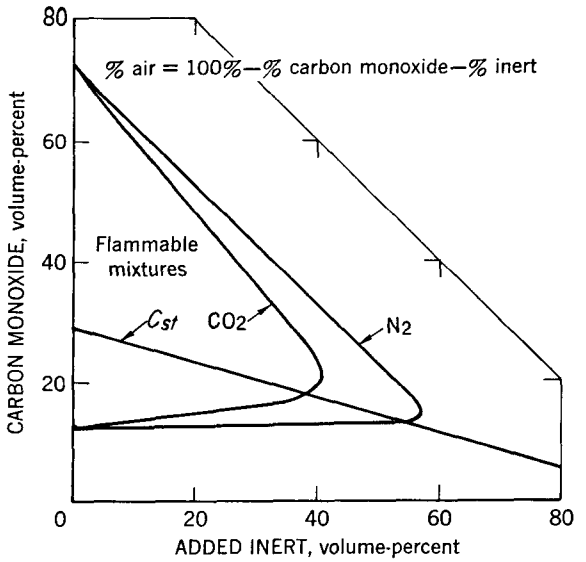

FIGURE 126.—Limits of Flammability of Carbon Monoxide-Carbon Dioxide-Air and Carbon Monoxide-Nitrogen-Air Mixtures at Atmospheric Pressure and 26° C.

at elevated pressures; the minimum spontaneous ignition temperature first decreases with initial increase in pressure and then increases as the pressure is increased still further (*120*, *248*).

Burning velocities were found to range from 20 cm/sec to 110 cm/sec in NPN-air mixtures containing 3.0 to 7.2 volume-percent NPN. Detonations were obtained in saturated NPN vapor-air mixtures from 30° to 65° C and 1 atmosphere pressure; the detonation velocity was from 1,500 to 2,000 meters per second. Stable detonations were obtained with liquid NPN at 90° C; the detonation velocity was from 4,700 to 5,100 meters per second.

Although many of the halogenated hydrocarbons are known to be flammable (*40*) still others such as methyl bromide, methylene chloride, and trichloroethylene (TCE) have been considered to be nonflammable or essentially nonflammable in air. As noted in connection with the methyl bromide data given in figure 28, Hill found methyl bromide to be flammable in air at 1 atmosphere pressure (*84*); the reported limits of flammability were from 10 to

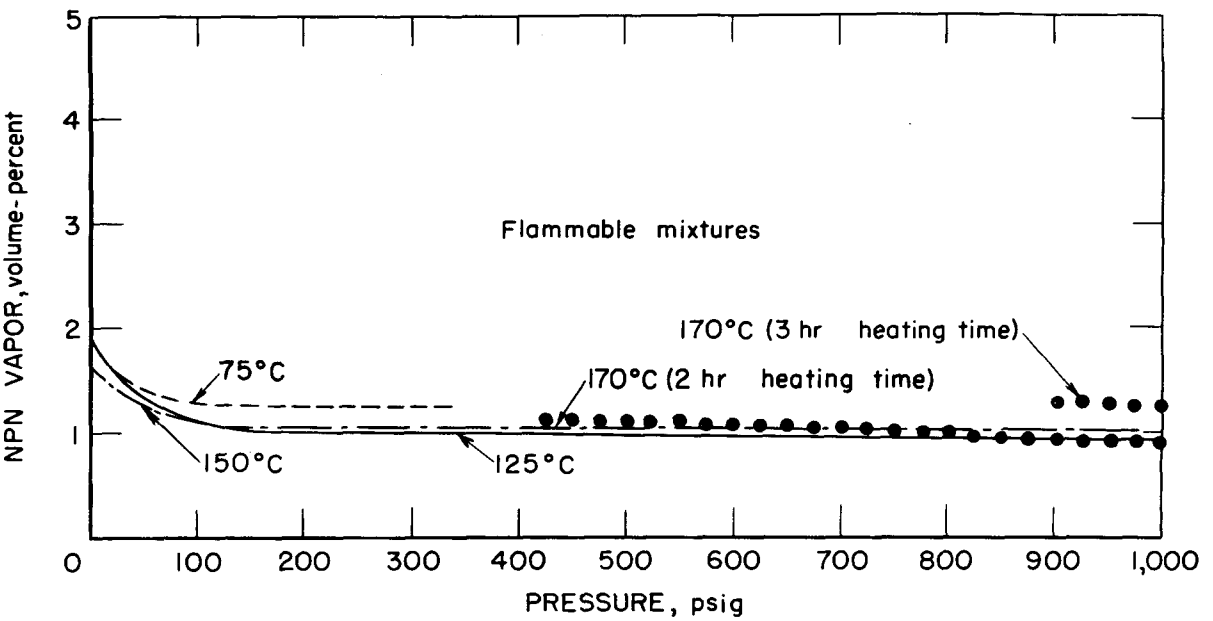

FIGURE 127.—Lower Limits of Flammability of NPN Vapor-Air Mixtures Over the Pressure Range From 0 to 1,000 Psig at 75°, 125°, 150°, and 170° C.

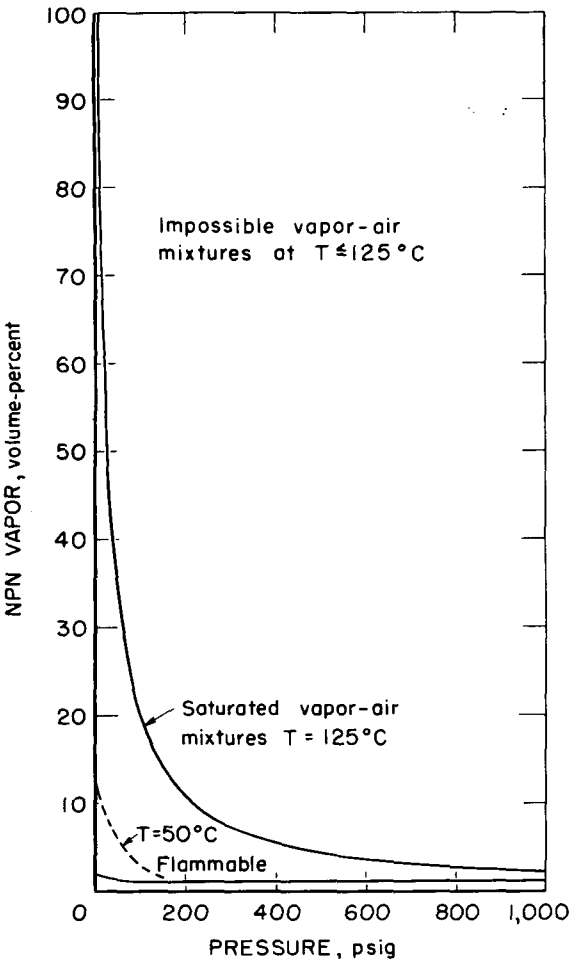

FIGURE 128.—Flammable NPN Vapor-Air Mixtures Formed Over the Pressure Range From 0 to 1,000 Psig at 50° and 125° C.

15 volume-percent methyl bromide. At an initial pressure of 100 psig, the flammable range was found to extend from 6 to 25 volume-percent. Similarly, methylene chloride and trichloroethane were found to be flammable in air at ambient temperatures although the flammable ranges were not determined. In general, much higher source energies are required with these combustibles than are required to ignite methane-air mixtures.

An approximate flammability diagram was prepared by Scott for trichloroethylene-air mixtures (*190*); a modification is reproduced in figure 131. The lower limit data were obtained in a vertical 7-inch-diameter flammability tube and the upper limit data in an 8-inch-diameter glass sphere with upward propagation of flame. Flammable mixtures of TCE and air were also obtained between 10.5 and 41 volume-percent TCE at 1 atmosphere and 100° C in an 8-inch-diameter glass sphere. Under the same conditions, flammable mixtures of TCE and oxygen were obtained between 7.5 and 90 volume-percent TCE. However, additional work must be conducted with this and the other halogenated hydrocarbons to determine the effect of vessel size, ignition source strength, temperature and pressure on their flammability characteristics.

Other useful flammability data may be found for various miscellaneous combustibles in many of the publications listed in the bibliography (*40, 154, 200, 208–214, 218*). These include data on the gases produced when metals react with water (*56*) and sulfur reacts with various hydrocarbons (*62*). Still other references consider the hazards associated with the production of unstable peroxides (*142, 157, 187, 233*) and other reactive materials (*66, 74, 80, 139*).

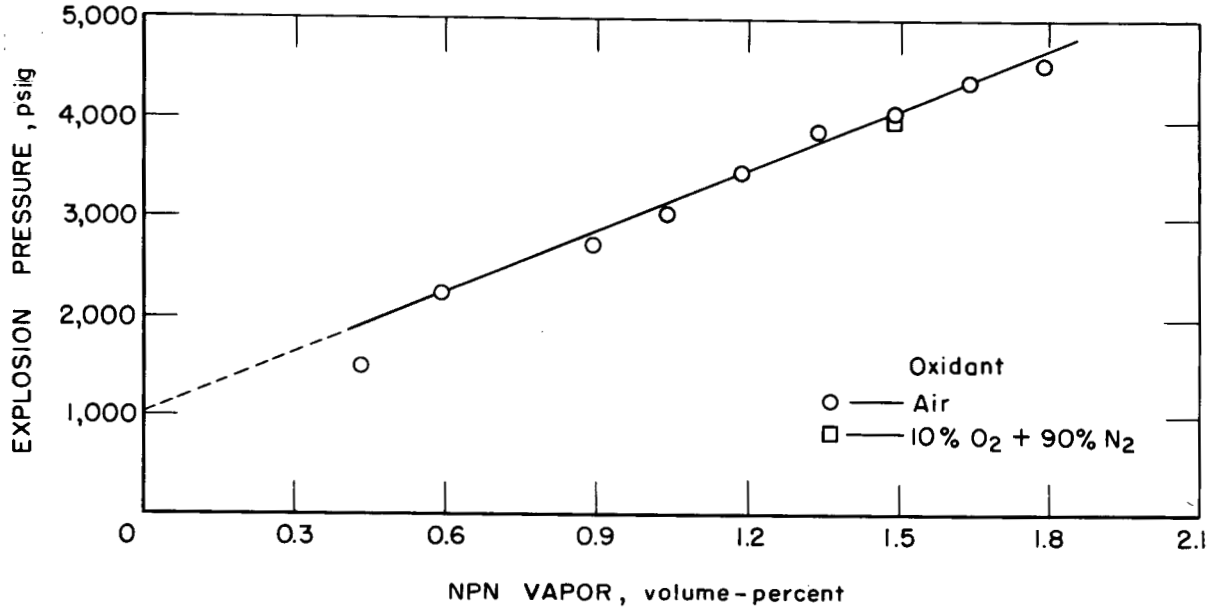

FIGURE 129.—Variation of Explosion Pressure Following Spontaneous Ignition With NPN Concentration, Initial Pressure 1,000 Psig.

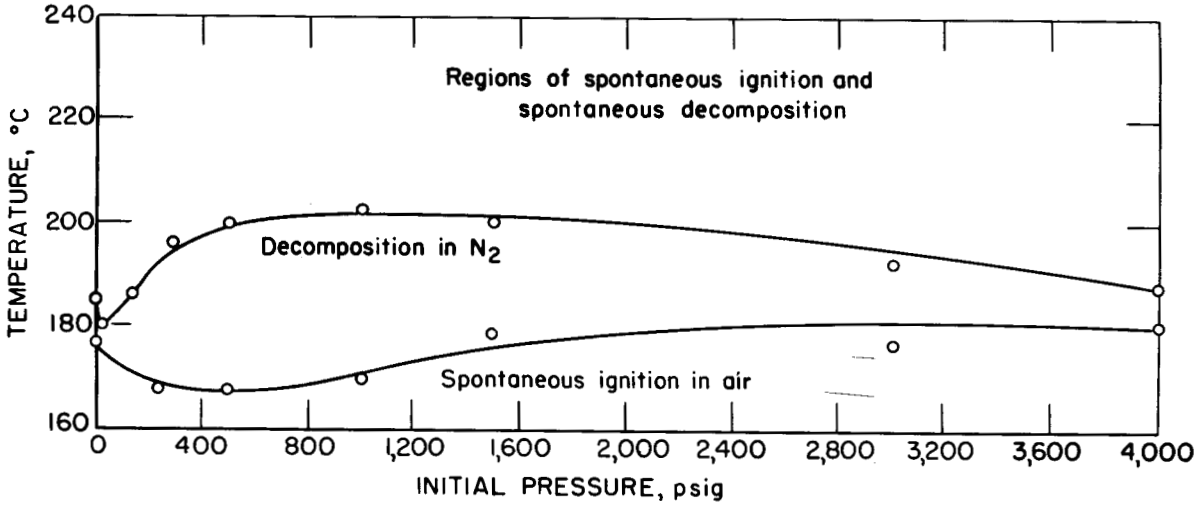

FIGURE 130.—Minimum Spontaneous Ignition and Decomposition Temperatures of *n*-Propyl Nitrate in Air as a Function of Pressure, Type 347 Stainless Steel Test Chamber.

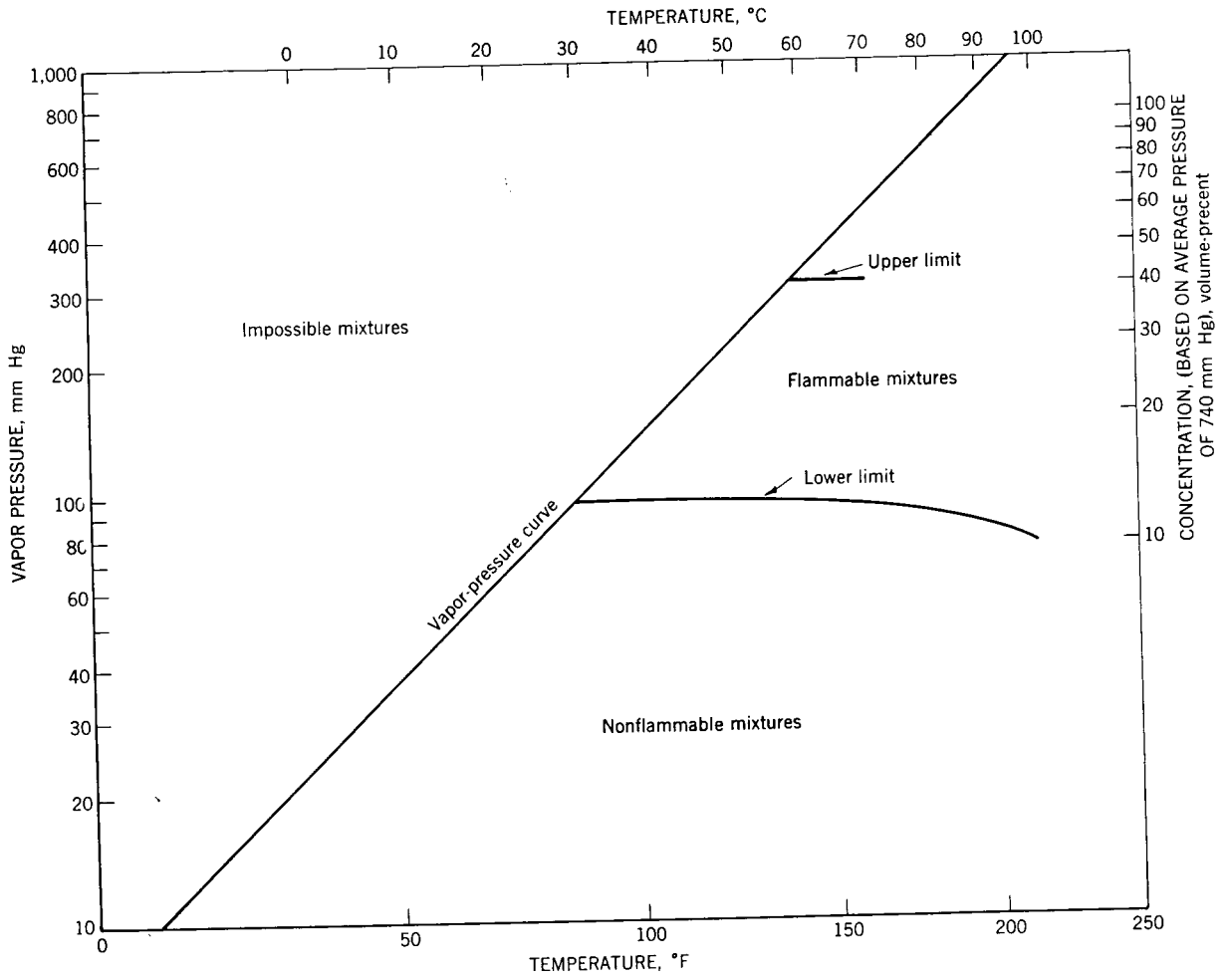

FIGURE 131.—Flammability of Trichloroethylene-Air Mixtures.

ACKNOWLEDGMENTS

Many of the unpublished data reported here were obtained by the predecessor of the author, the late G. W. Jones, former chief of the gas explosions branch. Other data were obtained by the author and his coworkers, particularly Messrs. George S. Scott, Joseph M. Kuchta, Aldo L. Furno and Henry E. Perlee. In addition, the author is indebted to Drs. David Burgess [6] and Robert W. Van Dolah for many fruitful discussions of the material contained in the sections on Definitions and Theory, Deflagration and Detonation Processes, and Preventive Measures.

[6] Presently with Reaction Motors Division, Thiokol Chemical Corporation, Denville, New Jersey.

BIBLIOGRAPHY

1. Affens, W. A., J. E. Johnson, and H. W. Carhart. Effect of Chemical Structure on Spontaneous Ignition of Hydrocarbons. J. Chem. Eng. Data, v. 6, 1961, pp. 613–619.
2. ————. Ignition Studies, Part V, Study of the Processes Occurring During the Spontaneous Ignition of the Hexane Isomers. NRL Rept. 5437, January 1960, 15 pp.
3. Agnew, J. T., and L. B. Graiff. The Pressure Dependence of Laminar Burning Velocity by the Spherical Bomb Method. Combustion and Flame, v. 5, 1961, pp. 209–219.
4. Alexander, D. S. Explosions in Butadiene Systems. Ind. and Eng. Chem., v. 51, 1959, pp. 733–738.
5. Anson, D. Influence of the Quality of Atomization on the Stability of Combustion of Liquid Fuel Sprays. Fuel, v. 32, 1953, pp. 39–51.
6. Ashman, L. E., and A. Büchler. The Ignition of Gases by Electrically Heated Wires. Combustion and Flame, v. 5, 1961, pp. 113–121.
7. Bartkowiak, Alphonse, Sotirios Lambiris, and Michael G. Zabetakis. Flame Propagation Through Kerosine Foams. Combustion and Flame, v. 3, 1959, pp. 347–353.
8. Bartkowiak, Alphonse, and Michael G. Zabetakis. Flammability Limits of Methane and Ethane in Chlorine at Ambient and Elevated Temperatures and Pressure. BuMines Rept. of Inv. 5610, 1960, 6 pp.
9. Berl, W. G., and W. Renich. The Combustion of Boron Hydrides. CM-942, Johns Hopkins Univ., Silver Spring, Md., 1958, 53 pp.
10. Block, Benjamin. Emergency Venting for Tanks and Reactors. Chem. Eng., January 1962, pp. 111–118.
11. Bollinger, Loren E., and Rudolph Edse. Thermodynamic Calculations of Hydrogen-Oxygen Detonation Parameters for Various Initial Pressures. ARS J., v. 31, 1961, pp. 251–256.
12. Bollinger, Loren E., Michael G. Fong, and Rudolph Edse. Experimental Measurements and Theoretical Analysis of Detonation Induction Distances. ARS J., 1961, pp. 588–594.
13. Bollinger, Loren E., James A. Laughrey, and Rudolph Edse. Experimental Detonation Velocities and Induction Distances in Hydrogen-Nitrous Oxide Mixtures. ARS J., v. 32, 1962, pp. 81–82.
14. British Chemical Engineering. Use of Bursting Discs at High Temperatures. December 1957, p. 677.
15. Brokaw, Richard S., and Joseph L. Jackson. Effect of Temperature, Pressure, and Composition on Ignition Delays for Propane Flames. 5th Symp. (Internat.) on Combustion, Reinhold Pub. Corp., New York, 1955, pp. 563–569.
16. Browne, Howard C., Harold Hileman, and Lowell C. Weger. Barricades for High Pressure Research. Ind. and Eng. Chem., v. 53, 1961, pp. 52A–58A.
17. Browning, J. A., and W. G. Krall. Effect of Fuel Droplets on Flame Stability, Flame Velocity, and Inflammability Limits. 5th Symp. (Internat.) on Combustion, Reinhold Pub. Corp., New York, 1955, pp. 159–163.
18. Browning, J. A., T. L. Tyler, and W. G. Krall. Effect of Particle Size on Combustion of Uniform Suspensions. Ind. and Eng. Chem., v. 49, 1957, pp. 142–148.
19. Buckley, William L., and Howard W. Husa. Combustion Properties of Ammonia. Chem. Eng. Prog., v. 58, 1962, pp. 81–84.
20. Burgess, D., A. Strasser, and J. Grumer. Diffusive Burning of Liquid Fuels in Open Trays. Fire Res. Abs. and Rev., v. 3, 1961, pp. 177–192.
21. Burgess, David, and Michael G. Zabetakis. Fire and Explosion Hazards Associated With Liquefied Natural Gas. BuMines Rept. of Inv. 6099, 1962, 34 pp.
22. Burgoyne, J. H. Mist and Spray Explosions. Chem. Eng. Prog., v. 53, 1957, pp. 121–M—124–M.
23. ————. Principles of Explosion Prevention. Chem. and Process Eng., April 1961, pp. 1–4.
24. Burgoyne, J. H., and L. Cohen. The Effect of Drop Size on Flame Propagation in Liquid Aerosols. Roy. Soc. (London), Proc. v. 225, 1954, pp. 375–392.
25. Burgoyne, J. H., and H. Hirsch. The Combustion of Methane at High Temperatures. Roy. Soc. (London), Proc. v. 227, 1954, pp. 73–93.
26. Burgoyne, J. H., and R. F. Neale. Some New Measurements of Inflammability Ranges in Air. Fuel, v. 32, 1953, pp. 5–16.
27. Burgoyne, J. H., and J. F. Richardson. The Inflammability of Oil Mists. Fuel, v. 28, 1949, pp. 2–6.
28. Burgoyne, J. H., and A. J. Steel. Flammability of Methane-Air Mixtures in Water-Base Foams. Fire Res. Abs. and Rev., v. 4, Nos. 1 and 2, 1962, pp. 67–75.
29. Burgoyne, J. H., and G. Williams-Leir. The Influence of Incombustible Vapours on the Limits of Inflammability of Gases and Vapours in Air. Roy. Soc. (London) Proc., v. 193, 1948, pp. 525–539.
30. Burgoyne, J. H., and M. J. G. Wilson. The Relief of Pentane Vapour-Air Explosions in Vessels. Proc. Symp. on Chem. Process Hazards, Inst. Chem. Eng. (London), 1960, pp. 25–29.
31. Butler, Judson C., and William P. Webb. Upper Explosive Limits of Cumene. Chem. Eng. Data, v. 2, 1957, pp. 42–46.
32. Cassutt, Leon H. Experimental Investigation of Detonation in Unconfined Gaseous Hydrogen-Oxygen-Nitrogen Mixtures. ARS J., 1961, pp. 1122–1128.
33. Cassutt, L. H., F. E. Maddocks, and W. A. Sawyer. A Study of the Hazards in the Storage and Handling of Liquid Hydrogen. Advances in Cryogenic Eng., ed. by K. D. Timmerhaus. Plenum Press, Inc., New York, v. 5, 1960, pp. 55–61.
34. Chemical and Engineering News. Explosive Decomposition of Propylene. V. 30, 1952, p. 1239.
35. Chemical Engineering. Pane Relievers Vent Explosive Popoffs. Jan. 22, 1962, pp. 70–72.
36. Chiantella, A. J., W. A. Affens, and J. E. Johnson. The Effect of High Temperatures on the Stability and Ignition Properties of Commercial Triaryl Phosphate Fluids. NRL Rept. 5839, 1962, 15 pp.

37. Coleman, E. H. Effects of Fluorinated Hydrocarbons on the Inflammability Limits of Combustible Vapours. Fuel, v. 31, 1953, pp. 445–447.
38. Conison, Joseph. How to Design a Pressure Relief System. Chem. Eng., 1960, pp. 109–114.
39. Copeland, N. A., and M. A. Youker. German Techniques for Handling Acetylene in Chemical Operations. FIAT Final Rept. No. 720, January 1946, 130 pp.
40. Coward, H. F., and G. W. Jones. Limits of Flammability of Gases and Vapors. BuMines Bull. 503, 1952, 155 pp.
41. Coward, H. F., G. W. Jones, C. G. Dunkle, and B. E. Hess. The Explosibility of Methane and Natural Gas. Carnegie Inst. of Technol., Min. and Met. Inv., Coop. Bull. 30, 1926, 40 pp.
42. Cubbage, P. A., and W. A. Simmonds. An Investigation of Explosion Reliefs for Industrial Drying Ovens. Gas Council, Res. Communication GC23 (London), 1955, 46 pp.
43. ————. An Investigation of Explosion Reliefs for Industrial Drying Ovens. Gas Council, Res. Communication GC43 (London), 1957, 41 pp.
44. Davenport, Donald E., George B. Huber, and Norman R. Zabel. Containment of Fragments From Runaway Nuclear Reactors. Progress in Nuclear Energy, v. 4, Pergamon Press, New York, 1961, pp. 484–503.
45. Davis, D. S. Emergency Vent Size for Tanks Containing Flammable Liquids. British Chem. Eng. Nomogram No. 62, v. 6, 1961, p. 644.
46. Diss, E., H. Karam, and C. Jones. Practical Way to Size Safety Disks. Chem. Eng., 1961, pp. 187–190.
47. Dixon-Lewis, G., and G. L. Isles. Limits of Flammability. 7th Symp. (Internat.) on Combustion, Butterworths Scientific Pub. (London), 1959, pp. 475–483.
48. Drell, Isadore L., and Frank E. Belles. Survey of Hydrogen Combustion Properties. Nat. Advisory Committee for Aeronautics Rept. 1383, 1958, 34 pp.
49. Dugger, Gordon L., and Dorothy D. Graab. Flame Velocities of Propane- and Ethylene-Oxygen-Nitrogen Mixtures. Nat. Advisory Committee for Aeronautics RM E52J24, January 1953, 23 pp.
50. Dugger, Gordon L., and Sheldon Heimel. Flame Speeds of Methane-Air, Propane-Air, and Ethylene-Air Mixtures at Low Initial Temperatures. Nat. Advisory Committee for Aeronautics TN 2624, February 1952, 25 pp.
51. Dugger, Gordon L., Robert C. Weast, and Sheldon Heimel. Effect of Preflame Reaction on Flame Velocity of Propane-Air Mixtures. 5th Symp. (Internat.) on Combustion, Reinhold Pub. Corp., New York, 1955, pp. 589–595.
52. Dunn, Robert G., and Bernard T. Wolfson. Single Generalized Chart of Detonation Parameters for Gaseous Mixtures. J. Chem. and Eng. Data, v. 4, 1959, pp. 124–127.
53. Dvorak, Karel, and Arnost Reiser. Influence of Water Vapor on the Flame Extinction of Methanol in Air. Chem. Listy, v. 49, 1955, pp. 467–472.
54. Edwards, D. H., G. T. Williams, and J. D. Breeze. Pressure and Velocity Measurements on Detonation Waves in Hydrogen-Oxygen Mixtures. J. Fluid Mech., November 1959, pp. 497–517.
55. Egerton, Sir Alfred C. Limits of Inflammability. 4th Symp. (Internat.) on Combustion, Williams & Wilkins Co., Baltimore, Md., 1953, pp. 4–13.
56. Epstein, Leo F. Correlation and Prediction of Explosive Metal-Water Reaction Temperatures. Nuclear Sci. and Eng., v. 10, July 1961, pp. 247–253.
57. Evans, Marjorie W., and C. M. Ablow. Theories of Detonation. J. Chem. Rev., v. 129, 1961, pp. 129–178.
58. Faeth, G. M., and D. F. White. Ignition of Hydraulic Fluids by Rapid Compression. Am. Soc. Naval Eng. J., v. 73, 1961, pp. 467–475.
59. Fitzgerald, F. Decomposition of Methylacetylene. Nature, 1960, p. 387.
60. Frank, Charles E., and Angus U. Blackham. Investigation of Hydrocarbon Ignition. Nat. Advisory Committee for Aeronautics TN 2549, 1952, 33 pp.
61. Fraser, R. P. Detonation Velocities in Liquid Fuel Vapours With Air or Oxygen at 100° C and Atmospheric Pressure. 7th Symp. (Internat.) on Combustion, Butterworths Sci. Pub. (London), 1958, pp. 783–788.
62. Furno, Aldo L., George H. Martindill, and Michael G. Zabetakis. Gas Explosion Hazards Associated With the Bulk Storage of Molten Sulfur. BuMines Rept. of Inv. 6185, 1963, 11 pp.
63. ————. Limits of Flammability of Hydrazine-Hydrocarbon Vapor Mixtures. J. Chem. Eng. Data, July 1962, pp. 375–376.
64. Gaydon, A. G., and H. G. Wolfhard. Flames, Their Structure, Radiation and Temperature. Chapman & Hall, Ltd. (London), 2d ed., 1960, 383 pp.
65. Gealer, Roy L., and Stuart W. Churchill. Detonation Characteristics of Hydrogen-Oxygen Mixtures at High Initial Pressures. AIChE, v. 6, September 1960, pp. 501–505.
66. Gerstein, M. A Study of Alkylsilane Flames. 7th Symp. (Internat.) on Combustion. Butterworths Sci. Pub. (London), 1959, pp. 903–905.
67. Gerstein, Melvin, Edward R. Carlson, and Francis U. Hill. Natural Gas-Air Explosions at Reduced Pressure. Ind. and Eng. Chem., v. 46, 1954, pp. 2558–2562.
68. Gibbs, G. J., and H. F. Calcote. Effect of Molecular Structure on Burning Velocity. J. Chem. Eng. Data, v. 5, 1959, pp. 226–237.
69. Glasstone, Samuel. Thermodynamics for Chemists. D. Van Nostrand Co., Inc., New York, 1946, 522 pp.
70. Glendinning, W. G., and A. M. MacLennan. Suppression of Fuel-Air Explosions. Nat. Fire Protect. Assoc. Quart., v. 45, July 1951, p. 61.
71. Gliwitzky, W. Prevention of Acetylene-Air Explosions by Addition of Carbon Dioxide and Nitrogen. Autogene Metalbearbeit, v. 33, 1940, pp. 2–5.
72. Grabowski, G. J. Industrial Explosion Protection. J. Am. Oil Chem. Soc., v. 36, 1959, pp. 57–59.
73. Gray, P., and J. C. Lee. Recent Studies of the Oxidation and Decomposition Flames of Hydrazine. 7th Symp. (Internat.) on Combustion, Butterworths Sci. Pub. (London), 1959, p. 61.
74. Greenlee, Kenneth. Butadiene-Crotonaldehyde Explosion. Chem. and Eng. News, v. 26, 1948, p. 1985.
75. Guest, P. G., V. W. Sikora, and Bernard Lewis. Static Electricity in Hospital Operating Suites: Direct and Related Hazards and Pertinent Remedies. BuMines Rept. of Inv. 4833, 1952, 64 pp.
76. Haber, F., and H. Wolff. Mist Explosions. Zeit. angew. Chem., v. 36, 1923, p. 373.
77. Hall, A. R., and R. A. M. Straker. The Methylacetylene (Propyne) Decomposition Flame at Pressures of 10, 20 and 40 Atmospheres. Rocket Propulsion Establishment (Westcott), TN 192, 1960, p. 11.
78. Hanna, N. E., M. G. Zabetakis, R. W. Van Dolah,

and G. H. Damon. Potential Ignition Hazards Associated With Compressed-Air Blasting Using a Compressor Underground. BuMines Rept. of Inv. 5223, 1956, 33 pp.

79. Harris, D. N., Glenn Karel, and A. L. Ludwig. Electrostatic Discharges in Aircraft Fuel Systems. 41st Ann. API Meeting Preprint, 1961, 10 pp.
80. Heck, W. B., Jr., and R. L. Johnson. Aluminum Alkyls. Ind. and Eng. Chem., v. 54, December 1962, pp. 35–38.
81. Heimel, Sheldon, and Robert C. Weast. Effect of Initial Mixture Temperature on the Burning Velocity of Benzene-Air, *n*-Heptane-Air, and Isooctane-Air Mixtures. 6th Symp. (Internat.) on Combustion, Reinhold Publishing Corp., New York, 1957, pp. 296–302.
82. Herzog, R. E., E. C. Ballard, and H. A. Hartung. Evaluating Electrostatic Hazard During the Loading of Tank Trucks. 41st Ann. API Meeting Preprint, 1961, 7 pp.
83. Hildebrand, Joel H., and Robert L. Scott. The Solubility of Nonelectrolytes. Reinhold Pub. Corp., New York, 3d ed., 1950, p. 243.
84. Hill, Howard W. Methyl Bromide-Air Explosion. Chem. Eng. Prog., v. 58, August 1962, pp. 46–49.
85. Holdsworth, M. P., J. L. vander Minne, and S. J. Vellenga. Electrostatic Charging During the White Oil Loading of Tankers. 41st Ann. API Meeting Preprint, 1961, 30 pp.
86. Holtz, John C., L. B. Berger, M. A. Elliott, and H. H. Schrenk. Diesel Engines Underground. BuMines Rept. of Inv. 3508, 1940, 48 pp.
87. Hsieh, M. S., and D. T. A. Townsend. An Examination of the Mechanism by Which "Cool" Flames May Give Rise to "Normal" Flames. Part I. The Inflammable Ranges of Ether-Air Mixtures in Closed Vessels. J. Chem. Soc. (London), 1939, pp. 337–340.
88. ————. An Examination of the Mechanism by Which "Cool" Flames May Give Rise to "Normal" Flames. Part II. The Inflammable Ranges of Higher Paraffin Hydrocarbons in Air: The Establishment of "Cool" Flame Ranges at Ordinary Temperatures and High Pressures. J. Chem. Soc. (London), 1939, pp. 341–345.
89. International Acetylene Association. Acetylene Transmission for Chemical Synthesis. Internat. Acetylene Assoc., New York (no date), 40 pp.
90. Jackson, J. L., and R. S. Brokaw. Variation of Spontaneous Ignition Delays With Temperature and Composition for Propane-Oxygen-Nitrogen Mixtures at Atmospheric Pressure. Nat. Advisory Committee for Aeronautics Res. Memo. E54B19, 1954, 29 pp.
91. Jacobs, R. B., W. L. Bulkley, J. C. Rhodes, and T. L. Speer. Destruction of a Large Refining Unit by Gaseous Detonation. Chem. Eng. Prog., v. 53, December 1957, pp. 565–573.
92. Johnson, J. Enoch, John W. Crellin, and Homer W. Carhart. A Study of the Autoignition Properties of Certain Diesel Fuels. Naval Res. Laboratory Rept. 3859, 1951, 29 pp.
93. ————. Ignition Studies. Part II—The Spontaneous Ignition Properties of Some Diesel Fuels and Pure Hydrocarbons. NRL Rept. 4202, 1953, 14 pp.
94. Jones, G. W. Fire and Explosion Hazards of Combustible Gases and Vapors. Ind. Hygiene and Toxicology, ed. by Frank A. Patty. Intersci. Pub., Inc., New York, v. 1, ch. 16, 2d rev. ed., 1958, pp. 511–548.
95. ————. Inflammation Limits and Their Practical Application in Hazardous Industrial Operations. Chem. Rev., v. 22, February 1938, pp. 1–26.
96. ————. The Inflammability of Refrigerants. Ind. Eng. Chem., v. 20, 1928, pp. 367–370.
97. Jones, G. W., and B. B. Beattie. Explosive Properties of Divinyl Ether. Ind. and Eng. Chem., v. 26, 1934, pp. 557–560.
98. Jones, G. W., E. S. Harris, and W. E. Miller. Explosive Properties of Acetone-Air Mixtures. BuMines Tech. Paper 544, 1933, 26 pp.
99. Jones, G. W., and R. E. Kennedy. Effect of Pressure on Ignition Temperature of Acetylene and Acetylene-Air Mixtures. BuMines Rept. of Inv. 3809, 1945, 7 pp.
100. ————. Extinction of Ethylene Flames by Carbon Dioxide and Nitrogen. Anesthesia and Analgesia, v. 9, 1930, pp. 6–10.
101. ————. Extinction of Propylene Flames by Diluting With Nitrogen and Carbon Dioxide and Some Observations on the Explosive Properties of Propylene. BuMines Rept. of Inv. 3395, 1938, 14 pp.
102. ————. Limits of Inflammability of Butadiene in Air. BuMines Rept. of Inv. 3565, 1941, 4 pp.
103. ————. Prevention of Butadiene-Air Explosions by Addition of Nitrogen and Carbon Dioxide. BuMines Rept. of Inv. 3691, 1943, 11 pp.
104. Jones, G. W., R. E. Kennedy, and W. E. Miller. Limits of Inflammability and Ignition Temperature of Ethyl Mercaptan in Air. BuMines Rept. of Inv. 3648, 1942, 6 pp.
105. Jones, G. W., R. E. Kennedy, and I. Spolan. Effect of High Pressures on the Flammability of Natural Gas-Air-Nitrogen Mixtures. BuMines Rept. of Inv. 4557, 1949, 16 pp.
106. Jones, G. W., R. E. Kennedy, and G. J. Thomas. Explosion Hazards of Combustible Anesthetics. BuMines Tech. Paper 653, 1943, 47 pp.
107. ————. Explosive Properties of Cyclopropane. BuMines Rept. of Inv. 3511, 1940, 17 pp.
108. ————. Inflammability of Ether-Oxygen-Helium Mixtures. BuMines Rept. of Inv. 3589, 1941, 15 pp.
109. Jones, E., and J. C. Kerr. Inflammability Limits of Ammonia, Nitrous Oxide, and Air. J. Soc. Chem. Ind., v. 68, 1949, pp. 31–34.
110. Jones, G. W., and W. E. Miller. Ignition Temperatures of Acetylene-Air and Acetylene-Oxygen Mixtures. BuMines Rept. of Inv. 3567, 1951, 5 pp.
111. Jones, G. W., W. E. Miller, and H. Seaman. Explosive Properties of Methyl-Formate-Air Mixtures. Ind. and Eng. Chem., v. 25, 1933, pp. 694–696.
112. Jones, G. W., and G. St. J. Perrott. Oxygen Required for the Propagation of Hydrogen, Carbon Monoxide, and Methane Flames. Ind. and Eng. Chem., v. 19, 1927, pp. 985–989.
113. Jones, G. W., and F. E. Scott. Extinction of Propane and Butane Flames by Dichlorodifluoromethane. BuMines Rept. of Inv. 3908, 1946, 8 pp.
114. ————. Inflammability of Dimethyl Ether-Dichlorodifluoromethane-Air Mixtures. BuMines Rept. of Inv. 4125, 1947, 4 pp.
115. Jones, G. W., W. P. Yant, W. E. Miller, and R. E. Kennedy. Limits of Inflammability of Diethyl Ether and Ethylene in Air and Oxygen. BuMines Rept. of Inv. 3278, 1935, 5 pp.
116. ————. The Ignition Temperatures of Diethyl Ether and Ethylene in Air and Oxygen. BuMines Rept. of Inv. 3284, 1935, 6 pp.
117. Jones, G. W., M. G. Zabetakis, and G. S. Scott. Elimination of Ethyl Mercaptan Vapor-Air

Explosions in Stench Warning Systems. BuMines Rept. of Inv. 5090, 1954, 8 pp.
118. Jost, Wilhelm. Explosion and Combustion Processes in Gases. McGraw-Hill Book Co., New York, 1946, 621 pp.
119. Kharasch, M. S. Heats of Combustion of Organic Compounds. NBS J. Res., v. 2, 1929, pp. 359–430.
120. Kennedy, R. E., G. S. Scott, and M. G. Zabetakis. Flammability Limits of Hydrocarbons at High Temperatures and Pressures. Chem. Eng. Prog., v. 53, 1957, pp. 125–126.
121. Kennedy, R. E., I. Spolan, W. K. Mock, and G. S. Scott. Effect of High Pressures on the Explosibility of Mixtures of Ethane, Air, and Carbon Dioxide and Ethane, Air, and Nitrogen. BuMines Rept. of Inv. 4751, 1950, 11 pp.
122. Kennedy, R. E., I. Spolan, and G. S. Scott. Explosibility of Mixtures of Propane, Air, and Carbon Dioxide and of Propane, Air, and Nitrogen at Elevated Pressures. BuMines Rept. of Inv. 4812, 1951, 9 pp.
123. Klinkenberg, A., and J. L. vander Minne. Electrostatics in the Petroleum Industry. Elsevier Publishing Co., New York, 1958, 191 pp.
124. Kobe, Kenneth A., and Ernest G. Long. Thermochemistry for the Petrochemical Industry. Part VI. Acetylenes and Diolefins. Petrol. Refiner, v. 28, 1949, p. 133.
125. Kogarko, S. M. Detonation of Methane-Air Mixtures and the Detonation Limits of Hydrocarbon-Air Mixtures in a Large-Diameter Pipe. Soviet Physics, Tech. Phys., v. 3, 1958, pp. 1904–1916. (Transl. of J. Tech. Phys., USSR, v. 28, pp. 2072–2078.)
126. Kuchta, Joseph M., Alphonse Bartkowiak, Irving Spolan, and Michael G. Zabetakis. Flammability Characteristics of High-Temperature Hydrocarbon Fuels. Wright Air Development Division Tech. Rept. 61–89, 1961, 29 pp.
127. Kuchta, Joseph M., Sotirios Lambiris, and Michael G. Zabetakis. Flammability and Autoignition of Hydrocarbon Fuels Under Static and Dynamic Conditions. BuMines Rept. of Inv. 5992, 1962, 21 pp.
128. Kunin, T. I., and V. I. Serdyukov. Limits and Temperatures of Explosion of Hydrogen-Chlorine Mixtures in Hydrogen Chloride. J. Gen. Chem., USSR, v. 16, 1946, p. 1421–1430.
129. Le Chatelier, H., and O. Boudouard. Limits of Flammability of Gaseous Mixtures. Bull. Soc. chim. (Paris), v. 19, 1898, pp. 483–488.
130. Lewis, Bernard, and Guenther von Elbe. Combustion, Flames and Explosions of Gases. 2d ed. Academic Press, Inc., New York, 1961, 731 pp.
131. Linnett, J. W. Methods of Measuring Burning Velocities. 4th Symp. (Internat.) on Combustion. Williams & Wilkins Co., Baltimore, Md., 1953, pp. 20–35.
132. Linnett, J. W., and C. J. S. M. Simpson. Limits of Inflammability. 6th Symp. (Internat.) on Combustion, Reinhold Pub. Corp., New York, 1957, pp. 20–27.
133. Lloyd, P. The Fuel Problem in Gas Turbines. Inst. Mech. Eng. Proc., War Emergency Issue No. 41, v. 159, 1948, p. 220.
134. Lowenstein, J. G. Calculate Adequate Rupture Disk Size. Chem. Eng., v. 65, 1958, pp. 157–158.
135. Luker, James A., and Leonard B. Adler. Effect of Reactor Length on the Formation of Detonation in Saturated Knallgas-Steam Mixtures. J. Chem. Phys., v. 36, 1962, pp. 718–721.
136. Luker, James A., and Melvin J. Leibson. Dynamic Loading of Rupture Disks With Detonation Waves. J. Chem. Eng. Data, v. 4, 1959, pp. 133–135.
137. Luker, James A., Paul L. McGill, and Leonard B. Adler. Knallgas and Knallgas-Steam Mixtures at High Initial Temperature and Pressure. J. Chem. Eng. Data, v. 4, 1959, pp. 136–142.
138. Manton, J., and B. B. Milliken. Study of Pressure Dependence of Burning Velocity by the Spherical Vessel Method. Gas Dynamics Symp. on Aerothermochem. Proc., 1955, pp. 151–157.
139. Marsel, J., and L. Dramer. Spontaneous Ignition Properties of Metal Alkyls. 7th Symp. (Internat.) on Combustion, Butterworths Sci. Pub. (London), 1959, p. 906.
140. Martindill, G. H., F. W. Lang, and M. G. Zabetakis. Flammability Characteristics of the Vapor System Hydrogen Peroxide-Xylene-Formic Acid-Water. J. Chem. Eng. Data, v. 5, 1960, pp. 355–358.
141. Matson, A. F., and R. E. Dufour. Limits of Flammability of Methyl Ethyl Ketone Vapor in Air at Initial Temperatures of 100°, 150° and 200°. Underwriters Laboratory Bull. Res. 38, 1947, pp. 5–18.
142. McDonald, J. S., and J. E. Owens. Investigation of Tetralin Explosion. Atomics Internat. Rept. NAA–SR–4803, Canoga Park, Calif., 1960, 58 pp.
143. Mellan, Ibert. Industrial Solvents. 2d ed. Reinhold Pub. Corp., New York, 1950, 758 pp.
144. Miller, S. A., and E. Penny. Hazards in Handling Acetylene in Chemical Processes, Particularly Under Pressure. Proc. Symp. on Chem. Process Hazards, Inst. of Chem. Eng. (London), 1960, p. 87.
145. Missen, R. W. Pressure Drop in Vapor-Relief Systems. Chem. Eng., 1962, pp. 101–102.
146. Moore, R. H. Fires and Explosions in Compressed Air Systems. Canadian Min. and Met. Bull. No. 609, v. 56, 1963, pp. 18–19.
147. Moran, H. E., Jr., and A. W. Bertschy. Flammability Limits for Mixtures of Hydrocarbon Fuels, Air, and Halogen Compounds. NRL Rept. 4121, 1953, 12 pp.
148. Moreton, D. H. Review of Synthetic Lubricants. Lubrication Eng., 1954, pp. 65–73.
149. Morgan, N. D. The Influence of Lubricants on Explosions in Compressed Air Systems. Canadian Min. and Met. Bull. 609, v. 56, pp. 19–21.
150. Morrison, Richard Boyd. A Shock-Tube Investigation of Detonative Combustion. Univ. of Michigan, UMM–97, 1955, 121 pp.
151. Moyle, Morton P., Richard B. Morrison, and Stuart W. Churchill. Detonation Characteristics of Hydrogen-Oxygen Mixtures. AIChE, March 1960, pp. 92–96.
152. Mulcahy, M. F. R. Oxidation of Lower Paraffins. Disc. Faraday Soc., 1947, No. 2, pp. 128–132.
153. Mullins, B. P. Spontaneous Ignition of Liquid Fuels. Butterworths Sci. Pub. (London), 1955, 117 pp.
154. Mullins, B. P., and S. S. Penner. Explosions, Detonations, Flammability and Ignition. Pergamon Press (London), 1959, 287 pp.
155. Murrin, R. W., and S. Goldhagen. Determination of the C-O Bond Energy From the Heats of Combustion of Four Aliphatic Ethers. Naval Powder Factory NPF TR 75, NAVord Report No. 5491, 1957, 14 pp.
156. National Advisory Committee for Aeronautics. Basic Considerations in the Combustion of Hydrocarbon Fuels With Air. Rep't 1300, ed. by Henry C. Barnett and Robert R. Hibbard, 1957, 259 pp.
157. National Board of Fire Underwriters. Fire and Explosion Hazards of Organic Peroxide. Res. Rept. No. 11, 1956, 60 pp.

158. National Fire Protection Association. Fire-Hazard Properties of Flammable Liquids, Gases and Volatile Solids. NFPA 325, 60 Battery march St., Boston 10, Mass., 1960, 126 pp.
159. Nuckolls, A. H. Underwriters' Laboratory Method for the Classification of the Hazards of Liquids. National Board of Fire Underwriters, Chicago, Ill., 1929, 20 pp.
160. Ordnance Corps, U.S. Department of the Army. Ordnance Safety Manual. ORDM 7-224, 1951; Sec. 17, May 15, 1958, 68 pp.
161. Palmer, K. N. The Quenching of Flame by Perforated Sheeting and Block Flame Arrestors. Proc. Symp. on Chemical Process Hazards, Inst. Chem. Eng. (London), 1960, p. 51.
162. ————. The Quenching of Flame by Wire Gauzes. 7th Symp. (Internat.) on Combustion, Butterworths Sci. Pub. (London), 1959, pp. 497–503.
163. Parker, W. G., and H. G. Wolfhard. Properties of Diborane Flames. Fuel, v. 35, 1956, pp. 323–331.
164. ————. Some Characteristics of Flames Supported by NO and NO_2. 4th Symp. (Internat.) on Combustion, Williams & Wilkins Co., Baltimore, Md.. 1953, pp. 420–428.
165. Penny, E. The Velocity of Detonation in Compressed Acetylene. Faraday Soc. Disc., No. 22, 1956, pp. 157–161.
166. Perlee, Henry E., Agnes C. Imhof, and Michael G. Zabetakis. Flammability Characteristics of Hydrazine Fuels in Nitrogen Tetroxide Atmospheres. J. Chem. Eng. Data, 1962, pp. 377–379.
167. Pieters, H. A. J., J. W. Hovers, and B. J. Rietveld. Determination of the Explosion Limits of Gases. Fuel, v. 26, 1947, pp. 80–81.
168. Porter, R. L. Unusual Pressure Relief Devices. Ind. and Eng. Chem., v. 54, January 1962, pp. 24–27.
169. Price, Fraser P. First and Second Limits of Explosion of Diborane-Oxygen Mixtures. J. Am. Chem. Soc., v. 72, 1950, pp. 5361–5365.
170. Randall, P. N., J. Bland, W. M. Dudley, and R. B. Jacobs. Effects of Gaseous Detonations Upon Vessels and Piping. J. Chem. Eng. Prog., v. 53, December 1957, pp. 574–580.
171. Randall, P. N., and I. Ginsburgh. Bursting of Tubular Specimens by Gaseous Detonation. ASME, Trans., Paper No. 60-WA-12, 1960, 9 pp.
172. Rasbash, D. J., and Z. W. Rogowski. Gaseous Explosions in Vented Ducts. Combustion and Flame, v. 4, December 1960, pp. 301–312.
173. ————. Relief of Explosions in Duct Systems. Proc. Symp. on Chem. Process Hazards, Inst. Chem. Eng. (London), 1960, p. 58.
174. Rebenstorf, Melvin A. Designing a High Pressure Laboratory. Ind. and Eng. Chem., v. 53, 1961, pp. 40A–42A.
175. Richardson, E. C., and C. R. Sutton. Explosive Properties of Lacquer-Solvent Vapors. Ind. and Eng. Chem., v. 20, 1928, pp. 187–190.
176. Roberts, A., B. R. Pursall, and J. B. Sellers. Methane Layering in Mine Airways. Coll. Guard., v. 205, October 1962, pp. 535–541.
177. ————. Methane Layering in Mine Airways. Part II, The Theory of Layering. Coll. Guard., v. 205, 1962, pp. 588–593.
178. ————. Methane Layering in Mine Airways. Part III. The Theory of Layering (Continued). Coll. Guard., v. 205, 1962, pp. 630–636.
179. ————. Methane Layering in Mine Airways. Part IV, Studying Layering Phenomena in a Laboratory Model. Coll. Guard., v. 205, 1962, pp. 723–732.
180. Roberts, A., B. R. Pursall and J. B. Sellers. Methane Layering in Mine Airways. Part V, Studying Layering Phenomena in a Laboratory Model. Coll. Guard., v. 205, 1962, pp. 756–763.
181. Rogers, D. T., and C. E. Schleckser. Engineering and Theoretical Studies of Static Electricity in Fuels. Proc. 5th World Petrol. Cong., New York, sec. 8, paper 10, 1959, pp. 103–121.
182. Rolingson, W. R., John MacPherson, P. D. Montgomery, and B. L. Williams. Effect of Temperature on the Upper Flammable Limit of Methane, Ammonia, and Air Mixtures. J. Chem. Eng. Data, v. 5, 1960, pp. 349–351.
183. Rossini, F. D. and others. Selected Values of Properties of Hydrocarbons. NBS Circ. C461, 1947, 483 pp.
184. Salooja, K. C. Studies of Combustion Processes Leading to Ignition in Hydrocarbons. Combustion and Flame, v. 4, 1960, pp. 117–136.
185. Sargent, H. B. How to Design a Hazard-Free System to Handle Acetylene. Chem. Eng., February 1957, pp. 250–254.
186. Schumb, W. C., C. N. Satterfield, and R. L. Wentworth. Hydrogen Peroxide. Reinhold Pub. Co., New York, 1955, 750 pp.
187. Scott, D. A. Hazards With Butadiene and its Properties. Am. Chem. Soc., v. 18, 1940, p. 404.
188. Scott, F. E., J. J. Burns, and B. Lewis. Explosive Properties of Hydrazine. BuMines Rept. of Inv. 4460, 1949, 18 pp.
189. Scott, F. E., R. W. Van Dolah, and M. G. Zabetakis. The Flammability Characteristics of the System H_2-NO-N_2O-Air. 6th Symp. (Internat.) on Combustion. Reinhold Pub. Co., New York, 1957, pp. 540–545.
190. Scott, G. S. Flammability of Trichloroethylene. BuMines Rept. of Inv. 6190, 1963, 5 pp.
191. Scott, G. S., G. W. Jones, and F. E. Scott. Determination of Ignition Temperatures of Combustible Liquids and Gases. Modification of the Drop Method. Anal. Chem., v. 20, 1948, pp. 238–241.
192. Scott, George S., Henry E. Perlee, George H. Martindill, and Michael G. Zabetakis. Review of Fire and Explosion Hazards of Flight Vehicle Combustibles. Aeronautical Systems Division Tech. Rept. 61-278, supp. 1, 1962, 43 pp.
193. Semenov, N. N. Some Problems in Chemical Kinetics and Reactivity. Princeton Univ. Press, Princeton, N.J., v. 2, 1959, 331 pp.
194. Setchkin, Nicholas P. Self-Ignition Temperatures of Combustible Liquids. J. Res. NBS, v. 53, 1954, Res. Paper 2516, pp. 49–66.
195. Simmonds, W. A., and P. A. Cubbage. The Design of Explosion Reliefs for Industrial Drying Ovens. Proc. Symp. on Chem. Process Hazards. Inst. Chem. Eng. (London), 1960, p. 69.
196. Simmons, R. F., and H. G. Wolfhard. The Influence of Methyl Bromide on Flames. Trans. Faraday Soc., v. 51, 1955, p. 1211.
197. Simon, Dorothy M., Frank E. Belles, and Adolph E. Spakowski. Investigation and Interpretation of the Flammability Region for Some Lean Hydrocarbon-Air Mixtures. 4th Symp. (Internat.) on Combustion, Williams & Wilkins Co., Baltimore, Md., 1953, pp. 126–138.
198. Singer, J. M., Joseph Grumer, and E. B. Cook. Burning Velocities by the Bunsen-Burner Method. I. Hydrocarbon-Oxygen Mixtures at One Atmosphere. II. Hydrocarbon-Air Mixtures at Subatmospheric Pressures. Proc. Aerothermochem. Gas Dynamics Symp., 1955, pp. 139–150.
199. Smith, Marion L., and Karl W. Stinson. Fuels

and Combustion. McGraw-Hill Book Co., New York, 1952, 340 pp.
200. Solov'ev, N. V., and A. N. Baratov. Dependence of the Lower Limit of Flammability on Molecular Structure. Russian J. Phys. Chem. (Zhur. Fiz. Khim.), v. 34, 1960, pp. 1661–1670.
201. Spakowski, A. E. Pressure Limit of Flame Propagation of Pure Hydrocarbon-Air Mixtures at Reduced Pressures. Nat. Advisory Committee for Aeronautics Res. Memo. E52H15, 1952, 33 pp.
202. Spalding, D. B. Some Fundamentals of Combustion. Butterworths Sci. Pub. (London), 1955, 250 pp.
203. Stenberg, John F., and Edward G. Coffey. Designing a High-Pressure Laboratory. Chem. Eng., 1962, pp. 115–118.
204. Stoner, R. G., and W. Bleakney. The Attenuation of Spherical Shock Waves in Air. J. Appl. Phys., v. 19, 1948, pp. 670–678.
205. Sullivan, M. V., J. K. Wolfe, and W. A. Zisman. Flammability of the Higher-Boiling Liquids and Their Mists. Ind. and Eng. Chem., v. 39, 1947, p. 1607.
206. Tamura, Z., and Y. Tanasawa. Evaporation and Combustion of Drop Contacting With a Hot Surface. 7th Symp. (Internat.) on Combustion, Butterworths Sci. Pub. (London), 1959, pp. 509–522.
207. Terao, Kunio. Selbstzundung von Kohlenwasserstoff-Luftgemischen in Stosswellen. J. Phys. Soc. of Japan, v. 15, 1960, pp. 2086–2092.
208. The Combustion Institute. Combustion and Flame. Butterworths Sci. Pub. (London), v. 1–7, 1957–63.
209. ————. 4th Symposium (International) on Combustion. The Williams & Wilkins Co., Baltimore, Md., 1953, 926 pp.
210. ————. 5th Symposium (International) on Combustion. Reinhold Pub. Corp., New York, 1955, 802 pp.
211. ————. 6th Symposium (International) on Combustion. Reinhold Pub. Corp., New York, 1957, 943 pp.
212. ————. 7th Symposium (International) on Combustion. Butterworths Sci. Pub. (London), 1959, 959 pp.
213. ————. 8th Symposium (International) on Combustion. The Williams & Wilkins Co., Baltimore, Md., 1962, 1164 pp.
214. The Institution of Chemical Engineers. Proceedings of the Symposium on Chemical Process Hazards. Inst. Chem. Eng. (London), 1960, 117 pp.
215. Thomas, A. Flame Propagation Through Air-Fuel Foams. 6th Symp. (Internat.) on Combustion, Reinhold Pub. Corp., New York, 1957, pp. 701–707.
216. Umland, A. W. Explosive Limits of Hydrogen-Chlorine Mixtures. J. Electrochem. Soc., v. 101, 1954, pp. 626–631.
217. U.S. Atomic Energy Commission. The Effects of Nuclear Weapons. Ed. by Samuel Glasstone, April 1962, p. 163.
218. Van Dolah, Robert W., Michael G. Zabetakis, David S. Burgess, and George S. Scott. Review of Fire and Explosion Hazards of Flight Vehicle Combustibles. BuMines Inf. Circ. 8137, 1962, 80 pp.
219. Wayman, D. H., and R. L. Potter. Detonations in Gaseous Fuming Nitric Acid-Hydrocarbon Mixtures. Combustion and Flame, Butterworths Sci. Pub. (London), 1957, v. 1, pp. 321–329.
220. Weber, J. P., J. Savitt, and K. Krc. Detonation Tests Evaluate High Pressure Cells. Ind. and Eng. Chem., v. 53, 1961, pp. 128A–131A.
221. Weil, N. A. Rupture Characteristics of Safety Diaphragms. J. Appl. Phys., 1959, pp. 621–624.
222. White, A. G. Limits for the Propagation of Flame in Inflammable Gas-Air Mixtures. III. The Effect of Temperature on the Limits. J. Chem. Soc., v. 127, 1925, pp. 672–684.
223. ————. Limits for the Propagation of Flame in Vapor-Air Mixtures. Part 1. Mixtures of Air and One Vapour at the Ordinary Temperature and Pressure. J. Chem. Soc., v. 121, 1922, pp. 1244–1270.
224. ————. Limits for the Propagation of Flame in Inflammable Gas-Air Mixtures. Part 1. Mixtures of Air and One Gas at the Ordinary Temperature and Pressure. J. Chem. Soc., v. 125, 1924, pp. 2387–2396.
225. ————. Limits for the Propagation of Flame at Various Temperatures in Mixtures of Ammonia With Air and Oxygen. J. Chem. Soc., v. 121, 1922, pp. 1688–1695.
226. White, A. G., and T. W. Price. The Ignition of Ether-Alcohol-Air and Acetone-Air Mixtures in Contact With Heated Surfaces. J. Chem. Soc., v. 115, 1919, pp. 1462–1505.
227. White, Douglas F. The Unintentional Ignition of Hydraulic Fluids Inside High Pressure Pneumatic Systems. ASNE J., 1960, pp. 405–413.
228. Winter, E. F. The Electrostatic Problem in Aircraft Fueling. J. Royal Aeronautical Soc., v. 66, 1962, pp. 429–446.
229. Wolfson, Bernard T. Harnessing Explosions. Office of Aerospace Res. Rept. No. 17, 1962, pp. 3–4.
230. Wolfson, Bernard T., and Robert G. Dunn. Generalized Charts of Detonation Parameters for Gaseous Mixtures. J. Chem. Eng. Data, v. 1, 1956, pp. 77–82.
231. Zabetakis, Michael G. Explosion of Dephlegmator at Cities Service Oil Company Refinery, Ponca City, Okla., 1959. BuMines Rept. of Inv. 5645, 1960, 16 pp.
232. ————. Gasfreeing of Cargo Tanks. BuMines Inf. Circ. 7994, 1961, 10 pp.
233. Zabetakis, M. J., M. P. Benoy, and P. M. Gussey. Explosion Hazards of Diethyl Ether. BuMines Rept. of Inv. 6051, 1962, 16 pp.
234. Zabetakis, M. G., and D. S. Burgess. Research on the Hazards Associated With the Production and Handling of Liquid Hydrogen. BuMines Rept. of Inv. 5707, 1961, 50 pp.
235. Zabetakis, M. G., J. C. Cooper, and A. L. Furno. Flammability of Solvent Mixtures Containing Methyl Ethyl Ketone and Tetrahydrofuran in Air. BuMines Rept. of Inv. 6048, 1962, 14 pp.
236. Zabetakis, M. G., and H. H. Engel. Flammable Materials: A Lecture Demonstration. BuMines Inf. Circ. 8005, 1961, 17 pp.
237. Zabetakis, M. G., A. L. Furno, and G. W. Jones. Minimum Spontaneous Ignition Temperatures of Combustibles in Air. Ind. and Eng. Chem., v. 46, 1954, pp. 2173–2178.
238. Zabetakis, M. G., P. M. Gussey, and G. S. Scott. Limits of Flammability of Methyl Ethyl Ketone and Methyl Isobutyl Ketone in Bromochloromethane-Air Mixtures. BuMines Rept. of Inv. 5680, 1960, 12 pp.
239. Zabetakis, M. G., and G. W. Jones. Flammability of Carbon Disulfide in Mixtures of Air and

Water Vapor. Ind. and Eng. Chem., v. 45, 1953, pp. 2079–2080.
240. ————. The Prevention of Industrial Gas Explosion Disasters. Chem. Eng. Prog., v. 51, 1955, pp. 411–414.
241. Zabetakis, Michael G., George W. Jones, George S. Scott, and Aldo L. Furno. Research on the Flammability Characteristics of Aircraft Fuels. Wright Air Development Center, Tech. Rept. 52–35, supp. 4, 1956, 85 pp.
242. Zabetakis, M. G., S. Lambiris, and G. S. Scott. Flame Temperatures of Limit Mixtures. 7th Symp. (Internat.) on Combustion, Butterworths Sci. Pub. (London), 1959, pp. 484–487.
243. Zebatakis, M. G., C. M. Mason, and R. W. Van Dolah. The Safety Characteristics of Normal Propyl Nitrate. BuMines Rept. of Inv. 6058, 1962, 26 pp.
244. Zabetakis, M. G., and J. K. Richmond. The Determination and Graphic Representation of the Limits of Flammability of Complex Hydrocarbon Fuels at Low Temperatures and Pressures. 4th Symp. (Internat.) on Combustion, Williams & Wilkins Co., Baltimore, Md., 1953, pp. 121–126.
245. Zabetakis, M. G., and B. H. Rosen. Considerations Involved in Handling Kerosine. Proc. Am. Petrol. Inst., sec. 3, v. 37, 1957, p. 296.
246. Zabetakis, M. G., G. S. Scott, and G. W. Jones. Limits of Flammability of Paraffin Hydrocarbons in Air. Ind. and Eng. Chem., v. 43, 1951, pp. 2120–2124.
247. ————. The Flammability Characteristics of the C_nH_{2n-6} Aromatic Series. BuMines Rept. of Inv. 4824, 1951, 9 pp.
248. Zabetakis, M. G., G. S. Scott, and R. E. Kennedy. Autoignition of Lubricants at Elevated Pressures. BuMines Rept. of Inv. 6112, 1962, 10 pp.
249. Zeldovich, Ia. B., S. M. Kogarko, and N. N. Simonov. An Experimental Investigation of Spherical Detonation of Gases. Zhurnal Tekh. Fiziki (J. Tech. Phys. (USSR)), v. 26, 1956, p. 1744.

761-928 O-65—8

APPENDIX A

TABLE A—*1. Summary of limits of flammability, lower temperature limits (T_L), and minimum autoignition temperatures* (AIT) *of individual gases and vapors in air at atmospheric pressure*

Combustible	Limits of flammability (volume-percent)		T_L (° C)	AIT (° C)
	L_{25}	U_{25}		
Acetal	1. 6	10	37	230
Acetaldehyde	4. 0	60	------	175
Acetic acid	[1] 5. 4	--------	40	465
Acetic anhydride	[2] 2. 7	[3] 10	47	390
Acetanilide	[4] 1. 0	--------	------	545
Acetone	2. 6	13	------	465
Acetophenone	[4] 1. 1	--------	------	570
Acetylacetone	[4] 1. 7	--------	------	340
Acetyl chloride	[4] 5. 0	--------	------	390
Acetylene	2. 5	100	------	305
Acrolein	2. 8	31	------	235
Acrylonitrile	3. 0	--------	−6	-----
Acetone Cyanohydrin	2. 2	12	------	-----
Adipic acid	[4] 1. 6	--------	------	420
Aldol	[4] 2. 0	--------	------	250
Allyl alcohol	2. 5	18	22	-----
Allyl amine	2. 2	22	------	375
Allyl bromide	[4] 2. 7	--------	------	295
Allyl chloride	2. 9	--------	−32	485
o-Aminodiphenyl	. 66	4. 1	------	450
Ammonia	15	28	------	-----
n-Amyl acetate	[1] 1. 0	[1] 7. 1	25	360
n-Amyl alcohol	[1] 1. 4	[1] 10	38	300
tert-Amyl alcohol	[4] 1. 4	--------	------	435
n-Amyl chloride	[5] 1. 6	[1] 8. 6	------	260
tert-Amyl chloride	[6] 1. 5	--------	−12	345
n-Amyl ether	[4]. 7	--------	------	170
Amyl nitrite	[4] 1. 0	--------	------	210
n-Amyl propionate	[4] 1. 0	--------	------	380
Amylene	1. 4	8. 7	------	275
Aniline	[7] 1. 2	[7] 8. 3	------	615
Anthracene	[4]. 65	--------	------	540
n-Amyl nitrate	1. 1	--------	------	195
Benzene	[1] 1. 3	[1] 7. 9	------	560
Benzyl benzoate	[4]. 7	--------	------	480
Benzyl chloride	[4] 1. 2	--------	------	585
Bicyclohexyl	[1] . 65	[8] 5. 1	74	245
Biphenyl	[9] . 70	--------	110	540
2-Biphenylamine	[4] . 8	--------	------	450
Bromobenzene	[4] 1. 6	--------	------	565
Butadiene (1,3)	2. 0	12	------	420
n-Butane	1. 8	8. 4	−72	405
1,3-Butandiol	[4] 1. 9	--------	------	395
Butene-1	1. 6	10	------	385
Butene-2	1. 7	9. 7	------	325
n-Butyl acetate	[5] 1. 4	[1] 8. 0	------	425
n-Butyl alcohol	[1] 1. 7	[1] 12	------	-----
sec-Butyl alcohol	[1] 1. 7	[1] 9. 8	-- 21	405
tert-Butyl alcohol	[1] 1. 9	[1] 9. 0	11	480
tert-Butyl amine	[1] 1. 7	[1] 8. 9	------	380
n-Butyl benzene	[1]. 82	[1] 5. 8	------	410
sec-Butyl benzene	[1] 0. 77	[1] 5. 8	------	420
tert-Butyl benzene	[1]. 77	[1] 5. 8	------	450
n-Butyl bromide	[1] 2. 5	--------	------	265
Butyl cellosolve	[8] 1. 1	[10] 11	------	245
n-Butyl chloride	1. 8	[1] 10	------	-----
n-Butyl formate	1. 7	8. 2	------	-----
n-Butyl stearate	[4]. 3	--------	------	355
Butyric acid	[4] 2. 1	--------	------	450
α-Butryolactone	[8] 2. 0	--------	------	-----
Carbon disulfide	1. 3	50	------	90
Carbon monoxide	12. 5	74	------	-----
Chlorobenzene	1. 4	--------	21	640
m-Cresol	[8] 1. 1	--------	------	-----
Crotonaldehyde	2. 1	[11] 16	------	-----
Cumene	[1]. 88	[1] 6. 5	------	425
Cyanogen	6. 6	--------	------	-----
Cycloheptane	1. 1	6. 7	------	-----
Cyclohexane	1. 3	7. 8	------	245
Cyclohexanol	[4] 1. 2	--------	------	300
Cyclohexene	[1] 1. 2	--------	------	-----
Cyclohexyl acetate	[4] 1. 0	--------	------	335
Cyclopropane	2. 4	10. 4	------	500
Cymene	[1]. 85	[1] 6. 5	------	435
Decaborane	. 2	--------	------	-----
Decalin	[1]. 74	[1] 4. 9	57	250
n-Decane	[12]. 75	[13] 5. 6	46	210
Deuterium	4. 9	75	------	-----
Diborane	. 8	88	------	-----
Diesel fuel (60 cetane)	--------	--------	------	225
Diethyl amine	1. 8	10	------	-----
Diethyl analine	[4]. 8	--------	80	630
1,4-Diethyl benzene	[1]. 8	--------	------	430
Diethyl cyclohexane	. 75	--------	------	240
Diethyl ether	1. 9	36	------	160
3,3-Diethyl pentane	[1]. 7	--------	------	290
Diethyl ketone	1. 6	--------	------	450
Düsobutyl carbinol	[1]. 82	[10] 6. 1	------	-----
Düsobutyl ketone	[1]. 79	[1] 6. 2	------	-----
2-4, Düsocyanate	--------	--------	120	-----
Düsopropyl ether	1. 4	7. 9	------	-----
Dimethyl amine	2. 8	--------	------	400
2,2-Dimethyl butane	1. 2	7. 0	------	-----
2,3-Dimethyl butane	1. 2	7. 0	------	-----
Dimethyl decalin	[1]. 69	[9] 5. 3	------	235
Dimethyl dichlorosilane	3. 4	--------	------	-----
Dimethyl ether	3. 4	27	------	350
n,n-Dimethyl formamide	[1] 1. 8	[1] 14	57	435
2,3-Dimethyl pentane	1. 1	6. 8	------	335
2,2-Dimethyl propane	1. 4	7. 5	------	450
Dimethyl sulfide	2. 2	20	------	205
Dimethyl sulfoxide	--------	--------	84	-----
Dioxane	2. 0	22	------	265
Dipentene	[8]. 75	[8] 6. 1	45	237
Diphenylamine	[4]. 7	--------	------	635

See footnotes at end of table.

Combustible	Limits of flammability (volume-percent)		T_L (° C)	AIT (° C)
	L_{25}	U_{25}		
Diphenyl ether	[4] 0.8			620
Diphenyl methane	[4] .7			485
Divinyl ether	1.7	27		
n-Dodecane	[4] .60		74	205
Ethane	3.0	12.4	−130	515
Ethyl acetate	2.2	11		
Ethyl alcohol	3.3	[11] 19		365
Ethyl amine	3.5			385
Ethyl benzene	[1] 1.0	[1] 6.7		430
Ethyl chloride	3.8			
Ethyl cyclobutane	1.2	7.7		210
Ethyl cyclohexane	[14] 2.0	[14] 6.6		260
Ethyl cyclopentane	1.1	6.7		260
Ethyl formate	2.8	16		455
Ethyl lactate	1.5			400
Ethyl mercaptan	2.8	18		300
Ethyl nitrate	4.0			
Ethyl nitrite	3.0	50		
Ethyl propionate	1.8	11		440
Ethyl propyl ether	1.7	9		
Ethylene	2.7	36		490
Ethyleneimine	3.6	46		320
Ethylene glycol	[4] 3.5			400
Ethylene oxide	3.6	100		
Furfural alcohol	[15] 1.8	[16] 16	72	390
Gasoline:				
100/130	1.3	7.1		440
115/145	1.2	7.1		470
Glycerine				370
n-Heptane	1.05	6.7	−4	215
n-Hexadecane	[4] .43		126	205
n-Hexane	1.2	7.4	−26	225
n-Hexyl alcohol	[1] 1.2			
n-Hexyl ether	[4] .6			185
Hydrazine	4.7	100		
Hydrogen	4.0	75		400
Hydrogen cyanide	5.6	40		
Hydrogen sulfide	4.0	44		
Isoamyl acetate	[1] 1.1	[1] 7.0	25	360
Isoamyl alcohol	[1] 1.4	[1] 9.0		350
Isobutane	1.8	8.4	−81	460
Isobutyl alcohol	[1] 1.7	[1] 11		
Isobutyl benzene	[1] .82	[10] 6.0		430
Isobutyl formate	2.0	8.9		
Isobutylene	1.8	9.6		465
Isopentane	1.4			
Isophorone	.84			460
Isopropylacetate	[4] 1.7			
Isopropyl alcohol	2.2			
Isopropyl biphenyl	[4] .6			440
Jet fuel:				
JP-4	1.3	8		240
JP-6				230
Kerosine				210
Methane	5.0	15.0	−187	540
Methyl acetate	3.2	16		
Methyl acetylene	1.7			
Methyl alcohol	6.7	[11] 36		385
Methyl amine	[4] 4.2			430
Methyl bromide	10	15		
3-Methyl butene-1	1.5	9.1		
Methyl butyl ketone	[5] 1.2	[1] 8.0		
Methyl cellosolve	[17] 2.5	[7] 20		380
Methyl cellosolve acetate	[8] 1.7		46	
Methyl ethyl ether	[4] 2.2			

Combustible	Limits of flammability (volume-percent)		T_L (° C)	AIT (° C)
	L_{25}	U_{25}		
Methyl chloride	[4] 7			
Methyl cyclohexane	1.1	6.7		250
Methyl cyclopentadiene	[1] 1.3	[1] 7.6	49	445
Methyl ethyl ketone	1.9	10		
Methyl ethyl ketone peroxide			40	390
Methyl formate	5.0	23		465
Methyl cyclohexanol	[4] 1.0			295
Methyl isobutyl carbinol	[4] 1.2		40	
Methyl isopropenyl ketone	[5] 1.8	[5] 9.0		
Methyl lactate	[1] 2.2			
α-Methyl naphthalene	[4] .8			530
2, Methyl pentane	[4] 1.2			
Methyl propionate	2.4	13		
Methyl propyl ketone	1.6	8.2		
Methyl styrene	[4] 1.0		49	495
Methyl vinyl ether	2.6	39		
Methylene chloride				615
Monoisopropyl bicyclohexyl	.52	[18] 4.1	124	230
2-Monoisopropyl biphenyl	[10] .53	[18] 3.2	141	435
Monomethylhydrazine	4			
Naphthalene	[19] .88	[20] 5.9		526
Nicotine	[1] .75			
Nitroethane	3.4		30	
Nitromethane	7.3		33	
1-Nitropropane	2.2		34	
2-Nitropropane	2.5		27	
n-Nonane	[21] .85		31	205
n-Octane	0.95		13	220
Paraldehyde	1.3			
Pentaborane	.42			
n-Pentane	1.4	7.8	−48	260
Pentamethylene glycol				335
Phthalic anhydride	[7] 1.2	[22] 9.2	140	570
3-Picoline	[4] 1.4			500
Pinane	[23] .74	[23] 7.2		
Propadiene	2.16			
Propane	2.1	9.5	−102	450
1,2-Propandiol	[4] 2.5			410
β-Propiolactone	[3] 2.9			
Propionaldehyde	2.9	17		
n-Propyl acetate	1.8	8		
n-Propyl alcohol	[12] 2.2	[1] 14		440
Propyl amine	2.0			
Propyl chloride	[4] 2.4			
n-Propyl nitrate	[17] 1.8	[17] 100	21	175
Propylene	2.4	11		460
Propylene dichloride	[4] 3.1			
Propylene glycol	[24] 2.6			
Propylene oxide	2.8	37		
Pyridine	[11] 1.8	[25] 12		
Propargyl alcohol	[5] 2.4			
Quinoline	[4] 1.0			
Styrene	[26] 1.1			
Sulfur	[27] 2.0		247	
p-Terphenyl	[4] .96			535
n-Tetradecane	[4] .5			200
Tetrahydrofurane	2.0			
Tetralin	[1] .84	[8] 5.0	71	385

See footnotes at end of table.

TABLE A—*1. Summary of limits of flammability, lower temperature limits (T_L) and minimum autoignition temperatures (AIT) of individual gases and vapors in air at atmospheric pressure*—Continued

Combustible	Limits of flammability (volume-percent)		T_L (° C)	AIT (° C)
	L_{25}	U_{25}		
2,2,3,3-Tetramethyl pentane	0.8	------	------	430
Tetramethylene glycol	------	------	------	390
Toluene	[1] 1.2	[1] 7.1	------	480
Trichloroethane	------	------	------	500
Trichloroethylene	[28] 12	[25] 40	30	420
Triethyl amine	1.2	8.0	------	-----
Triethylene glycol	[8] 9	[28] 9.2	------	-----
2,2,3-Trimethyl butane	1.0	------	------	420
Trimethyl amine	2.0	12	------	-----
2,2,4-Trimethyl pentane	.95	------	------	415
Trimethylene glycol	[4] 1.7	------	------	400
Trioxane	[4] 3.2	------	------	-----
Turpentine	[1] 7	------	-----	-----
Unsymmetrical dimethylhydrazine	2.0	95	------	-----
Vinyl acetate	2.6	------	------	-----
Vinyl chloride	3.6	33	------	-----
m-Xylene	[1] 1.1	[1] 6.4	------	530
o-Xylene	[1] 1.1	[1] 6.4	------	465
p-Xylene	[1] 1.1	[1] 6.6	------	530

[1] t=100° C.
[2] t=47° C.
[3] t=75° C.
[4] Calculated.
[5] t=50° C.
[6] t=85° C.
[7] t=140° C.
[8] t=150° C.
[9] t=110° C.
[10] t=175° C.
[11] t=60° C.
[12] t=53° C.
[13] t=86° C.
[14] t=130° C.
[15] t=72° C.
[16] t=117° C.
[17] t=125° C.
[18] t=200° C.
[19] t=78° C.
[20] t=122° C.
[21] t=43° C.
[22] t=195° C.
[23] t=160° C.
[24] t=96° C.
[25] t=70° C.
[26] t=29° C.
[27] t=247° C.
[28] t=30° C.
[29] t=203° C.

APPENDIX B

STOICHIOMETRIC COMPOSITION

The stoichiometric composition (C_{st}) of a combustible vapor $C_nH_mO_\lambda F_k$ in air may be obtained from the equation

$$C_nH_mO_\lambda F_k+\left(n+\frac{m-k-2\lambda}{4}\right)O_2\rightarrow nCO_2 \pm\left(\frac{m-k}{2}\right)H_2O+kHF.$$

Thus, $C_{st}=\dfrac{100}{1+4.773\left(n+\dfrac{m-k-2\lambda}{4}\right)}$ volume-percent, where 4.773 is the reciprocal of 0.2095, the molar concentration of oxygen in dry air. The following table lists the values of C_{st} for a range of $\left(n+\dfrac{m-k-2\lambda}{4}\right)$ values from 0.5 to 30.75:

N[1]	0	0.25	0.50	0.75
0			29. 53	21. 83
1	17. 32	14. 35	12. 25	10. 69
2	9. 48	8. 52	7. 73	7. 08
3	6. 53	6. 05	5. 65	5. 29
4	4. 97	4. 70	4. 45	4. 22
5	4. 02	3. 84	3. 67	3. 51
6	3. 37	3. 24	3. 12	3. 01
7	2. 90	2. 81	2. 72	2. 63
8	2. 55	2. 48	2. 40	2. 34
9	2. 27	2. 21	2. 16	2. 10
10	2. 05	2. 00	1. 96	1. 91
11	1. 87	1. 83	1. 79	1. 75
12	1. 72	1. 68	1. 65	1. 62
13	1. 59	1. 56	1. 53	1. 50
14	1. 47	1. 45	1. 42	1. 40
15	1. 38	1. 36	1. 33	1. 31
16	1. 29	1. 27	1. 25	1. 24
17	1. 22	1. 20	1. 18	1. 17
18	1. 15	1. 13	1. 12	1. 10
19	1. 09	1. 08	1. 06	1. 05
20	1. 04	1. 02	1. 01	1. 00
21	. 99	. 98	. 97	. 95
22	. 94	. 93	. 92	. 91
23	. 90	. 89	. 88	. 87
24	. 87	. 86	. 85	. 84
25	. 83	. 82	. 81	. 81
26	. 80	. 79	. 78	. 78
27	. 77	. 76	. 76	. 75
28	. 74	. 74	. 73	. 72
29	. 72	. 71	. 71	. 70
30	. 69	. 69	. 68	. 68

[1] $N=n+\dfrac{m-k-2\lambda}{4}$; where n, m, λ, and k are the number of carbon, hydrogen, oxygen, and halogen atoms, respectively, in the combustible.

For example, the stoichiometric mixture composition of acetyl chloride (C_2H_3OCl) in air may be found by noting that

$$N=n+\frac{m-k-2\lambda}{4}=2+\frac{3-1-2}{4}=2.0.$$

The entry for $N=2.0$ in the preceding table is 9.48 volume-percent, which is the value of C_{st} for this combustible in air.

APPENDIX C

HEAT CONTENTS OF GASES

(Kcal/mole[1])

T, ° K	CO_2	H_2O	O_2	N_2
298. 16	0	0	0	0
300	. 017	. 014	. 013	. 013
400	. 941	. 823	. 723	. 709
500	1. 986	1. 653	1. 4541	1. 412
600	3. 085	2. 508	2. 2094	2. 125
700	4. 244	3. 389	2. 9873	2. 852
800	5. 452	4. 298	3. 7849	3. 595
900	6. 700	5. 238	4. 5990	4. 354
1,000	7. 983	6. 208	5. 4265	5. 129
1,100	9. 293	7. 208	6. 265	5. 917
1,200	10. 630	8. 238	7. 114	6. 717
1,300	11. 987	9. 297	7. 970	7. 529
1,400	13. 360	10. 382	8. 834	8. 349
1,500	14. 749	11. 494	9. 705	9. 178
1,600	16. 150	12. 627	10. 582	10. 014
1,700	17. 563	13. 785	11. 464	10. 857
1,800	18. 985	14. 962	12. 353	11. 705
1,900	20. 416	16. 157	13. 248	12. 559
2,000	21. 855	17. 372	14. 148	13. 417
2,100	23. 301	18. 600	15. 053	14. 278
2,200	24. 753	19. 843	15. 965	15. 144
2,300	26. 210	21. 101	16. 881	16. 012
2. 400	27. 672	22. 371	17. 803	16. 884
2,500	29. 140	23. 652	18. 731	17. 758

[1] Gordon, J. S. Thermodynamics of High Temperature Gas Mixtures and Application to Combustion Problems. WADC Technical Report 57-33, January 1957, 172 pp.

APPENDIX D

DEFINITIONS OF PRINCIPAL SYMBOLS

Symbol:	*Definition*
A	Constant.
A'	Area.
a	Velocity of sound.
B	Constant.
C_{st}	Stoichiometric composition.
ΔH_c	Heat of combustion.
K	Ratio of duct area to vent area.
k	Thermal conductivity.
L	Lower limit of flammability.
L^*	Modified lower limit value.
L_{Ave}	Average carbon chain length for paraffin hydrocarbons and correlation parameter for aromatic hydrocarbons.
L_t	Lower limit of flammability at $t°$ C.
L/D	Length to diameter ratio.
M	Molecular weight.
M_1	Mach number.
NO_2^*	Equilibrium mixture of NO_2 and N_2O_4 at a specified temperature and pressure.
n	Number of moles.
P	Pressure.
P_m	Maximum pressure.
ΔP	Pressure rise.
p	Partial pressure.
S_u	Burning velocity.
T	Absolute temperature.
t	Temperature.
τ	Time delay before ignition.
U	Upper limit of flammability.
U_t	Upper limit of flammability at $t°$ C.
V	Volume.
V'	Critical approach velocity.
v	Liquid regression rate.
γ	Specific heat ratio.

SUBJECT INDEX

	Page
A	
Acetaldehyde	73
Acetylenic hydrocarbons	53
Air-fuel ratio	21
Alcohols	65
Aldehydes	73
Ammonia	77
n-Amyl alcohol	67
Aromatic hydrocarbons	59
Autoignition	4, 32, 41
B	
Barricades	17
Blast pressure	16
Burgess-Wheeler law	22
Burning velocity	42, 45
Butadiene	48, 53
n-Butane	21, 25, 32
Butene-1	48, 50, 52
n-Butyl alcohol	67
tert-Butyl alcohol	68
C	
Carbon chain	41
Carbon monoxide	97
Combustion equations	21, 117
Contact time	4
Cool flames	28
Copper acetylide	56
Critical C/N	11
Cyclopropane	64
D	
n-Decane	21, 25
Decane-dodecane blends	32, 43
Decomposition	51
Deflagration	15
Detonation	16, 57
Dimethyl ether	70
n-Dodecane	21, 25
E	
Engine oils	95
Esters	70
Ethane	21, 25, 28
Ethers	69
Ethyl alcohol	67
2-Ethyl butanol	67
Ethylene	48, 52
F	
Flame arrestors	18
Flame caps	2
Flame extinction	29
Flammability characteristics	20
Foam	8
Formic acid	61
Freon-12	69
Fuel-air ratio	21
Fuel blends	74
G	
Gas freeing	13
Gas mixtures	3
Gasoline	13, 82
H	
Halogenated hydrocarbons	102
Heat of formation	51
n-Heptane	21, 25, 35
Heterogeneous mixtures	3
n-Hexadecane	21, 25
n-Hexane	21, 25, 34
n-Hexyl alcohol	67
Hydraulic fluids	95
Hydrogen	77, 89
Hydrogen peroxide	61
I	
Ignition	3
Ignition temperature	4
Ignitibility limits	2
Inerting	18
Isobutylene	48
J	
JP-4	11, 88
K	
Kerosine	7
Ketones	73
L	
Layering	3
Le Chatelier's law	31
Limits of flammability	2
Liquid mixtures	31
Lower limit	2
Low pressure limits	12, 89
M	
Methane	9, 21
Methyl acetylene	55
Methyl alcohol	67
Methyl bromide	28, 61
3-Methyl butene-1	48
Methyl formate	71
Methylene bistearamide	7
Methylene chloride	102
Minimum oxygen value	11
Mists	3, 6
Mixer	4, 7
N	
Natural gas	27, 30
n-Nonane	21, 25
O	
n-Octane	21, 25
P	
Paraffin hydrocarbons	20, 36
n-Pentadecane	21
Pentane	24
n-Pentane	21, 25, 33
Perfluoromethane	28
Perfluoropropane	28
Peroxides	53, 70, 103
Predetonation distance	57
Pressure piling	58
Propadiene	48

	Page
Propane	21, 25, 31
Isopropyl alcohol	115
n-Propyl alcohol	67
n-Propyl nitrate	97
Propylene	48, 51

Q

Quantity-distance relationships	95

R

Raoult's law	31
Rectangular diagram	9
Regression rate	44
Relief diaphragms	18

S

Shock wave	17
Spark-energy requirements	3
Spontaneous ignition	3
Spray injection	97
Sprays	6
Sulfur compounds	74
Sulfur hexafluoride	28

T

Temperature limit	11
n-Tetradecane	21
Tetralin	7
Time delay	4
Town gas	19
Triangular diagram	9
Trichloroethylene	102
n-Tridecane	21
Tube diameter	3, 53, 57

U

n-Undecane	21
Unsaturated hydrocarbons	47
Upper limit	2, 23, 26

W

Wall quenching	3

X

o-Xylene	60

U.S. GOVERNMENT PRINTING OFFICE : 1965 O—761-928

A603: Limiting Oxygen - Impacts on Flammability

The limiting oxygen concentration and flammability limits of gases and gas mixtures

Isaac A. Zlochower*, Gregory M. Green

Pittsburgh Research Laboratory, National Institute for Occupational Safety and Health, Pittsburgh, PA 15236, USA

A B S T R A C T

This paper presents data on the limiting (minimum) oxygen concentration (LOC), in the presence of added N_2, of methane (CH_4), propane (C_3H_8), ethylene (C_2H_4), carbon monoxide (CO), and hydrogen (H_2), and some of their binary mixtures. It also addresses the issue of the flammable concentration (flammability) limits of these pure gases in air. The study is based on spark ignited explosions in large, spherical laboratory vessels (120-L and 20-L) using a 7% pressure-rise criterion for explosion propagation. The results of the study are compared with the older values which used long flammability tubes with a diameter $\geq$5 cm together with visual evidence of substantial upward propagation. They are also compared to results reported recently using a 12-L spherical flask with a visual flame propagation criterion. Finally, they are compared to results reported in Europe using more modest flammability criteria and smaller chambers.

The findings reported here show excellent agreement between the 120-L and 12-L results, good agreement with the 20-L results, and reasonable agreement with the earlier flammability tube values for the lower flammability limits. They disagree, however, with the more conservative European values. These results and those from the 12-L experiments also feature lower LOCs than are given by traditional flammability tubes. A model for the LOCs of such fuel mixtures based on the Le Chatelier mixture rule for lower flammable limits is seen to reasonably fit the observed results on binary mixtures and can accommodate more complex mixtures as well. One such set of ternary mixtures containing CH_4 and 1:1 CO:H_2 is well fitted by the model.

1. Introduction

Starting with basic definitions, the lower and upper flammability (or explosibility) limits (LFL and UFL, respectively) are the limiting fuel concentrations in air that can support flame propagation and lead to an explosion. Fuel concentrations outside those limits are non-flammable. The progressive addition of an inert gas to a fuel–air mixture causes the narrowing of the flammability range to the point where the two limits coincide. The limiting oxygen concentration (LOC) is the minimum O_2 concentration in a mixture of fuel, air, and an inert gas that will propagate flame. In this paper, the inert gas will be nitrogen. In practice, the limits (LFL, UFL, and LOC) represent an average between the neighboring concentrations inside and outside the experimental flammability limits (ASTM International, 2008a, 2008b).

There is currently a significant difference of opinion between American and European based standard-setting organizations as to the prescribed test vessels and criteria for flammability and LOC determinations (ASTM International, 2008a, 2008b; British and European Standard, 2003, 2007). The traditional criterion used in the US, which was the basis of an extensive database of flammability limits, required that flame and explosion propagation be distinguished from ignition phenomena (Coward & Jones, 1952; Kuchta, 1985). In order to demonstrate unambiguous flame propagation, U.S. standards required that flame be observed at some distance from the ignition source and to have traveled through a significant fraction of the enclosed volume. That requirement was relaxed in a more recent US standard that featured the use of a 5-L spherical glass flask, and mandated only that flame propagation be established by evidence of horizontal as well as vertical flame travel (ASTM International, 2008a). Where ambiguity resulted, the standard called for using a larger (12-L) flask with a more extensive flame evolution – a flame cone with an arc spanning at least 90° at the top of the flask, as measured from the point of ignition (ASHRAE, 2007; ASTM International, 2008a). The explosion overpressure in a closed system was, correspondingly, mandated to be 7%,[1] i.e.,

* Corresponding author. Tel.: +1 412 386 4960; fax: +1 412 386 6595.
E-mail address: iaz0@cdc.gov (I.A. Zlochower).

[1] A 7% pressure increase represents a 1 psi increase starting at 1 bar (14.5 psia) or 1 atm (14.7 psia).

a significant percentage of the initial value (ASTM International, 2008b). Although the exact flame travel distance or overpressure required for designation as a true flame propagation and explosion is somewhat subjective and apparatus-dependent, any attempt to minimize such requirements will lead to results that are subjective, apparatus-dependent, and overly conservative. Adding further to the problem, the flammability limits and LOCs when traditionally determined have no built-in safety factors. In practice, therefore, such factors must be imposed. For example, NFPA 69 requires that the fuel concentration only reach 25% of the LFL value (or 60% of the LFL for gaseous systems with automated in-line sensors and controls) (NFPA 69, 2008). Imposing these factors has been the long-standing practice in the US (MSHA, 1996; NFPA 69, 2008).

The current standard adopted by the European Union, based on the earlier German standard (DIN 51649, 1986), is a radical departure from the above considerations. In that standard (EN 1839T), a separation of flame 10 cm above the 0.2–0.5 s induction spark in an 8×30 cm cylinder defines a flammable mixture. The same is true if the flame extends to 24 cm without separation from the spark electrodes. The result is basically to substitute an ignitability criterion for flammability. For a closed spherical or cylindrical system with a minimum volume of 5-L and using such a centrally located induction spark, or fuse wire of 10–20 J nominal energy (EN 1839T), the corresponding criterion is a 5% pressure rise above that given by the source alone (British and European Standard, 2003). Other European researchers go further and insist that any separation of flame from the ignition spark bespeaks a flammable mixture (meaning ignitable). The same applies to an overpressure that is just measurable (2%) (De Smedt et al., 1999). The LFLs and LOCs resulting from such minimal flame propagation criteria are, understandably, lower than those resulting from the traditional ones since they have a built-in safety factor. Despite these concerns the primary purpose of this article is not to critique the European methodology, but to alert the readers to the current existence of incompatible flammability databases; the US database (Coward & Jones, 1952; Kuchta, 1985; NFPA, 2008; Zabetakis, 1965) and the European one (CHEMSAFE, 2007). More refined techniques often lead to the revision of earlier data and to progress in the field of study. Revisions based on new arbitrary criteria, however, tend to produce confusion. Moreover, the incompatible databases may lead to the misapplication of traditional safety factors to the already conservative European data. This caution has already been issued by Britton (2002) and is echoed in this paper.

2. Experimental

The flammability data reported here were obtained in the spherical 120-L and 20-L chambers used in earlier studies (Cashdollar, Zlochower, Green, Thomas, & Hertzberg, 2000). The internal diameter of the 120-L chamber is 60 cm and its pressure rating is 69 bar. Instrumentation includes a sensitive strain-gauge pressure transducer to measure the partial pressures as the gases are added and mixed, and a higher capacity strain-gauge pressure transducer to monitor the explosion pressure. The strain-gauges have a response time of 1 ms. The pressure transducers were mounted on the top and bottom flanges of the chamber. A fine wire thermocouple near the top of the chamber was used to record the steady-state temperature after the addition of each gaseous component. There were also ports with ball valves for connection to a vacuum pump and vent. An internal non-sparking fan at the bottom of the vessel was used to mix the gases. The gases were added via a manifold and controlled via manual switches in an isolated control room where the additions, pressure monitoring, mixing and spark ignition initiation, and PC recording were conducted.

The spark ignition system consisted of 3-mm diameter metal rod electrodes with a durable plastic spacer for rigidity. The pointed spark electrodes terminated below the center of the sphere and were bent to face each other with a gap of 6 mm. The electrical energy so delivered came from a 1300 μF capacitor charged to 300 V which was then discharged through a transformer to generate a strong spark. This spark was powered by a stored energy on the capacitor of 58 J based on the equation: stored energy $= 1/2CE^2$, where C is the capacitance and E is the voltage. The actual electrical energy in the spark gap was considerably less, however, because of the low efficiency of the transformer circuit (Hertzberg, Conti, & Cashdollar, 1985).

The calibrations of the pressure transducers were checked daily using the internal shunt calibration resistors provided by the manufacturer. Samples of the gas mixtures could be collected in evacuated test tubes through a sampling needle on the side of the chamber. These samples were then analyzed by gas chromatography (GC). During the initial evaluation of the mixing efficiency in the 120-L chamber, samples of H_2–air mixtures were collected after the gases had been added to the chamber and after 2 and 5 min of mixing by the fan. There was essentially no difference in the measured concentrations of H_2 for the gas mixtures over this time period, showing that there was good mixing of the gases even before the fan was turned on. The reported concentrations are in mole (volume) percent, based on the partial pressure of the component relative to the total pressure. It was noted that the addition of gas to a fully or partially evacuated chamber led to an increase in temperature due, presumably, to quasi-adiabatic compression of the prior atmosphere. This temperature rise was allowed to fall to a steady-state value. That temperature was then used to correct all the component partial pressures to a common (final) temperature using the ideal gas law.

The 20-L chamber, with a pressure rating of over 20 bar, is nearly spherical, having a diameter of 30 cm and a height of 35 cm. The ceramic encased electrodes were located slightly below the mid-height of the chamber, and the exposed, pointed steel tips were spaced 6 mm apart. The charging circuit was similar to that used for the 120-L sphere except that an 800 μF capacitor was charged to 300 V, giving a nominal stored energy of 36 J. The actual thermal energy deposited in the chamber, based on the observed pressure increase due to the spark, was 0.5–1 J. The partial pressures of the gaseous components were measured as above or via a sensitive, temperature-controlled capacitance manometer that had a resolution of 0.1 torr (0.13 mbar) over a range of 1000 torr (1.33 bar). This unit was calibrated by the manufacturer prior to use.

The data from the pressure transducers and the thermocouple were recorded using a high speed analog to digital (A/D) board in a personal computer (PC). This system can sample the data from various instrument channels, usually at speeds less than 20 kHz per channel. An in-house computer software program converted the raw data to engineering units, plotted the data vs. time, and allowed various data smoothing options. Maximum pressure and maximum rate of pressure-rise values were obtained from the pressure vs. time traces. The reproducibility of the flammability data was checked by repeated tests over a period of months and years.

The experimental determination of the flammability limits of the gases studied was done by fully evacuating the chamber and then admitting the fuel gas to the predetermined partial pressure required to produce the desired final concentration in air. Dry, oil-free air was admitted from a compressed gas cylinder to give the desired final pressure of 1 bar (the ambient pressure at the elevation of the laboratory was always less than that final pressure). The temperature in the chamber rose during the addition of both the fuel and air, as previously noted, and the gas was allowed to come to a steady-state temperature and pressure. The temperature of the fuel gas was then used to correct the fuel pressure to that

corresponding to the final temperature of the mixture according to the ideal gas law. The final concentration of the fuel gas was then calculated from its corrected pressure. Next, the non-sparking internal fan was started and run for at least 4 min to fully mix the gases. The fan was shut off and the generated turbulence was allowed to subside for 1 min. The capacitor spark ignition system was then charged to 300 V and discharged through an ignition coil to create the high voltage spark. The series of sparks thereby produced lasted for about 0.1 s.

The initial concentrations of fuel gas chosen were based on the literature values for the flammability limits or on prior determinations using such chambers. Once marginal explosion pressures were produced, the concentrations were changed in small steps (0.1–0.2%) for the LFL and UFL measurements of methane, propane, ethylene, and CO. The concentration step for the LFL of hydrogen was 0.5–1% owing to the low sensitivity of the explosion pressure to concentration near the LFL (Cashdollar et al., 2000).

The LOC measurements were made starting at fuel concentrations near the LFL and using oxygen concentrations (from the air and nitrogen additions) that were near the LFL multiplied by the stoichiometric oxygen/fuel ratio (the "R" column in Table 1). The oxygen concentration was varied in steps of 0.2% until the marginal explosion conditions were delineated and verified. Then the fuel concentration was changed and the minimum oxygen concentration again determined. The process was repeated until a global minimum oxygen concentration (LOC) with added N_2 was established.

3. Results and discussion: single fuels

Previous results (Cashdollar et al., 2000) for the LFL of H_2 in the 120-L sphere using spark ignition showed a slow, linear increase in explosion pressure with concentration below 7%, followed by an accelerated increase above 7%. The pressure rise became steep at 8% H_2. The LFL of H_2 is thus quite sensitive to the pressure criterion for explosion propagation. The 7% pressure-rise criterion for spark ignition yielded an LFL of 7% in this chamber. The explosion pressure rise also occurred gradually with low H_2 concentrations in the 20-L chamber (below 8% H_2), but with a steeper slope. In the 20-L chamber, the 7% pressure-rise criterion was satisfied at 6% H_2 in air. With a meter-long upward flame propagation criterion in vertical flammability tubes, the LFL was found to be 4%. The much shorter 30 cm tubes used in the EN 1839 (T) method gave an LFL of 3.6% (Schroder & Molnarne, 2005). The tube values are based on the buoyant rise of small flame kernels which represent only a small fraction of fuel consumed and a correspondingly minimal pressure rise. Measurements in a 14-L closed sphere gave an LFL of 4.2% (Schroder & Molnarne, 2005), but the use of fuse wire ignition rather than the weaker and more localized spark ignition is believed to have unduly influenced the pressure rise associated with partial propagation (5%). A more robust explosion pressure-rise criterion (7%) for hydrogen in larger chambers would appear to be better correlated with actual explosion hazards.

There is less data for the UFL in the 120-L sphere. However, the sharp drop in explosion pressure beyond 75.7% hydrogen (the pressure rise is near zero at 76%) argues against a significant dependence of UFL on the above pressure criterion. The UFL is estimated as 75.9% H_2, the midpoint between these values. Previously, a value of 76.8% was reported by Cashdollar et al. (2000), but that value was obtained in an 8-L chamber. The LFL in that chamber was also found to be lower (5%) than in the larger (20-L and 120-L) chambers. Similarly high UFLs were given in the tests run according to the EN 1839 standard (76.6%, tube and 77.0%, closed sphere). Given the sensitivity of hydrogen flammability to the experimental conditions and chamber volume, the above relative difference of 1% for the UFL is not surprising.

The data on explosion pressures at different oxygen vs. hydrogen concentrations in air–nitrogen mixtures is given in Fig. 1, where the legend symbols represent pressure-rise ranges. In other words, Fig. 1 and the subsequent figures for LOC data are pressure parameter plots for given O_2 and fuel concentrations, with the different symbols representing different pressure-rise levels. Fig. 1 shows a minimum oxygen concentration (LOC) of 4.6% that is independent of hydrogen concentration in the range of 10–30%. More typically, however, the minimum oxygen concentration for an inert fuel–air mixture occurs at a narrow range of fuel concentrations. Those "worst-case" fuel concentrations define the LOC for the fuel–air mixture containing the inert gaseous additive (e.g. N_2).

The results for the LFL of CO are similar to that of H_2, but feature a steeper rise in pressure with concentration. They are also dependent on the amount of water vapor present in the mixture. In contrast to the ordinary behavior of water as an effective inhibitor of explosions due to its large heat capacity, here it is an accelerant – at least at low concentrations. It functions, presumably, by supplying the H and OH free radicals for the branching chain reactions needed

Table 1
Flammability/LOC: 120-L and 20-L closed vessel results vs. 12-L glass sphere and flammability tube.

Fuel (F)	Vessel	Stoichiometric equation	Mole ratio (R) (O_2/F)	LFL (mol%)	UFL (mol%)	LOC (N_2) (mol%)	Explosion criterion
Hydrogen (H_2)	120-L	$2H_2 + O_2 = 2H_2O$	**0.5**	**7**	**75.9**	**4.6**	Pressure
	20-L			**6**		**4.7**	Pressure
	Flam.[a] tube			**4**	**75.0**	**5.0**	Visual
Carbon monoxide (CO)	120-L	$2CO + O_2 = 2CO_2$	**0.5**	**12.2**	**72.0**	**5.1**	Pressure
	12-L[b]			**12.2**	**72.5**		Visual
	Flam.[a] tube			**12.5**	**74.0**	**5.5**	Visual
Methane (CH_4)	120-L	$CH_4 + 2O_2 = CO_2 + 2H_2O$	**2**	**5.0**	**15.8**	**11.1**	Pressure
	20-L			**4.9**	**15.9**	**10.7**	Pressure
	12-L[b]			**4.9**	**15.8**	**11.3**	Visual
	Flam.[a] tube			**5.0**	**15.0**	**12.0**	Visual
Ethylene (C_2H_4)	120-L	$C_2H_4 + 3O_2 = 2CO_2 + 2H_2O$	**3**	**2.7**	**31.4**	**8.5**	Pressure
	12-L[b]			**2.7**	**31.5**	**8.6**	Visual
	Flam.[a] tube			**2.7**	**36.0**	**10.0**	Visual
Propane (C_3H_8)	120-L	$C_3H_8 + 5O_2 = 3CO_2 + 4H_2O$	**5**	**2.0**	**9.8**	**10.7**	Pressure
	12-L[b]			**2.0**	**10.0**	**10.5**	Visual
	Flam.[a] tube			**2.1**	**9.5**	**11.5**	Visual

[a] Flammability tube data summarized by Kuchta (1985).
[b] The data from a 12-L spherical flask by Kondo et al. (2006, 2008).

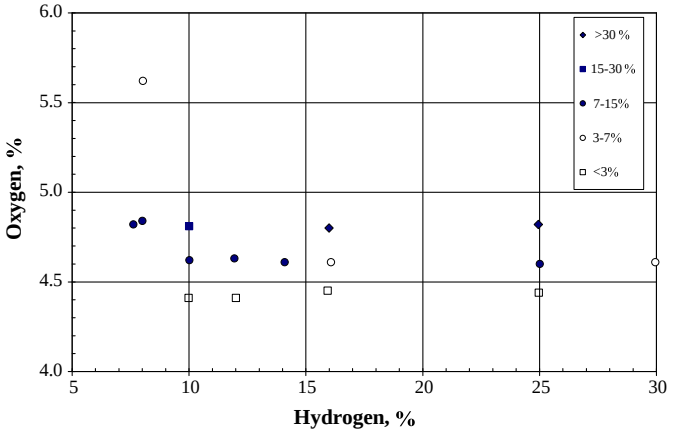

Fig. 1. LOC data on H_2 in air with added N_2 that was obtained in the 120-L sphere. Parametric pressure plot at different O_2 vs. H_2 concentrations, with the symbols representing different pressure-rise ranges.

for combustion and for rapid flame propagation. The measured LFL is 12.2% when the mixture is nearly saturated with water. Similarly, the UFL is 72% for near saturation. The results in the 12-L glass sphere for CO in moist air with added N_2 (LFL = 12.2%, UFL = 72.5%) that was reported by Kondo, Takizawa, Takahashi, Tokuhashi, and Sekiya (2008) agrees with the 120-L values (based on their listed uncertainty of 0.5% for the UFL). Fig. 2 shows an LOC in the 120-L sphere of about 5.1% O_2 for gas mixtures nearly saturated with water vapor. That LOC occurs near a 20% CO concentration.

The above results represent atypical fuels that are lighter and more diffusive than O_2 (H_2), or have branching chain reactions associated with flame propagation that are more difficult to establish (CO). Hydrogen, for example, is more concentrated at the flame front (i.e., the real fuel concentration at the flame front is higher than the nominal value) which clearly impacts the LFL value (Cashdollar et al., 2000; Hertzberg, 1989). More typical flammable gases – namely, the common hydrocarbons: methane (CH_4), the primary constituent of natural gas; propane (C_3H_8), the popular cooking and heating fuel; and ethylene (C_2H_4), a basic chemical feedstock for polyethylene and other plastics – were studied as well.

Cashdollar et al. (2000) have reported 120-L data on the LFL of methane in air which show a gradual increase in pressure from 4.6 to 5.0%. There is little reason, however, to dispute the choice of 5.0% as the LFL of methane. Both the pressure criterion of 7% and the existence of a discontinuous change in slope yield the same LFL value. The corresponding UFL is 15.8% based on the newer data. The same value is the average of the values reported by Cashdollar et al. (2000) for the 120-L and 20-L chambers (15.7 and 15.9%, respectively), while the LFL was 5.0% for both chambers. The 12-L glass sphere gave an LFL of 4.9% and a UFL of 15.8% (Kondo, Takizawa, Takahashi, & Tokuhashi, 2006).

Fig. 3 shows an LOC of 11.1% O_2 for 5.2–5.8% CH_4 in air–N_2 mixtures in the 120-L sphere, but the LOC was found to be 10.7% O_2 in the 20-L chamber. The 12-L sphere gave a value of 11.3%, as reported by Kondo et al. (2006). The lower value given by the 20-L chamber may indicate the need for a higher pressure-rise criterion in chambers appreciably smaller than 120-L (Brandes & Ural, 2008).

Past work (Cashdollar et al., 2000) gave an LFL value for propane of 2.05% with a sharp rise in pressure with concentration. The pressure drop with concentration near the UFL was more gradual. It was found to be 9.8% for the 7% pressure criterion. Current results in the 120-L sphere are consistent with the earlier findings. The LOC of propane is seen to be about 10.7% % at 2.5–2.7% propane (Fig. 4). The 12-L glass sphere results of Kondo et al. (2006) gave an LFL of 2.0%, a UFL of 10.0%, and an LOC of 10.5%, again in agreement with the 120-L results.

Ethylene also features a sharp rise in pressure with concentration at low concentrations and a slower decline in pressure near the UFL. The LFL is found to be 2.7% and the UFL is 31.4% using the 7% criterion. The LOC is seen to be 8.5% O_2 at 2.9–3.2% ethylene (Fig. 5). The 12-L results of Kondo et al. (2006) yielded an LFL of 2.7%, a UFL of 31.5%, and an LOC = 8.6%.

The 120-L and 20-L data are summarized in Table 1 together with the reported results from the 12-L sphere (Kondo et al., 2006, 2008) and flammability tubes (Kuchta, 1985). The reported results from the 12-L glass sphere are essentially identical to the results obtained here in the 120-L sphere despite the great difference in volume and propagation criterion.

A good reflection of the difference between the US and European standards is given by the LFLs of methane in air. Traditionally, this value has been listed as 5.0% based on the results of flame propagation studies using a large upward propagation distance in tall, wide containers (Britton, 2002; Coward & Jones, 1952), in closed, larger spherical vessels (120-L and 20-L), and in a very large spherical vessel (Cashdollar et al., 2000). The European Standard (Annex E) using a 5% pressure-rise criterion in a small vessel (EN 1839B) gave 4.6% as the LFL. Using the flame detachment criterion in a small

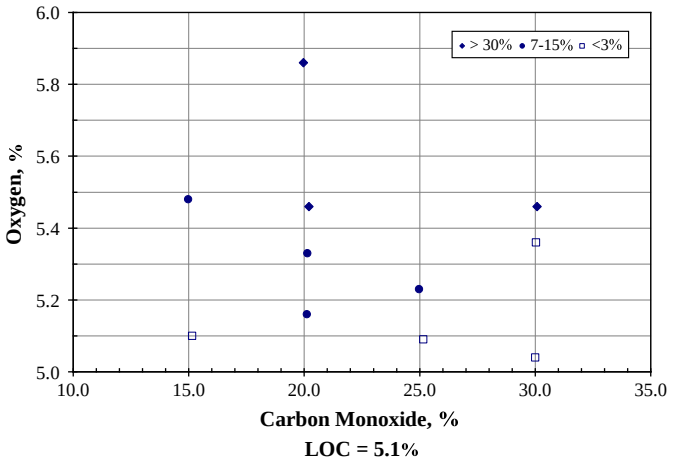

Fig. 2. 120-L data on the LOC of CO in nearly saturated moist air with added N_2. Parametric pressure plot at different O_2 vs. CO concentrations, with the symbols representing different pressure-rise levels.

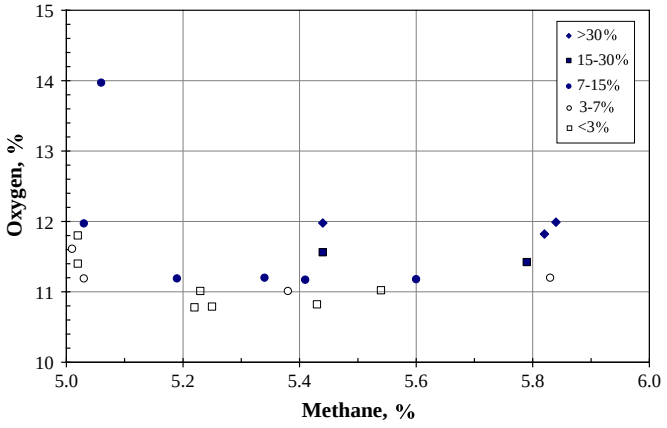

Fig. 3. 120-L data on the LOC of CH_4 in air with added N_2. Parametric pressure plot at different O_2 vs. CH_4 concentrations, with the symbols representing different pressure-rise ranges.

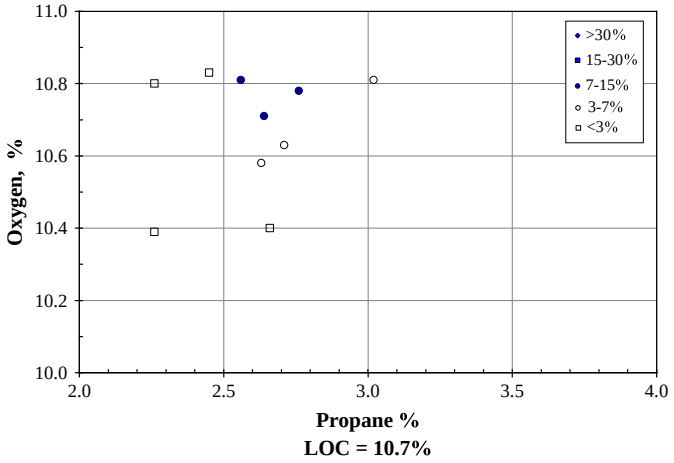

Fig. 4. The LOC of propane in air with added N_2; 120-L data. Parametric pressure plot at different O_2 vs. C_3H_8 concentrations, with the symbols representing different pressure-rise ranges.

cylindrical vessel (EN 1839T) yielded a value of 4.4% in this standard (British and European Standard, 2003). A similar difference was observed for the UFL measurements of methane in air. The European standard methods gave 16.6% and 16.8% values for the tube and "bomb" methods, respectively – cited in Annex E, while both the 120-L and 12-L spheres gave 15.8%. A further confirmation of the results reported here is given by the studies of Kondo's group on the effect of vessel size and shape on the experimental flammability limits of methane and propane. They found that cylindrical vessels did not yield values that were size independent until quite large dimensions were used. Their largest cylinder (45 × 100 cm) with a volume of 160-L gave values quite consistent with those reported here for full upward propagation of a flammable mixture (methane flammability limits = 5.0–15.8%; propane limits = 2.0–9.9%) (Takahashi, Urano, Tokuhashi, & Kondo, 2003).

The different values cited for the LFL of methane in the new databases which are based on the European standards (CHEMSAFE, 2007) should not be interpreted as an argument for the retention of older flammability values if new experiments in larger chambers using comparable flammability criteria produce new values. That is the case with experiments reported here, particularly in regards to LOC values. These experiments now generate systematically lower LOC values, as do the results in the 12-L glass sphere (Kondo et al., 2006). This agreement between the pressure-rise criterion used in the 120-L sphere and the visual criterion in the 12-L sphere lends encouragement to the assumption that values have been determined that are reasonably independent of vessel size and flame propagation criteria.

The above argument implies that the LOC values in the older literature are not sufficiently conservative and should not be used to generate safety protocols unless conservative safety factors are incorporated. The problem with the older LOC values is also recognized in the 2008 NFPA 69 standard which requires subtracting 2% (abs.) from the old values. While that is probably a conservative stance, it may involve unnecessary expense in the case of hydrogen – based on the results obtained in the 120-L sphere. Additional measurements using large chambers and appropriate flame propagation criteria will be needed to form a reliable database of LOC values.

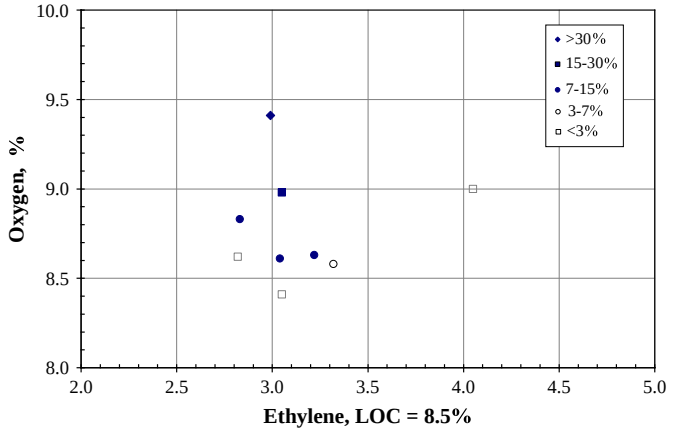

Fig. 5. The LOC of ethylene in air with added N_2; 120-L data. Parametric pressure plot for different O_2 vs. C_2H_4 concentrations, with the symbols representing different pressure-rise ranges.

4. Fuel mixtures

The LFL of fuel mixtures is predicted adequately by the Le Chatelier rule for fuel mixtures (Burgess et al., 1982; Coward & Jones, 1952; Kondo et al., 2008; Liekhus, Zlochower, Cashdollar, Djordjevic, & Loehr, 2000). That rule is less adequate, but still generally conservative, in predicting the UFL of mixtures (Kondo et al., 2008). The LOCs of such mixtures, however, have not been extensively studied. Prior work on mixtures of hydrogen and benzene (Thomas, 1996) established the utility of a calculation scheme that will be derived in this paper and used to compare to the experimental results on binary mixtures of hydrogen, CO, or ethylene with methane. Mixtures of propane and methane are not considered since their LOCs are too close to produce a significant variation with composition. The experimental method chosen was the same as for the single fuels, except that two different fuels were mixed together with air and nitrogen to establish the stated mixtures. Ternary mixtures of 1:1 hydrogen:CO with methane were also studied. Water was not added to the mixtures containing CO since the other fuel(s) had the H species needed for efficient CO combustion. The results are summarized in Table 2.

Table 2 shows the experimental and calculated values of the LOC of CH_4 mixtures with H_2 and/or CO, or with C_2H_4. The predicted LOCs involving mixtures of H_2 and/or CO with CH_4 follow the experimental values but fall to a maximum of 0.9% (abs.) below them. The calculations to be described in the next section are therefore seen as realistic but conservative. H_2 and CO are unusual fuels, however (high diffusivity or low reactivity) as noted earlier. The deviation of the experimental results from the derived formula is, therefore, not surprising. The one clear example of a mixture of more typical fuels with widely different LOCs is the mixture of methane and ethylene. The calculated values are very close to the experimental ones with a maximum difference of 0.15% (abs.).

5. LOC of fuel mixtures

As noted previously, the lower flammability limit (LFL) for mixtures of fuels is adequately given by the Le Chatelier rule:

$$L_{\text{mixt.}} = 1/\sum x_i/L_i \tag{1}$$

Where L_{mixt} is the LFL of the fuel mixture, L_i is the LFL of fuel component i, x_i is the mole fraction of the fuel component.

The LOC of fuel mixtures can be derived from (1) by defining L^*_{mixt} and L^*_i as,

$$L^*_i = (\text{LOC})_i/R_i, \quad L^*_{\text{mixt}} = (\text{LOC})_{\text{mixt}}/R^* \tag{2}$$

Where $(\text{LOC})_i$ is the experimental value for LOC of component i, $(\text{LOC})_{\text{mixt}}$ is the calculated LOC for the fuel mixture, R_i is the

Table 2
LOC: fuel mixtures containing methane: CH_4–H_2; CH_4–CO; CH_4–C_2H_4; CH_4–1:1 CO:H_2; experimental vs. calculated.

Fuel: % CH_4	Methane–H_2		Methane–CO		Methane–ethylene		CH_4–1:1 CO:H_2	
	$(LOC)_{exp}$	$(LOC)_{calc}$	$(LOC)_{exp}$	$(LOC)_{calc}$	$(LOC)_{exp}$	$(LOC)_{calc}$	$(LOC)_{exp}$	$(LOC)_{calc}$
0	4.6	4.6	5.1	5.1	8.6	8.6	4.8	4.8
10	6.5	5.6	6.1	6.1	8.6	8.7		
20							7.3	6.7
25	7.7	6.9	7.8	7.4	8.9	9		
35	8.3	7.65						
40							8.7	8.2
50	9.1	8.64	9.5	9.0	9.3	9.45		
60							9.7	9.4
75	10.3	10	10.9	10.2	10.05	10.1		
80							10.5	10.3
90	10.9	10.7	11	10.8				
100	11.1	11.1	11.1	11.1	11.1	11.1	11.1	11.1

stoichiometric molar ratio of oxygen to fuel i (see Table 1), R^* is the stoichiometric ratio of oxygen to the fuel mixture, as given by $\sum x_i R_i$.

For $L^*_{mixt} = 1/\sum x_i/L^*_i$ (modified Le Chatelier rule),
substituting (2) into the modified Le Chatelier and rearranging terms gives

$$(LOC)_{mixt.} = \sum x_i R_i / \sum x_i / L^*_i = \sum x_i R_i / \sum x_i R_i / (LOC)_i$$

For a 2-component mixture (a,b):

$$(LOC)_{mixt.} = (x_a R_a + x_b R_b) / \left[(x_a R_a / (LOC)_a) + (x_b R_b / (LOC)_b) \right]$$

For binary mixtures of methane (m) and hydrogen (h): $R_m = 2$, $R_h = 0.5$, $x_h = 1 - x_m$, $LOC_m = 11.1$, $LOC_h = 4.6$. *The result is:* $LOC_{m-h} = (1.5x_m + 0.5)/(0.0715x_m + 0.109)$.
For binary mixtures of methane and CO: $R_{co} = 0.5$, $x_{co} = 1 - x_m$, $LOC_{co} = 5.1$. *The result is:* $LOC_{m-co} = (1.5x_m + 0.5)/(0.0821x_m + 0.0980)$.
For binary mixtures of methane and ethylene: $R_{et} = 3$, $x_{et} = 1 - x_m$, $LOC_{et} = 8.6$. *The result is:* $LOC_{m-et} = (3 - x_m)/(0.349 - 0.169x_m)$.
For ternary mixtures of methane with 1:1 CO:H_2, $x_{co} = x_h = (1 - x_m)/2$. *The result is:* $LOC_{m-co:h} = (1.5x_m + 0.5)/(0.0768x_m + 0.1034)$.

The above equations lead to the calculated LOC results shown in Table 2. As noted previously, the calculated results for the mixture of hydrocarbons accurately predict the experimental values. The results for the unusual fuels, H_2 and CO, are below the experimental values, but barely outside experimental error. In any case, the calculated results are conservative. It remains to be seen how this calculation scheme will fit data on oxygenated and other non-hydrocarbon fuels.

6. Conclusions

The primary finding reported here is that the traditional flammability tube values for the LOCs are too high – at least for N_2 inerting that was the subject of this study. The differences from the 120-L results are typically less than 1% (e.g. 12 vs. 11.1% for CH_4, 11.5 vs. 10.7 for C_3H_8), but the difference is 1.5% for ethylene (10 vs. 8.5%). These results should be taken into account by the standard-setting organizations – or at least be subject to independent verification. A start in this direction is currently being made by standards committees based in the US (NFPA 69, 2008).

This study also generally confirms the results of the flammability tube measurements on the LFLs of these fuels (hydrogen being exceptional). The excellent agreement between the 120-L results using a 7% pressure-rise criterion with the reported results in the 12-L glass sphere which uses a visual criterion supports the contention that these results are realistic. The issue of the conflicting American and European flammability standards needs to be resolved so as to provide a consistent and reliable database for flammability.

Acknowledgement

This is to acknowledge the important contributions of Kenneth L. Cashdollar over the years to the flammability and LOC studies in the 120-L and 20-L chambers, and to his helpful suggestions and advice. Sad to say, Ken recently passed away and we will no longer have the benefit of his leadership, humanity, and superlative experimental and organizational skills. His many contributions to our organization and the field of explosion prevention will be sorely missed.

References

ASHRAE. (2007). Number designation and safety classification of refrigerants, ANSI/ASHRAE Standard 34-2007. American Society of Heating, Refrigerating, and Air-conditioning Engineers (ASHRAE), Atlanta GA.

ASTM International. (2008a). *Standard test method for concentration limits of flammability of chemicals (vapors and gases)*. E681-04. In: *ASTM International annual book of standards, Vol. 14.02*. West Conshohocken, PA: American Society for Testing and Materials.

ASTM International. (2008b). *Standard test methods for limiting oxygen (oxidant) concentration in gases and vapors*. E2079-07. In: *ASTM International annual book of standards, Vol. 14.02*. West Conshohocken, PA: American Society for Testing and Materials.

Brandes, E., & Ural, E. A. (2008). Towards a global standard for flammability determination. In *Proceedings of the 42nd annual loss prevention symposium – Global safety congress, paper 2E, April 6–10*. New Orleans, LA: American Institute of Chemical Engineers.

British and European Standard. (2003). *Determination of explosion limits of gases and vapours*. sections 4.1, Method T (BS EN 1839T) and 4.2, Method B (BS EN 1839B). rue de Stassart, 36, B-1050 Brussels, Belgium: CEN European Committee for Standardization.

British and European Standard. (2007). *Determination of limiting oxygen concentrations of gases and vapours*. EN 14756. rue de Stassart, 36, B-1050 Brussels, Belgium: CEN European Committee for Standardization.

Britton, L. G. (2002). Two hundred years of flammable limits. *Process Safety Progress, 21*, 1–11.

Burgess, D. S., Furno, A. L., Kuchta, J. M., & Mura, K. E. (1982). Flammability of mixed gases. *U.S. Bureau of Mines Report of Investigations, 8709*. 20 pp.

Cashdollar, K. L., Zlochower, I. A., Green, G. M., Thomas, R. A., & Hertzberg, M. (2000). Flammability of methane, propane, and hydrogen gases. *Journal of Loss Prevention in the Process Industries, 13*, 327–340.

CHEMSAFE. (2007). *Database of evaluated safety characteristics*. Frankfort/M, Germany: DECHEMA, BAM, and PTB.

Coward, H. F., & Jones, G. W. (1952). Limits of flammability of gases and vapors. *U.S. Bureau of Mines Bulletin, 503*. 155 pp.

De Smedt, G., de Corte, F., Notele, R., & Berghmans, J. (1999). Comparison of two standard test methods for determining explosion limits of gases at atmospheric conditions. *Journal of Hazardous Materials, A70*, 105–113.

DIN (German standard) 51649-1. (1986). *Determination of the explosion limits of gases and gas mixtures in air*. (Ger.). Berlin, Germany: Deutches Institut fur Normung.

Hertzberg, M. (1989). Selective diffusional demixing: occurrence and size of cellular flames. *Progress in Energy and Combustion Science, 15*, 203–239.

Hertzberg, M., Conti, R. S., & Cashdollar, K. L. (1985). Electrical ignition energies and thermal autoignition temperatures for evaluating explosion hazards of dust. *U.S. Bureau of Mines Report of Investigations, 8988*. 41 pp.

Kondo, S., Takizawa, K., Takahashi, A., & Tokuhashi, K. (2006). Extended Le Chatelier's formula and nitrogen dilution effect on the flammability limits. *Fire Safety Journal, 41*, 406–417.

Kondo, S., Takizawa, K., Takahashi, A., Tokuhashi, K., & Sekiya, A. (2008). A study on flammability limits of fuel mixtures. *Journal of Hazardous Materials, 155*, 440–448.

Kuchta, J. M. (1985). Investigation of fire and explosion accidents in the chemical, mining, and fuel-related industries – a manual. *U.S. Bureau of Mines Bulletin, 680*. 84 pp.

Liekhus, K. J., Zlochower, I. A., Cashdollar, K. L., Djordjevic, S. M., & Loehr, C. A. (2000). Flammability of gas mixtures containing volatile organic compounds and hydrogen. *Journal of Loss Prevention in the Process Industries, 13*, 377–384.

MSHA. (March 1996). *Safety standards for underground coal mine ventilation: Final rule*. 30 CFR, Part 75, Section 75.323. In: *Federal register, part III*. Department of Labor, Mine Safety and Health Administration.

NFPA 69. (2008). *Standard on explosion prevention systems* (2008 ed.). Quincy, MA: National Fire Protection Association.

Schroder, V., & Molnarne, M. (2005). Flammability of gas mixtures. Part I: fire potential. *Journal of Hazardous Materials, 121*, 37–44.

Takahashi, A., Urano, Y., Tokuhashi, K., & Kondo, S. (2003). Effect of vessel size and shape on experimental flammability limits of gases. *Journal of Hazardous Materials, 105*, 27–37.

Thomas, J. K. (1996). *Composite minimum oxygen concentrations for benzene–hydrogen–nitrogen–air mixtures*. WSRC-RP-96-619. Aiken, SC: Westinghouse Savannah River Co., Safety Engineering Div..

Zabetakis, M. G. (1965). Flammability characteristics of combustible gases and vapors. *U.S. Bureau of Mines Bulletin, 627*. 121 pp.

A604: Methane Lower Flammability Limit as Function of Pressure

The lower flammability limit of methane in air at elevated pressures and temperatures: a theoretical and numerical study

F. Van den Schoor, E. Van den Bulck
Katholieke Universiteit Leuven, Department of Mechanical Engineering, Celestijnenlaan 300A, B-3000 Leuven, Belgium, filip.vandenschoor@mech.kuleuven.be
Katholieke Universiteit Leuven, Department of Mechanical Engineering, Celestijnenlaan 300A, B-3000 Leuven, Belgium, eric.vandenbulck@mech.kuleuven.be

1. Introduction

In previous studies [1–3], four different methods for the calculation of flammability limits were evaluated. In this study, two of these methods will be used to calculate the lower flammability limit (LFL) of methane/air mixtures at initial pressures up to 30 bar and initial temperatures up to 200°C.

2. Theoretical study

A literature study shows that three different mechanisms, namely chemical kinetics (Section 2.1), heat loss (Section 2.2) and flow strain (Section 2.3), can be discerned that can cause flame extinction and, thus, can explain the occurrence of flammability limits. For each of these extinction mechanisms, it will be derived when an increase in pressure leads to a decrease of the LFL (and when not).

2.1 Chemical kinetics

A purely kinetic flame extinction mechanism can be thought to exist resulting from the competition between chain branching and chain terminating reactions [4]. Upon decreasing the equivalence ratio for lean near-limit mixtures, the flame temperature continuously decreases. This affects the reaction rate of the branching reactions more than that of the terminating reactions since the latter are generally less temperature sensitive than the former. Consequently, the concentration of chain carriers is continuously reduced, which given their importance in maintaining the combustion reaction might lead to flame extinction. The determining factor in this extinction mechanism is the reaction rate.

The dependence of the reaction rate on pressure is dictated by the overall reaction order n [5]. Although n is mostly positive, it can assume negative values as well [6]. As a result, the LFL is likely to decrease with pressure, but for certain mixtures (with $n < 0$) the opposite will occur.

2.2 Heat loss

Analogously to the kinetic mechanism, the competition between heat production in the reaction zone and heat loss to the surroundings may cause flame extinction since a decrease in flame temperature affects the reaction rate more than the heat loss rate.

Spalding [7] analytically solved the flame equations for a 1D planar premixed flame for a one-step reaction. His theory with inclusion of a heat loss term predicts the existence of flammability limits with a non-zero value of the burning velocity. Without including heat loss, however, it is predicted that the burning velocity goes to zero asymptotically and no flammability limits are found. The only important underlying assumption made by Spalding is

the necessity of an overall activation energy high enough to give a reaction rate dependence on temperature that is stronger than that of the heat loss rate. The determining factors in this extinction mechanism are the reaction rate and the (radiation) heat loss rate.

The dependence of the reaction rate on pressure is dictated by the overall reaction order *n* [5], while that of the radiation heat loss rate is set by an exponent *m* lying in the range 0 – 1 [8]. If no absorption of radiation is present, *m* = 1. As a result, only if *n* > 1, the LFL will decrease with pressure.

2.3 Flow strain

Flames can be extinguished by increasing the flame stretch rate. With increasing stretch rate the residence time reduces, the flame becomes thinner and complete reaction can no longer be achieved, eventually leading to a reduced flame temperature and extinction [9].

For a two-reactant mixture and a single-step reaction and for a flame propagating in an axisymmetric stagnation point flow, Buckmaster and Mikolaitis [10] calculated the limiting (minimum) value of the Karlovitz number that leads to extinction.

By assuming that the overall activation energy is (nearly) pressure independent or that the Lewis number is (close to) 1, and that the flame stretch rate is (nearly) pressure independent, the pressure dependence of the limiting burning velocity $S_{u,lim}$ is given by $S_{u,lim} \propto p^{-1/2}$, where *p* is the pressure [2]. Since the burning velocity $S_u \propto p^{n-2/2}$ [5], it follows that $S_u / S_{u,lim} \propto p^{n-1/2}$. As a result, only if *n* > 1, the LFL will decrease with pressure. Surprisingly, the same result was found in Section 2.2 based upon the competition between heat production and heat loss.

3. Numerical methods

The 1D planar premixed flame calculations, which enable determination of the flame temperature and the burning velocity, are performed using CHEM1D [11], a one-dimensional flame code. The radiation heat loss of CO_2, H_2O, CO and CH_4 is modelled by means of the optically thin limit. The GRI mechanism [12] is chosen as reaction mechanism.

The LFL is calculated numerically by using two different methods, namely (1) the calculation of planar flames with the inclusion of a radiation heat loss term in the energy conservation equation (based upon the heat loss extinction mechanism), and (2) the application of a limiting burning velocity (based upon the flow strain extinction mechanism).

In the first method, the LFL is determined by considering whether a transient flame calculation reaches a steady state or not. In the latter case, the maximum flame temperature and the burning velocity will decrease continuously in time [13], indicating that the mixture is non-flammable. Before doing transient flame calculations, an initial guess for the LFL is sought by carrying out a series of steady flame calculations in which the equivalence ratio φ is decreased in steps of 0.001 until a steady solution cannot be found upon a further decrease of φ. Next, steady solutions in the neighbourhood of this initial guess are calculated with 90% of the total radiation heat loss included. Finally, these solutions serve as initial conditions for the transient calculations, which are performed from their start with the radiation heat loss restored to the full 100%.

In the second method, the LFL is determined by finding the fuel concentration for which the burning velocity equals the limiting burning velocity. The limiting burning velocity for methane/air mixtures at 1 bar and 25°C of 2.3 cm/s found by Ronney [14], is used as a starting point for the calculations. This gives an LFL of 3.97 mol% at these conditions. Next,

the LFL at elevated temperatures is found be applying a constant limiting flame temperature (with inclusion of radiation heat loss) [2]. This gives values of 4.45 mol% and 4.80 mol% at 1 bar and 100 and 200°C, respectively. Finally, the pressure dependence of the limiting burning velocity namely $S_{u,lim} \propto p^{-1/2}$ is used to determine the LFL at elevated pressures.

Further details about the numerical methods can be found elsewhere [1].

4. Numerical results

The LFL of methane/air mixtures is calculated for initial pressures in the range 1 – 30 bar and for initial temperatures in the range 25 – 200°C.

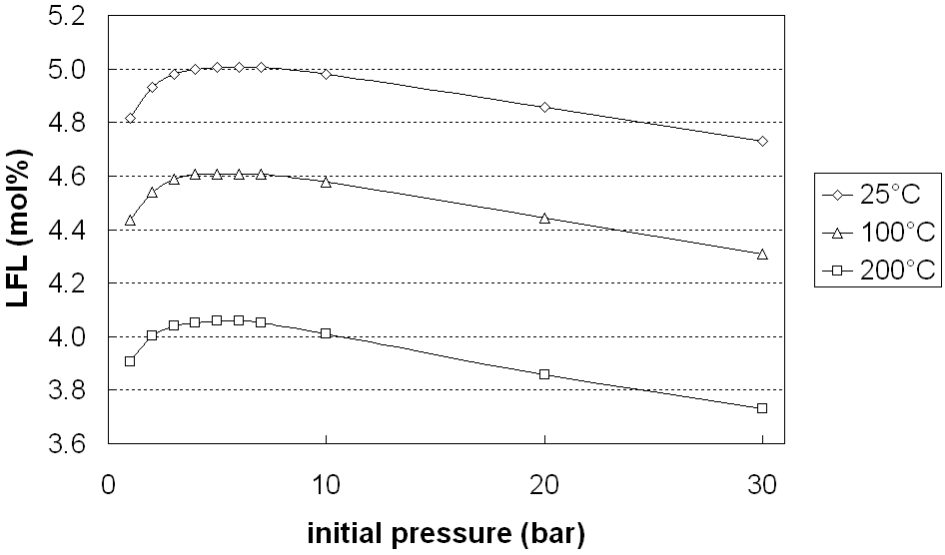

Figure 1: LFL of methane/air mixtures calculated with the first method

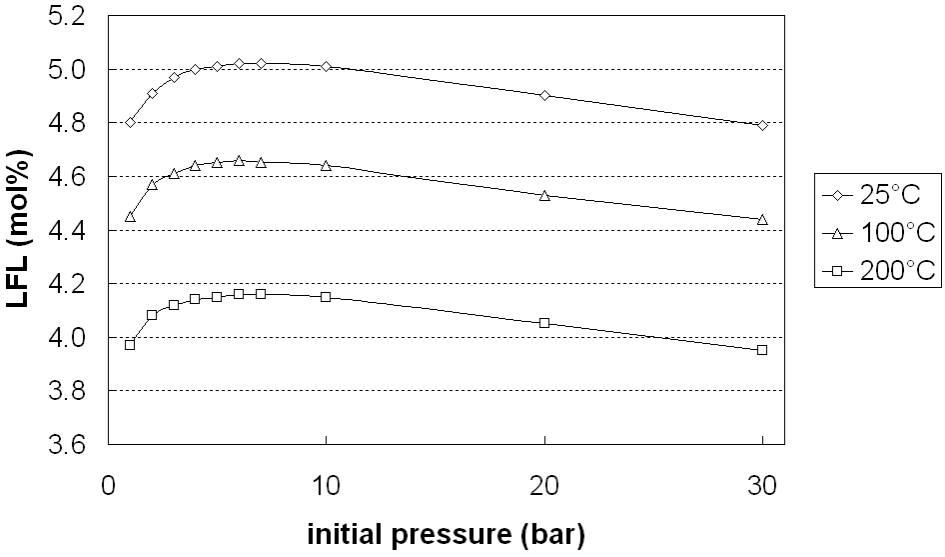

Figure 2: LFL of methane/air mixtures calculated with the second method

Figure 1 shows the results obtained by calculating planar flames with the inclusion of a radiation heat loss term in the energy conservation equation (first method). It can be seen that for the three initial temperatures the LFL first increases and subsequently decreases with increasing pressure. As described in Section 2.2, this behaviour of the LFL can be explained by the occurrence of an overall reaction order *n* which is less than 1.

Figure 2 shows the results obtained by applying a limiting burning velocity (second method). It can be seen that the behaviour of the LFL is essentially the same as that obtained by the first method. This was expected since the theoretical study showed that the same cut-off value for *n* applies with respect to both extinction mechanisms (Section 2.3).

5. Conclusions

It is found that

1. the lower flammability limit (LFL) of methane/air mixtures first increases and subsequently decreases with increasing pressure;
2. the numerical results corroborate the finding of the theoretical study that the observed behaviour of the LFL appears for both the heat loss and the flow strain extinction mechanisms at the same values of the overall reaction order *n*, namely $n < 1$.

Acknowledgements

The authors gratefully acknowledge the funding of this work by the Research Fund K.U.Leuven.

References

[1] F. Van den Schoor et al., J.Hazard. Mater. 150 (2008) 573–581.
[2] F. Van den Schoor et al., J. Hazard. Mater. 153 (2008) 1301–1307.
[3] F. Van den Schoor et al., Int. J. Hydrogen Energ. 33 (2008) 1399–1406.
[4] C.K. Law and F.N. Egolfopoulos, P. Combust. Inst. 23 (1990) 431–421.
[5] I. Glassman, Combustion, Third ed., Academic Press, San Diego (1996).
[6] C.K. Law, Combust. Sci. Technol. 178 (2006) 335–360.
[7] D.B. Spalding, P. Roy. Soc. Lond. A Mat. 240 (1957) 83–100.
[8] F. Van den Schoor, Influence of Pressure and Temperature on Flammability Limits of Combustible Gases in Air, doctoral dissertation, KULeuven (2007).
[9] C.K. Law, P. Combust. Inst. 22 (1988) 1381–1402.
[10] P.D. Ronney, P. Combust. Inst. 27 (1998) 2485–2506.
[11] CHEM1D, A one-dimensional laminar flame code, Eindhoven University of Technology. http://www.combustion.tue.nl/chem1d.
[12] J. Buckmaster and D. Mikolaitis, Combust. Flame 45 (1982) 109–119.
[13] K.N. Lakshmisha et al., P. Combust. Inst. 23 (1990) 433–440.
[14] G.P. Smith et al., GRI 3.0. http://www.me.berkeley.edu/gri-mech.

A605: USBM Bulletin 680 - Investigation of Fire & Explosion

Bulletin 680

Investigation of Fire and Explosion Accidents in the Chemical, Mining, and Fuel-Related Industries— A Manual

By Joseph M. Kuchta

UNITED STATES DEPARTMENT OF THE INTERIOR
Donald Paul Hodel, Secretary

BUREAU OF MINES
Robert C. Horton, Director

As the Nation's principal conservation agency, the Department of the Interior has responsibility for most of our nationally owned public lands and natural resources. This includes fostering the wisest use of our land and water resources, protecting our fish and wildlife, preserving the environment and cultural values of our national parks and historical places, and providing for the enjoyment of life through outdoor recreation. The Department assesses our energy and mineral resources and works to assure that their development is in the best interests of all our people. The Department also has a major responsibility for American Indian reservation communities and for people who live in island territories under U.S. administration.

Library of Congress Cataloging in Publication Data

Kuchta, J. M.
Investigation of fire and explosion accidents in the chemical, mining, and fuel-related industries.

(Bulletin/U.S. Dept. of the Interior, Bureau of Mines; 680)

Bibliography: p. 68

Supt. of Docs. no.: 128.3:680

1. Chemical industries—Fires and fire prevention. 2. Mine fires. 3. Fuel—Fires and fire prevention. 4. Explosions. I. Title. II. Series: Bulletin (United States. Bureau of Mines) ; 680.

TH9445.C47K8 1985 660.2'804 85—600188

For sale by the Superintendent of Documents, U.S. Government Printing Office
Washington, DC 20402

CONTENTS

	Page
Abstract	1
Introduction	2
Acknowledgments	2
Procedures for accident investigators	2
Initial actions	2
Investigative procedures	3
Background information	3
Site inspection	3
Witness interrogation	3
Evidence development and analysis	3
Conclusions and report	5
Theory and definitions	6
Physical gas laws	6
Stoichiometry	7
Thermodynamic relationships	8
Ignition processes	9
General concepts	9
Electrical ignition	10
Thermal ignition	11
Chemical ignition	12
Flame propagation processes	13
Flammable mixtures	13
Prediction of limits	14
Flame temperatures	14
Burning velocities	15
Explosion processes	16
Deflagrations	16
Physical explosions	17
Detonations	17
Properties of liquid and gaseous compounds	19
Vapor pressures and flashpoints	19
Saturated hydrocarbons	19
Other combustibles	20
Flammability limits in air and oxygen	25
Saturated hydrocarbons and derivatives	25
Unsaturated hydrocarbons, aromatics, and derivatives	28
Inorganic combustibles	29
Flammability limits in other atmospheres	30
Ignition requirements	33
Ignition energies	33
Quenching distances	34
Ignition temperatures	35
Flame temperatures and burning rates	37
Flame temperatures	37
Burning velocities	39
Detonation velocities	40
Liquid burning rates	41
Properties of gasolines, jet fuels, hydraulic fluids, and lubricants	41
Vapor pressures and flashpoints	43
Flammability limits in air	43
Flammability limits in other atmospheres	44
Ignition requirements	45
Ignition energies	45
Ignition temperatures	45
Flame temperatures and burning rates	47
Flame temperatures	47
Burning rates	48
Properties of metal and nonmetal elements	48
Flammability limits in air	48
Flammability limits in other atmospheres	49
Ignition requirements	49
Ignition energies	49
Ignition temperatures	50
Flame temperatures and burning rates	50
Flame temperatures	50
Burning rates	50
Properties of agricultural, carbonaceous, chemical, and plastic dusts	51
Flammability limits in air	52
Flammability limits in other atmospheres	53
Ignition requirements	54
Ignition energies	54
Ignition temperatures	54
Spontaneous heating temperatures	55
Flame temperatures and burning rates	57
Flame temperatures	57
Burning rates	57
Properties of fabric and sheet combustibles	58
Ignition temperatures	58
Burning rates	59
Fire and explosion damage	60
Fire temperature and radiation criteria	60
Explosion pressure criteria	62
Blast wave criteria	65
Crater and missile criteria	66
References	68
Appendix A.—Summary of combustion properties of liquid and gaseous compounds	71
Appendix B.—Definition of symbols	78
Appendix C.—Conversion factors	80
Subject index	82
Unit of measure abbreviations	84

ILLUSTRATIONS

1. Compressibility factor as a function of reduced pressure and reduced temperature 6
2. Variation of pressure ratio with volume ratio in adiabatic and isothermal compression of an ideal gas 8
3. Temporal and spatial characterization of various ignition sources 9
4. Spark energy versus fuel-air ratio for ignition of n-butane-air mixtures at 25° C and 1 atm 10
5. Ignition delay versus temperature for autoignition of n-decane in air at atmospheric pressure 11
6. Flammability and vapor pressure diagram for n-decane vapor-air system at various temperatures and atmospheric pressure 13
7. Flammability diagram for the aviation gasoline vapor (100/130 grade)-air-nitrogen system at 25° C and 1 atm 13
8. Flame speed, gas velocity, and burning velocity versus equivalence ratio for methane-air flame propagation at 25° C and 1 atm 15
9. Pressure history for the explosion of a stoichiometric methane-air mixture in a 3.65-m (12-ft) diam sphere at 25° C and 1 atm 16

ILLUSTRATIONS—Continued

Page

10. Pressure and flame profile histories for spark ignitions of 7.8 pct CH_4-74.1 pct air-18.1 pct N_2 mixture and 6.9 pct CH_4-65.8 pct air-27.3 pct N_2 mixture in a 3.65-m (12-ft) diam sphere at 25° C and 1 atm 17
11. Pressure-time transient for detonation of a stoichiometric acetylene-air mixture in a 45.7-m (150-ft) long tunnel with initiation end closed 18
12. Relation of ideal blast wave characteristics at the shock front to peak overpressure 18
13. Vapor pressure-temperature curves and flashpoints for five normal paraffins (C_1 to C_5) 19
14. Vapor pressure-temperature curves and flashpoints for eight normal paraffins (C_6 to C_{10}, C_{12}, C_{14}, C_{16}) 20
15. Vapor pressure-temperature curves and flashpoints for eight branched-chain paraffins 20
16. Vapor pressure-temperature curves for eight unsaturated hydrocarbons 21
17. Vapor pressure-temperature curves and flashpoints for seven alicyclic hydrocarbons 21
18. Vapor pressure-temperature curves and flashpoints for eight aromatic hydrocarbons 21
19. Vapor pressure-temperature curves and flashpoints for eight alcohols or hydroxy compounds 21
20. Vapor pressure-temperature curves and flashpoints for six glycols and glycerol 22
21. Vapor pressure-temperature curves and flashpoints for eight ethers 22
22. Vapor pressure-temperature curves and flashpoints for seven aldehydes 22
23. Vapor pressure-temperature curves and flashpoints for seven ketones 22
24. Vapor pressure-temperature curves and flashpoints for five acids and three acid anhydrides 23
25. Vapor pressure-temperature curves and flashpoints for seven esters 23
26. Vapor pressure-temperature curves and flashpoints for eight amines 23
27. Vapor pressure-temperature curves and flashpoints for ammonia, cyanogen, two cyanides, two hydrazines, and hydrogen peroxide 23
28. Vapor pressure-temperature curves and flashpoints for seven nitrated hydrocarbons 24
29. Vapor pressure-temperature curves and flashpoints for eight alkyl chlorides 24
30. Vapor pressure-temperature curves and flashpoints for six unsaturated and two aromatic chlorine compounds 24
31. Vapor pressure-temperature curves and flashpoints for seven brominated compounds 24
32. Vapor pressure-temperature curves and flashpoints for six sulfur and two boron compounds 25
33. Variation of lower and upper limits of flammability in air with number of carbon atoms for normal paraffins and their derivatives 26
34. Temperature effect on lower limits of flammability of 10 normal paraffins in air at atmospheric pressure .. 27
35. Temperature effect on upper limits of flammability of six normal paraffins and JP-6 jet fuel in air at atmospheric pressure 27
36. Pressure effect on limits of flammability of natural gas and ethane in air at 25° C 28
37. Variation of lower and upper limits of flammability in air with number of carbon atoms for normal alkenes and with number of chlorine atoms for chloroethenes 28
38. Limits of flammability of various methane-air-inert gas mixtures at 25° C and 1 atm 30
39. Limits of flammability of methane-, ethane-, propane-, n-butane-, and n-pentane-air-nitrogen mixtures at 25° C and 1 atm 30
40. Limits of flammability of methane-, ethane-, propane-, n-butane-, and n-pentane-air-carbon dioxide mixtures at 25° C and 1 atm 30
41. Limits of flammability of hydrogen-air mixtures with added nitrogen and carbon dioxide at 25° C and 1 atm 31
42. Limits of flammability of carbon monoxide-air mixtures with added nitrogen and carbon dioxide at 25° C and 1 atm 31
43. Limits of flammability of methane-air-Halon mixtures at 25° C and 1 atm 32
44. Effect of pressure on minimum oxygen requirements for propagation of natural gas, ethane, and propane in air-nitrogen mixtures at 25° C 32
45. Spark ignition energy versus combustible vapor concentration for six paraffins in air at atmospheric pressure 33
46. Minimum spark ignition energy of propane-oxygen-nitrogen mixtures as a function of oxygen concentration and mixture pressure 33
47. Correlation of minimum ignition energy with minimum quenching distance for a large variety of combustibles in air and other oxidant atmospheres 34
48. Autoignition temperatures and corresponding ignition delays of hydrocarbon fuels under static conditions in air at atmospheric pressure 36
49. Hot surface ignition temperatures as a function of heat source surface area for hydrocarbon fuels and an engine oil in air at 1 atm 37
50. Hot gas (air) ignition temperatures as a function of reciprocal jet diameter for hydrogen and various hydrocarbons at atmospheric pressure 37
51. Burning velocities of methane-, ethane-, propane-, and n-heptane-air mixtures at atmospheric pressure and room temperature 39
52. Burning velocity and vertical flame speed versus added N_2 for combustion of CH_4-air-N_2 mixtures in a 3.65-m (12-ft) diam sphere at 25° C and 1 atm 39

ILLUSTRATIONS—Continued

Page

53. Burning velocities of methane-, ethane-, and propane-oxygen mixtures at atmospheric pressure and room temperature ... 39
54. Effect of temperature on burning velocities of four paraffins in air at atmospheric pressure ... 40
55. Detonation velocities of methane-, ethane-, propane-, butane-, and hexane-oxygen mixtures at atmospheric pressure ... 40
56. Linear burning rates of combustible liquids as a function of pool diameter at ambient temperature ... 41
57. Vapor pressure (Reid)-temperature curves and flashpoints for aviation gas and five jet fuels ... 43
58. Limits of flammability of JP-4 vapor-air-inert gas (CO_2 or N_2) mixtures at 25° C and 1 atm ... 44
59. Limits of flammability of JP-1 vapor-air-inert gas (CO_2 or N_2) mixtures at 150° C and 1 atm ... 45
60. Effects of various inerting agents on limits of flammability of gasoline vapor-air mixtures at 25° C and 1 atm ... 45
61. Minimum autoignition temperatures of seven hydraulic fluids in oxygen-nitrogen mixtures at atmospheric pressure ... 46
62. Correlation of minimum autoignition temperatures of JP-6 fuel-oxygen-nitrogen mixtures with oxygen partial pressure at various mixture pressures ... 46
63. Minimum autoignition temperatures of phosphate ester, mineral oil, and water-glycol hydraulic fluids or lubricants in air at elevated pressures ... 47
64. Autoignition temperatures and corresponding ignition delays for JP-6 fuel under static and dynamic conditions in air at various pressures ... 47
65. Variation of hot gas (air) and hot surface ignition temperatures with reciprocal diameter of heat source for JP-6 fuel and MIL-L-7808 oil vapor-air mixtures at atmospheric pressure ... 47
66. Flame spread rate versus liquid fuel temperature for Jet A- and Jet B-type fuels in air at atmospheric pressure ... 47
67. Effect of average particle diameter on explosion parameters for atomized aluminum dust in air at 25° C and 1 atm ... 49
68. Lower dust explosion limits of oil shale (45 gal/ton), Pocahontas coal, and Pittsburgh coal in methane-air atmospheres with modified Hartmann apparatus ... 53
69. Calculated limits of explosibility of coal dust-incombustible mixtures for coals of 17, 29, and 36 pct volatility ... 54
70. Effectiveness of various powdered inhibitors on the furnace autoignition temperature of Pittsburgh coal dust in the Godbert-Greenwald furnace ... 55
71. CO-ΔO_2 ratio versus time in closed-vessel desorption experiments with seven coals of 10 to 20 mesh in air at 25° C ... 56
72. Variation of CO-ΔO_2 and CO-CO_2 ratios with temperature in a flowing airstream (15 cm^3/min) with three undried coals of 10 to 20 mesh ... 56
73. Representative gas contents of various ranked coals and their relative hazard potential for self-heating and gaseous explosion ... 57
74. Variation of burning rate with oxidizer concentration for dried sawdust with various solid oxidizers ... 58
75. Effect of oxygen pressure on the flame spread rates of sheet combustibles in oxygen atmospheres ... 59
76. Thermal irradiance of gasoline tank fires as a function of a dimensionless distance ratio ... 61
77. Effect of fuel concentration on explosion pressures of methane-air mixtures at 25° C and 1 atm ... 62
78. Explosion pressure growth for methane-air mixtures in 3.65-m (12-ft) diam sphere at 25° C and 1 atm ... 63
79. Explosion pressure growth for 9.5 pct methane-air mixtures and added nitrogen in 3.65-m (12-ft) diam sphere at 25° C and 1 atm ... 63
80. Explosion pressure growth for 9.5 pct methane-air mixtures and added bromotrifluoromethane (Halon 1301) in 3.65-m (12-ft) diam sphere at 25° C and 1 atm ... 63
81. Calculated pressure rise versus vent ratio ($A/V^{2/3}$) for stoichiometric methane-air ignitions with 0, 10, 20, and 30 pct added nitrogen at 25° C and 1 atm ... 64
82. Peak pressure rises and flame temperatures for H_2-air mixtures in 3.65-m (12-ft) diam sphere at 25° C and 1 atm ... 64
83. Peak pressure rises and flame temperatures for C_4H_{10}-air mixtures in 3.65-m (12-ft) diam sphere at 25° C and 1 atm ... 65
84. Peak overpressure versus scaled distance for hemispherical TNT surface bursts ... 65
85. Peak overpressure and approximate material and biological damage effects from hemispherical TNT surface bursts ... 67
86. Depth of penetration of mild steel versus striking velocity for steel fragments of various weights ... 67
87. Velocity-time profile and potential biological damage levels for head or body impacts ... 67

TABLES

1. Critical states and vaporization properties of common gases or liquids ... 7
2. Major components of dry air ... 7
3. Standard air atmosphere ... 8
4. Heat content (enthalpy) of combustion product gases at various temperatures ... 8

TABLES—Continued

Page

5. Shock wave and adiabatic compression temperatures of air ... 12
6. Limits of flammability of combustible vapors in air and oxygen at 25° C and 1 atm ... 25
7. Equivalence ratios and calorific values of lower limit mixtures of saturated hydrocarbons and derivatives in air at 25° C and 1 atm ... 26
8. Temperature effects on the flammability limits of four chlorinated hydrocarbons in air and oxygen at 1 atm ... 27
9. Equivalence ratios and calorific values of lower limit mixtures of unsaturated and aromatic hydrocarbons and derivatives in air at 25° C and 1 atm ... 29
10. Lower pressure limits of flammability for combustible vapors capable of propagation without an air atmosphere ... 29
11. Minimum oxygen requirements for propagation of combustible vapors in air-nitrogen and air-carbon dioxide mixtures at 25° C and 1 atm ... 31
12. Inerting requirements to prevent propagation of gaseous combustibles in air with nitrogen, carbon dioxide, Halon 1211, and Halon 1301 inhibitors at 25° C and 1 atm ... 32
13. Minimum spark ignition energies of combustible vapors in air and oxygen at 25° C and 1 atm ... 33
14. Comparison of minimum spark ignition quenching distances and maximum experimental safe gaps of combustible vapors in air at 25° C and 1 atm ... 34
15. Minimum autoignition temperatures of combustible gases and liquids in air and oxygen at 1 atm ... 35
16. Comparison of hot surface and hot gas ignition temperatures of hydrogen, carbon monoxide, and hydrocarbon fuels in air at 1 atm ... 37
17. Limit flame temperatures, maximum flame temperatures, and maximum burning velocities of gaseous combustibles in air at 1 atm ... 38
18. Calculated flame temperatures and pressure rises for adiabatic combustion of hydrogen, methane, and carbon monoxide in air at 25° C ... 38
19. Detonation velocities of several combustibles in air at 25° C and atmospheric pressure ... 40
20. Detonation velocities of various combustible mixtures at 25° C and atmospheric pressure ... 41
21. Burning rates and radiative characteristics of burning liquid pools ... 41
22. Summary of combustion properties of gasolines, diesels, and jet fuels ... 42
23. Summary of combustion properties of hydraulic fluids and lubricating oils ... 42
24. Effect of temperature on flammability limits of gasolines and jet fuels in air at atmospheric pressure ... 43
25. Effect of pressure on flammability limits and minimum oxygen requirements for propagation of gasolines and jet fuels in air and air-inert mixtures at 25° C ... 44
26. Effect of pressure and oxygen concentration on the minimum AIT's of aircraft combustible fluids in oxygen-nitrogen atmospheres ... 45
27. Summary of combustion properties of elemental metal and nonmetal dusts ... 48
28. Inerting requirements to prevent propagation of metal and nonmetal dusts in air-nitrogen, air-carbon dioxide, and air-inert dust mixtures (spark ignition) ... 49
29. Ignition temperatures of bulk metals in oxygen at atmospheric pressure ... 50
30. Adiabatic combustion temperatures of metals and nonmetals in oxygen at 1 atm ... 50
31. Summary of combustion properties of agricultural, carbonaceous, chemical, and plastic dusts ... 51
32. Inerting requirements to prevent propagation of combustible dusts in air-nitrogen, air-carbon dioxide, and air-inert dust mixtures at 25° C (spark ignition) ... 53
33. Incombustible requirements to prevent or suppress propagation of Pittsburgh coal dust with various dust inhibitors in small and large-scale experiments ... 54
34. Comparison of dust cloud minimum autoignition temperatures in standard and modified Godbert-Greenwald apparatus ... 55
35. Spontaneous heating temperatures and CO-ΔO_2 indexes of various dried coal dusts in air ... 55
36. Analyses of coals as received ... 56
37. Spontaneous heating temperatures of various woods, fibrous materials, and synthetic rubbers in air ... 57
38. Burning rates (horizontal) of flammable granular solids and oxidizer-sawdust mixtures in air at 1 atm ... 58
39. Ignition temperatures of flammable fabric or sheet materials in air and oxygen at atmospheric pressure ... 59
40. Flame spread rates (45° angle) of flammable fabric or sheet materials in air and oxygen at atmospheric pressure ... 59
41. Flammability data for mine conveyor belts and red oak standard in Bureau of Mines belt flammability apparatus ... 60
42. Temperature limits of various textiles ... 60
43. Melting points of metallic and nonmetallic substances ... 61
44. Color temperatures of iron or steel ... 61
45. Threshold radiation intensities for various thermal effects ... 61
46. Mechanical properties of metals and alloys ... 62
47. Properties of explosives ... 66
48. Peak overpressures for failure of structural materials ... 66
49. Scaled distance for building damage from statistical survey of chemical explosions ... 66

INVESTIGATION OF FIRE AND EXPLOSION ACCIDENTS IN THE CHEMICAL, MINING, AND FUEL-RELATED INDUSTRIES—A MANUAL

By Joseph M. Kuchta[1]

ABSTRACT

This Bureau of Mines manual is oriented to the technical needs of an investigation of fire or explosion accidents and includes various practical and theoretical information that is needed in analyzing accidents or evaluating conditions that might lead to an accident. It is applicable to accidents in the chemical, mining, transportation, and other fuel-related industries. Specific procedures for conducting an accident investigation are outlined, and various guidelines are given for developing the fire or explosion evidence. Ignitability, flammability, and physicochemical data are presented for over 500 combustible gases, liquids, and solids; empirical and theoretical expressions are also given for extrapolating the behavior of combustible-oxidant-diluent systems to various environmental conditions. In addition, various data pertinent to damage analysis are summarized to facilitate the task of the investigator in developing plausible accident scenarios.

[1]Research scientist, Pittsburgh Research Center, Bureau of Mines, Pittsburgh, PA (retired).

INTRODUCTION

Accidental fires and explosions generally occur when combustibles are produced, transported, or utilized in a hostile environment or under unsafe conditions. Proper investigation of such accidents is essential for determining their cause and assessing life or property loss and for preventing their recurrence. This requires a methodical and thorough investigation, knowledge of the basic properties of pertinent materials, understanding of the ignitability and flammability characteristics of the combustible-oxidant system, and understanding of combustion or explosion principles. The main purpose of this manual is to summarize useful guidelines and provide data that are frequently needed for investigating fires and explosions or evaluating conditions that may be conducive to such events. It is applicable to flammable liquids, gases, and solids that may be encountered in the chemical, mining, transportation, or other mineral-fuel-related industries.

Among the most widely used publications on the flammability characteristics of combustibles are the Bureau's bulletins by Zabetakis (*110*)[2] and Coward (*11*). However, these bulletins are limited to liquid and gaseous combustibles, and reference must be made to other publications for similar information on combustible solids. Furthermore, other combustion and physicochemical data that may be required in a hazard analysis are even more widely scattered throughout the literature. Some safety handbooks, such as that of the National Fire Protection Association (NFPA) (*72*), provide various data on many combustibles, but the information is not sufficiently comprehensive for the analysis of an accident; also, the data are rather meager for mining applications. This manual attempts to overcome the scope limitations of the earlier Bureau bulletins and brings together many other essential data for characterizing the reactivity and damage potential of various classes of combustibles.

Ignitability, flammability, and thermochemical data are presented for over 500 combustible gases, liquids, and solids. The main groups of combustibles include hydrocarbons and substituted hydrocarbons, gasolines and lubricating fluids, coals and other mine-related combustibles, and various agricultural, chemical, plastic, metallic, and carbonaceous solids; explosives are beyond the scope of this report, although certain data are included for comparison. Most of the ignitability and flammability data are taken from Bureau publications, but other authoritative sources were also relied upon to complete the data. Generally, the various data represent the most acceptable or conservative values from the standpoint of safety, unless otherwise specified.

This manual is organized to facilitate the task of finding the particular data or information of interest. The initial section outlines specific procedures for accident investigations; the second section presents pertinent definitions and basic concepts for understanding combustion data; the next sections discuss the large compilation of combustion data presented for various combustible classes; and the final section deals with the damage analyses of fire and explosion accidents. The main data compilations are given in summary tables which provide easy access to many useful properties of the combustibles; additional data in the text expand on this data base. Limitations of the experimental data are discussed, and both empirical and theoretical guidelines are given for extrapolating the data to other environmental conditions and for estimating the energy or damage potential of a combustible-oxidant system. Other publications can be referred to for more fundamental knowledge of the combustion processes discussed in this report (*21, 24, 66, 93, 98*).

ACKNOWLEDGMENTS

The Bureau of Mines data in this manual represent selected contributions of various research groups of the Pittsburgh Research Center over at least four decades. Particular acknowledgment is given to the members of the fire or explosion groups with whom the author was associated in advancing the art of safety technology. The author is especially indebted to Drs. Michael G. Zabetakis, presently with the University of Pittsburgh, Pittsburgh, PA, and David S. Burgess, retired, who provided practical and theoretical guidance in the author's research; Aldo F. Furno, Michael J. Sapko, Ralph W. Cato, and George H. Martindill, who conducted many of the ignitability and flammability studies; and Dr. Martin Hertzberg, who collaborated most recently in developing flammability concepts for combustible gases and dusts. Acknowledgment is also given to John Nagy and coworkers for their important contributions in the area of dust explosions.

PROCEDURES FOR ACCIDENT INVESTIGATION

INITIAL ACTIONS

A formal investigation of an accidental fire or explosion is ordinarily conducted by a cadre of technical specialists and responsible officials. In industrial cases, this typically includes plant representatives, safety officers, fire department officials, and experts in combustion and engineering technologies. Where military or civilian Government agencies have jurisdiction, as in mining and aircraft disasters, the makeup and procedures of the investigating team will necessarily be determined by the requirements of the proper agency. In all cases, the team members should meet as soon as possible to obtain a briefing of the accident, decide upon the plan(s) of action, and establish task groups to accomplish various specific objectives. The head of the investigating team must organize and coordinate these actions to ensure that all aspects of the accident are

[2]Italicized numbers in parentheses refer to items in the list of references preceding the appendix.

properly covered. Initial actions that should be taken are—
1. Isolation of accident site.
2. Protection of evidence.
3. Recovery of material evidence.
4. Photographic documentation of evidence.
5. Documentation of witness accounts.

Isolation of the accident site is important to ensure recovery and protection of all available evidence and also to minimize unnecessary human exposure to any hazards that may still exist. Confined areas should be entered with caution since flammable or toxic gases may be present even after a fire. Before removal of any fire or explosion debris, the accident area should be photographed, including detailed color exposures of suspect items; also, tagging and mapping of damaged materials is common practice to avoid subsequent confusion. Where materials are fragmented by an explosion, areas beyond the accident site may have to be searched to recover the items. Those involved in these early actions must protect the evidence from being inadvertently tampered with, destroyed, or lost.

Equally important are the accounts of all available witnesses, including those present in the immediate or remote vicinity of the accident and those who arrive later on the scene, such as firemen and medical personnel. Such accounts should be obtained as soon as possible after the accident with the witness calm and at ease. Of particular interest is what the witness saw, heard, or sensed before and after the accident, as well as the proximity and activity of the witness during the course of events. All witness accounts are recorded in writing, and further interrogations are made when necessary in developing the evidence.

INVESTIGATIVE PROCEDURES

The procedures for investigating accidents will vary from one case to another, but all involve the basic elements of factfinding and problem solving to develop a credible accident scenario. Frequently, the cause of an accident is difficult to pinpoint because the available evidence is incomplete, inconsistent, or only circumstantial. Therefore, it is necessary to have a methodical plan for accumulating and developing evidence, both direct and indirect, that will be needed to fully explain an accident. A recommended plan of investigation is summarized herein, including—
1. Accumulation of background information.
2. Inspection of accident site.
3. Interrogation of witnesses.
4. Development and analysis of evidence.
5. Conclusions and report.

Background Information

At the outset, the investigator should obtain all available background information pertaining to the accident. This includes a description of the accident site and systems or operations involved, conditions and events that led to the accident, performance histories of any suspect systems, and all the available evidence accumulated from any initial actions. Particularly important are what combustibles and oxidants were present and what abnormal or hazardous conditions existed that might account for the accident. A close examination should be made of witness accounts, maintenance records, operational logs and manuals, weather reports, previous accident reports, and other records that may be helpful in developing the evidence. Recent changes in equipment, procedures, or operating conditions can be especially significant. The investigator must be open-minded and reserve any judgment until all human and material factors have been fully considered.

Site Inspection

Inspection of the accident site is one of the most important steps in obtaining physical evidence. Initially, an examination is made of the overall operation involved and damage sustained by the immediate and remote surroundings. The investigator should prepare an areal map on which the damage patterns, including fragments from any explosion, can be spatially defined. Subsequently, a detailed examination is made to obtain evidence on the apparent origin, propagation, and localized damage of the fire or explosion. This should include examination of all electrical and mechanical systems as possible problem sources. The area with the greatest damage is generally given the most initial attention because it is normally the source of the combustible. The following items are typical of the evidence which an investigator must uncover or consider:
1. Combustible quantity, distribution, and consumption.
2. Combustible leakage or spillage.
3. Open flame heat sources.
4. Electrical and mechanical heat sources.
5. Chemical-type heat sources.
6. Fire condition, propagation, and damage.
7. Explosion condition, propagation, and damage.
8. Material and system failures.
9. Operator or human error.

Witness Interrogation

After inspection of the accident site, the investigator should review the witness accounts for consistency with the physical evidence and interrogate any witnesses, as may be necessary, to help clarify any inconsistencies. It is important to recognize that witness accounts of accidents are subject to sight and hearing limitations in resolving a rapid series of events. For example, it is not unusual for a witness to claim hearing two explosions when only one actually occurred, or to give poor estimates of distances to an object or between two moving objects because of confusion during an accident; similarly, the size and velocity of moving objects are frequently exaggerated. Therefore, witnesses should be requested to qualify their observations relative to known landmarks and events to help establish their evidence spatially and temporally. Interrogation of maintenance personnel on any equipment involved should always be included as a standard practice. At this time, the investigator needs to decide what facts are known and what evidence must be substantiated or developed.

Evidence Development and Analysis

Ideally, sufficient evidence should be accumulated to explain all phases of an accident, including the specific cause. The required physical evidence will vary with the type of accident. In fires or explosions, it is particularly important to account for the combustible source, probable ignition source, resultant propagation, and observed damage. The available evidence is analyzed by developing and testing hypotheses that may explain the sequence of events; any assumptions must be consistent with the fully established evidence and basic scientific principles. Some

important considerations in developing the evidence are reviewed in the following paragraphs.

1. Combustible Source.—In a fire situation, various combustible classes can be consumed as the fire spreads. These include ordinary combustible solids or dusts (class A), combustible liquids and gases (class B), combustibles of electrical equipment (class C), combustible metals (class D), or other miscellaneous materials; combustible fire classification is that of NFPA (*72*). Fires that spread rapidly are usually attributable to combustible gases, vapors of highly volatile liquid or solid combustibles, or finely divided solids that are highly flammable. Those that can be initiated without an external heat source are likely to involve pyrophoric, hypergolic, water-reactive, or self-heating combustibles. Soot formation is evidence of hydrocarbon or organic fuel fires, and extremely high temperatures can be indicative of combustion with high-energy fuels or high-strength oxidizers. Any widespread fire will always be accompanied by a wide distribution or dispersion of combustible.

In gaseous or dust explosions, the combustible sources are only those that can form flammable gas, vapor, or dust concentrations in the particular oxidant atmosphere and temperature environment; this implies some degree of confinement. Prime combustible suspects are fuel gases, low-flash-point liquids, gassy solids, and dispersed flammable dusts. The ignitability and flammability characteristics of the suspect combustible-oxidant system should be examined for supporting evidence. When possible, samples of the combustible system are taken for analysis to verify compositions. A likely combustible source also has to be present in sufficient concentration to account for the observed explosion pressure damage. The investigator must realize that relatively low combustible concentrations can be hazardous and that even an "empty" fuel tank may contain sufficient combustible vapor to account for the explosion. Where damage is unusually severe, combustible systems capable of detonation are to be suspected.

2. Ignition Source.—The possible sources of ignition can include electrical, mechanical, chemical, or nuclear forms of energy. Some of the specific types are (1) electrical arcs or sparks from lightning, static electricity, and defective electrical equipment; (2) hot surfaces from mechanical friction, electrical resistance heating, aerodynamic heating, and any vessel or reactor heating; (3) hot gases or flames from pilot burners, combustor exhaust systems, and gaseous compressor systems; and (4) chemical heating from pyrophoric, hypergolic, and spontaneous or self-heating reactions. Most fires or explosions are initiated by electrical sources. The static electricity source should be especially suspected as possible in the pumping of liquids or dusts and similar operations where triboelectrification can occur; this hazard will be greatest in the presence of plastic or nonconductive materials. The most common type of chemical self-heating involves slow oxidation and may be encountered with many combustibles of animal or vegetable oil origin and such ordinary combustibles as coal and charcoal. Self-heating, pyrophoric, and hypergolic ignitions require no external heat source.

In some accidents, the ignition source may be evident from localized heat damage such as weldlike fusion of metals from electrical arcing, discoloration or wear of metals from mechanical friction, and melting of metal materials due to abnormal process temperatures. The heat source in other cases, including electrostatic, self-heating, and hot gas ignitions, is not usually identifiable from the fire or explosion damage; therefore, the investigator must rely upon circumstantial evidence in such cases.

Both the nature of the available heat source and the physical state of the suspect combustible must be considered in determining the ignition source. For example, a flammable gas (such as hydrogen) may have a very low ignition energy but a relatively high ignition temperature; or a flammable liquid spray can have a high ignition energy compared to that possible with homogeneous vapor-air mixtures. Similarly the ignition energy requirements for a solid (such as coal dust) can be excessive for large particles, in which case the ignition temperature can be of greater significance. A proper assessment requires reference to ignition property data.

3. Propagation.—Propagation of a fire or explosion is deduced from the available physical evidence and known flammability properties of the combustible-oxidant system. Gas or dust explosions will propagate only into areas where flammable combustible-oxidant mixtures have accumulated but may then initiate fires of other combustibles. In comparison, fires do not require uniform combustible-oxidant mixtures and can propagate into areas where any concentration of combustible exists; also, the gaseous fire products may be flammable and produce an explosion in a confined environment, as in some coal mine disasters.

To fully characterize the propagation of fires or explosions, the investigator needs to define the consumption rates (burning rates) of the reactants and their flame propagation rates (flame speeds or flame spread rates). Such information may be available in the literature but is necessarily limited to certain temperature, pressure, and combustible-oxidant conditions. Therefore, it is often necessary to extrapolate laboratory data to conditions of interest by the prudent use of empirical rules or laws.

Typically, flame propagation rates of common hydrocarbon gas-air explosions are of the order of several meters per second, or about eight times the burning velocity of the particular mixture composition. In comparison, fires are usually associated with much lower spatial propagation rates, especially in the burning of bulk liquids and solids. However, all fires or flame propagation can accelerate by increased ventilation, turbulence, or wind effects, as in flight vehicles, ventilation ducts, or mine tunnels. The flame spread can be even greater when the fires are supported by strong buoyant forces, such as in a building stairwell or an elevator shaft. Highest propagation rates with liquids and solids will occur when they are finely dispersed or flash vaporized.

Very high propagation rates of the order of a 1,000 m/s or more are possible when deflagrations develop into detonations. Detonations are most likely to be encountered in combustion involving high pressures, high oxygen concentrations, or high-energy fuels. Even ordinary fuel-air systems are capable of detonation, but these require stronger ignition sources or longer flame runup distances.

4. Fire Damage.—Fire damage is largely attributable to the exposure of materials to excessive temperatures or heat. Fire temperatures of ordinary combustibles in air will generally be 1,000° to 2,000° C, but temperatures can be much higher in oxygen or with more exotic combustibles. An investigator's analysis of the fire damage should include consideration of such factors as—

1. Combustible loading and ventilation.
2. Size, shape, and distribution of materials.

3. Proximity and exposure duration of materials.
4. Fire temperatures, burning rates, and heat release.
5. Fire resistance properties of damaged materials.

Maximum fire temperatures will normally be evident where the air or oxygen ventilation is optimum for combustion, whereas the heat flux or heat release will depend additionally upon the combustible loading and burning rate. Most constructional materials cannot withstand the fire temperatures and heat loading from a fully developed hydrocarbon or carbonaceous fuel-air fire. Materials of low fire resistance, such as those having low melting points or ignition temperatures, will be consumed or largely destroyed; this will be especially the case for fine wires, sheet materials, or finely divided substances. However, one should also expect highly fire-resistant materials to fail when the fires are of severe intensity. On the other hand, even paper will not ignite if its exposure time to flame is too short or if its proximity to the heat source is too remote.

Ordinarily, material failures will be severest in fires involving large combustible loadings (as in fuel storage facilities), high ventilation or turbulence levels (as in aircraft flight applications), high oxidant concentrations (as in hyperbaric chambers), or high-energy combustibles (as in space rocket applications). Few materials will survive a torchlike fire, particularly one in oxygen; such intense fires are often evidenced by the erosion and fusion of metals. Similar metal damage can also occur in electrical fires, although any metal fusion due to electrical arcing will be more localized and display beadlike welds. Damage to powered equipment (motor, pumps, compressors, etc.) is often attributed to electrical or mechanical malfunctions but can be a result of the fire itself. Temperature limitations of materials and the extent of their fire exposure should be considered in making the fire damage assessment.

5. Explosion Damage.—Explosion damage is caused by the high pressures and winds that are generated by the sudden release of chemical or physical energy. Although the damage analyses may vary with the complexity of the explosions, they should at least include consideration of the following important items:

1. Combustible loading and confinement.
2. Explosion pressures, propagation rates, and energy release.
3. Pressure limitations of containment materials.
4. Nature of containment failure.
5. Blast wave or far-field effects.
6. TNT energy equivalence.

The most common explosions will involve the ignition of flammable vapor-air mixtures in a confined environment. If near-stoichiometric mixtures are present, the explosion pressure in a fully confined system can be approximately eight times the initial pressure ($P_2/P_1 = 8$). Such internal pressure loading will be evidenced by the rupture of the container unless it can sustain the explosion pressure. Similar damage can result in the absence of combustion, as in the failure of an overpressurized steam boiler, compressed gas cylinder, or cryogenic liquid receiver; the rupture of an evacuated chamber (implosion) or a decompressed aircraft compartment also falls into this category. Other explosions may produce damage from a combination of physical and chemical energy release. These include fuel tank explosions under high-impact conditions, furnace explosions of molten metal and water or combustible liquids, and boiling liquid-expanding vapor explosions (Bleves). In all cases, the explosion damage will be more severe when combustion involves high oxygen concentrations, elevated pressures, or highly turbulent environments. Detonations are more likely to occur in these situations, in which case the explosion pressure rise ratio (P_2/P_1) can be of the order of 18 to 1 for gaseous systems, or several orders of magnitude greater for condensed explosive systems.

Containment material failure or near-field damage is largely determined by the nature of the pressure loading, the degree of confinement, and the pressure or mechanical limitations of the container, fasteners, and adjacent materials. Explosions in highly confined systems have high damage potential because near-theoretical pressures can develop before any containment failure. In comparison, even an ordinary oven or building can sustain an explosion if it is adequately protected with large pressure relief panels or vent areas. Explosion venting guidelines are available for predicting the safe pressure limits of containments as a function of vent area. The containment failures in ordinary explosions will be evidenced by material stretching or thinning out (tension failure), whereas those in detonations will tend to be more severe and cleaner breaks (shear failure); an implosion will be characterized by a compression-type failure. The pressure limitations of a container can be estimated from a knowledge of the elastic limit or ultimate strength of the container material. However, one must allow for the fact that the dynamic stress is about two to three times the static stress for plastic deformation; pressure ratings of commercial vessels are usually specified for static-type loadings. Any container fragmentation should be expected to be greater for brittle materials than for highly ductile types.

Far-field effects are associated with the explosion damage that results from air blast waves and flying fragments. These effects will be especially evident where strong containments fail owing to detonations or highly energetic deflagrations. Here, the investigator should estimate the TNT energy equivalent of the exploding system from the available chemical energy or potential useful work (gas expansion); apply the cube-root scaling law for predicting blast pressures at any distance from any mass equivalent of TNT; and correlate the estimated blast pressures to published damage thresholds for structural and biological targets. Generally, one can expect a peak overpressure of 1 to 2 psi to cause the failure of most light structural materials, such as nonreinforced wood siding, corrugated steel paneling, or masonry block walls. In comparison, much higher overpressures can be tolerated when the structural design is reinforced, particularly for materials of good ductility. As a rule, pressure thresholds for far-field damage (external loading) will be greater than those for near-field damage, such as a containment failure (internal loading). Where condensed-phase detonable systems are involved, crater formation will also be possible besides far-field damage.

Conclusions and Report

All the available direct and indirect evidence is finally reviewed for accuracy and reliability to define the most likely sequence of events and probable cause(s) of the accident. Any hypotheses proposed to explain the accident should be logically and technically consistent with the

established evidence. A proper analysis will include consideration of both material and human factors. To complete the investigation, the investigator should prepare a summary report on the accident. This should include a description of the accident, accounts of witnesses, evidence from field inspection, analysis of evidence, and development of accident scenario to explain the cause of the accident. Most importantly, system malfunctions and hazardous conditions should be identified, and specific recommendations should be made to prevent recurrence of the accident, including both operative and protective measures.

THEORY AND DEFINITIONS

PHYSICAL GAS LAWS

Pressure-volume-temperature (PVT) relationships are important in determining material balances for a gaseous system. In most cases, one can assume *ideal gas behavior* and define the initial (1) and final (2) states of a gas as follows:

$$\frac{P_1V_1}{T_1} = \frac{P_2V_2}{T_2} \quad (1)$$

where T_1 and T_2 refer to absolute temperature, such as in kelvins (K). The general form of the ideal gas law is given by

$$PV = nRT = \frac{W}{M}RT \quad (2)$$

or

$$P = \frac{W}{V}\frac{RT}{M} = \rho\frac{RT}{M}, \quad (3)$$

where n, W, M, and ρ are the moles, weight, molecular weight, and density of the gas, respectively; R is a universal gas constant equal to 1.987 cal/(K·mol), 0.08205 L·atm/(K·mol), or 8.314 J/(K·mol) depending upon the P-V units. Thus, the volume of gas will vary directly with absolute temperature and inversely with total pressure. In calculating the moles of gas, it is useful to know that the *molar volume* of any ideal gas will occupy 22.414 L at 1 atm and 273 K (0° C).

For mixtures of ideal gases, the total pressure (P_t) is equal to the sum of the component partial pressures ($P_t = p_1 + p_2 + \ldots$) and proportional to the total number of moles ($N_t = n_1 + n_2 + \ldots$). Hence, the mole fraction (X) of a gaseous component (i) is

$$X_i = n_i/N_t = p_i/P_t, \quad (4)$$

and 100 X_i gives the mole or volume percent. For the vapors of ideal liquids, one uses Raoult's law:

$$X_i \text{ (liquid)} = n_i/N_t \text{ (liquid)} = p_i/p_i^\circ \text{ (vapor)}, \quad (5)$$

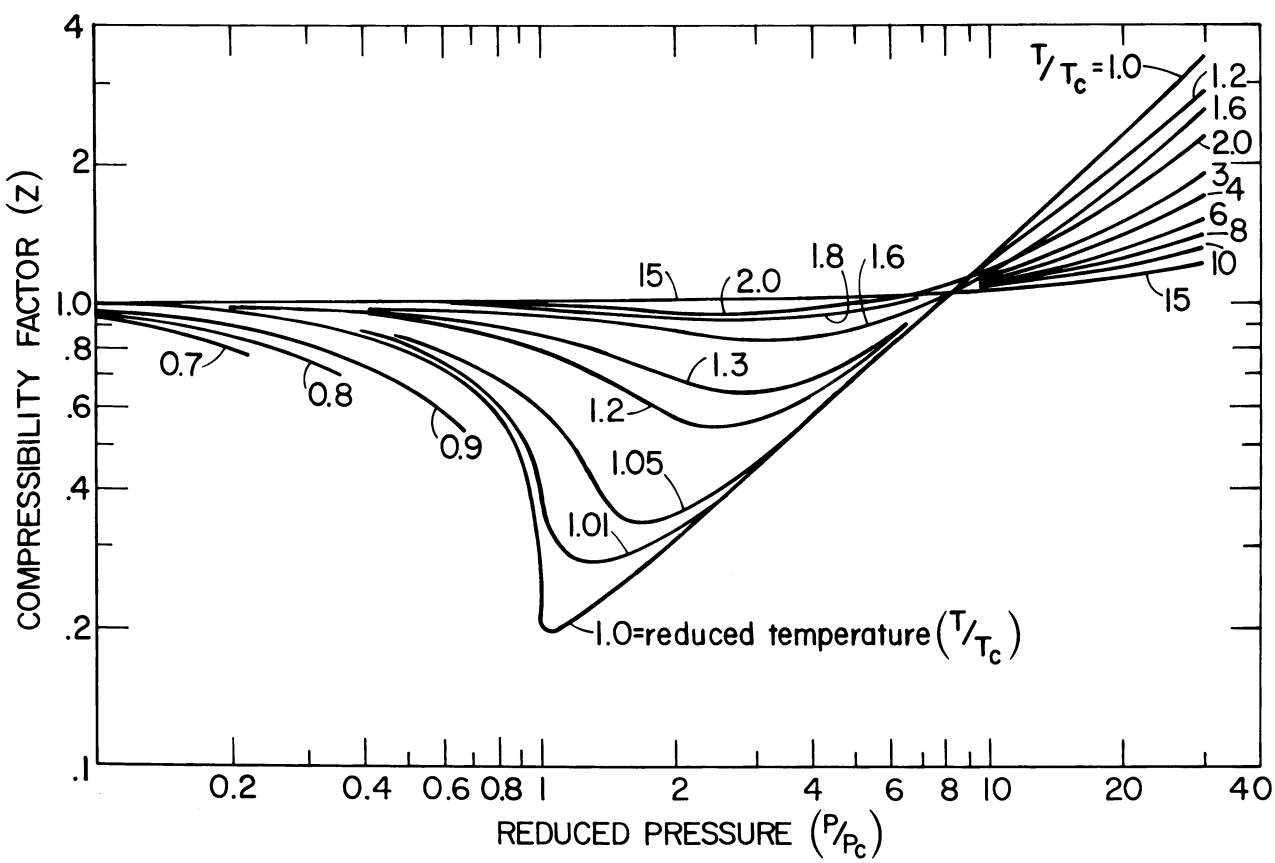

Figure 1.—Compressibility factor as a function of reduced pressure and reduced temperature.

where p_i is partial pressure of the i^{th} component in solution, p_i° is the vapor pressure of the pure component, and X_i is its mole fraction in solution.

Real gases deviate from ideal behavior, particularly when subjected to high pressures or cryogenic temperatures. In such cases, other equations must be used to determine the P-V-T relationships, such as the equation

$$PV = n Z RT, \quad (6)$$

where Z is a compressibility factor and depends upon the critical properties of the gas (P_c, T_c, and V_c). A fair approximation of the Z factor can be obtained for most gases from the generalized compressibility curves (*34*, p. 479) shown in figure 1 in terms of reduced pressure ($\pi = P/P_c$) and reduced temperature ($\Theta = T/T_c$); gases difficult to liquefy, such as hydrogen, give a more complex behavior. Critical states and vaporization properties are given in table 1 for a number of common gases and liquids (*27*, p. 502).

Table 1. — Critical states and vaporization properties of common gases or liquids (*27*, p. 502)

Substance	Boiling point (T_b), K	Heat of vaporization at T_b, kcal/mol	Critical temperature (T_c), K	Critical pressure (P_c), atm
Acetylene	184.7	NA	309.1	61.7
Ammonia	239.8	5.56	405.5	111.5
Benzene	353.3	7.40	561.6	47.7
n-Butane	272.6	5.30	426.0	36.0
i-Butane	263.0	5.08	407.1	37.0
Carbon dioxide	NA	NA	304.1	72.9
Carbon monoxide	81.1	1.41	134.4	34.6
Chlorine	239.5	4.80	417.0	76.0
Ethane	185.9	3.80	305.2	48.8
Ethylene	169.3	NA	282.8	50.7
Ethyl alcohol	351.6	9.40	516.2	63.1
Hydrogen	20.3	.216	33.2	12.8
Hydrogen bromide	206.2	3.95	363.0	84.0
Hydrogen chloride	189.5	3.60	324.5	81.6
Hydrogen cyanide	299.2	5.70	458.6	56.9
Hydrogen sulfide	213.4	4.49	373.5	88.9
Methane	111.7	1.95	191.1	45.8
Methyl alcohol	337.8	8.41	513.2	98.7
Nitrogen	77.3	1.36	126.0	33.5
Nitrogen oxide	121.4	NA	179.0	65.0
Nitrogen dioxide	NA	NA	431.0	99.0
Oxygen	90.2	1.61	154.3	49.7
Propane	231.0	4.50	369.9	42.0
Propylene	226.2	NA	364.8	45.0
Sulfur dioxide	263.2	6.08	430.3	77.7
Water	373.2	9.717	647.3	218.2

NA Not available.

STOICHIOMETRY

Combustion material balances will vary with the composition and concentration of the reactants and the nature of the products at the reaction conditions. Theoretically, the maximum heat release should occur at the *stoichiometric concentration* (C_{st}) that defines the optimum molar concentration of combustible for complete reaction with the particular oxidant; fuel-lean mixtures suffer from oxidant dilution and fuel-rich mixtures from incomplete reaction. The stoichiometry for complete combustion of a simple hydrocarbon in oxygen is given by the expression

$$C_cH_h + \left(c + \frac{h}{4}\right) O_2 \rightarrow c\,CO_2 + \frac{h}{2}\,H_2O, \quad (7)$$

and for substituted hydrocarbons by the general expression

$$C_cH_hO_mN_nX_x + \left(c + \frac{h\text{-}x\text{-}2m}{4}\right)O_2 \rightarrow c\,CO_2 + \left(\frac{h\text{-}x}{2}\right)H_2O + x\,HX + \frac{n}{2}\,N_2, \quad (8)$$

where X is any halogen atom. Thus, the C_{st} of methane (CH_4) in oxygen $\left(\frac{100}{(1 + c + h/4)}\right)$ is 33.3 mol pct. For combustion in air,

$$C_{st}\,(\text{in air}) = \frac{100}{1 + 4.773\left(c + \frac{h\text{-}x\text{-}2m}{4}\right)}\ \text{mol pct}, \quad (9)$$

where 4.773 is the reciprocal of the molar oxygen concentration in air (0.2095). By this equation, one obtains a C_{st} of 9.48 mol pct for methane in air. Similar expressions may be derived for incomplete or other combustion reactions in which H_2, CO, NO_2, or other possible products are assumed. For example, if NO_2 instead of N_2 is an assumed product, the oxygen term in equations 8 and 9 would be

$$\left(c + n + \frac{h\text{-}x\text{-}2m}{4}\right).$$

The volume percentages can be converted to a weight basis from a knowledge of the densities or molecular weights of the mixture components. As an example, the fuel-air weight ratio (F/A) of a stoichiometric mixture is given by

$$(F/A)_{st} = \frac{M}{28.97}\left[\frac{C_{st}\,(\text{vol pct})}{[100 - C_{st}\,(\text{vol pct})]}\right], \quad (10)$$

where M is the fuel molecular weight and 28.97 is the air molecular weight. Pertinent properties of air are summarized in tables 2 and 3.

Table 2. — Major components of dry air (*43*, *105*)

Constituent	Molecular weight	Density (0° C), g/L	Specific heat (20° C), cal/(g·° C)	vol pct
Nitrogen	28.01	1.251	0.249	78.09
Oxygen	32.00	1.429	.219	20.95
Argon	39.94	1.784	.124	.93
Carbon dioxide	44.01	1.977	.200	.033
Air	28.97	{ 1.293 (0° C) } { 1.205 (20° C) }	.240	100.0

Table 3. — Standard air atmosphere (*43*)

Altitude ft	Temperature, °C	Pressure, bars	Density, kg/m³
0	15	1.013	1.225
1,000	13	.977	1.190
5,000	5	.842	1.056
10,000	−5	.696	.905
15,000	−15	.571	.771
20,000	−24	.465	.654
30,000	−44	.301	.458
40,000	−55	.188	.300
50,000	−55	.116	.186
60,000	−55	.072	.115

THERMODYNAMIC RELATIONSHIPS

A knowledge of thermodynamic properties is essential in calculating the energy balance of a given system. The energy change may be in the form of work performed or heat transferred relative to the system surroundings. By the first law of thermodynamics (energy conservation), the energy change (ΔE) is

$$\Delta E = Q - W, \tag{11}$$

where Q is the heat absorbed (positive) and W is the work done by the system (positive); heat evolved or work on the system would be negative. For an *isothermal process* ($\Delta E = 0$), the total mechanical work ($W = \int PdV$) of expansion or compression of an ideal gas is

$$W = n\,RT\,\ln V_2/V_1 = n\,RT\,\ln P_1/P_2; \quad P_1V_1 = P_2V_2. \tag{12}$$

For an *adiabatic process* ($Q = O$), the total work ($W = -\int Cv\,dT$) is

$$W = n\,C_vT_1\,[1 - (P_2/P_1)^{R/C_p}];\ P_1V_1^{\gamma} = P_2V_2^{\gamma}, \tag{13}$$

where C_v and C_p are molar heat capacities, γ is C_p/C_v ratio, and their subscripts refer to constant volume (v) or constant pressure (p). Figure 2 shows how much greater the volume change of an ideal gas can be in an isothermal compression as compared to an adiabatic compression at various pressure ratios. In the adiabatic process, the temperature change is

$$T_2/T_1 = (V_1/V_2)^{R/C_v} = (P_2/P_1)^{R/C_p}. \tag{14}$$

Reactions may occur at constant volume or constant pressure. Under constant volume, where no mechanical work is performed ($W = O$), the heat change by equation 11 would be $Q_v = \Delta E$; at constant pressure, the heat change

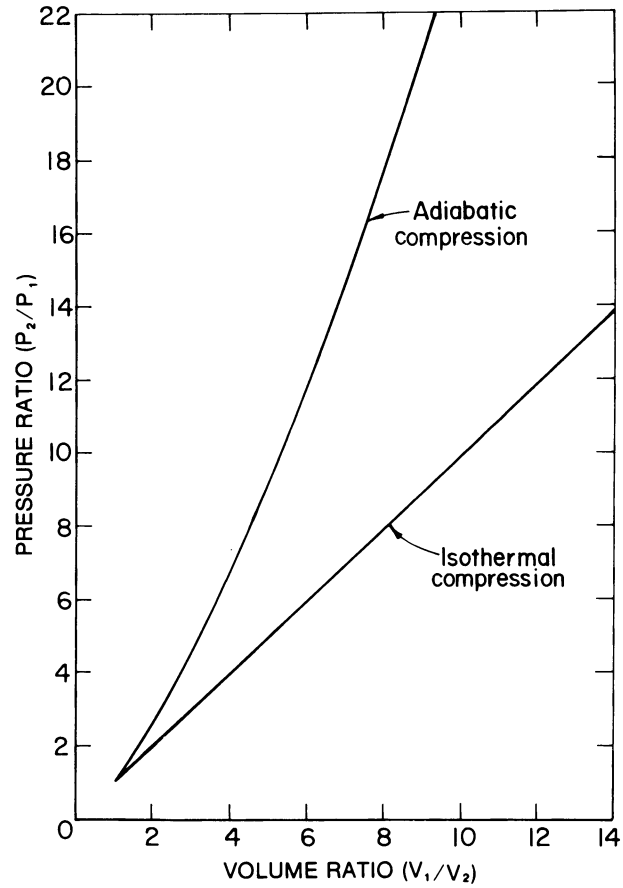

Figure 2.—Variation of pressure ratio with volume ratio in adiabatic and isothermal compression of an ideal gas.

is $Q_p = \Delta E + P\Delta V$. Since the heat content or enthalpy (H) of a system is

$$H = E + PV \tag{15}$$

and $\Delta H = H_2 - H_1 = Q_p$, the heat change at constant pressure becomes

$$\Delta H = \Delta E + P\Delta V = \Delta E + \Delta n\,RT, \tag{16}$$

where Δn is the change in the moles of gas after reaction of the system. Equations 15 and 16 are very useful because most standard thermodynamic properties are at constant pressure. The molar heat content of a number of common product gases is given at various temperatures in table 4;

Table 4. — Heat content (enthalpy) of combustion product gases at various temperatures[1]

Temperature, K	Heat content, kcal/mol						
	H_2	O_2	N_2	CO	CO_2	H_2O	NO
298.16	0	0	0	0	0	0	0
400	.71	.72	.71	.71	.94	.82	.73
600	2.10	2.21	2.13	2.14	3.09	2.51	2.19
800	3.51	3.78	3.60	3.63	5.45	4.30	3.72
1,000	4.94	5.43	5.13	5.18	7.98	6.21	5.31
1,200	6.40	7.11	6.72	6.79	10.63	8.24	6.96
1,400	7.91	8.83	8.35	8.45	13.36	10.38	8.64
1,600	9.45	10.58	10.01	10.13	16.15	12.63	10.36
1,800	11.04	12.35	11.71	11.84	18.99	14.96	12.09
2,000	12.66	14.15	13.42	13.56	21.86	17.37	13.84
2,200	14.31	15.97	15.14	15.30	24.75	19.84	15.60
2,400	16.00	17.80	16.88	17.05	27.67	22.37	17.37
2,600	17.71	19.66	18.63	18.81	30.61	24.94	19.14
2,800	19.45	21.54	20.39	20.58	33.56	27.55	20.93
3,000	21.21	23.45	22.16	22.36	36.53	30.20	22.72

[1]Data from reference 28 rounded off to 2 decimal places.

298.16 is the reference zero enthalpy state. These data are derived from the heat capacity relationship at constant pressure, $C_p = dH/dT$; the corresponding relation at constant volume is $C_v = dE/dT$; C_v is usually obtained from the approximation $C_p - C_v = R$. The constant-pressure heat capacity data are particularly important in calculating the final temperature of a reacting system, as discussed in a later section.

In a chemically reactive system, the reaction may evolve heat (exothermic) or absorb heat (endothermic). The heat of reaction (ΔH) is indicated by the enthalpy change of the reactants from their initial state to the final or product state. Here, the enthalpy change can be calculated by use of the heats of formation (ΔH_f – kcal/mol) of each specie; the standard values are defined at 25° C (298 K) and 1 atm. This is illustrated below for the complete combustion of methane at constant pressure with water formed as a liquid (l) or vapor (g):

$$\begin{matrix} CH_4 & + & 2O_2 & \rightarrow & CO_2 & + & 2H_2O(l); & \Delta H_{298} = \\ -17.9 & & 0 & & -94.05 & & 2(-68.3) & \end{matrix} \quad (17)$$

-212.8 kcal/mol.

$$\begin{matrix} CH_4 & + & 2O_2 & \rightarrow & CO_2 & + & 2H_2O(g); & \Delta H_{298} = \\ -17.9 & & 0 & & -94.05 & & 2(-57.8) & \end{matrix} \quad (18)$$

-191.8 kcal/mol,

ΔH_f values are given below each specie, and ΔH is equal to the sum difference of ΔH_f (products) $-\Delta H_f$ (reactants); negative ΔH indicates heat is evolved. The variation between the ΔH values (-212.8 versus -191.8) is equal to the latent heat of vaporization of water, i.e.,

$$H_2O\ (l) \rightarrow H_2O(g);\ \Delta H_{298} = 10.5 \text{ kcal/mol}. \quad (19)$$

Essentially, the larger ΔH represents the gross heat of combustion (ΔH_c), and the smaller ΔH is a net ΔH_c that is most meaningful when one is concerned with the product state at flame temperatures. Standard ΔH_f and ΔH_c (net) values are compiled in the summary data tables that are presented for each class of combustibles; the ΔH_f values can be used to calculate the ΔH_c values for other reactions of interest.

If the reactions occur under constant volume (closed system), the heats of reaction would not include any PV work ($\Delta V = O$) and would be defined by

$$\Delta E = \Delta H - \Delta n\, RT. \quad (20)$$

For example, the change in gaseous moles in equation 18 is zero and, therefore, $\Delta E = \Delta H$. However, in the case of equation 17 where $\Delta n = -2$,

$$\begin{aligned} \Delta E &= -212.8 + 2 \times 1.987 \times 10^{-3} \times 298 \\ &= -211.6 \text{ kcal/mol}. \end{aligned} \quad (21)$$

It is evident that unless Δn is large, differences between heats of reaction at constant volume and constant pressure will be small.

IGNITION PROCESSES

General Concepts

Ignition is usually considered to be a vapor-phase combustion reaction with the evolution of heat and emission of light that may or may not be visible to the naked eye. Such reactions are most often associated with the rapid oxidation of a combustible in air or oxygen. They may also occur with other oxidants, such as the halogens and nitrogen oxides, as well as without any oxidant when the combustible is capable of highly exothermic decomposition. The potential heat release for any reacting system can be calculated from thermodynamic considerations, but the combustion rate or intensity will depend upon the chemical kinetics at the reaction conditions. For example, in the constant-pressure reaction of hydrogen and oxygen,

$$H_2 + 1/2\ O_2 \rightarrow H_2O(g);\ \Delta H_{298} = -57.8 \text{ kcal/mol}, \quad (22)$$

the theoretical heat release is 28.9 kcal per gram of hydrogen. If this heat is produced rapidly and results in a branching chain reaction, high temperatures and flaming combustion are possible. However, if the heat is generated at a slow rate, as in a low-temperature oxidation process, flaming combustion is unlikely to occur unless the slow oxidation can initiate a self-accelerating reaction.

Most combustible-oxidant systems are not capable of sufficient self-reaction at ambient temperature to produce ignition. Generally, they require heating to some critical level by an external temperature or energy source. It is useful to consider the sources in terms of their spatial and temporal characteristics, as illustrated in figure 3. At one extreme (electrical sparks), the source is infinitesimally small and very high in temperature and heating rate; here, one is primarily concerned with energy density and the ignition energy. At the other extreme (heated vessels), the source is large, heating rate is very low, and temperature is also relatively low; here, one is mostly concerned with the concept of an ignition temperature. Thus, it is most meaningful to define ignition requirements in terms of energy for a highly concentrated heat source and in terms of temperature for a distributed heat source; an exception

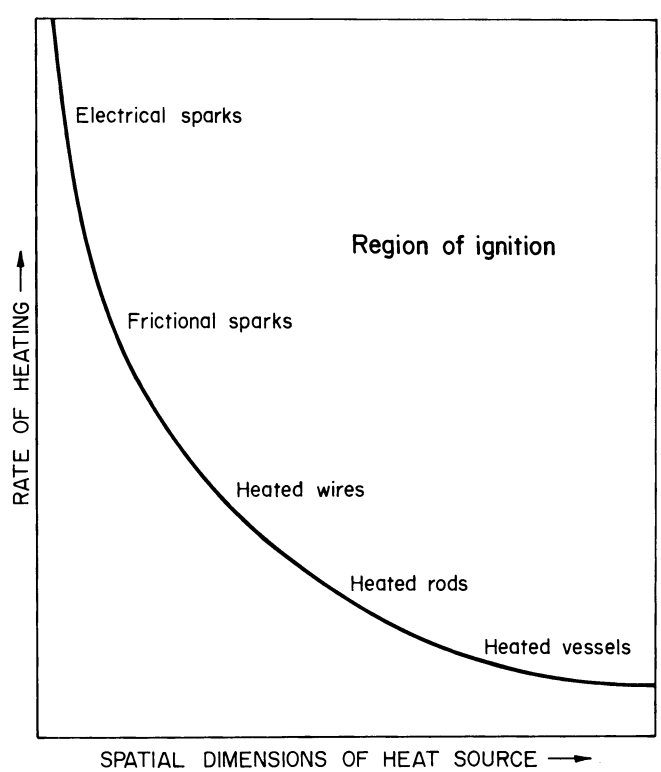

Figure 3.—Temporal and spatial characterization of various ignition sources.

is a large radiative heat source, which is usually defined in terms of energy.

Basically, ignition sources can be classified as either thermal or chemical types, the former being by far the most predominent type. In practice, electrical ignitions are treated as a separate category, although they are of a thermal nature; also, some ignitions are considered as thermal (self-heating) or chemical (pyrophoricity or hypergolicity) but are unique in that they do not require any external heat source. With this in mind, the various ignition sources may be categorized as follows:

Electrical ignitions:
1. High-voltage sparks or arcs.
2. Low-voltage sparks or arcs.

Thermal ignitions:
1. Hot surfaces:
   a. Heated vessels or walls.
   b. Heated wires or rods.
   c. Heated particles or frictional sparks.
2. Self-heating (spontaneous combustion).
3. Hot gases:
   a. Heated gas jets or pilot flames.
   b. Adiabatic or shock compression.
4. Thermal radiation.

Chemical ignitions:
1. Catalytic materials.
2. Pyrophoric and hypergolic mixtures.

Electrical Ignition

The simplest form of electrical ignition is a thermal process in which excessive surface heating is produced by the resistance to current flow in an electrical circuit. This resistance heating can be calculated from

$$E = VIt = I^2Rt, \quad (23)$$

where E is heat (J), V is potential difference (V), I is current (A), R is resistance (Ω), and t is time (s); Ohm's law (V = IR) is applied here. Ignitions by such heating may occur within a second or more and fall in the hot surface temperature category that is discussed later.

Other electrical ignitions involve sparks or arcs in which the energy approximates a point source and the heating duration may be as little as a fraction of a microsecond. These can be classified as a high-voltage or electrostatic type and low-voltage or break spark type. In the case of *electrostatic sparks*, they are formed when the electrical charge of a conductor is sufficient to bridge ("jump") the gap to another conductor or nonconductor. The energy of electrostatic discharge is given by

$$E = 1/2\ CV^2, \quad (24)$$

where E is the stored energy (J), C is capacitance of the charged conductor (F), and V is the potential difference (V); the capacitance is related to the electrical charge (Q) by C = Q/V, where Q is in coulombs. In the case of *break sparks*, they are formed when current-carrying conductors are abruptly separated to result in a collapsing field, such as when an electrical switch is opened. The energy of break sparks or arcs is given by

$$E = 1/2\ LI^2, \quad (25)$$

where L is the inductance (H). Although such energies can be orders of magnitude greater than those associated with capacitative spark discharges, the differences are not so noticeable when the breaking circuit involves a short gap length, as in the rapid separation of very fine wires.

Capacitative spark-type discharges are generally relied upon to determine the *minimum ignition energy* (MIE) of a combustible vapor-oxidant system. The MIE value occurs at an optimum spark gap length (electrode separation) and varies with temperature, pressure, and combustible-oxidant concentration; the optimum gap is referred to as the *minimum ignition quenching distance*. Figure 4 shows how the spark ignition energy can vary with the fuel-air weight ratio (F/A) for the butane-air system (*41*). Although stoichiometric butane combustion occurs at an F/A of 0.065 (3.12 vol pct), the MIE falls on the rich side of stoichiometric for this fuel. This figure also shows that whereas the minimum spark energy for ignition may be only a few tenths of a millijoule, it tends to be infinitely large as the mixture ratio approaches the limits of flammability.

The minimum ignition quenching distances in this context imply an optimum electrode design that maximizes

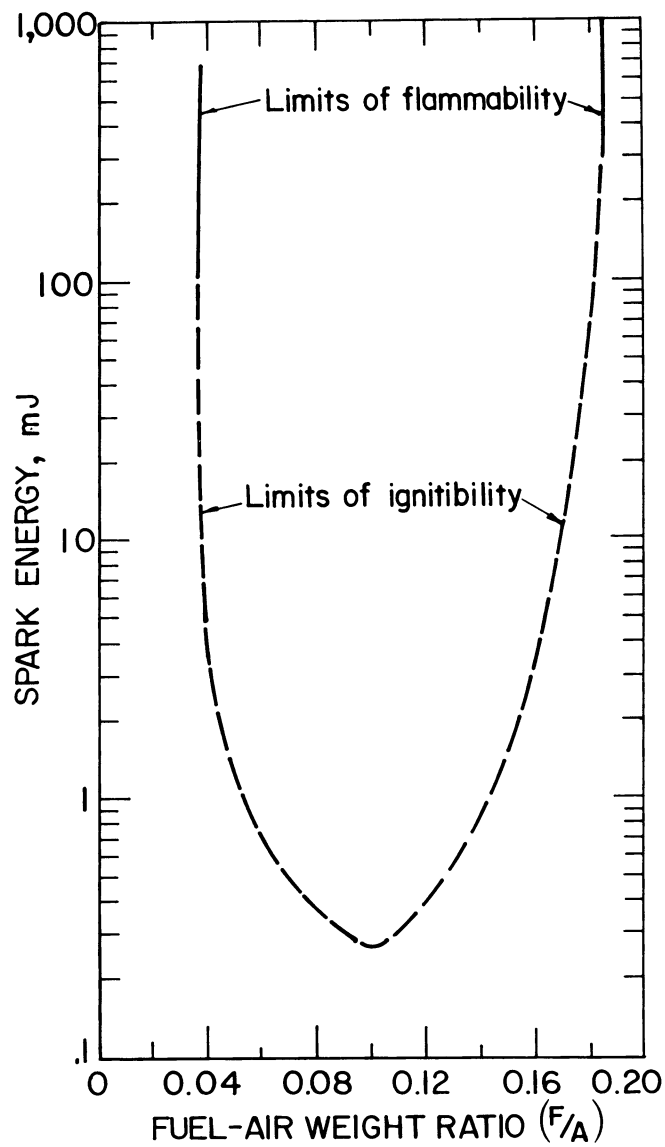

Figure 4.—Spark energy versus fuel-air ratio for ignition of n-butane-air mixtures at 25° C and 1 atm.

the spark energy efficiency in a quiescent mixture. They should not be confused with *minimum ignition quenching diameters* since these involve flowing mixtures and larger quenching surfaces; quenching diameters are roughly 1-1/2 times greater than corresponding quenching distances for many ordinary fuels, largely because of greater heat losses. In contrast, the so-called *maximum experimental safe gaps* involve much more severe combustion conditions, including both elevated pressures and large flame runup distances, which result in high turbulence, high flame speeds, and pressure piling (*71*). Thus, safe gap values tend to be much smaller than the ignition quenching distances that involve combustion at low flame propagation rates.

Generation of *static electricity* is commonly known to occur by triboelectrification, i.e., from the frictional action of two electrically unlike materials. The materials can be liquids, solids, and/or gases, one of which needs to be a relatively poor conductor for the charge to accumulate. This frequently occurs in the pumping of fluids, pneumatic transport of solids, and processes involving plastics. Even a human body can accumulate hazardous static charges (*101*). For example, by equation 24, an average human with a capacitance of 300×10^{-12} F and charge of 10,000 V could conceivably produce a static discharge of 0.015 J (15 mJ), which is much greater than the MIE of most combustible-air systems. The ability of a nonconductor (or conductor) to accumulate a static charge will depend upon its resistivity $\frac{(\text{resistance} \times \text{area})}{(\quad \text{length} \quad)}$ as well as that of the surrounding medium. Obviously, charge dissipation will be greater in a liquid than in a dry gaseous medium, indicating the importance of humidity.

Thermal Ignition

Most thermal sources other than sparks or arcs tend to be much less localized spatially and temporally. These are discussed below, together with the concept of an ignition temperature or critical heating, which is basic to thermal ignition theory.

1. *Hot Surfaces.*—In the simplest terms, thermal ignition is a combustion reaction in which the limiting condition is determined primarily by the rate of chemical heat release versus the rate of heat loss to the surroundings. The rate of chemical heat release (q_1) by the Semenov theory (*93*), which assumes a uniform temperature distribution, is given by

$$q_1 = VQZ\, a^n e^{-E/RT}, \tag{26}$$

where V is vessel volume, Q is heat reaction, Z is rate frequency factor, a is reactant concentration, n is order of reaction, E is activation energy, R is universal gas constant, and T is the reactant absolute temperature. Also, the rate of heat loss (q_2) is defined by

$$q_2 = \alpha\, S\, (T - T_o), \tag{27}$$

where α is heat transfer coefficient, S is wall surface area, and T_o is wall temperature. The critical heating condition for ignition is that temperature and pressure at which $q_1 = q_2$. Based on this theory, ignition temperature will be a function of the S/V ratio of the vessel, or roughly its reciprocal diameter ($S/V \propto d^2/d^3 = 1/d$). The variation of the *time delay to ignition* (τ) with temperature is given by the following useful expression:

$$\tau P^n = A\, e^{E/RT}, \tag{28}$$

which at constant pressure (P) yields

$$\log \tau = \frac{0.22\,E}{T} + A', \tag{29}$$

where A and A′ are system constants and E is the apparent activation energy of the global processes controlling τ, i.e., the temperature coefficient of ignition delay. The lowest temperature that can accelerate the reaction to ignition occurs when the ignition delay (or induction period) is maximized and the vessel S/V ratio is minimized; this temperature is commonly referred to as the *minimum autoignition temperature* (AIT).

Figure 5 illustrates typical AIT data obtained for the n-decane-air system by injecting various quantities of liquid fuel in an open heated vessel; a plot of log τ versus 1/T is more useful to define E and A in equation 29. Corresponding data under flowing conditions, where the contact time with the heated surface is shorter (<1 s), would be characterized by smaller τ and greater AIT values. In all such ignitions, the AIT's will be sensitive to fuel composition, fuel-oxygen ratio, pressure, and nature of the container surface. Generally, hot surface ignition temperatures increase with decreasing diameter or area of the heat source, although this dependence may not be uniform over a wide temperature range.

2. *Self-heating.*—A more rigorous thermal theory is one developed by Frank-Kamenetskii (*21*, p. 209) in which a nonuniform temperature distribution is assumed. It is particularly suitable for predicting the size of the reactant mass that may undergo self-heating at various ambient temperatures. Here, time delay to ignition can be of the order of hours or days in the case of adiabatic self-heating, as opposed to only minutes or seconds in the case of isothermal heating by an external source. The *self-heating*

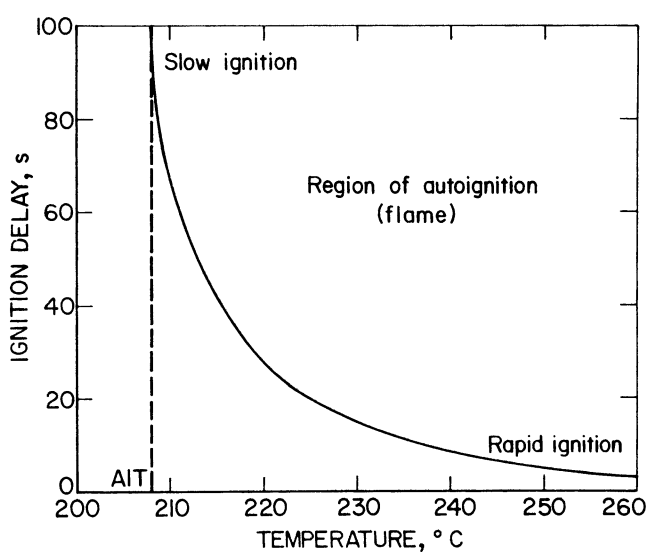

Figure 5.—Ignition delay versus temperature for autoignition of n-decane in air at atmospheric pressure.

rate (q) is defined as the sum of the chemical heat release rate (q_1) and the conductive heat loss rate (q_2):

$$\underset{(q)}{\rho C \frac{\partial T}{\partial t}} = \underset{(q_1)}{\rho Q Z e^{-E/RT}} + \underset{(q_2)}{\lambda \nabla^2 T} \qquad (30)$$

where ρ is density, C is specific heat, λ is thermal conductivity, ∇^2 is a differential operator, and other quantities have the same meaning as above. For steady state conditions ($\partial T/\partial t = 0$), $q_1 = q_2$ and the critical mass radius (r_c) that will self-heat is

$$r_c = \left[\frac{\delta_c \lambda RT^2}{\rho E Q Z e^{-E/RT}}\right]^{1/2}, \qquad (31)$$

where δ_c is a shape factor that is equal to 3.33 for a sphere, 2.0 for a cylinder, and 0.88 for plane-parallel slabs. For adiabatic conditions ($\partial T/\partial x = 0$), $q = q_1$ and the critical temperature rise rate for self-heating is

$$dT/dt = \frac{QZ}{C} e^{-E/RT} \qquad (32)$$

Thus, autoignition by self-heating is strongly dependent upon the dimensions of the reactant mass, whereas autoignition by external heating depends more upon the dimensions of the heat source (heated vessels, wires, rods, etc.). In real self-heating situations, convective heat transport cannot be fully neglected as done in equation 30. For example, the self-heating of conical coal piles is due in part to the favorable "chimney effect" that can occur during the weathering of coal; furthermore, the *heat of wetting* itself can be greater than the heat of oxidation at ambient temperature. In all ignitions of combustible solids, the reactions will be particularly sensitive to particle size, bed porosity, moisture conditions, and the air ventilation rate.

3. *Hot Gases.*—As with heated surfaces, ignitions by hot gas sources also differ in their temporal and spatial characteristics. *Shock wave heating* (nonisentropic) is the most localized in space and time (e.g., <1 ms), whereas *adiabatic compression heating* (isentropic) is more spatially distributed and, therefore, should effect ignitions of combustible mixtures at lower temperatures. Table 5 compares the air temperatures possible in shock wave and adiabatic compression heating at various pressure ratios; it is apparent that shock compression temperatures are noticeably greater than adiabatic compression temperatures at a given pressure ratio. According to this table, it would appear that a combustible-air mixture with an AIT of 200° C could be ignited at a shock pressure ratio of at least 5 or an adiabatic compression ratio of 10. However, in both cases, much higher pressure ratios would be required because of the short duration of heating involved (milliseconds) as opposed to those associated with minimum AIT's (minutes). Essentially, ignition will not occur unless the elevated heating conditions are maintained for a duration that exceeds the ignition delay at the given temperature.

Table 5. — Shock wave and adiabatic compression temperatures of air (*66*, p. 516)

(P_1 = 14.7 psia; T_1 = 0° C)

Compression ratio (P_2/P_1)	Gas compression temperature (T_2)	
	Shock wave °C	Adiabatic compression °C
2	62	57
5	208	152
10	432	242
50	1,988	521
100	3,588	677
1,000	18,840	1,435

Other hot gas ignitions can involve *heated jets* of air, inert gas, or gaseous combustion products, including luminous and nonluminous flames. They are intermediate on the temporal and spatial scale of heating by hot gases. Although these ignitions involve more complex heat and mass transport processes than in hot surface ignitions, they are also a thermal type and depend upon the enthalpy or heat flux of the heat source. The heat flux of the hot gas jet will depend upon its temperature, diameter, velocity, and composition. Reported ignition temperatures by hot gas jets tend to be higher than those by hot surfaces, but the differences are not likely to be great when compared at the same heat source diameter and fuel contact time with the heat source.

4. *Thermal Radiation.*—Ignitions under this category include those in which a combustible is raised to its AIT by exposure to the thermal radiation of a hot gas, hot surface, or other infrared heat sources, including a fire. Solid or condensed combustibles have the greatest capacity to absorb radiative heating and, therefore, are most likely to be ignited by this heating mode. The radiative ignition requirements for any combustible are usually defined in terms of a critical heat flux. For ordinary combustible solids, the critical *radiant heat flux* for ignition can be a relatively small value (1 to 2 cal/(cm^2·s)), depending upon the ignition temperature of the solid. Such critical radiation intensities can be easily encountered when the combustible is exposed to a nearby flame source since the maximum radiation intensity can be 10 to 30 cal/(cm^2·s) near the flame surface. Generally, approximately 15 to 40 pct of the theoretical thermal output of a large flame source will be radiated to the surroundings (7). Assuming spherical geometry and a flame point source, the radiant heat flux (h_x) at various distances (x) from a flame source, such as a burning pool of radius r, can be estimated by

$$h_x = \frac{h_r \pi r^2}{4 \pi x^2}, \qquad (33)$$

where h_r is the maximum radiative heat flux at the flame surface. The assumption of a hemispherical pool fire model will yield twice the irradiances predicted by equation 33. Factors that can determine the level of thermal flame radiation include fuel-oxidant stoichiometry, soot formation (fuel-rich hydrocarbon flames), and radiative properties of the gaseous combustion products. Hydrogen flames are typical of a low-radiative emitter, and benzene flames, which tend to produce considerable soot, are representative of a high-radiative emitter.

Chemical Ignition

This category represents a special case of autoignition in which the heat of chemical reaction alone can produce ignition at or below ambient temperature. One type is a *pyrophoric reaction* where the combustible ignites spontaneously upon mere exposure to air, as in the self-reaction of alkali metals, metal alkyls, or metal hydrides. Such reactions are usually promoted by the presence of moisture and can involve the formation and ignition of a flammable gas; the combustibles in this case are also referred to as water-reactive substances.

Another type is a *hypergolic reaction* where spontaneous ignition occurs when a combustible is intimately mixed

with a highly reactive oxidizer. These ignitions can occur with ordinary and high-energy fuels and particularly with such high-strength oxidizers as fluorine, hydrogen peroxide, nitrogen tetroxide, and concentrated acids. Their heats of reaction can be calculated from available heats of formation. In the case of acid-base systems, heats of neutralization are typically about 13 to 14 kcal/mol for a strong acid and strong base in aqueous solution. If one also considers the heats of solution, the total heat release can be about 25 to 35 kcal/mol and sufficient to initiate a combustion reaction.

Chemical ignitions also result from *catalytic reactions*. The most common catalysts in organic reactions are finely divided metals, but many different substances can serve as catalysts, depending upon the chemical reactants. Contaminants that accumulate on the walls of a reaction vessel may serve as either ignition catalysts or inhibitors.

FLAME PROPAGATION PROCESSES

Flammable Mixtures

A flammable gaseous mixture of combustible and oxidant is one that, when ignited, will propagate flame beyond the influence of the ignition source. All combustible gases and combustible vapors of liquids or solids form flammable mixtures over a limited range of combustible concentrations, depending upon temperature, pressure, and nature of the oxidant. The critical combustible concentrations are known as the *limits of flammability* or explosion limits of the system and are defined as the fuel-lean or *lower limit* (L) and the fuel-rich or *upper limit* (U). These limits are usually in volume percent and refer to homogeneous combustible vapor-oxidant mixtures. Since the flammability limits vary with temperature and since the vapor formation of a combustible in its liquid or solid state is strongly dependent on temperature, it is useful to construct a flammability concentration-temperature diagram of the type shown in figure 6. A three-dimensional plot to include the pressure effect would be required to completely define the flammability domains.

As shown in figure 6, the flammable mixtures of a combustible liquid-air system may consist of mists (droplets + saturated vapor + air), saturated vapor-air mixtures (vapor pressure curve), or neat vapor-air mixtures (region beyond saturated vapor temperatures). The temperature range over which the liquid can form flammable vapor concentrations is defined by its *temperature limits* of flammability (T_L and T_U); intersections of these temperature limits with the vapor pressure curve define the *concentration limits* of flammability (L and U) at liquid-vapor equilibrium conditions. At higher temperatures, flammability domains for the neat vapor-air mixtures become widened, particularly on the fuel-rich side. Eventually, the temperature can be sufficient to produce autoignition of the mixtures, as illustrated in figure 6.

The lower temperature limit (T_L) is of great practical interest because it defines the minimum temperature to which a combustible liquid or solid must be heated to form a flammable vapor-air mixture, i.e., the lower limit of flammability (L). In practice, this temperature corresponds approximately to the *flashpoint* of the combustible, which is determined under less ideal conditions (downward flame propagation and nonuniform mixtures) than those used in flammability limit determinations (upward propagation and uniform mixtures). *Closed cup flashpoints* are the most reliable values. It is evident from figure 6 that flammable mists, sprays, or foams can form below the flashpoint or T_L of the combustible. However, their ignition energy requirements are much more severe than for neat vapor-air mixtures. The flammability characteristics of mists can be expected to approximate their vapor behavior when the droplet size of the mist is less than about 10 μm.

Various flammability diagrams are used to present complete limit of flammability data for combustible vapor-oxidant-inert systems (*110*). Most data are presented in the form of a rectangular plot, as in figure 7 for the aviation gasoline vapor-air-nitrogen system (*42*). In this plot, the flammability limits in the oxidant alone (air) are found on the ordinate (1.3 and 7.1 pct combustible); also, the variations of these limits with added inert (N_2) are indicated

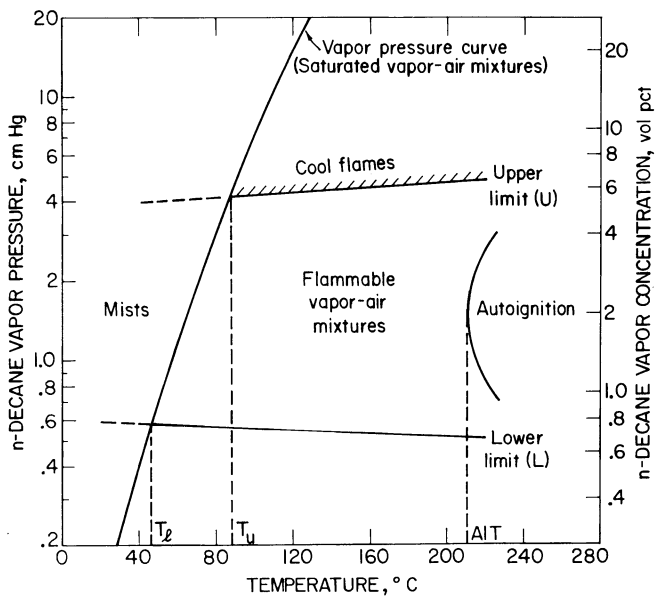

Figure 6.—Flammability and vapor pressure diagram for n-decane vapor-air system at various temperatures and atmospheric pressure.

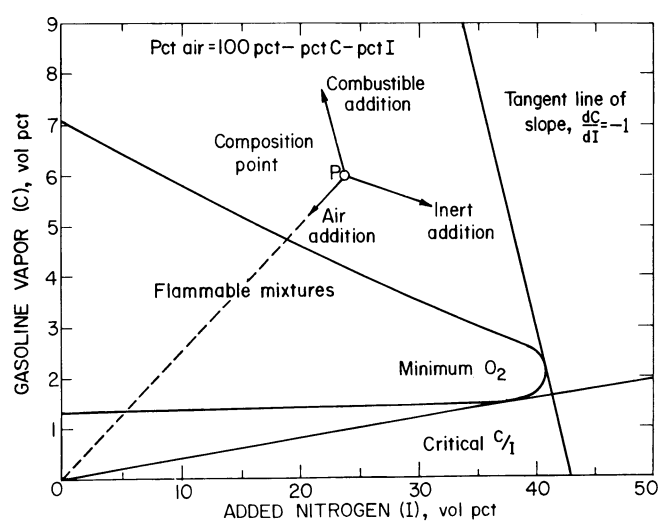

Figure 7.—Flammability diagram for the aviation gasoline vapor (100/130 grade)-air-nitrogen system at 25° C and 1 atm.

by the lower and upper boundaries defining the complete range of possible flammable mixtures for the total system. Any mixture composition point is defined by the following relation:

$$\text{Pct oxidant (air)} = 100 \text{ pct} - \text{pct combustible (C)} - \text{pct inert (I)} \quad (34)$$

The variation of a composition by the addition or reduction of any mixture component is illustrated for a composition (P) outside the flammable zone. Note that additions of air to this composition point could result in the formation of flammable mixtures (see dashed line), but that additions of combustible or inert could not form mixtures that fall into the flammable zone.

Also of great practical interest are the *minimum oxygen concentration* (minimum O_2) and critical *combustible-inert ratio* (critical C/I) below which flammable mixtures cannot form. The minimum O_2 is obtained by drawing a constant oxidant tangent line of negative slope ($dC/dI = -1$) to the nose of the flammability diagram, whereas the critical C/I is found by constructing a tangent line from the origin to the lean side of the nose of the curve. The former is important in determining inerting requirements, and the latter in assessing fire extinguishing requirements.

Generally, limits of flammability are widened by increased temperature, pressure, oxygen concentration, and energy of the ignition source. The limits are also widened by turbulence and buoyancy effects, which increase the flame propagation rate. Essentially, flammability limits may be classified according to their propagation mode, upward or downward. *Upward limits* have the greatest practical value because they include the buoyancy effect and reflect the maximum flammability hazard; *downward limits* exclude buoyancy and are of greater fundamental significance. In addition to buoyancy, the differences between molecular diffusivities of the combustible and oxidant can contribute to the wide variations often observed between these limits; recent papers by Burgess (*5*) and Hertzberg (*30*) provide in-depth discussions of the relevant processes of "selective diffusional demixing" and buoyancy. As with ignition limits, flammability limits are narrowed by heat losses to vessel walls, and propagations can become impossible at some *quenching diameter*.

Prediction of Limits

If the flammability limits of the components of a mixture are known, the limits of the mixture may be calculated by *Le Chatelier's law* (*65*). The specific form of this law for lower limits of complex mixtures in air is

$$L = \frac{100}{C_1/L_1 + C_2/L_2 + \cdots C_i/L_i}, \quad (35)$$

where C_1, C_2---C_i are the proportions of each combustible gas in the mixture, free from air, L_1, L_2---L_i are the lower limits of each combustible gas in air, and L is the lower limit of the complex mixture in volume percent. Although this law predicts fairly reliable lower limits for mixtures of many common fuel gases, it tends to be less reliable for upper-limit calculations because of the more complex reactions. Also, its application to limits of upward propagation that are greatly influenced by preferential diffusion (H_2-air) and to limits of materials that involve chemical flame inhibition (extinguishing agents) presents uncertainties (*5*). The application of Le Chatelier's law to mixtures that include various added inerts is much more complicated and is given in a comprehensive treatment by Coward (*11*).

One of the most useful expressions for predicting the variation of lower flammability limits with temperature is a modified Burgess-Wheeler law suggested by Zabetakis (*110*) for combustible-air mixtures:

$$L_T/L_{25} = 1 - \frac{0.75}{L_{25}\Delta H_c}(T - 25°), \quad (36)$$

where L_T and L_{25} are the lower limits (vol pct) at temperatures T(° C) and 25° C, ΔH_c is net heat of combustion (kcal/mol), and 0.75 is essentially a molar heat capacity constant × 100. If the combustion heat release $\frac{(L_{25}\Delta H_C)}{(100)}$ can be assumed to be a constant value, as it is for many hydrocarbons, the lower limits of the combustibles should decrease linearly with increasing temperature and converge at some limit temperature which corresponds to zero concentration ($L_T = 0$). For hydrocarbons, this limit temperature is about 1,300° C. (See "Flame Temperatures," below). Equation 36 can also be used to calculate the ideal flashpoint of a combustible if its L_{25} value and vapor pressure-temperature relationship are known; construction of a flammability diagram such as figure 6 facilitates this determination. A similar expression is also proposed for upper limits that increase drastically with temperature. However, these calculated values are not always reliable because of cool flames, soot formation, or other incomplete combustion modes associated with fuel-rich flames.

Flame Temperatures

Flames are formed when the gaseous reaction products are heated above some critical temperature that can produce luminous combustion. Those formed by homogeneous gaseous mixtures are defined as *premixed flames* and have well-defined flame temperatures and propagation rates. The maximum flame temperature, $(T_f)_M$, of a mixture is found under adiabatic conditions at or near stoichiometric fuel-oxidant concentrations. In comparison, the *limit flame temperature*, $(T_f)_L$, is the minimum temperature at which a normal flame can be sustained and is, therefore, the value for a lower limit mixture. A simple expression for estimating the flame temperature of a lower limit mixture (L, volume percent) in air under constant pressure is given by

$$(T_f)_L = T_1 + \Delta T = T_1 + \frac{L\Delta H_c}{100\,\overline{C}_p}, \quad (37)$$

where T_1 is ambient temperature, ΔT is temperature rise, ΔH_c is heat of combustion, and $\overline{C}_p$ is average molar heat capacity of the gaseous products between T and the flame temperature $(T_f)_L$. Note that this equation can be derived from Zabetakis' equation 36 by substituting $100\,\overline{C}_p$ for the 0.75 constant and letting L_T/L_{25} equal zero. A general procedure for obtaining reliable estimates of flame temperatures for combustible-oxidant-diluent systems is outlined below.

For the lower limit mixture of methane (5 pct) in air at 25° C (298 K), the reaction for complete combustion of 1 mol (n) of mixture may be written as

$$0.05\ CH_4 + 0.20\ O_2 + 0.75\ N_2 \rightarrow 0.05\ CO_2 + 0.10\ H_2O(g) + 0.10\ O_2 + 0.75\ N_2. \quad (38)$$

The heat of reaction (combustion) is defined from standard heats of formation (ΔH_f) at 298 K as

$$\Delta H_{298} = \Sigma n \Delta H_f \text{ (products)} - \Sigma n \Delta H_f \text{ (reactants)} \quad (39)$$

where ΔH_{298} is the heat release per mol of reactant (kcal/mol). The approximate temperature rise of the product gases for constant pressure combustion is

$$\Delta T \text{(products)} = \frac{\Delta H_{298}}{\Sigma n \, Cp \text{ (products)}} \cong \frac{\Delta H_{298}}{\overline{C}_p \text{(mixture)}} \quad (40)$$

where

$$\overline{C}_p \text{ (mixture)} = 0.05 \, \overline{C}_p (CO_2) + 0.10 \, \overline{C}_p (H_2O) + 0.10 \, \overline{C}_p (O_2) + 0.75 \, \overline{C}_p (N_2). \quad (41)$$

The heat content (H) data in table 3 can be used to determine the average heat capacity values $\frac{(H_2 - H_1)}{(T_2 - T_1)}$ that will satisfy equation 40 at the assumed T_2 flame temperature. Since the lower limit combustion enthalpy (ΔH_{298}) of many C-H-O-N combustibles is 10 to 11 kcal per mol of mixture and $\overline{C}_p$ of their products is about 8×10^{-3} kcal/(mol·K), their limit flame temperature can be assumed to be close to 1,300° C. Noticeable deviations from this generalization occur for combustible systems of very high or very low reactivity. Rigorous solutions are necessary for precise flame temperature calculations (*24*, p. 283; *66*, p. 590).

The temperature rise for constant volume combustion is given by

$$\Delta T \text{(products)} \cong \frac{\Delta E_{298}}{\overline{C}_v \text{(mixture)}} = \frac{\Delta H_{298} - \Delta n RT_1}{\overline{C}_v \text{(mixture)}} \quad (42)$$

where ΔE_{298} is constant volume heat release, Δn is molar change of gaseous reactants and products, and $\overline{C}_v = \overline{C}_p - R$. These temperature rises tend to be at least 20 pct higher than those found under constant pressure.

Another category of flaming combustion is *diffusion flames*, which are encountered in most fires, such as burning of a liquid pool, solid surface, or flared fuel gas. These heterogeneous flames have a wide spectrum of combustible concentrations and, therefore, do not have definitive flame temperatures or flammability limits, per se. Flames of dispersed dusts also involve diffusional and heterogeneous burning. However, if they are uniformly mixed in air, their flames can have some of the fundamental properties of premixed flames even though they may be less well defined. No simple theory is available for predicting dust flame temperatures, but the values for carbonaceous dusts are roughly equivalent to those of the hydrocarbon vapors that can form as a result of heating of the dust.

Cool flames are also a special category of combustion and are usually associated with low-temperature oxidations and two-stage ignitions. They are formed by many hydrocarbons including ethers, aldehydes, alcohols, and paraffins. These flames are ordinarily pale blue and are believed to result from aldehyde and/or peroxide formation. They are most often found with fuel-rich mixtures that are outside the normal flammability domain of the fuel vapor-air system. Because only a small fraction of the available enthalpy is used to form cool flames, their temperatures are very low, typically of the order of a few hundred degrees Celsius. They cannot be ignored because they may produce normal ignitions if brought into contact with flammable vapor-oxidant compositions.

Burning Velocities

The linear rate at which a laminar combustion wave (reaction zone) propagates relative to the unburned gas of a flammable mixture is the *burning velocity* (S_u). This velocity is a fundamental property of the mixture and depends primarily upon the thermal diffusivity $\frac{(\lambda)}{(\rho C_p)}$, chemical reaction rate, and heat of combustion. Although the mechanism of flame propagation is very complex, it is well known that certain physical processes can quench propagation and account for the existence of a limit burning velocity and corresponding limit of flammability. For example, if only natural convection and buoyancy effects are considered, the *limit burning velocity*, $(S_u)_L$, for a lower limit mixture can be predicted with reasonable accuracy by the equation proposed by Hertzberg (*30*):

$$(S_u)_L = (2 \, \alpha \, g \, \rho_b/\rho_\mu)^{1/3}, \quad (43)$$

where g is gravitational constant, α is thermal diffusivity, and ρ_b/ρ_μ is density ratio of burned and unburned gas. This equation defines the horizontal propagation limit where the buoyancy force just balances the combustion force of the product gases and predicts $(S_u)_L$ values to be less than 10 cm/s for a variety of fuel-air mixtures.

Of great practical interest is the *flame speed* (S_f) associated with combustion, i.e., the flame velocity sensed by an observer. It may be defined as

$$S_f = S_u + S_g, \quad (44)$$

where S_g is a gas velocity component associated with the expansion and buoyancy of the product gases. Figure 8, which was obtained by Andrews (*3*), illustrates the expected relationship between S_u, S_f, and S_g for spherical CH_4-air

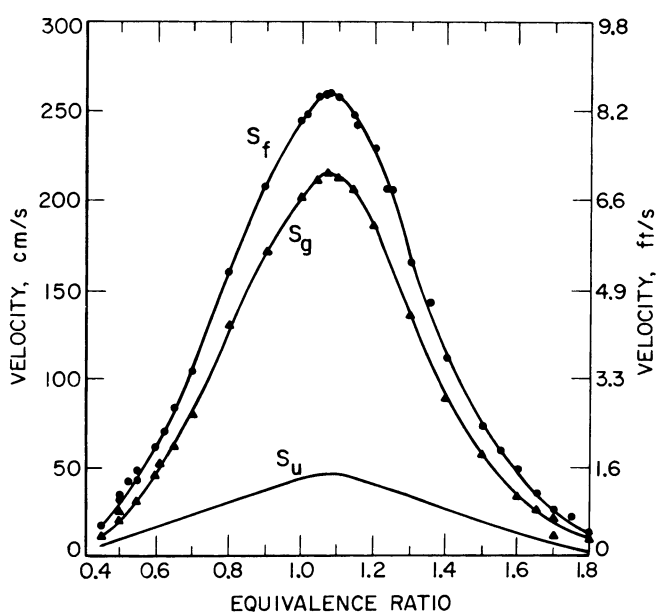

Figure 8.—Flame speed (S_f), gas velocity (S_g), and burning velocity (S_u) versus equivalence ratio for methane-air flame propagation at 25° C and 1 atm.

propagations as a function of equivalence ratio (fraction of stoichiometric). Note that maximum S_f and S_u values occur on the rich side of stoichiometric and their ratio (S_f/S_u) is about 6. Under adiabatic conditions, the maximum S_f/S_u ratio is closer to approximately 7.5, which is typical of the combustion product *expansion ratio* (E) for most combustibles. Thus, the flame speed may be calculated from the following expressions:

$$S_f = S_u E \tag{45}$$

$$S_f = S_u \, \rho_u/\rho_b = S_u \frac{M_u T_b P_u}{M_b T_u P_b} \tag{46}$$

where the u and b subscripts refer to the unburned and burned states, respectively. The burning velocity itself generally increases consistently with increasing initial temperature, whereas the pressure effect is usually positive in oxygen but negative in air for many combustibles. In oxygen, burning velocities are considerably greater because of increased reaction rates and heats of reaction, particularly at stoichiometric combustible concentrations, which are much higher in oxygen than in air.

The foregoing discussion is applicable primarily to laminar flame propagation of mixtures initially at rest. With the mixtures under dynamic conditions, S_u can be expected to vary with the degree of turbulence and S_f will increase from the combined effects of turbulence and any added flow. If the propagations occur in a long tube or duct, the flames can accelerate and may even develop into detonations (see next section), depending upon the length-diameter ratio. Since turbulent flames involve severe velocity gradients and distorted flame fronts, they are not amenable to simple generalizations like laminar flames.

In the case of burning liquid pools, the burning rate (regression rate) is a strong function of the pool diameter because of the radiation feedback effect. With increased heat feedback, the rates of vaporization and reaction are enhanced. Zabetakis (*111*) has shown that the burning rate for large pools (v_∞, cm/min) is given by

$$v_\infty = k_\infty \, \Delta H_c/\Delta H_v, \tag{47}$$

where ΔH_c is net heat of combustion, ΔH_v is sensible heat of vaporization, and k_∞ is a constant that is 0.0076 for hydrocarbon fuels.

EXPLOSION PROCESSES

Deflagrations

The term "explosion" is best defined as a sudden release of pressure or energy. One of the most common types is the deflagration of a flammable mixture which is characterized by subsonic propagation rates relative to the unburned gas. The *explosion pressure* (P_2) of a deflagration is greatest in adiabatic combustion under total confinement, i.e., constant volume. By applying equation 42 to calculate the temperature rise (ΔT), the pressure rise ratio ($P_b/P_u = P_2/P_1$) for constant-volume adiabatic combustion of a mixture can be obtained from

$$P_2/P_1 = \frac{n_2 T_2}{n_1 T_1}, \tag{48}$$

This equation predicts that the maximum P_2/P_1 ratio for the confined deflagration of most combustible-air systems is about 8:1 to 9:1.

Assuming ideal propagation after central ignition in a spherical enclosure, the pressure rise (ΔP) may be estimated from the expression suggested by Zabetakis (*110*):

$$\Delta P = K \, P_1 \, S_u^3 \, t^3/V, \tag{49}$$

where t is time, V is enclosure volume, and K is a constant that includes an expansion term and is obtained from an evaluation of the P-V data. Actual pressure rises are less than those predictable by equation 49 because flame propagation rarely is uniformly spherical, heat losses increase with proximity of the flame front to the vessel walls, and S_u is not constant nor maximum throughout constant-volume combustion. Nevertheless, this equation is fairly reliable for rapid-burning mixtures, such as stoichiometric mixtures, which can readily form spherical flames and are least affected by wall and buoyancy effects. Figure 9 (*47*) illustrates the pressure history for the deflagration of a stoichiometric CH_4-air mixture in the Bureau's large spherical vessel (3.65-m diam); here, an S_u of 45 cm/s is appropriate for determining the K factor applicable in equation 49. In such spherical explosions, where propagation is near ideal, the time to reach maximum pressure (P_2) is approximated by the following expression:

$$t_2 = \frac{\text{vessel radius}}{S_f} = \frac{\text{vessel radius}}{E \, S_u} \tag{50}$$

where the E and S_u values for constant-pressure combustion may be used.

Explosion pressures of mixtures less optimum than stoichiometric are generally lower because of decreased enthalpy and burning velocity, but also because of the restricted mode of flame propagation—upward, horizontal, or downward. As shown by Sapko (*92*), the spatial mode of propagation varies greatly with mixture composition and is strongly related to buoyancy effects. Figure 10 shows the flame and pressure histories obtained in the Bureau's large vessel for a partly inerted CH_4-air-N_2 mixture (upward and only slight downward propagation) and a near-limit

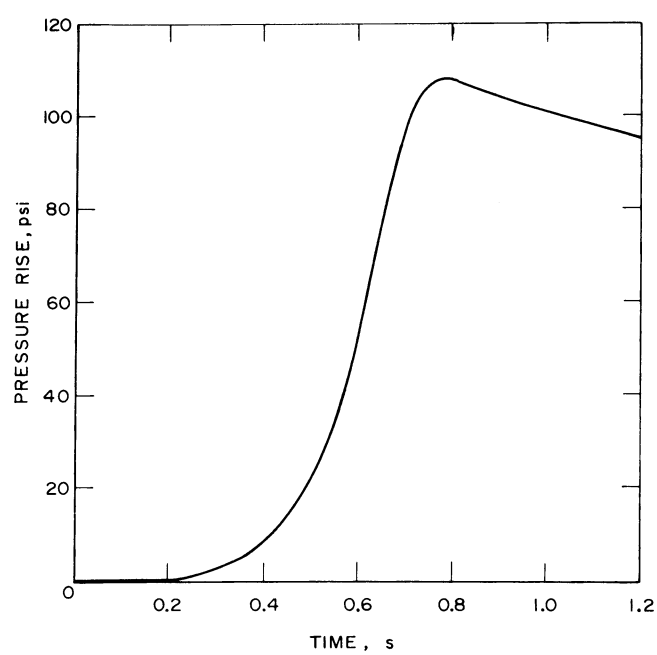

Figure 9.—Pressure history for the explosion of a stoichiometric methane-air mixture in a 3.65-m (12-ft) diam sphere at 25° C and 1 atm.

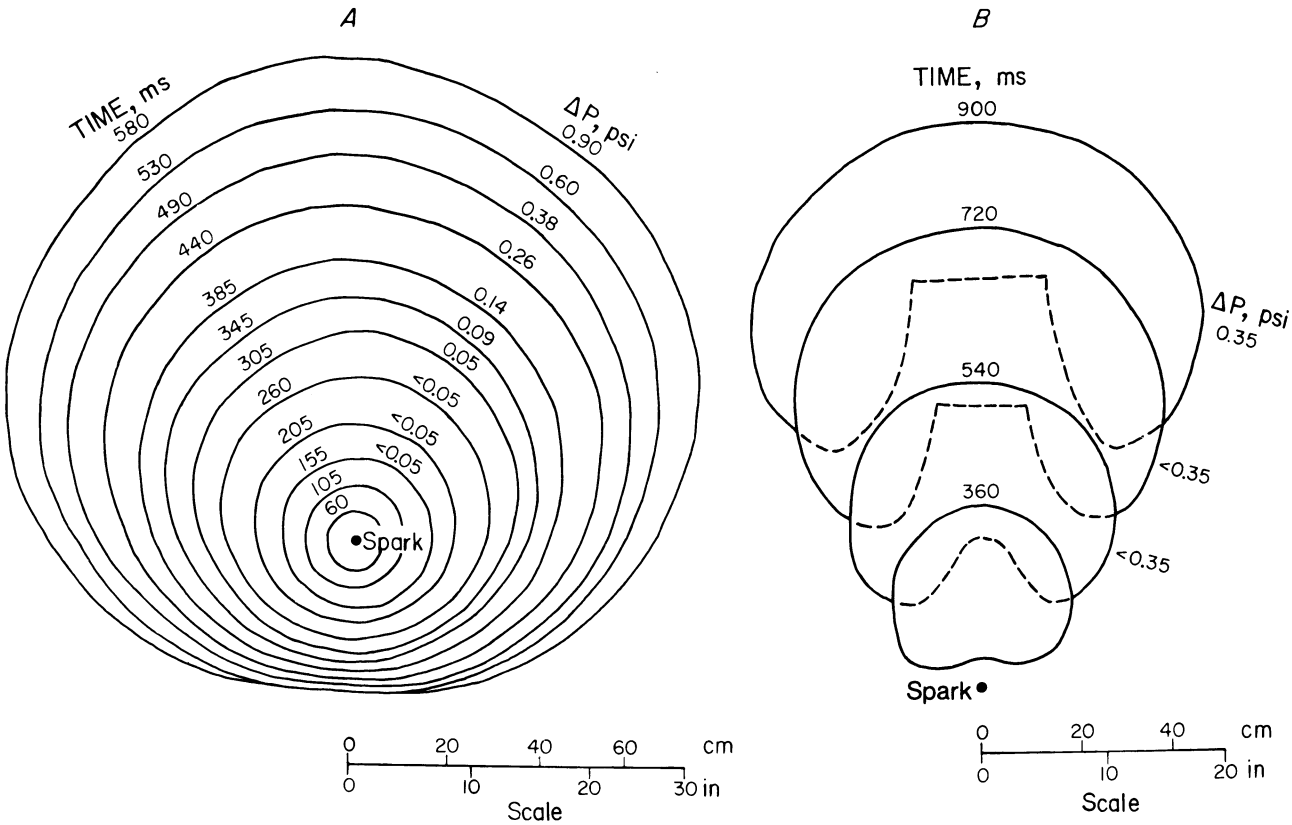

Figure 10.—Pressure and flame profile histories for spark ignitions of (*A*) 7.8 pct CH_4-74.1 pct air-18.1 pct N_2 mixture and (*B*) 6.9 pct CH_4-65.8 pct air-27.3 pct N_2 mixture in a 3.65-m (12-ft) diam sphere at 25° C and 1 atm.

CH_4-air-N_2 mixture (only upward propagation). Buoyant velocities of the highly inerted flames will vary roughly with the square root of the fire ball radius, which is predicted by theory for rising gas bubbles.

The maximum work output or energy release of a combustible explosion is given by equation 12 or 13, depending upon whether an isothermal or adiabatic condition is assumed. Since neither condition is fully attained in real situations, the actual energy release will fall somewhere between the values for the two possible cases.

Physical Explosions

Many explosions are the physical type in which no combustion takes place. These would include outward burstings of confined gas systems due to overpressurization by mere physical processes; inward burstings (implosions) due to insufficient pressurization are also a physical type. The potential energy release associated with such physical eruptions may be treated simply as the thermodynamic expansion or compression of an inert gas. Some explosions involve a combination of physical and chemical energy release, such as in a boiling liquid-expanding vapor explosion, which culminates in a large fireball. Liquefied petroleum gases are normally involved in these explosions and result when the fuel container is excessively heated by an external fire and ruptures from overpressurization. The fireball diameter may be estimated by the following expression (*32*):

$$d = 3.86\ W^{0.32}, \qquad (51)$$

where d is fireball diameter (m) and W is fuel weight (kg).

Detonations

The most severe type of explosion is a detonation that is characterized by supersonic propagation rates relative to the unburned reactant. Detonations are commonly associated with liquid or solid explosives but can also occur with many gaseous fuel-oxidant systems under certain initiation or propagation conditions. Detonations are unique in that their combustion wave is coupled to a shock wave which results in very high pressures under either confined or unconfined conditions. The *detonation pressure* (P_2) for gaseous mixtures can be estimated by the following expression:

$$P_2 = 2\ P_v \qquad (52)$$

where P_v is the maximum pressure for constant-volume combustion (equation 48). Thus, the maximum pressure rise ratio (P_2/P_1) for gaseous detonations is about 18:1, depending upon the energy of the mixture.

Figure 11 by Burgess (*6*) is typical of the pressure history that can result in a well-developed gaseous detonation; these data are for a stoichiometric acetylene-air mixture in a 45.7-m-long tunnel (0.61-m diam) with one end open. Three pressure levels are worth noting here: C–the initial spike (Von Neumann) or shock front, which is of very short duration with an insignificant impulse ($\int$ Pdt); D–the well-defined Chapman-Juguet (C-J) pressure, which corresponds to complete combustion within the detonation front but which also produces little impulse; and E–the static pressure, which reflects the expansion of gas and beyond which the pressure remains at a plateau until relieved.

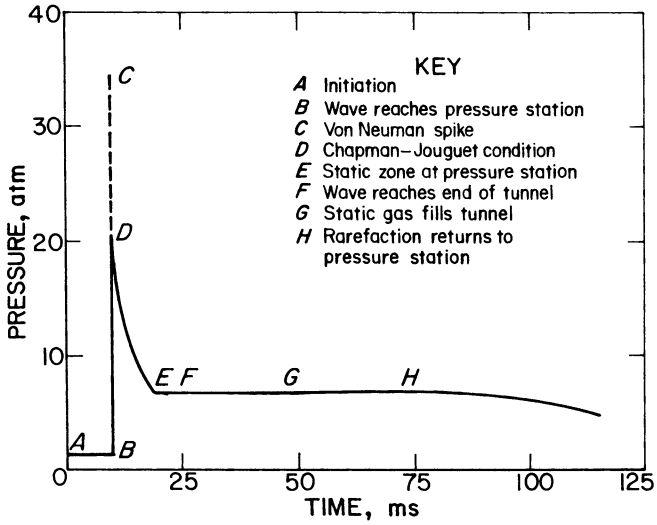

Figure 11.—Pressure-time transient for detonation of a stoichiometric acetylene-air mixture in a 45.7-m (150-ft) long tunnel with initiation end closed. Instrument station 18.3 m (60-ft) from initiator point.

The pressure at the C-J condition is the detonation pressure (P_2) referred to in equation 52. In comparison, the reflected pressure is often about 2.5 times the C-J detonation pressure. Although detonation pressures are of great concern, it is the static pressures (E-H plateau) of the expanded gases that produce the greatest pressure energy because of their much greater duration and impulse; this is fully realized in a closed system.

Many more rigorous expressions than equation 52 are available for calculating detonation parameters. The following expression (*106*) relates the pressure rise ratio (P_2/P_1) across the C-J detonation front with the *detonation velocity* (v*):

$$P_2/P_1 = \frac{1 + \gamma_1(v^*/c_1)^2}{1 + \gamma_2}, \qquad (53)$$

where γ_1 is ratio of specific heats (C_p/C_v) and c_1 is sonic velocity $(\gamma_1 RT_1)^{1/2}$ of the reacting gas; γ_2 refers to the molecular and dissociated products and varies somewhat with any shifting product composition. Although precise γ_2 values require elaborate thermochemical computations, they may be roughly estimated from specific heat tables for any assumed reaction products and their adiabatic flame temperatures; the latter temperature is usually a few hundred degrees less than the detonation temperature. The term v^*/c_1 is the *Mach number* (M) of the detonation wave, which theoretically propagates at a constant velocity as it moves through the unreacted gas, usually several times the sonic velocity of the unburned gas. For most practical applications, the estimation of P_2 by equation 52 is sufficiently reliable and adequate.

Any strong explosion that discharges into the free atmosphere, as in a detonation or deflagration failure of an enclosure, propagates for some distance as an *air blast wave*, which is characterized as an air shock wave ($M \geq 1$). Blast waves associated with detonations propagate over much greater distances and at greater velocities than those of deflagrations. The damage potential of an air blast wave can be characterized by its overpressure (ΔP_s), which is

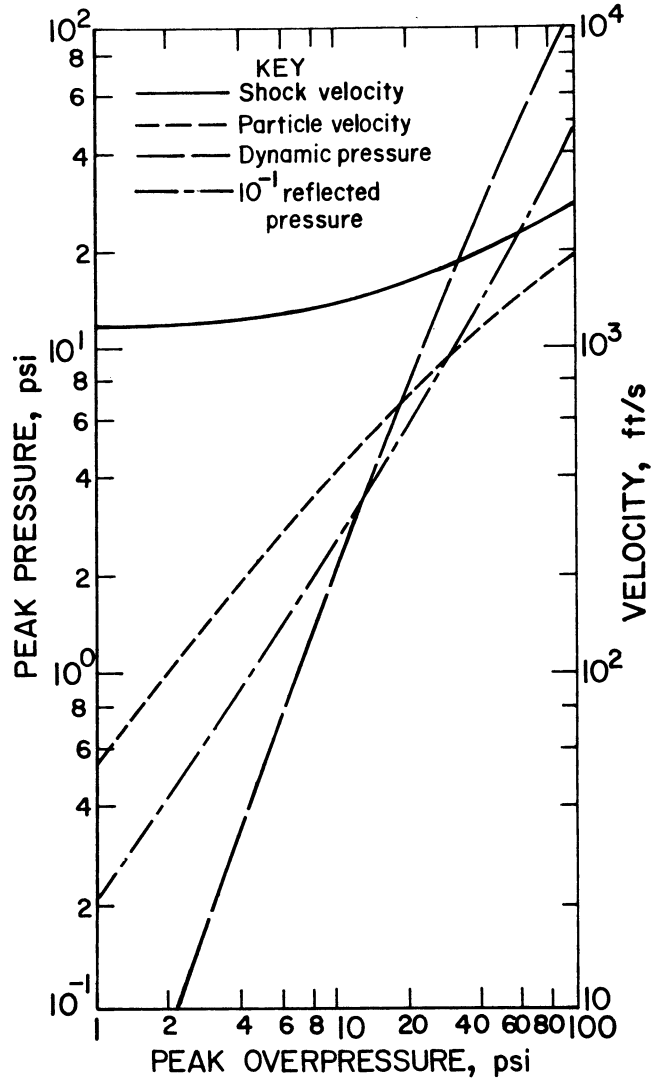

Figure 12.—Relation of ideal blast wave characteristics at the shock front to peak overpressure.

the static or side-on shock pressure (P_s) minus the ambient pressure (P_o). By air shock theory (26),

$$\Delta P_s = P_o \frac{2\gamma(M_o^2 - 1)}{\gamma - 1}, \qquad (54)$$

where γ is the specific heat ratio of air ($\sim$ 1.4) and M_o is the ratio of the shock wave velocity (v_s) to the sonic velocity of air (v_s/c_o); c_o is 331 m/s at 0° C. The total pressure that is sensed by an object exposed to a shock wave is the sum of the static shock pressure (ΔP_s) and the dynamic pressure ($1/2\ \rho v^2$) associated with the wind velocity (particle velocity, v). Figure 12 (*26*, p. 123) shows the normal relationship of such pressure and velocity parameters for an ideal air blast wave. Note that the dynamic pressure is negligible for weak shocks but becomes equal to the peak static overpressure of a strong shock at approximately 70 psi.

The blast wave pressure at various distances from the explosion source should be proportional to the cube root of the explosion energy yield if the chemical energy conversion to pressure energy is ideal, as in the case of TNT and other high explosives. The *TNT equivalence* of a strong

explosion can be computed by invoking the cube root scaling law (*26*, p. 127) that relates the blast pressure potential to the exploding charge weight (W) and distance (d) from the exploding charge, relative to TNT:

$$d/d_o = (W/W_o)^{1/3}, \quad (55)$$

where d_o and W_o refer to TNT. It is convenient to express W_o in terms of unit TNT mass, such as 1 ton or 1 gram, which is defined to yield about 10^9 cal/ton or 1,100 cal/g (*101*); thus $d = d_o W^{1/3}$ for a unit mass of TNT ($W_o = 1$). Corresponding blast pressures can then be compared in terms of a scaled distance ($d/W^{1/3}$).

TNT equivalents of solid and liquid explosives can be reliably estimated from their calculated heats of detonation and the value for TNT. However, in the case of gaseous explosions, the fraction of available chemical energy (ΔH_c) that is converted into blast energy or pressure energy can vary greatly with the degree of confinement and ability of the gas mixture to detonate (*6*). Assuming adiabatic expansion, the work that can be converted into blast pressure energy is given approximately by

$$W = \frac{P_2V_2 - P_1V_1}{\gamma - 1}, \quad (56)$$

where P_2 is elevated pressure of the gaseous products and P_1 is ambient pressure of the gases after expansion. In weakly confined gaseous deflagrations where the container walls fail before the maximum potential combustion pressure is achieved, P_2 will be small and little of the chemical energy (<10 pct) will result in blast pressure energy. In strongly confined deflagrations in which the containment fails, a small fraction of the chemical energy (~10 pct) will be used to cause wall failure, and the pressure energy will be slightly less than ΔH_c. The TNT equivalent for such strong gaseous deflagrations, as well as gaseous detonations, can be assumed to approximate the ΔH_c of the mixture for constant-volume combustion.

PROPERTIES OF LIQUID AND GASEOUS COMPOUNDS

This section covers selected combustion properties of a great number of liquid and gaseous organic compounds, as well as some common inorganic fuels. Pertinent physical properties of the combustibles and their flashpoints, autoignition temperatures, and flammability limits in air are given in the summary tabulations in appendix A. The data are grouped according to the chemical class of combustible to make apparent the effects of chemical structure within a homologous series and between chemical families of combustibles. These data are summarized in the text and supplemented with other data of interest for evaluating ignitability and flammability hazards.

VAPOR PRESSURES AND FLASHPOINTS

Since the flashpoint of a combustible liquid or solid depends upon its volatility and the vapor concentration required to form a lower limit of flammability in air, vapor pressure-temperature curves are important in assessing the flammability hazard. Accordingly, vapor pressure curves and flashpoint data are presented herein for selected combustibles of each chemical class of compounds. Flashpoints obtained by closed cup methods, which best approximate the lower temperature flammability limit (T_L), are reported here provided such data were available. Any reported open cup values may be assumed less conservative, particularly if the vapor concentration indicated by the flashpoint is appreciably higher than the lower limit (L) obtained from limit-of-flammability experiments.

Saturated Hydrocarbons

Vapor pressure curves and flashpoint data are given in figures 13 and 14 for the straight-chain paraffins and in figure 15 for branched-chain paraffins; the vapor pressures are predominantly from Stull (*99*) and the flashpoints from Bureau, NFPA, and other references cited in appendix A. Corresponding vapor concentrations, assuming 1 atm total pressure (76 cm Hg), are also included in the figures to permit estimation of lower flammability limits from the flashpoints. According to these data, normal alkanes with more than eight carbon atoms (above octane) will not form flammable vapor-air mixtures below 30° C and atmospheric pressure; also chain branching increases the volatility and decreases the flashpoint, as evident in comparing the values for n-octane (14° C) and 2,2,4-trimethylpentane or isooctane (−12° C). Generally, flashpoints of a paraffin series increase with increasing molecular weight, whereas the corresponding vapor pressures and lower flammability limits vary inversely.

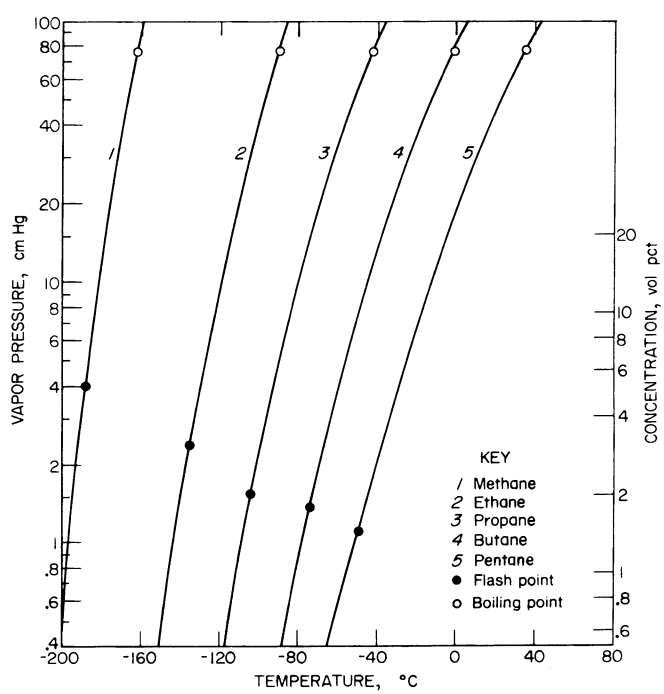

Figure 13.—Vapor pressure-temperature curves and flashpoints for five normal paraffins (C_1 to C_5).

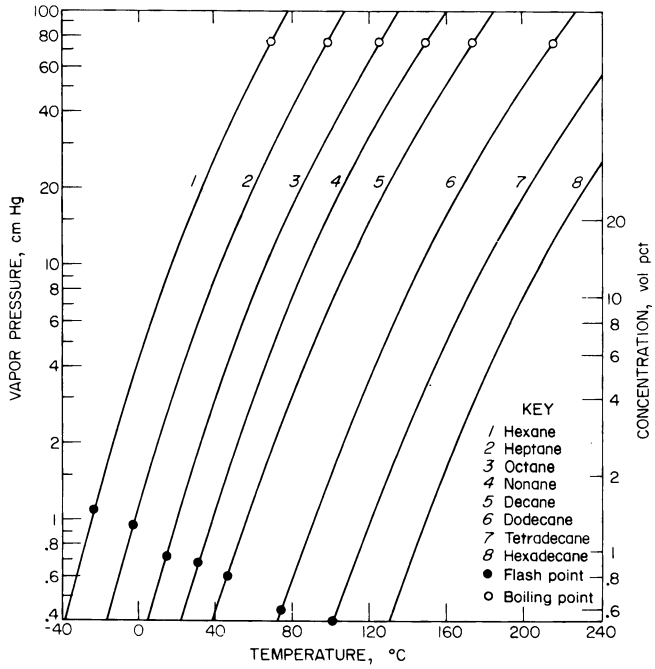

Figure 14.—Vapor pressure-temperature curves and flashpoints for eight normal paraffins (C_6 to C_{10}, C_{12}, C_{14}, C_{16}).

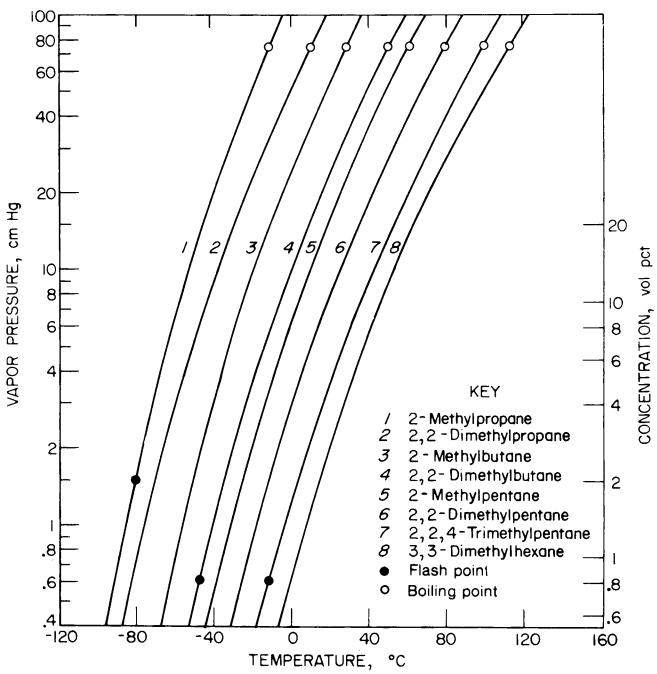

Figure 15.—Vapor pressure-temperature curves and flashpoints for eight branched-chain paraffins.

Based on similar data, Affens (*1*) has derived the following expressions for predicting the flashpoints (T_F, ° C) of the normal paraffins:

$$(T_F + 277.3)^2 = 10{,}410\ n, \quad (57)$$

$$(T_F + 277.3)^2 = 741.7/P_F, \quad (58)$$

and

$$(T_F + 277.3)^2 = 77{,}291\ (1/L_{25}) - 3{,}365, \quad (59)$$

where n is number of carbon atoms, P_F is vapor pressure (atm) at T_F, and L_{25} is the lower flammability limit (vol pct) in air at 25° C. Agreement between calculated and literature values is good except for methane. Additional correlations of this type can be made by substituting known relationships between number of carbon atoms and molecular weights, boiling points, or heats of combustion. The method proposed by Zabetakis (*110*) is equally reliable and is based upon equation 36, which predicts lower limits of mixtures as a function of their calorific values ($L_{25}\Delta H_c$) and temperature. This method also requires vapor pressure data but is attractive in that either actual calorific values or an assumed constant may be used in calculating the flashpoint.

Other Combustibles

Vapor pressure curves and flashpoint data for other families of combustibles are presented in figures 16-32. As with the paraffins, the flashpoints of each homologous series generally increase with increasing number of carbon atoms and decrease with chain branching. Ellis (*17*) finds the correlations with carbon atoms and heats of combustion to be practically linear for certain normal alkyl compounds (paraffins, cyclohexanes, ketones, alcohols, acetates) and alkyl benzenes but not for their isomers. The addition of functional groups can have a large and varied effect on flash point as illustrated below:

For butane:	° C	For benzene:	° C
C_4H_{10}	−74	C_6H_{10}	−11
$C_4H_9NH_2$	−12	C_6H_5Cl	29
C_4H_9Cl	−9	C_6H_5Br	51
C_3H_7CHO	−7	$C_6H_4Cl_2$	66
C_4H_9SH	2	$C_6H_5NH_2$	70
C_4H_9Br	18	C_6H_5OH	79
C_4H_9OH	29	$C_6H_5NO_2$	88
C_3H_7COOH	72		

The effects of any functional group on the flashpoint will depend upon the changes produced in both volatility and the lower flammability limit. As a rule, the flashpoints of such hydrocarbon derivatives will be noticeably greater than those of their parent hydrocarbons.

For blends of any combustible liquids, flashpoint predictions are more complex and will depend upon their deviations from ideal mixture laws (equations 4 and 5) and Le Chatelier's mixture flammability law (equation 35). Anomalous behavior is most likely to occur with dissimilar molecular species, such as mixtures of a hydrocarbon and a halogenated, oxygenated, or nitrated hydrocarbon. Ellis (*17*) has shown that the flashpoints of many solvent blends are often lower than expected because of polarity, hydrogen bonding, or solubility parameter differences. In practice, the greatest concern is necessarily for the liquid mixture component of highest volatility. Where a highly volatile component is present in only small concentrations as an additive or contaminant, the flashpoint will be subject to the evaporative history of the mixture. Depending upon the evaporation period, the actual flashpoint hazard may be underestimated when the volatile additive is nonflammable and overestimated when the additive is more flammable than the main liquid components. Such uncertainties are often encountered in evaluating cleaning solutions, paint mixtures, water-based lubricants, and modified fuels or chemicals. In the case of controversy, their flashpoints should be confirmed by limit-of-flammability-type experiments.

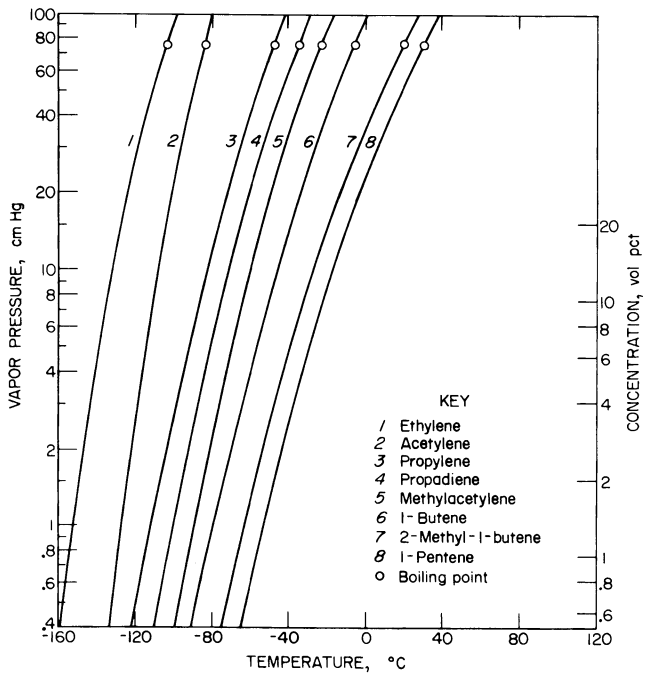

Figure 16.—Vapor pressure-temperature curves for eight unsaturated hydrocarbons.

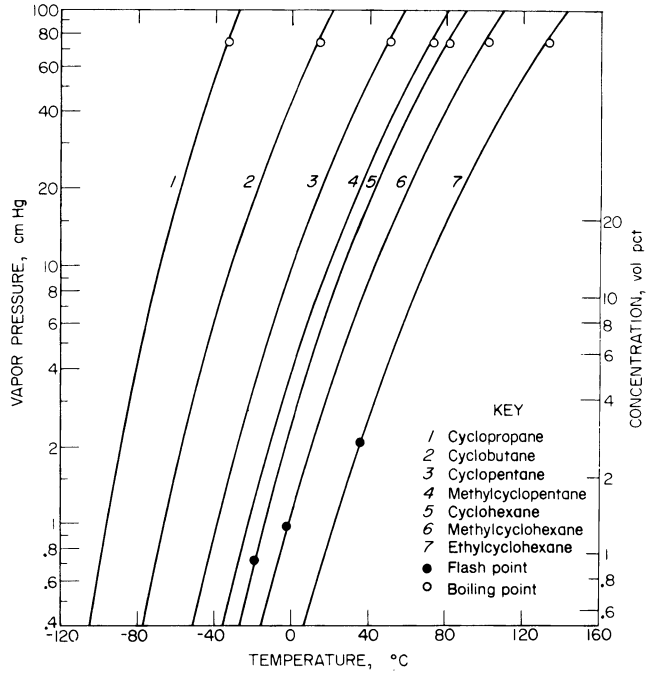

Figure 17.—Vapor pressure-temperature curves and flash-points for seven alicyclic hydrocarbons.

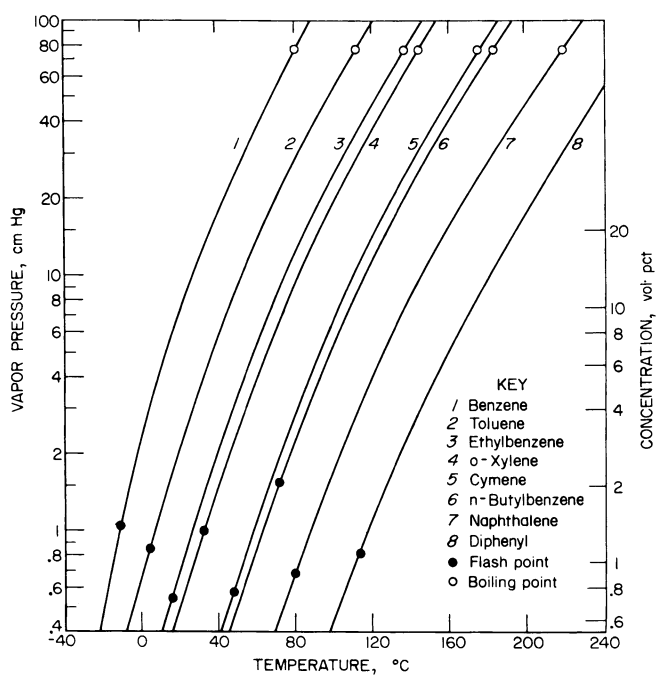

Figure 18.—Vapor pressure-temperature curves and flash-points for eight aromatic hydrocarbons.

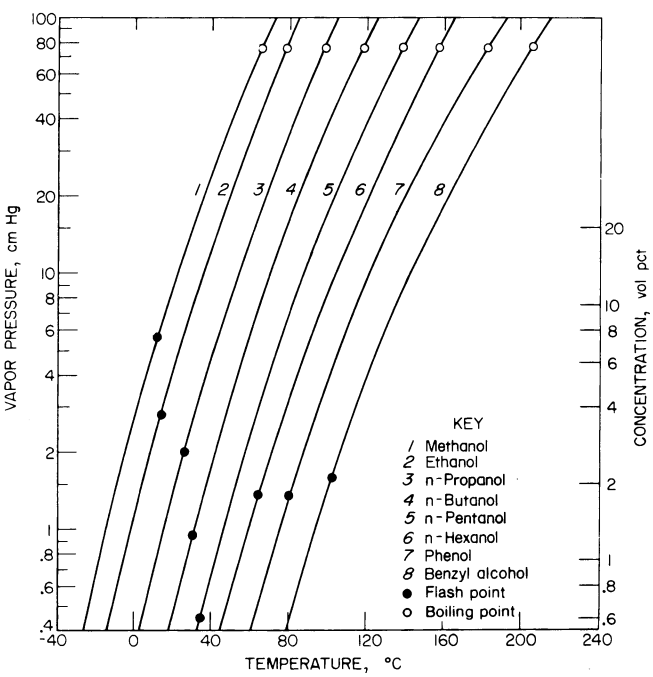

Figure 19.—Vapor pressure-temperature curves and flash-points for eight alcohols or hydroxy compounds.

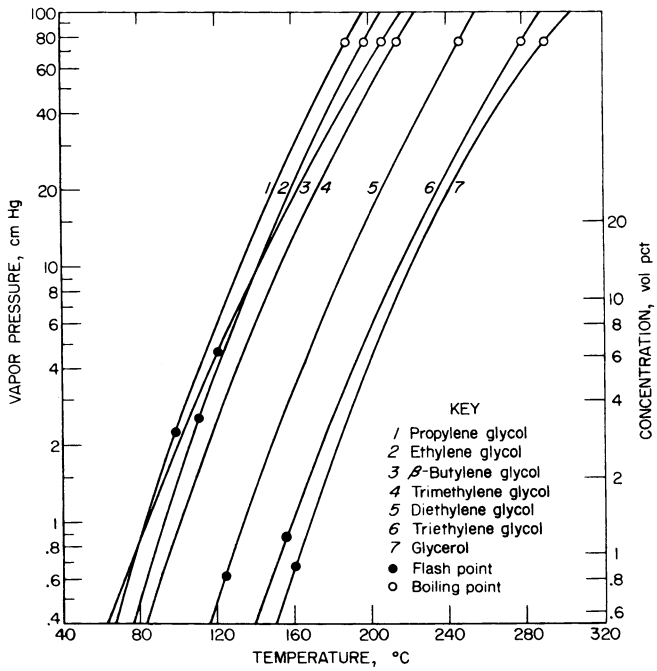

Figure 20.—Vapor pressure-temperature curves and flash-points for six glycols and glycerol.

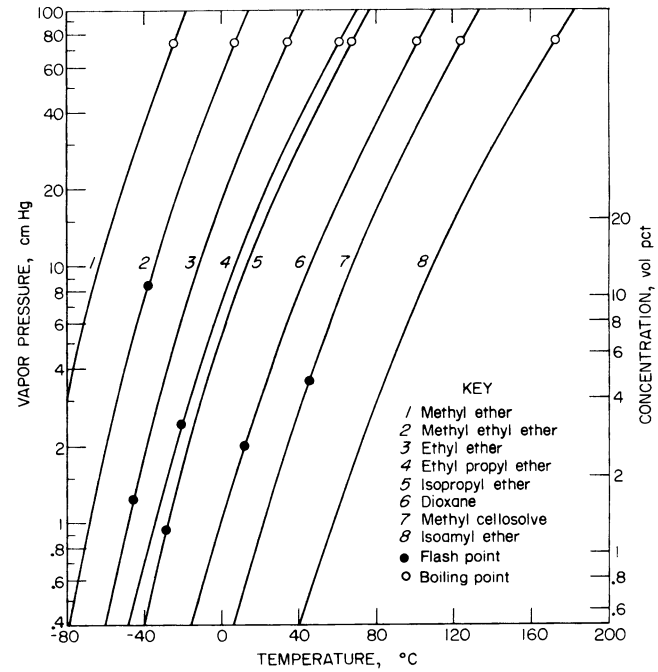

Figure 21.—Vapor pressure-temperature curves and flash-points for eight ethers.

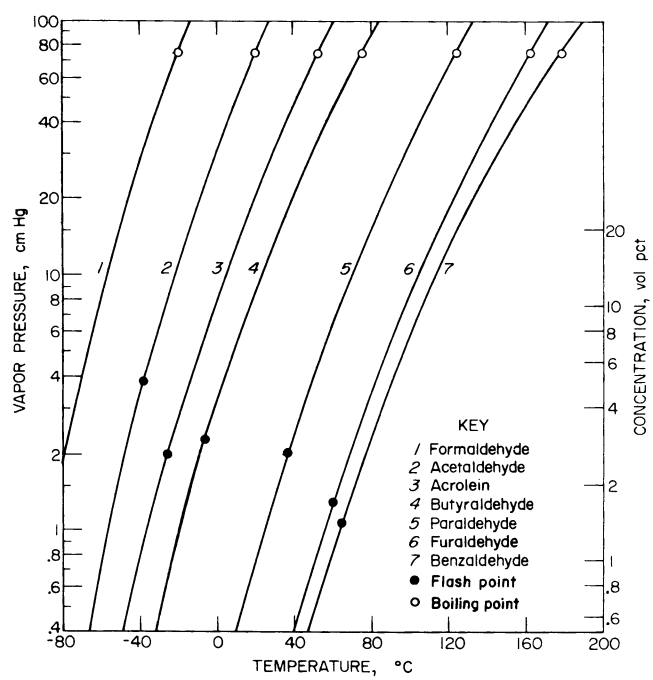

Figure 22.—Vapor pressure-temperature curves and flash-points for seven aldehydes.

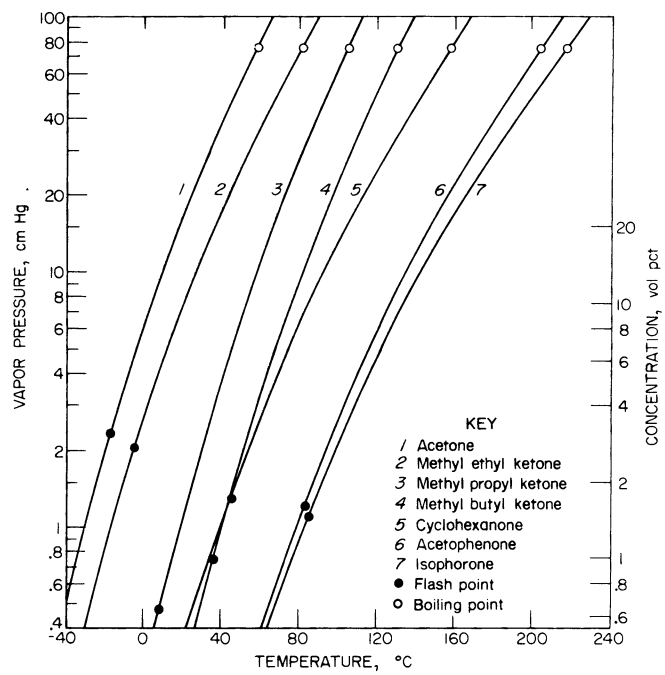

Figure 23.—Vapor pressure-temperature curves and flash-points for seven ketones.

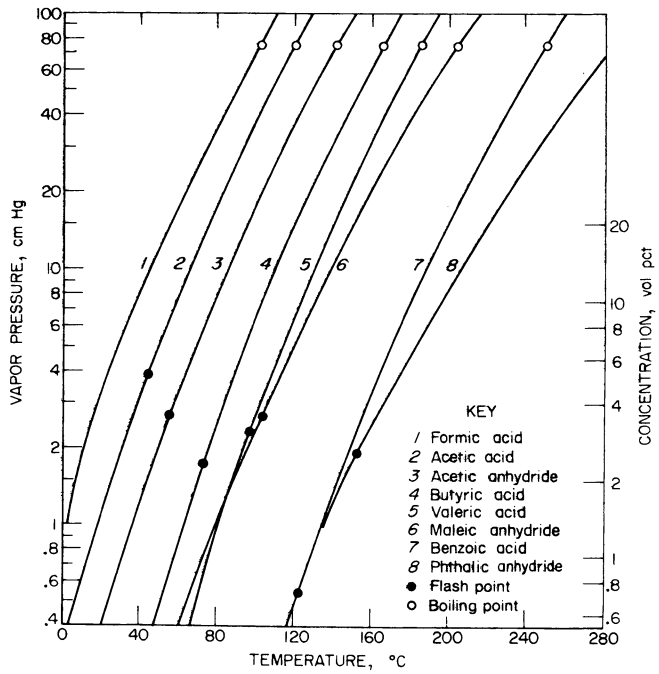

Figure 24.—Vapor pressure-temperature curves and flash-points for five acids and three acid anhydrides.

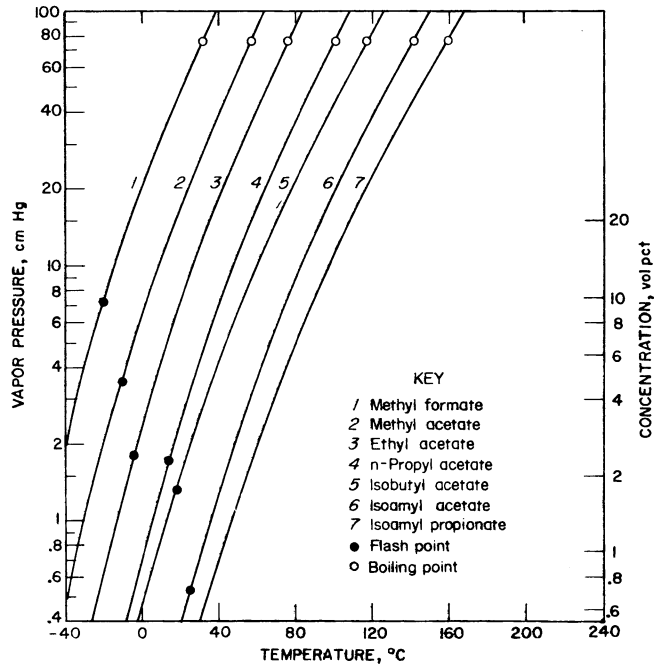

Figure 25.—Vapor pressure-temperature curves and flash-points for seven esters.

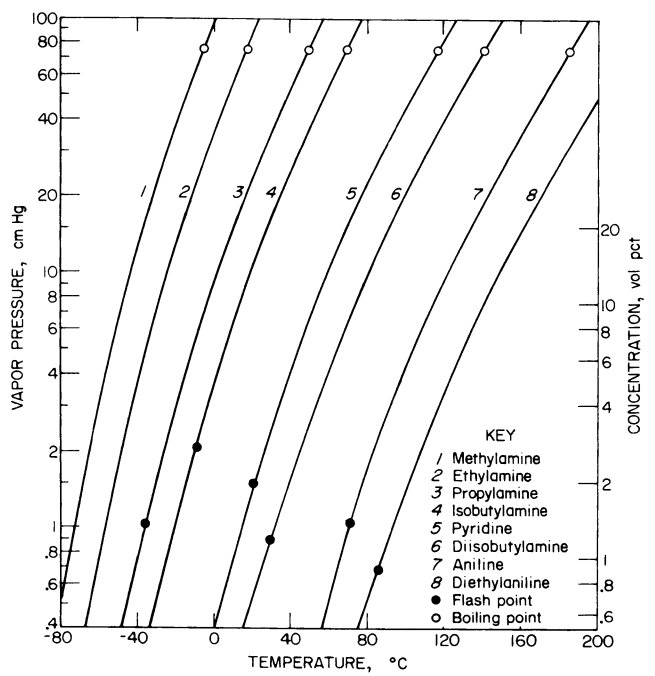

Figure 26.—Vapor pressure-temperature curves and flash-points for eight amines.

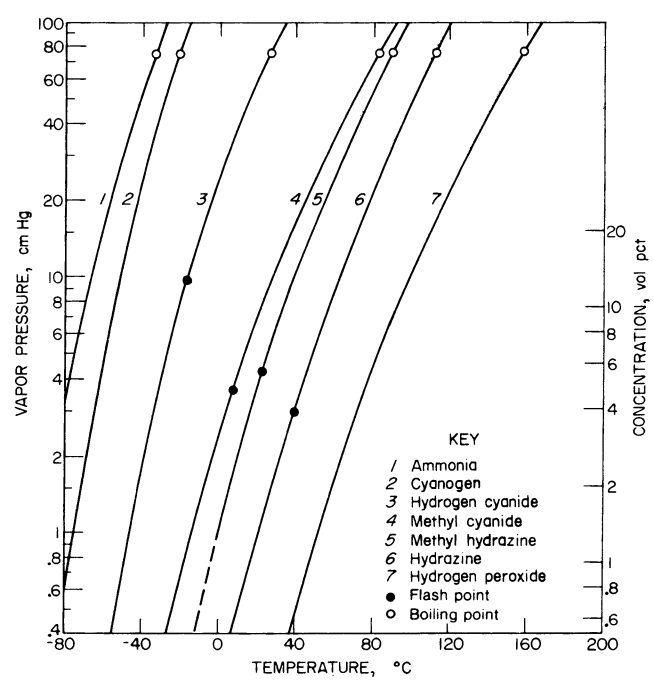

Figure 27.—Vapor pressure-temperature curves and flash-points for ammonia, cyanogen, two cyanides, two hydrazines, and hydrogen peroxide.

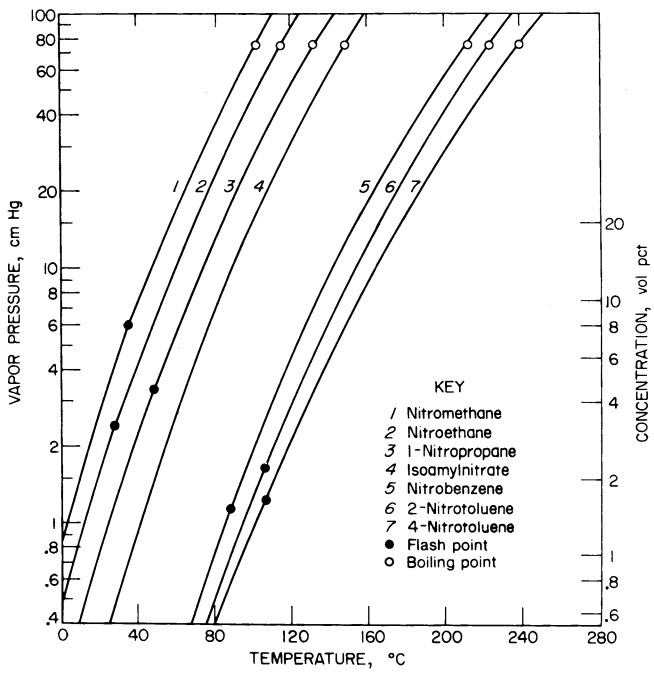

Figure 28.—Vapor pressure-temperature curves and flash-points for seven nitrated hydrocarbons.

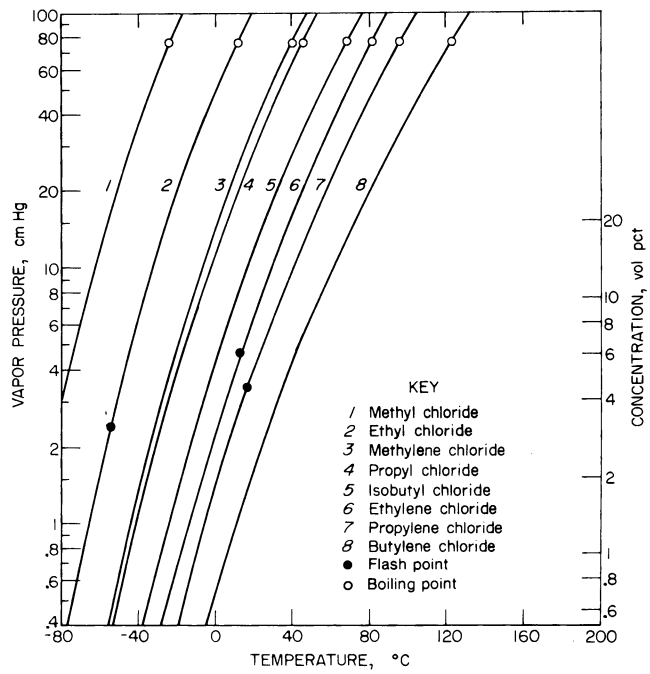

Figure 29.—Vapor pressure-temperature curves and flash-points for eight alkyl chlorides.

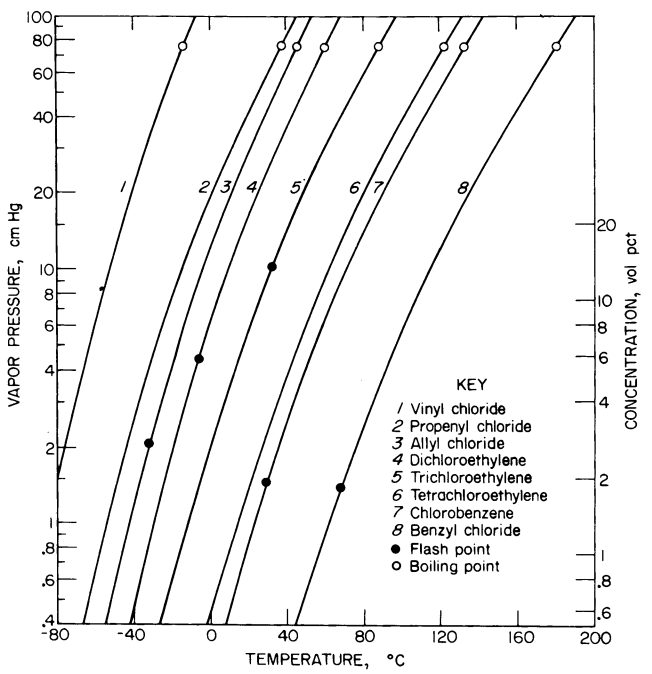

Figure 30.—Vapor pressure-temperature curves and flash-points for six unsaturated and two aromatic chlorine compounds.

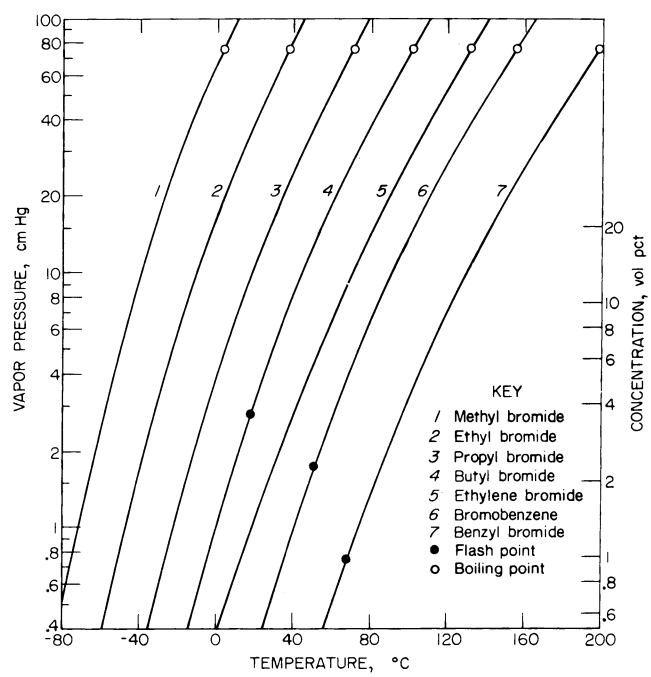

Figure 31.—Vapor pressure-temperature curves and flash-points for seven brominated compounds.

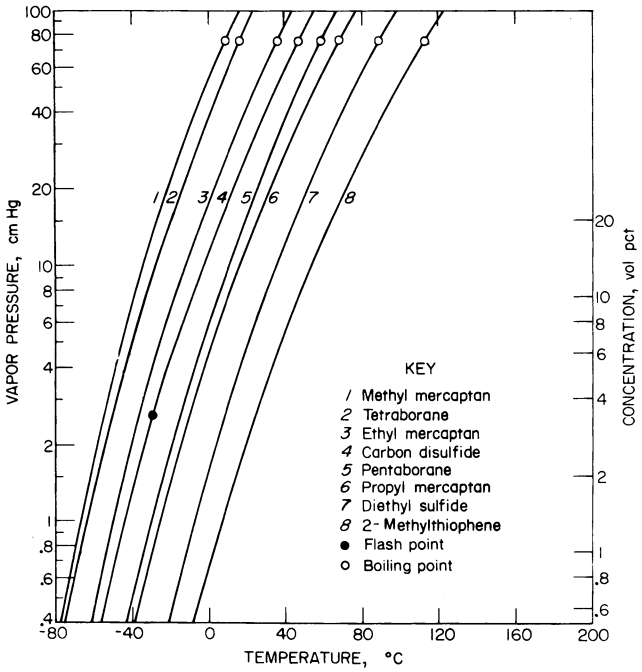

Figure 32.—Vapor pressure-temperature curves and flash-points for six sulfur and two boron compounds.

FLAMMABILITY LIMITS IN AIR AND OXYGEN

Lower limits (L_{25}) and upper limits (U_{25}) of flammability of individual gases or vapors in air are systematically tabulated in appendix A for the members of many families of combustibles. These limits define the range of flammable vapor-air concentrations for ignitions of quiescent uniform mixtures at atmospheric pressure and 25° ± 5° C and with propagation in the *upward* optimum mode; some data are given at temperatures higher than 25° C, mostly because of vapor pressure limitations. Unless otherwise specified, these data and those presented in the text were taken largely from compilations of earlier Bureau bulletins (*11*, *110*) and other cited Bureau publications; most Bureau flammability limit determinations were made in cylindrical tubes of at least 5-cm diameter with an electrical spark ignition source, as described in reference 117. Any data uncertainties because of possible inadequate ignition energies or apparatus dimensions (wall effects) would be greatest for combustibles having large ignition energies and quenching distances, such as the halogenated hydrocarbons. Typically, the reported limits have a precision of ± 0.1 at 1 vol pct and ± 0.5 at 10 vol pct, which is adequate for most safety applications. Thus, previously accepted data were not rejected because of subtle differences observed in later studies.

Limits of flammability in oxygen or other oxidizers are much less complete than those in air for most families of combustibles. A comparison of limit data in air and oxygen is made in table 6 for a number of hydrocarbons, halogenated hydrocarbons, and other combustibles at atmospheric pressure and 25° C (or the indicated temperature). The range of flammable concentrations for each combustible is considerably greater in oxygen than in air, except for acetylene, which can propagate flame even in the absence of air. The increased hazard with oxygen is reflected primarily by the great increase of upper limits of flammability (U_{25}). Although lower limits (L_{25}) in oxygen should be equal to or less than those in air, some of the reported data are inconsistent in this respect; this is not totally unexpected since all data were not obtained from a single source or by the same apparatus. The flammability limits in such oxidants as chlorine and nitrogen tetroxide also tend to be wider than in air, although these data are meager (*54*, *110*). Flammability trends of the different classes of combustibles are briefly summarized in the next sections.

Table 6. — Limits of flammability of combustible vapors in air and oxygen at 25° C and 1 atm[1]

Combustible	Flammability limits, vol pct			
	Air		Oxygen	
	L_{25}	U_{25}	L_{25}	U_{25}
HYDROCARBONS				
Methane	5.0	15.0	5.0	61
Ethane	3.0	12.4	3.0	66
Propane	2.1	9.5	2.3	55
n-Butane	1.8	8.4	1.8	49
n-Hexane	1.2	7.4	1.2	[2]52
n-Heptane	1.1	6.7	.9	[2]47
Acetylene	2.5	100	≤2.5	100
Ethylene	2.7	36	2.9	80
Propylene	2.4	11	2.1	53
α-Butylene	1.6	10	1.8	58
Cyclopropane	2.4	10.4	2.5	60
Benzene	[2]1.3	[2]7.9	≤1.3	NA
HALOGENATED HYDROCARBONS				
Methyl chloride	10.7	17.4	~8.0	~66
Ethyl chloride	3.8	15.4	4.0	67
n-Butyl chloride	1.8	[2]10	1.8	[2]52
Methylene chloride	[2]15.9	[2]19.1	13.6	[2]68
Ethylene chloride	6.0	[2]17.3	5.6	[2]68
Methyl chloroform	6.8	NA	6.6	[2]57
Trichloroethylene	[3]12.0	[2]41	7.5	[2]91
Vinyl chloride	3.6	33	4.0	70
Isocrotyl chloride	2.9	9.3	4.2	[4]66
Ethyl bromide	6.7	11.3	6.7	44
Isocrotyl bromide	6.4	12	6.4	[4]50
OTHER COMBUSTIBLES				
Acetaldehyde	4.0	60	4.0	93
Acetone	2.6	13	≤2.6	[2]60
Ammonia	15.0	28	~15	~79
Carbon monoxide	12.5	74	≤12.5	94
Ethyl ether	1.9	36	2.0	[4]~82
Hydrogen	4.0	75	4.0	94
Isopropyl ether	1.4	7.9	≤1.4	[4]69
Methanol	6.7	[5]36	≤6.7	[4]93
Vinyl ether	1.7	27	≤1.7	[4]~85

NA Not available.
[1]Based upon data in references 11, 54, 78, and 110.
[2]Data at 100° C.
[3]Data at 30° C.
[4]Temperature unknown but >25° C.
[5]Data at 60° C.

Saturated Hydrocarbons and Derivatives

The lowest member of the paraffin series is methane, which has a lower limit of 5 pct and an upper limit of 15 pct in normal ambient air. For most homologous series of organic combustibles, their flammability limits in air or oxygen decrease with increasing molecular weight or number of carbon atoms. This is illustrated in figure 33 where lower and upper limits are plotted versus carbon atoms for the vapor-air mixtures of the normal paraffins and their corresponding alcohols, aldehydes, amines, and chlorides; the curves approximate the limits given in table 6 or appendix A at 1 atm and ≥25° C. The indicated limits

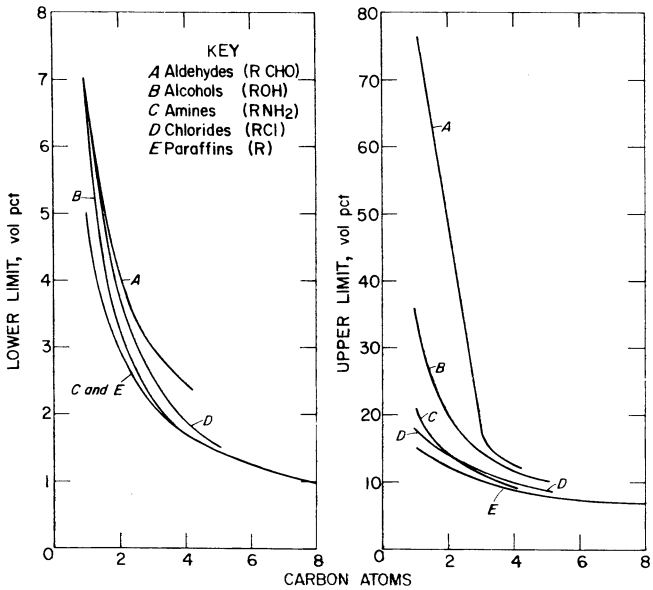

Figure 33.—Variation of lower and upper limits of flammability in air with number of carbon atoms for normal paraffins and their derivatives. Data at 25° C or reported temperature.

for the straight-chain paraffins can be assumed to be practically the same as for their branched-chain isomers and only slightly wider than for their cyclic homologs.

In comparison, many other paraffin derivatives have a wider range of flammability than their parent hydrocarbons, particularly because of large differences between their upper limits. Such derivatives include the primary or simple aldehydes, alcohols, and ethers, many of which form cool flames readily and have substantially wider limits than their corresponding paraffins; primary amines and certain esters (formates), which have a flammability range roughly comparable to that of the ethers; alkyl nitrates, nitrites, and hydrazines, which may undergo highly exothermic decomposition with or without air; and the alkyl mercaptans. Other derivatives such as the primary acids and simple ketones have flammability limits comparable to or slightly wider than those of the normal paraffins, whereas those of the halogenated homologs are narrower or wider, depending upon the number of carbon and halogen atoms. As a rule, the effect of a monosubstituted group tends to be minimum at a carbon chain length of about four or more; for example, compare the limits of n-butane (C_4H_{10}) and n-butyl chloride (C_4H_9Cl) in table 6.

The lower limit (L_{25}, volume percent) of paraffin combustibles in air may be approximately predicted by the expression suggested by Lloyd (*70*):

$$L_{25} \cong 0.55\ C_{st}, \qquad (60)$$

where C_{st} is the volume percent for stoichiometric combustion to CO_2 and H_2O. Limit equivalence ratios (L_{25}/C_{st}) given in table 7 show that this equation is fairly reliable for the normal paraffins (n-alkanes), as well as for many of their isomeric, cyclic, and substituted derivatives. However, most aldehydes, alkane bromides, alkane dichlorides, and nitroalkanes have L_{25}/C_{st} values that are much lower or higher than those for paraffins; C_{st} values for all the combustibles are included in appendix A for calculating

Table 7. — Equivalence ratios (L_{25}/C_{st}) and calorific values ($L_{25}\Delta H_c/100$) of lower limit mixtures of saturated hydrocarbons and derivatives in air at 25° C and 1 atm

Formula	L_{25}, vol pct	L_{25}/C_{st}	$L_{25}\Delta H_c/100$, kcal/mol
n-ALKANES (PARAFFINS)			
CH_4	5.0	0.53	9.6
C_2H_6	3.0	.53	10.2
C_3H_8	2.1	.52	10.3
C_4H_{10}	1.8	.58	11.4
C_5H_{12}	1.4	.55	10.9
C_6H_{14}	1.2	.56	11.1
C_7H_{16}	1.1	.59	11.8
C_8H_{18}	[1].95	.58	11.6
ISOALKANES			
C_4H_{10}	1.8	0.58	11.4
C_5H_{12}	1.4	.55	10.9
C_8H_{18}	.95	.58	11.6
CYCLOALKANES			
C_3H_6	2.4	0.54	11.2
C_4H_8	1.8	.53	11.1
C_5H_{10}	1.5	.55	11.1
C_6H_{12}	1.3	.57	11.5
C_7H_{14}	1.1	.56	11.4
N-ALKYL ALCOHOLS			
CH_3OH	6.7	0.55	10.7
C_2H_5OH	3.3	.51	10.1
C_3H_7OH	[1]2.2	.49	9.9
C_4H_9OH	[1]1.7	.50	10.1
$C_5H_{11}OH$	[1]1.4	.51	10.4
$C_6H_{13}OH$	[1]1.2	.53	10.7
ALKYL ALDEHYDES			
HCHO	7.0	0.40	8.7
CH_3CHO	4.0	.52	10.6
C_2H_5CHO	2.9	.58	11.9
C_3H_7CHO	2.5	.68	13.9
ALKYL KETONES			
$(CH_3)_2CO$	2.6	0.52	10.5
$(C_2H_5)_2CO$	1.9	.52	10.4
ALKYL ETHERS			
$(CH_3)_2O$	3.4	0.52	10.7
$(C_2H_5)_2O$	1.9	.56	11.5
$(C_4H_9)_2O$	1.5	.87	17.9
$(C_5H_{11})_2O$	.7	.51	10.5
N-ALKYL AMINES			
CH_3NH_2	4.9	0.58	11.4
$C_2H_5NH_2$	3.5	.66	13.3
$C_3H_7NH_2$	2.0	.52	10.5
$C_4H_9NH_2$	1.7	.57	11.4
ALKYL ESTERS			
$HCOOCH_3$	5.0	0.53	10.9
$HCOOC_2H_5$	2.8	.50	10.3
$HCOOC_4H_9$	1.7	.54	11.1
CH_3COOCH_3	3.2	.57	11.5
$CH_3COOC_2H_5$	2.2	.55	11.1
$CH_3COOC_3H_7$	1.8	.58	11.7
$CH_3COOC_4H_9$	[1]1.4	.55	11.0
n-ALKYL HALIDES			
CH_3Cl	7.0	0.56	10.7
C_2H_5Cl	3.8	.58	11.4
C_3H_7Cl	2.6	.59	11.6
C_4H_9Cl	1.8	.53	10.7
CH_3Br	10.0	.82	15.2
C_2H_5Br	6.7	1.03	19.9
C_4H_9Br	[1]2.5	.74	14.8
ALKANE DICHLORIDES			
CH_2Cl_2	[1]15.9	0.92	18.3
$C_2H_4Cl_2$	[1]4.5	.58	11.7
$C_3H_6Cl_2$	3.4	.68	13.7
NITROALKANES			
CH_3NO_2	[1]7.3	0.33	11.9
$C_2H_5NO_2$	3.4	.40	10.5
$C_3H_7NO_2$	[1]2.2	.42	10.0

[1]Limits at elevated temperatures.

other limit equivalence ratios. Corresponding correlations of upper limits with C_{st} values are less consistent or more difficult to quantify. Excluding possible cool flames, the upper limits (U_{25}, volume percent) of normal paraffins obey the following expression given in Bulletin 627 (*110*):

$$U_{25} = 4.8\ C_{st}^{1/2}. \quad (61)$$

The limits of these hydrocarbons in air can also be correlated with the number of carbon atoms per molecule (n) as follows (*1*):

$$1/L_{25} = 0.1347\ n + 0.04353;$$
$$1/U_{25} = 0.01337\ n + 0.05151. \quad (62)$$

For most saturated hydrocarbons, their lower limits on a weight basis are approximately 45 ± 5 mg per liter of air at standard conditions (0° C and 1 atm); upper limits typically fall between 200 and 400 mg/L, excluding methane (*110*).

With increased temperature, the lower limits of saturated hydrocarbon vapor-air mixtures decrease in the manner shown in figure 34 for 10 paraffins (*110*); AIT data are included, as is an updated value for methane (630° C). Limits in this figure are extrapolated from room temperature to 1,300° C, assuming the White concept of a constant limit flame temperature (*107*). Applying the modified Burgess-Wheeler law (equation 36), Zabetakis (*110*) assumed a constant calorific value for both lower and upper limits and obtained the following correlations for predicting temperature effects:

$$L_T/L_{25} = 1 - 0.000721\ (T - 25°) \quad (63)$$

$$U_T/U_{25} = 1 + 0.000721\ (T - 25°) \quad (64)$$

where T refers to elevated temperature in ° C. Equation 63 is fairly reliable for the lower limits of the paraffins and many of their derivatives, although a calorific value ($L_{25}\Delta H_c/100$) closer to 11 kcal/mol would be more representative of the data given in table 7; most inconsistencies with calorific values occur with the aldehyde, bromide, and dichloride derivatives. Upper limit predictions based on ideal $U_{25}\Delta H_c/100$ values (not shown) are more tenuous because of incomplete combustion and possibility of cool flames. Data by Cato (*9*) indicate that the upper limits of paraffins above n-butane can increase by much greater amounts than predictable by equation 64 (fig. 35). This behavior appears likely to occur with low-AIT hydrocarbons or other combustibles highly capable of cool or blue flames. Temperature effects reported by Kuchta (*54*) for the flammability limits of four chlorinated hydrocarbons in air and oxygen are summarized in table 8.

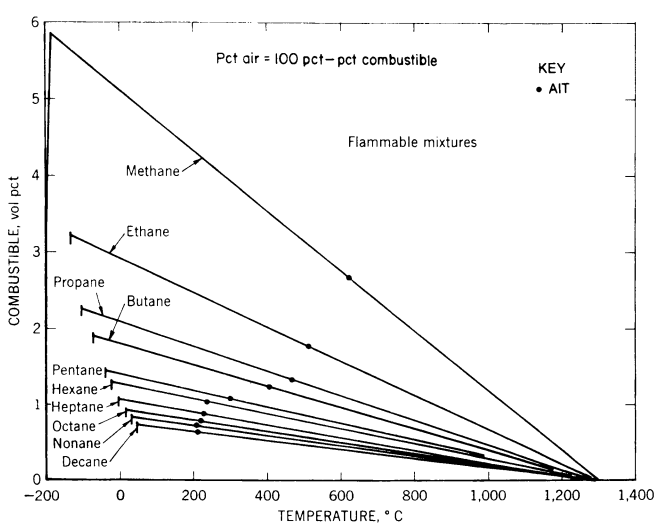

Figure 34.—Temperature effect on lower limits of flammability of 10 normal paraffins in air at atmospheric pressure.

Table 8. — Temperature effects on the flammability limits of four chlorinated paraffins in air and oxygen at 1 atm (*54*)

	Temp, °C	Flammability limits, vol pct			
		Air		Oxygen	
		L_{25}	U_{25}	L_{25}	U_{25}
n-BUTYL CHLORIDE					
(C_4H_9Cl) . . .	25	[1]1.9	8.4	1.8	49
	100	2.0	10.3	1.7	52
	200	1.8	12.0	1.6	56
METHYLENE CHLORIDE					
(CH_2Cl_2) . . .	25	NA	NA	13.6	NA
	100	15.9	19.1	11.7	68
	200	14.9	19.2	11.0	72
ETHYLENE CHLORIDE					
($C_2H_4Cl_2$)	25	6.0	NA	5.6	NA
	100	4.5	17.3	4.0	67.5
	200	3.9	21.2	3.5	69
METHYL CHLOROFORM					
($C_2H_3Cl_3$)	25	[1]6.8	[2]>10.5	6.6	NA
	100	6.3	13.0	5.5	57
	200	5.9	14.3	4.1	60

NA Not available.
[1]Interpolated values from flammability diagrams.
[2]Value limited by vapor pressure of fuel.

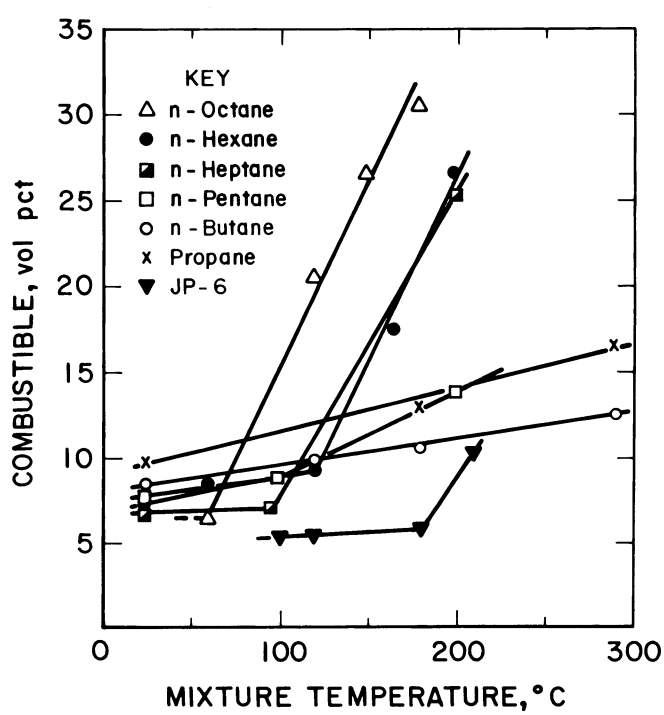

Figure 35.—Temperature effect on upper limits of flammability of six normal paraffins and JP-6 jet fuel in air at atmospheric pressure.

Flammability limits of hydrocarbon vapor-air mixtures vary only slightly with reduced pressure except at very low pressures, such as below 1/4 atm, where ignition energy or quenching distance becomes the most critical factor. Thus, limits of combustibles which are sensitive to ignition energies can be substantially narrowed by reduced pressures. At elevated pressures, the lower limits of combustibles generally decrease slightly, but the upper limits tend to increase greatly. Figure 36 illustrates the effect of high pressures on the limits of natural gas (85 pct CH_4 and 15 pct C_2H_6) and ethane in air at 25° C, as reported by Kennedy (*44*). For such combustibles, the upper limits are increased at least threefold at 500 psig, above which the pressure effect diminishes; in comparison, the lower limits at 500 psig are decreased by only 1/10 or less of their values at atmospheric pressure.

Unsaturated Hydrocarbons, Aromatics, and Derivatives

The main classes of unsaturated hydrocarbons are alkenes (olefins) and alkynes (acetylenes). Flammability limits of the alkene series decrease with increasing number of carbon atoms (fig. 37), similar to the alkane series, but tend to be wider because of higher upper limits; note especially the U_{25} values in air or oxygen for ethylene (C_2H_4) versus ethane (C_2H_6) in table 6. The equivalence ratios and calorific values of their lower limits in air at 25° C are in fair agreement with those of the normal paraffins, except for ethylene, which gives noticeably lower values (table 9); values for two alkadienes, propadiene (C_3H_4) and butadiene (C_4H_6), are also included in table 9.

Many of the alkene derivatives also have wide flammability ranges, including the ethers, amines or imines, and chlorine derivatives. Data in figure 37 for three chloroethylenes show that the lower limits in air increase consistently with the number of chlorine atoms; however, their upper limits display an anomalous behavior, namely those corresponding to ethylenes with two and three chlorine atoms, i.e., dichloroethylene ($C_2H_2Cl_2$) and trichloroethylene (C_2HCl_3), respectively. Differences in heats of formation (appendix A) of these chloroethenes cannot account for this anomaly. Instead, differences in test temperatures (25° versus 100° C) and vessel diameters (5 versus 20 cm), which were more favorable for trichloroethylene, are more likely to explain these results; such variables can greatly affect the flammability of halogenated combustibles. The diameter effect is best illustrated in the flammability evaluation of trichloroethylene by Perlee (*82*). The dichloroethenes and trichloroethenes, as well as bromoethenes, have lower limit equivalence ratios and calorific ratios for combustion in air that are markedly higher than the values for their unsubstituted alkenes (table 9). Other ethene derivatives, particularly allyl alcohol (C_3H_5OH) and allyl amine ($C_3H_5NH_2$), are more consistent with the data for normal alkenes.

Alkynes present a greater flammability hazard than alkenes because of their greater thermal instability and ability to form decomposition flames with or without air. For example, acetylene vapors have a flammable range from 2.5 to 100 pct in air at 25° C and atmospheric pressure, provided the vessel diameter is at least about 15 cm (*110*); upper limits of 75 or 80 pct are occasionally given in the literature for this fuel, but these represent quenched limits from determinations in small-diameter tubes (*11*). The

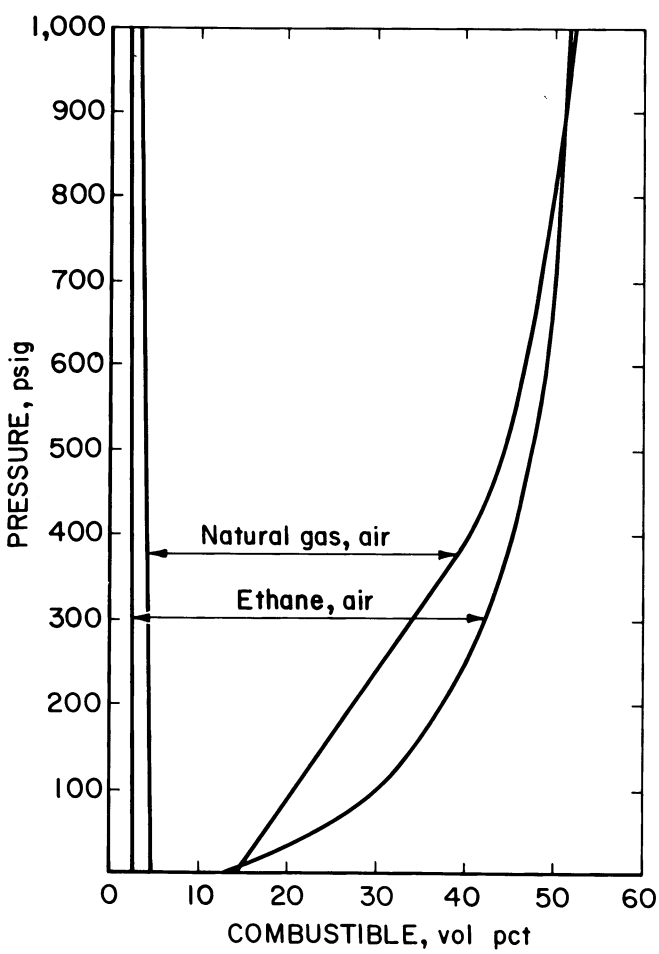

Figure 36.—Pressure effect on limits of flammability of natural gas and ethane in air at 25° C.

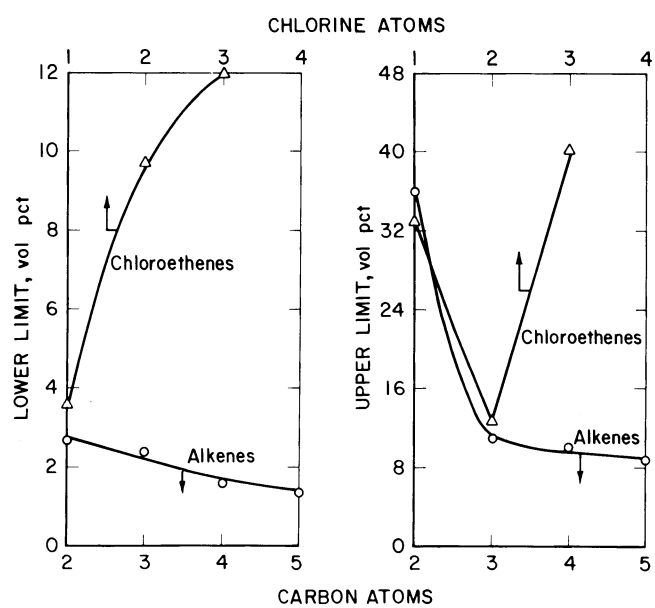

Figure 37.—Variation of lower and upper limits of flammability in air with number of carbon atoms for normal alkenes and with number of chlorine atoms for chloroethenes. Data at 25° C or reported temperature.

Table 9. — Equivalence ratios (L_{25}/C_{st}) and calorific values ($L_{25}\Delta H_c/100$) of lower limit mixtures of unsaturated and aromatic hydrocarbons and derivatives in air at 25° C and 1 atm

Formula	L_{25}, vol pct	L_{25}/C_{st}	$L_{25}\Delta H_c/100$, kcal/mol
n-ALKENES OR ALKADIENES			
C_2H_4	2.7	0.41	8.5
C_3H_6	2.4	.54	11.0
C_3H_4	2.2	.44	9.8
C_4H_8	1.6	.47	9.7
C_4H_6	2.0	.54	11.5
C_5H_{10}	1.4	.52	10.6
ALKENE DERIVATIVES			
C_2H_4O	3.6	0.47	10.5
C_2H_4NH	3.6	.60	13.0
C_2H_3Cl	3.6	.47	9.9
$C_2H_2Cl_2$	9.7	1.02	22.5
C_2HCl_3	[1]12.0	.98	25.2
C_3H_5Cl	2.9	.58	12.2
C_3H_5Br	4.4	.89	18.4
C_3H_5O	2.8	.56	12.1
C_3H_5OH	2.5	.50	10.6
$C_3H_5NH_2$	2.2	.52	10.8
$(C_2H_3)_2O$	1.7	.42	9.3
n-ALKYNES			
C_2H_2	2.5	0.32	7.5
C_2HCH_3	1.7	.34	7.5
ALKYNE (PROPARGYL) DERIVATIVES			
C_3H_3OH	2.2	0.39	9.0
C_3H_3Br	3.0	.53	11.7
ALKYL BENZENES			
C_6H_6	[2]1.3	0.48	9.8
$C_6H_5CH_3$	[2]1.2	.53	10.8
$C_6H_5C_2H_5$	[2]1.0	.51	10.5
$C_6H_5C_4H_9$	[2].82	.54	11.0
BENZENE DERIVATIVES			
$C_6H_5NH_2$	[2]1.2	0.46	9.4
$C_6H_5NO_2$	[2]1.8	.56	12.8
C_6H_5Cl	1.4	.48	10.0
$C_6H_4Cl_2$	[2]2.2	.71	14.8
C_6H_5Br	[2]1.6	.55	11.4
$(C_6H_5)_2NH$	.7	.50	10.5
$(C_6H_5)_2O$	.8	.54	11.3

[1]Limit at 30° C.
[2]Limits at elevated temperatures.

lower limit equivalence ratios for acetylene (C_2H_2) and methyl acetylene (C_2HCH_3) in table 9 are in good agreement but much lower than found for alkenes or alkanes. Halogenated alkynes such as propargyl bromide (C_3H_3Br), propargyl chloride (C_3H_3Cl), and chloroacetylene (C_2HCl) are capable of propagating flame without air at substantially lower pressures than acetylene. Even ethylene and ethylene oxide (C_2H_4O) can propagate a decomposition flame, although ethylene requires relatively high pressures (~1,000 psia). Table 10 summarizes the lower pressure limits that were reported in references 20 and 110 for various hazardous combustibles. For the hydrocarbon combustibles, their pressure limits correlate with their heats of formation (ΔH_f) and are lowest for the most endothermic (positive ΔH_f) compounds. Consistency of such correlations for any combustible will vary with the complexity of the decomposition products.

Table 10. — Lower pressure limits of flammability for combustible vapors capable of propagation without an air atmosphere[1]

Combustible	ΔH_f (25° C), kcal/mol	Vessel diameter, cm	Lower pressure limit (25° ± 5° C), cm Hg
Propargyl bromide	~40	20.3	~0.15
Chloroazide	NA	~6.4	.2
Hydrazine	22.8	2.5	1.2
Ethyl nitrate	−36.8	[2]5.3	≤2.5
Propargyl chloride	NA	20.3	3.0
Monochloroacetylene	51.1	5.1	6.0
Ethylene oxide	−12.6	20.3	52.5
Acetylene	54.2	15.2	~76
Propadiene	45.9	20.3	169
Methylacetylene	44.3	10.2	300
Ethylene	12.5	5.1	~5,170

NA Not available.
[1]Selected data from references 20 and 110.
[2]Flat flame burner data.

Aromatic hydrocarbons have flammability limits that are comparable to or narrower than the values for their paraffin homologues with the same number of carbon atoms. Thus, their L_{25}/C_{st} and $L_{25}\Delta H_c/100$ values in table 9 tend to approximate the data for normal paraffins in table 7; data for dichlorobenzene ($C_6H_4Cl_2$) are the most inconsistent in these correlations.

Inorganic Combustibles

Some inorganic fuels have much wider flammability limits in ambient air than the saturated and unsaturated hydrocarbons, excluding those of high thermal instability such as the acetylenes. Such inorganics include hydrogen and carbon monoxide, which have flammability ranges of 4.0 to 75 pct and 12.5 to 74 pct, respectively, in air at 25° C and atmospheric pressure. The lower limit of 4.0 pct for hydrogen is thermodynamically impossible but is consistent with the greater diffusivity of hydrogen relative to oxygen or air. As shown by Burgess (*5*), preferential diffusion effects can account for the wide difference of upward and downward lower limits for hydrogen (4.0 versus 8.5 pct) and the small differences of such limits for carbon monoxide and methane. Earlier data by Furno (*22*) showed that similar diffusional effects can also explain the widening of upper limits of such hydrocarbons as normal butane; in this case, the greater diffusivity of oxygen allows greater fuel concentrations to be burned.

Of the nitrogen-containing inorganics, hydrazine has the widest flammability range (4.7 to 100 pct) in air and ammonia the narrowest (15 to 28 pct). As noted in table 10, hydrazine can form a decomposition flame at very low pressures, 1.2 cm Hg in a 2.5-cm-diameter tube. The flammability limits of cyanogen (6.6 to 32 pct) are nearly as wide as those for ethylene, and those for hydrogen cyanide (5.6 to 40 pct) are somewhat wider. It is worth noting that some organic nitrates and nitrites also have wide flammability limits; see appendix A and table 10. Other inorganic fuels with a wide flammability range are hydrogen sulfide (4.0 to 44 pct), carbon disulfide (1.3 to 50 pct), and diborane (0.8 to 88 pct).

The difference between the flammability limits of all combustibles tend to be less pronounced in oxygen than in air. This is evident by the available data in table 6. Similarly, the difference will be much less at highly elevated pressures, which in effect correspond to higher oxygen partial pressures.

FLAMMABILITY LIMITS IN OTHER ATMOSPHERES

The flammability limits of combustible vapors are of interest in various oxidant-inert or diluent atmospheres for defining inerting and extinguishing requirements. Complete flammability diagrams have been reported by Bureau investigators for many combustible-oxidant-inert systems. Figure 38 shows the flammability diagram given by Zabetakis (*110*) for the methane-air system with various added inerts at 25° C and atmospheric pressure. As expected, the flammability range is progressively narrowed by the addition of inert, particularly on the fuel-rich side, until propagation is not possible at some inert concentration. Helium is seen to be the least effective inert, and the halogenated hydrocarbons (CH_3Br and CCl_4) are the most effective "inerting" agents; the order of effectiveness of the other agents ($CO_2 > H_2O > N_2$) is of greater interest because of their wider use. Composites of the flammability data obtained by Coward (*11*) for five paraffin hydrocarbons are shown in figures 39 (air + N_2) and 40 (air + CO_2). These data are representative of the variations in N_2 and CO_2 inerting requirements for hydrocarbon-type combustibles, excluding such thermally unstable materials as the acetylenic hydrocarbons. Similar flammability diagrams by Jones (*40*) are given in figures 41 and 42 for hydrogen and carbon monoxide, respectively; their inerting requirements with N_2 and CO_2 are substantially greater than for most hydrocarbons.

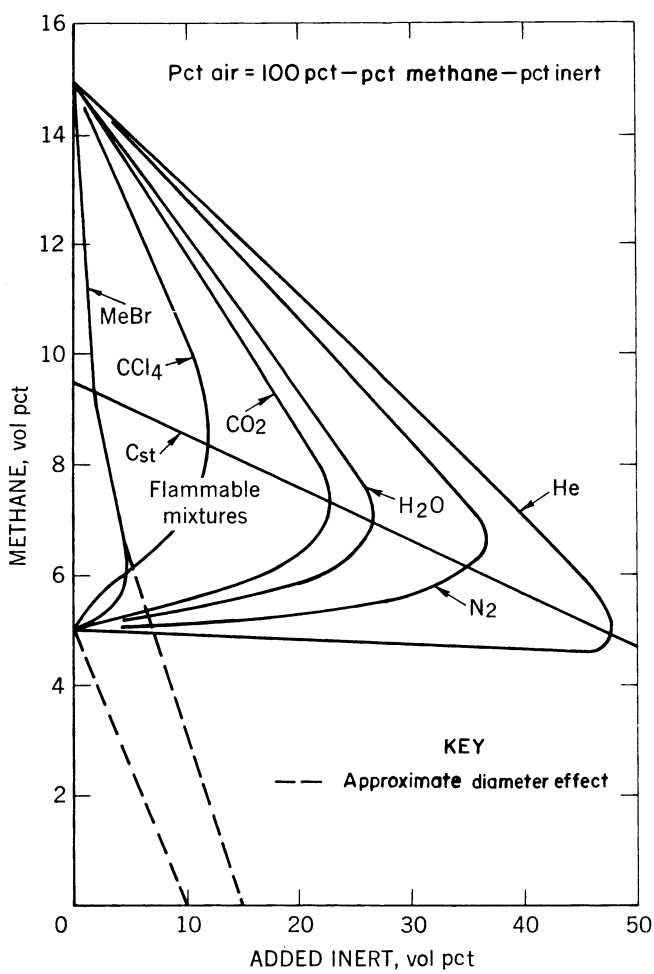

Figure 38.—Limits of flammability of various methane-air-inert gas mixtures at 25° C and 1 atm.

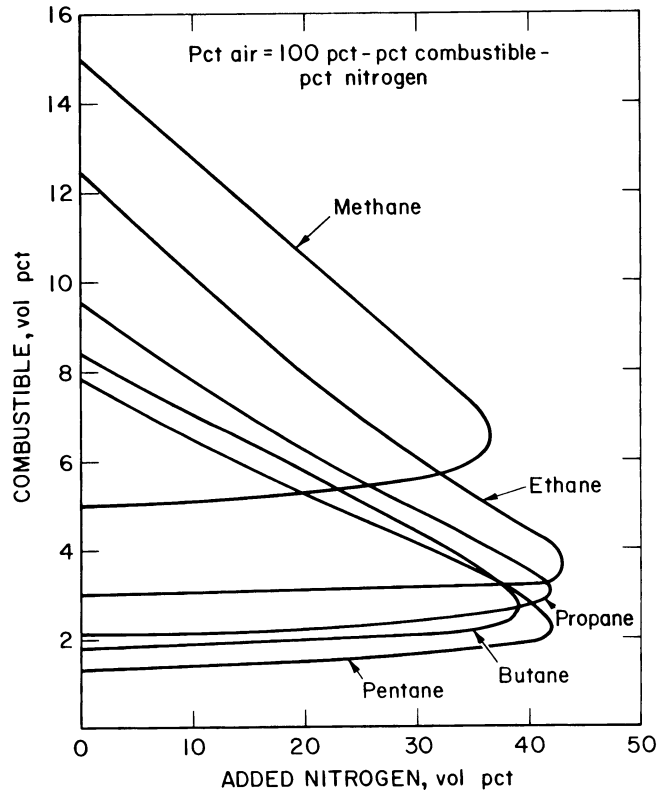

Figure 39.—Limits of flammability of methane-, ethane-, propane-, n-butane-, and n-pentane-air-nitrogen mixtures at 25° C and 1 atm.

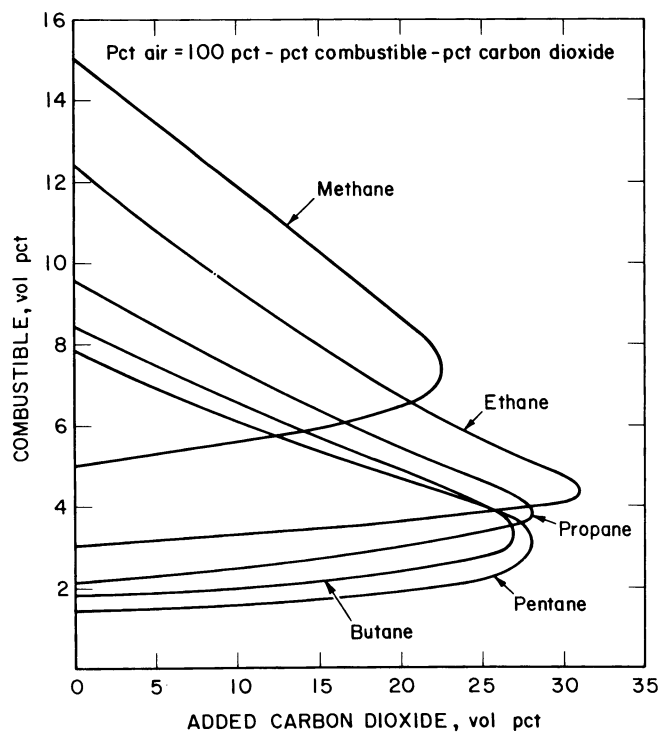

Figure 40.—Limits of flammability of methane-, ethane-, propane-, n-butane-, and n-pentane-air-carbon dioxide mixtures at 25° C and 1 atm.

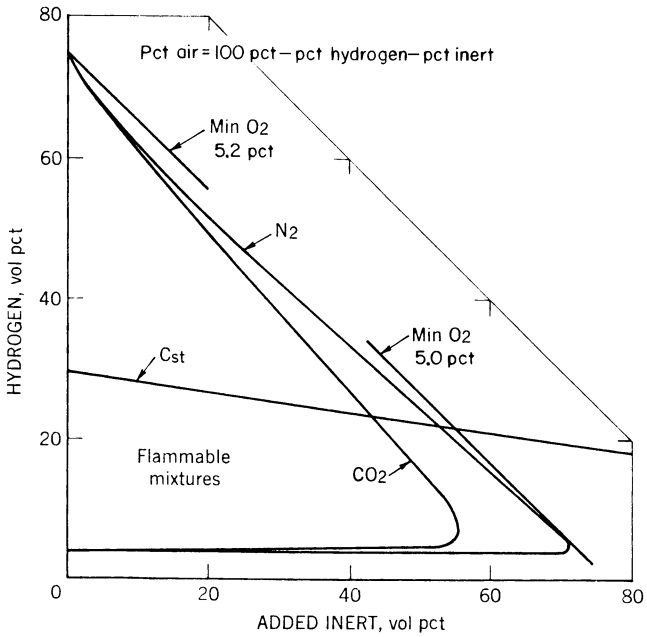

Figure 41.—Limits of flammability of hydrogen-air mixtures with added nitrogen and carbon dioxide at 25° C and 1 atm.

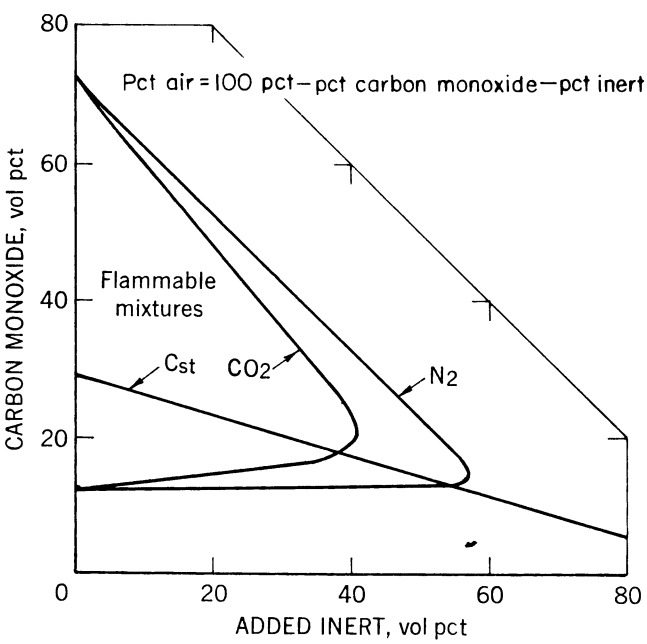

Figure 42.—Limits of flammability of carbon monoxide-air mixtures with added nitrogen and carbon dioxide at 25° C and 1 atm.

It is beyond the scope of this manual to reproduce all the complete flammability diagrams that are available for many other combustibles. Instead, such data are summarized here by listing the minimum oxygen concentrations, as defined in figure 7, below which propagation will not occur (table 11) and corresponding inert concentrations above which propagation is prevented (table 12). For the saturated hydrocarbons, their minimum O_2 values fall between 11 and 12 pct in air-N_2mixtures and between 13.5 and 14.5 pct in air-CO_2 mixtures. Practically the same range of values is found for most unsaturated hydrocarbons and hydrocarbon derivatives; those that differ significantly tend to have somewhat lower minimum O_2 values except for most of the halogenated hydrocarbons (excluding trichloroethylene). Combustibles such as hydrogen, carbon monoxide, carbon disulfide, hydrogen sulfide, and unsymmetrical dimethyl hydrazine (UDMH) stand out by their very low oxygen requirements (5 to 7.5 pct) for propagation.

Essentially the same data trends are expected in comparing the corresponding inert concentrations at the critical oxygen concentrations. The available data in table 12 for the N_2 and CO_2 inerts are consistent in this respect, except for the CO_2 value (29 pct) listed for hydrogen sulfide; this unexpected low value appears questionable. This table also includes inerting data with two Halon extinguishants, both of which are much more effective than CO_2 or N_2. Excluding ethylene, CO_2 is roughly 1-1/2 times more effective (volume basis) than N_2 in inerting the vapor-air mixtures of the saturated and unsaturated hydrocarbons. For

Table 11. — Minimum oxygen requirements for propagation of combustible vapors in air-nitrogen and air-carbon dioxide mixtures at 25° C (unless otherwise indicated) and 1 atm[1]

Combustible	Minimum oxygen concentration, vol pct	
	Air-N_2	Air-CO_2
HYDROCARBONS		
Methane	12	14.5
Ethane	11	13.5
Propane	11.5	14.5
n-Butane	12	14.5
Isobutane	12	15
n-Pentane	12	14.5
Isopentane	12	14.5
n-Hexane	12	14.5
n-Heptane	11.5	14.5
Ethylene	10	11.5
Propylene	11.5	14
α-Butylene	11.5	14
Isobutylene	12	15
Butadiene	10.5	13
3-Methyl-l-butene	11.5	14
Benzene	11	14
Cyclopropane	11.5	14
Gasoline (70/100)	12	15
Gasoline (115/145)	12	14.5
Kerosene	10 (150° C)	13 (150° C)
JP-1 fuel	10.5 (150° C)	14 (150° C)
JP-3 fuel	12	14.5
JP-4 fuel	11.5	14.5
Natural gas (Pittsburgh)	12	14.5
HALOGENATED HYDROCARBONS		
n-Butyl chloride	14	NA
Methylene chloride	17 (100° C)	NA
Ethylene chloride	13	NA
Methyl chloroform	14	NA
Trichloroethylene	9 (100° C)	NA
OTHER COMBUSTIBLES		
Acetone	11.5	.14
t-Butanol	NA	16.5 (150° C)
Carbon disulfide	5	7.5
Carbon monoxide	5.5	[2]7 (5.5)
Ethanol	10.5	13
2-Ethyl butanol	9.5 (150° C)	NA
Ethyl ether	10.5	13
Hydrogen	5	[2]6 (5.2)
Hydrogen sulfide	7.5	[2]13 (11.5)
Isobutyl formate	12.5	15
Methanol	10	12
Methyl acetate	11	13.5
Methyl ether	10.5	13
Methyl formate	10	12.5
Methyl ethyl ketone	11	13.5
UDMH (dimethylhydrazine)	7	NA

NA Not available.
[1]Based upon data in references 11, 42, 54, 68, and 110.
[2]Figure in parentheses is value at upper limit in air alone.

Table 12. — Inerting requirements to prevent propagation of gaseous combustibles in air with nitrogen (N_2), carbon dioxide (CO_2), Halon 1211 (CF_2ClBr) and Halon 1301 (CF_3Br) inhibitors at 25° C (unless otherwise indicated) and 1 atm

Combustible	Minimum inerting concentration, vol pct			
	N_2[1]	CO_2[1]	Halon 1211[2]	Halon 1301[2]
HYDROCARBONS				
Methane	36	23	[3]4.0 (5.3)	[3]2.0 (4.7)
Ethane	44	31	5.8	NA
Propane	42	28	5.9	6.5
n-Butane	40	27	5.9	[4]2.9
Isobutane	40	26	5.2	8.0
n-Pentane	42	28	[4]4.5	NA
n-Hexane	41	28	5.8	NA
n-Heptane	42	28	6.5 (50° C)	8.0
Ethylene	48	39	9.6	11.0
Propylene	42	28	6.2	NA
α-Butylene	43	30	NA	NA
Isobutylene	39	26	NA	NA
Butadiene	47	34	NA	NA
Cyclopropane	41	30	NA	NA
Cyclohexane	NA	NA	5.7	NA
Benzene	44	28	4.8	4.3
Gasoline	41	28	[4]4.2	NA
Kerosene	43	28	[4]4.2	[4]2.8
JP-4	43	29	NA	6.6
OTHER COMBUSTIBLES				
Acetone	41	28	4.9	5.3
Carbon disulfide	72	59	[4]2.7	12.0
Carbon monoxide	58	41	NA	[4]1.0
Ethanol	44	31	6.2 (50° C)	4.0
Ethyl acetate	NA	NA	[4]6	4.6
Ethyl ether	48	33	NA	6.3
Hydrogen	71	57	27	20
Hydrogen sulfide	NA	29	NA	NA
Methanol	46	32	24.7 (50° C)	NA
Methyl ether	47	33	NA	NA
Methyl ethyl ketone	45	32	5.8	NA
Methyl formate	45	32	NA	NA

NA Not available.
[1]References 11, 47, and 110.
[2]References 79 and 80; includes 10-pct safety factor.
[3]Data in parentheses from reference 47.
[4]Data for flame extinguishment (less conservative value).

the same combustibles, Halon 1211 (CF_2ClBr) is about five times more effective than CO_2 and roughly comparable in effectiveness to Halon 1301 (CF_3Br). The effectiveness of the Halons is attributable to their chemical flame inhibiting action, whereas that of CO_2 and N_2 is due merely to their capacity to absorb heat. Data discrepancies are most likely to occur with the Halons because their propagations are more sensitive to vessel size and ignition energy effects. Bureau of Mines investigators (*47*) showed that the parenthetical values of 5.3 pct Halon 1211 and 4.7 pct Halon 1301 in table 12 for methane-air mixtures are more realistic than the given NFPA data (*79-80*). Figure 43 shows the complete flammability diagrams obtained by the Bureau authors with such Halons, including Halon 1202 (CF_2Br_2), in a 10-cm-diam tube (spark ignition). With a very strong and diffuse ignition source, such as an incendiary, the Halon requirements can be substantially greater. Thus, some reservation is appropriate in the use of these Halon data.

Data on the effects of temperature and pressure on inerting requirements are rather meager. The modified Burgess-Wheeler law (equation 63) may be used to obtain rough estimates of temperature effects on minimum O_2 values in air-N_2 or air-CO_2 mixtures, but its reliability for different combustibles and temperature ranges is uncertain. Ordinarily, the oxygen requirements with N_2 or CO_2 inerts decrease only slightly with moderate increases of temperature or pressure. Figure 44 (*110*) is representative

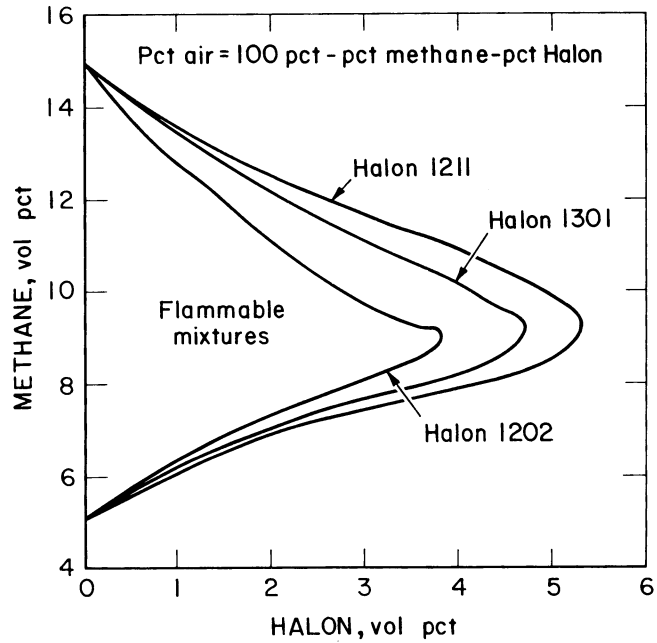

Figure 43.—Limits of flammability of methane-air-Halon mixtures at 25° C and 1 atm.

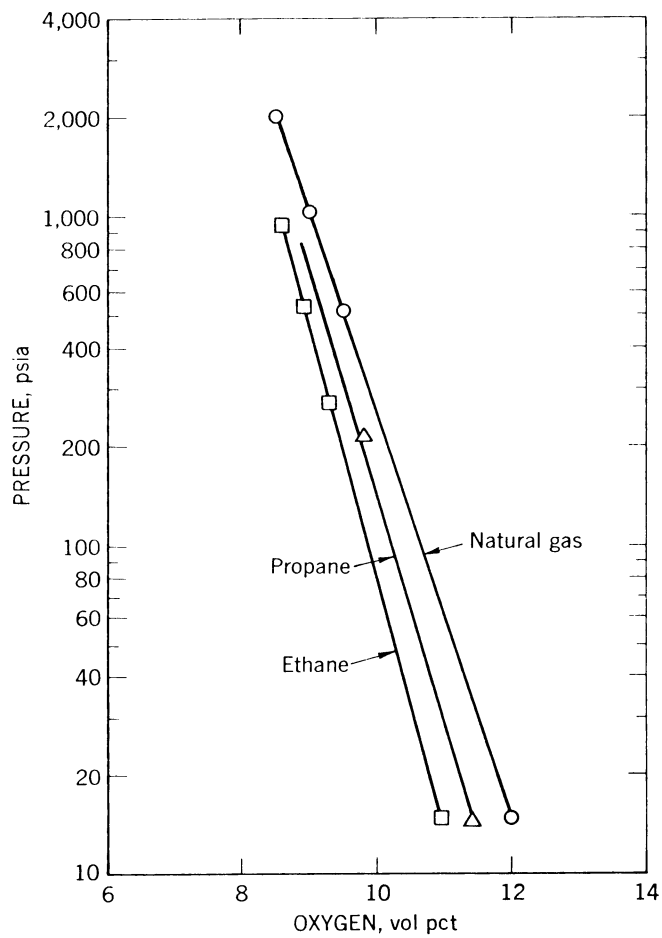

Figure 44.—Effect of pressure on minimum oxygen requirements for propagation of natural gas, ethane, and propane in air-nitrogen mixtures at 25° C.

of the pressure effect on the minimum O_2 requirements for saturated hydrocarbons in air-N_2 mixtures.

With Halon-type agents, their effectiveness may decrease greatly in propagations at even moderate pressures, depending upon their thermal stability. Both Halons and inert gases are least likely to be effective against combustibles that can propagate flame without an oxidant, such as those in table 10. Also, one must bear in mind that the inerting data are primarily applicable to the prevention of flame propagation or explosion and not for fire extinguishment, which can require much greater concentrations of extinguishants.

IGNITION REQUIREMENTS

Ignition Energies

Electrical spark ignition energies provide a measure of the thermal requirements for ignition by a highly localized source. Figure 45 presents such data from the classic studies summarized by Lewis (*66*, p. 323) for the vapor-air mixtures of six normal paraffins at 25° C and atmospheric pressure. The minimum ignition energies (MIE) for these saturated hydrocarbons are approximately 0.25 mJ and occur at fuel-air ratios greater than stoichiometric, except for methane; see also figure 4. Differences in fuel diffusivities account largely for the variation of optimum fuel-air ratios for ignition with increasing molecular weight. Lewis (*66*), Litchfield (*67-69*), and Calcote (*8*) have reported ignition energy data in air and oxygen for various combustibles, many of which are summarized in table 13. The MIE values of most combustibles fall between 0.1 and 0.3 mJ in normal ambient air. Combustibles with much lower values are acetylene, hydrogen, and carbon disulfide, and those with much higher values are ammonia and halogenated hydrocarbons, excluding butyl chloride; the MIE value for acetone is also very high but is suspect.

Corresponding MIE's in oxygen are at least an order of magnitude lower than in air. They are also very sensitive to pressure. Figure 46 shows the effects of both pressure and oxygen concentration on the MIE's of propane-oxygen-nitrogen mixtures (*66*, p. 333). The MIE's generally vary

Table 13. — Minimum spark ignition energies of combustible vapors in air and oxygen at 25° C (unless otherwise indicated) and 1 atm[1]

Combustible	Minimum ignition energy, mJ	
	Air	Oxygen
HYDROCARBONS		
Methane	0.30	0.003
Ethane	.26	.002
Propane	.26	.002
n-Butane	.26	.009
n-Hexane	.29	.006
Acetylene	.017	.0002
Ethylene	.07	.001
Propylene	.28	NA
Cyclopropane	.18	.001
Benzene	.22	NA
HALOGENATED HYDROCARBONS		
n-Butyl chloride	0.33	0.007 (88° C)
Methylene chloride	133 (88° C)	.124 (88° C)
Ethylene chloride	2.37	.011 (88° C)
Methyl chloroform	NI	.092 (88° C)
Trichloroethylene	295 (88° C)	18.0 (88° C)
OTHER COMBUSTIBLES		
Acetaldehyde	0.38	NA
Acetone	1.15	0.0024
Ammonia	> 1,000	NA
Carbon disulfide	.015	NA
Ethyl ether	.20	.0013
Ethylene oxide	.062	NA
Hydrogen	.017	.0012
Hydrogen sulfide	.077	NA
Methanol	.14	NA
Propylene oxide	.14	NA

NA Not available. NI No ignition.

[1]Based upon data in references 8, 66 (p. 323), and 67-69; mixture composition stoichiometric or near-optimum for ignition.

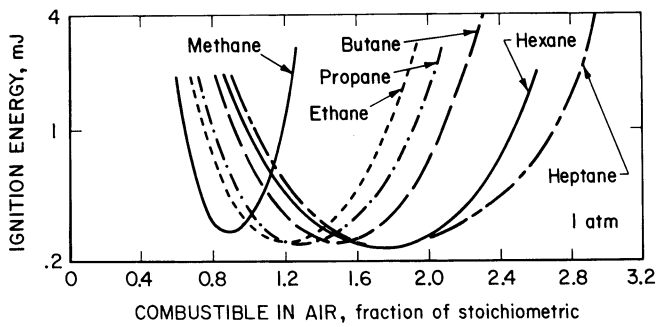

Figure 45.—Spark ignition energy versus combustible vapor concentration for six paraffins in air at atmospheric pressure.

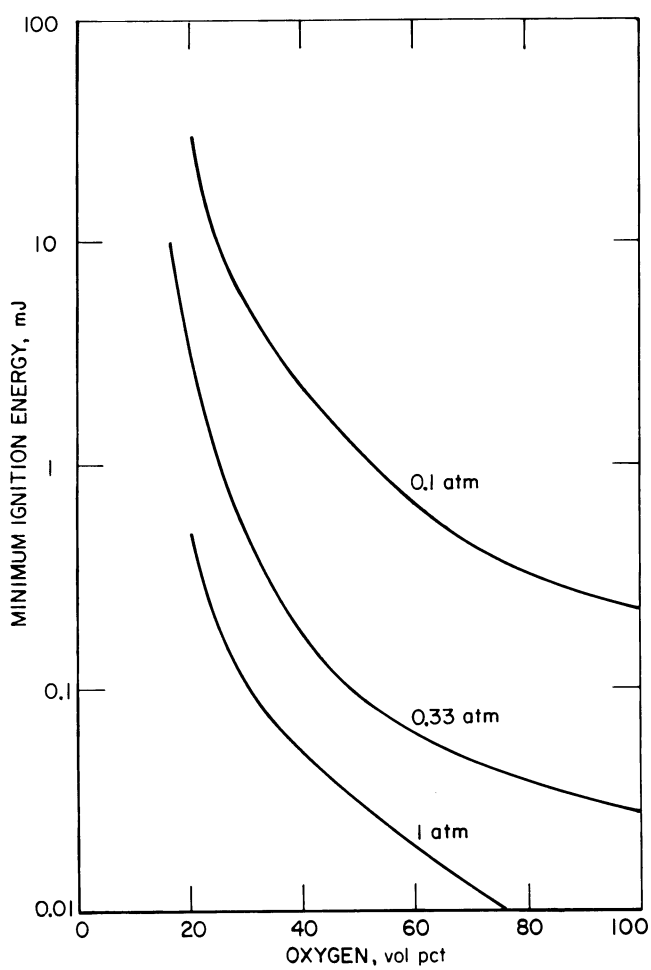

Figure 46.—Minimum spark ignition energy of propane-oxygen-nitrogen mixtures as a function of oxygen concentration and mixture pressure.

inversely with approximately the square of pressure. With increasing temperature, they decrease roughly by a factor of 2 for a 100° C temperature change (*69*). The low ignition energy requirements of combustible vapor mixtures are of great concern since sparks or arcs from ordinary electrical equipment have much greater energies (order of joules); even spark energies from static electricity are often greater (order of tens of millijoules) than MIE values, as discussed under theory and definition. Applications of spark ignition data to safety engineering, including intrinsic safety, are elaborated on by Litchfield (*67*).

Quenching Distances

Minimum ignition quenching distances for the combustible vapors in normal ambient air or oxygen are included in table 14. These data were obtained by the above-cited authors and refer to quenching of the spark flame kernel between flat plate electrodes. As with MIE values, minimum quenching distances occur at near-stoichiometric fuel-air ratios and fall in a narrow range (~1.5 to 2.5 mm) for many combustibles. Notable exceptions again are acetylene, carbon disulfide, and hydrogen, which are the most readily ignitable; other exceptions are ammonia and some of the halogenated materials, which are least ignitable.

Although corresponding data in oxygen are less available, the minimum quenching distances are much lower, being only a few tenths of a millimeter for hydrocarbons and hydrogen (table 14). For most combustibles, quenching distances vary inversely with the first power of pressure but with an ill-defined power of temperature (*69*). A useful correlation for estimating the minimum ignition quenching distance from the MIE, or vice versa, is given graphically by figure 47 (*102*). This figure is a composite of Bureau data for various combustible-oxidant-diluent mixtures over a wide range of pressures and oxygen concentrations; here, the MIE varies approximately with the square of the quenching distance. Quenching diameters obtained in tubes are about 1.5 times greater than these flat plate quenching distances.

Such ignition quenching data are useful in predicting flame propagation hazards of combustible mixtures and designing flame arresting devices. An effective flame arrester must quench the propagating flame at the arrester face and remove sufficient heat from the product gases to prevent ignition beyond the arrester; thus, both flame velocity and arrester physical specifications are important. In practice, flame velocities can be much greater than those developed in the above quenching distance experiments. Palmer (*81*) found the approach velocity of the flame to be most critical and developed semiempirical expressions for predicting the effectiveness of various flame arresters.

Table 14. — Comparison of minimum spark ignition quenching distances and maximum experimental safe gaps (MESG) of combustible vapors in air at 25° C and 1 atm[1]

Combustible	Ignition quenching[2] distance, mm	MESG[3], mm
HYDROCARBONS		
Methane	2.03 (0.30 in O_2)	1.14
Ethane	1.5	.91
Propane	1.75	.92
n-Butane	2.4 (0.15 in O_2)	.98
n-Hexane	1.5 (0.20 in O_2)	.93
Acetylene	.64 (0.18 in O_2)	.37
Ethylene	1.22 (0.23 in O_2)	.65
1,3-Butadiene	1.25	.79
Cyclopropane	NA	.91
Benzene	1.95	.99
HALOGENATED HYDROCARBONS		
Allyl chloride	<2.75	1.17
n-Butyl chloride	2.2	1.06
Methylene chloride	5.46	NA
Ethylene chloride	4.57	1.8
Vinyl chloride	NA	.96
OTHER COMBUSTIBLES		
Ammonia	NI	3.18
Carbon disulfide	.55	.20
Carbon monoxide	NA	.91
Ethyl ether	1.85	.83
Isopropyl ether	3.0	.94
Ethylene oxide	1.18	.59
Hydrogen	.64 (0.25 in O_2)	.20
Methanol	1.5	.92
Methyl amine	NA	1.10
Propylene oxide	1.3	.70
Vinyl acetate	2.35	.94

NA Not available. NI No ignition at 1 J.
[1]Mixture composition—stoichiometric or near-optimum for ignition.
[2]Reference 8, 66 (p. 323), and 67-69.
[3]Reference 71.

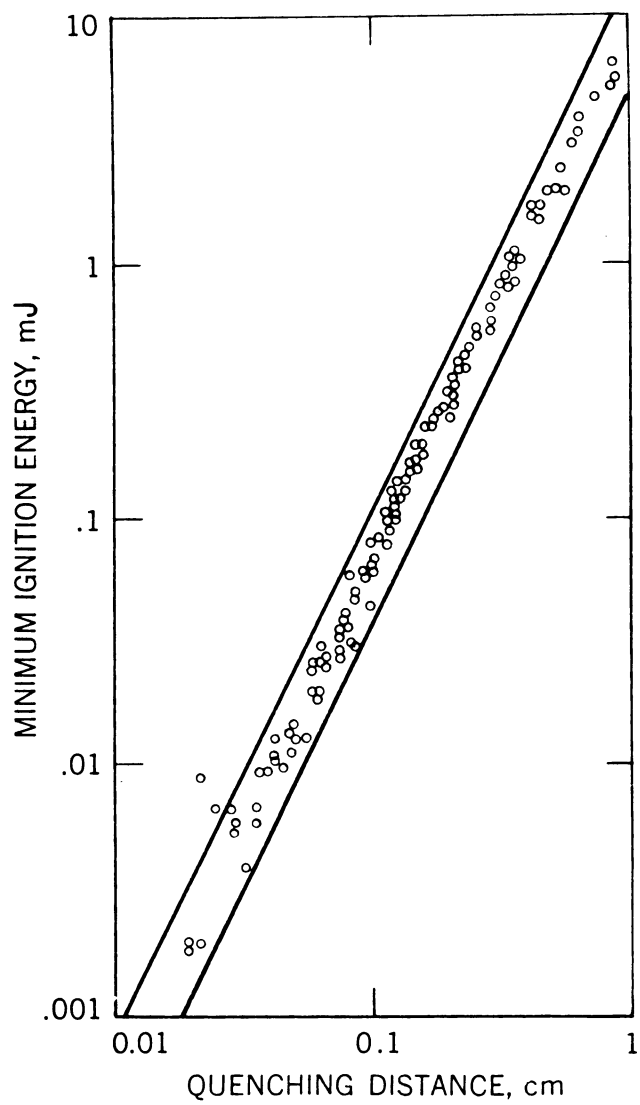

Figure 47.—Correlation of minimum ignition energy with minimum quenching distance for a large variety of combustibles in air and other oxidant atmospheres.

Based on this work and others, a simple relationship is given in a British guide (*73*) for predicting the critical approach velocity:

$$v = 0.5\ a\ y/d^2, \quad (65)$$

where v is flame velocity (ft/s), y is arrester thickness (in), d is diameter of apertures (in), and a is the face area not blocked by the arrester material (wire gauze, metal ribbon, etc.). This expression is primarily applicable to ordinary flame propagations and to moderate pressures.

In the case of explosionproof enclosures, ignition quenching distance data are not sufficiently conservative to protect against the high-velocity jets of flame or hot gas that can be produced at high explosion pressures. Instead, it is necessary to use the maximum experimental safe gap (MSEG) data, which are designed to prevent ignition by any jets of hot gas escaping through the flange gap of such enclosures; hot gas ignition temperatures are given in the next section. The MSEG values included in table 14 are proposed by British Government laboratories (*71*) and were obtained at an initial pressure of 1 atm and gap passage length of 2.54 cm (1 in). Underwriters' Laboratories (*15*) in this country reports lower MSEG values for some of the combustibles, particularly acetylene, hydrogen, carbon disulfide, and ammonia. Their lower values reflect the effects of a shorter gap length (3/4 in) and more severe explosion pressures that were developed by using turbulent mixtures and a long flame runup to simulate pressure piling.

Ignition Temperatures

Minimum autoignition temperatures (AIT's) are widely relied upon for assessing the ignitability hazard of combustible vapors in a heated environment without an external ignition source. Relatively complete listings of AIT's for liquid and gaseous compounds in atmospheric air are given in appendix A. These listings also update any previously reported data that could not be confirmed, including the widely cited values for methane (540° C) and hydrogen (400° C). The data refer to ignitions under static conditions that were obtained in open glass vessels, usually of at least 200 cm^3 volume and with induction or contact times (ignition delays) of the order of minutes; data obtained in smaller vessels or with shorter contact times are less conservative for safety applications. Appearance of any flame was normally used as the criterion of ignition in such determinations. Precision of these data can be assumed to be approximately ±10° at 300° C. They should not be confused with flashpoints, which relate to the volatility and not the ignitability of the combustible.

AIT's of combustibles are lower in oxygen than in air, but the differences are not great for most hydrocarbon combustibles. Selected data from Bureau (*23, 110, 112*) and NFPA (*72, 78*) compilations are given in table 15 for some representative organic and inorganic combustibles at atmospheric pressure. The effects of chemical structure are evident from the data in this table and appendix A. Generally, the AIT's of straight-chain hydrocarbons decrease with increasing number of carbon atoms and increase with chain branching (note isobutane) and ring formation (note cyclopropane); Zabetakis (*112*) showed they can be correlated with the average chain length. Similar trends occur with the various families of hydrocarbon derivatives, although the data are less consistent, depending upon the functional group. The AIT's of most hydrocarbons and their derivatives in air fall between the values for methane (630° C) and n-decane (210° C); notable exceptions are acetaldehyde, methyl hydrazine, and various alkyl ethers, nitrites, or nitrates, which can autoignite below 200° C. Among inorganic compounds, the AIT's are lowest for carbon disulfide and diborane (≤100° C) and highest for carbon monoxide and ammonia (>600° C); the updated values for hydrogen are 520° C in air and 400° C in oxygen. With nitrogen tetroxide as the oxidant, the AIT's are comparable to those in oxygen for such paraffins as butane, hexane, and heptane, but lower by 100° to 200° C for hydrogen and highly chlorinated hydrocarbons (*23*); also, hydrazine fuels are hypergolic with this oxidant.

Table 15. — Minimum autoignition temperatures (AIT's of combustible gases and liquids in air and oxygen at 1 atm

Combustible	Minimum AIT, °C	
	Air[1]	Oxygen[2]
HYDROCARBONS		
Methane	630	555
Ethane	515	505
Propane	450	NA
n-Butane	370	285
Isobutane	460	320
n-Pentane	260	260
n-Hexane	225	220
n-Heptane	225	210
n-Octane	220	210
n-Decane	210	200
Acetylene	305	295
Ethylene	490	485
Propylene	460	425
1,3-Butadiene	420	335
Cyclopropane	500	455
Gasoline (100/130)	440	315
Kerosene	230	215
HALOGENATED HYDROCARBONS		
Ethyl chloride	520	470
n-Butyl chloride	250	245
Methylene chloride	615	535
Ethylene chloride	440	430
Methyl chloroform	485	470
Trichloroethylene	420	405
OTHER COMBUSTIBLES		
Acetaldehyde	175	160
n-Amyl acetate	360	235
Carbon disulfide	~100	<105
Carbon monoxide	610	590
Ethyl ether	195	180
Glycerol	370	320
Hydrazine	270	150
Hydrogen	520	~400
Hydrogen sulfide	260	220
Propanol	440	330
Vinyl ether	360	165

NA Not available.
[1]References 72, 110, and 112.
[2]References 23 and 78.

Figure 48 (*57*) illustrates the dependence of ignition delays on autoignition temperatures in stagnant air for various hydrocarbon fuels, including cyclics and aromatics. Although the data display an exponential dependence as predicted by the Semenov theory (equation 29), the temperature dependence for each fuel changes to a less sensitive one (decreased slope) at some high temperature; this indicates a change in reaction mechanisms or rate-controlling factors. Global activation energies (E) derived from the slopes and use of equation 29 are 11 to 22 kcal/mol in the high-temperature region and 33 to 46 kcal/mol in the low-temperature region for most of these fuels. Similar data under flow conditions, where contact times can be of the order of milliseconds, are rather meager for individual compounds. The following expressions from the above Bureau work (*57*) give the approximate variation of ignition delay

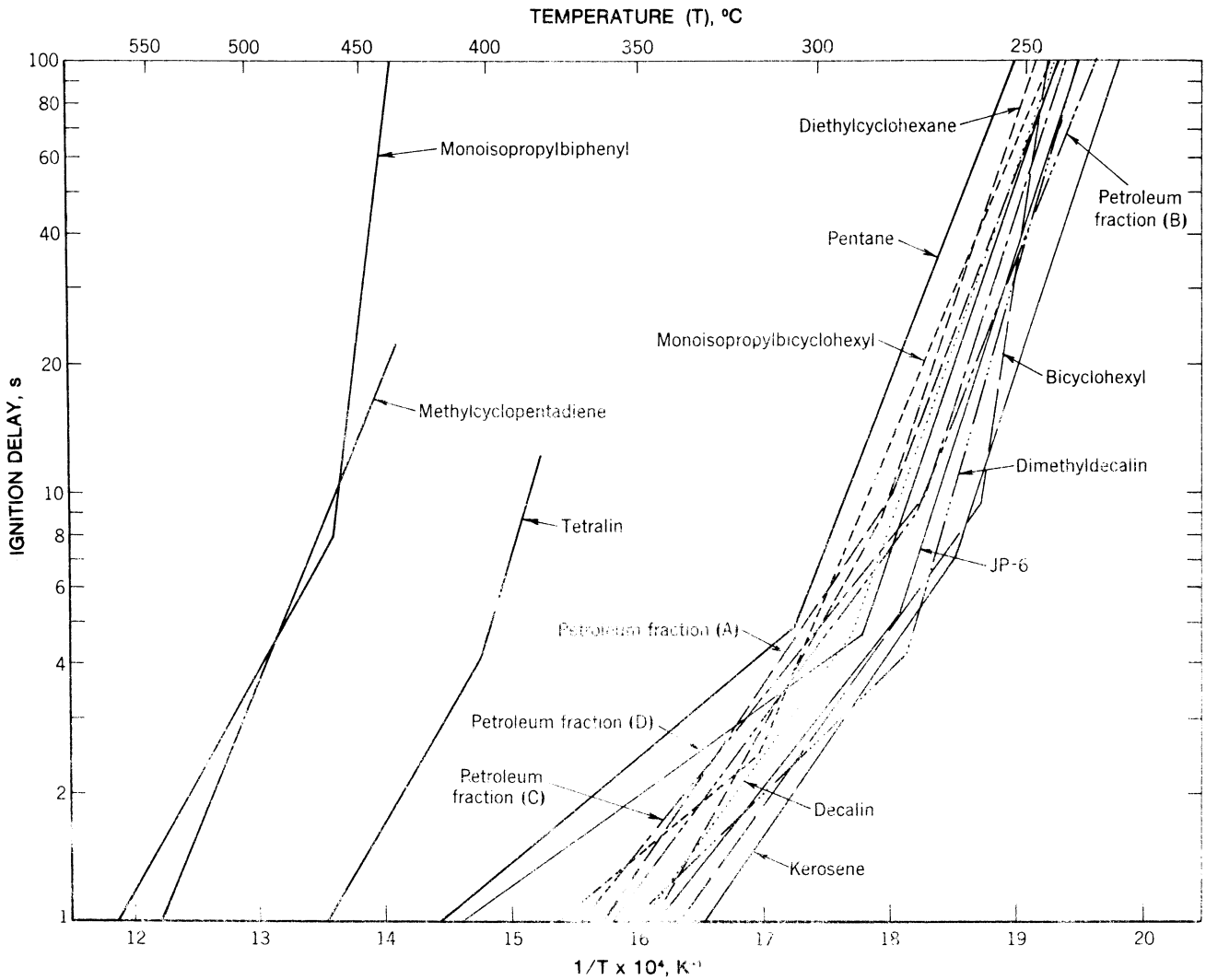

Figure 49.—Autoignition temperatures and corresponding ignition delays of hydrocarbon fuels under static conditions in air at atmospheric pressure.

(τ, ms) with temperature (T, K) for n-pentane (C_5H_{12}) and decalin ($C_{10}H_{18}$) in heated air streams at 2 atm:

Pentane (350°-670° C) .. $\ln \tau = 5400/RT + 1.13$ (66)

Decalin (370°-600° C) .. $\ln \tau = 6600/RT - 0.37$ (67)

where R is 2 cal/(K·mol). The low gross activation energies indicate that physical factors rather than chemical factors were rate controlling.

Autoignition temperatures decrease with increasing pressure, but the decrease is often small for moderate pressure changes, depending upon the combustible and oxidant. According to data for high-molecular-weight hydrocarbons (57), their AIT's in air at 5 atm roughly approximate their corresponding values in oxygen at atmospheric pressure (table 16), i.e., an atmosphere of equivalent oxygen partial pressure. Also, the values in air for hydrocarbons of low AIT (~250° C) are approximately doubled when the pressure is reduced to 0.5 atm (57, 112). However, as shown by Furno (23) for selected paraffins, chlorinated hydrocarbons, and hydrazine fuels, the pressure effect is greatly diminished by the use of large vessels (4,900 cm^3).

Ignitions by any heated surface are a function of the heat source dimensions. For autoignitions in heated vessels, a vessel diameter of at least 5 cm or surface-to-volume ratio (S/V) less than 1 cm^{-1} is required to obtain the AIT values given in appendix A. With larger vessels, Setchkin (94) has shown that the AIT's do not decrease greatly, although the size effect can still be significant for some combustibles. Heated wire, rod, or tube ignition temperatures are normally much higher than the heated vessel AIT's; such data are compared in table 16 for some representative combustibles. Figure 49 was obtained by Furno data (57) and illustrates the dependence of ignition temperature on surface area of the heat source with different sources and combustibles; heat source diameters ranged from 0.8 to 7.5 cm for the vessels (cylindrical) and from 0.04 to 2.5 cm for the wires or rods. For the three paraffins in this figure, their ignition temperatures (T, °C) in air are given by the following expressions for heat source surface areas (A, cm^2) less than 80 cm^2:

n-Hexane	$T = 951 - 98.5 \ln A;$	(68)
n-Octane	$T = 921 - 96.0 \ln A;$	(69)
n-Decane	$T = 893 - 89.5 \ln A.$	(70)

Table 16. — Comparison of hot surface and hot gas ignition temperatures of hydrogen, carbon monoxide, and hydrocarbon fuels in air at 1 atm

Combustible	Ignition temperature, ° C			
	Heated[1] glass vessel (~4.5-cm diam)	Heated[2] Inconel wire (1-cm diam)	Heated[3] Nichrome wire (0.1-cm diam)	Heated[4] air jet (1-cm diam)
Methane	630	NA	1,220	1,040
Ethane	515	NA	980	840
Propane	450	NA	1,050	885
n-Butane	370	NA	1,010	910
n-Hexane	225	670	900	765
n-Octane	220	660	860	755
n-Decane	210	650	835	750
Acetylene	305	NA	850	655
Ethylene	490	NA	900	765
Propylene	460	NA	1,090	930
Isobutylene	445	NA	1,060	960
Carbon monoxide	610	NA	780	785
Hydrogen	520	NA	750	640
JP-6 fuel	230	695	930	805
MIL-L-7808 oil	390	585	695	750

NA Not available.
[1]AIT data from table 15 and appendix A.
[2]Reference 50.
[3]References 50 and 103.
[4]References 51 and 103.

Linear correlations extending to the larger surface areas (~180 cm^2) associated with heated vessel AIT's appear to occur only with combustibles requiring high autoignition temperatures; note data for the engine oil.

Heat source dimensions are equally important in ignitions by jets of hot gases that may come into contact with a combustible vapor-air mixture. Comprehensive studies on hot gas ignitions have been made by Vanpee and Wolfhard (*103-104, 108*). Their results on the effect of jet diameter on ignition temperature with heated laminar air jets are shown in figure 50 for hydrogen and the lower members of the alkane and alkene series; similar data for higher alkane members are also available (*51*). Minimum ignition temperatures obtained with a 1-cm-diam heated air jet are included in table 16 for the various combustibles. As noted, the hot gas ignition temperatures correlate best with the heated wire or rod ignition temperatures, all of which are noticeably higher than the heated vessel AIT's. In comparing all such ignition temperatures for a given combustible, Kuchta (*51*) found the differences are not necessarily great when they are compared at the same heat source diameter. Hot gas ignition temperatures are especially useful in evaluating the ignition hazard of possible hot gases evolved from flame arrestors, explosionproof seals, and permissible explosive firings in mines.

FLAME TEMPERATURES AND BURNING RATES

Flame Temperatures

Assessment of the potential heat release and pressure development in the combustion of gaseous mixtures requires a knowledge of flame temperatures. Table 17 includes such data for the constant-pressure combustion of various combustibles in ambient air at atmospheric pressure; the

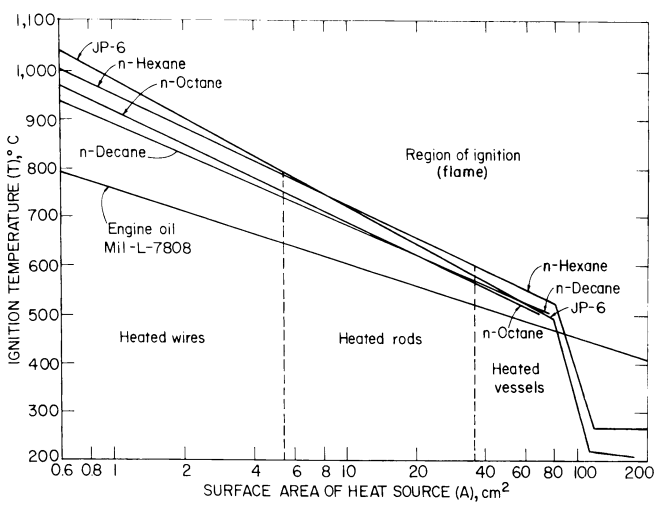

Figure 49.—Hot surface ignition temperatures as a function of heat source surface area for hydrocarbon fuels and an engine oil in air at 1 atm.

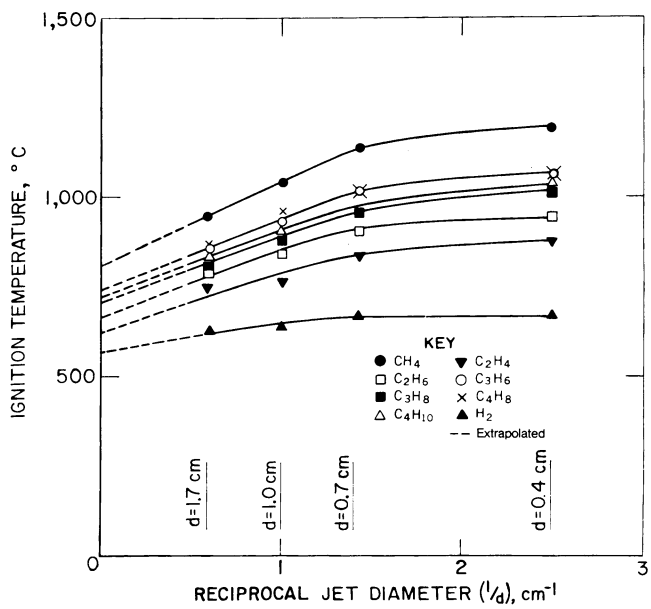

Figure 50.—Hot gas (air) ignition temperatures as a function of reciprocal jet diameter for hydrogen and various hydrocarbons at atmospheric pressure.

Table 17. — Limit flame temperatures, maximum flame temperatures, and maximum burning velocities of gaseous combustibles in air at 1 atm

Combustibles	Limit flame temperature, $(T_f)_L$		Maximum flame[1] temperature, $(T_f)_M$		Maximum burning[2] velocity (S_u), cm/s
	Diffusion[3], °C	Premixed[4], °C	Measured, °C	Calculated, °C	
HYDROCARBONS					
Methane	1,518	1,377 (1,260)	1,875	1,927	45
Ethane	1,363	1,327 (1,230)	1,895	1,922	47.5
Propane	1,422	1,367 (1,310)	1,925	1,967	45.5
n-Butane	1,434	1,492 (1,390)	1,895	2,007	46
n-Pentane	NA	1,362	NA	2,002	44.5
n-Heptane	NA	~1,400 (1,370)	NA	2,002	42.5
Acetylene	NA	1,002	2,325	2,307	157
Ethylene	1,335	1,202	1,975	2,067	74.5
Propylene	1,489	1,337	1,935	2,047	51
Butylene	1,494	NA	1,930		43
1,3-Butadiene	NA	1,317	NA	2,104	54.5
Cyclopropane	NA	1,377	NA	2,077	55.5
Cyclohexane	NA	NA	NA	1,952	43.5
Benzene	1,540	1,442	NA	2,092	48
Natural gas	NA	~1,350	NA	1,950	38.5
OTHER COMBUSTIBLES					
Acetone	NA	1,427	NA	1,934	42.5
Acrolein	NA	1,267	NA	2,067	66
Carbon monoxide	1,177	NA	2,100	2,032	52
Ethanol	1,405	NA	NA	NA	NA
Ethyl ether	1,386	1,337	NA	2,032	50
Ethylene oxide	NA	1,242	NA	2,152	89.5
Hydrogen	811	712	2,045	2,072	326
Methanol	1,258	NA	NA	1,862	57
Propylene oxide	NA	1,282	NA	2,087	67

NA Not available.
[1]References 66, p. 705 (measured values) and 2, 18, and 95 (calculated values); values for near-stoichiometric mixtures.
[2]References 2, 25, and 95; values for near-stoichiometric mixture.
[3]Reference 103 (diffusional burner flame method).
[4]Reference 18 (flammability tube method); parenthetical values from reference 115.

maximum flame temperatures were obtained with near-stoichiometric mixtures. Measured values by Lewis (*66*, p. 628) differed only slightly (<100° C) from calculated values for common hydrocarbons in spite of the lack of adiabatic conditions in measuring such temperatures. Calculated data by Fenn (*18*), Simon (*95*), and others (*2*) are included in table 17. Excluding acetylene (2,325° C), the maximum flame temperatures of hydrocarbons and their derivatives fall in a narrow range, nominally between 1,900° and 2,100° C; hydrogen and carbon monoxide also fall within this temperature range. Corresponding flame temperatures under constant-volume conditions are about 20 pct higher, largely because of the heat capacity differences of the gaseous products under constant volume and constant pressure; see equations 40 and 42.

Limit flame temperatures for the constant-pressure propagation of combustible vapor-air mixtures (lower limit mixtures) are also included in table 17. It is evident that the premixed flame data by Fenn (*18*) and Zabetakis (*115*) are more conservative than the diffusional flame data by Vanpee (*103*). A temperature of at least 1,200° C is required by most of these combustibles, excluding acetylene (~1,000° C) and hydrogen (~800° C). Lowest flame temperatures occur at the lower flammability limit that correspond to upward propagation and constant-pressure combustion. However, in the special case of hydrogen, which has a very high diffusivity coefficient, the calculated flame temperature for its lower limit in air with upward propagation (4.0 pct) would be less than 400° C. Thus, a value of 700° to 800° C is more meaningful and would be characteristic of the concentration required for downward propagation (~8 pct). The variation of theoretical flame temperatures and pressure rises for the adiabatic combustion of hydrogen, methane, and carbon monoxide in atmospheric air is shown in table 18 as a function of combustible concentration. Furno (*22*) and Burgess (*5*) showed that the experimental and theoretical explosion pressures come into agreement only when upward and downward propagation can occur. Knowing the flame temperature at constant volume, the explosion pressure can be estimated by use of equation 48. Thus, for a 5 pct methane-air mixture, the calculated explosion pressure is

$$P_2 = P_1 \frac{n_2}{n_1} \frac{T_2}{T_1} = 1 \times 1 \times \frac{1{,}810}{300} = 6.03\,\text{atm}, \qquad (71)$$

where P is in atm, T is in K, and n_2/n_1 is 1. A maximum P_2/P_1 ratio of approximately 8 is typical of near-stoichiometric mixtures.

Table 18. — Calculated flame temperatures and pressure rises for adiabatic combustion of hydrogen, methane, and carbon monoxide in air at 25° C (*5*)

Fuel concentration, vol pct	Pressure rise (ΔP), psig	Flame temperature (T_f), K	
		Constant volume	Constant pressure
H_2-air:			
4	21.4	746	628
6	30.9	951	788
8	39.8	1,151	944
12	56.2	1,528	1,249
15	67.2	1,794	1,472
CH_4-air:			
4.5	68.5	1,688	1,382
5	74.6	1,810	1,485
6	86.0	2,040	1,683
7	96.4	2,248	1,870
8	105.4	2,425	2,043
CO-air:			
10	53.2	1,450	1,194
11	57.4	1,547	1,275
12	61.5	1,643	1,355
13	65.4	1,736	1,434
14	69.2	1,828	1,512

Burning Velocities

Like flame temperatures, burning velocity (S_u) of a flammable mixture is a fundamental property and depends primarily upon the temperature, pressure, and composition of the mixture. The burning velocities of limit vapor-air mixtures are only a few centimeters per second and become maximum at near-stoichiometric combustible concentrations. Figure 51 illustrates the combustible concentration effect obtained by Gibbs (*25*) for several paraffins in air at ambient temperature and pressure. Maximum S_u values are given for these and other combustibles in table 17. The maximum values for the paraffins and most of their derivatives fall in the 40- to 50-cm/s range, whereas those for unsaturated hydrocarbons are usually greater. Values for acetylene (155 cm/s), hydrogen (325 cm/s), ethylene (75 cm/s), and ethylene oxide (90 cm/s) stand out among the fast-burning combustibles.

With the addition of inert diluents, burning velocities decrease depending upon the concentration and heat capacity of the diluent. Figure 52 (*92*) shows the effect of added nitrogen on both burning velocity (S_u) and flame speed (S_f) of methane-air-N_2 mixtures. Greater S_u reduction occurs with inerts of greater heat capacity than N_2 and even more so with diluents that are chemical flame inhibitors; Johnson (*39*) found that 2.4 pct Halon 1301 (CF_3Br) gave approximately the same S_u reduction (~85 pct) as 34 pct N_2 for CH_4-air flames at near-atmospheric pressure. Assuming nonturbulent flames, the maximum flame speeds of most combustibles at optimum fuel-air ratios can be roughly estimated by

$$S_f = 8\ S_u, \qquad (72)$$

where 8 approximates the expansion ratio (see equation 45) for combustion at 25° C and atmospheric pressure.

Burning velocities are much higher in oxygen than in air. For the paraffins, the maximum values at normal ambient conditions are about an order of magnitude greater in oxygen, as shown in figure 53 from the work by Singer (*96*). For such fuels as acetylene, hydrogen, and carbon monoxide, the corresponding values are about 7, 4, and 2-1/2 times greater, respectively, in oxygen than in air.

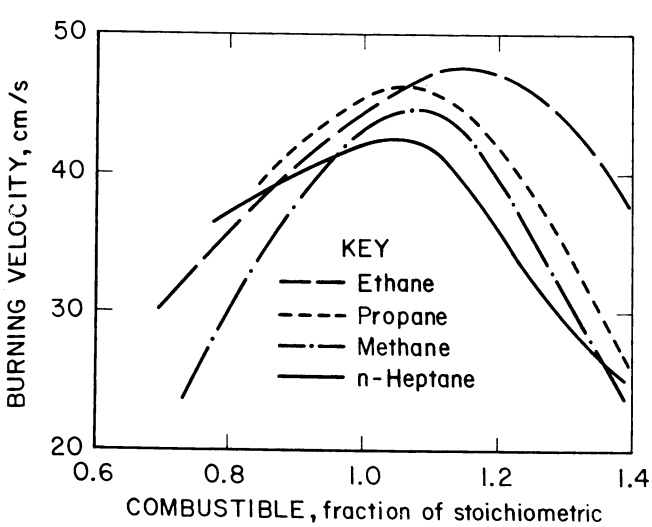

Figure 51.—Burning velocities of methane-, ethane-, propane-, and n-heptane-air mixtures at atmospheric pressure and room temperature.

These data are summarized in the comprehensive works by Lewis (*66*, p. 705) and Gaydon (*24*, p. 56), who have developed basic theories on flame propagation. With increasing temperature, the burning velocities increase (fig.

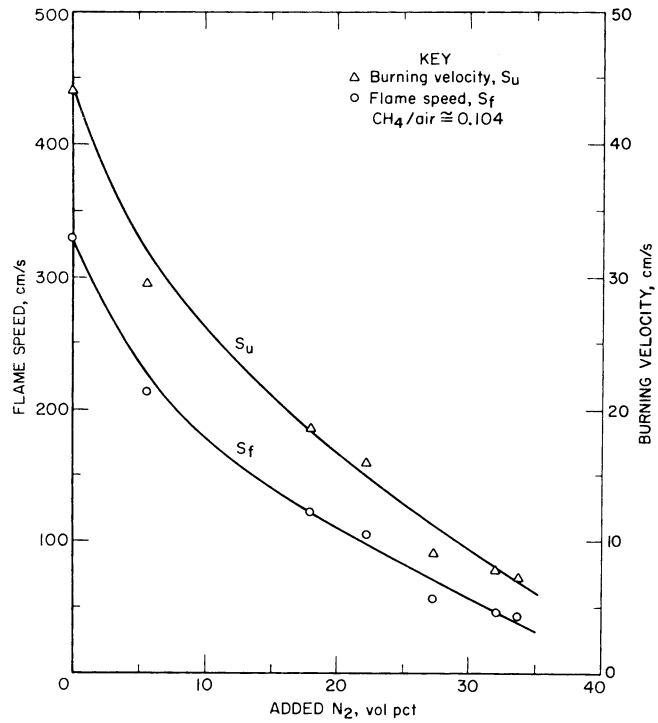

Figure 52.—Burning velocity and vertical flame speed versus added N_2 for combustion of CH_4-air-N_2 mixtures in a 3.65-m (12-ft) diam sphere at 25° C and 1 atm.

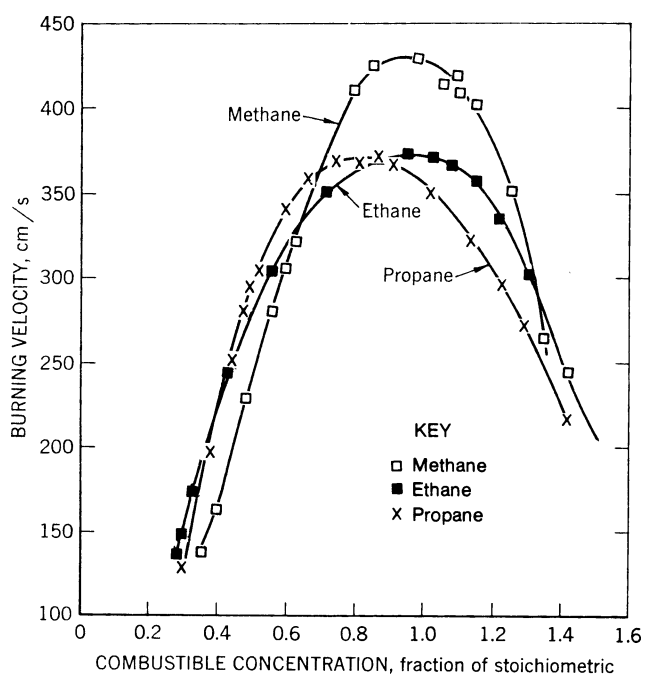

Figure 53.—Burning velocities of methane-, ethane-, and propane-oxygen mixtures at atmospheric pressure and room temperature.

54). The following expression by Dugger (*16*) has been found reliable for at least paraffinic hydrocarbons in ambient air:

$$S_u = 10 + 0.000342\ T^2 \quad (73)$$

where S_u is in cm/s and T is in K. Pressure effects on S_u are more difficult to predict. Data summaries (*24, 66, 110*) indicate that S_u decreases with increased pressure for low-burning-velocity mixtures (<50 cm/s) and increases for high-velocity mixtures (>100 cm/s); intermediate mixtures display little effect of pressure.

Detonation Velocities

Detonations involve supersonic propagation rates and are more likely to occur in oxygen than in air. Figure 55 gives the detonation velocities obtained by Morrison (*74*) for vapors of various paraffins in oxygen as a function of combustible concentration. Maximum velocities are 2,500 to 2,700 m/s for these combustibles. For acetylene, hydrogen, and ammonia, the maximum values are closer to 3,000 m/s or more (*66*, p. 524). In all cases, the maximum values occur at combustible concentrations greater than stoichiometric.

Many combustibles can also undergo detonation in air, although this requires much higher initiation energies, higher pressures, or conditions that promote turbulent combustion and pressure piling. Propagations in long tunnels, especially with irregular wall surfaces, offer favorable conditions for detonations. Although detonations of the paraffins are obtained most readily with the higher members, even methane-air mixtures have been found detonable in recent work. Table 19 lists the detonation velocities obtained by Burgess (*6*) in an air atmosphere for a few hydrocarbon fuels; data for methane and hydrogen are taken from references 46 and 66, p. 524. Although the velocities in air are lower than in oxygen, they are all above 1,500 m/s over the given range of concentrations, below or above which they decrease as the detonability limits are approached; detonability limits normally fall within flammability limits but can be wider for some combustibles with the use of large booster (initiator) charges. In addition to the initiator strength, the length and diameter (or l/d ratio) of the explosion container can be critical for the development of a detonation at a given pressure; detailed discussions of these factors are given in references 66 and 110.

Table 19. — Detonation velocities of several combustibles in air at 25° C and atmosphere pressure[1]

Combustible	Combustible concentration, vol pct	Initiator	Detonation velocity, m/s
Acetylene	19-77	10 g PETN	1,950-2,100
Ethylene oxide	10-18	10 g tetryl	1,890-1,910
	20.5-22	100 g tetryl	2,300-2,350
Hydrogen	~30	NA	1,975
Methane	7-13	50-70 g Amatol	1,550-1,600
Propane	4-7	10 g PETN	1,800-1,890
MAPP gas[2]	6-8	10 g PETN	1,800-1,850

NA Not available.
[1]Based upon data in references 6, 46, and 66, p. 524.
[2]Methylacetylene, propadiene, and propane of near-equal fractions.

Additional detonation velocities for various combustible mixtures are listed in table 20. Although these data were compiled by Laffitte (*61*) almost 50 years ago, they are in fair to good agreement with more recent data, including those given in figure 55 for the paraffins. Where data discrepancies occur, the values in table 20 are on the low side. It is worth noting that the detonation velocities of benzene and ethyl alcohol at stoichiometric oxygen concentrations are comparable to those of most hydrocarbons, excluding acetylene. Other combustibles such as carbon monoxide and carbon disulfide have relatively low detonation velocities in oxygen even at stoichiometric concentrations; the value for carbon monoxide (1264 m/s) is near marginal for a true detonation. Because of the magnitude of detonation velocities, explosion protection systems designed to protect against deflagrations (subsonic) can hardly be expected to be effective against detonations (supersonic).

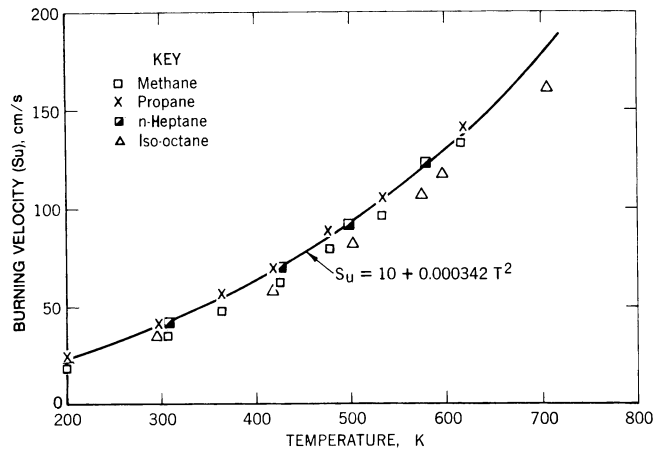

Figure 54.—Effect of temperature on burning velocities of four paraffins in air at atmospheric pressure.

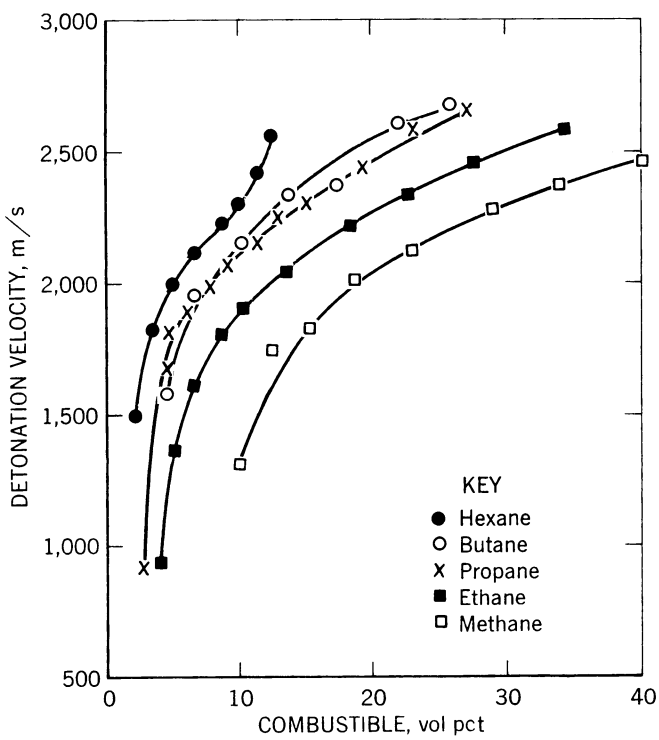

Figure 55.—Detonation velocities of methane-, ethane-, propane-, butane-, and hexane-oxygen mixtures at atmospheric pressure.

Table 20. — Detonation velocities of various combustible mixtures at 25° C and atmospheric pressure (*61*)

Mixture	Detonation velocity, m/s	Mixture	Detonation velocity, m/s
$2H_2+O_2$	2,821	$C_3H_8+3\ O_2$	2,600
$2\ CO+O_2$	1,264	$C_3H_8+6\ O_2$	2,280
$CS_2+3\ O_2$	1,800	$i\text{-}C_4H_{10}+4\ O_2$	2,613
$CH_4+2\ O_2$	2,146	$i\text{-}C_4H_{10}+8\ O_2$	2,270
$CH_4+1.5\ O_2+2.5\ N_2$	1,880	$C_5H_{12}+8\ O_2$	2,371
$C_2H_6+3.5\ O_2$	2,363	$C_5H_{12}+8\ O_2+24\ N_2$	1,680
$C_2H_4+3\ O_2$	2,209	$C_6H_6+7.5\ O_2$	2,206
$C_2H_4+2\ O_2+8\ N_2$	1,734	$C_6H_6+22.5\ O_2$	1,658
$C_2H_2+1.5\ O_2$	2,716	$C_2H_5OH+3\ O_2$	2,356
$C_2H_2+1.5\ O_2+N_2$	2,414	$C_2H_5OH+3\ O_2+12\ N_2$	1,690

Liquid Burning Rates

Whereas burning velocities of combustible gases are relevant to explosion hazard evaluations, burning rates of combustible liquids—including liquefied gases—are important in assessing their fire hazards. The burning rate of a liquid pool is normally defined as a linear regression rate but can also be expressed as a mass or molar consumption rate per unit area. Data uncertainties are greatest for cryogenic fuels, which represent the extreme in vaporization rates.

Burgess (*7*) defined the liquid regression rates of various combustibles in ambient air as a function of pool diameter (fig. 56). With increasing pool diameter, the regression rates increase because of increased radiation feedback to the burning pool, resulting in greater vaporization and reaction. A pool diameter of about 1 m is required before the rates become maximum and level off for most of the fuels. Burgess gives the following expression for predicting the maximum burning rates:

$$v_\infty = 0.0076\ \Delta H_c/\Delta H_v, \qquad (74)$$

where v_∞ is the extrapolated rate at infinite pool diameter (cm/min) and $\Delta H_c/\Delta H_v$ is the ratio of net heat of combustion and sensible heat of vaporization (ΔH_v). For most hydrocarbon fuels, $\Delta H_c/\Delta H_v$ is about 100. This equation has been found to underestimate the burning rates of liquefied natural gas (LNG) in full-scale tests with 6-m-diam pools.

Table 21 (*7*) lists the calculated or experimental v_∞ values for various liquid fuels and the corresponding fractions of thermal energy that may be radiated in large-diameter pool fires. For hydrocarbon flames, the fraction of heat radiated to the surroundings can be expected to be between 25 and 40 pct, as compared to only 17 pct for methanol flames. Note that the burning rate of LNG is roughly comparable to that of butane, hexane, and gasoline. (See also figure 56.) The data for liquid hydrogen, which has by far the highest burning rate (1.4 cm/min), indicate that only about 25 pct of the thermal energy is radiated; however, these data are uncertain because of the limited range of testing. The special hazards associated with liquid hydrogen fires and explosions are summarized by Zabetakis (*111*).

Table 21. — Burning rates and radiative characteristics of burning liquid pools (*7*)

Combustible	Linear burning rates[1] (v_∞), cm/min	Thermal output		
		Total, kcal/(cm²·min)	Radiative	
			kcal/(cm²·min)	pct
n-Butane	0.79	5.1	1.4	28
n-Hexane	.73	5.1	2.0	39
Ethylene	NA	NA	NA	38
Benzene	.60	5.1	1.8	35
Xylene	.58	5.0	NA	NA
Gasoline	NA (~0.8)	NA	NA	NA
LNG	.66 (~0.9)	3.2	.8	25
Methanol	.17	.64	.11	17
Hydrogen	1.40	2.8	.7	25
UDMH	.38	2.2	.6	27

NA Not available.
[1]Computed rates for infinite diameter; parenthetical values from tests with 3-m diam pools.

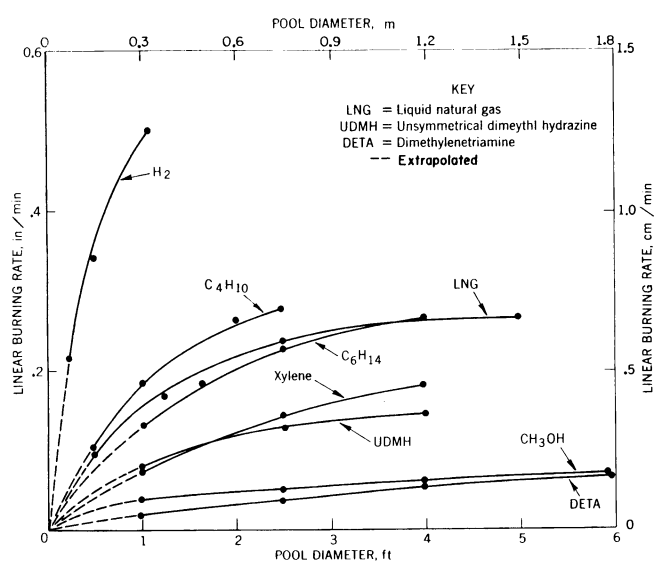

Figure 56.—Linear burning rates of combustible liquids as a function of pool diameter at ambient temperature.

PROPERTIES OF GASOLINES, JET FUELS, HYDRAULIC FLUIDS, AND LUBRICANTS

This section summarizes the combustion properties of composite liquid fuels, hydraulic fluids, and lubricating oils. Most of the data are derived from Bureau studies sponsored by the Air Force. Table 22 gives some of the common physical and combustion properties of various gasolines, diesels, and jet fuels. Table 23 gives corresponding combustion data for hydraulic fluids and lubricating oils. The flashpoints, minimum AIT's, and limits of flammability were determined by the same or modified methods previously described for the neat organic and inorganic combustibles.

Table 22. — Summary of combustion properties of gasolines, diesels, and jet fuels: Gaseous combustion in air at atmospheric pressure[1]

Fuel	Mol wt (av)	Sp gr (water = 1)	BP (90 pct), °C	C_{st}[2] (in air), vol pct	ΔH_c (net, 25° C)		Flash-point, °C	Minimum AIT, °C	Flammable limits	
					Btu/lb	cal/g			L_{25}, vol pct	U_{25}, vol pct
JP-1	151	0.81	210	1.3	18,480	10,265	46	230	NA	NA
JP-3	112	.76	227	(2.6)	18,710	10,395	NA	240	1.4	7.9
JP-4	125	.78	199	(2.4)	18,710	10,395	−18	240	1.3	8.2
JP-5	169	.83	238	1.1	18,440	10,245	66	225	[3].6	[3]4.5
JP-6	147	.84	260	(1.3)	18,620	10,345	38	230	[3].7	[3]4.8
JP-8	164	.8	238	NA	18,400	10,225	46	225	NA	NA
Jet A	NA	.8	249	NA	18,590	10,328	47	225	([4])	([4])
Jet B	NA	.8	199	NA	18,780	10,435	−7 to −18	230	([5])	([5])
Kerosene	NA	.8	254	(1.3)	18,600	10,335	52	230	[3].7	[3]4.8
Gasoline 100/130	NA	.7	116	(2.4)	19,000	10,555	−45	440	1.3	7.1
Gasoline 115/145	NA	.7	120	(2.2)	19,000	10,555	−45	470	1.2	7.1
Diesel fuel (60 cetane)	NA	.8	~325	NA	NA	NA	40 to 55	225	NA	NA

NA Not available.
[1]Flammability data from references 41-42, 47, and 114; physical property values are average or typical.
[2]Values in parentheses calculated by $C_{st} = L_{25}/0.55$.
[3]Values at 100° to 150° C.
[4]Similar to JP-5.
[5]Similar to JP-4.

Table 23. — Summary of combustion properties of hydraulic fluids and lubricating oils[1]

Fluid	Sp gr (water = 1)	Flash-point, °C	Fire point, °C	Minimum AIT, °C
MINERAL OILS				
MIL-H-5606 (oil)	0.9	90	107	225
MIL-2190 (oil)	.86	232	NA	350
MLO-60-294 (oil)	.88	196	221	370
Mobil DTE-103 (oil)	.92	199	NA	370
Pyrogard D (invert emulsion)	NA	NA	NA	>315
GLYCOLS				
Propylene glycol	NA	110	113	445
Houghto-Safe 271 (water-glycol)	1.05	NA	NA	410
Ucon 50 HB-260 (polyglycol)	1.04	235	260	395
PHOSPHATE ESTERS				
Cellulube 220 (ester base)	1.15	235	352	560
Skydrol (ester base)	NA	182	243	>700
Pydraul 150 (ester base)	1.13	193	243	525
Pydraul AC (ester base)	1.35	232	396	595
Houghto-Safe 1055 (aryl ester)	1.15	263	360	550
Tricresyl phosphate	1.17	243	NA	600
POLYOL AND DIBASIC ACID ESTERS				
MIL-L-7808 (acid diester)	NA	225	238	390
MIL-L-9236 (polyol ester)	NA	221	246	390
MLO-54-581 (acid diester)	NA	224	246	390
Plexol 201 (acid diester)	.91	216	232	~380
SILANES				
MLO-56-280 (diphenyl-dodecyl)	NA	291	329	415
MLO-56-610 (decyl-dodecyl)	NA	279	302	400
SILICATES AND SILICONES				
MLO-54-540 (silicate)	NA	163	221	375
MLO-54-856 (silicate)	NA	157	227	380
Oronite 8200 (silicate)	.93	196	227	380
Versilube F-50 (silicone)	1.05	288	338	480
Dow Corning 400 (siloxane)	NA	124	138	320
Dow Corning 500 (siloxane)	≤.95	243	NA	480
Dow Corning 550 (silicone)	1.07	316	NA	NA
CHLORINATED SILICONES AND HYDROCARBONS				
MLO-53-446 (silicone)	NA	304	377	420
Arachlor 1248 (diphenyl)	1.41	193	>315	~640
Pydraul A-200 (hydrocarbon)	1.42	177	360	650
AROMATIC ETHERS				
5P4E (polyphenoxy)	NA	293	349	610
OS-124 (polyphenyl)	1.20	288	349	600
MCS-293	1.19	220	270	490
MISCELLANEOUS FLUIDS				
SAE No. 10 lube oil	<1.0	171	193	380
SAE No. 60 lube oil	<1.0	249	327	380
Linseed oil	.95	224	279	440

NA Not available.
[1]Based upon data in references 47 and 52 and vendors' literature.

VAPOR PRESSURES AND FLASHPOINTS

Jet aircraft fuels can be classified as low- or high-volatility petroleum mixtures. The low-volatility grades are typically kerosenes, such as JP-1, JP-5, JP-6, and JP-8, which have a 10 pct boiling point of at least 177° C (350° F); commercial Jet A fuel also falls in this category. The high-volatility grades are blends of kerosene and high-octane aviation gasoline, such as JP-3 and JP-4, which have a 10 pct boiling point of about 110° C (230° F) or lower; commercial Jet B fuel and motor gasolines also fall in this category. In practice, the compositions of the different grades of fuels can vary with the sources and seasonal period of production. Their vapor compositions will necessarily depend upon the fractional distillation of the lighter ends that comprise such fuels.

Reid vapor pressure curves and flashpoint data are given for representative grades of aviation gasoline and five jet fuels in figure 57 (*47*). The Reid vapor pressures are normally determined at 38° C (100° F) and are slightly lower than true vapor pressures because the vapor-liquid ratio is not ideal in Reid determinations. The flashpoints are at least 38° C (100° F) for the low-volatility fuels and about −18° C (0° F) or less for high-volatility fuels. Diesel fuels fall in the flashpoint range of the low-volatility fuels. Thus, the vapors of the low-volatility fuels, including Jet A, which is used on most commercial passenger aircraft, will not form homogeneous flammable vapor-air mixtures at a normal ambient temperature of 20° C (68° F) and atmospheric pressure. However, flammable mists can form below the flashpoints of the liquids; see figure 6 and discussion. Assuming ideal behavior, the lower limit fuel concentrations at the flashpoint temperatures can be calculated from the vapor pressure data and equation 4. These may be compared to the experimental values given in table 22, which generally represent the limits of the completely vaporized fuels.

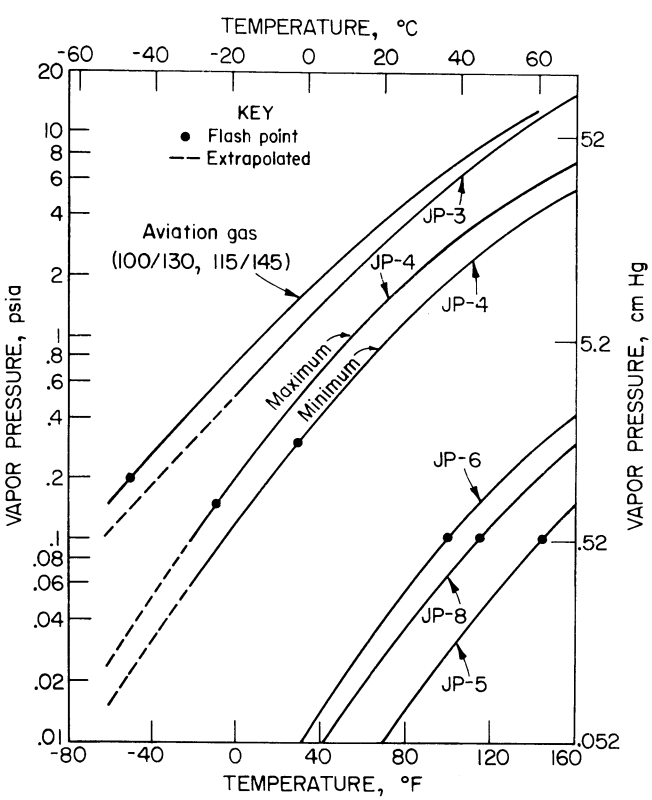

Figure 57.—Vapor pressure (Reid)-temperature curves and flashpoints for aviation gas and five jet fuels.

Both flashpoint and firepoint data are listed in table 23 for the hydraulic fluids and lubricating oils. The firepoint is the temperature at which flame can be sustained after the vapors have been ignited; differences between flashpoints and firepoints tend to be great for combustible liquids of low volatility and high fire resistance (high AIT). The flashpoints of hydraulic fluids and lubricating fluids are much higher than those of gasolines and jet fuels. Flashpoints of about 200° C or more are typical of the highly fire-resistant fluids for each chemical class of fluids. In the case of mineral-oil-based fluids, their flashpoints will be largely determined by the paraffinic and naphthenic constituents that are present; MIL-H-5606 oil, which has a flashpoint of only 90° C, is largely paraffinic and presents the greatest flammability hazard among these fluids. In the case of water-glycols, flashpoints will not exist until the excessive water has been removed. It is evident from these data that a high-temperature environment is required to realize a flashpoint hazard with the vapors of these fluids at normal pressure conditions.

FLAMMABILITY LIMITS IN AIR

Limits of flammability of completely vaporized fuel blends can differ from those obtained only with their lighter fractions, as in flashpoint determinations, since the limits vary inversely with the molecular weights of the combustible vapors. Data reported here are mainly those obtained with all fractions of the composite fuel present. As with flashpoint, the flammability limits of the gasolines and jet fuels in table 22 fall into two separate groups. The fuels of high volatility have a flammability range of approximately 1.3 (L_{25}) to 8 (U_{25}) vol pct or less in normal ambient air; those of low volatility have a limiting range of approximately 0.6 to 5 vol pct at ambient temperatures (100° or 150° C) above their flashpoints. These limits are comparable to those found for high-molecular-weight paraffins ($>C_4$) and the benzenes or naphthalenes (appendix A).

Bureau investigators have determined the flammability limits of aircraft-type fuels in air under various environmental conditions. Their data on the effects of mixture temperature and pressure for various gasolines and jet fuels are summarized in tables 24 and 25, respectively. Table 24 shows that the flammability limits of such fuel vapor-air mixtures on a weight basis vary only slightly with a moderate temperature increase; the lower limits at 25° C were at least 48 mg/L and the upper limits were at

Table 24. — Effect of temperature on flammability limits of gasolines and jet fuels in air at atmospheric pressure[1]

Fuel	Flammability limits, mg/L[2]			
	25° C		150° C	
	Lower	Upper	Lower	Upper
Av gas 100/130	56	350	53	348
Av gas 115/145	56	330	48	337
JP-1	NA	NA	48	380
JP-3	61	370	48	387
JP-4	48	330	47	330
JP-6	NA	NA	[3]46	290

NA Not available.
[1]Based upon data in references 41, 57, and 114.
[2]Mg fuel per liter of air at 0° C and at 1 atm.
[3]Data at 100° C.

Table 25. — Effect of pressure on flammability limits and minimum oxygen requirements for propagation of gasolines and jet fuels in air and air-inert mixtures at 25° C[1]

Fuel	Flammability limits, vol pct (in air)			Minimum oxygen, vol pct	
	Press, atm	Lower	Upper	Air-CO_2	Air-N_2
Motor gasolines[2]	1	1.4	7.6	14.9	12.1
Av gas 100/130	1	1.3	7.15	14.8	11.9
	.53	1.25	6.75	14.1	11.2
	.27	1.3	6.85	14.1	11.6
	.13	1.4	7.6	14.8	11.9
Av gas 115/145	1	1.2	7.1	14.6	11.9
	.53	1.25	6.9	14.6	11.6
	.27	1.25	7.0	14.8	11.6
	.13	1.5	7.85	14.9	12.0
JP-1	1	NA	NA	[3]13.9	[3]10.5
JP-3	1	1.45	7.95	14.3	11.8
JP-4	1	1.3	8.2	14.3([3]13.8)	11.5([3]10.9)
	.5	1.3	7.85	14.5	11.4
	.27	1.35	8.05	14.6	11.7
	.13	1.35	8.1	14.9	12.4

NA Not available.
[1]Based upon data in references 11, 41, and 42.
[2]73-100 octane ratings.
[3]Data at 150° C.

least 330 mg/L, which are consistent for fuels containing hydrocarbons. Conversion of weight concentration limits to volume percent can be made by equation 10; a fuel molecular weight of about 100 or more is a reasonable assumption for the vapors of these combustibles. Equations 63 and 64 may be used to estimate the volume concentration limits of these fuels at other temperatures. However, the AIT limitation on upper limit predictions cannot be neglected, as shown in figure 35 for the JP-6 fuel.

Pressure effects on the flammability limits of aircraft fuel vapor-air mixtures are similar to those observed for the neat hydrocarbons. Jones data (table 25) at 25° C showed little effect of reduced pressure down to nearly 1/10 atm or a pressure altitude of about 15 km (50,000 ft). Below such pressures, the ignition energy source becomes a serious limitation on flame propagation. At elevated pressures, the limits can be assumed to be widened similarly to that shown in figure 36 for hydrocarbon combustibles.

Meager flammability limit data are available for hydraulic fluids and lubricating oils. Although these fluids require rather high temperatures to form flammable vapor-air mixtures, their flammability limits can differ widely, depending upon the thermal stability and combustibility of the organic compounds that comprise the fluids. For example, the Oronite 8515 hydraulic fluid (silicate ester) is reported to have a lower limit of 64 mg/L, compared to 45 mg/L for the MIL-L-7808 engine oil (dibasic acid ester) in ambient air at 260° C (*52*). The lower limits of these fluids in air may be roughly estimated by use of equations 9 and 60 if the chemical formula of the fluid is known.

FLAMMABILITY LIMITS IN OTHER ATMOSPHERES

Jones and Zabetakis (*41-42, 114*) have published complete flammability diagrams for the vapors of various gasolines and jet fuels in air atmospheres diluted with nitrogen or carbon dioxide. Such flammability diagrams are shown in figure 58 for the highly volatile JP-4 fuel and in figure 7 for 100/130 grade aviation gasoline at 25° C and atmospheric pressure. A flammability diagram is also shown in figure 59 for the low-volatile JP-1 fuel at 150° C on a weight basis; the corresponding diagram for JP-4 did not differ greatly. Consistent with the data for hydrocarbons, the flammability limits are progressively narrowed with increased inert and more effectively with carbon dioxide than with nitrogen. For the fuels listed in table 25, the minimum oxygen concentrations required for flame propagation are 14 to 15 pct for air-CO_2 mixtures and 11.5 to 12 pct for air-N_2 mixtures at 25° C. Data in table 25 also indicate that the minimum oxygen values are lower at 150° C and are only slightly greater, if at all, at subatmospheric pressures to 0.13 atm. Such data are especially useful in evaluating the explosion hazard and inerting requirements of aircraft fuels in flight applications.

Inerting requirements for gasoline vapor-air mixtures are greatly reduced by the use of halogenated-type materials. The flammability diagram of figure 60 compares the effectiveness of various inerting agents for motor-type

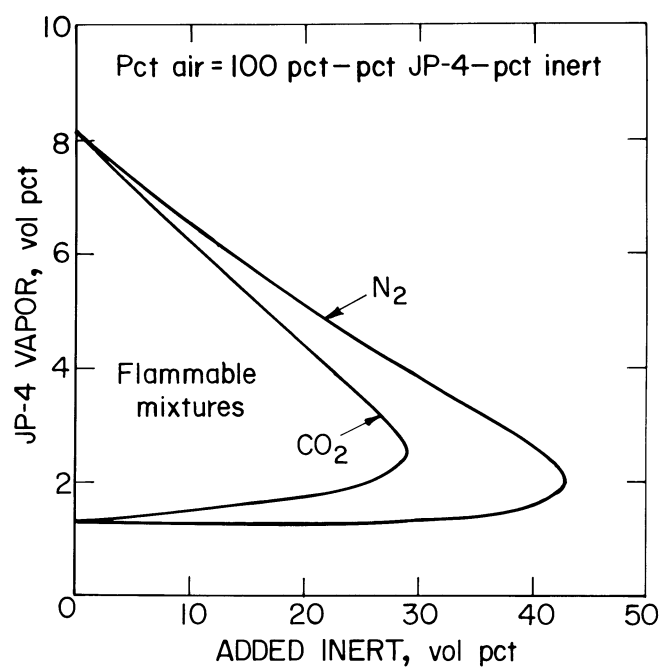

Figure 58.—Limits of flammability of JP-4 vapor-air-inert gas (CO_2 or N_2) mixtures at 25° C and 1 atm.

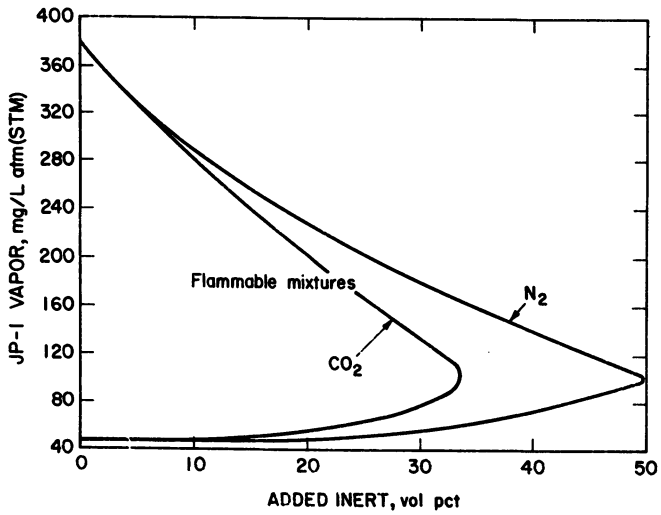

Figure 59.—Limits of flammability of JP-1 vapor-air-inert gas (CO_2 or N_2) mixtures at 150° C and 1 atm.

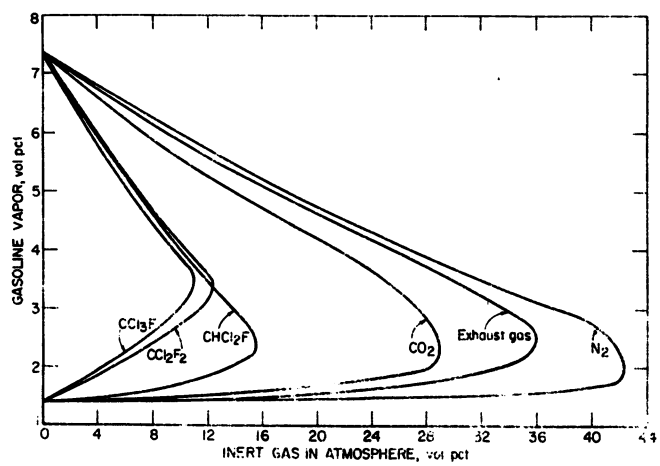

Figure 60.—Effects of various inerting agents on limits of flammability of gasoline vapor-air mixtures at 25° C and 1 atm.

gasolines (*11*); this figure represents the averaged data for motor gasolines of 73, 92, and 100 octane rating. Minimum oxygen values are 11.6 pct with nitrogen, 14.4 pct with carbon dioxide, and at least 17.2 pct with the halogenated methanes. Water vapor would be expected to be less effective than carbon dioxide and more effective than nitrogen or the exhaust gas (85 pct N_2 + 15 pct CO_2). Other data for gasoline, kerosene, and JP-4 fuels are compared in table 12 with nitrogen, carbon dioxide, Halon 1211 (CF_2ClBr), and Halon 1301 (CF_3Br) as the inerting agents. As previously mentioned, the inerting requirements for premixed flames are not as severe as the extinguishing requirements for fully established fires of the same fuels.

IGNITION REQUIREMENTS

Ignition Energies

Few data are available on the precise determination of the minimum spark ignition energies of gasoline-type fuels. Nevertheless, since such fuels are comprised of hydrocarbons, the MIE values of their optimum vapor-air mixtures can be safely assumed to be about 0.2 to 0.3 mJ at 25° C and atmospheric pressure; note data of table 13. If the fuel is in the form of a fine spray or mist, the MIE will tend to be of the order of several millijoules, depending upon temperature (*48*). At temperatures greater than the flashpoint of the fuel, the spark ignition energies of the fuel sprays become drastically reduced and closer to that of the fuel vapor.

Ignition Temperatures

Autoignition temperatures of composite combustible liquids have been determined in heated vessels by the same procedures previously described for neat organic combustibles. As noted in table 22, minimum AIT's in quiescent air at atmospheric pressure are between 225° and 250° C for all the jet fuels and diesel fuels, whereas those for aviation gasolines are closer to 450° C. Although these combustibles contain a wide variety of hydrocarbons, their AIT variation may be compared to that observed for normal octane (220° C) and isooctane (415° C) or ethylcyclohexane (260° C) and ethylbenzene (430° C). The effect of chemical structure on AIT is also evident in comparing the data for the hydraulic fluids and lubricants (table 23). Those classified as aromatic ethers, phosphate esters, and chlorinated hydrocarbons have the highest AIT's, ~500° to 700° C; mineral oils have the lowest values, ~225° to 370° C, and depend greatly upon their paraffinic and naphthenic content; and glycols, silanes, silicates, ordinary silicones, and dibasic acid esters have intermediate values, ~350° to 475° C. Generally, the autoignition hazard for each chemical class is increased with the addition of aliphatic groups as opposed to aromatic groups.

The AIT's of aircraft liquid fuels, lubricants, and hydraulic fluids have been investigated by Zabetakis and coworkers under various environmental conditions. As with other combustibles, the minimum AIT's of the aircraft combustibles generally increase with decreasing pressure and oxygen concentration; such data are summarized in table 26 (*53, 113-114, 116*) for ignitions in air and oxygen.

Table 26 — Effect of pressure and oxygen concentration on the minimum AIT's of aircraft combustible fluids in oxygen-nitrogen atmospheres[1]

Combustible	Minimum AIT, ° C			
	Air			Oxygen
	1/4 atm	1/2 atm	1 atm	1 atm
FUELS				
Kerosene	NA	NA	230	215
Av gas 100/130	NA	553	440	315
Av gas 115/145	NA	573	470	NA
JP-1	NA	462	228	NA
JP-3	NA	449	238	NA
JP-4	521	444	242	NA
JP-5	512	496	232	222
HYDRAULIC FLUIDS AND LUBRICANTS				
H-5606	456	438	225	[illegible]
MIL-53-446	442	424	419	408
MLO-54-540	510	448	373	230
MLO-54-581	548	480	390	274
MLO-54-645	520	452	380	256
MLO-54-856	516	460	380	266
MLO-829[illegible]	522	450	380	244
MIL-L-7[illegible]	NA	NA	402	270

NA Not available.
[1]Based upon data in references 53, 113-114, and 116.

The effect of reduced pressure on AIT's in air is greatest for the aircraft combustibles having the lowest AIT's at atmospheric pressure. Conversely, the effect of increased oxygen concentration is greatest for the combustibles of high AIT in normal atmospheric air. An exception is the MLO-53-446 chlorinated silicone hydraulic fluid, which was not sensitive to the above pressure and oxygen variations. Figure 61 (*116*) shows the oxygen effect on AIT for seven hydraulic fluids. Kuchta (*48*) found that the oxygen and pressure effects on AIT for jet fuels and lubricants or hydraulic fluids correlate well with the oxygen partial pressure of the atmosphere. Such a correlation is shown in figure 62 (*49*) for the JP-6 fuel in various oxygen-containing

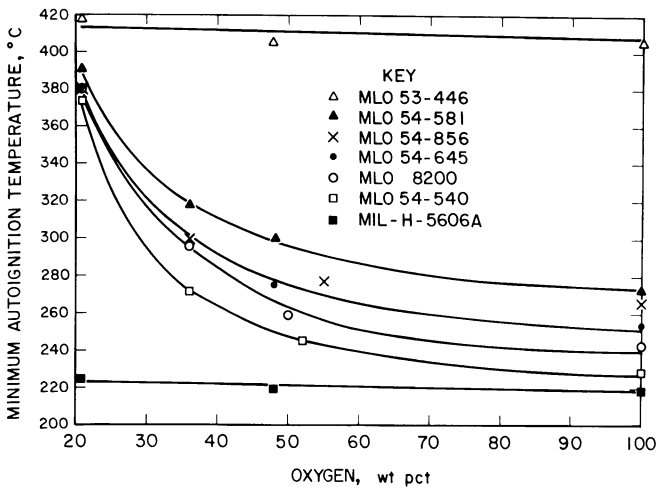

Figure 61.—Minimum autoignition temperatures of seven hydraulic fluids in oxygen-nitrogen mixtures at atmospheric pressure (glass vessels).

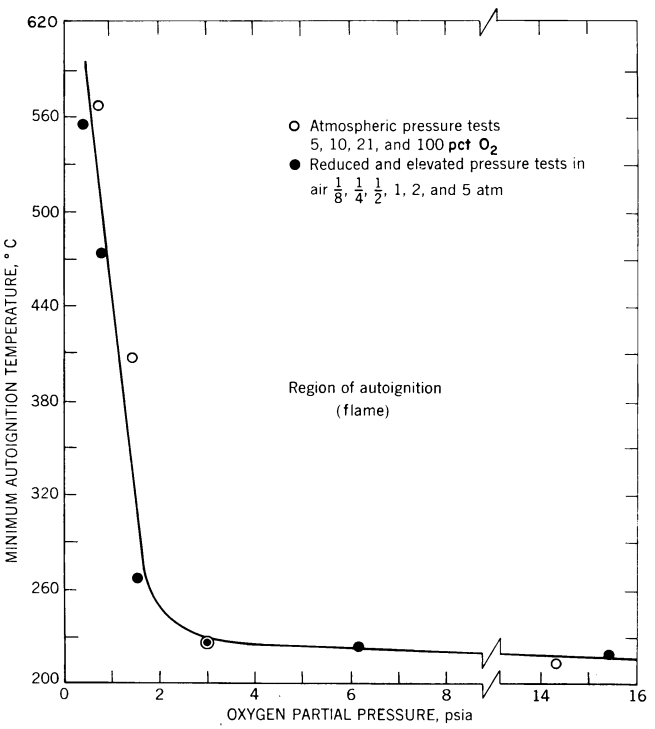

Figure 62.—Correlation of minimum autoignition temperatures of JP-6 fuel-oxygen-nitrogen mixtures with oxygen partial pressure at various mixture pressures.

atmospheres at reduced and moderately elevated pressure. Below an oxygen partial pressure of about 0.2 atm (~3 psia), the AIT can be expected to increase sharply for organic fuels or fluids of this type.

At highly elevated pressures, the AIT's of aircraft fluids are noticeably lower than at 1 atm but tend to become constant. In figure 63 (*110*), the AIT's of phosphate ester, mineral oil, and water-glycol fluids in air are reduced by up to one-half with a pressure increase to about 100 atm; above this pressure, the AIT's varied only slightly. Similar pressure effects were observed for the MIL-L-7808, Mobil DTE-103, and Houghto-Safe-1055 lubricants in autoignitions at pressures to 1000 atmospheres (*48*); their AIT's (interpolated values) were approximately 200°, 230°, and 275° C, respectively, at 150 atm, above which they leveled off. The compression ignition hazard of these fluids in air can be assessed from such AIT data and adiabatic compression temperature data (table 5) at the pressures of interest.

All of the above-cited AIT data were obtained under static conditions with maximum contact times with the heated surface of the vessel. The much higher AIT's that can result with shorter contact times (ignition delays) are illustrated in figure 48; note data for JP-6, kerosene, and the petroleum fractions. A similar plot obtained for the JP-6 fuel in heated air streams at various pressures is shown in figure 64 (*57*); data in static air are also included. The AIT (T, K) variation with ignition delay (τ, ms) under flow conditions at 2 atm is given by

$$\text{JP-6 (370-600° C)} \quad \ln \tau = 5800/RT + 0.44, \qquad (74)$$

where R is in cal/(K·mol); in these experiments, the air velocity was between 6 and 50 m/s in a 5-cm-diam tube. With increasing pressure, the ignition delays at a given temperature decrease and, therefore, increase the autoignition hazard.

With small heated surfaces such as wires or rods, the ignition temperatures are also higher than heated vessel AIT's and follow the data trends displayed by JP-6 jet fuel and MIL-L-7808 engine oil in table 16 and figure 49 (*50*). The wire ignition temperatures (T, °C) of such aircraft combustibles in air under near-stagnant conditions are given by the following expressions as a function of the heat source surface area (A, cm^2):

$$\text{JP-6} \quad T = 985 - 112 \ln A;\ A < 80\ cm^2 \qquad (75)$$

$$\text{MIL-L-7808} \quad T = 752 - 64 \ln A;\ A < 190\ cm^2 \qquad (76)$$

or in terms of radius of the heat source (r, cm):

$$\text{JP-6} \quad \ln r = 12{,}000/T - 12.9;\ r < 0.7\ cm \qquad (77)$$

$$\text{MIL-L-7808} \quad \ln r = 14{,}000/T - 17.7;\ r < 1.3\ cm \qquad (78)$$

where T is in K. These data indicate the importance of the heat source dimensions in comparing ignition temperatures. So-called hot manifold or hotplate ignition temperatures are also higher than vessel AIT's, depending upon the size of the heated surface and the flow or convective conditions that determine the contact time. For jet fuels and the MIL-H-5606 fluid, the hotplate-type ignition temperatures tend to be about double their vessel AIT's in quiescent air. Reference 48 summarizes these and other ignition properties of jet fuels and various aircraft fluids.

Ignitions of fuels and lubricants by jets of hot gases are not common but can occur as a result of seal failures or pinhole leaks in pressurized systems. They are also of interest in designing flame arrestors and explosionproof equipment. Ignition temperature data obtained with hot

air jets for the JP-6 fuel and MIL-L-7808 oil (*51*) have been replotted in figure 65, together with wire and vessel ignition temperatures, as a function of heat source diameters. As with neat hydrocarbons, the highest ignition temperatures occur with the hot air jets, depending upon their diameter; see also table 16. The fact that vessel AIT's become greater than wire ignition temperatures at small heat source diameters is due to increased wall quenching.

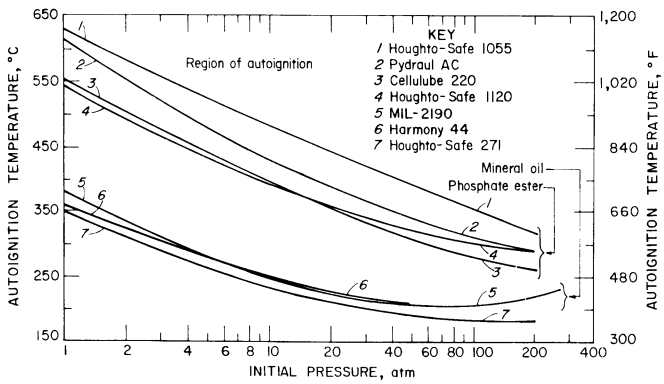

Figure 63.—Minimum autoignition temperatures of phosphate ester, mineral oil, and water-glycol hydraulic fluids or lubricants in air at elevated pressures.

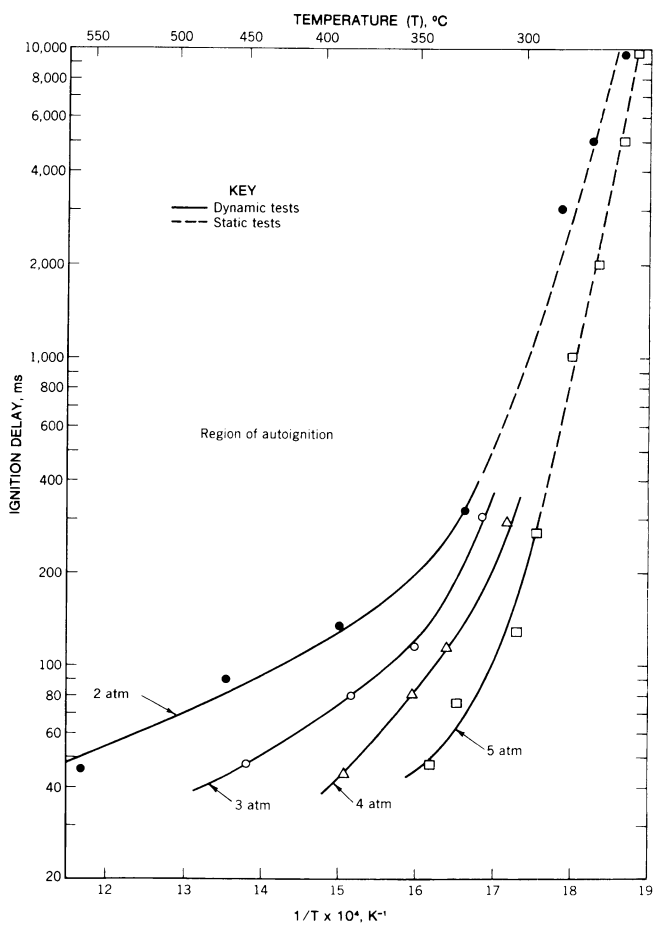

Figure 64.—Autoignition temperatures and corresponding ignition delays for JP-6 fuel under static and dynamic conditions in air at various pressures.

FLAME TEMPERATURES AND BURNING RATES

Flame Temperatures

Maximum flame temperatures of the optimum vapor-air mixtures of petroleum-derivable combustibles can be assumed to be comparable to those of the neat hydrocarbons, 1,900° to 2,000° C (table 17). Similarly, their limit

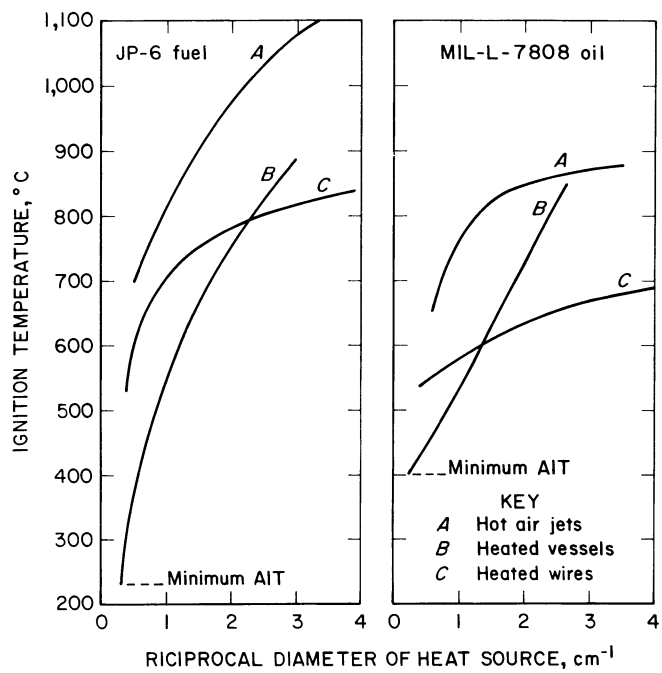

Figure 65.—Variation of hot gas (air) and hot surface ignition temperatures with reciprocal diameter of heat source for JP-6 fuel and MIL-L-7808 oil vapor-air mixtures at atmospheric pressure.

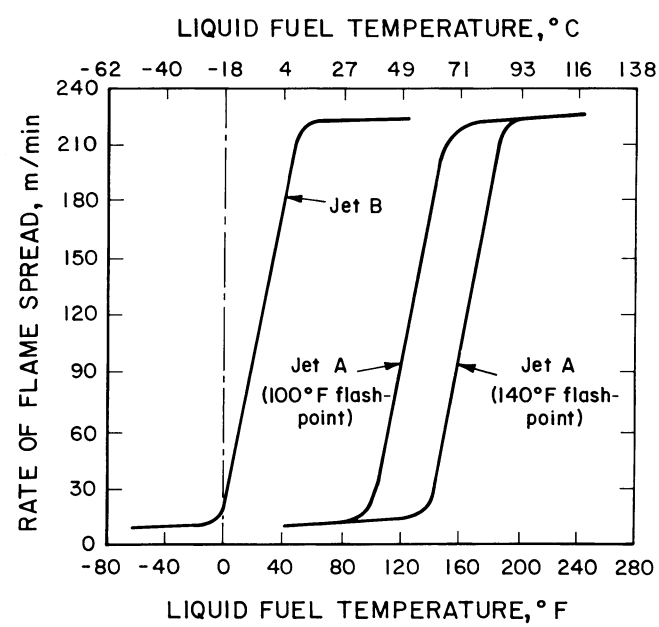

Figure 66.—Flame spread rate versus liquid fuel temperature for Jet A- and Jet B-type fuels in air at atmospheric pressure.

flame temperatures should be in the 1,200° to 1,300° C range. Such flame temperature estimates are fairly reliable for gasolines, jet fuels, and the mineral oil hydraulic fluids.

Burning Rates

The liquid burning rates (regression rates) of petroleum-based fuels are necessarily dependent upon the size of the burning pool. At an infinite pool diameter, the rate for a gasoline-type fuel should be about 0.6 to 0.8 cm/min (table 21). For smaller pools, the rates for xylene in figure 56 are most relevant for the gasoline or jet fuels. This figure also indicates that higher rates will occur for fuels containing higher concentrations of low-molecular-weight paraffins. The burning rates may be estimated by equation 74.

Flame spread rates of liquid fuels are strongly dependent upon their volatility or flashpoint. Figure 66 (*47*) shows the reported variation of flame spread rate (horizontal) with fuel temperature for Jet A and Jet B-type fuels. It is important to note that the flame spread rates increase drastically when the fuel temperature is above the flashpoint of the given fuel. Also, the maximum rates are of the order of flame speeds (~10 ft/s) encountered with premixed hydrocarbon vapor-air systems. The indicated maximum rates can be realized in real situations when the liquid fuel is heated substantially above its flashpoint, or when it is finely dispersed to produce flash vaporization, as in an aircraft crash situation. The rates are also enhanced when the fuel is in the form of a thin liquid film. Much higher rates than those in figure 66 are possible under windy conditions.

PROPERTIES OF METAL AND NONMETAL ELEMENTS

Physical properties of elemental metals and nonmetals are given in table 27 together with ignition temperature and explosion limit (flammability limit) data for the combustion of their dusts. The dust combustion data were taken from the comprehensive compilations by Nagy, Jacobson, and other Bureau coworkers but were limited primarily to the elemental substances of relatively high purity. Their data for various combustibles are conveniently summarized in an NFPA handbook (*72*).

FLAMMABILITY LIMITS IN AIR

Lower explosion limits of the dusts in table 27 (*36, 76*) were determined in normal ambient air by the widely known Hartmann apparatus (*13*), equipped with a 7-cm-diam explosion tube (1.23 L) and a high-voltage spark source (~24 W) for ignition. A dust particle size of less than 74 μm (minus 200 mesh) was used to obtain most of these limits. These data show that a dust explosion hazard may arise with a wide variety of metallic or nonmetallic elements, including aluminum, tin, iron, zinc, and silicon. Aluminum, magnesium, titanium, and sulfur are among the widely used substances having a relatively low dust explosion limit, less than 0.1 g/L or 0.1 oz/ft^3. In comparison, the dusts of such elemental substances as carbon and copper could not be ignited under the given conditions. Because of apparatus limitations, including the lack of uniform dust dispersions, the reported limits cannot be

Table 27. — Summary of combustion properties of elemental metal and nonmetal dusts: Dust combustion in air at atmospheric pressure[1]

Combustible	At wt	Density, g/cm^3	MP, °C	ΔH_c[2] (25° C), kcal/mol	Ignition temperature[3]		Lower explosion[3] limit (L_{25}), g/L
					Layer, °C	Cloud, °C	
Aluminum, atomized	26.98	2.70	660	199.5 (Al_2O_3)	490	670	0.075
Antimony (96 pct), milled	121.75	6.68	631	83.3 (Sb_2O_3)	330	420	.420
Barium	137.34	3.51	725	133.0 (BaO)	NA	NA	NA
Boron (85 pct), amorphous	10.82	2.32	2,300	151.0 (B_2O_3)	400	470	<.100
Cadmium (98 pct), atomized	112.40	8.64	321	60.9 (CdO)	250	570	NI
Carbon, lampblack	12.01	2.27	>3,500	94.1 (CO_2)	NA	730	NI
Chromium (97 pct), milled	52.00	7.20	1,857	134.9 (Cr_2O_3)	400	580	.230
Cobalt (97.8 pct), milled	58.93	8.90	1,495	57.2 (CoO)	370	760	NI
Copper (99.5 pct), electrolytic	63.55	8.92	1,083	37.1 (CuO)	NA	700	NI
Iron (98 pct)	55.85	7.86	1,535	98.3 (Fe_2O_3)	290	320	.120
Lead (99 pct), atomized	207.20	11.34	328	52.4 (PbO)	270	710	NI
Lithium	6.94	.53	181	71.2 (Li_2O)	NA	NA	NA
Magnesium, milled	24.31	1.74	649	143.8 (MgO)	430	560	.030
Manganese	54.94	7.20	1,244	124.5 (MnO_2)	240	460	.125
Molybdenum (99.8 pct)	95.94	10.20	2,617	180.3 (MoO_3)	360	720	NI
Nickel	58.71	8.90	1,453	58.4 (NiO)	NA	NA	NA
Phosphorus, white	30.97	1.83	44	180.0 (P_2O_5)	NA	NA	NA
Potassium	39.10	.86	64	43.2 (K_2O)	NA	NA	NA
Silicon (96 pct), milled	28.06	2.40	1,420	205.4 (SiO_2)	950	780	.160
Sodium	22.99	.97	98	49.7 (Na_2O)	NA	NA	NA
Sulfur	32.06	~2.0	113	71.0 (SO_2)	220	190	.035
Tantalum	180.95	>14.0	300	250.0 (Ta_2O_5)	300	630	<.200
Thorium (1.2 pct O_2)	232.04	11.70	1,750	292.0 (ThO_2)	280	270	.075
Tin (96 pct), atomized	118.69	>5.0	232	138.8 (SnO_2)	430	630	.190
Titanium (99 pct)	47.90	4.5	1,660	183.5 (Ti_2O_3)	510	330	.045
Tungsten	183.85	19.35	3,410	136.3 (WO_2)	430	NA	NI
Uranium	238.03	19.05	1,132	250.0 (UO_2)	100	20	.060
Vanadium (86.4 pct)	50.94	5.96	1,890	145.0 (V_2O_3)	490	500	.220
Zinc (97 pct)	65.38	7.14	420	83.2 (ZnO)	540	690	.480
Zirconium (97 pct)	91.22	6.49	1,852	258.2 (ZrO_2)	20	190	.045

NA Not available. NI No ignition with electric spark source.
[1]Flammability data from references 36 and 76.
[2]Values calculated from ΔH_f (25° C) data of reference 105.
[3]Combustible particle size less than 74 μm (−200 mesh); g/L equates to oz/ft^3.

assumed as absolute. Sample purity itself can have a large effect on these limits.

The ignition and explosion parameters of dusts are strongly dependent upon their particle size. Figure 67 (*36*) shows the effect of average particle diameter on the lower explosion limit and other parameters for atomized aluminum-air mixtures in the Hartmann apparatus; the minus 200-mesh data in table 27 would correspond to those for a 30-μm average particle diameter. Note that the explosion limit increases greatly when the average particle diameter is greater than approximately 50 μm. Also, the maximum explosion pressures are not any greater than those previously cited for organic combustible vapor-air mixtures. However, dusts do not necessarily have well-defined upper flammability limits and are capable of high explosion pressures even with highly fuel-rich mixtures. Data by the above authors indicate that, for most metals, dust concentrations of 1 to 2 g/L (1 to 2 oz/ft^3) are required to achieve near-maximum explosion pressures in an air atmosphere. With increasing ignition energies, the range of possible explosive concentrations will tend to widen.

Table 28. — Inerting requirements to prevent propagation of elemental metal and nonmetal dusts in air-nitrogen, air-carbon dioxide, and air-inert dust (fuller's earth) mixtures (spark ignition) (*77*)

Combustible	Lower explosion limit $(L_{25})_3$ kg/m^3	Minimum oxygen limit, vol pct		Minimum inert dust limit, wt pct
		Air-N_2	Air-CO_2	
Aluminum, atomized, <74 μm	0.075	9	3	80
Aluminum, atomized, <44 μm	.045	NA	2	90
Iron, 98 pct, <53 μm	.12	NA	11	50
Magnesium, milled, <74 μm	.03	2	[1]<1	90
Silicon, 98 pct, milled, < 74 μm	.11	11	12	70
Sulfur, 99 pct, <44 μm	.035	NA	12	85
Tin, 96 pct, atomized, <53 μm	.19	NA	16	30
Titanium, 96 pct, <44 μm	.045	4	[1]<1	85
Zinc, 95 pct, <74 μ	.50	10	10	35
Zirconium, 97 pct, <44 μm	.045	2	[1]<1	90+

NA Not available.
[1]Reported ignitions with only diluent present.

FLAMMABILITY LIMITS IN OTHER ATMOSPHERES

Explosion limits of the elemental dusts are narrowed by the reduction of oxygen concentration, addition of inert gas, or addition of inert dust. Table 28 summarizes some explosion inerting data from the Bureau studies (*77*) for the dusts of several metals or nonmetals in normal air at atmospheric pressure; these data apply to electrical spark ignitions. With an inert dust of fuller's earth of less than 74 μm (minus 200 mesh) or 44 μm (minus 325 mesh), the more reactive substances require about 80 wt pct or more of inert to prevent an explosion; only 30 to 50 pct inert dust is required for the much less reactive substances. Gaseous inerts are not any more effective in preventing their explosions. For the more reactive metal dusts, the critical oxygen concentrations in air-CO_2 atmospheres extend down to less than 1 vol pct; note that the magnesium, titanium, and zirconium dusts ignited in the diluent alone. Corresponding minimum O_2 values in air-N_2 atmospheres tend to be higher than those for air-CO_2 atmospheres for these materials. With all such dusts, the inerting requirements will vary with their particle size and purity or contamination.

IGNITION REQUIREMENTS

Ignition Energies

Available ignition energy data for combustible dusts are not as precisely defined as those for combustible gases because of great experimental uncertainties. Nevertheless, the reported data in the above cited works provide a relative estimate of the spark ignition energy requirements for various dusts. The minimum ignition energies of dust-air clouds are one or more orders of magnitude greater than those of combustible gas-air mixtures, depending greatly upon the dust particle size. Figure 67 includes the variation of minimum spark ignition energy with average particle diameter for an atomized aluminum dust cloud. For metal dusts of minus 200 mesh (<74 μm), the minimum ignition energies are as low as several millijoules for the most reactive metals and as high as several joules for the least reactive ones; those of moderate reactivity have values mostly of about 100 mJ or more.

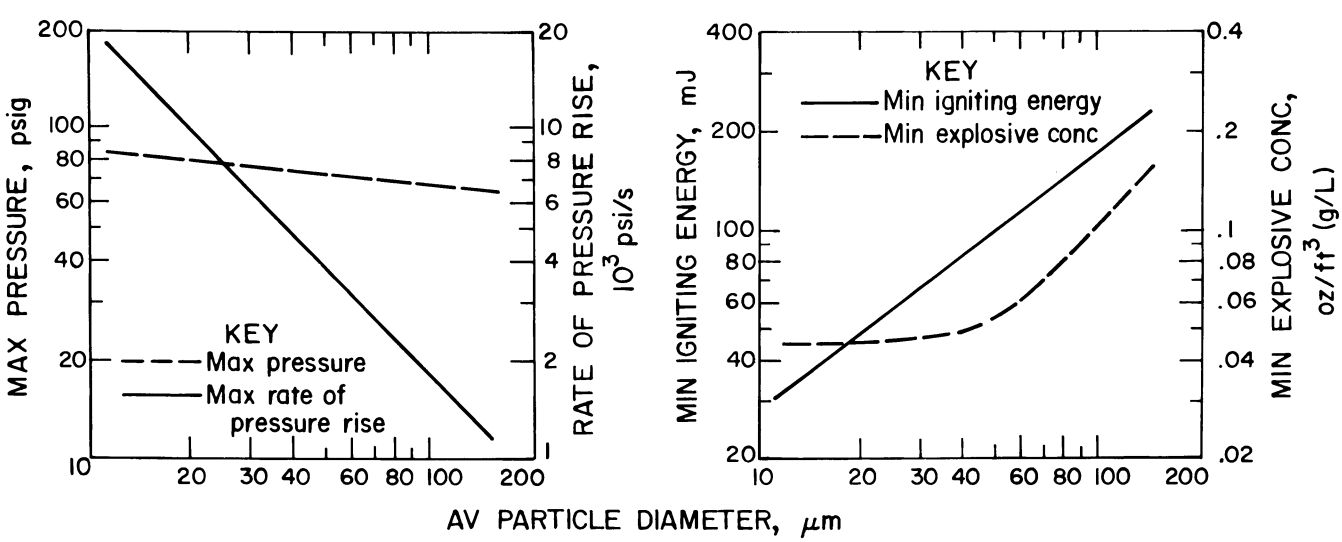

Figure 67.—Effect of average particle diameter on explosion parameters for atomized aluminum dust in air at 25° C and 1 atm.

Ignition Temperatures

The dust ignition temperatures given in table 27 were determined largely by Jacobson (*36*) using the Godbert-Greenwald apparatus, 3.65-cm-diam furnace. As noted, ignition temperatures of the metallic and nonmetallic dusts in air are generally lower when the heated dust is a layered mass, as opposed to a dispersed mass (cloud); most obvious exceptions are titanium and uranium. Most of these ignition temperatures were obtained with dusts of less than 74 μm (minus 200 mesh) but do not necessarily represent the lowest possible ignition temperatures for finer size dusts or for large dust layers that approximate adiabatic conditions. The most temperature sensitive materials are those that can undergo pyrophoric reaction at room temperature; these include uranium, zirconium, sodium, potassium, lithium, and white phosphorus. Their reaction is normally enhanced by increased humidity.

Metals in bulk form are much more difficult to ignite than those that are finely divided and, therefore, their ignition temperatures are usually found in an oxygen-enriched atmosphere. Ignition temperatures of metals in oxygen are given in table 29 (*29, 62*) with samples in rod or block form that have been preheated in oxygen or argon. Although all data are not consistent, the ignition temperatures tend to be near or above the melting point of the pure metal; also, most values are higher when the metals are preheated in oxygen, rather than an inert gas (argon). The oxygen preheating reflects the effect of the formation of metal oxides on the surface, thereby making ignition usually more difficult because of higher melting points and lower reactivities of the oxide coatings. This effect is least for metals of low melting point or for metals whose oxides are of similar or lower melting point.

FLAME TEMPERATURES AND BURNING RATES

Flame Temperatures

Maximum flame (or combustion) temperatures of metals and nonmetals are difficult to calculate precisely because the oxide species may be uncertain at the high temperatures and because thermodynamic data may be unavailable. Table 30 lists the calculated adiabatic temperatures by Grosse (*29*) for the combustion of such substances in an atmosphere of oxygen. These temperatures are necessarily above the melting point and boiling points of the oxides that may be formed by the elemental substances. Also, the values are roughly consistent with the variation of the molar heats of combustion (table 27) of the elements. As with hydrocarbons, the combustion temperatures are greatly reduced by any dissociation of the reaction products; the high heat capacities of metal oxides are also a contributing factor.

Table 29. — Ignition temperatures of bulk metals in oxygen at atmospheric pressure (metal sample in rod or block form) (*29,62*)

Metal	Melting point, °C		Metal ignition temperatures, °C	
	Metal	Oxide	Preheated in oxygen (*62*)	Preheated in argon (*29*)
Aluminum	660	2,045 (Al_2O_3)	NA	>1,000
Antimony	631	656 (Sb_2O_3)	NA	720
Barium	725	1,923 (BaO)	550	175
Bismuth	271	820 (Bi_2O_3)	735	775
Cadmium	321	[1]900 (CdO)	NA	760
Calcium	839	2,580 (CaO)	790	550
Iron	1,535	1,565 (Fe_2O_3)	1,315	930
Lead	328	888 (PbO)	850	870
Lithium	181	>1,700 (Li_2O)	NA	190
Magnesium	649	2,800 (MgO)	635	625
Molybdenum	2,617	795 (MoO_3)	780	750
Potassium	64	[1]350 (K_2O)	NA	69
Sodium	98	460 (Na_2O)	NA	118
Strontium	769	2,430 (SrO)	1,075	720
Thorium	1,750	3,050 (ThO_2)	NA	500
Tin	232	1,127 (SnO_2)	940	865
Zinc	420	1,975 (ZnO)	905	900

NA Not available.
[1]Decomposition.

Table 30. — Adiabatic combustion temperatures of metals and nonmetals in oxygen at 1 atm (*29*)

Substance	Adiabatic combustion temperature, K	Substance	Adiabatic combustion temperature, K
Aluminum	3,800	Magnesium	3,350
Antimony	1,700	Manganese	3,400
Barium	3,000	Molybdenum	3,000
Beryllium	4,300	Potassium	1,700
Bismuth	2,000	Silicon	2,500
Boron	2,900	Sodium	2,000
Cadmium	1,700	Strontium	3,500
Calcium	3,800	Thorium	4,700
Iron	3,000	Tin	2,700
Lead	1,800	Titanium	3,300
Lithium	2,600	Zinc	2,200
		Zirconium	4,800

Burning Rates

The burning rates of granular combustibles are usually determined in the horizontal burning mode, although both rates of consumption and flame spread are greater in the upward burning mode. Most of the available data for elemental metals or nonmetals are limited to substances that are readily ignitable. Bureau investigators (*60*) reported horizontal burning rates in air of about 200 cm/min for such granular materials as titanium and phosphorus (red) of 100 to 200 mesh; in comparison, the rates for magnesium ranged from 2 to 75 cm/min, depending upon the dust particle size. For comparison with other flammable solids, these data are included in the burning rate tabulations of the next section for various industrial dusts.

PROPERTIES OF AGRICULTURAL, CARBONACEOUS, CHEMICAL, AND PLASTIC DUSTS

This section covers combustion properties of various industrial dusts that are classified as agricultural, carbonaceous, chemical, and plastic types. Coal, which is a carbonaceous material, is given special emphasis because of the high fire or explosion risks in the coal mining industry and because of the great usefulness of the many mine safety data that have been generated. Table 31 summarizes selected ignition and flammability data that were obtained

Table 31. — Summary of combustion properties of agricultural carbonaceous, chemical, and plastic dusts[1]

Combustible	Ignition temperature		Lower explosion limit (L_{25}),[2] g/L
	Layer, °C	Cloud, °C	
AGRICULTURAL DUSTS			
Alfalfa meal	NA	530	0.105
Cellulose	270	480	.055
Cereal grass	230	620	.20
Corn	250	400	.055
Cornstarch (minus 325-mesh)	350	390	.04
Cotton linter, raw	NA	520	.50
Cottonseed meal	310	540	.055
Grain (wheat, corn, oats, barley)	230	430	.055
Gum, arabic	260	500	.06
Lycopodium	310	480	.025
Pea flour	260	560	.05
Potato starch, dextrinated	NA	440	.045
Rice	450	510	.085
Soybean meal	340	550	.06
Sucrose	400	370	.045
Tobacco stem	230	420	NI
Wheat, untreated	220	500	.065
Wood, birch bark	250	450	.020
Wood flour, white pine	260	470	.035
CARBONACEOUS DUSTS			
Asphalt, brown petroleum resin	500	510	0.025
Carbon, activated, petroleum sludge	490	760	NI
Carbon black, acetylene	900	NA	NI
Charcoal, activated, lignite	370	670	2.00
Charcoal, hardwood mixture	180	530	.14
Coke, bituminous coal	440	710	NI
Coke, petroleum	NA	670	1.00
Gilsonite, Utah	500	580	.02
Oil shale (17 gal/ton), Colorado	350	440	NI
Oil shale (10 gal/ton), Tennessee	260	630	NI
Pitch, coal tar	NA	650	.045
Pitch, petroleum	NA	630	.045
Coal, lignite, California	200	450	.03
Coal, lignite, North Dakota	180	440	.045
Coal, bituminous, Fox Hill, CO	180	440	.045
Coal, bituminous, No. 7, Illinois	160	600	.04
Coal, bituminous, Whitesburg, KY	190	595	.05
Coal, bituminous, Bruceton, PA	170	610	.055
Coal, bituminous, Pocahontas No. 3, West Virginia	220	640	NI
Coal, bituminous, Laramie No. 3, Wyoming	180	575	.04
CHEMICAL DUSTS			
Acetoacetanilide	NA	560	0.03
Adipic acid	NA	550	.035
Anthranilic acid	NA	580	.03
Azealic acid	NA	610	.025
Benzoic acid	NA	620	.03
Benzotriazole	NA	440	.03
o-Chloroacetoacetanilide	NA	640	.035
Dehydroacetic acid	NA	430	.03
Diallyl phthalate	NA	480	.03
Dimethyl isophthalate	NA	580	.025
Dimethyl terephthalate	NA	570	.03
3,5-Dinitrobenzoic acid	NA	460	.05
Diphenyl	NA	630	.015
Ethyl hydroxyethyl cellulose	NA	390	.02
Fumaric acid	NA	520	.085
Hexamethylenetetramine	NA	410	.015
Hydroxyethyl cellulose	NA	410	.025
Isatoic anhydride	NA	700	.035
Nitrosoamine	NA	270	.025
Paraformaldehyde	NA	410	.04
Paraoxybenzaldehyde	430	380	.02
Paraphenylenediamine	NA	620	.025
Pentaerythritol	NA	450	.03
Phthalic anhydride	NA	650	.015
Phthalimide	NA	630	.03
Salicylanilide	NA	610	.04
Sorbic acid	460	470	.02
Stearic acid, aluminum salt	440	420	.015
Stearic acid, zinc salt	NA	510	.02
Sulfur	220	190	.035
Terephthalic acid	NA	680	.05

Table 31. — Summary of combustion properties of agricultural carbonaceous, chemical, and plastic dusts[1] — Continued

Combustible	Ignition temperature		Lower explosion limit (L_{25}),[2] g/L
	Layer, °C	Cloud, °C	
PLASTIC DUSTS (RESINS AND MOLDING COMPOUNDS)			
Acetal, linear, polyformaldehyde	NA	440	0.035
Acrylamide polymer	NA	480	.03
Acrylonitrile polymer	460	500	.025
Cellulose acetate	NA	420	.04
Cellulose triacetate	NA	430	.04
Cellulose propionate (0.3 pct free hydroxyl)	NA	460	.025
Epoxy (no catalyst or additives)	NA	540	.02
Ethyl cellulose (5- to 10-μm)	350	370	.025
Ethylene-maleic anhydride copolymer	NA	540	.095
Ethylene oxide polymer	NA	350	.03
Melamine formaldehyde, laminating type	NA	790	.065
Methyl cellulose	340	360	.03
Methyl methacrylate, polymer	NA	440	.035
Phenol formaldehyde, 1-step	NA	640	.04
Phenol formaldehyde, 2-step	NA	580	.025
Phenol furfural	NA	530	.025
Polycarbonate	NA	710	.025
Polyethylene, high-pressure process	380	450	.02
Polyethylene wax, low-molecular weight	NA	400	.02
Polymethylene, carboxy	NA	520	.325
Polypropylene (no antioxidant)	NA	420	.02
Polystyrene, clear	NA	490	.02
Polyurethane foam, non-fire-retardant	440	510	.03
Polyurethane foam, fire-retardant	390	550	.025
Polyvinyl acetate	NA	550	.04
Polyvinyl acetate alcohol	440	520	.035
Polyvinyl butyral	NA	390	.02
Polyvinyl chloride, fine	400	660	NI
Styrene-butadiene latex	NA	440	.025
Urea formaldehyde molding compound	NA	460	.085
Vinylidene chloride molding compound	NA	900	NI
OTHER DUSTS			
Nylon, polyamide	430	500	0.03
Rayon flock, viscose	250	520	.055
Rosin, DK	NA	390	.015
Rubber, crude, hard	NA	350	.025
Rubber, synthetic, hard (33 pct S)	NA	320	.03
Rubber, chlorinated	290	940	NI
Shellac	NA	400	.02

NA Not available. NI No ignition with electric spark source.
[1]Flammability data from references 14, 37-38, and 76.
[2]Combustible particle size less than 74 μm (−200 mesh); g/L equates to oz/ft^3.

by Nagy, Jacobson, and coworkers (*14, 37-38, 76*) for the various classes of combustible dusts in a normal ambient air atmosphere.

FLAMMABILITY LIMITS IN AIR

It is evident from tables 31 and 27 that practically all industrial dusts are capable of forming flammable dust-air mixtures. The table 31 data were also obtained with the previously described Hartmann apparatus (1.23 L) and spark ignition source using largely particle size dusts of less than 74 μm (minus 200 mesh). With some exceptions, particularly among carbonaceous dusts, the lower explosion limits (L_{25}) of the various classes of dusts are less than 0.06 g/L (0.06 oz/ft^3). Many of the chemical and plastic dusts have lower limits as low as 0.02 or 0.03 g/L. Because the dust dispersions in this apparatus were not uniform, the assumed concentration limits in tables 27 and 31 should be regarded as nominal values. As with metal dusts, the organic combustible dusts have no well-defined upper limits.

The lower explosion limits of high-volatile bituminous coal dusts are 0.04 to 0.06 g/L in air by the above spark ignition method. Recent work by Hertzberg (*31*) with a modified Hartmann apparatus—larger volume (8 L), stronger ignition source, and more uniform dust dispersion—yielded limit values that were 2 or more times greater for such coals. They reported a limit of 0.135 g/L for Pittsburgh (Bruceton) coal dust of minus 200 mesh using electrical match ignition energies of the order of 200 J. This dust concentration was verified by optical measurements, whereas the earlier values represent gross concentrations derived from the mass loadings that were dispersed. Nevertheless, full-scale experiments in the Bruceton Experimental Mine indicate explosions can occur with a Pittsburgh coal dust loading of 0.049 g/L or more (*90*). Thus, the limit data in table 31, which were obtained by the standard Hartmann apparatus, are not overly conservative for safety purposes.

The lower limits of carbonaceous dust-air mixtures decrease greatly with increased volatility of the dust or increased methane content of the atmosphere. Figure 68 shows such data for the high-volatile (~35 pct) Pittsburgh coal, low-volatile (~16 pct) Pocahontas coal, and an oil shale assayed at 45 gal/ton. These data were reported by Richmond (*90*) and refer to electrical match ignitions in the modified Hartmann apparatus. With the standard apparatus and spark ignition source, the Pocahontas coal and most coals of lower volatility gave ignitions in oxygen but not in air (*76*). For the more volatile coals given in table 31, their lower explosion limits in oxygen were at least 1/2 lower than their listed values in air. Anthracite coal dusts also do not ignite in air with ordinary electrical spark sources.

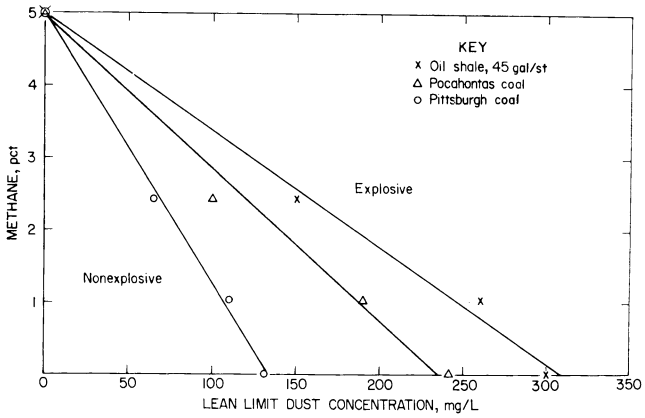

Figure 68.—Lower dust explosion limits of oil shale (45 gal/ton), Pocahontas coal, and Pittsburgh coal in methane-air atmospheres with modified Hartmann apparatus.

FLAMMABILITY LIMITS IN OTHER ATMOSPHERES

Selected inerting data for the various classes of organic industrial dusts are given in table 32. These data were obtained by Nagy and other Bureau investigators in electrical spark ignition experiments with near-optimum concentrations of the dispersed dusts in air; dust particle size was nominally less than 74 μm. With CO_2 as the inert, the minimum oxygen values to prevent propagation ranged from 11 to 18 pct. The values for cornstarch, acetal resin, and methyl methacrylate dusts were lowest (11 pct), and those for carbonaceous dusts were consistently highest (15 to 18 pct). The data with N_2 as the inert are meager but clearly indicate the smaller effectiveness of this agent. Similar to the lower limits, the minimum oxygen values are greatly dependent upon the volatiles and pyrolysis products that can be formed by the combustible dusts.

Dust explosions can also be prevented by adding a dry powder inert or inhibitor to the combustible dust. With an inert such as calcined fuller's earth, the above Bureau investigators found that except for melamine formaldehyde at least 60 wt pct is required for inerting the combustible dusts in table 32 that have lower explosion limits (L_{25}) of less than 0.1 g/L in air; the most reactive dusts required about 90 pct. For the combustible dusts with lower limits greater than 0.1 g/L, the inert dust limit was between 25 and 55 pct. The Pittsburgh coal dust from the Bruceton Mine (L_{25} = 0.055 g/L) required 60 pct inert to prevent propagation in these laboratory experiments. The effectiveness of the calcined fuller's earth is comparable to that of a limestone rock dust ($CaCO_3$).

Certain salts of alkali metals and other chemical flame inhibitors are more effective than purely inert materials in preventing or suppressing dust explosions. Table 33 (*31*,

Table 32. — Inerting requirements to prevent propagation of combustible dusts in air-nitrogen, air-carbon dioxide, and air-inert dust (fuller's earth) mixtures at ~25° C (spark ignition)[1]

Combustible	Lower explosion limit (L_{25}), g/L	Minimum oxygen limit, vol pct air-CO_2	Minimum inert dust limit, wt pct
AGRICULTURAL DUSTS			
Cellulose	0.055	13	80
Cornstarch	.045	11	90
Cottonseed meal	.055	15	75
Lycopodium	.025	13	90+
Soybean meal	.06	15	65
Sucrose	.045	14 (10 in N_2)	85
Wood flour	.035	17	80
CARBONACEOUS DUSTS			
Asphalt, brown petroleum	0.025	NA	90
Charcoal, hardwood	.14	17	55
Gilsonite, Utah	.02	NA	90
Pitch, coal tar	.035	NA	75
Coal, lignite, California	.03	NA	85
Coal, lignite, North Dakota	.045	15	75
Coal, bituminous, Pratt, AL	.12	18	40
Coal, bituminous, No. 7, Illinois	.04	15	75
Coal, bituminous, Whitesburg, KY	.05	NA	60
Coal, bituminous, Bruceton, PA	.055	17	60
CHEMICAL AND PLASTIC DUSTS			
Acetal resin, polyformaldehyde	0.035	11	90+
Acrylonitrile polymer	.03	13	90+
Ascorbic acid	NA	15 (12 in N_2)	NA
Cellulose acetate	.04	13 (9 in N_2)	85
Diallyl phthalate	.03	NA (10 in N_2)	NA
Epoxy resin (no additives)	.02	12	90
Ethylene-maleic anhydride copolymer	.095	14 (11 in N_2)	70
Ethylene oxide polymer	.03	12	90
Hexamethylenetetramine	.015	14	90+
Melamine formaldehyde (no plasticizer)	.085	17	55
Methyl methacrylate polymer	.03	11	80
Nylon polyamide	.03	13	90
Paraformaldehyde	.04	12 (8 in N_2)	90
Phenolformaldehyde, 1-step	.025	14	90
Phthalic anhydride	.015	14	90
Polyethylene, high-pressure process	.02	13	90+
Polystyrene, clear	.02	14	90+
Polyvinyl acetate	.04	17	75
Rubber, crude, hard	.025	15	90
Urea formaldehyde, spray-dried	.135	16	25

NA Not available.

[1]Based upon data in references 37, 38, 76, and 77.

Table 33. — Incombustible requirements to prevent or suppress propagation of Pittsburgh coal dust with various dust inhibitors in small- and large-scale experiments, weight percent[1]

	$NH_4H_2PO_4$ (ABC powder)	NaCl (salt)	KCl	$NaHCO_3$	$CaCO_3$ (rock dust)	$KHCO_3$ (Purple K)
Hartmann apparatus[2]	NA	50	NA	NA	60	>60
Large gallery[3]	25	30	35	>60	70	~75
Experimental mine[3]	NA	<50	NA	NA	75	>75

[1]Includes inhibitor and ash in coal (6 to 8 pct)
[2]Data from reference 31 with modified apparatus.
[3]Data from reference 88; gallery values taken from graph.

88) compares the effectiveness of six dry powder-type extinguishants against Pittsburgh coal dust explosions in recent small- and large-scale Bureau experiments; note that agent effectiveness was least in the full-scale mine experiments. These data indicate the following ratings for the extinguishants:

$$NH_4H_2PO_4 > NaCl > KCl >> NaHCO_3 > CaCO_3 > KHCO_3.$$

The poor effectiveness of purple K ($KHCO_3$) relative to rock dust ($CaCO_3$) contradicts many earlier data that were obtained under marginal ignition or apparatus-limited conditions; therefore, such data are not reported here. The ABC powder ($NH_4H_2PO_4$ - orthoammonium phosphate) has proved to the most effective dust explosion suppressant. Similar inerting or extinguishing effectiveness of these agents may be assumed applicable to the other combustibles in table 32 that have chemical constituents like those of coal.

Inerting requirements for dust explosions vary with the coal volatility. Figure 69 shows a calculated explosibility diagram by Richmond (*89*) for three coal dusts of different volatility and varying incombustible content; the incombustible included rock dust and ash content (6 to 8 pct) of the coal dusts. The predicted inerting limits from the nose of each curve are 63, 76, and 80 pct for pulverized coals of 17 pct (Pocahontas), 29 pct (Sewell), and 36 pct (Pittsburgh) volatility, respectively. Corresponding limits for such volatile coals in the Bureau's mine experiments were 43, 65, and 73 pct rock dust with a relatively "weak" ignition source; a weak source was defined as a methane-air zone plus coal dust which produces a flame speed of about 50 m/s and flame travel of about 15 m. Calculated values are reported to give best agreement with experimental values obtained with "strong" ignition sources, which are also encountered in mine explosions.

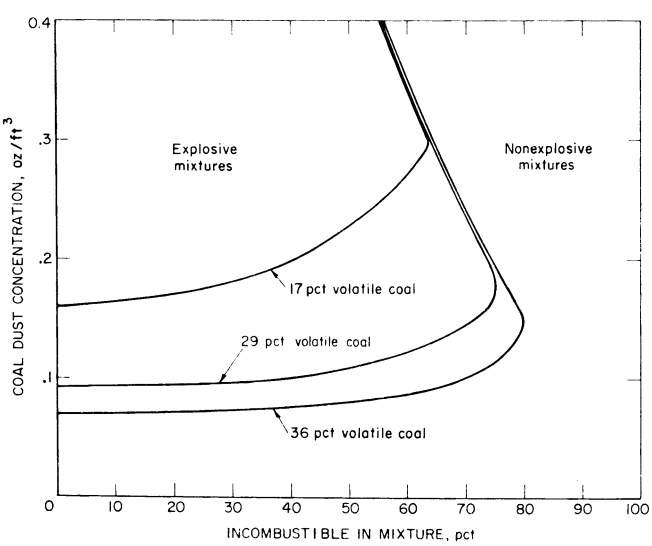

Figure 69.—Calculated limits of explosibility of coal dust-incombustible mixtures for coals of 17, 29, and 36 pct volatility.

IGNITION REQUIREMENTS

Ignition Energies

As with metal dusts, spark ignition energy data for organic dusts are subject to great experimental uncertainties, particularly in the measurement of absolute minimum values. The most complete data for the various classes of combustible dusts are included in the previously cited reports by Nagy, Jacobson, and coworkers. In summary, their data with dust clouds in air indicated that the minimum spark ignition energies of many agricultural, carbonaceous, chemical, and plastic dusts (minus 74 μm) are about 100 mJ or less. Those that required much higher ignition energies included low-volatility carbonaceous materials, fire-resistant chemicals and plastics, and materials with mineral fillers. Coals of high volatility typically had ignition energies of about 50 mJ in air and 10 mJ in oxygen. Coals of low volatility appear to have ignition energies of the order of joules in air and millijoules in oxygen; most such coals did not ignite in air under the spark ignition conditions of the particular study (*76*).

Ignition Temperatures

Bureau data on the minimum ignition temperatures of the various organic dusts in air are also summarized in table 31 (*14, 37-38, 76*). These data were obtained using layered and dispersed dusts (minus 74 μm) in the Godbert-Greenwald apparatus (0.3 L). The dust cloud ignition temperatures are between 400° and 600° C for most of the combustibles investigated; sulfur (190° C), nitrosamine (270° C), and synthetic or crude rubber (320°-350° C) are the few materials that have noticeably lower values. The dust layer ignition temperatures should be noticeably lower than the dust cloud values, although some data are inconsistent. These data are primarily applicable to heating durations of the order of a second for dust clouds and a few minutes for dust layers. Lower ignition temperatures result when the heating duration (residence times) are longer. Table 34 shows the reductions of dust cloud autoignition temperatures that are possible by increasing the volume of the Godbert-Greenwald furnace to 1.2 L and the dust residence time to several seconds. In the case of the dust layer ignition temperatures, these should not be confused with spontaneous heating temperatures that are associated with extended reaction times and adiabatic conditions.

The effectiveness of various dry powder inhibitors on the ignition temperature of Pittsburgh coal dust (minus

Table 34. — Comparison of dust cloud minimum autoignition temperatures in standard and modified Godbert-Greenwald apparatus

	Autoignition temperature, ° C	
	Standard apparatus[1] (0.3 L)	Modified apparatus[2] (1.2 L)
Anthracite coal	840 (4 pct volatile)	780 (6.6 pct volatile)
Bituminous coal (Pocahontas)	640	625
Bituminous coal (Pittsburgh)	610	560
Subbituminous coal (Wyoming)	NA	455
Gilsonite (Utah)	580	490
Lycopodium	480	435
Polyethylene	450	400

NA Not available.
[1]References 37-38, 76.
[2]Reference 10.

74 μm) was determined in the Godbert-Greenwald apparatus by Liebman and Richmond. Their data are shown in figure 70, which was taken from reference 10. These data provide an explanation for the greater effectiveness of NaCl, KCl, and $NH_4H_2PO_4$ as compared to $CaCO_3$, $NaHCO_3$, and $KHCO_3$ in suppressing coal dust explosions; note the agreement between this figure and table 33.

Spontaneous Heating Temperatures

Agricultural and carbonaceous dusts are the most common types of organic materials that may undergo spontaneous heating at normal or slightly elevated temperatures. Spontaneous heating is also referred to as self-heating or spontaneous combustion. It is usually associated with slow oxidation (days) of a combustible under near-adiabatic conditions, as in a large storage bin or pile. Agricultural dusts containing vegetable oils or other highly oxidizable oils are particularly susceptible to self-oxidation. Many coals and charcoals present a similar hazard.

Of the organic combustibles capable of spontaneous heating, coals by far have been the most completely investigated. The most recent and comprehensive study on various U.S. coals was that by Kuchta (*58*), who used a small adiabatic-type apparatus to determine the actual spontaneous heating temperatures. The data showed that dried

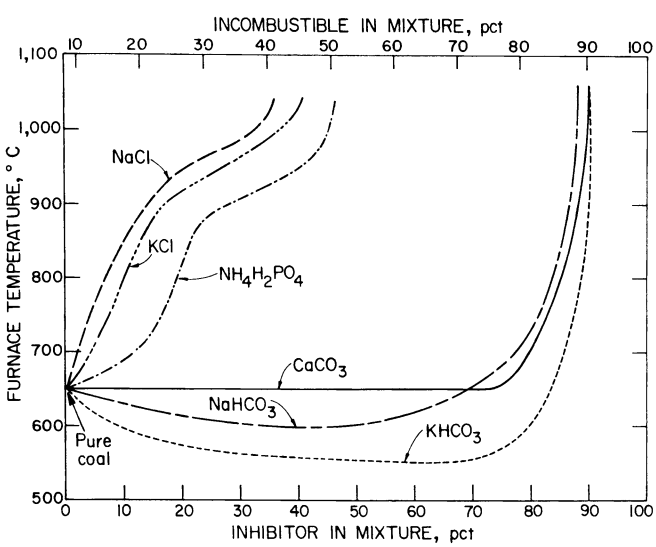

Figure 70.—Effectiveness of various powdered inhibitors on the furnace autoignition temperature of Pittsburgh coal dust in the Godbert-Greenwald furnace.

lignite and subbituminous coals of 100 to 200 mesh could readily self-heat in moist air at 30° C, as compared to 60° to 70° C for western bituminous coals and 80° to 100° C for eastern coals (table 35); heating durations were generally limited to a maximum of about 2 days. Although some western bituminous coals showed a slight tendency to self-heat at 30° C, the exothermic reactions were not sustainable in this apparatus. The heat of wetting (condensation) is believed to be important as a triggering mechanism in these reactions; temperature rises of at least 10° C were reported in experiments with a dried coal and moist nitrogen. Sondreal (*97*) found that the calorific heats of wetting can be as high as 26, 20, 7 and 1 cal/g for dried lignite, subbituminous, Illinois bituminous, and Pittsburgh bituminous coals, respectively. Thus, the weathering of coals increases their spontaneous combustion hazard.

Table 35. — Spontaneous heating temperatures and CO-ΔO_2 indexes of various dried coal dusts in air (*58*)

Coal	Spontaneous heating[1] temperature, °C	CO/ΔO_2[2], ppm/vol pct
LIGNITE		
Beluga, Alaska	32	198
Gascoyne strip, North Dakota	30	244
Husky strip, North Dakota	30	246
Sandow strip, Texas	30	228
SUBBITUMINOUS		
Dravo, seam No. 80, Wyoming	30	285
Jim Bridger, Wyoming	32	188
Sarpy Creek, Rosebud, Montana	30	178
Sarpy Creek, Stray No. 2, Montana	30	216
BITUMINOUS		
Pittsburgh, Pennsylvania	80	74
Pocahontas No. 3, West Virginia	90	66
Powhatan, No. 3, Ohio	105	49
Sahara, No. 20, Illinois	60	75
Scotia, Kentucky	70	48
Somerset No. 1, Colorado	60	119
Sunnyhill No. 9, Ohio	70	110
Sunnyside No. 1, Utah	70	178

[1]100- to 200-mesh coals.
[2]10- to 20-mesh coals.

The tendency of coals to self-heat may be roughly predicted from their CO-ΔO_2 index, which is a measure of the coal's ability to adsorb oxygen from the atmosphere and form or evolve carbon monoxide. Closed vessel desorption experiments (*58*) showed that the CO-ΔO_2 index is greatest for dried crushed coals and becomes near-maximum after several days' exposure in air (fig. 71). Table 35 includes the CO-ΔO_2 index values that were obtained in such experiments after 7 days with 10- to 20-mesh samples of the coals in air at 25° C; here, the CO formation or desorption is in parts per million, and oxygen reduction (ΔO_2) is in volume percent. Essentially, the most reactive coals have a CO-ΔO_2 index close to 200 or more, and the least reactive ones less than about 100. Proximate and ultimate analyses of the coals are included in table 36. The CO-ΔO_2 ratios correlate best with the oxygen content of the coals. They are strongly dependent upon temperature and about an order of magnitude less than corresponding CO-CO_2 ratios (fig. 72) (*58*). Such data can be useful in predicting the temperature of the given coals during their incipient combustion before autoignition. In a mining environment, the CO-ΔO_2 index is often found to be at least 1/2 lower than the laboratory closed-vessel value; this is attributable to experimental artifact or complex dilution effects in mine ventilation networks.

Table 36. — Analyses of coals as received

Mine	Location	Heating value, Btu/lb	Proximate analysis, wt pct				Ultimate analysis, wt pct					
			Moisture	Volatile matter	Fixed carbon	Ash	Hydrogen	Carbon	Nitrogen	Oxygen	MAF[1] oxygen	Sulfur
LIGNITE												
Beluga	Alaska	7,000	24.5	31.1	28.9	15.5	5.9	42.0	0.7	35.8	23.3	0.1
Gascoyne strip	North Dakota	7,150	34.0	29.5	30.2	6.3	6.7	43.0	.8	41.9	19.6	1.3
Husky strip	North Dakota	7,280	34.1	30.7	29.0	6.2	7.0	42.7	.6	42.8	20.9	.6
Monticello	Texas	7,430	29.4	31.9	27.7	11.0	6.4	43.3	1.2	37.6	19.2	.6
Center strip	North Dakota	7,660	32.0	32.5	30.9	4.6	6.7	46.1	.7	41.5	20.6	.4
Darco strip	Texas	7,850	31.1	30.5	32.5	5.9	6.6	46.1	.8	39.7	19.1	1.0
Sandow strip	Texas	8,940	21.1	39.5	29.1	10.3	6.4	50.8	.9	30.6	17.3	1.0
SUBBITUMINOUS												
Sarpy Creek, Rosebud	Montana	9,330	22.0	32.5	39.4	6.1	6.2	54.6	0.7	31.9	17.2	0.5
Sarpy Creek, Stray No. 2	Montana	9,460	18.5	33.5	37.8	10.2	5.9	54.5	.7	27.9	16.1	.8
Dravo, seam No. 82	Wyoming	10,620	14.7	33.0	47.7	4.6	5.8	61.7	1.4	25.6	15.7	.9
Jim Bridger	Wyoming	10,740	15.7	31.6	49.9	2.8	5.8	62.6	1.0	27.4	16.4	.4
P&M, Mammoth	Montana	11,130	11.2	38.2	46.9	3.7	5.4	65.9	1.1	23.5	16.0	.4
Dravo, seam No. 80	Wyoming	11,190	11.7	38.0	46.9	3.4	6.0	64.1	1.7	24.2	16.2	.6
BITUMINOUS												
Sunnyhill No. 9	Ohio	11,520	8.2	35.9	46.3	9.6	5.4	65.5	1.3	15.7	10.2	2.5
Inland No. 6	Illinois	12,370	6.2	30.5	55.4	7.9	5.2	70.8	1.6	14.0	9.8	.5
Prince	Nova Scotia	12,580	3.2	35.1	52.4	9.3	4.9	69.7	1.3	10.1	8.2	4.7
Sahara No. 21	Illinois	12,650	4.5	32.7	54.2	8.6	5.2	71.1	1.5	11.2	8.2	2.4
Sahara No. 20	Illinois	12,760	6.5	33.8	52.4	7.3	5.2	71.5	1.6	12.3	7.5	2.1
Napoleon	Ohio	12,830	6.2	43.3	45.1	5.0	5.7	70.6	1.4	14.2	9.8	3.1
Sunnyside No. 1	Utah	13,060	4.7	37.4	53.2	4.7	5.5	73.5	1.5	13.6	10.3	1.2
Somerset No. 2	Colorado	13,250	2.7	37.6	53.7	6.0	5.4	74.4	1.5	12.2	10.7	.5
Somerset No. 1	Colorado	13,770	3.8	39.1	54.2	2.9	5.8	76.5	1.6	12.6	9.9	.6
York Canyon	New Mexico	13,680	1.4	35.9	53.9	8.8	5.3	75.7	1.6	8.2	7.6	.4
Allison	Ohio	13,660	2.5	43.5	46.3	7.7	5.4	73.2	1.3	7.1	5.6	5.3
Powhatan No. 3	Ohio	13,690	2.9	41.5	50.7	4.9	5.6	76.3	1.7	9.2	7.1	2.3
Vail	Ohio	13,780	4.1	41.2	50.3	4.4	5.6	75.6	1.6	10.2	7.3	2.6
Scotia	Kentucky	13,850	1.6	35.1	54.1	9.2	5.1	76.0	1.2	7.9	7.3	.6
Bruceton	Pennsylvania	14,500	1.5	38.9	55.8	3.8	5.6	79.7	1.8	7.9	6.9	1.2
Pocahontas No. 3	West Virginia	14,360	2.7	16.3	75.9	5.1	4.5	84.1	1.1	4.6	2.6	.6

[1]Moisture and ash free.

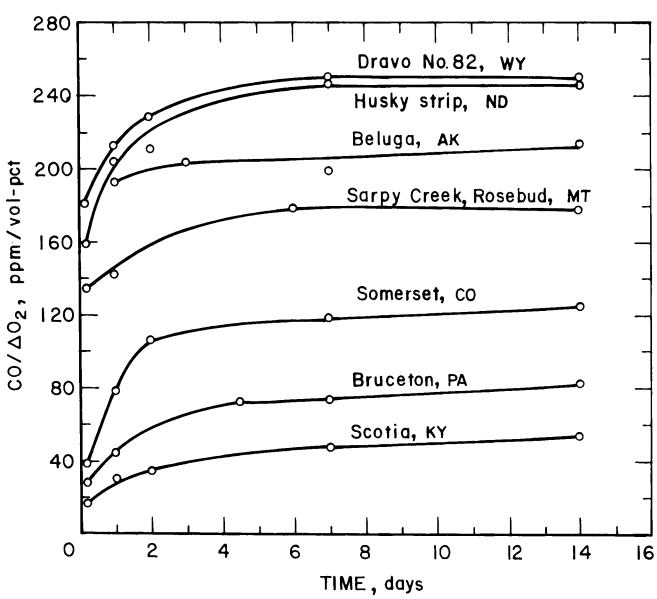

Figure 71.—CO-ΔO_2 ratio versus time in closed-vessel desorption experiments with seven coals of 10 to 20 mesh in air at 25° C.

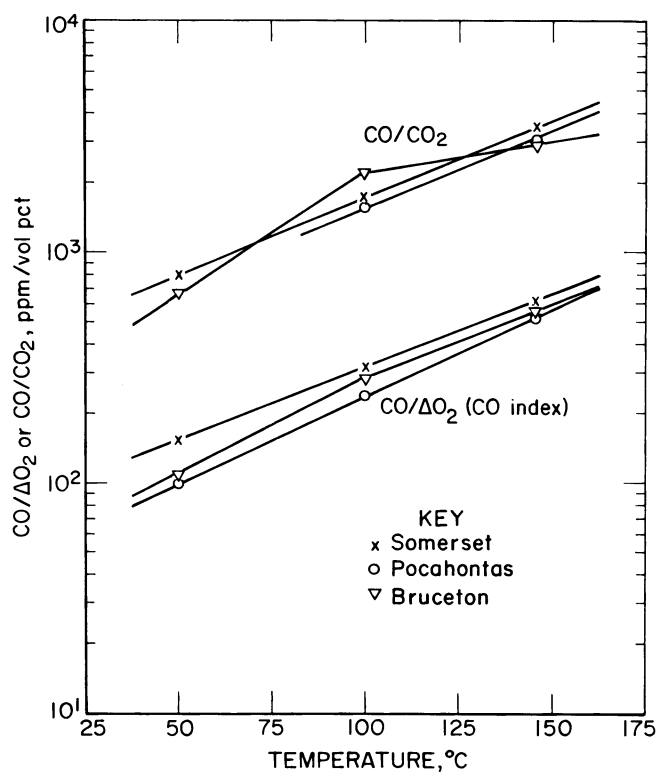

Figure 72.—Variation of CO-ΔO_2 and CO-CO_2 ratios with temperature in a flowing airstream (15 cm_3/min) with three undried coals of 10 to 20 mesh.

The total gas content of a coal can be useful in predicting both spontaneous heating and explosion hazards, even though methane or other gases in the coal are not known to be vital to the spontaneous combustion process. Figure 73 illustrates this point with ASTM designations for coal rankings. The gas content data are average values of gas desorption measurements by Diamond (*12*) for virgin core samples from 125 coalbeds; they represent total gas desorptions of cored and crushed samples for periods up to 1 month or when the degasification rates become very low. Of practical significance is that the self-heating hazard increases whereas the gas explosion hazard decreases with decreasing gas content or rank of the coal; the coals in table 36 are listed in the order of increasing calorific value, which also indicates their approximate ASTM coal ranking. Although all coals are capable of self-heating at some threshold temperature, the incidence rate is small for those with a gas content of about 4 cm^3/g or greater; this corresponds to a high-volatile A bituminous or higher rank coal. In evaluating the gas explosion potential of any coal, one can assume that most of its gases will be released during the mining stage; also, the residual gases will be released at a slower rate for the higher rank coal.

Other organic dusts that are widely known to undergo self-heating at normal ambient temperature are those containing linseed, cottonseed, rapeseed, or olive-type vegetable oils. Cereal grains, hay, and even grass clippings have this capability during their curing or storage. Most other organic solids require elevated temperatures to self-heat and present a potential ignition hazard. Table 37 lists the spontaneous heating temperatures that were obtained by the National Bureau of Standards (*72*) for various woods, fibrous materials, and synthetic rubbers. The data for rubber materials indicate the great effect of particle size or physical form of the combustible solid.

Table 37. — Spontaneous heating temperatures of various woods, fibrous materials, and synthetic rubbers in air

Material	Sample type	Spontaneous heating temperature, °C
WOODS AND FIBROUS MATERIALS		
Douglas fir	Shavings	260
Spruce	Shavings	261
Long leaf pine	Shavings	230
Short leaf pine	Shavings	228
White pine	Shavings	264
Paper, filter	Cuts	232
Paper, newsprint	Cuts	230
Cotton, absorbent	Roll	266
Cotton, batting	Roll	230
Cotton, sheeting	Roll	240
Nylon, parachute	Roll	475
Silk, parachute	Roll	570
Viscose rayon, parachute	Roll	280
Wool, blanket	Roll	205
Cane fiberboard	Piece	240
Wood fiberboard	Piece	~220
SYNTHETIC RUBBERS		
GR-S, black	Buffings	160
GR-S, black	Coagulum	295
GR-S (R-60), black	Buffings	190
GR-S (R-60), black	Coagulum	310
GR-S, indulin	Crumb	440

[1]Data from reference 72, 13th ed., 1969, sec. 5, p. 213.

Sulfide ores, such as iron sulfide, are well known to oxidize spontaneously in moist air. Temperatures in such reactions can be sufficient to ignite timbers, coals, and other organic material.

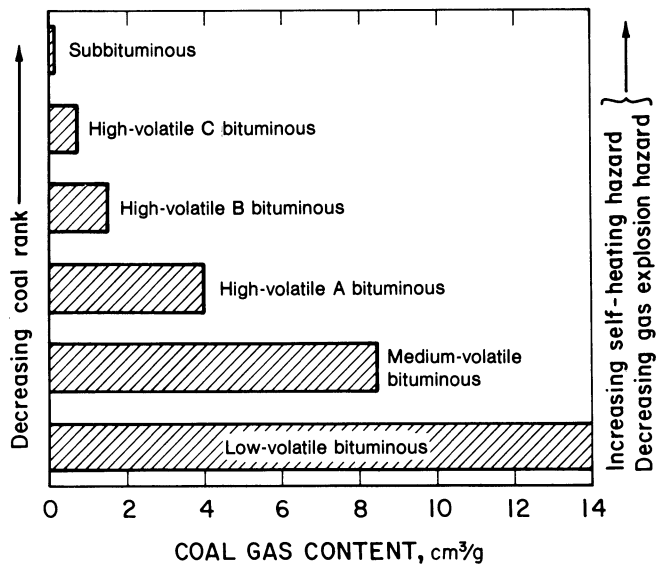

Figure 73.—Representative gas contents of various ranked coals and their relative hazard potential for self-heating and gaseous explosion.

FLAME TEMPERATURES AND BURNING RATES

Flame Temperatures

The flame temperatures of most organic dusts have not been determined, and those that have been are not as precisely defined as for organic liquid vapors or gases. Nevertheless, their flame temperatures should be comparable to those of the hydrocarbons or other classes of chemical constituents that are present. For example, Hertzberg (*31*) obtained a maximum flame temperature of approximately 2,100° C in explosions of Pittsburgh coal dust-air mixtures, which is comparable to the *constant-volume* combustion values calculated for many stoichiometric hydrocarbon vapor-air mixtures. The maximum value of 2,100° C was found at a coal dust concentration of 300 mg/L, and a near-lower-limit value of 1,300° to 1,400° C was obtained at a dust concentration of 150 mg/L. Corresponding flame temperatures for other carbonaceous or organic dusts should roughly fall in this temperature range if their chemical constituents are largely hydrocarbons or hydrocarbon derivatives similar to those found in coals. For any composite dust, the flame temperature will decrease with increasing amounts of incombustible material.

Burning Rates

Compared to hydrocarbon vapor-air mixtures, the fundamental burning velocities (S_u) of organic dust-air mixtures appear to be noticeably lower, although only meager data are available. For Pittsburgh coal dust-air mixtures, the calculated S_u values from measured flame speeds ranged from 4 to 18 cm/s for dust concentrations of 150 to 500 mg/L (*31*). The maximum S_u of 18 cm/s is at least 1/2 lower than those reported for gaseous hydrocarbons (table 17).

In the case of fires with combustible solids, their burning rates or flame spread rates are useful in determining how rapidly the fires may propagate. Table 38 gives horizontal burning rates that were obtained by Bureau investigators for small beds of various flammable granular

Table 38. — Burning rates (horizontal) of flammable granular solids and oxidizer-sawdust mixtures in air at 1 atm (decreasing order of flammability)

Material	Particle size, mesh	Burning rate, cm/min
FLAMMABLE SOLIDS (1.25- BY 1.25- BY 12.5-CM BED) (*60*)		
Phosphorus sesquisulfide	50-150	[1]290
Phosphorus, red	100-200	225
Titanium	100-200	190
Camphor	10-30	89
Magnesium	>80	[1]76
Sodium methylate	70-150	74
Picric acid, 10 to 20 pct H_2O	10-50	19
2,4-Dinitroaniline	40-70	16.5
Ammonium dichromate	30-100	10.2
Phthalic anhydride	20-70	[1]9.7
Sodium borohydride	10-30	8.6
Tetraphenyl tin	50-200	6.9
Charcoal, willow wood	40-50	[1].8
OXIDIZERS + SAWDUST (2.5- BY 5- BY 18-CM BED) (*55*)		
Sodium peroxide (70 pct)	40-150	2,160
Calcium hypochlorite-69.5 pct Cl_2 (80 pct)	20-100	305
Potassium bromate (60 pct)	70-100	290
Chromium trioxide (80 pct)	20-100	230
Ammonium perchlorate (80 pct)	20-100	105
Sodium perchlorate (70 pct)	20-100	76
Potassium nitrate (40 pct)	40-100	71
Sodium nitrate (40 pct)	40-150	61
Sodium chlorate (60 pct)	20-70	48
Potassium permanganate (60 pct)	20-100	30
Lead nitrate (50 pct)	50-150	12
Potassium persulfate (80 pct)	30-150	10
Potassium dichromate (70 pct)	30-100	8.9
REFERENCE SAWDUST (2.5- BY 5- BY 18-CM BED)		
Red oak, select grade (dried)	20-50	6.9

[1]0.65- by 1.25- by 12.5-cm bed.

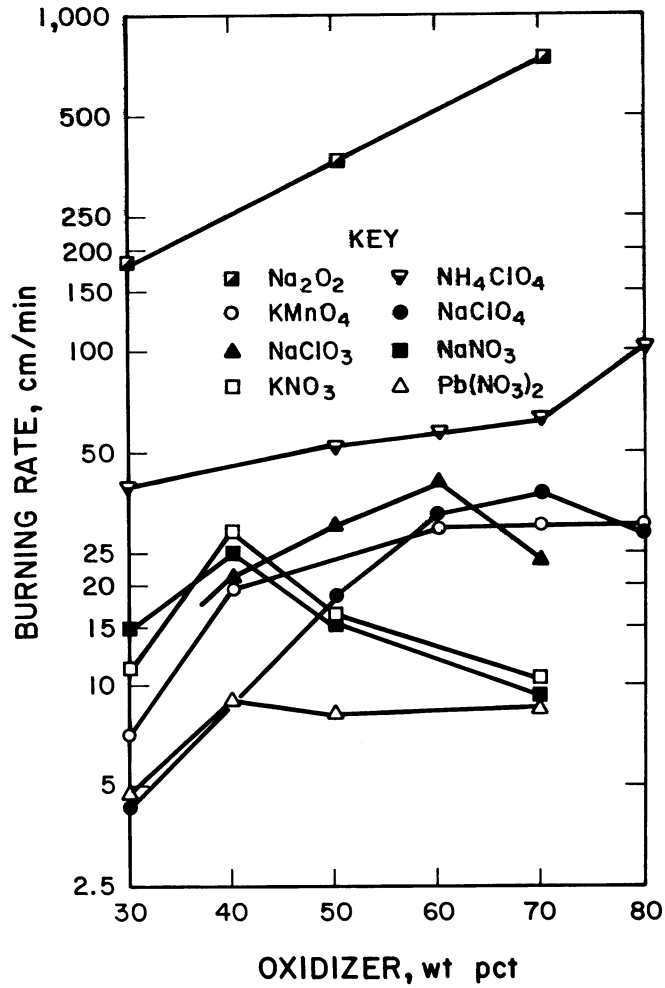

Figure 74.—Variation of burning rate with oxidizer concentration for dried sawdust (red oak) with various solid oxidizers.

solids (*60*); these data actually represent flame spread measurements over the burning surface. Although particle size was not held constant, the data provide a good indication of the flame spread potential of each material, including such hazardous metal dusts as magnesium and titanium. Higher burning rates are normally expected with finer dusts, provided particle agglomeration does not occur. Materials having a burning rate less than 10 cm/min are considered to present a low flame spread hazard. With the exception of sodium borohydride, the flame spread ratings found by these authors were consistent with ignitability ratings by a flame source.

Table 38 also includes burning rates for mixtures of dried sawdust of a select grade red oak with a number of oxidizers (*55*). The rates are maximum values obtained at optimum oxidizer concentrations; oxidizer concentration effect is shown in figure 74. These data are indicative of the increased fire hazard that may result when a cellulosic packaging material, such as wood, is involved in fires with oxidizer cargoes. Note that the burning rate of the sawdust (~7 cm/min) is substantially increased with the addition of most oxidizers, including the alkali metal nitrates, chlorates, and perchlorates. The highest rate (2,160 cm/min) by far was obtained with the very strong oxidizer of sodium peroxide. In any application of these data, one must allow for the increased flame spread that can result from scaling and ventilation effects.

PROPERTIES OF FABRICS AND SHEET COMBUSTIBLES

IGNITION TEMPERATURES

Combustibles in sheet form can require relatively high temperatures for their ignition. Bureau data (*56*) for 10 representative fabric- or sheet-type combustibles are given in table 39. Such common materials as paper drapes and cotton or rubber sheeting require about 400° C for ignition in air when uniformly heated (vessel ignitions); other sheet combustibles such as wool, cellulose acetate, polyvinyl chloride, and Nomex require over 500° C for ignition; Nomex is a fire-resistant nylon. When the heating is nonuniform, as with a hotplate, the ignition temperatures are substantially higher than the vessel ignition temperatures; also, they are lower in oxygen than in air, as one would predict. Although fire-retardant additives usually increase the ignition temperature, some may actually increase the ignition hazard; note data for the treated cotton sheeting that contained an ammonium salt fire retardant. In addition, the values in oxygen (1 atm) were found comparable to or less than those in air at 6 atm, indicating the dependence on oxygen partial pressure.

Table 39. — Ignition temperatures of flammable fabric or sheet materials in air and oxygen at atmospheric pressure (*56*)

Material	Density, g/m²	Ignition temperature, °C		
		Heated vessel with air	Hotplate	
			Air	Oxygen
Cellulose acetate sheet	363	550	>600	425
Conductive rubber sheeting	500	390	480	360
Conductive Tygon tubing	NA	415	NA	NA
Cotton sheeting	160	385	465	360
Cotton sheeting, fire retardant	NA	430	575	310
Nomex sheeting	102	515	>600	520
Paper drapes	53	400	470	410
Plexiglass sheet	807	450	595	430
Polyvinyl chloride sheet	495	560	>600	390
Wool blanket	712	540	>600	500

NA Not available.

BURNING RATES

Flame spread rates of sheet combustibles provide a measure of their surface burning rates. Such data are given in table 40 from the above-cited work (*56*) where the upward flame propagations were determined with small samples (5- by 25-cm) at a 45° angle in air and oxygen at atmospheric pressure. Under these conditions, many of the combustibles failed to sustain propagation in air. Even in oxygen, only the paper drapes (19.6 cm/s) and wool blanket (100 cm/s) gave relatively high rates; the high value for wool is attributable to "nap" burning. The rates in oxygen atmospheres correlate well with total pressure or oxygen partial pressures (fig. 75); the pressure dependence was greatest for cotton sheeting (rate α $P^{0.95}$) and least for rubber sheeting (rate α $P^{0.55}$). In comparison, the rates in various oxygen-nitrogen atmospheres were not as sensitive to oxygen partial pressure.

Flame spread rates are always greater when the combustibles are burned in a vertical orientation in the upward mode. For example, upward verticle rates for cotton sheeting in air were 20 times greater than horizontal rates and 40 times greater than vertical downward rates. The rates can also be greatly influenced by the combustible loading, combustible distribution, air ventilation rate, and other fire enhancement factors. Hence, the laboratory-scale data cannot be assumed to provide a measure of the maximum fire hazard that may be encountered in a large-scale fire situation.

The fire resistance characteristics of several mine conveyor belts are given in table 41. These data were obtained by the Bureau (*59*) in a moderately scaled apparatus (48 by 48 by 168 cm) with a flame ignitor input of 50 kcal/min (~1.6 cal/(cm²·s)) and air velocity of 30 m/min. Horizontal flame spread rates under such conditions ranged from 0 to 12 cm/min depending upon the type of belt, as compared to 21 cm/min for a red oak standard. To define the overall fire resistance rating for each belt, a flammability index (FI) is given that includes the contributions of the flame spread rate (FS), heat release rate (Q_f), and critical ignitor input (I, time-integrated heat flux); this index (FI = FS $\times$ Q_f/I) is also normalized with respect to red oak. The fire resistance ratings by this method were found to be more reliable than those obtained by small laboratory-scale methods. The use of air velocities greater than 30 m/min can give higher flame spread rates, although ignitions become increasingly difficult to achieve. Also, a belt height-chamber height ratio of about 0.75 appears optimum for sustained propagation in a tunnel-type fire. Both ignition and flame propagation stages must be considered in determining belt fire resistance.

Table 40. — Flame spread rates (45° angle) of flammable fabric or sheet materials in air and oxygen at atmospheric pressure (*56*)

Material	Density, g/m²	Flame spread rate, cm/s	
		Air	Oxygen
Cellulose acetate sheet	363	NP	2.8
Conductive rubber sheeting	500	NP	3.3
Cotton sheeting	160	2.0	8.1
Cotton sheeting, fire-retardant	NA	NP	4.3
Nomex sheeting	102	NP	4.3
Paper drapes	53	5.1	19.6
Plexiglass sheet	807	.5	1.3 (42 pct O_2)
Polyvinyl chloride sheet	495	NP	2.5
Wool blanket	712	NP	100
Wood strips, white pine	1,670	.5	2.8

NA Not available. NP No sustained propagation.

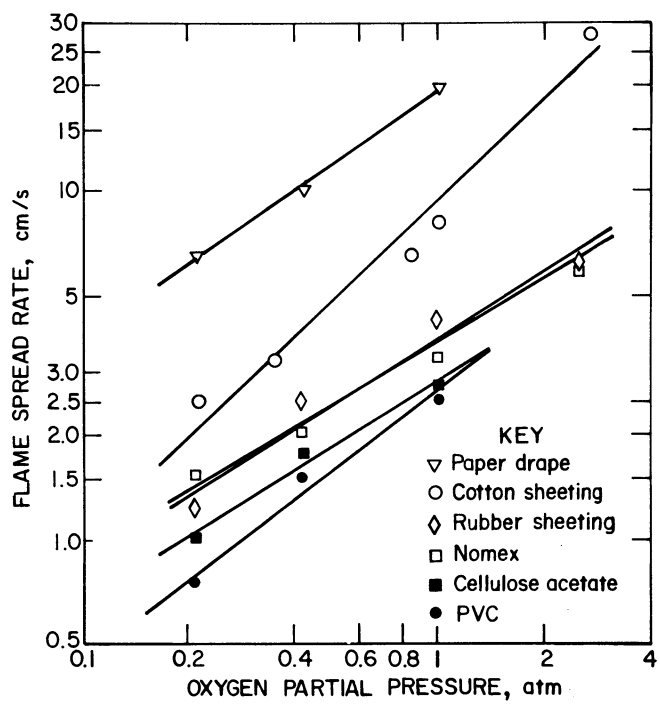

Figure 75.—Effect of oxygen pressure on the flame spread rates of sheet combustibles in oxygen atmospheres.

Table 41. — Flammability data for mine conveyor belts and red oak standard in Bureau of Mines belt flammability apparatus (*59*)[1]

Combustible	Flame spread rate (FS), cm/min	Heat release rate (Q_f), cal/(cm^2·min)	Critical ignitor input (I), cal/cm^2	Flammability index[2] (FI)	Normalized flammability index (FI*)
REFERENCE STANDARD MATERIAL					
Red oak	20.8	230	145	33	100
CONVEYOR BELTS					
Non-fire-resistant rubber (Goodyear)	10.9	213	145	16	48
Neoprene (Goodyear-A)	10.6	165	240	7.3	22
Polyvinyl chloride (Fenner America)	12.2	122	335	4.4	13
Fire-resistant rubber (Goodyear)	5.8	60	335	1.0	3.0
Neoprene (Goodyear-B)	7.2	76	820	.7	2.1
Polyvinyl chloride (Scandura)	7.3	75	1,295	.4	1.2
Polyvinyl chloride (Georgia Duck)	NI	NI	>1,440	0	0
Polyvinyl chloride[3] (German Clouth)	0-4.6	0-71	≥865	0-.4	0-1.2
Neoprene (German Clouth)	NI	NI	>2,400	0	0

NI No ignition at given ignitor input.
[1]Ignitor input — 50 kcal/min (1.6 cal/(cm^2·s), Air velocity — 30 m/min.
[2]$FI = \frac{FS \times Q_f}{I}$.
[3]Only 1 ignition in 4 trials.

FIRE AND EXPLOSION DAMAGE

FIRE TEMPERATURE AND RADIATION CRITERIA

Fire damage to materials results primarily from exposure to the high levels of temperature and thermal radiation produced by the fire. Qualitative guidelines for analyzing fire damage are summarized in the section on investigative procedures. Supporting data for such analyses are found in this section and in the other sections that characterize the fire properties of various materials. Considering that maximum flame temperatures of many combustible-oxidant systems can be 2,000° C or more, as in table 17, constructional and appurtenant materials cannot withstand a large-scale fire for long durations without being consumed or severely damaged. Fortunately, most fires involve diffusional flames, which are less severe than premixed flames. The extent of any fire damage will be largely determined by the fire loading on the exposed material and its meltability, combustibility, and massiveness or fineness. Fire loading itself is the temperature and heat flux generated by the fire under the particular static or dynamic environmental conditions.

Some useful temperature limits of various textile fibers and metallic or nonmetallic composite materials are given in tables 42 and 43, respectively. Melting points of pure elements and compounds are included in the summary tables of this manual for each class of combustibles; the ignition temperature data are also useful in determining temperature limitations of materials. Among the highest melting point substances are graphite (3,700° C), molybdenum (2,617° C), tantalum (2,996° C), tungsten (3,410° C), and the refractory compounds. Steel is one of the most common materials of construction and has a melting point of about 1,400° C or more. The brightness or color of such metals in a fire can be used to estimate their temperatures (table 44).

Damage may occur even in the absence of flaming combustion, as in the self-heating of coals, which may result in a loss of their calorific values. Generally, if the temperature rise from self-heating is small (~10° C), any calorific loss of the coal that does occur will be very small. However, if the temperature rise is about 30° or more, the calorific loss can be noticeable, depending upon the heating duration and maximum resultant temperature. Proximate and ultimate coal analyses on a moisture-free basis are most useful in determining the self-heating effect on calorific values.

Thermal radiation from a fire can cause property damage and human injury if the incident radiant flux is of sufficient intensity. Data by Lawson (*64*) define the threshold radiation intensities required for igniting various combustible solids and for sensing pain by a human body (table 45). These data are for relatively moderate exposure times and, therefore, do not necessarily represent the lowest values possible for extended exposure periods. For example, the value for ignition of wood (0.8 cal/(cm^2·s)) is higher than the usually accepted value of approximately 0.5 cal/(cm^2·s) for exposure times of many minutes. The value of 0.1 cal/(cm^2·s) for sensing pain can also be considered as an approximate threshold for second-degree burns at exposure times of minutes.

Table 42. — Temperature limits of various textiles (*4*)[1]

Fiber	Temp, °C	Effect	Fiber	Temp, °C	Effect
Acetate	260	Melts.	Polyester	250	Melts.
Asbestos	810	NS.	Polyethylene	110-120	Melts.
Cotton	150	Decomposes.	Polypropropylene	160-170	Melts.
Flax	135	NS.	Silk	150	Decomposes.
Glass	730	Softens.	Viscose rayon	175-205	Decomposes.
Jute	135	NS.	Wool	135	Decomposes.
Nylon	215-260	Melts.			

NS Not specifically defined.
[1]Rounded values.

Table 43. — Melting points of metallic and nonmetallic substances[1]

Substance	Melting point, °C
METAL	
Aluminum alloy 38	565
Aluminum alloy 3003	650
Aluminum bronze, ASTM B36	1,040
Bismuth solder	95-130
Carbon steel, SAE 1020	1,515
Cast iron, gray, ASTM A48	1,175
Cast iron, ductile, ASTM A339	1,150
Brass, red, ASTM B30	995
Brass, yellow, ASTM B36	930
Cupronickel, constantan	1,260
Hastelloy C	1,290
Inconel X, annealed	1,400
Magnesium alloy, AZ 3113	625
Monel K	1,330
Nickel-silver alloy, 18 pct	1,110
Stainless steel, type 304	1,425
Tin solder	135-175
Titanium, commercial	1,815
NONMETAL	
Borax	560
Glass, borosilicate	[2]820
Graphite	3,700
India rubber	125
Paraffin	55
Porcelain	1,550
Quartz, clear	[2]~1,660
Spermaceti (wax)	50
Stearine (wax)	50

[1]Based upon data in references 4, 83, 105; rounded values.
[2]Softening point.

Table 44. — Color temperatures of iron or steel (*4*)[1]

Metal color	Temp, °C
Dark blood red, black red	530
Dark red, blood red	565
Dark cherry red	635
Medium cherry red	675
Cherry, full red	745
Light cherry, light red	845
Orange	900
Light orange	940
Yellow	995
Light yellow	1,080
White	1,205

[1]Rounded values.

Table 45. — Threshold radiation intensities for various thermal effects (*64*)

Effect	Threshold radiation intensity	
	cal/(s·cm^2)	Btu/(h·ft^2)
Wood ignites spontaneously	0.8	10,600
Hemp, jute, and flax ignite spontaneously	1.0	13,300
Textiles ignite spontaneously	.85	11,300
Fiberboard ignites spontaneously	.75	10,000
Wood ignites by flying brands	.1	1,300
Painted wood ignites by flying brands	.4	5,300
Humans feel pain after a short time	.1	1,300

The fire radiation received by an object is a function of its distance from the fire source and the size and intensity of the radiant energy source. Yumoto (*109*) defined the irradiance (I) of hydrocarbon-type fuel fires (gasolines) as a dimensionless function of the irradiance distance and diameter of the burning fuel tank. These data are replotted in figure 76 and extrapolated to an ignition threshold for wood (0.45 cal/ (cm^2·s)) and to the radiant intensity at a dimensionless ratio (d_o/r_o) of 1 (~5 cal/(cm^2·s)), which theoretically corresponds to the source intensity; d_o is the irradiance distance and r_o is the radius of the fuel tank. The negative slope of 2 indicated by these data is consistent with the inverse square dependence with distance that is predicted by equation 33. Thus, if the ignition radiant thresholds are known for hydrocarbon- or carbonaceous-type combustibles as in table 45, figure 76 can be applied to obtain a rough estimate of the distance from a gasoline pool fire source at which ignition could occur. Similar estimates for other liquid fuels can be made using equation 33 and the data in table 21. The variations of irradiances with windy conditions, nonuniform flame symmetry, and different flame emissivities are important in any rigorous treatment.

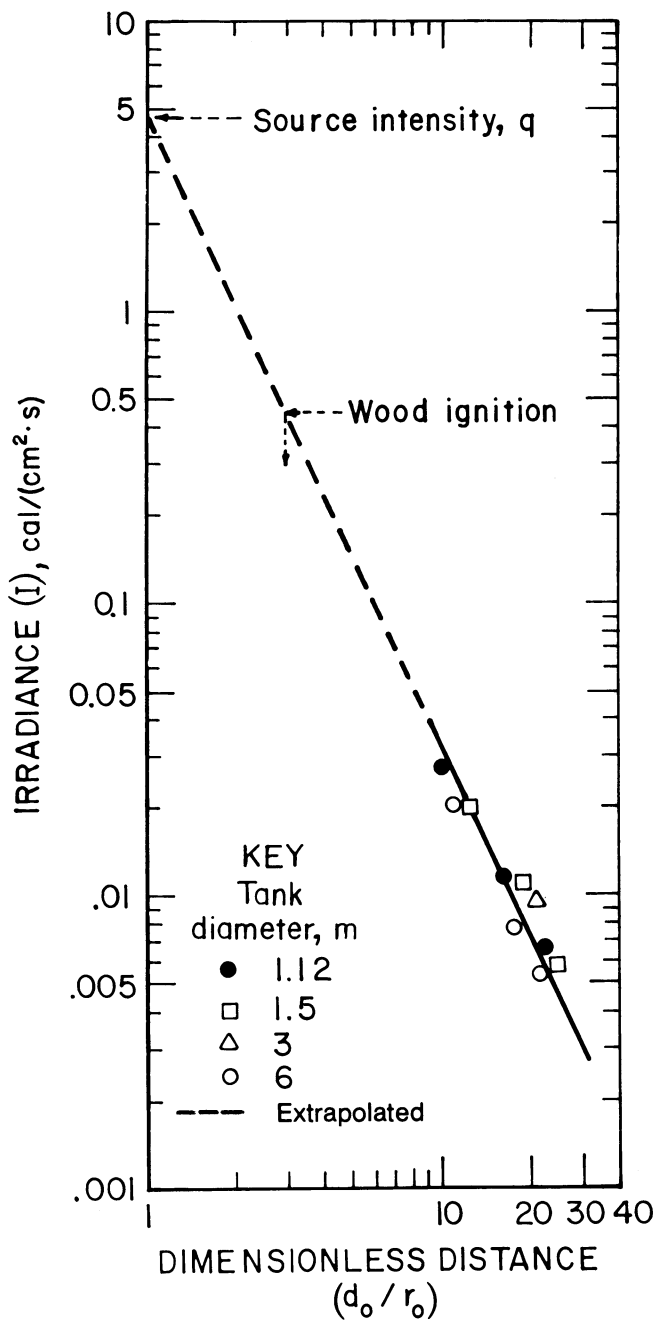

Figure 76.—Thermal irradiance of gasoline tank fires as a function of a dimensionless distance ratio (irradiance distance-tank fire radius).

EXPLOSION PRESSURE CRITERIA

Pressure damage from combustible gas explosions (deflagrations) will depend upon the explosion pressure of the combustible mixture, strength of the confinement material (including fasteners), and degree of any venting. Expressions for calculating explosion temperatures and pressures are given in the section on theory and definitions. Although maximum pressures occur with near-stoichiometric combustible concentrations for complete combustion, even near-limit concentrations yield explosion pressures that may exceed the pressure limits of the confinement material. The methane-air data in figure 77 (*47*) are typical of the fuel concentration effect on explosion pressure for many hydrocarbon combustibles. They are characterized by a maximum pressure rise ratio (P_2/P_1) of about 8 at near-stoichiometric concentrations, as predicted by theory; some calculated adiabatic values are given in table 18.

Failure of a cylindrical or spherical container in such explosions may be estimated from the equations for the two possible types of stress failure:

Hoop stress (tangential) $S_h = Pr/t$ (79)

Tensile stress (longitudinal) $S_t = Pr/2t$ (80)

where S is stress (psi), P is pressure (psi), r is container radius (in), and t is container thickness (in); efficiency of any welds is neglected in the above equations but is usually near unity. The most severe explosions will involve hoop stress failure with minimum "thinning down" of the container in areas adjacent to the failure. Table 46 gives the yield and tensile strengths of various metals and alloys that define the maximum stresses for deformation and failure of the materials, respectively. These values are for uniform static loadings; for dynamic loadings, they are at least twice as large.

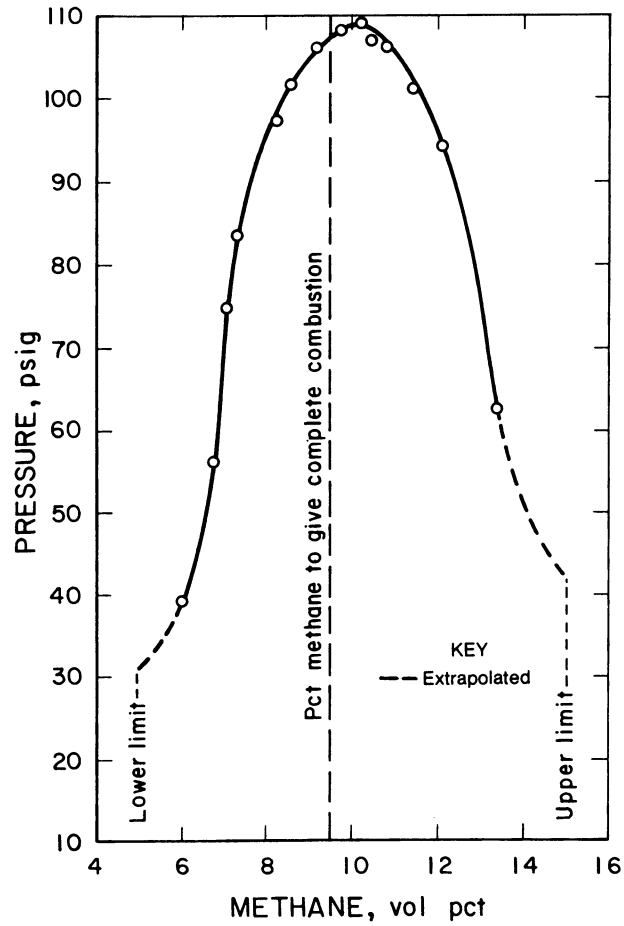

Figure 77.—Effect of fuel concentration on explosion pressures of methane-air mixtures at 25° C and 1 atm.

Table 46. — Mechanical properties of metals and alloys (*83*)

Material	Condition	Yield strength, kpsi	Tensile strength, kpsi
Aluminum alloy (1100)	Annealed	5	13
Aluminum alloy (1100)	Cold-rolled-H 18	22	24
Aluminum alloy (5052)	Annealed	13	28
Aluminum alloy (5052)	Cold-rolled stabilized-H 38	37	42
Aluminum alloy (380)	Die-cast	26	43
Aluminum bronze (612)	Hard	65	105
Brass, red (230)	Cold-rolled	60	75
Copper (102)	Cold-drawn	40	45
Cupronickel (55-45)	Cold-drawn	50	65
Duranickel	Annealed	45	100
Hastelloy (B)	Rolled	56	120
Hastelloy (G)	Sheet	46	102
Incoloy (800)	Annealed	40	90
Inconel (600)	Cold-drawn	100	130
Inconel (610)	As-cast	38	80
Iron, wrought	Hot-rolled	30	48
Iron, gray cast	As-cast	NA	≥25
Magnesium alloy (AZ80A)	Extruded	36	49
Monel (400)	Cold-drawn	80	110
Nickel alloy (220)	Annealed	20	70
Permanickel	Annealed, age-hardened	125	175
Stainless steel (201)	Annealed, strip	50	115
Stainless steel (304)	Annealed	30	85
Stainless steel (304)	Cold-rolled	≤160	≤185
Stainless steel (321 and 347)	Cold-rolled	≤120	≤150
Stainless steel (420)	Heat-treated	200	250
Stainless steel (cast 12 Cr)	Tempered at 315° C	150	200
Stainless steel (cast 20 Cr)	Annealed	60	95
Steel, carbon (SAE 1020)	Hot-rolled	42	68
Tantalum (10W)	Annealed	158	160
Tin	As-cast	NA	2
Titanium (pure)	Annealed	75	85
Zircaloy (2)	Annealed	50	75

NA Not available.

In the case of containments equipped with bolt or screw fasteners, their failure will be determined by the uniform or nonuniform distribution of the pressure loading on all the bolts; the root thread area is used in calculating the loading on a threaded fastener. One should not neglect the stress due to tightening a bolt since this initial load can exceed the tensile strength of ordinary carbon steel material (~60,000 psi) in bolts of less than about 1.25 cm (1/2 in) diameter.

The time at which a vessel or confining structure will fail owing to a gaseous explosion can vary greatly with the combustible-oxidant-diluent mixture and container volume. Figures 78, 79, and 80 (*39*) show the explosion pressure growth rates obtained by Bureau investigators (Johnson, Furno, and Kuchta) in a 3.65-m (12-ft) diameter sphere. In this size vessel, the time to achieve maximum pressure was less than 1 s for the optimum CH_4-air mixture, compared with about 20, 12, and 6 s for near-limit compositions of CH_4-air, CH_4-air-N_2, and CH_4-air-CF_3Br, respectively; note that the effectiveness of the CF_3Br inhibitor tends to be minimal when the pressure rises are above about 30 psig. For ideal spherical explosions at constant flame speeds, the maximum pressure rise rates (dP/dt) or times (t) to maximum pressure may be approximately extrapolated to larger vessel volumes (V) as follows:

$$\frac{(dP/dt)_1}{(dP/dt)_2} = \frac{t_2}{t_1} = \left(\frac{V_2}{V_1}\right)^{1/3} \qquad (81)$$

where the subscripts 1 and 2 refer to the small and large size vessels, respectively. However, this cubic dependence on volume becomes unreliable with the less optimum mixtures or nonspherical propagations, as discussed earlier in connection with equation 49.

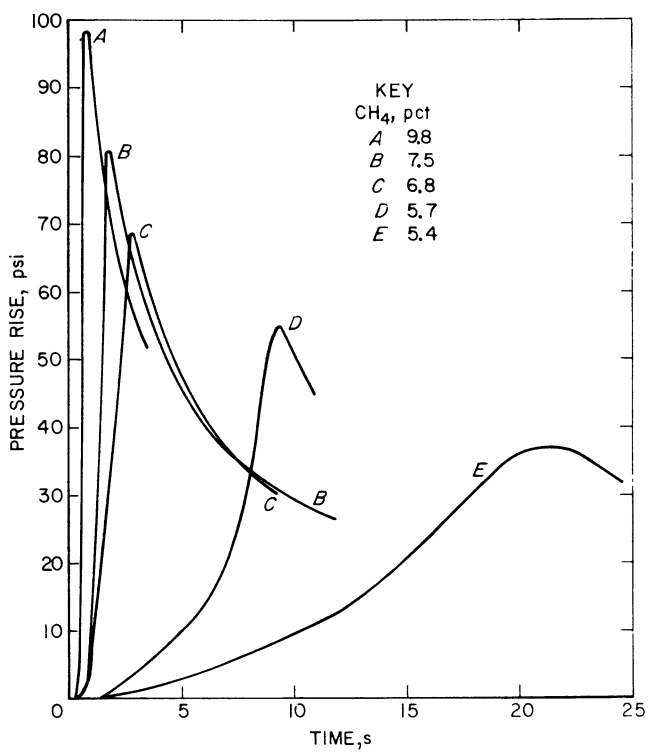

Figure 78.—Explosion pressure growth for methane-air mixtures in 3.65-m (12-ft) diam sphere at 25° C and 1 atm.

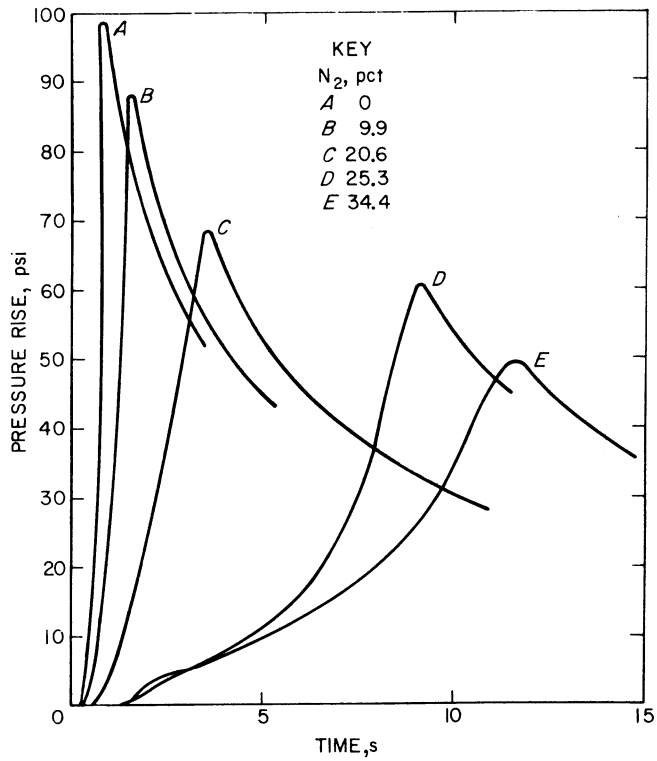

Figure 79.—Explosion pressure growth for 9.5 pct methane-air mixtures and added nitrogen in 3.65-m (12-ft) diam sphere at 25° C and 1 atm.

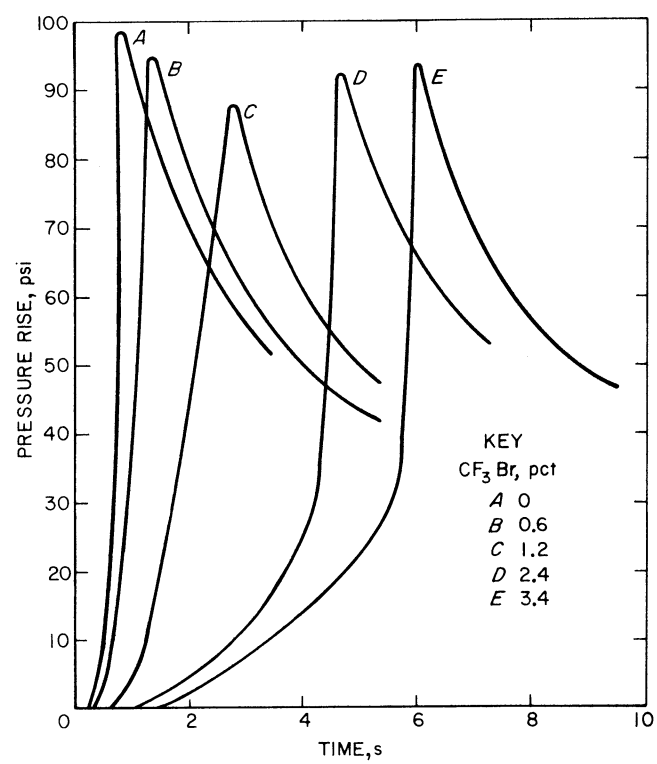

Figure 80.—Explosion pressure growth for 9.5 pct methane-air mixtures and added bromotrifluoromethane (Halon 1301) in 3.65-m (12-ft) diam sphere at 25° C and 1 atm.

Where such explosions are vented, the maximum pressures developed can be limited to a few pounds per square inch or less if the vent area is at least as large as the cross-sectional area of the particular enclosure. The following expression derived by Bureau investigators (*92*) predicts the unrestricted venting requirements for ignitions of hydrocarbon vapor-air-nitrogen mixtures in large spherical or cubical enclosures:

$$A = 13.03 \times 10^{-3} V^{2/3} (E\text{-}1) S_u / c_d \left(\frac{E \rho_u}{P\text{-}P_o}\right)^{1/2} \quad (82)$$

where A is vent area (m^2), V is enclosure volume (m^3), E is expansion ratio of combustion products, S_u is mixture burning velocity (cm/sec), c_d is vent discharge coefficient, ρ_u is density of unburned gas mixture (g/cm^3), P_o is initial pressure (psig), and P is vent control pressure (psig). Predicted pressure rise ($P\text{-}P_o$) as a function of the vent ratio ($A/V^{2/3}$) is shown in figure 81 for methane-air ignitions with 0 to 30 pct added nitrogen; a c_d value of 0.8 is assumed. The calculated venting requirements are most reliable for enclosures with a length-diameter ratio close to unity and are at least as conservative as those found experimentally for deflagrations of hydrocarbon-air systems. They are particularly useful in the venting of large enclosures or buildings which can tolerate at most a few pounds per square inch of overpressure before structural failure.

Rasbash (*86*) developed the following expression for venting large buildings using propane-air mixtures:

$$P_m = 1.5\ P_v + 0.5\ K;\ K = 1 \text{ to } 5 \quad (83)$$

where P_m (psi) is maximum pressure during venting, P_v (psi) is pressure when venting starts, and K is ratio of smallest cross-sectional area of building to total vent area. The expression is limited to building length-width ratios of up to 3 and vent materials that rupture or open below 1 psi. For venting ducts, the maximum pressure (P_m, psi) is given by

$$P_m = 1.8\ K \quad ;\ K = 2 \text{ to } 32 \quad (84)$$

$$P_m = 0.35\ L/D + 0.9\ K;\ K = 1 \text{ to } 2 \quad (85)$$

where L/D is length-diameter ratio of duct and K is ratio of duct cross-sectional area to vent area. These equations were derived by Rasbash (*85*) and limited to unobstructed ducts, gas mixture flame speeds of less than 3 m/s, and L/D ratios between 6 and 30; higher pressures result with obstructed ducts. In both ducts and buildings or enclosures, the maximum pressure will tend to be minimal when the area vent ratio (K) is unity or less.

In vented and unvented systems, explosion pressures will be greater with turbulent mixtures than with quiescent ones. On the other hand, the explosion pressure hazard is greatly reduced when the mixture is of borderline flammability and only capable of upward flame propagation. Furno's data (*22*) for lean H_2-air mixtures (fig. 82) and rich C_4H_{10}-air mixtures (fig. 83) are classic examples; note that pressure rises are minimal until fuel concentrations are capable of both upward and downward propagation. In comparison, lean CH_4-air or CO-air mixtures do not have greatly different upward limits and downward limits of propagation. Burgess (*5*) found such trends consistent with preferential diffusion effects and showed the stoichiometric ratio of upward-downward limits to correlate with the square root ratio of the oxygen-fuel diffusivities.

Gaseous detonations may be assumed to produce explosion pressures of about twice the values for constant-volume deflagrations (equation 52) and maximum pressure rise ratios (P_2/P_1) of about 18:1; reflected pressures are higher but are not greatly destructive because of their very short duration. Container failures due to detonations will be typically characterized by fine fragmentation of brittle materials, shear or hoop stress failures of ductile materials, "peeling back" of failed ductile materials as in tube failures, and relatively far field damage due to flying fragments and blast waves. Blast wave damage is treated in the next section. One should understand that gaseous deflagrations at high pressures can produce localized material damage that can be as severe as that of gaseous detonations.

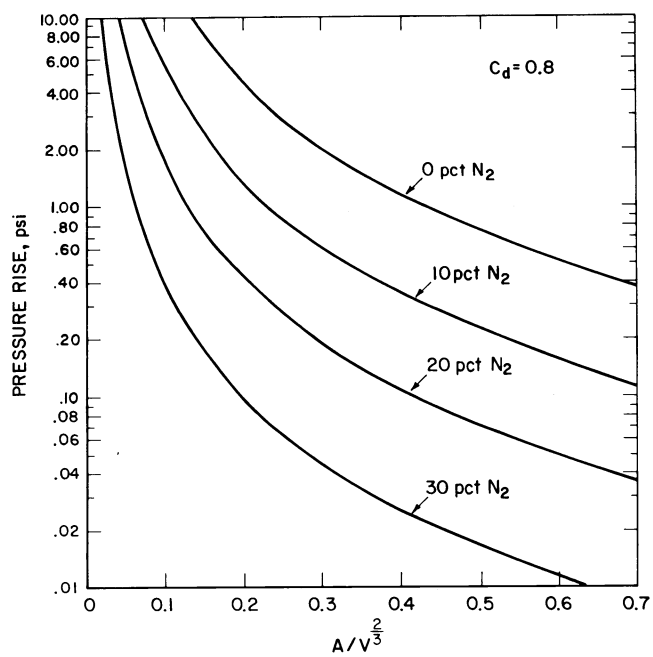

Figure 81.—Calculated pressure rise versus vent ratio ($A/V^{2/3}$) for stoichiometric methane-air ignitions with 0, 10, 20, and 30 pct added nitrogen at 25° C and 1 atm.

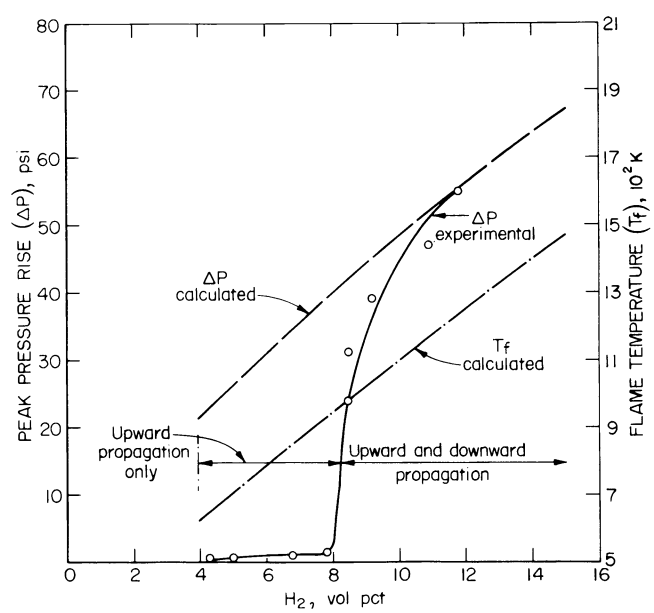

Figure 82.—Peak pressure rises and flame temperatures for H_2-air mixtures in 3.65-m (12-ft) diam sphere at 25° C and 1 atm.

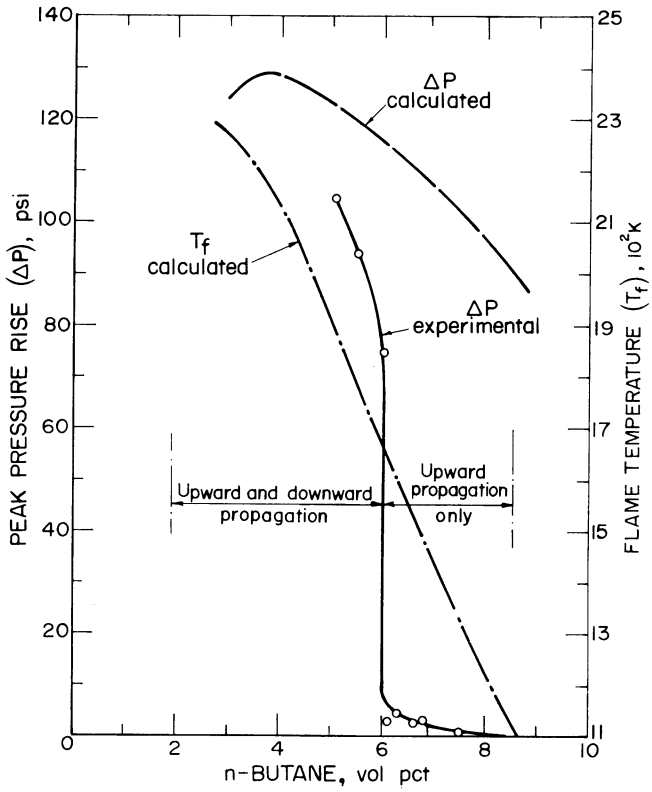

Figure 83.—Peak pressure rises and flame temperatures for C_4H_{10}-air mixtures in 3.65-m (12-ft) diam sphere at 25° C and 1 atm.

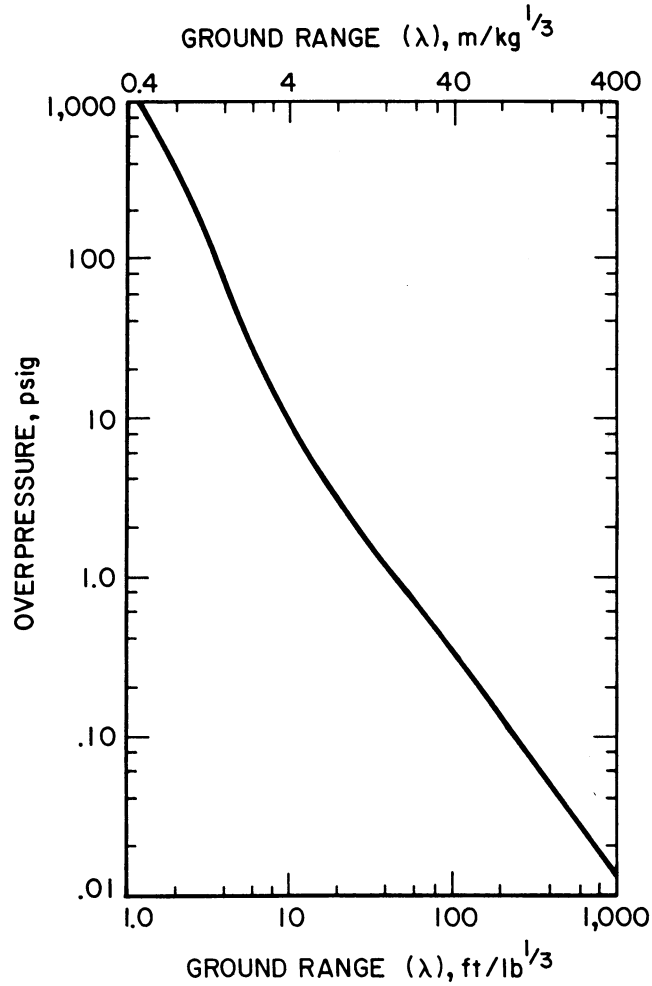

Figure 84.—Peak overpressure versus scaled distance (λ) for hemispherical TNT surface bursts.

BLAST WAVE CRITERIA

The blast wave pressures from weakly confined gaseous deflagrations are small because a large fraction of the available chemical energy is not converted to pressure energy before the container walls fail (see equation 56). In such cases, any pressure energy will be largely dissipated by convection, and the TNT equivalent will be small and not very meaningful. In the case of strongly confined gaseous deflagrations and particularly detonations, their blast pressure energy and TNT equivalence will tend to approximate the energy yield given by their heats of combustion (ΔH_c). By application of the cube root scaling law (equation 55), the blast overpressures of TNT charges are normally plotted as a function of a scaled distance (λ),

$$\lambda = d/W^{1/3}, \qquad (86)$$

where d is distance (ft) and W is charge weight (lb). Figure 84 shows the plot obtained by Kingery (*45*); the peak overpressures refer to the static or side-on pressures of the blastwave. Thus, if a combustible mixture has a TNT equivalence of 454 g (1 lb), the peak overpressure (static) would be approximately 10 psi at a distance of 3.1 m (10 ft); the theoretical chemical energy of the mixture or equivalent TNT (1,100 cal/g) would be 499 kcal (454 g × 1,100 cal/g). Detonation properties of TNT and other explosives are summarized in table 47 (*63*); the listed heat of detonation for TNT (1,400 cal/g) is a high value because of a high TNT density and assumption of condensed $H_2O(l)$ in the explosion products.

Blast wave damage that may occur to structural materials or buildings is given in table 48 (*26*, p. 163) in terms of peak overpressure and in table 49 (*19*) as a function of scaled distance (λ). Figure 84 can be invoked to assess the damage potential in each case as a function of both overpressure and scaled distance relative to TNT. It is important to note in table 48 that most ordinary constructional materials can fail with only a few pounds per square inch overload; these values refer to external pressure loading but can even be lower for internal loading, as in a vessel explosion. Other data by the same author (*26*, p. 253) indicated that an average sized aircraft would suffer severe damage at a blast overpressure of approximately 3 psi and only light damage at 1 psi. With any structural material, the greatest pressure damage will occur to components of minimum thickness and maximum width or length without any material supports or reinforcement.

Biological effects of blast overpressures by Richmond (*87*) are included in figure 85. Note that the lethal overpressure values are for a 400-ms pulse duration and that about 50 psig would be lethal at a 50-pct probability level for a human or animal target. However, since the biological damage is impulse sensitive, the values for both lethal and other biological damage will vary with the pressure pulse duration. Accordingly, the indicated overpressures for biological damage can be substantially greater when the pulse duration is of much shorter duration than 400 ms.

Table 47. — Properties of explosives (*63*)

Explosive	Molecular weight	Nominal density, g/cm³	Heat of[1] detonation, cal/g	Detonation velocity, m/s	Detonation[1] pressure, kbar
PRIMARY HIGH EXPLOSIVES					
Lead azide, PbN_6	291.3	4.8	367	5,180	NA
Lead styphnate, $PbC_6HN_3O_8$	450.3	3.1	457	5,200	NA
Mercury fulminate, $C_2N_2O_2Hg$	284.6	4.4	427	5,000	NA
SECONDARY HIGH EXPLOSIVES					
Baratol, 24 pct TNT + 76 pct Ba $(NO_3)_2$	NA	2.55	560	4,870	140
Comp B, 36 pct TNT + 63 pct RDX	NA	1.72	1,530	7,990	295
LX-04-1, 85 pct HMX + 15 pct Viton A	NA	1.86	1,420	8,460	360
Nitrocellulose, guncotton (≥13.35 pct N)	274.1	1.20	1,260	7,300	210
Nitroglycerine, propanetriol trinitrate	227.1	1.60	1,590	7,700	253
Nitromethane	61.0	1.13	1,940	6,320	140
PETN, pentaerythritol tetranitrate	316.2	1.76	1,650	8,300	305
Pentolite, 50 pct TNT + 50 pct PETN	NA	1.67	1,520	7,470	248
RDX, Trinitrotriazacyclohexane	222.1	1.77	1,620	8,640	338
Tetranitromethane	196.0	1.65	550	NA	144
Tetryl, trinitrophenylmethylnitramine	287.0	1.71	1,520	7,850	250
TNT, trinitrotoluene	227.1	1.64	1,400	6,930	220

[1]Calculated or observed values; heats of detonation refer to maximum calculated values with water formed as liquid; detonation pressures refer to Chapman-Jouquet state.

Table 48. — Peak overpressures for failure of structural materials (*26*, p. 163)

Structural material	Usual failure	Peak blast overpressure, psi
Glass windows	Shattering	0.5-1.0
Corrugated asbestos siding	Shattering	1.0-2.0
Corrugated steel or aluminum paneling	Connection failure and buckling	1.0-2.0
Wood siding panels (standard house construction)	Connection failure and buckling	1.0-2.0
Concrete or cinderblock walls, 8 or 12 in thick (not reinforced)	Shattering	2.0-3.0
Brick walls, 8 or 12 in thick (not reinforced)	Shearing and flexure failures	7.0-8.0

Table 49. — Scaled distance for building damage from statistical survey of chemical explosions (*19*)

Category	Building damage	Scaled distance (λ)	
		ft/lb$^{1/3}$	m/kg$^{1/3}$
A	Demolished, not standing	7.4	2.9
B	Severe damage; standing but substantially destroyed, some walls gone	16.6	6.6
C	Moderate damage; walls bulged, roof cracked or bulged, studs and rafters broken	25.0	9.9
D	Slight damage; doors, sashes, or frames removed; plaster or wallboard broken; shingles or siding off	28.1	11.2
E	Minor damage to glass or miscellaneous small items (similar to that resulting from high wind)	42.7	17.0

An overpressure of 1 psi is reported by Glasstone (*26*) for knocking over a human body but again would be overly conservative for combustible explosions where pressure pulse durations are relatively short.

CRATER AND MISSILE CRITERIA

Ground craters can result only from high-energy explosions, as with solid or condensed-phase explosives that are detonated near the ground surface. By the cube root scaling law, the crater diameter (d) is given by

$$d = d_o W^{1/3}, \quad (87)$$

where W is charge weight and d_o is scaled diameter for a unit weight of the reference explosive. According to Van Dolah (*101*), d_o is approximately 1.5 for a 1-lb charge of TNT with the diameter dimensions in feet. The crater dimensions will depend upon the physical nature of the ground surface and depth of the exploding charge. The crater depth is nominally 1/4 the crater diameter. Many potentially explosive materials such as black powder, smokeless gun propellants, and even ammonium nitrate do not readily detonate and form craters. However, both ammonium nitrate and black powder are capable of detonation and crater formation when they are combusted in massive quantities under high degrees of confinement or with a high explosive ignition stimulus.

Missile damage from the fragmentation of a vessel involving gaseous explosions will depend upon the mass, shape, and velocity of the fragment(s) and the nature of the target material. In such assessments, it is often necessary to assume what fraction of the available chemical energy (strong confinement) or pressure energy (weak confinement) will be converted into kinetic energy ($E = 1/2\ mv^2$) for propelling the fragment; the average velocity (v) of the fragment (gravitational mass m) can then be calculated. High (*33*) gives the following guidelines for estimating the distribution of available energy:

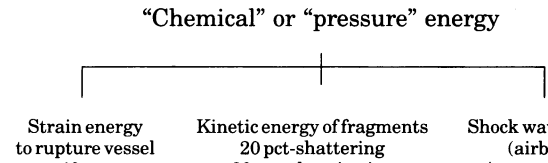

In practice, the pressure energy for estimating kinetic energies gives more realistic values than the chemical energy when the vessel shatters before maximum explosion pressures are realized. Chemical energy refers to theoretical

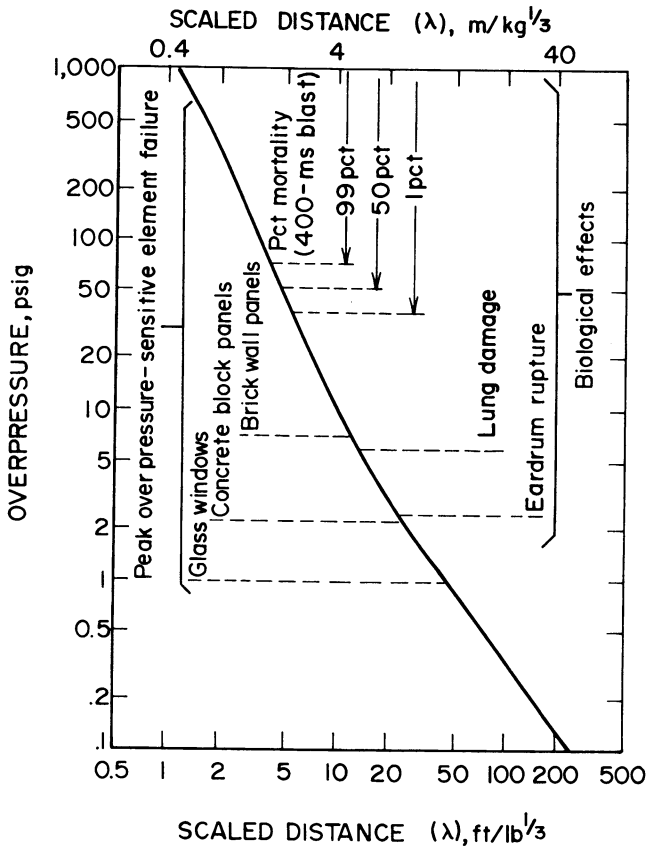

Figure 85.—Peak overpressure and approximate material and biological damage effects from hemispherical TNT surface bursts.

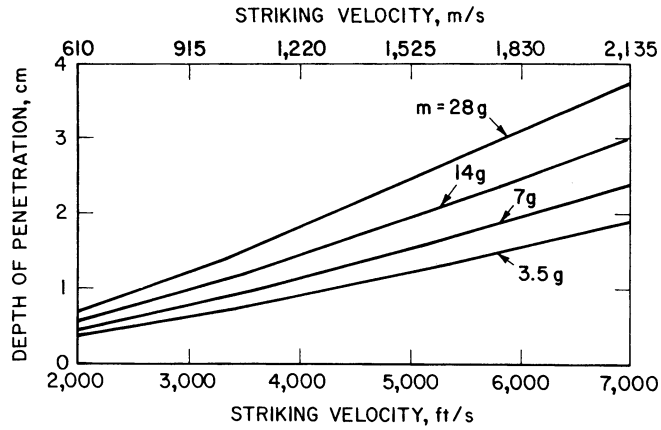

Figure 86.—Depth of penetration of mild steel versus striking velocity for steel fragments of various weights.

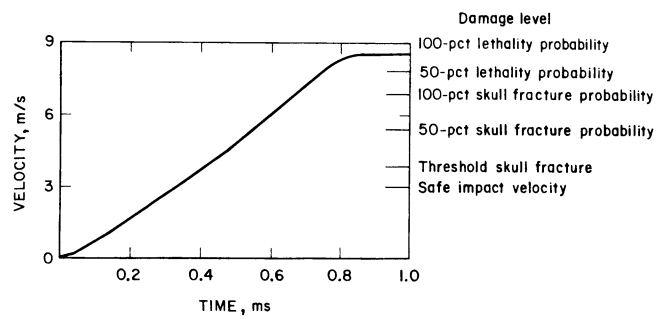

Figure 87.—Velocity-time profile and potential biological damage levels for head or body impacts.

heats of combustion (ΔH_c) or detonation, and pressure energy refers to calculated work outputs (W) assuming adiabatic expansion of products to atmospheric pressure, as given by equation 56,

$$W = \frac{P_2V_2 - P_1V_1}{\gamma - 1}$$

The initial velocity (v_o) of an explosion fragment can be estimated from its distance from the exploding vessel, which is its range (R). From equations of motion, the maximum range is obtained when the trajectory angle (α) of the missile is 45°:

$$R = \frac{v_o^2 \sin 2\alpha}{g}\ ; \qquad (88)$$

also, the maximum height (h) is

$$h = \frac{v_o^2 \sin^2\alpha}{2g}\ , \qquad (89)$$

where g is the gravitational constant (980 cm/s^2 or 32 ft/s^2). The final or striking velocity of the fragment will be less than v_o because of air drag effects, which are greatest for materials with the largest face areas; this effect will be noticeable over small trajectory ranges.

A useful equation (Demarre's) for predicting the penetration of irregular steel fragments into mild steel plates or similar targets is

$$P_d = kW^{1/3}\left(\frac{v}{1000}\right)^{4/3} \qquad (90)$$

where k is 0.112 for mild steel when the dimensions of the penetration depth (P_d, in), fragment weight (W, oz), and striking velocity (v, ft/s) are in the specified English units. Figure 86 (*84*) shows the predicted values by this equation for fragment weights of 1/8 oz (~3.5 g) to 1 oz (~28 g). The velocity range of 2,000 to 3,000 ft/s (~600 to 900 m/s) is comparable to the muzzle velocity of a ·30-caliber rifle weapon. Compared to a concrete-type target, steel may be considered to offer about 10 times greater penetration resistance (*101*).

Human targets have low impact-velocity thresholds for biological damage. Figure 87 (*87*) compares the blast-induced translational velocities of a nylon sphere (1/8-in diam) with various velocity damage thresholds that can result from head or total body impacts; the sphere data reflect the velocity change for the impacts. Of particular significance is that the threshold impact velocity is only about 15 ft/s (~4.5 m/s) for a skull fracture and 30 ft/s (~9 m/s) for a 100-pct lethal probability. Because of many uncertainties in making such correlations, the human damage levels should not be considered as precise values but as approximate values that are generally on the conservative side on the basis of available data.

In the case of cased explosives, the prediction of kinetic energy velocities is complicated by the distribution of energy to the case material and the explosive products. The conversion of available energy to kinetic energy is much greater than in gaseous deflagrations and can be 60 pct or so. Damage by explosives, which is beyond the scope of this report, has been summarized by Van Dolah and other Bureau investigators (*101*).

REFERENCES

1. Affens, W.A. Flammability Properties of Hydrocarbon Fuels. Part I—Interrelations of Flammability of n-Alkanes in Air. U.S. Nav. Res. Lab., NRL Rep. 6270, May 25, 1965, 24 pp.

2. American Gas Association. Combustion of Gas. Catalog H20010, Sept. 1967, pp. 2-48 to 2-61.

3. Andrews, G.E., and D. Bradley. The Burning Velocity of Methane-Air Mixtures. Combust. and Flame, v. 19, 1972, pp. 275-288.

4. Baumeister, T., and L.S. Marks. Standard Handbook for Mechanical Engineers. McGraw-Hill, 7th ed., 1969, sec. 4, 89 pp.

5. Burgess, D.S., A.L. Furno, J.M. Kuchta, and K.E. Mura. Flammability of Mixed Gases. BuMines RI 8709, 1982, 20 pp.

6. Burgess, D.S., J.N. Murphy, N.E. Hanna, and R.W. Van Dolah. Large-Scale Studies of Gas Detonations. BuMines RI 7196, 1968, 53 pp.

7. Burgess, D.S., and M.G. Zabetakis. Fire and Explosion Hazards Associated With Liquefied Natural Gas. BuMines RI 6099, 1962, 34 pp.

8. Calcote, H.F., C.A. Gregory, C.M. Barnett, and R.B. Gilmer. Spark Ignition: Effect of Molecular Structure. Ind. and Eng. Chem., v. 44, 1952, pp. 2656-2662.

9. Cato, R., W.H. Gilbert, and J.M. Kuchta. Effect of Temperature on Upper Limits of Flammability of Hydrocarbon Fuel Vapor-Air Mixtures. Fire Technol., v. 3, No. 1, 1967, pp. 14-19.

10. Conti, R.S., K.L. Cashdollar, M. Hertzberg, and I. Liebman. Thermal and Electrical Ignitability of Dust Clouds. BuMines RI 8798, 1983, 40 pp.

11. Coward, H.F., and G.W. Jones. Limits of Flammability of Gases and Vapors. BuMines 503, 1952, 155 pp.

12. Diamond, W.P., and J.R. Levine. Direct Method Determination of the Gas Content of Coal: Procedures and Results. BuMines RI 8515, 1981, 36 pp.

13. Dorsett, H.G., Jr., M. Jacobson, F.J. Nagy, and R.P. Williams. Laboratory Equipment and Test Procedures for Evaluating Explosibility of Dusts. BuMines RI 5624, 1960, 21 pp.

14. Dorsett, H.G., Jr., and J. Nagy. Dust Explosibility of Chemicals, Drugs, Dyes and Pesticides. BuMines RI 7132, 1968, 23 pp.

15. Dufour, R.E., and W.C. Westerberg. An Investigation of 15 Flammable Gases or Vapors With Respect to Explosionproof Electrical Equipment. Fire J v. 62, No. 4, 1968, p. 8

16. Dugger, G.L., R.C. Weast, and S. Heimel. Effect of Preflame Reaction on Flame Velocity of Propane—Air Mixtures. Paper in Fifth Symposium (International) on Combustion. Reinhold, 1955, pp. 589-595.

17. Ellis, W.H. Solvent Flash Points—Expected and Unexpected. J. Coat. Technol., v. 48, No. 614, 1976, pp. 44-57.

18. Fenn, J.B. Lean Flammability Limit and Minimum Spark Ignition Energy. Ind. and Eng. Chem., v. 43, 1951, pp. 2865-2869.

19. Filler, W.S., J.M. Rossi, and H.R.J. Walsh. Barricade Effectiveness Evaluated From Records of Accidental Explosions. Armed Services Explosives Safety Board Work Group, Rep. AD 487554 L, July 1966, 56 pp.

20. Forshey, D.R., J.C. Cooper, G.H. Martindill, and J.M. Kuchta. Potential Hazards of Propargyl Halids and Allene. Fire Technol., v. 5, No. 2, 1960, pp. 100-111.

21. Frank-Kamenetskii, D.A. Diffusion and Heat Exchange in Chemical Kinetics. Princeton Univ. Press, 1955, 370 pp.

22. Furno, A.L., E.B. Cook, J.M. Kuchta, and D.S. Burgess. Some Observations on Near-Limit Flames. Paper on Thirteenth Symposium (International) on Combustion. The Combustion Institute, 1971, pp. 593-599.

23. Furno, A.L., A.C. Imhof, and J.M. Kuchta. Effect of Pressure and Oxidant Concentration on Autoignition Temperatures of Selected Combutibles in Various Oxygen and Nitrogen Tetroxide Atmospheres. J. Chem. and Eng. Data, v. 13, No. 2, 1968, pp. 243-249.

24. Gaydon, A.G., and H.G. Wolfhard. Flames, Their Structure, Radiation, and Temperature. Chapman and Hall, 2d ed., 1960, 383 pp.

25. Gibbs, G.J., and H.F. Calcote. Effect of Molecular Structure on Burning Velocity. J. Chem. and Eng. Data, v. 4, July 1959, pp. 226-237.

26. Glasstone, S. The Effects of Nuclear Weapons. U.S. Atomic Energy Commission, Apr. 1962, 730 pp.

27. _____. Thermodynamics for Chemists. Van Nostrand, 1947, 522 pp.

28. Gordon, J.S. Thermodynamics of High Temperature Gas Mixtures and Application to Combustion Problems. WADC Tech. Rep. 57-33, Jan. 1957, 172 pp.

29. Grosse, A.V., and J.B. Conway. Combustion of Metals in Oxygen. Ind. and Eng. Chem., v. 50, 1958, pp. 663-672.

30. Hertzberg, M. The Theory of Flammability Limits. Radiative Losses and Selective Diffusional Demixing. BuMines RI 8607, 1982, 38 pp.

31. Hertzberg, M., K.L. Cashdollar, and J.J. Opferman. The Flammability of Coal Dust-Air Mixtures. Lean Limits, Flame Temperatures, Ignition Engines, and Particle Size Effects. BuMines RI 8360, 1979, 70 pp.

32. High, R.W. The Saturn Fireball. Ann. NY Acad. Sci., v. 152, art. 1, 1968, pp. 441-451.

33. High, W.G. The Design and Scale Model Testing of a Cubicle To House Oxidation or High Pressure Equipment. Chem. and Ind., 1967, pp. 899-910.

34. Hougen, O.A., and K.M. Watson. Chemical Process Principles. Part II. Wiley, 1947, pp. 437-804.

35. Humphrey, H.B., and G. Morgis. Safety With Solvents. BuMines IC 7757, 1956, 25 pp.

36. Jacobson, M., A.R. Cooper, and J. Nagy. Explosibility of Metal Powders. BuMines RI 6516, 1964, 25 pp.

37. Jacobson, M., J. Nagy, and A.R. Cooper. Explosibility of Dusts Used in the Plastics Industry. BuMines RI 5971, 1962, 30 pp.

38. Jacobson, M., J. Nagy, A.R. Cooper, and F.J. Ball. Explosibility of Agricultural Dusts. BuMines RI 5753, 1961, 23 pp.

39. Johnson, A.L., A.L. Furno, and J.M. Kuchta. Infrared Spectral Radiances and Explosion Properties of Inhibited Methane-Air Flames. BuMines RI 8246, 1977, 22 pp.

40. Jones, G.W., and G. St. J. Perrot. Oxygen Required for the Propagation of Hydrogen, Carbon Monoxide, and Methane Flames. Ind. and Eng. Chem., v. 19, 1927, pp. 985-989.

41. Jones, G.W., M.G. Zabetakis, J.K. Richmond, G.S. Scott, and A.L. Furno. Research on the Flammability Characteristics of Aircraft Fuels. Wright Air Dev. Cent., Tech. Rep. 52-35, 1952, 93 pp.

42. _____. Wright Air Development Center Technical Report 52-35. Supplement I, 1954, 57 pp.

43. Keenan, J.H., and J. Kaye. Gas Tables. Wiley, 1949, 238 pp.

44. Kennedy, R.E., I. Spolan, W.K. Mock, and G.S. Scott. Effect of High Pressures on the Explosibility of Ethane, Air, and Carbon Dioxide and of Ethane, Air, and Nitrogen. BuMines RI 4751, 1950, 11 pp.

45. Kingery, C., and B. Pannill. Peak Overpressure Versus Scaled Distance for TNT Surface Burst (Hemispherical Charges). Ballistics Res. Lab., Aberdeen, MD, BRL Memo. Rep. 1518, 1964, 22 pp.

46. Kogarko, S.M. Detonation of Methane-Air Mixtures and the Detonation Limits of Hydrocarbon-Air Mixtures in a Large Diameter Pipe. Soviet Phys., Tech Phys., v. 3, 1958, pp. 1904-1916.

47. Kuchta, J.M. Fire and Explosion Manual for Aircraft Accident Investigators. Wright-Patterson Air Force Base, Tech. Rep. AFAPL-TR-73-74, 1973, 117 pp.

48. _____. Summary of Ignition Properties of Jet Fuels and Other Aircraft Combustible Fluids. Air Force Aeropropulsion Lab., Wright-Patterson Air Force Base, Tech. Rep. AFAPL-TR-75-70, Sept. 1975, 54 pp.

49. Kuchta, J.M., A. Bartkowiak, and M.G. Zabetakis. Autoignition of Hydrocarbon Jet Fuel. BuMines RI 6654, 1965, 25 pp.

50. _____. Hot Surface Ignition Temperatures of Hydrocarbon Fuel Vapor-Air Mixtures. J. Chem. and Eng. Data, v. 10, 1965, pp. 282-288.

51. Kuchta, J.M., and R.J. Cato. Hot Gas Ignition Temperatures of Hydrocarbon Fuel Vapor-Air Mixtures. BuMines RI 6857, 1966, 14 pp.

52. _____. Ignition and Flammability Properties of Lubricants. SAE Trans., v. 77, 1968, pp. 1008-1020.

53. Kuchta, J.M., R.J. Cato, G.H. Martindill, and W. Gilbert. Ignition Characteristics of Fuels and Lubricants. Air Force Aeropropulsion Lab., Tech. Rep. AFAPL-TR-66-21, Mar. 1966, 71 pp.

54. Kuchta, J.M., A.L. Furno, A. Bartkowiak, and G.H. Martindill. Effect of Pressure and Temperature on Flammability Limits of Chlorinated Combustibles in Oxygen-Nitrogen and Nitrogen Tetroxide-Nitrogen Atmospheres. J. Chem. and Eng. Data, v. 13, 1968, pp. 421-428.

55. Kuchta, J.M., A.L. Furno, and A.C. Imhof. Classification Test Methods for Oxidizing Materials. BuMines RI 7594, 1974, 13 pp.

56. Kuchta, J.M., A.L. Furno, and G.H. Martindill. Flammability of Fabrics and Other Materials in Oxygen-Enriched Atmospheres. Part I. Ignition Temperatures and Flame Spread Rates. Fire Technol., v. 5, 1969, pp. 203-216.

57. Kuchta, J.M., S. Lambiris, and M.G. Zabetakis. Flammability and Autoignition of Hydrocarbon Fuels Under Static and Dynamic Conditions. BuMines RI 5992, 1962, 21 pp.

58. Kuchta, J.M., V.R. Rowe, and D.S. Burgess. Spontaneous Combustion Susceptibility of U.S. Coals. BuMines RI 8474, 1980, 37 pp.

59. Kuchta, J.M., M.J. Sapko, F.J. Perzak, and K.E. Mura. Improved Fire Resistance Test for Belt Materials. Fire Technol., v. 17, No. 2, 1981, pp. 120-130.

60. Kuchta, J.M., and A.F. Smith. Classification Test Methods for Flammable Solids. BuMines RI 7593, 1972, 13 pp.

61. Laffitte, P. Science of Petroleum. Oxford Univ. Press, v. 4, 1938, p. 2995.

62. Laurendeau, N.M., and I. Glassman. Ignition Temperatures of Metals in Oxygen Atmospheres. Combus. Sci. and Technol., v. 3, 1971, pp. 77-82.

63. Lawrence Radiation Laboratory. Properties of Chemical Explosives. Univ. CA, Livermore, CA, AEC Contract W-7405-eng-48, Rep. WCRL-14952, Dec. 16, 1965, 75 pp.

64. Lawson, D.I., and D. Hird. Radiation From Burning Buildings. Fire Office Committee, London Fire Protection Assoc., June 1953, 12 pp.

65. Le Chatelier, H., and O. Boudouard. Limits of Flammability of Gaseous Mixtures. Bull. Soc. Chim. (Paris), v. 19, 1898, pp., 483-488.

66. Lewis, B., and G. von Elbe. Combustion, Flames and Explosions of Gases. Academic, 2d ed., 1961, 731 pp.

67. Litchfield, E.L. Minimum Ignition-Energy Concept and Its Application to Safety Engineering. BuMines RI 5671, 1960, 10 pp.

68. Litchfield, E.L., J.M. Kuchta, and A.L. Furno. Flammability of Propellant Combinations. BuMines Explosives Res. Rep. 3958, June 30, 1965, 83 pp.; available from BuMines library, P.O. Box 18070, Cochran Mills Rd., Pittsburgh, PA 15236: attention Ms. K. Stabryla.

69. _____. Flammability of Propellant Combinations. BuMines Explosives Res. Rep. 3997, Oct. 30, 1966, 69 pp.; available from BuMines library, P.O. Box 18070, Cochran Mills Rd., Pittsburgh, PA 15236: attention Ms. K. Stabryla.

70. Lloyd, P. The Fuel Problem in Gas Turbines. Inst. Mech. Eng. Proc., War Emergency Issue No. 41, v. 159, 1948, p. 220.

71. Lunn, G.A., and H. Phillips. A Summary of Experimental Data on the Maximum Experimental Safe Gap. Safety in Mines Research Establishment (Sheffield, England), SMRE Rep. R2, 1973, 39 pp.

72. McKinnon, G.P., and K. Towers (eds.). Fire Protection Handbook. National Fire Protection Assoc., Boston, MA, 14th ed., 1977, sec. 3, 210 pp.

73. Ministry of Labour, United Kingdom. Guide to the Use of Flame Arrestors and Explosion Reliefs. New Series No. 34, H.M. Stat. Office, Aug. 1965, 55 pp.

74. Morrison, R.B. A Shock Tube Investigation of Detonative Combustion. Univ. of MI, UMM-97, 1955, 121 pp.

75. Nagy, J. The Explosion Hazard in Mining. MSHA, IR 1119, 1981, 69 pp.

76. Nagy, J., H.G. Dorsett, Jr., and A.R. Cooper. Explosibility of Carbonaceous Dusts. BuMines RI 6597, 1965, 30 pp.

77. Nagy, J., H.G. Dorsett, Jr., and M. Jacobson. Preventing Ignition of Dust Dispersions by Inerting. BuMines RI 6543, 1964, 29 pp.

78. National Fire Protection Association. Fire Hazards in Oxygen-Enriched Atmospheres. NFPA 53 M, 1979, 94 pp.

79. _____. Halogenated Extinguishing Agent Systems—Halon 1211. NFPA 12 B, 1972, 45 pp.

80. _____. Halogenated Extinguishing Agent Systems—Halon 1301. NFPA 12 A, 1971, 70 pp.

81. Palmer, K.N. The Quenching of Flame by Wire Gauzes. Paper in 7th Symposium (International) on Combustion. Butterworths, 1959, pp. 497-503.

82. Perlee, H.E., G.S. Scott, and G.H. Martindill. Flammability Characteristics of Trichloroethylene. BuMines RI 6766, 1966, 8 pp.

83. Perry, R.H., and C.H. Chilton (eds.). Chemical Engineer's Handbook. McGraw-Hill, 5th ed., New York, 1973, sec. 23, 74 pp.

84. Petes, J. Blast and Fragmentation Characteristics, Prevention of and Protection Against Accidental Explosion of Munitions, Fuels, and Other Hazardous Materials. Ann. NY Acad. Sci., v. 152, Oct. 1968, p. 283-316.

85. Rasbash, D.J., and Z.W. Rogowski. Relief of Explosions in Duct Systems. Paper in Proceedings Symposium on Chemical Process Hazards. Inst. Chem. Eng., London, 1961, pp. 58-68.

86. Rasbash, D.J., and K.L. Stretch. Explosions in Domestic Structures. Structural Eng., v. 47 No. 10, 1969, pp. 403-411.

87. Richmond, D.R., and C.S. White. Biological Effects of Blast and Shock. Lovelace Foundation, DASA-1177, Apr. 1966, p. 39.

88. Richmond, J.K., I. Liebman, A.E. Bruszak, and L.F. Miller. A Physical Description of Coal Mine Explosions. Part II. Paper in 17th Symposium (International) on Combustion. The Combustion Institute, 1978, pp. 1257-1268.

89. Richmond, J.K., I. Liebman, and L.F. Miller. Effect of Rock Dust on Explosibility of Coal Dust. BuMines RI 8077, 1975, 34 pp.

90. Richmond, J.K., M.J. Sapko, and L.F. Miller. Fire and Explosion Properties of Oil Shale. BuMines RI 8726, 1982, 39 pp.

91. Rossini, F.D., and others. Selected Values of Properties of Hydrocarbons. NBS Circ. C461, 1947, 483 pp.

92. Sapko, M., A.L. Furno, and J.M. Kuchta. Flame and Pressure Development of Large-Scale CH_4-Air-N_2 Explosions: Buoyancy Effects and Venting Requirements. BuMines RI 8176, 1976, 32 pp.

93. Semenov, N.N. Thermal Theory of Combustion and Explosion. Nat. Advisory Committee for Aeronautics, Tech Memo 1024, Aug. 1942, 55 pp.

94. Setchkin, N.P. Self-Ignition Temperatures of Combustible Liquids. J. Res. NBS, v. 53, 1954, Res. Paper 2516, pp. 49-66.

95. Simon, D.M. Flame Propagation. Ind. and Eng. Chem., v. 43, 1951, p. 2718.

96. Singer, J.M., J. Grumer, and E.B. Cook. Burning Velocities by the Bunsen-Burner Method. Paper in Proceedings, Aerothermochemical Gas Dynamics Symposium. Northwestern University, 1955, pp. 139-150.

97. Sondreal, E.A., and R.C. Ellman. Laboratory Determination of Factors Affecting Storage of North Dakota Lignite: Computer Simulation of Spontaneous Heatings. BuMines RI 7887, 1974, 83 pp.

98. Spalding, D.B. Some Fundamentals of Combustion. Butterworth, 1955, 250 pp.

99. Stull, D.R. Vapor Pressure of Pure Substances—Organic Compounds. Ind. and Eng. Chem., v. 39, 1947, pp. 517-536.

100. Stull, D.R., E.F. Westrum, and G.C. Sinke. The Chemical Thermodynamics of Organic Compounds. Wiley, 1969, 865 pp.

101. Van Dolah, R.W., and D.S. Burgess. Explosion Problems in the Chemical Industry. ACS, 1970, 172 pp.

102. Van Dolah, R.W., M.G. Zabetakis, D.S. Burgess, and G.S. Scott. Review of Fire and Explosion Hazards of Flight Vehicle Combustibles. BuMines IC 8137, 1963, 80 pp.

103. Vanpee, M., and A.E. Bruszak. The Ignition of Combustible Mixtures by Laminar Jets of Gases. BuMines RI 6293, 1963, 84 pp.

104. Vanpee, M., and H.G. Wolfhard. Ignition by Hot Gases. BuMines RI 5627, 1960, 12 pp.

105. Weast, R.C. (ed.). Handbook of Chemistry and Physics. Chemical Rubber Co., Cleveland, OH, 53d ed., 1972-73, sec. B, 551 pp; sec. C, 777 pp; sec. D, 235 pp; sec. F, 309 pp.

106. Weir, A., Jr., and R.B. Morrison. Equilibrium Temperature and Composition Behind a Detonative Wave. Ind. and Eng. Chem., v. 46, 1954, p. 1056.

107. White, A.G. Limits for the Propagation of Flame in Inflammable Gas-Air Mixtures III. The Effect of Temperature on the Limits. J. Chem. Soc., v. 127, 1925, pp. 672-684.

108. Wolfhard, H.G. The Ignition of Combustible Mixtures by Hot Gases. Jet Propulsion, v. 28, 1958, pp. 798-804.

109. Yumoto, T. Fire Spread Between Two Oil Tanks. J. Fire and Flammability, v. 8, 1977, pp. 494-505.

110. Zabetakis, M.G. Flammability Characteristics of Combustible Gases and Vapors. BuMines B 627, 1965, 121 pp.

111. Zabetakis, M.G., and D.S. Burgess. Research on the Hazards Associated With the Production and Handling of Liquid Hydrogen. BuMines RI 5707, 1961, 50 pp.

112. Zabetakis, M.G., A.L. Furno, and G.W. Jones. Minimum Spontaneous Ignition Temperatures of Combustibles in Air. Ind. and Eng. Chem., v. 46, 1954, pp. 2173-2178.

113. Zabetakis, M.G., A.L. Furno, and J.J. Miller. Research on the Flammability Characteristics of Aircraft Hydraulic Fluids. Wright Air Devel. Cent., Tech. Rep. 57-151, 1957, pp. 28.

114. Zabetakis, M.G., G.W. Jones, G.S. Scott, and A.L. Furno. Research on the Flammability Characteristics of Aircraft Fuels. Wright Air Devel. Cent., Tech. Rep. 52-35, Supplement 4, 1956, 85 pp.

115. Zabetakis, M.G., S. Lambiris, and G.S. Scott. Flame Temperatures of Limit Mixtures. Paper in 7th Symposium (International) on Combustion. Butterworth, 1959, pp. 484-487.

116. Zabetakis, M.G., G.S. Scott, A.C. Imhof, and S. Lambiris. Research on the Flammability Characteristics of Aircraft Hydraulic Fluids. Part II. Wright Air Devel. Cent., Tech. Rep. 57-151, 1959, p. 29.

117. Zabetakis, M.G., G.S. Scott, and G.W. Jones. Limits of Flammability of Paraffin Hydrocarbons in Air. Ind. and Eng. Chem., v. 43, 1951, pp. 2120-2124.

APPENDIX A. — SUMMARY OF COMBUSTION PROPERTIES OF LIQUID AND GASEOUS COMPOUNDS[1] (GASEOUS COMBUSTION IN AIR AT ATMOSPHERIC PRESSURE)

Combustible	Formula	Mol wt	Sp gr (air = 1)	BP, °C	C_{st} (in air), vol pct	ΔH_f (25° C), kcal/mol	ΔH_c (net, 25° C), kcal/mol	Flash-point, °C	Minimum AIT, °C	Flammable limits	
										L_{25}, vol pct	U_{25}, vol pct
PARAFFINIC HYDROCARBONS (STRAIGHT-CHAIN ALKANES)											
Methane	CH_4	16.04	0.55	−164	9.48	−17.9	191.8	[2] −188	630	5.0	15.0
Ethane	C_2H_6	30.07	1.04	−89	5.65	−20.2	341.3	[2] −135	515	3.0	12.4
Propane	C_3H_8	44.11	1.52	−42	4.02	−24.8	488.5	[2] −104	450	2.1	9.5
n-Butane	C_4H_{10}	58.12	2.01	−.5	3.12	−30.2	635.4	[2] −74	370	1.8	8.4
n-Pentane	C_5H_{12}	72.15	2.49	36	2.55	−35.0	782.0	[2] −49	260	1.4	7.8
n-Hexane	C_6H_{14}	86.18	2.98	69	2.16	−40.0	928.9	−23	225	1.2	7.4
n-Heptane	C_7H_{16}	100.21	3.46	98	1.87	−44.9	1,075.8	−3	225	1.1	6.7
n-Octane	C_8H_{18}	114.23	3.94	126	1.65	−49.8	1,222.8	14	220	.95	[3] 6.5
n-Nonane	C_9H_{20}	128.26	4.43	151	1.47	−54.7	1,369.7	31	205	[4] .85	NA
n-Decane	$C_{10}H_{22}$	142.29	4.91	174	1.33	−59.7	1,516.6	46	210	[4] .75	[5] 5.6
n-Dodecane	$C_{12}H_{26}$	170.33	5.88	215	1.12	−69.5	1,810.5	74	204	[2] .60	NA
n-Tetradecane	$C_{14}H_{30}$	198.38	6.85	253	.97	−79.4	2,104.3	107	200	[2] .50	NA
n-Hexadecane	$C_{16}H_{34}$	226.45	7.82	287	.85	−89.2	2,398.2	[2] 126	205	[2] .43	NA
PARAFFINIC HYDROCARBONS (BRANCHED-CHAIN ALKANES)											
2-Methylpropane (isobutane)	C_4H_{10}	58.12	2.07	−12	3.12	−32.2	634	[2] −81	460	1.8	8.4
2-Methylbutane (isopentane)	C_5H_{12}	72.15	2.49	28	2.55	−36.9	780	< −50	420	1.4	7.6
2-Methylpentane	C_6H_{14}	86.18	3.0	60	2.16	−41.7	927	NA	306	1.2	7.0
2,2-Dimethylpropane (neopentane)	C_5H_{12}	72.15	2.5	10	2.55	−39.7	777	NA	450	1.4	7.5
2,2-Dimethylbutane	C_6H_{14}	86.18	3.0	50	2.16	−44.4	925	−48	425	1.2	7.0
2,3-Dimethylpentane	C_7H_{16}	100.21	3.5	90	1.87	−47.6	1,073	NA	335	1.1	6.8
2,2,3-Trimethylbutane	C_7H_{16}	100.21	3.46	81	1.87	−49.0	1,072	NA	420	1.0	NA
2,2,4-Trimethylpentane (isooctane)	C_8H_{18}	114.23	3.9	99	1.65	−53.6	1,219	−12	415	.95	6.0
2,2,3,3-Tetramethylpentane	C_9H_{20}	128.26	4.4	134	1.47	−56.7	1,368	NA	430	.80	[6] 4.9
3,3-Diethylpentane	C_9H_{20}	128.26	4.4	146	1.47	−55.4	1,369	NA	290	[7] .70	[6] 5.7
UNSATURATED HYDROCARBONS (ALKENES AND DIENES)											
Ethylene (ethene)	C_2H_4	28.05	0.97	−104	6.53	12.5	316.2	NA	490	2.7	36
Propylene (propene)	C_3H_6	42.08	1.45	−47	4.45	4.9	460.4	NA	460	2.4	11
α-Butylene (1-butene)	C_4H_8	56.12	1.94	−6.3	3.37	−.03	607.7	NA	385	1.6	10
β-Butylene (2-butene)	C_4H_8	56.12	1.94	3.7	3.37	−1.7	606.0	NA	325	1.7	9.7
n-Amylene (1-pentene)	C_5H_{10}	70.14	2.42	30	2.72	−5.0	754.3	−18 oc	275	1.4	8.7
3-Methyl-1-butene	C_5H_{10}	70.14	2.42	20	2.72	−6.9	752.3	NA	365	1.5	9.1
Propadiene (allene)	C_3H_4	40.07	1.38	−35	4.97	45.9	443.7	NA	NA	2.2	NA
1,3-Butadiene	C_4H_6	54.09	1.87	−4.4	3.67	26.3	576.3	NA	420	2.0	12
2-Methyl-1,3-butadiene (isoprene)	C_5H_8	68.11	2.40	34	2.90	18.1	720	−54	460	2.0	9
UNSATURATED HYDROCARBONS (ACETYLENES)											
Acetylene (ethyne)	C_2H_2	26.04	0.91	−84	7.73	54.2	300.1	NA	305	2.5	100
Methylacetylene (propyne)	C_3H_4	40.07	1.40	−23	4.97	44.3	442.1	NA	340	1.7	NA
CYCLIC HYDROCARBONS (SATURATES)											
Cyclopropane (trimethylene)	C_3H_6	42.08	1.45	−33	4.45	12.7	465	[2] 92	500	2.4	10.4
Cyclobutane	C_4H_8	56.12	1.94	12	3.37	6.4	614	NA	NA	1.8	NA
Cyclopentane	C_5H_{10}	70.14	2.42	49	2.72	−18.5	740.8	NA	380	1.5	NA
Cyclohexane	C_6H_{12}	84.16	2.91	81	2.27	−29.4	881.7	−20	245	1.3	7.8
Cycloheptane	C_7H_{14}	98.19	3.39	118	1.96	−28.5	1,034	NA	NA	1.1	6.7
Ethylcyclobutane	C_6H_{12}	84.16	2.91	71	2.27	NA	880	NA	210	1.2	7.7
Ethylcyclopentane	C_7H_{14}	98.19	3.39	104	1.96	−30.4	1,033	NA	260	1.1	6.7
Methylcyclohexane	C_7H_{14}	98.19	3.39	101	1.96	−37.0	1,026	−4	250	1.1	6.7
Ethylcyclohexane	C_8H_{16}	112.21	1.71	132	1.71	−41.1	1,174	35	260	[8] .95	[8] 6.6
Diethylcyclohexane	$C_{10}H_{20}$	140.26	NA	174	1.38	NA	NA	49	240	[3] .80	[7] 6.0
Pinane	$C_{10}H_{18}$	138.26	NA	169	1.42	NA	NA	NA	NA	[9] .74	[9] 7.2
Bicyclohexyl	$C_{12}H_{22}$	166.31	5.7	238	1.18	−77.6(l)	1,687	74	245	[7] .65	[10] 5.1
Isopropyl bicyclohexyl	$C_{15}H_{28}$	208.37	NA	283	.94	−54.9(l)	2,165	124	230	[10] .52	[11] 4.1

See footnotes on page 77.

APPENDIX A. — SUMMARY OF COMBUSTION PROPERTIES OF LIQUID AND GASEOUS COMPOUNDS[1] (GASEOUS COMBUSTION IN AIR AT ATMOSPHERIC PRESSURE) — Continued

Combustible	Formula	Mol wt	Sp gr (air = 1)	BP, °C	C_{st} (in air), vol pct	ΔH_f (25° C), kcal/mol	ΔH_c (net, 25° C), kcal/mol	Flash-point, °C	Minimum AIT, °C	Flammable limits	
										L_{25}, vol pct	U_{25}, vol pct
CYCLIC HYDROCARBONS (UNSATURATES)											
Methylcyclopentadiene	C_6H_8	80.10	NA	NA	2.55	NA	799	49	445	[7]1.3	[7]7.6
Cyclohexene	C_6H_{10}	82.15	2.8	83	2.40	−1.3	852	NA	310	[7]1.2	NA
Dipentene (dl-limonene)	$C_{10}H_{16}$	136.24	4.7	178	1.47	−13.2(l)	1,390	45	237	[10].75	[10]6.1
α-Pinene (turpentine)	$C_{10}H_{16}$	136.24	4.7	156	1.47	−4.1(l)	1,399	33	255	[7].7	NA
AROMATIC HYDROCARBONS (BENZENES)											
Benzene (benzol)	C_6H_6	78.12	2.69	80	2.72	19.8	757.5	−11	560	[7]1.3	[7]7.9
Toluene	C_7H_8	92.15	3.18	111	2.27	12.0	901.5	4	480	[7]1.2	[7]7.1
Ethylbenzene	C_8H_{10}	106.17	3.67	136	1.96	7.1	1,049	15	430	[7]1.0	[7]6.7
o-Xylene (1,2-dimethylbenzene	C_8H_{10}	106.17	3.67	144	1.96	4.5	1,046	32	530	[7]1.1	[7]6.4
m-Xylene	C_8H_{10}	106.17	3.67	139	1.96	4.1	1,046	29	465	[7]1.1	[7]6.4
p-Xylene	C_8H_{10}	106.17	3.67	138	1.96	4.3	1,046	27	530	[7]1.1	[7]6.6
Cumene (isopropylbenzene)	C_9H_{12}	120.20	4.15	152	1.72	.94	1,194	44	425	[7].88	[7]6.5
p-Cymene	$C_{10}H_{14}$	134.22	4.63	177	1.53	−6.9	1,342	47	435	[7].85	[7]6.5
n-Butylbenzene	$C_{10}H_{14}$	134.22	4.6	183	1.53	−3.3	1,342	71	410	[7].82	[7]5.8
sec-Butylbenzene	$C_{10}H_{14}$	134.22	4.6	173	1.53	−4.2	1,341	52	420	[7].77	[7]5.8
tert-Butylbenzene	$C_{10}H_{14}$	134.22	4.6	169	1.53	−5.4	1,340	60	450	[7].77	[7]5.8
Isobutylbenzene	$C_{10}H_{14}$	134.22	4.6	173	1.53	−5.2	1,340	55	430	[7].82	[9]6.0
p-Diethylbenzene	$C_{10}H_{14}$	134.22	4.6	183	1.53	−5.3	1,340	57	430	[7].80	NA
Styrene (vinylbenzene)	C_8H_8	104.16	3.6	145	2.05	35.2	1,019	32	490	[8]1.1	[6]6.1
Methylstyrene	C_9H_{10}	118.18	4.1	163	1.79	28.3	1,164	57 oc	495	[6].7	NA
AROMATIC HYDROCARBONS (POLYNUCLEAR)											
Naphthalene	$C_{10}H_8$	128.19	4.4	218	1.71	36.1	1,208	79	526	[5]0.88	[8]5.9
1-Methylnaphthalene	$C_{11}H_{10}$	142.20	NA	245	1.53	27.9	1,351	NA	530	[2].80	NA
Tetralin (tetrahydronaphthalene)	$C_{10}H_{12}$	132.21	4.6	208	1.58	6.6	1,294	71	385	[7].84	[10]5.0
Decalin (decahydronaphthalene)	$C_{10}H_{18}$	138.25	4.8	196	1.42	−40.4	1,420	57	250	[7].71	[7]4.9
Dimethyl decalin	$C_{12}H_{22}$	166.30	NA	232	1.18	NA	NA	84	235	[7].67	5.4
Diphenyl (biphenyl)	$C_{12}H_{10}$	154.20	5.31	255	1.42	43.5	1,461	113	540	[7].60	[10]5.8
Diphenylmethane (ditane)	$C_{13}H_{12}$	168.24	5.82	264	1.29	21.3(l)	1,591	130	485	[2].70	NA
2-Isopropylbiphenyl	$C_{15}H_{16}$	196.28	NA	269	1.09	11.8(l)	1,883	140	435	[9].53	[11]3.2
Anthracene	$C_{14}H_{10}$	178.24	6.15	340	1.25	55.2	1,661	121	540	[2].65	NA
p-Terphenyl (diphenylbenzene)	$C_{18}H_{14}$	230.31	NA	376	.97	NA	NA	207 oc	535	[2].96	NA
ALCOHOLS (ALKANOLS AND CYCLOALKANOLS)											
Methanol	CH_3OH	32.04	1.11	65	12.25	−48.1	159	11	385	6.7	[3]36
Ethanol	C_2H_5OH	46.07	1.59	79	6.53	−56.1	306	13	365	3.3	[3]19
n-Propanol	C_3H_7OH	60.11	2.07	97	4.45	−61.6	448	25	440	[4]2.2	[7]14
Isopropanol (2-propanol)	C_3H_7OH	60.11	2.1	82	4.45	−61.6	448	12	399	2.2	[7]12
n-Butanol	C_4H_9OH	74.12	2.56	117	3.37	−65.6	596	29	365	[7]1.7	[7]12
sec-Butanol	C_4H_9OH	74.12	2.6	100	3.37	−69.9	595	24	405	[7]1.7	[7]9.8
tert-Butanol	C_4H_9OH	74.12	2.6	82	3.37	−74.7	591	11	480	[7]1.9	[7]9
Isobutanol (2-methyl-1-propanol)	C_4H_9OH	74.12	2.6	108	3.37	−79.7(l)	586	28	427	[7]1.7	[7]11
n-Pentanol (amyl alcohol)	$C_5H_{11}OH$	88.15	3.04	137	2.72	−72.3	742	38	300	[7]1.4	[7]10
tert-Pentanol	$C_5H_{11}OH$	88.15	3.0	102	2.72	−78.7	738	41	435	[2]1.4	NA
Isopentanol (3-methyl-1-butanol)	$C_5H_{11}OH$	88.15	3.0	129	2.72	−85.2(l)	732	43	350	[7]1.4	[7]9
n-Hexanol	$C_6H_{13}OH$	102.18	3.53	158	2.27	−76.4	892	63	300	[7]1.2	NA
Methyl isobutyl carbinol	$C_6H_{13}OH$	102.18	NA	133	2.27	−103.8(l)	865	41	NA	[6]1.0	[6]5.5
Diisobutyl carbinol	$C_9H_{19}OH$	144.26	5.0	176	1.53	NA	NA	74	NA	[7].82	[7]6.1
Cyclohexanol	$C_6H_{11}OH$	100.16	3.5	161	2.40	−70.4	935	68	300	[5]1.2	NA
1-Methyl cyclohexanol	$C_7H_{13}OH$	114.19	3.9	155	2.05	−88.2(l)	975	65	295	[5]1.0	NA
ALCOHOLS (GLYCOLS)											
Ethylene glycol (1,2-ethanediol)	$C_2H_4(OH)_2$	62.07	2.14	198	7.73	−93.1	268	111	400	[2]3.5	NA
Propylene glycol	$C_3H_6(OH)_2$	76.11	2.52	189	4.97	−119.3(l)	394	99	410	[5]2.6	[6]12.5
Trimethylene glycol	$C_3H_6(OH)_2$	76.11	2.6	214	4.97	NA	NA	NA	400	[2]1.7	NA
Tetramethylene glycol	$C_4H_8(OH)_2$	90.12	NA	235	3.67	NA	NA	NA	390	NA	NA
βButylene glycol	$C_4H_8(OH)_2$	90.12	3.1	204	3.67	−122.9(l)	542	121	395	[2]1.9	NA
Pentamethylene glycol	$C_5H_{10}(OH)_2$	104.15	NA	260	2.90	−105.1(l)	712	129	335	NA	NA

Combustible	Formula	Mol wt	Sp gr (air = 1)	BP, °C	C_{st} (in air), vol pct	ΔH_f (25° C), kcal/mol	ΔH_c (net, 25° C), kcal/mol	Flash-point, °C	Minimum AIT, °C	Flammable limits	
										L_{25}, vol pct	U_{25}, vol pct
ALCOHOLS (GLYCOLS) — continued											
Triethylene glycol	$C_6H_{12}O_2(OH)_2$	150.17	5.17	278	2.72	−191.4(l)	777	156	371	[10]0.9	[9]9.2
Glycerol (1,2,3-propanetriol)	$C_3H_5(OH)_3$	92.11	3.17	290	5.65	−159.8(l)	354	160	370	NA	NA
ALCOHOLS (UNSATURATES AND AROMATICS)											
Propargyl alcohol (2-propynol)	C_3H_3OH	56.07	1.93	114	5.65	10.1	408	36 oc	NA	[4]2.2	[7]14
Allyl alcohol (2-propenol)	C_3H_5OH	58.08	2.0	97	4.97	−31.6	424	21	378	2.5	18
Aldol (3-hydroxybutanal)	$C_2H_4OHC_2H_3O$	88.12	3.0	NA	4.02	−102.9(l)	504	66 oc	250	[2]2.0	NA
Furfuryl alcohol	$CH_2OHC_4H_3O$	98.10	3.4	171	3.67	−66.1(l)	578	75 oc	390	[3]1.8	[7]16
Phenol (carbolic acid)	C_6H_5OH	94.11	3.2	182	2.90	−23.0	715	79	NA	NA	NA
Benzyl alcohol	C_7H_7OH	108.15	3.72	205	2.40	−38.5(l)	851	101	436	NA	NA
m-Cresol (3-methylphenol)	C_7H_7OH	108.15	3.7	202	2.40	−31.6	858	94	559	[10]1.1	NA
ETHERS (ALKYLS)											
Methyl ether (dimethyl ether)	$(CH_3)_2O$	46.07	1.59	−23	6.53	−44.0	316	NA	350	3.4	27
Methyl ethyl ether	$CH_3OC_2H_5$	60.10	2.1	11	4.44	−51.7	462	−37	190	2.0	10
Ethyl ether (diethyl ether)	$C_2H_5)_2O$	74.12	2.56	35	3.37	−60.3	605	−45	160	1.9	36
Ethyl propyl ether	$C_2H_5OC_3H_7$	88.15	3.28	64	2.72	NA	750	−20	NA	1.7	9
Isopropyl ether	$(C_3H_7)_2O$	102.18	3.53	68	2.27	−76.2	893	−28	NA	1.4	7.9
Butyl ether	$(C_4H_9)_2O$	130.22	4.5	142	1.72	−79.8	1,193	25	194	1.5	[6]7.6
Amyl ether (dipentyl ether)	$(C_5H_{11})_2O$	158.29	5.5	190	1.38	−82.5(l)	1,494	57 oc	170	[2].7	NA
Hexyl ether	$(C_6H_{13})_2O$	186.34	5.5	223	1.15	NA	NA	77 oc	185	[2].6	NA
ETHERS (UNSATURATES AND MISCELLANEOUS)											
Ethylene oxide (epoxyethane)	C_2H_4O	44.05	1.5	14	7.72	−12.6	291	NA	429	3.6	100
Propylene oxide	C_3H_6O	58.08	2.0	34	4.97	−22.2	433	−37	464	2.8	37
Methyl vinyl ether	$CH_3OC_2H_3$	58.08	2.0	12	4.97	NA	411	NA	287	2.6	39
Vinyl ether (diethenyl ether)	$(C_2H_3)_2O$	70.09	2.42	28	4.02	−3.0	547	NA	360	1.7	27
Furan (epoxybutadiene)	C_4H_4O	68.07	2.3	31	4.44	−8.3	484	NA	NA	2.3	14.3
Tetrahydrofuran (epoxybutane)	C_4H_8O	72.10	2.5	67	3.67	−44.0	563	−14	321	2.0	NA
p-Dioxane (diethylene dioxide)	$(C_2H_4O)_2$	88.12	3.0	101	4.02	−75.3	532	12	265	2.0	22
Trioxane (metaformaldehyde)	$(CH_2O)_3$	90.08	NA	115	6.53	−124.4(s)	331	45 oc	414	[6]3.6	[6]29
Acetal	$C_2H_4(OC_2H_5)_2$	118.18	4.1	103	2.40	−117.2(l)	852	37	230	1.6	10
Phenyl ether	$(C_6H_5)_2O$	170.21	5.86	258	1.47	−3.5(l)	1,414	115	620	[2].8	NA
ETHERS (CELLOSOLVES)											
Methyl cellosolve (2-methoxyethanol)	$CH_3OC_2H_4OH$	76.11	2.6	125	4.97	−114.8	399	46	380	[8]2.5	[10]20
Ethyl cellosolve	$C_2H_5OC_2H_4OH$	90.12	3.0	135	3.67	NA	NA	94	235	[6]1.8	[6]14
Butyl cellosolve	$C_4H_9OC_2H_4OH$	118.18	4.08	171	2.40	NA	NA	71	245	[10]1.1	[9]11
ALDEHYDES (ALKYLS)											
Formaldehyde (methanal)	HCHO	30.03	1.0	−20	17.32	−27.7	124	NA	430	7.0	73
Acetaldehyde (ethanal)	CH_3CHO	44.05	1.52	21	7.73	−39.8	264	−38	175	4.0	60
Propionaldehyde	C_2H_5CHO	58.08	2.01	49	4.97	−45.9	409	−7 oc	207	2.9	17
Butyraldehyde	C_3H_7CHO	72.12	2.5	76	3.67	−49.0	558	−7	230	2.5	12.5
ALDEHYDES (MISCELLANEOUS)											
Acrolein (2-propenal)	C_2H_3CHO	56.07	1.90	53	5.64	−25.1(l)	373	−26	235	2.8	31
Crotonaldehyde (2-butenal)	C_3H_5CHO	70.09	2.4	104	4.02	−34.5(l)	515	13	232	2.1	[3]16
Furaldehyde	$(C_4H_3O)CHO$	96.09	3.3	162	4.02	−46.6(l)	539	60	316	[6]2.1	[6]19.3
Benzaldehyde	C_6H_5CHO	106.13	3.7	178	2.55	−18.5(l)	813	64	192	NA	NA
Paraldehyde (paraacetaldehyde)	$(CH_3CHO)_3$	132.16	4.56	128	2.72	−164.2(l)	747	36 oc	238	1.3	NA
KETONES (ALKYLS)											
Acetone (propanone)	$(CH_3)_2CO$	58.08	2.01	56	4.97	−52.0	403	−18	465	2.6	13
Methyl ethyl ketone (2-butanone)	$CH_3COC_2H_5$	72.12	2.49	80	3.67	−57.0	548	−6	516	1.9	11

See footnotes on page 77.

APPENDIX A. — SUMMARY OF COMBUSTION PROPERTIES OF LIQUID AND GASEOUS COMPOUNDS[1] (GASEOUS COMBUSTION IN AIR AT ATMOSPHERIC PRESSURE) — Continued

Combustible	Formula	Mol wt	Sp gr (air = 1)	BP, °C	C_{st} (in air), vol pct	ΔH_f (25° C), kcal/mol	ΔH_c (net, 25° C), kcal/mol	Flash-point, °C	Minimum AIT, °C	Flammable limits	
										L_{25}, vol pct	U_{25}, vol pct
KETONES (ALKYLS) — continued											
Diethyl ketone (3-pentanone)	$(C_2H_5)_2CO$	86.14	2.97	102	2.90	− 61.8	692	13 oc	450	1.6	NA
Methyl propyl ketone	$CH_3COC_3H_7$	86.14	2.97	102	2.90	−61.8	692	7	505	1.6	8.2
Methyl butyl ketone	$CH_3COC_4H_9$	100.16	3.46	128	2.40	−78.9	840	35 oc	533	[4]1.2	[7]8
Methyl isobutyl ketone	$CH_3COC_4H_9$	100.16	3.5	117	2.40	−92.9(l)	818	23	460	1.4	7.5
Diisobutyl ketone	$(C_4H_9)_2CO$	142.23	4.9	168	1.59	NA	NA	60	NA	[7].79	[7]6.2
KETONES (MISCELLANEOUS)											
Methyl isopropenyl ketone	$CH_2COC_3H_5$	83.11	2.9	98	3.24	NA	NA	NA	NA	[4]1.8	[4]9
Cyclohexanone	$C_5H_{10}CO$	98.15	3.4	156	2.55	−55.0	798	44	420	[7]1.1	NA
Acetyl acetone (pentanedione)	$(CH_3CO)_2CH_2$	100.13	3.5	139	3.37	−127.6(l)	574	41 oc	340	[2]1.7	NA
Acetophenone (acetylbenzene)	$C_6H_5COCH_3$	120.16	4.1	202	2.16	−20.8	963	82 oc	570	[2]1.1	NA
Isophorone	$C_8H_{14}CO$	138.20	NA	215	1.72	NA	NA	84 oc	460	[6].84	NA
ACIDS (ALKYLS AND AROMATICS)											
Formic acid (methanoic)	HCOOH	46.03	1.6	101	29.53	−90.5	61	[12]69	[12]601	NA	NA
Acetic acid (ethanoic)	CH_3COOH	60.05	2.1	118	9.48	−103.9	200	43	465	[7]5.4	[7]16
Butyric acid (butanoic)	C_3H_7COOH	88.12	3.0	164	4.02	−127.6(l)	480	−72	450	[6]2.0	[6]10
Valeric acid (pentanoic)	C_4H_9COOH	102.13	NA	186	3.12	−117.2	412	96 oc	400	NA	NA
Benzoic acid	C_6H_5COOH	122.13	4.21	249	2.72	−69.4	762	121	570	NA	NA
Adipic acid (hexandioic)	$C_4H_8(COOH)_2$	146.14	5.04	338	3.12	−236.5(s)	617	196	420	[2]1.6	NA
Stearic acid	$C_{17}H_{35}COOH$	284.50	NA	360	.80	−213.1(l)	2,520	196	395	NA	NA
ANHYDRIDES (MISCELLANEOUS)											
Maleic anhydride	$(CHCO)_2O$	98.06	NA	202	6.53	−112.4(s)	322	102	477	[6]1.4	[6]7.1
Acetic anhydride	$(CH_3CO)_2O$	102.09	3.5	140	4.97	−137.6	412	54	390	[4]2.7	[2]10
Phthalic anhydride	$C_6H_4(CO)_2O$	148.12	NA	295	2.72	−110.1(s)	758	152	570	[10]1.2	[11]9.2
ESTERS (ALKYLS)											
Methyl formate (methyl methanoate)	$HCOOCH_3$	60.05	2.07	32	9.48	−83.6	219	−19	465	5.0	23
Ethyl formate	$HCOOC_2H_5$	74.08	2.56	55	5.65	−88.7	367	−20	455	2.8	16
n-Butyl formate	$HCOOC_4H_9$	102.13	3.53	107	3.12	NA	650	18	322	1.7	8.2
Methyl acetate	CH_3COOCH_3	74.08	2.56	57	5.65	−97.9	358	−10	502	3.2	16
Ethyl acetate	$CH_3COOC_2H_5$	88.12	3.04	77	4.02	−105.9(l)	504	−4	427	2.2	11
n-Propyl acetate	$CH_3COOC_3H_7$	102.13	3.53	102	3.12	NA	650	14	450	1.8	[5]8
Isopropyl acetate	$CH_3COOC_3H_7$	102.13	3.5	88	3.12	−124.0(l)	635	4	460	[2]1.7	NA
n-Butyl acetate	$CH_3COOC_4H_9$	116.16	4.01	127	2.55	−126.1(l)	785	22	425	[4]1.4	[7]8
Isobutyl acetate	$CH_3COOC_4H_9$	116.16	4.0	118	2.55	−124.0(l)	787	18	421	2.4	10.5
n-Amyl acetate (pentyl acetate)	$CH_3COOC_5H_{11}$	130.19	4.50	149	2.16	NA	970	25	360	[7]1.0	[7]7.1
Isoamyl acetate	$CH_3COOC_5H_{11}$	130.19	4.5	142	2.16	NA	NA	25	360	[7]1.1	[7]7
Methyl propionate	$C_2H_5COOCH_3$	88.12	3.04	80	4.02	−113.0(l)	494	−2	469	2.4	13
Ethyl propionate	$C_2H_5COOC_2H_5$	102.13	3.53	99	3.12	−114.2(l)	645	12	440	1.8	11
n-Amyl propionate	$C_2H_5COOC_5H_{11}$	144.22	NA	169	1.87	NA	NA	41 oc	380	[2]1.0	NA
Methyl butyrate	$C_3H_7COOCH_3$	102.13	3.52	102	3.12	−119.0(l)	640	14	NA	NA	NA
Ethyl butyrate	$C_3H_7COOC_2H_5$	116.16	4.0	121	2.55	−123.0(l)	788	26	463	NA	NA
n-Butyl stearate	$C_{17}H_{35}COOC_4H_9$	340.60	NA	223	.65	NA	NA	160	355	[2].3	NA
ESTERS (MISCELLANEOUS)											
β-Propiolactone	$C_2H_4CO_2$	72.06	2.5	162	6.53	−67.6	330	74	NA	[3]2.9	NA
γ-Butyrolactone	$C_3H_6CO_2$	86.09	NA	206	4.45	−99.2(l)	450	98 oc	NA	[10]2.0	NA
Vinyl acetate (ethenyl ethanoate)	$CH_3COOC_2H_3$	86.09	3.0	72	4.44	−83.6(l)	466	−8	427	2.6	13.4
Methyl acrylate	$C_2H_3COOCH_3$	86.09	3.0	80	4.44	NA	NA	−3	468	2.8	[6]25
Methyl lactate	$C_2H_4OHCOOCH_3$	104.12	3.6	145	4.45	−152.3(l)	455	49	385	[7]2.2	NA
Ethyl lactate	$C_2H_4OHCOOC_2H_5$	118.13	4.1	155	3.37	−158.6(l)	601	46	400	[7]1.5	NA
Methyl cellosolve acetate	$CH_3COOC_2H_4OCH_3$	118.13	4.1	145	3.37	NA	NA	~44	NA	[10]1.7	[6]8.2
Cyclohexylacetate	$CH_3COOC_6H_{11}$	142.20	4.9	174	1.96	NA	NA	58	335	[2]1.0	NA
Benzyl benzoate	$C_6H_5COOC_7H_7$	212.24	7.3	323	1.29	−65.1(s)	1,598	148	480	[2].7	NA

Combustible	Formula	Mol wt	Sp gr (air = 1)	BP, °C	C_{st} (in air), vol pct	ΔH_f (25° C), kcal/mol	ΔH_c (net, 25° C), kcal/mol	Flash-point, °C	Minimum AIT, °C	Flammable limits	
										L_{25}, vol pct	U_{25}, vol pct
AMINES (ALKYLS)											
Methylamine (aminomethane)	CH_3NH_2	31.06	1.1	−6.3	8.52	−5.5	233	NA	430	4.9	20.7
Ethylamine	$C_2H_5NH_2$	45.09	1.6	17	5.29	−11.0	379	NA	385	3.5	14
n-Propylamine	$C_3H_7NH_2$	59.11	2.0	48	3.83	−17.3	525	−37	318	2.0	10.4
n-Butylamine	$C_4H_9NH_2$	73.14	2.5	78	3.01	−22.0	672	−12	312	1.7	9.8
tert-Butylamine	$C_4H_9NH_2$	73.14	2.5	44	3.01	−28.7	665	NA	380	[7]1.7	[7]8.9
n-Amylamine (aminopentane)	$C_5H_{11}NH_2$	87.16	3.0	103	2.48	NA	NA	7 oc	NA	2.2	NA
Dimethylamine	$(CH_3)_2NH$	45.09	1.6	7.4	5.29	−4.5	386	NA	400	2.8	14.4
Diethylamine	$(C_2H_5)_2NH$	73.14	2.5	56	3.01	−17.3	677	NA	312	1.8	10
Trimethylamine	$(CH_3)_3N$	59.11	NA	2.9	3.83	−5.7	537	NA	NA	2.0	12
Triethylamine	$(C_2H_5)_3N$	101.19	3.5	89	2.10	−23.8	974	7 oc	NA	1.2	8
AMINES (UNSATURATES AND AROMATICS)											
Ethyleneimine (aziridine)	C_2H_4NH	43.07	1.5	56	6.05	29.5	362	−11	320	3.6	46
Allylamine (3-aminopropene)	$C_3H_5NH_2$	57.09	2.0	58	4.22	6.9	491	−29	375	2.2	22
Aniline (phenyl amine)	$C_6H_5NH_2$	93.13	3.2	184	2.63	20.8	787	70	615	[10]1.2	[10]8.3
Diethylaniline	$C_6H_5N(C_2H_5)_2$	149.24	5.0	216	1.47	9.6	1,384	85	630	[2].8	NA
Biphenylamine	$(C_6H_5)_2NH$	169.23	5.8	302	1.40	48.2	1,495	153	635	[2].7	NA
2-Biphenylamine	$C_6H_4NH_2C_6H_5$	169.23	NA	299	1.40	29.1(s)	1,476	NA	450	[2].8	NA
AMINES (PYRIDINE DERIVATIVES)											
Pyridine (azine)	C_5H_5N	79.10	2.7	116	3.24	33.5	648	20	482	[3]1.8	[4]12
3-Methyl pyridine (β-picoline)	$C_5H_4(CH_3)N$	93.13	3.2	144	2.63	25.4	792	NA	500	[2]1.4	NA
Quinoline (benzazine)	C_9H_7N	129.16	4.5	238	1.91	35.7(l)	1,084	NA	480	[2]1.0	NA
Nicotine	$C_{10}H_{14}N_2$	162.24	5.6	246	1.53	10.2(l)	1,355	NA	244	[7].75	NA
AMIDES AND CYANIDES											
Hydrogen cyanide	HCN	27.03	0.9	26	14.34	31.2	154	−18	538	5.6	40
Methyl cyanide (acetonitrile)	CH_3CN	41.05	1.4	82	7.08	21.0	296	6 oc	524	4.4	16
Cyanogen	C_2N_2	52.04	NA	−22	9.47	73.8	262	−62	NA	6.6	32
Vinyl cyanide (acrylonitrile)	C_2H_3CN	53.06	1.8	78	5.29	44.2	413	0 oc	481	3.0	17
Dimethyl formamide	$HCON(CH_3)_2$	73.09	2.5	149	4.69	NA	NA	57	435	[7]1.8	[7]14
Acetone cyanohydrin	C_3H_6OHCN	85.11	2.9	NA	3.84	NA	NA	74	687	[6]2.2	[6]12
Acetanilide (phenylacetamide)	$C_6H_5NHCOCH_3$	135.17	4.65	304	2.10	−50.3(s)	962	174 oc	540	[2]1.0	NA
HYDRAZINES											
Hydrazine	N_2H_4	32.05	1.1	114	17.32	22.8	138	38	270	[6]4.7	[6]100
Methylhydrazine	$CH_3N_2H_3$	46.07	1.6	87	7.73	20.4	259	21	185	4.0	NA
1,1-Dimethylhydrazine (UDMH)	$(CH_3)_2N_2H_2$	60.11	2.1	63	4.97	20.3	440	−6	250	2.0	[7]95
NITRATED COMPOUNDS (NITRO ALKYLS AND AROMATICS)											
Nitromethane	CH_3NO_2	61.04	2.1	101	21.83	−17.9	163	35	418	[6]7.3	NA
Nitroethane	$C_2H_5NO_2$	75.07	2.6	115	8.52	−24.2	308	28	414	3.4	NA
1-Nitropropane	$C_3H_7NO_2$	89.09	3.1	131	5.29	−29.8	454	49 oc	421	[6]2.2	NA
2-Nitropropane	$C_3H_7NO_2$	89.09	3.1	120	5.29	−33.5	451	28	428	[6]2.5	NA
Nitrobenzene (nitrobenzol)	$C_6H_5NO_2$	123.11	4.3	211	3.24	3.8(l)	713	88	482	[5]1.8	NA
o-Nitrotoluene	$C_7H_7NO_2$	137.14	4.7	220	2.63	−.4(l)	860	106	NA	NA	NA
NITRATED COMPOUNDS (NITRITES AND NITRATES)											
Ethyl nitrite	$C_2H_5NO_2$	75.07	2.6	17	8.52	−24.8	308	−35	90	3.0	50
Ethyl nitrate	$C_2H_5NO_3$	91.07	3.1	87	10.68	−36.8	296	10	NA	4.0	NA
n-Propyl nitrate	$C_3H_7NO_3$	105.10	NA	110	6.05	−41.6	443	20	175	[8]1.8	[8]100
n-Amyl nitrite	$C_5H_{11}NO_2$	117.15	4.0	105	3.01	NA	NA	NA	210	[2]1.0	NA
n-Amyl nitrate	$C_5H_{11}NO_3$	133.15	NA	~155	3.24	NA	NA	52 oc	195	[6]1.1	NA

See footnotes on page 77.

APPENDIX A. — SUMMARY OF COMBUSTION PROPERTIES OF LIQUID AND GASEOUS COMPOUNDS[1] (GASEOUS COMBUSTION IN AIR AT ATMOSPHERIC PRESSURE) — Continued

Combustible	Formula	Mol wt	Sp gr (air = 1)	BP, °C	C_{st} (in air), vol pct	ΔH_f (25° C), kcal mol	ΔH_c (net, 25° C), kcal mol	Flash-point, °C	Minimum AIT, °C	Flammable limits	
										L_{25}, vol pct	U_{25}, vol pct
CHLORINATED COMPOUNDS (ALKYLS)											
Methyl chloride (chloromethane)	CH_3Cl	50.49	1.8	−24	12.25	−20.6	153	NA	632	10.7	17.4
Methylene chloride (dichloromethane)	CH_2Cl_2	84.94	2.9	40	17.32	−22.8	115	NA	615	[7]15.9	[7]19.1
Ethyl chloride	C_2H_5Cl	64.52	2.2	12	6.52	−26.7	299	−50	519	3.8	15.4
Ethylene chloride (1,2-dichloroethane)	$C_2H_4Cl_2$	98.96	3.4	83	7.72	−31.0	259	13	440	[7]4.5	[7]17.3
Methyl chloroform (trichloroethane)	$C_2H_3Cl_3$	133.41	4.6	74	9.48	−24.2	230	NA	485	6.8	NA
n-Propyl chloride	C_3H_7Cl	78.54	2.7	47	4.44	−31.1	447	NA	520	2.6	11
Propylene chloride	$C_3H_6Cl_2$	112.99	3.9	96	4.97	−39.6	402	16	557	3.4	14.5
n-Butyl chloride	C_4H_9Cl	92.57	3.2	78	3.37	−35.2	594	−9	250	1.8	[7]10
Isobutyl chloride	C_4H_9Cl	92.57	3.2	69	3.37	−38.1	591	NA	NA	2.0	8.8
n-Amyl chloride (chloropentane)	$C_5H_{11}Cl$	106.60	3.7	108	2.72	−41.8	740	13 oc	260	[4]1.6	[7]8.6
tert-Amyl chloride	$C_5H_{11}Cl$	106.60	3.7	86	2.72	−43.1	738	−12	345	[5]1.5	7.4
CHLORINATED COMPOUNDS (UNSATURATES)											
Chloroacetylene	C_2HCl	60.48	NA	−30	9.48	51.1	261	NA	NA	NA	100
Vinyl chloride (chloroethene)	C_2H_3Cl	62.50	2.2	−13	7.72	8.4	276	NA	472	3.6	33
Dichloroethylene (1,2-dichlorethene)	$C_2H_2Cl_2$	96.94	3.4	60	9.47	.5	232	6	460	9.7	12.8
Trichlorethylene	C_2HCl_3	131.39	4.5	87	12.25	−1.4	210	32	420	12.0	[7]40
Tetrachloroethylene	C_2Cl_4	165.83	5.72	121	17.32	−3.4	185	NA	NA	NA	NA
Propargyl chloride (3-chloropropyne)	C_3H_3Cl	74.51	NA	65	7.73	NA	NA	NA	NA	NA	100
Allyl chloride (3-chloropropene)	C_3H_5Cl	76.53	2.6	45	4.97	−.2	420	−32	485	2.9	11
Isopropenyl chloride	C_3H_5Cl	76.53	2.63	23	4.97	NA	NA	NA	NA	4.5	16
Isocrotyl chloride	C_4H_7Cl	90.55	NA	68	3.67	NA	NA	NA	NA	4.2	19
2-Chloro-2-butene	C_4H_7Cl	90.55	3.1	71	3.67	NA	NA	−19	NA	2.9	9.3
CHLORINATED COMPOUNDS (ACETYL AND ALCOHOL DERIVATIVES)											
Acetyl chloride	C_2H_3OCl	78.50	2.7	51	9.48	−58.3	210	4	390	[2]5.0	NA
Ethylene chlorohydrin (2-chloroethanol)	C_2H_4ClOH	80.52	2.78	128	7.73	−70.3(l)	256	60 oc	425	[6]4.9	[6]15.9
CHLORINATED COMPOUNDS (BENZENES)											
Chlorobenzene	C_6H_5Cl	112.56	3.9	132	2.90	12.4	714	29	640	1.4	7.1
Benzyl chloride (chlorotoluene)	C_7H_7Cl	126.59	4.4	179	2.40	−16.8(l)	837	67	585	[6]1.1	NA
o-Dichlorobenzene	$C_6H_4Cl_2$	147.01	5.1	181	3.12	7.2	673	66	648	[6]2.2	[6]9.2
BROMINATED COMPOUNDS (ALKYLS)											
Methyl bromide (bromomethane)	CH_3Br	94.94	3.3	3.6	12.24	−9.0	152	NA	537	10	15
Ethyl bromide	C_2H_5Br	108.97	3.8	38	6.52	−15.3	297	NA	511	6.7	11.3
n-Propyl bromide	C_3H_7Br	123.00	4.3	71	4.45	−21.0	443	NA	490	NA	NA
n-Butyl bromide	C_4H_9Br	137.03	4.7	102	3.37	−25.7	590	18	265	[7]2.5	[7]6.6
n-Amyl bromide (bromopentane)	$C_5H_{11}Br$	151.05	NA	130	2.72	−30.9	737	32	NA	NA	NA
BROMINATED COMPOUNDS (UNSATURATES AND BENZENES)											
Propargyl bromide (3-bromopropyne)	C_3H_3Br	118.97	4.1	88	5.65	~40	389	10	324	3.0	100
Allyl bromide (3-bromopropene)	C_3H_5Br	120.98	4.2	70	4.97	11.8	418	−1	295	4.4	7.3
Isocrotyl bromide	C_4H_7Br	135.00	NA	NA	3.67	NA	NA	NA	NA	6.4	12
Bromobenzene	C_6H_5Br	157.02	5.4	156	2.90	25.1	713	51	565	[2]1.6	NA
SULFUR COMPOUNDS											
Hydrogen sulfide	H_2S	34.08	1.18	−61	12.25	−4.8	124	NA	260	4.0	44
Carbon disulfide	CS_2	76.14	2.63	46	6.53	28.0	252	−30	100	1.3	50
Methyl mercaptan (methanethiol)	CH_3SH	48.11	1.66	6	6.53	−5.5	276	NA	NA	3.9	22
Ethyl mercaptan	C_2H_5SH	62.13	2.15	35	4.45	−11.0	421	NA	300	2.8	18
Butyl mercaptan	C_4H_9SH	90.19	3.10	97	2.72	−21.1	715	2	NA	NA	NA
Dimethyl sulfide	$(CH_3)_2S$	62.13	2.15	37	4.45	−9.0	423	NA	205	2.2	20
Dimethyl sulfoxide	$(CH_3)_2SO$	78.13	NA	189	4.98	−34.6	398	95	NA	[6]2.6	[6]28.5

Combustible	Formula	Mol wt	Sp gr (air = 1)	BP, °C	C_{st} (in air), vol pct	ΔH_f (25° C), kcal/mol	ΔH_c (net, 25° C), kcal/mol	Flash-point, °C	Minimum AIT, °C	Flammable limits	
										L_{25}, vol pct	U_{25}, vol pct
BORON COMPOUNDS											
Diborane	B_2H_6	27.67	0.96	−93	6.53	7.5	478	NA	~40	0.8	88
Tetraborane	B_4H_{10}	53.32	1.84	16	3.67	NA	NA	NA	NA	.4	NA
Pentaborane	B_5H_9	63.12	2.18	58	3.37	15.0	1,030	NA	NA	.42	NA
Decaborane	$B_{10}H_{14}$	122.22	4.23	213	1.87	8.0 (s)	NA	NA	NA	.2	NA
MISCELLANEOUS GASES											
Hydrogen	H_2	2.02	0.07	−253	29.53	0	57.8	NA	520	4.0	75
Deuterium	D_2	4.03	NA	−250	29.53	0	NA	NA	NA	4.9	75
Ammonia	NH_3	17.03	.59	−33	21.83	−11.0	75.7	NA	650	15	28
Carbon monoxide	CO	28.01	.97	−192	29.53	−26.4	67.6	NA	609	12.5	74
Natural gas (Pittsburgh)	Mixture	~17	~.6	NA	~8.6	NA	NA	NA	~500	~4.8	~13.5
Natural gas (others)	Mixture	~17	.6-.7	NA	8.5-10	NA	NA	NA	480-630	3.8-6.5	13-17
Coal gas	Mixture	NA	.4-.5	NA	15.5-18	NA	NA	NA	NA	~5.3	~32

NA Not available. l liquid. g gas. s solid. oc open cup.

[1]Flammability data represent the values selected from the various publications cited in the text. The flammability limits (L_{25} and U_{25}) are mainly from references 11, 54, 72, and 110; minimum autoignition temperatures (AIT's) from references 23, 72, 110, and 112; and flashpoints from references 1, 35, 72, and 110. Flashpoints are generally closed-cup values; AIT's refer to incipient flame combustion; and L_{25} and U_{25} limits refer to combustible vapor-air mixtures at 25° ± 5° C. Most ΔH_f data are from references 91, 100, and 105 with combustible in gaseous state. Both C_{st} and ΔH_c are calculated values for ideal combustion to H_2O, CO_2, SO_2, B_2O_3, N_2, HCl, or HBr. Boiling points (BP), specific gravities (Sp gr), and molecular weights (mol wt) are from handbook references 72 and 105.

[2]Calculated.

[4]45° to 55° C.

[5]80° to 95° C.

[6]Temperature uncertain (>25° C).

[7]100° to 115° C.

[8]120° to 135° C.

[9]160° to 175° C.

[10]140° to 155° C.

[11]200° C.

[12]90% solution.

APPENDIX B.— DEFINITION OF SYMBOLS

COMBUSTION OR THERMODYNAMIC SYMBOLS WITH TYPICAL UNITS

A — Area, m^2 or cm^2, or rate constant
AIT — Minimum autoignition temperature, °C
a — Reactant concentration, mol/L
BP — Boiling point, °C
C — Concentration, vol pct or wt pct; or specific heat, cal/(g·° C)
C_p — Heat capacity at constant pressure, cal/ (mol·° C)
C_{st} — Stoichiometric concentration, vol pct or wt pct
C_v — Heat capacity at constant volume, cal/ (mol·° C)
C/I — Combustible-inert ratio
$CO/\Delta O_2$ — Ratio of CO formation to O_2 reduction
c — Velocity of sound, m/s
c_d — Vent discharge coefficient
D — Detonation velocity, m/s
d — diameter, m or cm
E — Energy (chemical or mechanical), cal or J, or gas expansion ratio
ΔE — Energy change, cal or J
F/A — Fuel-air ratio
FI — Flammability index (fire resistance)
FS — Flame spread rate, cm/s
g — Gravitational constant, 980.6 cm/s^2
H — Heat content or enthalpy, kcal/mol
ΔH — Heat of reaction, kcal/mol
ΔH_c — Heat of combustion, kcal/mol
ΔH_f — Heat of formation, kcal/mol
ΔH_v — Heat of vaporization, kcal/mol
h — Height, m or cm
h_r — Radiative heat flux, cal/(cm^2·s)
I — Ignitor heat input, cal/cm^2, or irradiance, cal/(cm^2·s)
K — Ratio of duct area to vent area
k — Empirical constant
L — Lower limit of flammability, vol pct
L/D — Length-diameter ratio
M — Molecular weight, g/mol, or Mach number
MESG — Maximum experimental safe gap, cm
MIE — Minimum ignition energy, J
N_t — Total moles
n — Moles of a component
P_F — Fuel vapor pressure at flash point, atm or psia
P_t — Total pressure, atm or psia
P_v — Combustion pressure at constant volume, atm or psia
ΔP — Pressure rise, atm or psi
p — Partial pressure, atm or psi
Q — Heat (chemical or mechanical), cal or J
q — Rate of heating, cal/s or °C/s
R — Universal gas constant, 1.987 cal/(k·mol)
r — Radius, m or cm
S — Surface area, m^2 or cm^2
S_f — Flame speed, cm/s
S_g — Gas velocity, cm/s
S_h or S_t — Vessel hoop or tensile stress, psi
S_u — Fundamental burning velocity, cm/s
T — Temperature, °C or K
T_F — Flashpoint, °C
T_f — Flame temperature, °C or K
T_L — Lower temperature limit of flammability, °C
T_u — Upper temperature limit of flammability, °C
ΔT — Temperature rise, °C or K
t — Time, s, or thickness, cm
U — Upper limit of flammability, vol pct
V — Volume, m^3 or cm^3
v — Regression rate, cm/min, or flame velocity, cm/s

W — Weight, g or kg, and work, cal or J
X — Mole fraction
x — Distance, m or cm
Z — Rate frequency constant or compressiblity factor

GREEK SYMBOLS

α — Thermal diffusivity $\frac{(\lambda)}{(\rho C_p)}$, cm^2/s
γ — Ratio of specific heats (C_p/C_v)
δ_c — Vessel shape factor (thermal theory)
Θ — Reduced temperature (T/T_c)
λ — Thermal conductivity, cal/(cm·s·°C), or scaled distances, $m/kg^{1/3}$
π — Reduced pressure (P/P_c)
ρ — Density, g/cm^3
τ — Ignition delay, s

SUBSCRIPTS

$_1$ or $_0$ — Initial or zero state
$_2$ — Final state
$_b$ — Burned state
$_c$ — Critical state
$_f$ — Flame
$_g$ — Gas
$_i$ — i^{th} fraction
$_{l,L}$ — Lower limit
$_m$ — Maximum
$_p$ — Constant pressure
$_T$ — Temperature
$_t$ — Total
$_{u,U}$ — Upper limit or unburned state
$_v$ — Vapor

ELECTRICAL SYMBOLS WITH TYPICAL UNITS

C — Capacitance, F
E — Voltage, V, or energy, J
I — Current, A
L — Inductance, H
Q — Electrical charge, C
R — Resistance, ohms, Ω
t — Time, s
V — Potential difference, V

APPENDIX C. — CONVERSION FACTORS

TO CONVERT FROM —	TO —	MULTIPLY BY —
Square centimeter	Square inch	0.155
Square foot	Square inch	144
Square foot	Square meter	9.290×10^{-2}
Square inch	Square centimeter	6.452
Square inch	Square meter	6.452×10^{-4}
Square yard	Square meter	0.836
	DENSITY	
Gram per cubic centimeter	Pound per cubic foot	62.428
Ounce per cubic inch	Kilogram per cubic meter	1.730×10^{3}
Ounce per cubic foot	Kilogram per cubic meter	1.001
Kilogram per cubic meter	Gram per liter	1.000
Pound per cubic inch	Gram per cubic centimeter	27.680
Pound per cubic inch	Kilogram per cubic meter	27.680×10^{3}
Pound per cubic inch	Pound per cubic foot	17.28×10^{2}
Pound per cubic foot	Kilogram per cubic meter	16.018
	ENERGY OR WORK	
British thermal unit (Btu)	Joules (International)	1.055×10^{3}
Btu	Calorie, gram	252.16
Btu	Foot pound	778
Calorie, gram	Joule	4.187
Erg	Dyne centimeter	1.000
Erg	Joule	1.00×10^{-7}
Foot pound	Joule	1.356
Foot pound	Btu	1.285×10^{-2}
Foot poundal	Joule	4.214×10^{-2}
Kilocalorie	Btu	3.968
Kilocalorie	Foot pound	3.087×10^{3}
Kilowatt hour	Joule	3.600×10^{6}
Watt second	Joule	1.000
	ENERGY PER AREA-TIME	
Btu per square foot-second	Watt per square meter	1.135×10^{4}
Btu per square foot-hour	Watt per square meter	3.153
Calorie per square centimeter-minute	Watt per square meter	6.973×10^{2}
Calorie per square centimeter-second	Btu per square foot-second	3.690
Kilowatt per square foot	Btu per square foot-second	0.948
	FLOW	
Cubic foot per minute	Cubic meter per second	4.179×10^{-4}
Cubic foot per minute	Gallon (liquid) per second	0.125
Cubic foot per minute	Liter per second	0.472
Cubic inch per minute	Cubic meter per second	2.731×10^{-7}
Pound per minute	Kilogram per second	7.560×10^{-3}
	FORCE	
Dyne	Gram	1.02×10^{-3}
Dyne	Newton	1.00×10^{-5}
Gram (force)	Dyne	9.807×10^{2}
Kilogram (force)	Newton	9.807
Pound (force)	Newton	4.448
Pound (force)	Poundal	32.174
	HEAT	
Btu per hour-square foot-°F	Watt per square meter-kelvin	5.678
Btu square foot	Joule per square meter	1.136×10^{4}
Btu per pound °F	Joule per kilogram kelvin	4.187×10^{3}
Btu per pound	Joule per kilogram	2.326×10^{3}
Calorie per gram	Joule per kilogram	4.187×10^{3}
Calorie per square centimeter	Joule per square meter	4.184×10^{4}
Calorie per square centimeter-second	Watt per square meter	4.184×10^{4}
Square foot per hour (thermal diffusivity)	Square meter per second	2.581×10^{-5}
	LENGTH	
Centimeter	Inch	0.284
Foot	Meter	3.048×10^{-1}
Inch	Meter	2.540×10^{-2}
Meter	Inch	39.37
Micrometer	Meter	1.00×10^{-6}
Mile (statute)	Meter	1.609×10^{3}
Mile (statute)	Foot	5.280×10^{3}
Mile (statute)	Kilometer	1.609
Mile (nautical)	Meter	1.852×10^{3}
Yard	Meter	9.144×10^{-1}

TO CONVERT FROM —	TO —	MULTIPLY BY —
	MASS	
Ounce	Gram	28.35
Pound	Kilogram	45.36×10^{-2}
Slug	Pound	32.174
Ton (short, 2,000 lb)	Kilogram	9.072×10^{2}
Ton (long, 2,240 lb)	Kilogram	1.016×10^{3}
	POWER	
Btu per second	Horsepower	1.414
Btu per second	Watt	1.054×10^{3}
Calorie per second	Watt	4.184
Foot pound per second	Watt	1.356
Horsepower (metric)	Watt	7.355×10^{2}
Kilowatt	Btu per second	9.483×10^{-1}
Kilowatt	Kilocalorie per second	0.239
Watt	Joule per second	1.00
	PRESSURE OR STRESS (FORCE PER AREA)	
Atmosphere (760 torr)	Centimeter of mercury (°C)	76.0
Atmosphere	Feet of water	33.93
Atmosphere	Pound per square inch	14.696
Atmosphere	Newton per square meter	1.013×10^{5}
Bar	Newton per square meter	1.00×10^{5}
Dyne per square centimeter	Newton per square meter	1.00×10^{-1}
Inch of mercury	Pound per square inch	0.491
Inch of water (60°F)	Newton per square meter	2.488×10^{2}
Inch of water	Pound per square inch	3.609×10^{-2}
Pascal	Newton per square meter	1.00
Pound per square foot	Newton per square meter	1.488
Pound per square inch	Gram per square centimeter	70.31
Pound per square inch	Pound per square foot	144.00
Pound per square inch	Newton per square meter	6.895×10^{3}
Torr (mm Hg, 20° C)	Newton per square meter	1.333×10^{2}
	TEMPERATURE	
Celsius (T_c, °C)	Fahrenheit (T_F, °F)	$T_F = 1.8(T_c) + 32$
Celsius (T_c, °C)	Kelvin (T_K, K)	$T_K = T_c + 273$
Fahrenheit (T_F, °F)	Celsius (T_c, °C)	$T_c = (T_F - 32)/1.8$
	VELOCITY	
Foot per second	Meter per second	3.048×10^{-1}
Foot per second	Mile per hour	6.818×10^{-1}
Inch per second	Meter per second	2.540×10^{-2}
Meter per second	Foot per second	3.281
Mile per hour (statute)	Meter per second	4.470×10^{-1}
Mile per hour (statute)	Foot per second	1.467
	VISCOSITY	
Centipoise	Gram per centimeter second	1.00×10^{-2}
Centipoise	Newton second per square meter	1.00×10^{-3}
Centistoke	Square meter per second	1.00×10^{-6}
	VOLUME	
Barrel (oil, 42 gal)	Cubic meter	1.590×10^{-1}
Cubic foot	Cubic meter	2.832×10^{-2}
Cubic foot	Liter	28.316
Cubic inch	Cubic meter	1.639×10^{-5}
Cubic inch	Cubic centimeter	1.639×10^{-1}
Cubic yard	Cubic meter	7.646×10^{-1}
Gallon (liquid)	Liter	3.785
Liter	Cubic centimeter	1.000×10^{3}
Quart (liquid)	Cubic meter	9.464×10^{-4}

SUBJECT INDEX

Page

A

Accident investigation 2
Acetylenic hydrocarbons .. 17, 25, 28, 29, 33-41
Acids 23
Adiabatic process 8, 12, 16
Agricultural dusts 51, 53
Air composition 7
Aircraft fuels 41-48
Alcohols 21, 25, 26, 29, 31-35, 38
Aldehydes 22, 25, 26, 29, 33, 35
Alkanes 19, 25-28, 30-41
Alkenes 21, 25, 28, 31-41
Alkynes 21, 25, 28, 31-41
Amines 23, 26, 29, 34
Ammonia 23, 25, 33, 34
Anhydrides 23
Aromatic hydrocarbons ... 21, 25, 29, 31-36, 38
Autoignition temperature 11, 35, 42, 45, 55

B

Benzenes 21, 25, 29-34, 38, 41
Biological damage 67
Bituminous coals 51, 53-57
Blast waves 18, 65
Boron compounds 25
Brominated compounds 24-26, 29
Burgess-Wheeler law 14, 27
Burning rate (liquids & solids) .. 16, 41, 48, 57, 59
Burning velocity (flame) 15, 39, 40

C

Calorific value 26, 29
Carbon monoxide 25, 31-38, 41
Carbonaceous dusts 51, 53
Chapman-Jouget state 17
Chemical dusts 51, 53
Chemical ignition 10, 12
Chlorinated compounds .. 24, 25-28, 29, 31-35
CO index 55
Coal compositions 56
Coal dust 51, 53, 55
Coal ranking 57
Combustible solids 48, 51, 58
Combustion equations 7, 9, 14
Compressibility factors 6
Compression pressure 8, 12
Conveyor belts 60
Crater damage 66
Critical C/I 13
Critical gas properties 7
Cyanides 23
Cyclic hydrocarbons 21, 25, 26, 31-38

Page

D

Decomposition flames 29
Deflagration 16
Detonation pressure 17, 66
Detonation velocity 18, 40, 66
Diesel fuels 42

E

Electrical ignition 10
Engine oils 37, 42, 45-47
Enthalpy 8
Equivalence ratio 15, 26, 29
Esters 23, 26, 31-35
Ethers 22, 25, 26, 29-35, 38
Expansion ratio 16
Explosion pressure 5, 16, 38, 62
Explosion processes 5, 16
Explosion suppression 30, 53
Explosion venting 64
Explosives 66
Extinguishing requirements 32, 45, 54, 63

F

Fabrics 57, 58, 60
Fire damage 4, 60
Fire extinguishants 32, 45, 54, 63
Fire resistance 5, 59
Flame arrestors 34
Flame speed 15, 39
Flame spread rate 47, 59
Flame temperature 14, 37, 47, 50, 64
Flammable mixtures 13
Flammable solids 48, 51, 58
Flashpoint 13, 19-25, 43
Frictional ignition 10
Fuel-air ratio 7

G

Gas laws 6
Gasolines 13, 31, 32, 35, 41-45
Glycols 22, 35

H

Halogenated compounds 24, 25-29, 31-35
Heat content 8, 15
Heat of combustion 9, 14, 42, 48
Heat of detonation 66
Heat of formation 9

Page

Heat of vaporization 7, 9
Hot gas ignition 12, 37
Hydraulic fluids 41, 42, 45-47
Hydrazines 23, 29, 31, 35, 41
Hydrogen 9, 25, 31-41, 64

I

Ignition delay 11, 36, 47
Ignition energy 9, 33, 49, 54
Ignition processes 4, 9
Ignition quenching distance 10, 34
Ignition temperature 9, 35, 45, 50, 54, 58
Inerting 14, 30, 32, 44, 49, 53, 63
Isothermal process 8

J

Jet fuels 27, 31, 32, 36, 37, 41-48

K

Kerosene 31, 32, 35, 36, 42-45
Ketones 22, 25, 26, 31-33, 38

L

Le Chatelier's law 14
Lignites 51, 53, 55, 56
Limit flame temperature 14, 27, 38
Limits of flammability ... 13, 25, 30, 43, 48, 52
Liquefied gases 41
Lower pressure limit 29
Lubricants 41, 42, 45, 47

M

Metal alloys 61, 62
Metal elements 48, 50, 61, 62
Methane 9, 14-19, 25-27, 30-41, 62-64
Mine fires 55, 59
Mine explosions 52, 54
Minimum oxygen value 14, 31, 44, 49, 53
Missile damage 66

N

Natural gas 28, 32, 38
Nitrated compounds 24, 26, 29
Nonmetal elements 48-50

Page

O

Oil shale 51, 53, 54
Olefins 21, 25, 28, 31-41
Overpressures 18, 65
Oxidizer materials 58
Oxygen atmospheres 25, 33, 35, 39, 50, 59

P

Paper 57, 59
Paraffin hydrocarbons ... 19, 20, 25-28, 30-41
Physical explosions 17
Plastics 51, 53
Pool burning 12, 16, 41, 61
Pressure energy 8, 19, 66

Q

Quenching distance 10, 34

R

Radiation 12, 41, 60, 61
Raoult's law 6
Regression rate 16, 41
Rock dust 54
Rubber 52, 53, 59, 60

S

Safe gap 11, 34
Saturated hydrocarbons .. 19-21, 25-28, 30-41
Sawdust 58
Scaled distance 19, 65
Self-heating temperature 11, 55, 57
Shock wave 12, 18
Spark ignition 10, 33
Spontaneous combustion 10, 55
Static electricity 10
Stoichiometry 7
Stress failure 62
Subbituminous coals 51, 53, 55-57
Sulfur compounds 25, 31-35

T

Temperature limit of flammability 13, 19
Temperature limit of materials 60, 61
Tensile strength 62
Thermal stability 12, 28

Page

Thermal theory 11
Thermodynamic relationships 8
TNT equivalent 5, 18, 65

U

Unsaturated hydrocarbons ..21, 25, 28, 29, 31-41

V

Vapor pressure 13, 19-25, 43

Page

Vent ratio 64
Vessel rupture 5, 62, 66
Volatility 19, 43, 52

W

Wall quenching 10, 14, 25, 34, 47
Wire ignition 9, 37
Wood 57, 60, 61

UNIT OF MEASURE ABBREVIATIONS USED IN THIS REPORT

A	ampere
atm	atmosphere
Btu	British thermal unit
Btu/(h·ft^2)	British thermal unit per hour per square foot
Btu/lb	British thermal unit per pound
C	coulomb
°C	degree Celsius
cal	calorie
cal/cm^2	calorie per square centimeter
cal/(cm^2·min)	calorie per square centimeter per minute
cal/(cm^2·s)	calorie per square centimeter per second
cal/(cm·s·°C)	calorie per centimeter per second per degree Celsius
cal/g	calorie per gram
cal/(g·°C)	calorie per gram per degree Celsius
cal/(K·mol)	calorie per kelvin per mole
cal/(mol·°C)	calorie per mole per degree Celsius
cal/s	calorie per second
cal/ton	calorie per short ton
cm	centimeter
cm Hg	centimeter mercury (pressure)
cm/min	centimeter per minute
cm/s	centimeter per second
cm/s^2	centimeter per square second
cm^3/g	cubic centimeter per gram
cm^3/s	cubic centimeter per second
F	farad
ft	foot
ft/lb	foot per pound
ft/s	foot per second
g	gram
g/cm^3	gram per cubic centimeter
g/L	gram per liter
g/m^2	gram per square meter
gal/ton	gallon per short ton
H	henry
h	hour
in	inch
in/min	inch per minute
J	joule
J/(K·mol)	joule per kelvin per mole
K	kelvin (degree)
kbar	kilobar
kcal	kilocalorie
kcal/(cm^2·min)	kilocalorie per square centimeter per minute
kcal/mol	kilocalorie per mole
kcal/mol·K)	kilocalorie per mole per kelvin
kg	kilogram
kg/m^3	kilogram per cubic meter
km	kilometer
kpsi	kilopounds per square inch
L	liter
L·atm/(K·mol)	liter atmosphere per kelvin per mole
m	meter
m/kg	meter per kilogram
m/min	meter per minute
m/s	meter per second
mg	milligram
mg/L	milligram per liter
mJ	millijoule
ms	millisecond
μm	micrometer
mol pct	mol percent
oz/ft^3	ounce per cubic foot
pct	percent
psi	pound per square inch
psia	pound per square inch, absolute
psig	pound per square inch, gauge
psi/s	pound per square inch per second
s	second
V	volt
vol pct	volume percent
W	watt
wt pct	weight percent
Ω	ohm

U.S. GOVERNMENT PRINTING OFFICE : 1986 O - 159-315